Mud Volcano Systems: Structure, Evolution and Processes

ROBERTS, KATIE,SARAH

DEPARTMENT OF EARTH SCIENCES, DURHAM UNIVERSITY

Mud Volcano Systems: Structure, Evolution and Processes

A thesis submitted to Durham University for the degree of Doctor of Philosophy in the Faculty of Science.

Katie Sarah Roberts

2011

Abstract

Mud volcano systems erupt sediment and fluid onto the Earth's surface producing edifices up to 25 km^3 in volume however, little is known about how such volumes are transported through the Earth's crust. This thesis investigates whether transport is through mud-dyke-sill complexes, or is diapiric. Structural field mapping of exhumed mud volcano intrusive domains onshore in Azerbaijan, shows that feeder complexes are 200-800 m wide and roughly circular. These complexes consist of various fracture networks and a megabreccia of country rock blocks tens-of-metres-across that have rotated up to 90° in a matrix of mud. A structural domain model categorises regions within the feeder complex which formed during stoping processes.

Structural mapping is combined with nearest neighbour and 2-point-azimuth statistical analysis of vent distributions described from nine mud volcanoes in Azerbaijan and Lusi mud volcano, East Java. Vent distributions are non-random, showing alignments with: 1) anticline crestal faulting, 2) fractures 3) ring faults, and 4) detachment faults indicating that fracture systems and regional stresses significantly influence feeder complex architecture. Lusi's vent alignments change orientation from 2006-2010 implying regions 10 km east and west of the main vent are more likely to be impacted by new vents due to the onset of elongate-caldera collapse.

Kilometre-scale, elongate scarps are identified as 'sector collapses' on mud volcanoes in Azerbaijan due to morphological similarity to those on igneous volcanoes. Shape parameters distinguish sector collapses and eruptive mud breccia flows allowing identification in field and satellite-based mapping. The updip domains are characterised by vents showing there is linkage to deeper mud volcano fluid flow pathways. A model of a deflating mud chamber triggering 'thin-skinned' sector collapse is proposed. This sector collapse model, vent alignment orientation analysis and intrusive domain structural model are ultimately integrated into a comprehensive schematic model of the mud volcano system.

Table of Contents

Abstract ..... *i*

List of Tables ..... *vi*

List of Figures ..... *vii*

List of Abbreviations ..... *xvi*

List of Symbols ..... *xvii*

Declaration ..... *xviii*

Acknowledgements ..... *xix*

1 Introduction 1

1.1 Introduction 1

1.2 Aims and Rationale 3

1.3 Thesis Outline 6

1.4 Methodology 9

1.4.1 Remote Sensing 9

1.4.2 Structural Field Mapping 9

1.4.3 Statistical Analyses 10

1.5 Geographical, Tectonic and Stratigraphic Setting 13

1.5.1 The South Caspian Basin (SCB) and Eastern Azerbaijan 14

1.5.2 Sidoarjo, East Java, Indonesia 18

2 The Characterisation of Mud Volcano Systems 24

2.1 Introduction 24

2.2 The Source Domain 25

2.2.1 Mechanisms of Sediment Deformation and Mobilisation 26

2.3 The Intrusive Domain 35

2.3.1 Mud Diapirism 37

2.3.2 Mud Sill/Dyke Igneous Style Intrusive Complex 42

2.3.3 Faulting 46

2.4 The Extrusive Domain 50

2.4.1 Edifice 51

2.4.2 Classification Schemes 52

2.4.3 Mud Volcano Activity 55

2.4.4 Calderas 59

2.4.5 Flows 60

2.4.6 Deposits 61

2.5 The Roof Domain 64

3 Structure of Exhumed Mud Volcano Feeder Complexes, Azerbaijan 65

3.1 Introduction 66

3.2 Geological Setting 67

3.3 Methods and Datasets 69

3.4 Observations 70

3.4.1 Kichik Kharami Mud Volcano 70

3.4.2 Pirsaatadag Mud Volcano 77

3.4.3 Alyaty Ridge 79

3.4.4 Structural Sub-Domains Associated with Feeder Complexes 81

3.5 Interpretation 84

3.5.1 Degree of Fracturing 84

3.5.2 Blocks of Country Rock within the Feeder Complex 85

3.6 Discussion: Block Rotation Processes 86

3.6.1 Flow Rotation 87

3.6.2 Stoping 89

3.6.3 Rotation Due to Multiple Intrusive Episodes 91

3.6.4 Caldera Collapse 91

3.6.5 Diapirs 92

3.7 Implications 92

3.8 Conclusions 93

4 Structural Controls on Mud Volcano Vent Distributions: Examples from Azerbaijan and Lusi, East Java 95

4.1 Introduction 96

4.1.1 Mud Volcanoes and Vent Complexes 97

4.2 Geological Settings 99

4.2.1 Azerbaijan 99

4.2.2 Lusi, Sidoarjo, East Java 99

4.3 Database and Methodology 100

4.3.1 Structural Mapping 100

4.3.2 Statistical Analyses 101

4.4 Observations 104

4.4.1 Alyaty Ridge 104

4.4.2 Kichik Kharami Mud Volcano 106

4.4.3 Pirsaatadag Mud Volcano 108

4.4.4 Akhtarma-Karadag Mud Volcano 110

4.4.5 Dashgil Mud Volcano 111

4.4.6 Durovdag Mud Volcano 113
4.4.7 Lusi Mud Volcano, East Java 115
4.4.8 Nearest Neighbour Analysis 117
4.5 Discussion 117
4.5.1 Alignments 118
4.5.2 Distributions - Fractionation of Vent Eruptive Phases 123
4.5.3 Time Dependent Changes – Lusi Mud Volcano 124
4.6 Conclusions 130

5 Sector Collapse of Mud Volcanoes, Azerbaijan 132
5.1 Introduction 133
5.2 Geological Setting 133
5.3 Methods and Datasets 134
5.4 Observations 135
5.4.1 Lökbatan Mud Volcano 135
5.4.2 Akhtarma-Karadag and Pilpilya Mud Volcanoes 138
5.5 Interpretation 142
5.5.1 Amphitheatre 142
5.5.2 Sector Collapse Fault 144
5.5.3 Levees 145
5.5.4 Debris Avalanche Deposit 146
5.5.5 Eruptive Flow Versus Sector Collapse 149
5.6 Discussion: Mechanisms for Mud Volcano Sector Collapse 152
5.7 Conclusions 159

6 Discussions and Conclusions 161
6.1 Introduction 161
6.2 Discussion 161
6.2.1 Comparison to Igneous Volcanic Systems 162
6.2.2 Influence of Regional and Local Structure and Stresses 167
6.2.3 Fluid Flow Pathways within Mud Volcano Systems 173
6.2.4 Geo-Hazard Prediction 174
6.2.5 Mud Volcano System Model 176
6.2.6 Limitations 178
6.3 Conclusions 179
6.3.1 General Conclusions 182
6.4 Future Work 183

6.4.1 Field Studies 183
6.4.2 Modelling 186
6.4.3 Seismic Imaging Techniques 186

Appendix I: Azerbaijan Locations, Structural Maps and Eruption History 188
Appendix II: Supporting Material for Chapter 3 197
Appendix III: Supporting Material for Chapter 4 204
Appendix IV: Supporting Material for Chapter 5 212
Appendix V: Published Journal Articles 220
References 222
Electronic Appendices and Electronic Copy of Thesis ..... Disc

List of Tables

Chapter 2: The Characterisation of Mud Volcano Systems

Table 2.1:	Mechanisms for generating overpressure from Kopf (2002).	30
Table 2.2:	Classification system based on the character of mud volcano activity with respect to morphological expression, distinguishing three types of mud volcanoes. After Dimitrov (2002).	55
Table 2.3:	Different vent types found on mud volcanoes.	58

Chapter 3: Structure of Exhumed Mud Volcano Feeder Complexes, Azerbaijan

Table 3.1:	Dimensions of mud volcanoes (A, B and C), that extrude along Alyaty Ridge.	79
Table 3.2:	Table of structural features present in each field area.	80

Chapter 4: Structural Controls on Mud Volcano Vent Distributions: Examples from Azerbaijan and Lusi, East Java

Table 4.1:	Classification of vents mapped during the study.	98
Table 4.2:	Showing different mud volcanoes nearest neighbour statistical analysis results.	117

Chapter 5: Sector Collapse of Mud Volcanoes, Azerbaijan

Table 5.1:	Dimensions of sector collapse structures discussed in the text. The 'angle of repose' is measured from the slope angle of the sector failure.	147
Table 5.2:	Causes of mud volcano collapse adapted from Voight & Elsworth (1997).	157

Chapter 6: Discussions and Conclusions

Table 6.1:	Comparison of igneous and mud volcanic systems. Google Earth Images © 2010 DigitalGlobe and © 2010 GeoEye, © 2010 Google.	163

List of Figures

Chapter 1: Introduction

Fig. 1.1:	Distribution of mud volcanoes on Earth. From Kopf (2002).	2
Fig. 1.2:	Schematic of the 2-point azimuth technique. Line segments are drawn between each vent and any vents to the east of that vent. The azimuth of the line segment from north is measured. Each azimuth orientation is then plotted in a frequency histogram.	13
Fig. 1.3:	Geological setting and study area location in Azerbaijan: A) Location of Azerbaijan. B) Tectonic map of the SCB showing the position of major structural elements and position of the onshore project study area (red box). Map location is shown as a blue box in Fig. 1.3A. Modified from Jackson *et al.* (2002).	14
Fig. 1.4:	Location of mud volcanoes in the Azerbaijan and the Caspian Sea region. 1- Mud volcanoes, 2- deep faults, 3- boundaries of mud volcano areas, 4- political margins. I to VII Mud volcano areas: I- interflow of Kura and Iori rivers, II- Shamakha-Gobustan, III- Lower Kura, IV- Pre-Caspian, V- Absheron-Prebalkhan, VI- Baku archipelago, VII- Western Turkmenia. From Guliyev & Panahi (2004).	15
Fig. 1.5:	Regional 2-D reflection seismic line showing main tectono-stratigraphic elements, approximately six times vertical exaggeration. Inset shows the interpretation at vertical = horizontal scale. ACG is one of the main hydrocarbon producing fields in the SCB. From Stewart & Davies (2006).	17
Fig. 1.6:	Schematic cross-section across Shah Deniz in the SCB showing the relationship of the deep structure with the shallower structure and mud volcanoes. From Fowler *et al.* (2000).	18
Fig. 1.7:	Geological map and mud volcano distribution in east and Central Java. Red dots are the identified mud volcano locations. From Istadi *et al.* (2009). Inset shows global location with red rectangle marking the extent of the figure from Istadi *et al.* (2009).	20
Fig. 1.8:	The Porong collapse structure. A) Seismic base map overlays satellite image. The areal extent of the Porong collapse structure in shaded dark colour, which covers a much larger area compared to the Lusi interpreted overpressured shale area. Porong was an adjacent mud volcano that has been used as an analogue to build the subsidence model for Lusi. From Istadi *et al.* (2009). B) Seismic section of Lusi – Banjar Panji-1 – Tanggulangin-1 – Porong-1 – Porong collapse structure. The Porong collapse structure located approximately 7 km from Lusi is a palaeo-mud volcano where subsidence is evident and the multiple faults present likely served as conduits for the mudflow. Similarly, the multiple faults near the BJP-1 well (200 m from Lusi) may have been reactivated and served as conduit for the mud eruptions and escaping gas, hence the appearance of gas bubbles along fault lines.	21

Chapter 2: The Characterisation of Mud Volcano Systems

Fig. 2.1:	Summary diagram outlining the basic subsurface configuration and structural domains of a large mud volcano system. Onshore mud volcano systems usually lack a roof domain and are not below sea level. Modified from Stewart & Davies (2006).	25
Fig. 2.2:	Summary diagram of mud volcano timing with respect to stratigraphy and start of structural growth. Note the delay in the appearance of the first mud volcanoes from the start of structural growth. Delay of the order of 0.5 to 1 million years assuming relative constant deposition rates from the Akchagyl Ash Beds date of 2.4–2.6 Ma. From Fowler *et al.* (2000).	28

Fig. 2.3:	Schematic diagram of a mud diapir, mud volcano extrusions, and diatremes, including possible fluid sources (numbered 1–8). (1) Pore fluid expulsion during compaction. (2) Biogenic methane from degradation of organic matter. (3) Lateral fluid flux through stratigraphic horizons or fault zones. (4) Fluid migration along deep seated thrusts. (5) Thermogenic methane and higher hydrocarbon concentrations. (6) Fluids from mineral dehydration (opal, smectite). (7) Hydrothermal fluids, alteration of crustal rock. (8) Fluid expulsion from internal deformation within the diapiric intrusion. Geochemically mature fluids may be found among categories 3, 4, and 7, while in categories 1, 6, and 8, water from dissociated gas hydrates may provide 'freshened' fluids. Modified from Kopf (2002).	32
Fig. 2.4:	A) Horizontal seismic section (depth slice) through a downward-tapering cone, showing an abrupt change from regional structure to faulting and folding of strata in the downward-tapering cone. B) Seismic coherency data emphasising stratal discontinuities in a mud volcano system. The cube is located below the mud volcano and contains a downward-tapering cone. Discontinuities (bright blue) can be interpreted as faults and fracture zones. This visualisation of structural complexity can be useful in well planning through or around mud volcano substructure. Modified from Stewart & Davies (2006).	37
Fig. 2.5:	Schematic cross sections illustrating some of the characteristics of shale diapirs and pipes (A and B). Variations on shale bulges developing in response to sedimentary loading by deposition in the hanging wall of a reactive diapir (Fig. 2.5A), and in a withdrawal syncline (Fig. 2.5B); C) development of shale diapirs similar to classic salt diapirs with reactive, active, and passive phases and D) shale diapirs commonly do not develop like Fig. 2.5C but may superficially resemble them. Instead a complex of gas rich fluids and shale intrusions may intrude laterally and vertically (pipes) into the country rock from mobile shale masses at depth. The well developed synformal depocentres in Fig. 2.5C are not seen in Fig. 2.5D. Modified from Morley *et al.* (1998).	40
Fig. 2.6:	Summary of how diapirs can 'apparently pierce' overburden sediments on seismic reflection profiles. A) Condensed sequence and/or attenuation by ductile creep. B) Non-deposition of sediment and active erosion/dissolution at the sea-bed. C) Extensional faulting and condensed sequence. D) Dissolution above sea-level with surface run-off creates pot-holes crevasse system with stoping of sediments into dissolved channels and caverns. Modified from Davison *et al.* (1996).	41
Fig. 2.7:	Sketch of an outcrop in Jerudong (Brunei) cut by numerous dykes. Some of the dykes follow older normal faults, but most dykes are independent of the normal faults. The dykes have steep dips in their present orientation. Upon rotation of bedding to horizontal, dyke dips become much lower. Hence assuming dykes were intruded sub-vertically, dyke emplacement is inferred to be post folding. Photographs show jogs and splays in mudstone dykes in sandstones, these dykes are natural hydraulic fractures and do not follow pre-existing faults. Modified from Morley (2003).	43
Fig. 2.8:	A) 'Variance Cube' slice illustrating a change in fault pattern around a 'mud pillow' structure from the Gjallar Ridge, offshore mid-Norway. The variance cube highlights lateral discontinuities such as faults in the seismic data. It was calculated by cross correlating adjacent traces over a 100-ms window and assigning a value from 0 (perfect match) to 1 (no match). The radial pattern in the proximity of the structure and the polygonal pattern away from the structure suggest that the polygonal faults developed when the structure either had formed or was forming. Modified from Hansen *et al.* (2005). B) Sidescan sonar image of a mud volcano from Nigeria. Modified from Graue (2000). C) 30-kHz side-scan sonar image of the mud volcano Yuma (dark tones indicate high acoustic back-scatter), shown with the same horizontal scale, in the Gulf of Cadiz. Note the concentric ring-like structures that are centred on the main	49

	summit with the small dome to its left. Modified from Murton & Biggs (2003). D) Seabed dip map in Nigeria. Mud volcanoes are seen as 1–2 km circular features. Note the cuspate faults and numerous pockmarks. Modified from Graue (2000). E) 3-D view of the concentric fault system and margins of the caldera with downward-tapering cone in ACG field, SCB. Elements of the seismic reflection cube are left to indicate the quality of seismic data on which the interpretation is based. Modified from Stewart & Davies (2006). F) Artificially illuminated rendering of the Akchagyl structure map viewed from the northeast to southwest. The rendering illustrates the radial fault pattern and associated fault blocks that offset the Akchagyl horizon, and subtle erosional channels on the eastern (facing) flank of the anticline (vertical exaggeration – 50:1) modified from Corthay & Aliyev (2000).	
Fig. 2.9:	Sketches of radial and concentric fault patterns and kinematics. Driving mechanism is salt flow and volume change of central cylinder. Volume and line length balance assumed. All sketches are plan views except D. Salt is pink. A) Expansion of central zone forces fold with circumferential trend, and circumferential extension accommodated by radial faults. B) Radial fault clustering at each end of elliptical hole or intrusion. C) Contraction of central zone allows concentric, inward-facing extensional faults. Secondary structures accommodate circumferential contraction. D) Sheared sediments close to diapir margin (vertical section). These faults are parallel to the salt sediment interface, i.e. concentric in plan view. From Stewart (2006).	50
Fig. 2.10:	Sizes and shapes of various terrestrial mud volcanoes (note the figure of a man in both frames). Locations: A= Maghaehu Stream, New Zealand; B= Volcanito, near Cartegena, Colombia; C= Moruga Bouff, Trinidad; D= El Totumo, near Cartegena, Colombia; E= Chandragup, Makran Coast, Pakistan; F= Napag, Makran Coast, Pakistan; G= Gharniarigh-Tapeh, Goran region, northern Iran. From Judd & Hovland (2007).	51
Fig. 2.11:	Schematic diagrams of A) cone-shaped and B) pie-shaped mud feature with main applicable terms from Kopf (2002).	53
Fig. 2.12:	Types of mud volcanoes based on the shape and appearance on the seismic line. A) Concave; B) Convex; C) Flat; D) Buried. From Yusifov (2004).	53
Fig. 2.13:	Schematic showing end-member geometries of stacked mud volcanoes in a subsiding basin. Volcanoes are kilometre-scale. No sub-volcanic structure is implied. A) A single mud volcano bicone at a shallow structural level, connected by a long feeder to the mud source. B) Episodic reactivation, edifice building and burial create a stack of bicones of various sizes, the youngest shown here yet to be fully buried. C) A single episode of pulsed extrusion, punctuated by brief periods of relatively high rates of background sedimentation, creates an interdigitating margin and 'Christmas tree' appearance. Geometries A or C could be misinterpreted as plutonic intrusions. Modified from Stewart & Davies (2006).	57
Fig. 2.14:	Mud volcano calderas. A) Photograph of a small caldera to the west of Bahar mud volcano, Azerbaijan. B) Schematic block diagram illustrating the principal structural and morphological elements of a typical circular mud volcano summit caldera identified. Dashed lines indicate areas of tentative interpretation. From Evans *et al.* (2008).	60
Fig. 2.15:	Different scales of mud flow from mud volcanoes. A) Koturdag mud volcano with a 1.3 km long mud flow emanating from its caldera. Image © 2010 GeoEye, © 2010 Google. B) Photograph of a gryphon with a centimetre-scale mud flow flowing from a small depression at its crest. Note in both pictures the compressional ridges at the base of each flow and the levees building up on either side of the flows in their lower reaches.	61
Fig. 2.16:	Photographs of eruptive deposits on mud volcanoes in Azerbaijan. A) A salse erupting oil with a gryphon erupting mud into it at Pirsaatadag mud volcano. B) A sandstone clast within the kilometre-scale mud flow on Kichik Kharami mud	64

	volcano. Note the rucksack for scale. C) Cinder mound marking the location of the gaseous eruption of Lökbatan mud volcano in 2001. Note the camera case for scale. D) Salt deposits around a salse on Kichik Kharami mud volcano. E) Nodular concretions found on top of Kichik Kharami, Koturdag C and Pirsaatadag mud volcanoes.	

Chapter 3: Structure of Exhumed Mud Volcano Feeder Complexes, Azerbaijan

Fig. 3.1:	Map of the Caspian coastline in Azerbaijan showing the location of the study areas (localities marked with stars) and the trends of anticlines axes (indicated by black line with dash across). Inset map of Azerbaijan shows map location as red box.	68
Fig. 3.2:	Schematic regional seismic section depicting the relationship between exhumed intrusive domains onshore to the deeply buried, folded mud volcanoes offshore. Yellow and green marker in the Pliocene offshore strata represent hydrocarbon reserves.	69
Fig. 3.3:	Case Study 1- Kichik Kharami Mud Volcano. A) Location of Kichik Kharami to the south of an anticline axis. Red rectangle marks the area seen in Fig. 3.3C. Image © 2010 DigitalGlobe, © 2010 Google. B) Outcrop at centre of Kichik Kharami volcano showing a large 'block' of highly fractured sandstone surrounded by a mud matrix. C) Structural map of Kichik Kharami. The central red area marks the zone where fluid is currently being extruded (i.e. the 'active vent zone'). The orange area outlines the zone where both sinuous and conjugate fracture systems are found (i.e. the 'peripheral fracture zone'). The grey transparent zone represents the area where bedding strike measurements vary greatly from the surrounding anticlinal bedding (i.e. the 'central zone of block rotation'). Any other areas that do not fall into these coloured zones are part of the 'un-intruded zone' which contains only conjugate faulting/fracturing. Purple areas mark areas where old mud flows cover outcrop. Image © 2010 DigitalGlobe, © 2010 Google.	72
Fig. 3.4:	A) Mud infilling pre-existing joints and fractures within the country rock, found in both the peripheral fracture zone and the un-intruded zone. B) Sinuous fractures only found in the peripheral fractured zone, often contain small clasts of country rock as seen in the inset picture. Pen for scale. C) Mud plugs consisting of dense mud breccia flows and D) Breccia pipes where country rock clasts have been incorporated into the vent walls to form a breccia.	74
Fig. 3.5:	Histograms showing the change in fracture densities per metre with distance from the centre of the mud volcano feeder complexes. A) Kichik Kharami mud volcano, B) Pirsaatadag Mud Volcano and C) Alyaty Ridge.	75
Fig. 3.6:	A) Stereonet showing anticline bedding around Kichik Kharami mud volcano. B) Stereonet showing the varying bedding measurements found at the centre of Kichik Kharami mud volcano. C) Stereonet showing anticline bedding around Pirsaatadag mud volcano. D) Stereonet showing the varying bedding measurements found at the centre of Pirsaatadag mud volcano. E) Stereonet showing anticline bedding around Alyaty Ridge. F) Stereonet showing the varying bedding measurements found at the centre of Alyaty Ridge.	76
Fig. 3.7:	A) Case Study 2: Outcrop at centre of Pirsaatadag volcano with rotated bedding strike orientation. B) Structural map of Pirsaatadag Mud Volcano. The central red area marks the zone where fluid is currently being extruded (i.e. the 'active vent zone'). The orange area outlines the zone where both sinuous and conjugate fracture systems are found (i.e. the 'peripheral fracture zone'). The grey transparent zone represents the area where bedding strike measurements vary greatly from the surrounding anticlinal bedding (i.e. the 'central zone of block rotation). Any other areas that do not fall into these coloured zones are part of the 'un-intruded zone' which contains only conjugate faulting/fracturing.	79

	Image ©2010 GeoEye, ©2010 Google. C) Case Study 3: Outcrop at the centre of Alyaty Ridge (compass clinometer at centre of picture for scale). D) Structural map of Alyaty Ridge. The central red areas at the centre of Koturdag A, B and C volcanoes mark the zones where fluid is currently being extruded (i.e. the 'active vent zone'). The orange area outlines the zone where both sinuous and conjugate fracture systems are found (i.e. the 'peripheral fracture zone'). Any other areas that do not fall into these coloured zones are part of the 'un-intruded zone' which contains only conjugate faulting/fracturing. The green area represents an area of contorted bedding and the blue areas indicate areas where scarps have formed due to slope failures down the flank of the anticline. Purple areas mark areas where old mud flows cover outcrop. Image ©2010 GeoEye, ©2010 Google.	
Fig. 3.8:	Schematic of the mud volcano 'feeder complex'. The 'active vent zone' is highlighted in red, this represents the area of the mud volcano that is currently erupting fluid. The 'peripheral fractured zone', in orange, marks the region where both sinuous and conjugate fracture sets are present in the country rock. The 'central zone of block rotation', in purple, indicates the area where blocks of country rock with bedding strike measurements vary from the normal bedding orientations seen in the un-intruded anticlinal bedding. The 'un-intruded zone', in grey, denotes the region that has been unaffected by the intrusion of the mud volcano system. Here only conjugate fractures that contain no fill are found. The full yellow lines represent areas of bedding that follow the general anticlinal trend, whereas dashed yellow lines indicate areas where bedding strikes could be rotated away from the regional trend. Sinuous blue lines indicate active fluid flow to the vents erupting at the surface.	82
Fig. 3.9:	Mechanisms. A) Schematic of the 'caldera collapse', mechanism modified from Cole *et al.* (2005), B) schematic map view of the intrusive mud rotation and C) schematic cross section of the 'flow rotation' mechanism.	88
Fig. 3.10:	Schematic of the 'hybrid stoping' mechanism modified from Geshi *et al.* (2002). A) Intrusion stage before the surface collapse. Evacuation of mud from the reservoir caused stoping of the roof rock of the reservoir. Underground stoping formed a cavity at the top of the stoping column. B) The early stage of summit subsidence. The roof rocks of the cavity cannot carry their own weight and collapse into the cavity. Release of mud and fluids fills the cavity. C) The late stage of the summit subsidence. Continuous evacuation of mud from the reservoir caused the subsidence of the roof of the reservoir. The top of the stoping column was filled with the collapsed materials from the outward migrating caldera wall. D) Explosive stage. Invasion of fluids to the stoping column causes eruption and conduit consists of large blocks of country rock rotating freely within it.	90

Chapter 4: Structural Controls on Mud Volcano Vent Distributions: Examples from Azerbaijan and Lusi, East Java

Fig. 4.1:	A) Major structural elements of eastern Azerbaijan after Jackson *et al.* (2002), showing the location of the mud volcanoes in this study (localities marked with blue stars; see inset for global location). B) Major structural elements of the East Java Basin, after The Geological Survey of Indonesia (1963), showing the location of Lusi mud volcano (marked with a star) and main faults marked in red (see inset for global location).	97
Fig. 4.2:	A) Gryphons (purple triangles on Fig. 4.3, Fig. 4.5, Fig. 4.6 and Fig. 4.7). Conical vents erupting mud, a few centimetres to 4 m high. B) Salses (blue triangles on Fig. 4.3, Fig. 4.5, Fig. 4.6 and Fig. 4.7). 'Lakes' of muddy water, with cones 1-2 m high and diameters of a few centimetres to over 50 m (Guliyev *et al.* 2000). C)	102

	Cinder mounds (orange triangles on Fig. 4.3, Fig. 4.5, Fig. 4.6 and Fig. 4.7). Erupt only gaseous phases. Resemble heaps of fired clay, up to 4 m high and 10-20 m long displaying an orangey-red ceramic appearance (Hovland *et al.* 1997; Planke *et al.* 2003). D) Mud plugs (purple triangle labelled in Fig. 4.3A). Breccia with a putty-like malleable consistency extruding from craters like 'paste from a tube', on Koturdag A mud volcano (Guliyev *et al.* 2000; Planke *et al.* 2003). E) Pools (green triangles on Fig. 4.3, Fig. 4.5, Fig. 4.6 and Fig. 4.7). Bubbling pools of fluid, less than 2 cm in diameter (Mazzini *et al.* 2009). Extinct or dormant vents (black triangles on Fig. 4.3, Fig. 4.5, Fig. 4.6 and Fig. 4.7). Vents that were once actively extruding fluids but have since dried up and are no longer active.	
Fig. 4.3:	A) Part of Alyaty Ridge with three mud volcanoes intruded along its axis. Koturdag A is located to the 0.6 km north of the fold axis. Yellow dashed lines represent the bedding orientation. Triangles: Purple- gryphons, orange- cinder mounds, black- extinct vents, blue- salses and green- pools. Image © 2010 DigitalGlobe, © 2010 GeoEye and © 2010 Geocentre Consulting, © 2010 Google. B) Rose diagram of fault and fracture orientations measured along Alyaty Ridge. C) Histogram of frequencies of azimuthal direction for 2-point azimuth technique of all vent types grouped together for Koturdag A, B and C. D) Histogram of frequencies of azimuthal direction for 2-point azimuth technique of individual vent types separated into their different distributions for Koturdag B. E) Histogram of frequencies of azimuthal direction for 2-point azimuth technique of individual vent types separated into their different distributions for Koturdag C.	105
Fig. 4.4:	A) Kichik Kharami mud volcano. B) Zoomed in image of the centre of the mud volcano seen in Fig. 4.4A. Vents can be seen clustering in concentric rings at the centre of the volcano whereas they form along lines orientated in NW-SE and NE-SW directions further out from the centre of the volcano. Triangles: Purple- gryphons, orange- cinder mounds, black- extinct vents, blue- salses and green- pools. Images © 2010 DigitalGlobe and © 2010 Geocentre Consulting, © 2010 Google. C) Rose diagram of fault and fracture orientations from country rock in and around Kichik Kharami. D) Histogram of frequencies of azimuthal direction for 2-point azimuth technique of individual vent types separated into their different distributions. E) Histogram of frequencies of azimuthal direction for 2-point azimuth technique of all vent types grouped together.	107
Fig. 4.5:	A) Pirsaatadag mud volcano. Triangles: Purple- gryphons, orange- cinder mounds, black- extinct vents, blue- salses and green- pools. Image © 2010 GeoEye and © 2010 Geocentre Consulting, © 2010 Google. B) Rose diagram of fault and fracture orientations from country rock in and around Pirsaatadag. C) Histogram of frequencies of azimuthal direction for 2-point azimuth technique of individual vent types separated into their different distributions. D) Histogram of frequencies of azimuthal direction for 2-point azimuth technique of all vent types grouped together.	109
Fig. 4.6:	A) Akhtarma-Karadag mud volcano. This volcano is dominated by gryphons at its western edge next to two small cinder mounds. The majority of the salses and larger gryphons extrude along an elongate ring detachment fault found along the length of the edifice (see Chapter 5; Roberts *et al.* 2011). The salses are found furthest away from the main centre of eruption further to the east of the volcano. Triangles: Purple- gryphons, orange- cinder mounds, black- extinct vents, blue- salses and green- pools. Image © 2010 GeoEye. B) Histogram of frequencies of azimuthal direction for 2-point azimuth technique of individual vent types separated into their different distributions. C) Histogram of frequencies of azimuthal direction for 2-point azimuth technique of all vent types grouped together.	111
Fig. 4.7:	A) Dashgil mud volcano zoomed in on the active vent zone. Gryphons can be seen clustering in the western section of the volcano. Cinder mounds form an elongate ridge at the southern limit of the active vent zone and two large salses	112

	are found at the southeast end of the volcano. Triangles: Purple- gryphons, orange- cinder mounds, black- extinct vents, blue- salses and green- pools. Red lines show faults and black lines show breaks in slope, with triangles pointing towards the downthrown side. Image © 2010 GeoEye and © 2010 Geocentre Consulting, © 2010 Google. B) Histogram of frequencies of azimuthal direction for 2-point azimuth technique of individual vent types separated into their different distributions. C) Histogram of frequencies of azimuthal direction for 2-point azimuth technique of all vent types grouped together.	
Fig. 4.8:	A) Durovdag mud volcano. Showing that this volcano is dominated by gryphons at its northern edge. This purple area had such a large concentration of gryphons that the whole of this area has been coloured purple to represent the intense number of gryphons found in this region, approximately one gryphon every 5 m^2. Due to the un-stable nature of this area separate readings could not be taken and so the area has been considered as one large vent. The majority of the salses cluster in a ring around the outer edge of the mud volcano with only a few small vents and extinct vents at the centre of the edifice. Triangles: Purple- gryphons, orange- cinder mounds, black- extinct vents, blue- salses and green- pools. B) Histogram of frequencies of azimuthal direction for 2-point azimuth technique of individual vent types separated into their different distributions. C) Histogram of frequencies of azimuthal direction for 2-point azimuth technique of all vent types grouped together.	114
Fig. 4.9:	Lusi mud volcano, East Java. A) November, 2006. Histogram of frequencies of azimuthal direction for 2-point azimuth technique of active vents in 2006. B) 30th September 2009. Histogram of frequencies of azimuthal direction for 2-point azimuth technique of active vents in 2009. C) January, 2010. Histogram of frequencies of azimuthal direction for 2-point azimuth technique of active vents in 2010. Blue dashed line shows trace of Kendensari River. The blue triangles represent 'bubbles' that are or were currently active at that time. Red dashed lines indicate faults described by Istadi *et al.* (2009). Images courtesy of CRISP.	116
Fig. 4.10:	Schematics of the structures that may cause the varying vent distributions. A) Dashgil type, some form of phase segregation is occurring at depth allowing the gryphons to erupt in the area of caldera collapse, the cinder mounds to follow a linear area of weakness and so erupt in a line and the watery salses erupt further away from the main vent zone. B) Kichik Kharami type, where small salses line up along pre-existing conjugate fractures and also concentrically at the centre of the edifice where caldera collapse may be initiating. C) Durovdag type, where some form of phase segregation is occurring at depth allowing the gryphons to erupt in the central zone of caldera collapse beneath the main vent, with the watery salses erupting further away from the main vent zone along concentric ring faults produced during caldera collapse. D) Koturdag type, where mud volcanoes can be seen aligning along anticline axes but have varying vent fluid compositions along the length of the anticline. E) Akhtarma-Karadag type, some form of phase segregation is occurring at depth allowing the gryphons to erupt in the area of caldera collapse, the cinder mounds to follow a linear area of weakness and so erupt in a line and the watery salses to erupt further away from the main vent zone along the detachment fault.	120
Fig. 4.11:	Schematic model depicting mud volcano elongation, elongated vent distributions, mud chamber elongation and summit caldera elongation patterns. Mud dykes preferentially trend perpendicular to σ_{Hmax} taking advantage of the crestal faulting along the anticline. Summit calderas and mud chambers also become elongate perpendicular to σ_{Hmax}. After Paulsen & Wilson (2010a).	121
Fig. 4.12:	Schematic diagram of the mode of formation of Lusi mud volcano and how its vent systems have evolved through time. A) November 2006 with its initial NE-SW vent alignment. B) January 2010 with the initiation of caldera collapse with vents aligning along re-activated E-W trending anticline crestal faulting. C) Predicted future development including elongate caldera collapse structure with	129

	vents aligning along caldera ring faults.	

Chapter 5: Sector Collapse of Mud Volcanoes, Azerbaijan

Fig. 5.1:	Digital elevation map of the Caspian coastline in Azerbaijan showing the location of the study areas (localities marked with red triangles). Red dashed lines indicate presence of faults. Inset map of Azerbaijan shows map location as red box. White colouring indicates highest topographic areas with blue representing the lowest topographic areas.	135
Fig. 5.2:	A) Lökbatan mud volcano, Baku, Azerbaijan. B) The western flank of this volcano collapsed in 2001 during an eruption. Red arrow indicates the direction of the main failure. Amphitheatre shaped depression is shaded in orange. Old mud breccia flows are coloured in purple. Levees are dark brown. Edges of collapse structure are marked by the dashed red line. Image © 2010 DigitalGlobe, © 2010 Google.	137
Fig. 5.3:	A) Akhtarma-Karadag mud volcano and west of it Pilpilya mud volcano with a collapse structure. Image © 2010 GeoEye, © 2010 Google. B) Interpretation of Fig. 5.3A. Red arrow indicates the direction the main slope failure has/could occur in. On Pilpilya the collapse and most recent flow can be seen to fail down the volcanoes western flank. C) IKONOS image of Akhtarma-Karadag mud volcano. D) Interpretation of Fig. 5.3C. Dotted black line shows fault trace. Purple areas represent gryphons and orange areas indicate regions where cinder mounds are present. Image © 2010 GeoEye.	140
Fig. 5.4:	Photos of the Akhtarma-Karadag mud volcano, Azerbaijan. A) At northern side of ring fault, June, 2006 and B) April, 2009 with an inset photo of en-echelon faulting seen along the main ring fault. Rucksack for scale. The photos show a section of the ring fault (marked by the dashed red line) that has an offset on it. There is also a large gryphon that is erupting along this fault line. C) Photo taken at the head of the ring fault in June, 2005 and D) Photo taken at the head of the ring fault in June, 2006.	142
Fig. 5.5:	Schematic of sector collapse of an igneous volcano after Ui *et al.* (2000). A) Longitudinal section of a sector collapse. The dashed line indicates the previous morphology of the volcano before the collapse took place. B) Cross section across the debris avalanche high on the flanks of the volcano- 'debris avalanche block facies', location (B). C) Cross section across the debris avalanche low down on the flanks of the volcano- 'debris avalanche matrix facies', location (C). D) 3-D schematic of mud volcano sector collapse with localities of cross sections B and C drawn on. White dashed line marks sector collapse fault.	143
Fig. 5.6:	A) Schematic diagram showing the positions of fault tips during caldera collapse and B) fault forming due to sector collapse of mud volcanoes.	145
Fig. 5.7:	Structure of mud breccia flows compared to collapse deposits. A) Mud breccia flow emanating from Koturdag crater (3 times vertical exaggeration). Image © 2010 GeoEye, © 2010 Google. Koturdag mud volcano is located 30 km southwest of Pilpilya. B) Elongate collapse structure on Lökbatan (3 times vertical exaggeration). Image © 2010 DigitalGlobe, © 2010 Google. C) Photograph of the elongate collapse structure on Lökbatan. D) Schematic of structural features seen in Fig. 5.7C. E) Photograph of the mud breccia flow emanating from Koturdag crater. F) Schematic of the structural features seen in Fig. 5.7E.	148
Fig. 5.8:	Graph showing the relationship between length and widths of various structures on mud volcano edifices. Dashed line represents the transition zone between mud breccia flows and sector collapse geometries (depicting a 2:1 ratio).	150
Fig. 5.9:	Schematic ternary diagram showing the positions of mud breccia flows, sector collapses, slope failures and hybrid failures occurring on mud volcanoes in	151

	relation to the scarp length and width and the size of the feature. The internal structure of each deposit can also be seen in the block diagrams.	
Fig. 5.10:	Schematic diagrams showing primers and triggers of mud volcano sector collapse events. A) Inflation of mud chamber and volcano causing instability. B) Addition of overburden when mud breccia is erupted onto the volcano flanks. C) Change in pore pressure within the mud volcano. D) Erosion and removal of support. E) Precipitation increasing pore fluid and loading and therefore pore pressures. F) Earth tides exerting different gravitational forces on the mud source causing more or less violent eruptions. G) Seismicity shaking the ground and changing pore pressure in the mud volcanoes. H) Eruption of mud volcano.	153
Fig. 5.11:	Rose diagrams of orientations of A) long axes of mud volcano calderas, B) mud breccia flows and C) sector collapse troughs.	155
Fig. 5.12:	Schematic sector collapse formation. A) Dormant mud volcano edifice. B) Ring fault forms after small eruption and evacuation of material from depth. C) Large eruption causes subsidence to occur due to expulsion of fluids at the surface resulting in sector collapse along ring fault. Green dashed line represents position of anticline axis.	158

Chapter 6: Discussions and Conclusions

Fig. 6.1:	Photograph showing a horizontal cross section through a sedimentary blowout pipe of late-Pleistocene age on the Greek island of Rhodes; the inset sketch illustrates the feature in three-dimensions. The inner central zone comprises relatively large (<5-10 cm) angular mud clasts floating in a muddy matrix; the outer zone has smaller (<5 cm) clasts. These zones are surrounded by 20 cm of heavily fractured country rock (limestone) and a further 4 m of less fractured rock. From Judd & Hovland (2007).	169
Fig. 6.2:	A) Sketch illustrating emplacement of radial dykes and parasitic vents in a direction parallel to the maximum horizontal compression (MHC), producing elongation of the edifice and a dilatational stress within the volcano, promoting collapse in a direction normal to the MHC. The sketch on the right-hand side illustrates typical morphology of sector collapses. From Siebert (1984). B) Schematic block diagram showing the relations between the orientation of the principal stress axes and the main fracture sets in a sealed-type thrust fold. The steep brittle discontinuities may potentially operate as conduits transferring fluids from depth up to surface. Notably, the intersection of 'ac' and 'bc' fracture families may represent a locus potentially very favourable for localising fluidising pipes feeding mud volcanoes. The thick 'ac' joint indicates the setting at Nirano mud volcano field, Italy (NMVF), where this joint family is controlling mud volcanism. 'H' - maximum horizontal stress; 'h' - minimum horizontal stress; 'V' - maximum vertical stress. MA, Marnoso Arenacea; LU, Ligurian units; ELU, Epi- Ligurian units; PQ, Pliocene-Quaternary deposits. From Bonini (2007). C) Schematic fold and its major and minor structures from relationships seen in the clastic dyke swarm in Western Isla Grande, Southern Andes. From Winslow (1983).	172
Fig. 6.3:	Schematic depicting the new structural model for the intrusive and extrusive domains of a mud volcano system from the results of this study. This figure highlights how each of the findings of this study relate to each other and link together to form one complete system.	177

List of Abbreviations

ACG - Azeri-Chirag-Gunashli
BMV - Base mud volcano
BJP-1 - Banjar Panji-1
BPLS - Badan Penanggulangan Lumpur Sidoarjo
DOI - Digital Object Identifier
DTC - Downward Tapering Cone
E - East
ENE - East-north-east
ESE - East-south-east
GIA - Geological Institute of Azerbaijan
GPS - Global positioning system
Km - Kilometres
Lusi - Lumpur Sidoarjo
m - Metres
mi - Miles
µm - Micro-metres
MHC - Maximum horizontal compression
Ma - Million years
N - North
NE - Northeast
NNE - North-north-east
NNW - North-north-west
NOAA - National Oceanic and Atmospheric Administration
NW - Northwest
S - South
SCB - South Caspian Basin
SE - Southeast
SW - Southwest
SSE - South-south-east
SSW - South-south-west
TMV - Top mud volcano
ka - Thousand years
3-D - Three-dimensional
2-D - Two-dimensional
UTM - Universal transverse mercator
W - West
WGS - World geodetic system
WNW - West-north-west
WSW - West-south-west

List of Symbols

g - Acceleration due to gravity

ρ_b - Average bulk density

ρ_{parent} - Bulk density of parent bed

ρ_{os} - Bulk density of overlying sediments

BF_{parent} - Buoyancy of parent bed

σ'_h - Effective horizontal stress

σ' - Effective stress

ρ_f - Fluid density

P_{frac} - Fracture pressure

σ_h - Horizontal stress

ε_{mf} - Intergranular porosity at minimum fluidisation

σ_2 - Intermediate stress

σ_1 - Maximum stress

σ_{Hmax} - Maximum horizontal stress

U_{mf} - Minimum fluidisation velocity

σ_{Hmin} - Minimum horizontal stress

σ_3 - Minimum stress

σ_n - Normal stress

S - Overburden stress

P_f - Pore fluid pressure

ϕ - Porosity

ρ_s - Sediment/grain density

ϕ - Shape

d - Size

T - Tensile strength

T_h - Tensile strength parallel to bedding

T_v - Tensile strength perpendicular to bedding

h_{parent} - Thickness of parent bed

σ_v - Vertical stress

h - Vertical thickness

μ - Viscosity of fluid

Declaration

No part of this thesis has previously been submitted for a degree at this or any other university. The work described in this thesis is entirely that of the author, except where reference is made to previously published or unpublished work.

Katie S. Roberts
Durham University
Department of Earth Sciences
November 2010

Acknowledgements

The majority of thanks go to my amazing supervisory team of Richard Davies and Simon Stewart who not only devised the project but have provided constant support and inspiration throughout the whole process. I am so grateful for everything they have helped me achieve. Thanks also to their wives and families who have had to put up with both of them reading my work for the past three years. Ken McCaffrey and Jonathan Henton are also thanked for their participation in the project. I am very grateful to BP for funding this Ph.D. project and for logistical backup during field seasons especially by Simon Grant. I would like to acknowledge Google Earth, ArcGIS, Landmark, Matlab by The Mathworks, CRISP, BPLS, who supplied the Lusi 'bubble' GPS vent coordinates and the GIA for data, software and aerial imagery.

Thank you to my co-authors Mark Tingay and Robert Evans (and his field assistants) who were of great help throughout the project. A plethora of people who either reviewed the papers that compose this thesis or provided me with stimulating conversation; Chris Morley, Mads Huuse, Richard Jolly, Ed Llewellin, Claire Horwell, Geoff Wadge, Jenny Moss, Jon Gluyas, Chris Jackson, Tim Needham, Jonny Imber, Marco Bonini, Mark Allen and Richard Jones (and GRL). Gary and Dave, the office staff, Katie Daniels, Dave Sales and Alan Carr are all thanked for their assistance. Thanks to Steve and Rach for their brief but extremely helpful assistance during fieldwork. Fran Watson gets special thanks for her patience in teaching me how to use Matlab.

A big thank you to all my friends in the department, particularly Jen, Sarah, Dom, Steve, Mark P., Dean, Ben, Kirstie, Jo, Amelie and Juan-Carlos for all their encouragement. Rhian Meara is also thanked for keeping me sane throughout the writing up process. To Mr Mark, who has at times felt like my third supervisor, has been a brilliant field assistant and who has been generally amazing during the past three years, massive thanks. Last, but never least my family, Tricia, Alan, Lindsey, Ebby, Schmedley and my Grandparents who have always believed in me, provided me with love, guidance and to whom I will be forever grateful.

1 Introduction

1.1 Introduction

Mud volcano systems are a dynamic type of piercement structure that are integral components in many sedimentary basins globally. A 'mud volcano' is commonly described as a topographically expressed surface edifice from which mud and fluid erupt or flow (Milkov 2000). They form when sediment and fluid erupt onto the Earth's surface in the form of volcanoes measuring up to 25 km^3 in volume (Davies & Stewart 2005). This scale of geo-fluid transport has only been previously noted in igneous volcanic systems (Holmes 1998) and sand injectite complexes (Jolly & Lonergan 2002; Huuse *et al.* 2005, 2007), but in contrast, mud volcano systems have received relatively little investigation. Several thousands of mud volcanoes have been identified on the Earth's surface (Fig. 1.1) and more recently possible extraterrestrial examples (Fortes & Grindrod 2006; Skinner & Tanaka 2009; Oehler & Allen 2010). Close association can be seen with mud volcano systems and hydrocarbon provinces, rapid rates of sedimentation and burial (Kopf *et al.* 2003). They usually occur in tectonically active settings such as convergent margins (Kopf 2002), foreland basins (Deville *et al.* 2006), strike-slip provinces (Barber *et al.* 1986) and in some passive-margin settings (Graue 1999; Hansen *et al.* 2005; Cartwright *et al.* 2007). The intrusive domain (Stewart & Davies 2006) is the least understood part of mud volcano anatomy and also the most important as they penetrate sealing successions within basins making them extremely effective seal bypass systems (Cartwright *et al.* 2007). It is therefore critical to identify conduit geometry as this, in conjunction with viscosity, controls the fluid and sediment flux and surface expression of the edifice as well as any potential geo-hazards (Kopf 2002; Cartwright *et al.* 2007; Judd & Hovland 2007).

Fig. 1.1: Distribution of mud volcanoes on Earth. From Kopf (2002).

Distribution of fluid overpressure and regional stresses within the crust often determine what type of fracture networks form during or before an intrusive event (Sibson 1996). These networks can act to either augment or prevent fluid flow depending on their relative permeability to that of the surrounding country rock (Aydin 2000; Eichhubl & Boles 2000). Recognising that a fracture system is present in an intrusive domain is not sufficient to help distinguish structural permeability properties (Sibson 1996) which vary widely within the intrusive domain and are extremely complex (Aydin 2000). In order to predict the permeability and fluid flow pathways within an intrusive fracture network individual fault/fracture types must

be classified depending on their geometry (orientation and dimensional properties), spacing, distribution, connectivity and hydraulic properties, which result in both limitations and advantages for fluid and sediment transport (Aydin 2000).

The study of mud volcano systems has been enhanced by recent advances in industrial 3-D seismic reflection data carried out in order to survey hydrocarbon prospects that are usually in close proximity (Cartwright 2007). The main problem with seismic data is that it doesn't image the centres of the intrusive domains due to acoustic blanking most likely caused by the high gas content within the systems (Judd & Hovland 1992). What little is visible may not actually exist i.e. it may be a seismic artefact or might also be below seismic resolution. This has resulted in the structure of the intrusive domains remaining undetermined (e.g. Judd & Hovland 1992; Kopf 2002). Mud volcanoes have a significant impact on the petroleum plays through which they penetrate and may act as a conduit or a baffle to fluid flow within a basin as well as having a major influence on overpressure locally (Osborne & Swarbrick 1997; Cartwright *et al.* 2007). Mud volcano systems pose the threat of shallow hazards for drilling and other problems by introducing local uncertainties in pore and fracture pressure, depending on the degree of connectivity within the system (Reilly & Flemings 2010). Understanding these hazards is particularly significant after the formation of Lusi mud volcano (East Java) in 2006 which was potentially the result of a blow out in the nearby Banjar Panji-1 well (Davies *et al.* 2007, 2008; Tingay *et al.* 2008).

1.2 Aims and Rationale

The primary focus of this thesis is the documentation of the structural evolution and geometry of kilometre-scale mud volcano systems with particular focus on the intrusive domain and associated fluid flow pathways exposed in outcrop onshore in Azerbaijan and at Lusi mud volcano, East Java. A major problem when attempting to understand the intrusive domain of mud volcano systems is the lack of smaller-scale structural studies that would not be imaged in seismic data (Huuse *et al.*

2007). This thesis addresses the lack of resolution at the centre of the intrusive domain using field mapping and aerial imagery to assess sub-seismic scale (<12 m) vent geometry, distribution, structure and observed fluid flow pathways in both Azerbaijan and East Java. How conduit geometry controls the surface expression and fluid/sediment flux within these systems will also be investigated. Azerbaijan is ideal for the study of mud volcanoes since there are a large number both on- and offshore that are well-imaged by seismic data and many are easily accessible onshore. Onshore the mud volcano edifices of Azerbaijan are a comparable size to those offshore and most are now covered by high quality topographic data and satellite imagery. Therefore it is possible to compare the structures observed offshore with those seen onshore. Lusi mud volcano is interesting to evaluate as the evolution of the system though time can be recorded due to the system being younger than its counterparts in Azerbaijan.

Recently multi-disciplinary studies of mud volcanoes globally have increased in number (Planke *et al.* 2003; Davies & Stewart 2005; Stewart & Davies 2006; Evans *et al.* 2007; Evans *et al.* 2008; Kopf *et al.* 2009; Mazzini *et al.* 2009; Bonini & Mazzarini 2010; Calvès *et al.* 2010; Deville *et al.* 2010), however, hardly any focus solely on the metre- to kilometre-scale intrusive structure of the mud volcano system and how it impacts upon the strata that host them (Morley 2003; Davies & Stewart 2005; Stewart & Davies 2006). The majority of mud volcanic studies have focused on constraining their methane flux (Dimitrov 2002; Etiope & Klusman 2002; Etiope *et al.* 2002, 2004; Kopf 2002; Etiope & Milkov 2004 and references therein), describing their surface morphology and structure (Snead 1964; Hovland *et al.* 1997; Delisle *et al.* 2001; Planke *et al.* 2003; Martinelli & Judd 2004; Chow *et al.* 2006; Bonini 2008; Kopf *et al.* 2009; Mazzini *et al.* 2009), and analysing their internal structure on seismic reflection data (Davies & Stewart 2005; Stewart & Davies 2006; Evans *et al.* 2007, 2008). No studies have attempted to thoroughly assess the structural influence of intrusion or fluid flow pathways in field outcrops for better understanding of the subsurface processes that control their architecture and evolution. The research presented in this thesis focuses on the field architecture, structural mapping, extrusive morphologies and vent distributions of

both the intrusive and extrusive domains of mud volcano systems at present and over time. The main aims and methodologies of the project are identified below:

1) **Mud transport is through linked mud dykes that have dimensions similar to their igneous counterparts (a few metres to tens of metres wide) and that these collectively form highly efficient conduit systems capable of transporting and re-cycling tens of cubic kilometres of mud and fluid from depths of 1-5 km. If the hypothesis is correct it would counter the common conception of kilometre wide mud diapir systems.**
    i. Determine the structure of these intrusive systems.
    ii. Establish how these intrusive systems affect the reservoir potential of the country rock through which they pass.
    iii. Define a descriptive model for the intrusive features seen within the systems.
    iv. Analyse the way these intrusive features formed and determine the controls on their internal structure.
    v. Reconstruct the intrusive history of a large mud volcano system.
    vi. Develop a model of formation for the mud volcano systems.

2) **Identify evidence for faults and fluid flow at the surface and relate these to sub-surface fluid flow. Investigate mud volcano vent distributions on several edifices in order to determine which fluid flow pathways are exploited.**
    i. Use statistical analyses to pick out dominant vent alignments and their orientations.
    ii. Identify possible structures that have similar orientations.
    iii. Relate the vent populations to possible controls on subsurface fluid flow within the feeder systems.
    iv. Investigate the evolution of fluid flow pathways over time i.e. Lusi mud volcano, East Java.
    v. Relate this relatively young mud volcano system to those in Azerbaijan and how their structural settings may influence their evolution.

3) **Characterise the morphology and structures on edifices at the upper terminations of mud volcano systems that may be influenced by the intrusive domain i.e. sector collapse scarps.**
   i) Describe morphology of structures found on mud volcano edifices.
   ii) Relate these features to structural influences in the region and in the intrusive domain.
   iii) Investigate how this impacts the evolution of the edifice.
   iv) Develop a model of formation that includes what external factors may be influencing the structures.

1.3 Thesis Outline

In this section Chapters 2-6 are described individually. The main data sections, Chapters 3-5, have been written as stand-alone manuscripts and have all been submitted for publication; these are recast for the thesis when appropriate. As such, each chapter contains introduction, geological background, observations, interpretation, discussion and conclusions sections. The geological background sections for each chapter represent a content-specific geological history which is also outlined in Chapter 1, and may therefore be skipped at the reader's discretion. The thesis only contains manuscripts for which I am the first author, and I have been responsible for primary data collection, interpretation and paper writing.

Chapter 2 – *The mud volcano system.*

This chapter represents a summary of the mud volcano system components based primarily on published references, but also incorporating regional-scale remote-sensed and field studies of Azerbaijan carried out as part of the present study.

Chapter 3 – *Outcrop scale structural analysis of the exhumed mud volcano systems, Azerbaijan.*

This chapter investigates outcrop-scale features seen within intrusive systems of kilometre-scale mud volcano systems exposed onshore in Azerbaijan. Field

mapping focuses on the size, shape and internal structure of country rock outcrops as well as fluid flow pathways within the feeder complexes, an aspect poorly described in previous studies. This is a structural study of a selection of exhumed mud volcano systems in Azerbaijan detailing fault and fracture patterns and relationships as well as bedding orientations affected by the intrusion of these feeder complexes. This study is based on detailed structural- and field-mapping. The analyses are used to determine distinct deformation events, which are fitted into a model of intrusion and formation. A metre-scale model of the 3-D geometry and structure of the mud volcano intrusive complex is presented and confirms the presence of a system that has more in common with igneous intrusive complexes than those of a diapiric system. Prof. Davies (Ph.D. supervisor, Durham University) and Prof. Stewart (Ph.D. supervisor, Heriot-Watt University) appear as co-authors as they provided supervision and manuscript editing advice (Roberts *et al.* 2010). Prof. Stewart also drafted the first version of Fig. 3.2.

Chapter 4 – *Outcrop and regional scale study of mud volcano vent patterns and alignments in Azerbaijan and Lusi mud volcano, East Java.*

The aim of this chapter is to investigate the distribution of a variety of fluid escape structures at outcrop-scale within kilometre-scale mud volcano edifices, and to use the observations to suggest the structural controls on fluid flow pathways within the feeder complexes. These observations are made on a selection of mud volcanoes onshore Azerbaijan, and at the Lusi mud volcano in East Java between 2006 and 2010. Statistical tests have been carried out on the vent distributions in order to ascertain the geometry of the subsurface feeder system and how it is compartmentalising the country rock through which it is intruding. This chapter provides an in-depth analysis of the vent alignments on mud volcano edifices and relates them to regional and local structure using statistical analyses. This is the first study of its kind carried out on mud volcano edifices as it is primarily used in relation to igneous volcanic systems. The evolution and 'switching' of vent alignments through time at Lusi mud volcano is also documented with the structural controls being identified. Prof. Davies and Prof. Stewart appear as co-authors and provided supervision and manuscript editing advice. Dr Mark Tingay

(University of Adelaide) appears as a co-author as he provided references for the geological history of East Java, information about the stress regimes in the region and manuscript editing. Vent location data from Lusi mud volcano were kindly provided by Badan Penanggulangan Lumpur Sidoarjo (BPLS; Roberts *et al. Accepted for publication*).

Chapter 5 – *Outcrop scale structural and aerial analysis of sector collapse events on mud volcano flanks.*

This chapter describes collapse phenomena and related morphological features seen on mud volcano edifices, considers the priming and triggering events, formation mechanisms and potential similarities with the processes by which sector collapse occurs in igneous volcanoes. Further consideration is given regarding collapse of mud volcanoes to distinguish between features that are wholly or partly due to slope failure versus features that are largely the product of incision and erosion of the flanks during an eruptive event. Using the orientation and size scale ranges of these features their importance in mud volcano edifice growth and how the underlying structure and fluid flow pathways may affect their evolution are documented. Analysis of these structures at the surface allows inference of processes possibly occurring in the feeder complex below. Prof. Stewart and Prof. Davies again appear as co-authors providing supervision and manuscript editing advice, Prof. Stewart also adapted Fig. 5.8. Dr Robert Evans (former Cardiff University) is a co-author as he provided photographs for Figs. 5.4C and D, manuscript editing and carried out some basic mapping of this study area which was referred to during this study (Roberts *et al.* 2011).

Chapter 6 – *Discussion, conclusions, and future work.*

This chapter elaborates on the discussion sections of the preceding chapters and conclusions drawn throughout the body of the thesis are summarised. This chapter also identifies areas of interest for possible future research, and suggests further relevant studies of importance for both the scientific and industrial communities.

1.4 Methodology

Datasets in this thesis have been collected at multiple scales, including: 1) kilometre-scale remote-sensing mapping using high-resolution aerial imagery and topography; 2) meso-scale field mapping and 3) statistical analysis.

1.4.1 Remote Sensing

Remote-sensing analyses were conducted using ArcGIS software, incorporating topographic and two-dimensional (2-D) aerial and satellite images (0.5-6 m resolution; IKONOS and CRISP imagery) as well as using Google Earth software. All remote-sensed analyses have been conducted within the WGS 1984, UTM zone 39°N (projected) coordinate system in Azerbaijan and UTM zone 49°S for Lusi mud volcano, East Java. Structural data was imported onto the imagery so that a clear structural map could be drawn. Vent GPS positions and types were each plotted onto satellite imagery with corresponding symbols in order to conduct several spatial statistical analyses (see section 1.4.3).

1.4.2 Structural Field Mapping

Detailed structural mapping, mud sampling, hand specimen collection and data collection were carried out at 20 mud volcanoes in Azerbaijan (see mud volcano location map in Appendix I). Field measurements were primarily concerned with outcrop-scale structural geometries, since large-scale features such as strike and dip variations in country rock and antiform/synform structures could be mapped remotely.

Mapping of the mud volcanoes in Azerbaijan was carried out using a handheld global positioning system (GPS) receiver, with a positional accuracy of 5 m therefore, vent alignments also have an accuracy of 5 m. Orientation data such as bedding, fracture and fold orientations have been collected in a standard compass-bearing system then loaded into GEOrient software to plot stereographic and rose projections. At the time of study, magnetic deviation was calculated to the nearest

½ degree as 5.4°E (source: National Oceanic and Atmospheric Administration (NOAA)). Planar data were collected as strike, dip and dip direction; within the thesis text. All locality coordinates are geo-referenced in UTM zone 39°N and UTM zone 49°S for Lusi mud volcano, East Java on the WGS 1984 geoid.

The GPS co-ordinates with their corresponding structural datasets were integrated as layers in ArcMap software. The locations of the vents in the Lusi mud volcano were provided by Badan Penanggulangan Lumpur Sidoarjo (BPLS) and recorded using a hand-held GPS with an accuracy of between 5-12 m. Some uncertainties may arise when mapping vents at Lusi as it is unknown how many of these vents are either linked to a deeper feeder system or simply shallow eruptions linked to the massive and rapid subsidence occurring in the area. Some large areas covered in mud meant vent locations could not be mapped which possibly accounts for the high proportion of vents located near roads, dam walls and high density populated urban areas. Vent types were classified as being either: gryphons, salses, cinder mounds, pools, mud plugs or breccia pipes (see Chapter 2, section 2.4.3 for vent descriptions).

Mud volcanoes in Azerbaijan were only selected for mapping if they were exhumed and exposure of country rock at the centre of the systems was >60%. This enabled the relationship between faulting, folding, regional structure and the Azerbaijan mud volcanoes to be determined. There is less structural information from outcrops at the Lusi mud volcano and limited 2-D seismic coverage. Therefore the volcanoes in Azerbaijan were used to inform the interpretation of controls on structure and vent distributions at Lusi and globally.

1.4.3 Statistical Analyses

Two statistical approaches were used to characterise geographic spatial patterns within vent fields. Supported by field studies, these techniques have revealed that shifts in the locus of activity are common and that vents often form clusters and define alignments at several scales in igneous vent systems (Bleacher *et al.* 2009).

The aim of these spatial studies was to provide insight into the link between the distribution of vents and causal processes.

1.4.3.1 Nearest Neighbour Technique

The nearest neighbour technique (Clark & Evans 1954; Bleacher *et al.* 2009) tests randomness in spatial distributions by calculating the ratio of the observed mean distance to the expected mean distance for a hypothetical random distribution to determine whether the points are clustered. This was carried out in ArcGIS which measures the distance from every vent point to its nearest neighbouring vent point. The *spatial statistics tools* for *analysing patterns* in ArcMap were used, within this the *average nearest neighbour* feature was chosen. This calculates the nearest neighbour index based on the average distance from each feature to its nearest neighbouring feature. The *Euclidean distance method* was selected as this measures distances as a straight line between the two points. The *nearest neighbour index* (*Rn*) can be represented using;

$$Rn = \frac{D(Obs)}{0.5\sqrt{\frac{a}{n}}} \qquad \textbf{Eq. 1.1}$$

Where *D(Obs)* is the mean observed nearest neighbour distance, *n* is the number of vents and *a* is the aerial extent of vent coverage in the study area (Mitchell 2005; Moss & Cartwright 2010). A ratio of 1 indicates a random distribution and a ratio of <1 is clustered, the nearer to 0 the more clustered the distribution. A ratio of >1 is a regular distribution. The equations used to calculate the average nearest neighbour distance index and Z score are based on the assumption that the points being measured are free to locate anywhere within the study area (Mitchell 2005). In addition, the index and Z score for this statistic are sensitive to changes in the study area or changes to the *area* parameter (Mitchell 2005). For all these reasons, comparing results from this statistic are most appropriate when the study area is fixed. The default area value in this study is the area of the minimum enclosing rectangle around the point set (Mitchell 2005).

In order to determine if there is no pattern to the vent distribution, the *Z* score is calculated. The *Z* score (*Z*) is a test of statistical significance which evaluates for a normal distribution of the nearest neighbour distances. Very high or very low *Z* scores indicate that it is very unlikely that the observed pattern has occurred by chance. *Z* scores are a measure of standard deviation away from the mean;

$$Z = \frac{D(Obs) - 0.5\sqrt{\frac{a}{n}}}{SE} \qquad \textbf{Eq. 1.2}$$

Where *SE* is the standard error as below;

$$SE = \frac{0.26136}{\sqrt{n^{2}/_{a}}} \qquad \textbf{Eq. 1.3}$$

Where *a* is the aerial extent of vent coverage in the study area (Mitchell 2005; Moss & Cartwright 2010).

1.4.3.2 2-Point Azimuth Technique

The 2-point azimuth technique (Lutz 1986; Wadge & Cross 1988; Connor 1990; Bleacher *et al.* 2009) was applied as a fundamental statistical measure of the significance of alignments between vents in the study area. The 2-point azimuth technique quantitatively ascertains structurally controlled trends within a field of vents that are spatially distributed. This method was carried out by implementing an algorithm from Bleacher *et al.* (2009). This algorithm was input into Matlab to obtain the large data files produced (see Appendix III for script). Only points to the east of each point were measured to avoid any duplication (Fig. 1.2). The data from Matlab was then loaded into Microsoft Office Excel where histograms of azimuth values (0°=north, 90°=east, 180°=south) were produced with 10° bins. Vent alignments of 0° and 180° are considered to have the same orientation. Peaks in the frequency distribution of the azimuths are suggested to result from preferred formation of vents in response to structural controls within a region (Bleacher *et al.*

2009). It should be kept in mind that where vent spacing is <5 m the alignments identified will be less reliable. However there are clear visual and statistical alignments in vents that are consistent and geologically sensible in areas where the vent spacing drops below 5 m.

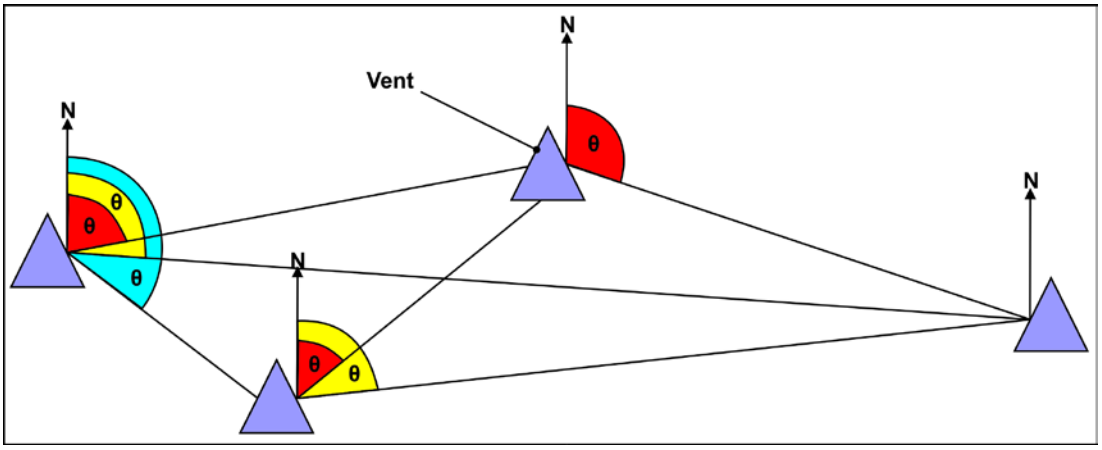

Fig. 1.2: Schematic of the 2-point azimuth technique. Line segments are drawn between each vent and any vents to the east of that vent. The azimuth of the line segment from north is measured. Each azimuth orientation is then plotted in a frequency histogram.

1.5 Geographical, Tectonic and Stratigraphic Setting

The mud volcano systems investigated in this project are located along the west coast of the Caspian Sea in Azerbaijan and the 'Lusi' mud volcano which is in Sidoarjo, East Java. Each of these areas are described separately below, as well as in more detail at the beginning of Chapters 3, 4 and 5 and so may be omitted at the readers discretion. This section introduces the location of the project study areas, provides a brief discussion of the distribution of mud volcanism in the study areas and summarises the sequence of events that have influenced their geological histories.

1.5.1 The South Caspian Basin (SCB) and Eastern Azerbaijan

1.5.1.1 Location and Formation

Mud volcano systems from onshore in east Azerbaijan are investigated in this study (Fig. 1.3).

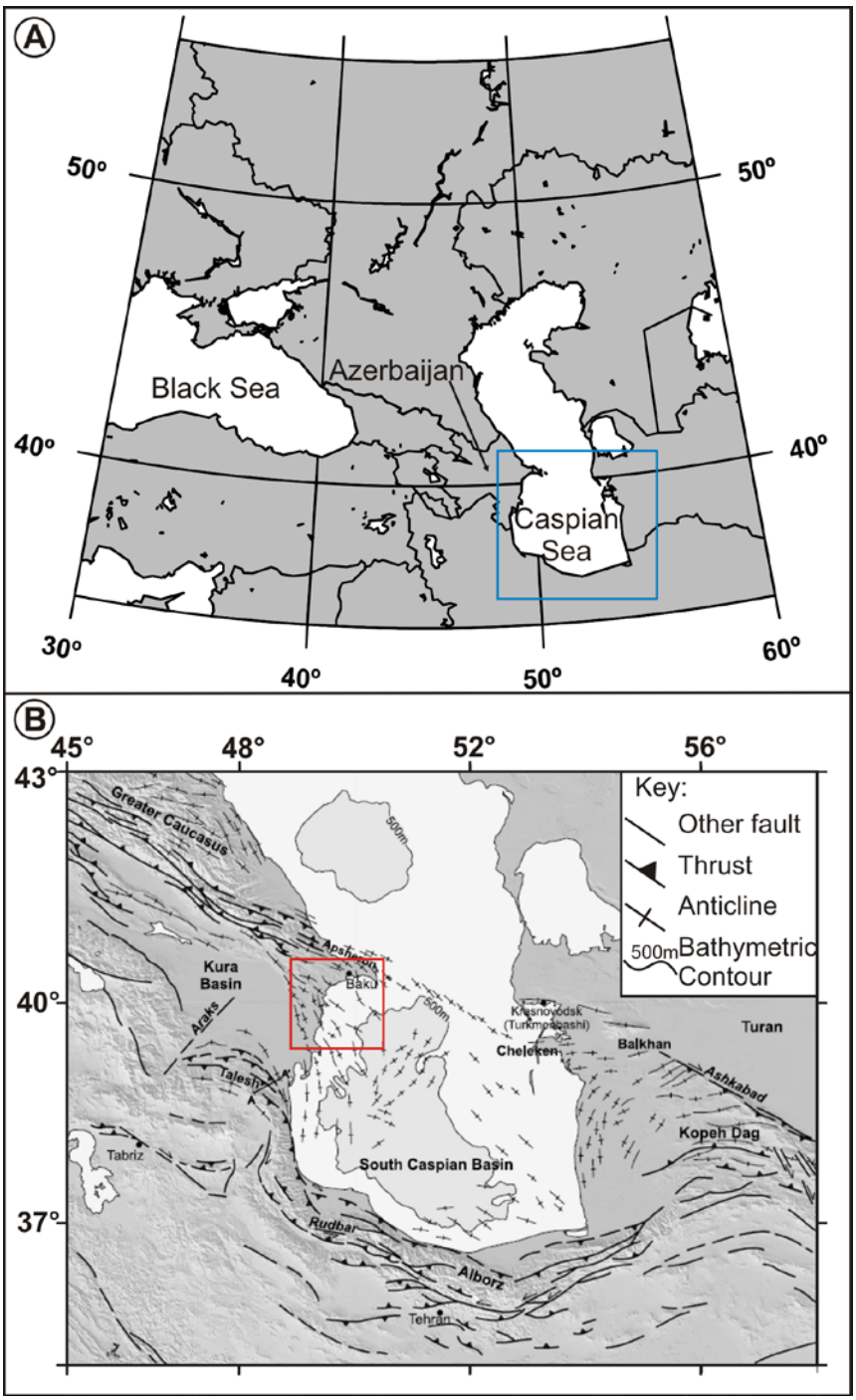

Fig. 1.3: Geological setting and study area location in Azerbaijan: A) Location of Azerbaijan. B) Tectonic map of the SCB showing the position of major structural elements and position of the

onshore project study area (red box). Map location is shown as a blue box in Fig. 1.3A. Modified from Jackson *et al.* (2002).

The mud volcano systems in this study are found within the Shamakha Gobustan and Lower Kura 'mud volcano areas' of Guliyev & Panahi (2004; Fig. 1.4). Mud volcanism in the SCB is extensive and the area is thought to host approximately 30% of the world's known population of mud volcano systems (Guliyev *et al.* 2000). This distribution of mud volcano systems is believed to be the result of the presence of their regional source layer, the Oligocene to Miocene age Maykop Formation. Pinch-out of this formation in the west against the NNW-SSE trending Talysh-Vandam structural high restricts the mud volcanism to areas east of the high (Cooper 2001). In the north, mud volcanism is restricted by the absence of the Maykop Formation north of the Apsheron Sill (Fig. 1.4; Yusifov & Rabinowitz 2004).

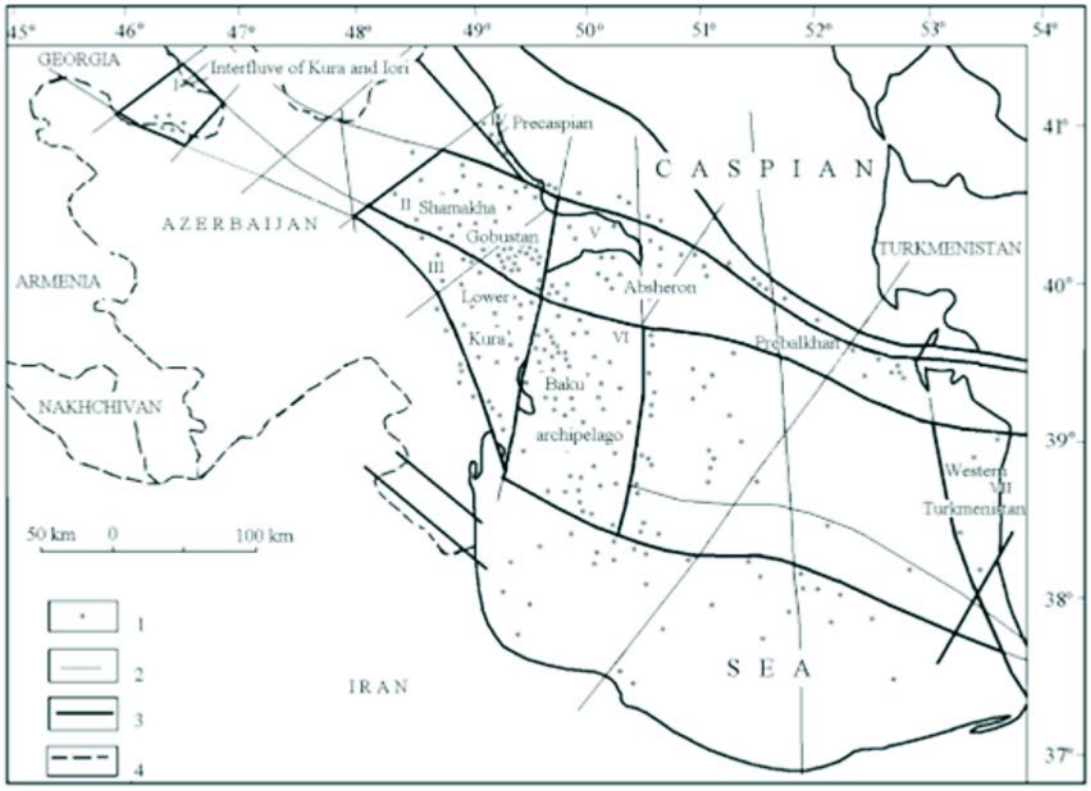

Fig. 1.4: Location of mud volcanoes in the Azerbaijan and the Caspian Sea region. 1- Mud volcanoes, 2- deep faults, 3- boundaries of mud volcano areas, 4- political margins. I to VII Mud volcano areas: I- interflow of Kura and Iori rivers, II- Shamakha-Gobustan, III- Lower Kura, IV- Pre-Caspian, V- Absheron-Prebalkhan, VI- Baku archipelago, VII- Western Turkmenia. From Guliyev & Panahi (2004).

Approximately 170 onshore mud volcano systems have been identified from aerial imagery (see Appendix I) in Azerbaijan during this study and some of these have erupted approximately 300 times since records began (Aliyev *et al.* 2002; Appendix I). These edifices range from small fields of metre-scale vents (gryphons, salses and cinder mounds, see section 2.4.3) to kilometre-scale conical edifices that can be up to 6 km wide and 400 m high. Offshore studies have revealed 99 mud volcano systems in the north-western portion of the SCB alone and many more are known to exist elsewhere within it (Yusifov & Rabinowitz 2004). Approximately 75% are located in the crest of anticlines with the remainder located on the flanks of anticlines or in synclines (Yusifov & Rabinowitz 2004). Mud volcano formation began in the mid-Miocene and became more intensive in the Pliocene during active compression and folding within the region (Fowler *et al.* 2000; Yusifov & Rabinowitz 2004).

1.5.1.2 Geological History

Deep seismic events (>80 km) at the northern side of the SCB (Allen *et al.* 2002) indicate that it is subducting beneath the Central Caspian with a westward component of motion that initiated in the Pliocene (3-5 Ma; Fig. 1.5; Jackson *et al.* 2002). Backstripping of the stratigraphy by Allen *et al.* (2002) revealed that ~2.4 km of tectonic subsidence had occurred during the Pliocene and Quaternary which they attributed to subduction. This subsidence increased accommodation space within the SCB, this and the fact that it is bounded on all sides by compressional orogens allowed >13 km of sediment to accumulate post-Oligocene (Jackson *et al.* 2002). During the Oligo-Miocene the regional source rock i.e. the Maykop Formation was deposited, which was subsequently overlain by several thick deltaic sequences including the sand rich Productive Series, in the Late Miocene (Jackson *et al.* 2002). The Productive Series form the ~6 km thick (Allen *et al.* 2002) regional reservoir rock and were deposited rapidly in 1-2 ka (Jackson *et al.* 2002). This rapid deposition and burial lead to disequilibrium compaction of the Maykop Formation and overpressuring which resulted in mechanical weakening of the rock (Jackson *et al.* 2002). Fluids from below the Maykop Formation entrained the weakened rock

providing the driving force for the mud volcanoes within the region (Jackson *et al.* 2002; Kopf *et al.* 2003). It also resulted in low temperature gradients within the basin allowing hydrocarbons to be generated at depths of 8-12 km (Devlin *et al.* 1999).

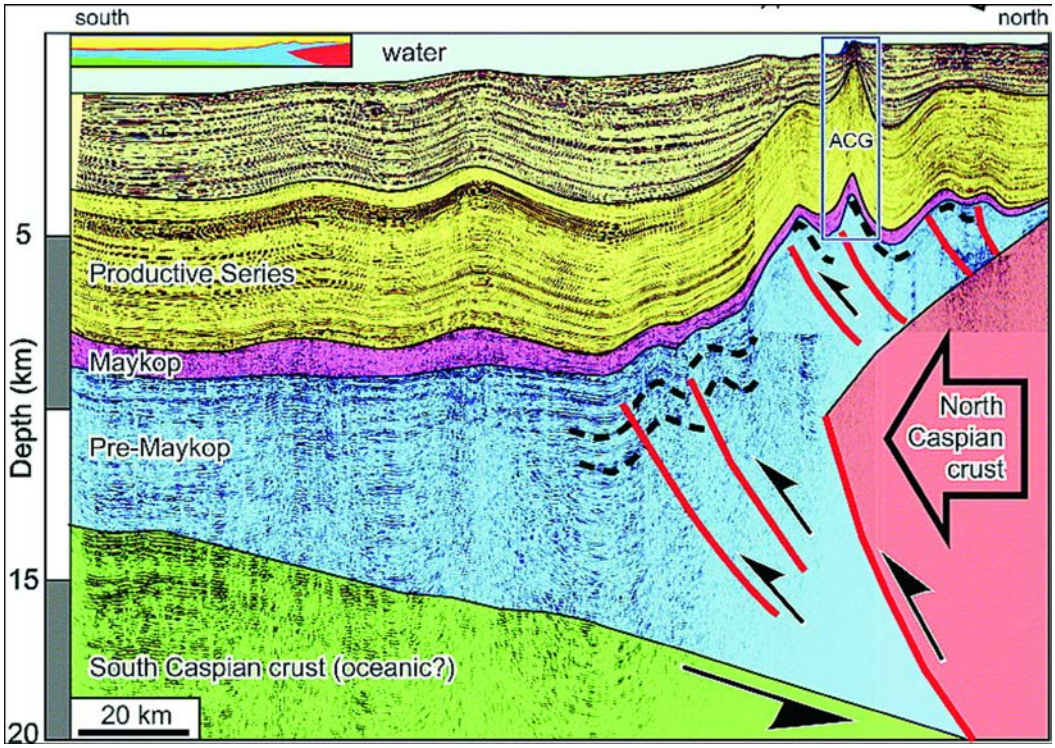

Fig. 1.5: Regional 2-D reflection seismic line showing main tectono-stratigraphic elements, approximately six times vertical exaggeration. Inset shows the interpretation at vertical = horizontal scale. ACG is one of the main hydrocarbon producing fields in the SCB. From Stewart & Davies (2006).

Large amplitude buckle folding of the Productive Series offshore initiated at around ~3.4 Ma (Devlin *et al.* 1999) whereas onshore may have occurred up to 2 Ma earlier, as indicated by stratal pinchouts onto fold flanks (Aliyev 1960). The anticlines contain low angle reverse faulting in their lower sections and normal faulting in their upper regions (Fig. 1.6; Devlin *et al.* 1999). Folding is thought to detach in the underlying overpressured Maykop Formation (Jackson *et al.* 2002). These structures provide many of the structural traps exploited by the hydrocarbon industry as well as accommodating the numerous mud volcano systems (Fig. 1.6; Devlin *et al.* 1999).

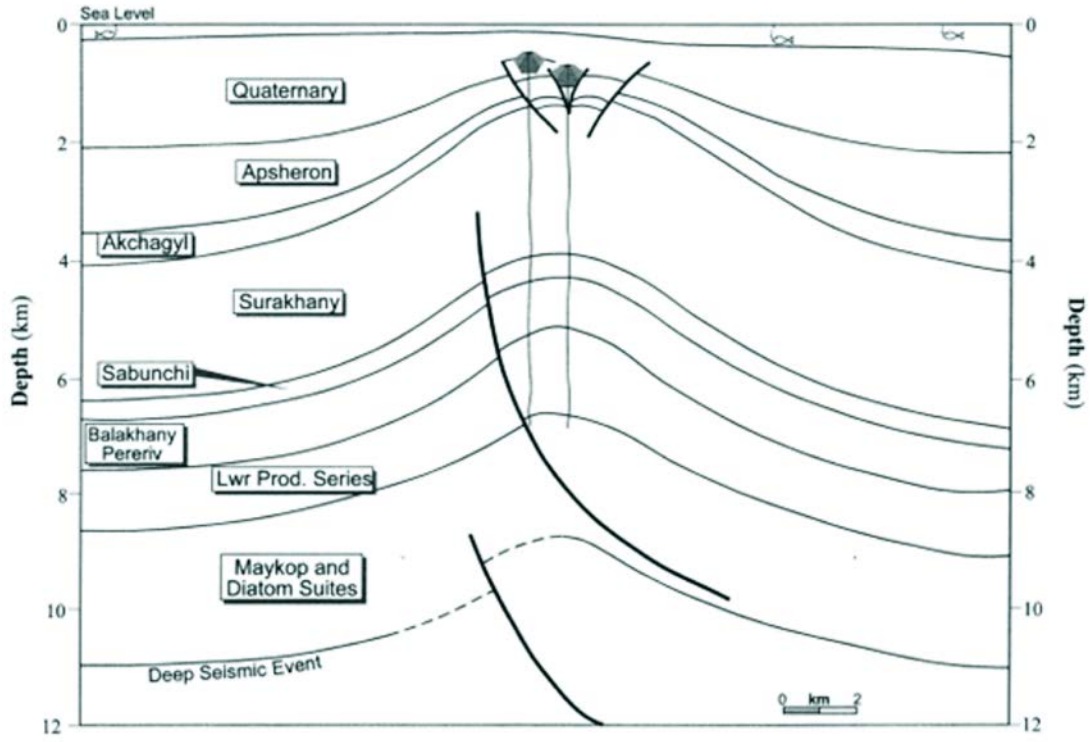

Fig. 1.6: Schematic cross-section across Shah Deniz in the SCB showing the relationship of the deep structure with the shallower structure and mud volcanoes. From Fowler *et al.* (2000).

1.5.2 Sidoarjo, East Java, Indonesia

1.5.2.1 Location and Formation

'Lusi' (Lumpur Sidoarjo) mud volcano erupted in the Porong district of Sidoarjo, approximately 25 km south of Surabaya, at 5 am on the 29th May 2006 (Fig. 1.7). It has been erupting continuously ever since, claimed 17 lives, displaced approximately 40,000 people, and inundated 7 km^2 of a populated area (Tingay 2010). There are two contending theories as to what triggered the eruption; 1) that the mudflow resulted from a blowout in the Banjar Panji-1 well located 150 m away (Davies *et al.* 2008; Tingay *et al.* 2008), and 2) that the disaster was initiated by the M_w6.3 Yogyakarta earthquake that occurred on the 27th May 2006 (Mazzini *et al.* 2007; Sawolo *et al.* 2009). In order to predict the longevity and evolution of Lusi greater knowledge of the subsurface anatomy is essential (in particular the ongoing subsidence of the area, the reactivation of faults and possibility of caldera collapse (Tingay 2010).

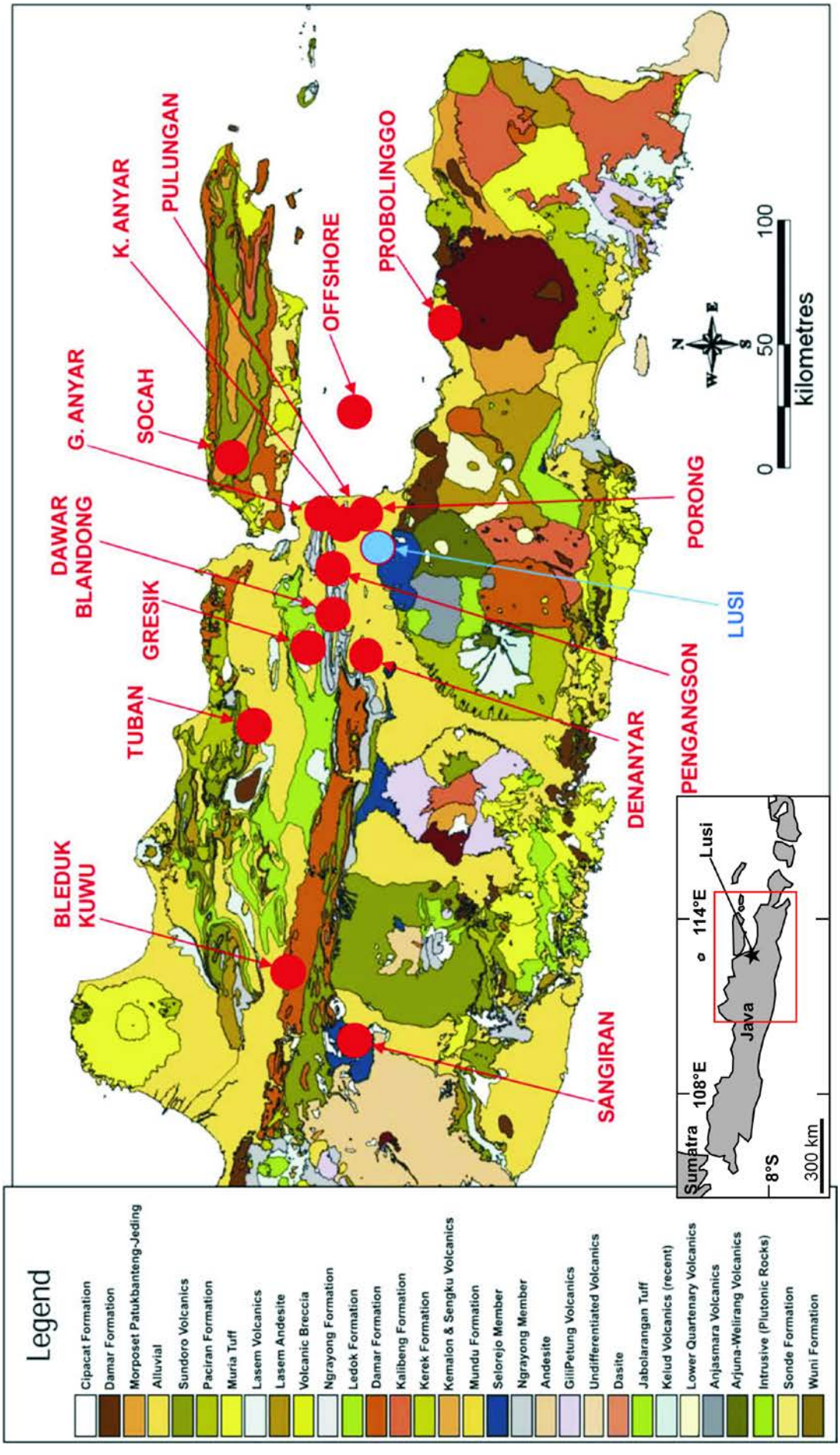
BLEDUK KUWU
TUBAN
GRESIK
DAWAR BLANDONG
G. ANYAR
SOCAH
K. ANYAR
PULUNGAN
OFFSHORE
PROBOLINGGO
PORONG
LUSI
PENGANGSON
DENANYAR
SANGIRAN
0
50
100
kilometres
N
S
W
E
Sumatra
Java
Lusi
108°E
114°E
8°S
300 km
Legend
Cipacat Formation
Damar Formation
Morposet Patukbanteng-Jeding
Alluvial
Sundoro Volcanics
Paciran Formation
Muria Tuff
Lasem Volcanics
Lasem Andesite
Volcanic Breccia
Ngrayong Formation
Ledok Formation
Damar Formation
Kalibeng Formation
Kerek Formation
Kemalon & Sengku Volcanics
Mundu Formation
Selorejo Member
Ngrayong Member
Andesite
GiliPetung Volcanics
Undifferentiated Volcanics
Dasite
Jabolarangan Tuff
Kelud Volcanics (recent)
Lower Quartenary Volcanics
Anjasmara Volcanics
Arjuna-Welirang Volcanics
Intrusive (Plutonic Rocks)
Sonde Formation
Wuni Formation

Fig. 1.7: Geological map and mud volcano distribution in east and Central Java. Red dots are the identified mud volcano locations. From Istadi *et al.* (2009). Inset shows global location with red rectangle marking the extent of the figure from Istadi *et al.* (2009).

There are fourteen naturally occurring mud volcanoes found in this region that correlate with the presence of the thick and rapidly deposited clay-bearing Kalibeng Formation sediments, with at least four located in close proximity to Lusi (Fig. 1.7; Istadi *et al.* 2009). One way to predict the growth of Lusi is to study the stratigraphically identical Porong and Kedeco-11C carbonate mounds (located on a trend to the ENE from Lusi). Both these structures contain circular collapse structures with faulting propagating out of the crest of the carbonate mounds (Fig. 1.8; Kusumastuti *et al.* 2002; Istadi *et al.* 2009). These large collapse structures are over 1 km wide and 300 m deep and are possibly 'Lusi-type' mud eruptions that occurred during the Quaternary and were sourced by adjacent and slightly shallower reefal mounds (Kusumastuti *et al.* 2002; Istadi *et al.* 2009).

Lusi differs from other naturally occurring mud volcanoes in that it is erupting hot (70-100°C) fluid rich mud (initially 60-80% water, reducing over time to 30-50% water at present, solid fraction is 80-90% clays with minor silts and sand-sized grains; Tingay 2010) and has had an average flow rate of approximately 64,000 m^3/day over the first three years (Istadi *et al.* 2009; Tingay 2010). Most naturally occurring mud volcano systems flow at rates of only a few tens to hundreds of cubic metres per day, but can occasionally have eruptions that are short-lived (1-14 days) and extremely violent (100,000-1,000,000 m^3/day; Tingay 2010). The temperature, flux and geochemistry of the water indicates a source depth of >1700m (Mazzini *et al.* 2007). The eruption of mud from Lusi is predominately from the circular 'main vent' which is approximately 100 m in diameter, this along with the extremely high flow rate suggest that the feeder system under Lusi is either conical in shape or comprised of several very large open and intersecting fractures (Tingay 2010).

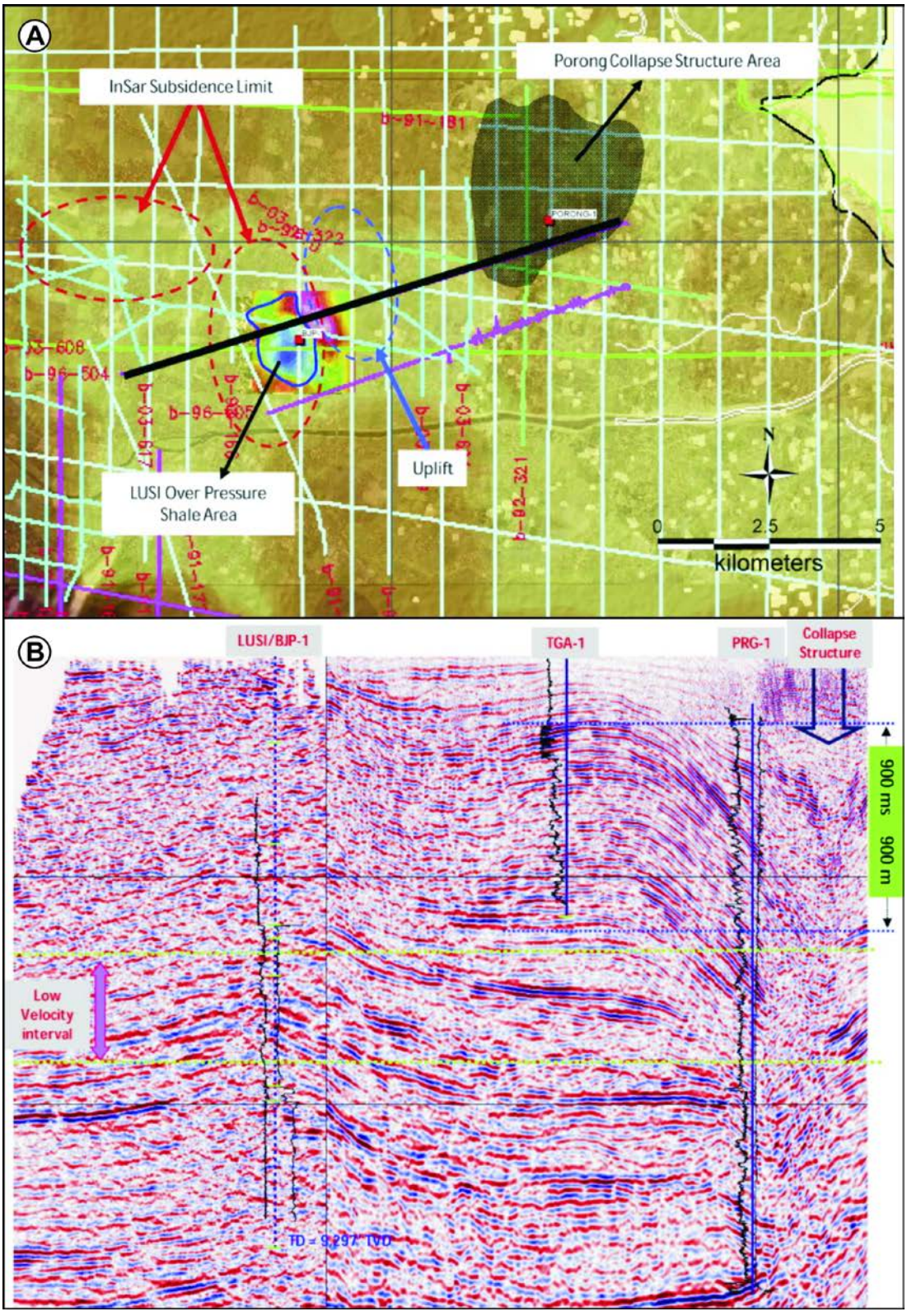

Fig. 1.8: The Porong collapse structure. A) Seismic base map overlays satellite image. The areal extent of the Porong collapse structure in shaded dark colour, which covers a much larger area compared to the Lusi interpreted overpressured shale area. Porong was an adjacent mud volcano that has been used as an analogue to build the subsidence model for Lusi. From Istadi *et al.* (2009). B) Seismic section of Lusi – Banjar Panji-1 – Tanggulangin-1 – Porong-1 – Porong collapse structure.

The Porong collapse structure located approximately 7 km from Lusi is a palaeo-mud volcano where subsidence is evident and the multiple faults present likely served as conduits for the mudflow. Similarly, the multiple faults near the BJP-1 well (200 m from Lusi) may have been reactivated and served as conduit for the mud eruptions and escaping gas, hence the appearance of gas bubbles along fault lines.

1.5.2.2 Geological History

Lusi is located within the East Java Basin, in a present-day, inverted, back-arc setting which is dominated by NE-trending basement highs and intervening half-grabens that formed during the Tertiary period (Carter *et al.* 2005). During the Eocene NE-SW oriented rift basins formed and filled with continental clastics that host both source rock and productive reservoirs (Kusumastuti *et al.* 2002). In the Oligocene to early Miocene east-west trending normal faults formed (Kusumastuti *et al.* 2002; Istadi *et al.* 2009). Carbonate platforms developed on some palaeo-basement highs. Compression during the late Miocene-Pleistocene resulted in inversion associated with E-W trending fault movement (Istadi *et al.* 2009). This produced the E-W orientation of the anticline structures (Istadi *et al.* 2009). Subsequent Pliocene-Pleistocene sedimentation consisted of an eastward-prograding mudstone-dominated volcaniclastic wedge derived from the Java volcanic arc (Istadi *et al.* 2009). The mudstone deposited during the Pleistocene named the Kalibeng Formation is overpressured at 900-1870 km depth at Lusi (Istadi *et al.* 2009). This is the source of the solid fraction of the mud erupted at Lusi (Mazzini *et al.* 2007). The water has an unknown source estimated to be from >1700 m depth by its temperature and isotopic composition (Davies *et al.* 2007; Mazzini *et al.* 2007), but is generally considered to be primarily from the Miocene carbonates (2833-3500 m) with a contribution from the remobilisation of the Upper Kalibeng Formation (Davies *et al.* 2007). Some fluids may also be sourced from shallow aquifers in the Pleistocene Pucangan Formation at 280-900 m depth (Tingay *et al.* 2008).

The stratigraphy under Lusi comprises:

(1) Recent alluvium (alternating sands and shales; 0-290 m depth)

(2) Pleistocene Pucangan Formation (alternating sands and shales; 290-900 m depth)

(3) Pleistocene Upper Kalibeng undercompacted smectite-illite muds (900-1870 m depth)

(4) Plio-Pleistocene low-porosity extrusive igneous rocks (1870-2833 m depth)

(5) Miocene Tuban Formation which comprises a series of mudstones with thin limestone, siltstone and sandstone units (~2833-~3500 m depth; Tingay 2010).

(6) Early Miocene Kujung Formation, composed predominantly of carbonates and mudstones. It is sub-divided into three members - Kujung III, II, and I (from oldest to youngest).

(7) Late Eocene-early Oligocene clastics, known as the Ngimbang or 'CD' Formation.

(8) Metamorphic and igneous pre-Tertiary basement (Carter *et al.* 2005).

2 The Characterisation of Mud Volcano Systems

2.1 Introduction

The study of mud volcanism or 'sedimentary volcanism' was first carried out by Russian and Azerbaijani scientists mainly in relation to their occurrence with hydrocarbon provinces (Abikh 1863; Arhangelski 1932; Goubkin & Fedorov 1938; Dadashev 1963; Kalinko 1964). The earliest works often focus on mud volcanoes in the Crimea and Azerbaijan (Abruitski 1853; Ansted 1866). The term 'mud volcano system' was first formally defined by Stewart & Davies (2006) who described it as a set of structures associated with a constructional edifice (mud volcano) and feeder complex that connects the volcano to its source stratigraphic unit and any deeper fluid sources. Fig. 2.1 shows a basic structural model of a kilometre-scale mud volcano system based on 3-D seismic mapping in the South Caspian Basin (Stewart & Davies 2006). This system can be subdivided into a series of 'structural domains', within which a characteristic set of processes occur that control the architecture of that part of the system. The basic mud volcano system consists of three principal structural domains (Fig. 2.1); the deepest 'source domain', overlain by the 'intrusive domain' and finally the 'extrusive domain'. If the system becomes buried a fourth structural domain forms called the 'roof domain' which overlies the whole system. Each individual domain and the processes which occur within them are now described with a particular focus on the intrusive domain.

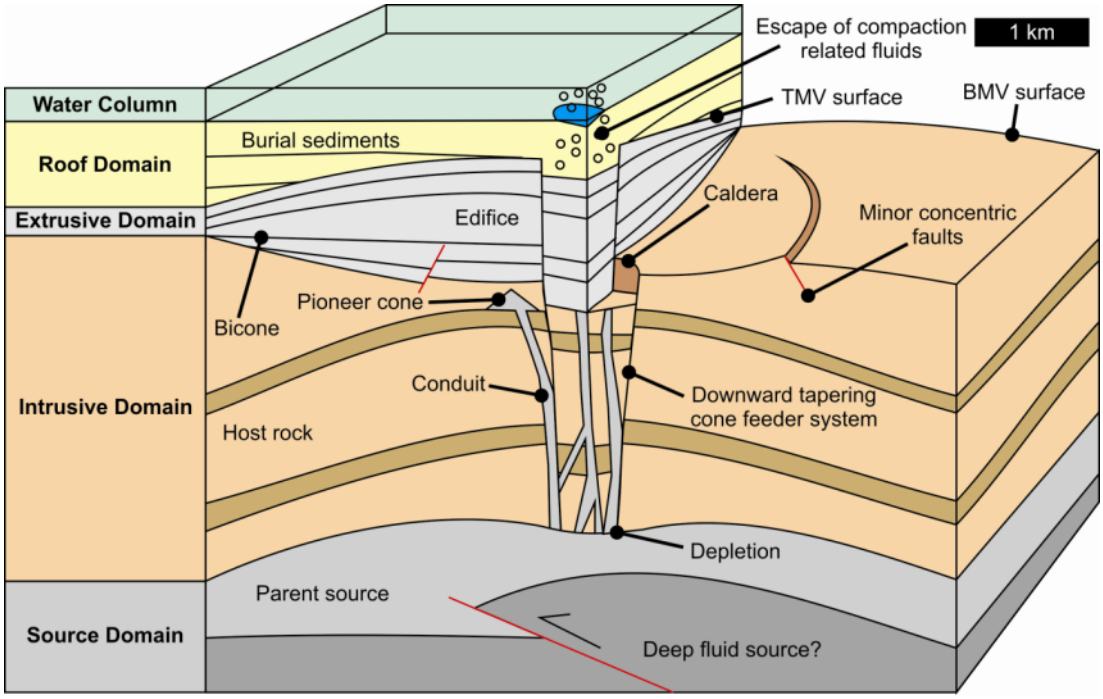

Fig. 2.1: Summary diagram outlining the basic subsurface configuration and structural domains of a large mud volcano system. Onshore mud volcano systems usually lack a roof domain and are not below sea level. Modified from Stewart & Davies (2006).

2.2 The Source Domain

This is the deepest domain at the root of the whole system (Fig. 2.1). It includes the 'parent bed', 'source layer' or 'parent formation' of the remobilised sediment as well as any deeper source of fluids that entrain the sediments during their ascent. The upper boundary of the source domain is defined by the deepest stratigraphic unit that has been intruded and invaded by allochthonous fluids and sediment (Evans 2008). The parent bed usually consists of a thick sequence of undercompacted clays or shales (Kopf 2002). The erupted mud breccia can be easily related to the regional geology and to clay or shale-bearing lithologies at depth by using chemical analysis, identification of mud matrix, clast type or microfossil assemblages (Kopf 2002; Deville *et al.* 2006). Difficulties in determining the exact source are only usually experienced along accretionary margins, where it is not obvious what type of sediment enters the subduction zone and the accretionary wedge may comprise similar argillaceous deposits (Kopf 2002). The depth of origin of mud extruded from volcanoes gives a good indication of the

vertical distances that mud can be transported and, therefore, the vertical extent of any potential seal breach (Cartwright *et al.* 2007). Evans *et al.* (2008) noted that mud volcano caldera margins are generally coincident with the thinnest sections of the parent bed, implying that collapse was initiated as material was evacuated from depth. The source domain also includes any deeper structure, such as the leading edges of thrust sheets emerging from accretionary prisms (Jackson *et al.* 2002; Allen *et al.* 2003; Knapp *et al.* 2004), which may have an influence on which parts of the parent bed mobilise to form the mud volcano system, as well as any zones beneath the parent bed that have contributed fluids to the system. For example in the South Caspian Basin Kopf *et al.* (2003) used the geochemical signatures of mud volcano fluids to estimate their depth of origin to be beneath the regional parent bed. Geochemical and biostratigraphical analyses were also carried out on the eruptive products in Templars Firs, Wootton Bassett mud springs in the UK to determine their parent bed (Bristow *et al.* 2000).

2.2.1 Mechanisms of Sediment Deformation and Mobilisation

2.2.1.1 Overpressure

Pore fluid within the parent bed is overpressured if its pressure exceeds that of the hydrostatic gradient at a specific depth (Osborne & Swarbrick 1997). Overpressure can result in sediments becoming undercompacted as the pore fluids support a greater weight of the lithostatic load, minimising the contact between grains. Overpressure can also inhibit increases in shear strength and tensile strength, keep the bulk density low and where trapped pore fluid is water, heat is retained (Judd & Hovland 2007). There are many processes that can cause overpressure in the parent bed including;

a) Disequilibrium Compaction

As a shale/mud succession becomes buried fluid is initially expelled from the sediment, so the pore pressure increases following the hydrostatic pressure gradient (Osborne & Swarbrick 1997). However, as burial continues, the

permeability of the sediment decreases and fluid will start to be retained; the depth at which this occurs is the 'fluid isolation depth' (Osborne & Swarbrick 1997). If no fluid escapes below the fluid isolation depth, the pore pressure would then rise along a pressure-depth path that is parallel to the lithostatic gradient. This results in the pore pressure within the sediments becoming higher than the hydrostatic pressure. When the burial load is eventually taken up by the pore fluid, the sediment remains with fixed porosity despite the increasing burial depth. The sediment is now considered overpressured and under-compacted because it shows greater porosity than expected at a certain depth (Maltman & Bolton 2003).

This mechanism is the most likely form of overpressure generation in the South Caspian Basin (Osborne & Swarbrick 1997). This is especially likely as disequilibrium compaction most commonly occurs in less permeable lithologies e.g. the argillaceous Maykop Formation (Devlin *et al.* 1999), and in regions of rapid burial which the South Caspian Basin had (e.g. >5 km of sediment was deposited in 1-2 Ma; Nadirov *et al.* 1997; Jackson *et al.* 2002). Maykop pore pressure gradients of 0.020-0.023 MPa m^{-1} developed in response to the rapid burial (Yusifov & Rabinowitz 2004) reducing effective stress and promoting mechanical weakening of the sediment.

b) Tectonic Compression

This mechanism is poorly understood however, may be important in the South Caspian Basin where tectonic compression has occurred and now forms the anticlinal structures through which the mud volcano systems intrude (Fig. 2.2; Stewart & Davies 2006). The predominant location of mud volcano systems within anticlines is thought to reflect the importance of regional compression through the increase of lateral stress on the parent bed at depth. Little is known however about the specific ways in which compression influences the Maykop parent bed at depth and exactly why mud volcanoes are mostly located within anticline crests. In many regions the folding appears to be synchronous with mud volcano formation (Fig. 2.2; Fowler *et al.* 2000; Yusifov & Rabinowitz 2004). The horizontal stresses would be equal to or less than the vertical stresses in basins where no lateral compression

is occurring (Osborne & Swarbrick 1997). Lateral compression can increase pore pressures in the same way as vertical stress can cause overpressuring through disequilibrium compaction (Osborne & Swarbrick 1997). One of the main issues in this process is that even though it results in a rapid increase in overpressuring it may also produce accelerated pressure release during faulting and fracturing events.

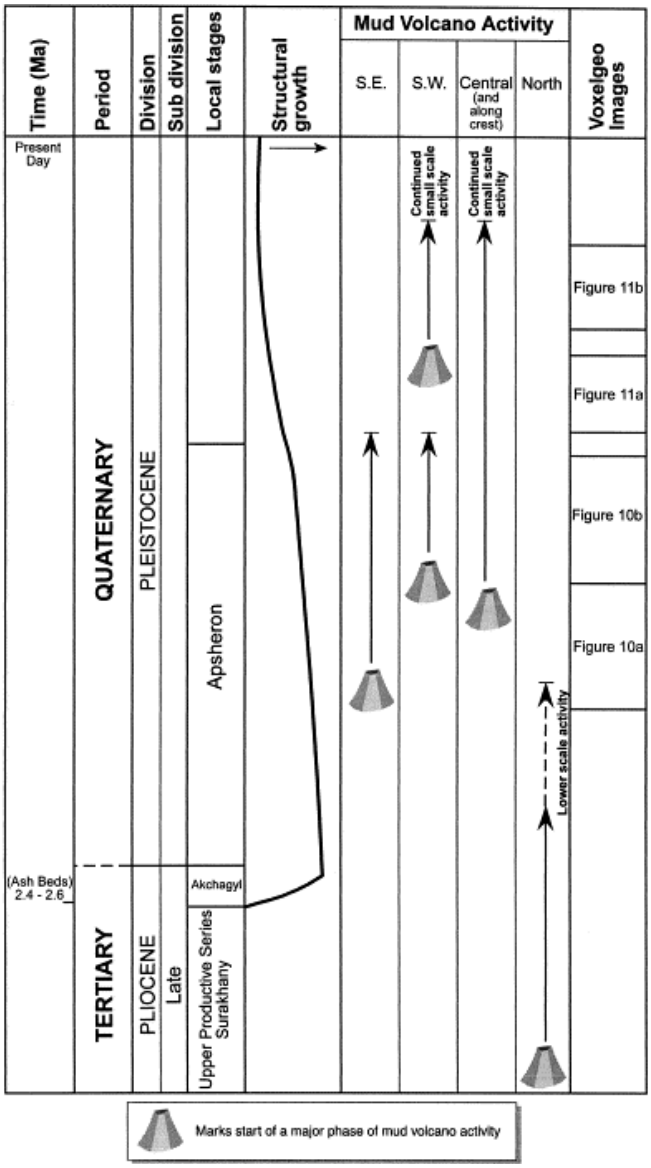

Fig. 2.2: Summary diagram of mud volcano timing with respect to stratigraphy and start of structural growth. Note the delay in the appearance of the first mud volcanoes from the start of structural growth. Delay of the order of 0.5 to 1 million years assuming relative constant deposition rates from the Akchagyl Ash Beds date of 2.4–2.6 Ma. From Fowler *et al.* (2000).

c) Volume Changes

There are numerous mechanisms which result in an increase in fluid volume or change in the solid-to liquid ratio within a sedimentary section (Osborne & Swarbrick 1997). These processes include; (a) aquathermal expansion, (b) mineral diagenesis (including dehydration), and (c) release of hydrocarbons from kerogen. In mud volcano systems the two main volumes changes cited for causing overpressure are methane gas expansion and hydrocarbon cracking. At temperatures between 120-180°C almost complete thermal cracking from oil to lighter, gaseous hydrocarbons i.e. methane occurs (Hunt 1979). Production of gaseous phases usually results in a volume expansion which in turn causes overpressuring in a closed system (Osborne & Swarbrick 1997). This can lead to a negative feedback as increasing pressure can also retard the reaction and therefore may not produce significant amounts of overpressure (Osborne & Swarbrick 1997). In the Maykop Formation the maturation of hydrocarbons within it and the addition of other fluids injected from below is highly likely to have contributed to the development of overpressure (Osborne & Swarbrick 1997; Kopf *et al.* 2003). Maturation of the Maykop and expulsion of oil and gas is thought to have taken place in the last 1 to 3.5 Ma (Abrams & Narimanov 1997; Lerche *et al.* 1997; Lerche & Bagirov 1999).

Several of these mechanisms can occur in a mud volcano system and so it may be difficult to distinguish which is the prominent driving factor. A more detailed list of mechanisms can be seen in Table 2.1 from Kopf (2002).

Origin	Mechanism	Environment
Burial	• Sedimentary loading, compaction/settling • Slumping, sliding	• Any sedimentary setting (i.e. deltas, active and passive margins) • Marine slopes of active and passive margins
Tectonic	• Tectonic loading • Deep level ducting • Smectite dehydration	• Any compressional margin, thrust zones and wedges • Accretionary complexes • Accretionary complexes
Thermogenic	• Opal/quartz reactions • Smectite dehydration • Other diagenesis • Metamorphism • Methanogenesis/hydrocarbon generation • Thermal expansion; hydrothermal pressuring	• Any setting with biosilica • Any setting with abundant clay deposition • Deeper subduction zone • Deep subduction zones and other collision zones • Any setting and reservoirs • Magmatic arcs and ridges
Biogenic	• Methanogenesis	• Shallow marine settings and accretionary prisms
Other	• Osmosis	• Clay-bearing sedimentary environments

Table 2.1: Mechanisms for generating overpressure from Kopf (2002).

2.2.1.2 Buoyancy

A second driving force for mobilised sediment is the buoyancy of the fluid-sediment mix which is a function of the bulk-density contrast (Judd & Hovland 2007). Sediments that are under-consolidated or overpressured (as discussed in section 2.2.1.1) or in which 'buoyant fluids' are accumulating, have a low bulk density compared to overlying 'normally consolidated' sediments. In both these cases bulk density decreases with depth i.e. there is a density inversion;

$$BF_{parent} = \left(\rho_{parent} - \rho_{os}\right) \times g \times h_{parent} \qquad \textbf{Eq. 2.1}$$

Where BF_{parent} is the buoyancy of the parent bed or parent formation, ρ_{parent} is the bulk density of the parent bed, ρ_{os} is the bulk density of the overlying sediment, g is the acceleration due to gravity and h_{parent} is the height or thickness of the parent bed. Density inversion can either cause the underlying sediment to 'push' through the capping sequence flowing as a coherent sediment mass (i.e. a diapir) or the

excess pore fluid pressure will lead to fluidisation and escape as a fluid transporting particles of the parent bed i.e. as a diatreme (Judd & Hovland 2007). The buoyancy force exerted by the sediment mud must be greater than the downward force of the overlying sediment and the cohesion in order for the mass to be able to break through into the overlying successions (Judd & Hovland 2007). Once the mass begins to ascend there is a pressure reduction in the fluid contained within it allowing gases to come out of solution and in so decreasing the density (Judd & Hovland 2007).

All of these mechanisms serve to weaken the sediments contained within the parent bed however they do not necessarily provide a means of mobilising the sediment. A sediment becomes mobilised once it is in a condition of insufficient strength to resist the forces driving it to move (Maltman & Bolton 2003). Once the parent bed has been overpressured it must become mobilised in order to travel to the surface. This can be caused by several processes including fluidisation and liquefaction. In mud volcano systems the sediments are thought to be entrained within fluid that most likely enters the overpressured sediments from other sources (Fig. 2.3). Chemical signatures of these fluids help to identify where they originated within the system.

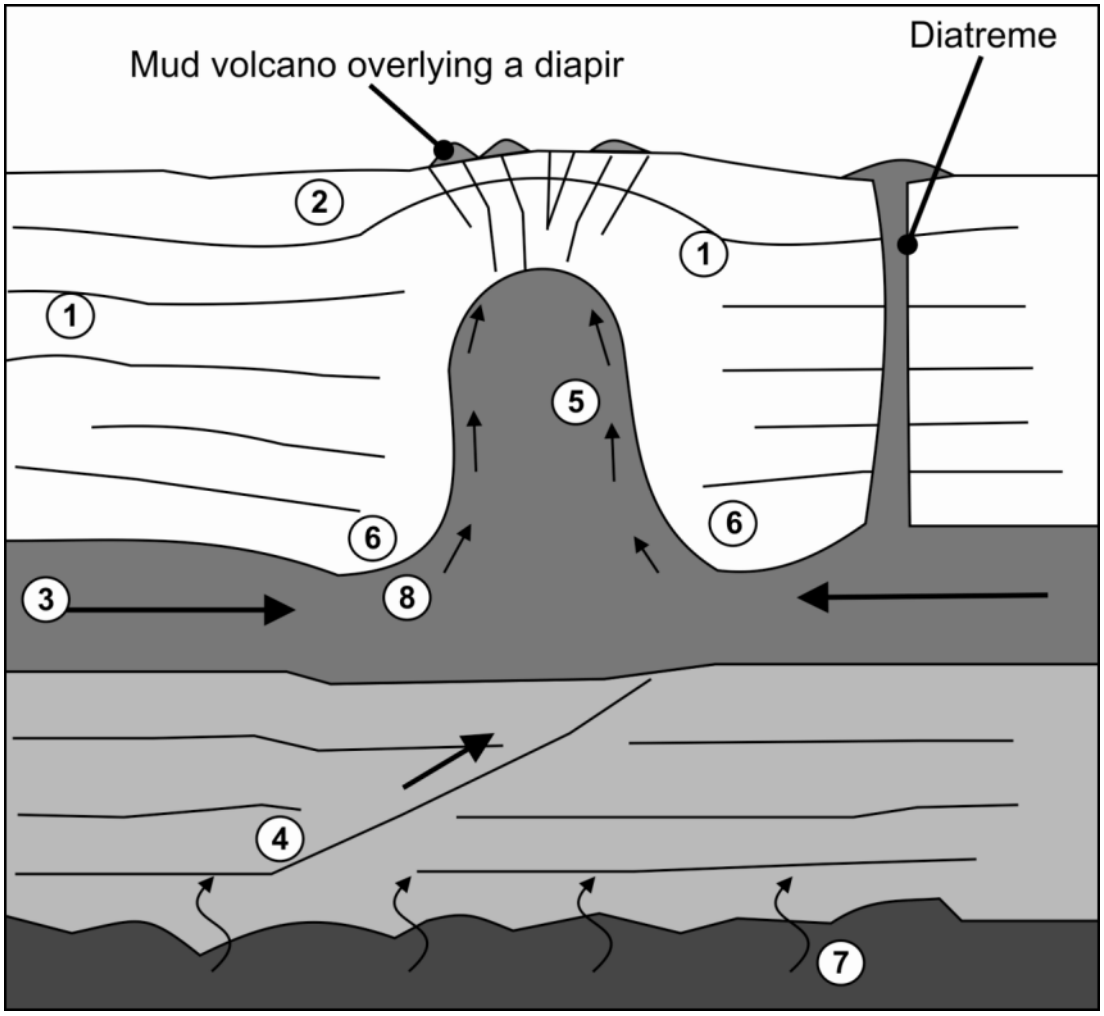

Fig. 2.3: Schematic diagram of a mud diapir, mud volcano extrusions, and diatremes, including possible fluid sources (numbered 1–8). (1) Pore fluid expulsion during compaction. (2) Biogenic methane from degradation of organic matter. (3) Lateral fluid flux through stratigraphic horizons or fault zones. (4) Fluid migration along deep seated thrusts. (5) Thermogenic methane and higher hydrocarbon concentrations. (6) Fluids from mineral dehydration (opal, smectite). (7) Hydrothermal fluids, alteration of crustal rock. (8) Fluid expulsion from internal deformation within the diapiric intrusion. Geochemically mature fluids may be found among categories 3, 4, and 7, while in categories 1, 6, and 8, water from dissociated gas hydrates may provide 'freshened' fluids. Modified from Kopf (2002).

2.2.1.3 Fluidisation

This occurs when the drag exerted by moving pore fluids exceed the particle weight, the particles are lifted and the grain framework is destroyed (Lowe 1975). This usually requires rapid influx of external fluids into the sediment (Maltman 1994). This can occur once the minimum fluidisation velocity (U_{mf}) is reached;

$$U_{mf} = \frac{\varepsilon_{mf}^3(\rho_s - \rho_f)g(\varphi d)^2}{5(1-\varepsilon_{mf})\mu 36} \quad \textbf{Eq. 2.2}$$

Where ε_{mf} is the intergranular porosity at minimum fluidisation, d and ϕ are the grain size and shape respectively and ρ_s and ρ_f are the density of the grains and fluid, respectively, g is the acceleration due to gravity and μ is the fluid viscosity. When the fluid velocity exceeds the settling velocity of the grains, the grains will be lifted and carried away in the flow. The most easily fluidised sediments are fine grained sands and undercompacted clays and silts (Judd & Hovland 2007). Unconsolidated clay particles require the lowest fluid velocities to become fluidised (0.07 cm/s; Lowe 1975; Judd & Hovland 2007). Coarse sand and gravel grain fluidisation requires much higher fluid velocities (approximately 10 cm/s or higher; Huuse *et al.* 2005).

2.2.1.4 Liquefaction

This process occurs when there is no internal friction or cohesion between the particles in the sediment as the pore fluid temporarily sustains the entire stress exerted on the sediment (Maltman 1994), essentially behaving as a fluid. This usually occurs when the effective stress is zero when the upward force of flowing fluid equals the buoyant weight of the particles (Lowe 1975; Judd & Hovland 2007). Both liquefaction and fluidisation are forms of 'liquidisation' processes i.e. both lead to a reduction in the sediment strength resulting in it behaving as a liquid.

2.2.1.5 Hydroplastic Deformation

This type of deformation characterises grain supported sediments with a significant yield stress and at pore fluid velocities below those required for fluidisation (Lowe 1975). A sediment does not have to be subject to complete liquidisation in order to become mobilised. If the sediment has moderate overpressure or a large proportion of cohesive clay minerals it will retain a degree of strength and behave plastically rather than as a fluid (Maltman 1994) i.e. it becomes mechanically

'hydroplastic' (Maltman & Bolton 2003). Yield stress may originate from either cohesive forces or frictional resistance. This state usually arises from an increase in pore-fluid pressure and results in a reduction in strength. Deformation becomes possible when the moisture content exceeds the 'plastic limit' but has not reached the 'liquid limit' (Judd & Hovland 2007).

2.2.1.6 Critical State Deformation

Deformation at a sediment's 'critical state' takes place before the onset of liquidisation. This is a state where the sediment is able to undergo very large amounts of shear even at low deforming stress due to a particular combination of porosity, fluid-pressure and stress (Maltman & Bolton 2003). The sediment behaves in a weak, ductile manner rather than as a fluid. In any one instance of subsurface sediment mobilisation liquefaction, fluidisation, hydroplastic and critical state deformation are likely to work together (Barber *et al.* 1986; Maltman & Bolton 2003).

Although the mechanical states described above make sediment capable of mobilisation, in themselves they are not sufficient to bring about bulk movement as a driving force is required. Liquidised sediments, by definition, behave as fluids and as such will be subject to fluid pressure gradients. For example, the fluid potential within an overpressured sediment layer is no longer balanced by the elevation head meaning that the fluid will attempt to move to lower values of the fluid pressure gradient (i.e. move from high pressure areas to lower pressure areas, Brown 1994). The sediment will undergo bulk movement if the pressure gradient is high enough to trigger movement. Movement will continue as long as the pressure gradient is maintained and the sediment remains in a mechanical state capable of mobilisation. In most sedimentary basins pressure decreases upwards as it is usually the lithostatic load that imparts the majority of the loading force on the sediment. This means that most liquidised sediments will have a tendency to move upwards. Locally however, the fluid potential gradient can decrease in any

direction making it possible for mobilised sediment to move in any direction, even downwards.

2.3 The Intrusive Domain

The 'intrusive domain' of the mud volcano system connects the extrusive and source domains (Fig. 2.1). Included within this is the conduit system that transports fluids and sediment from the source domain to the surface and the host rock that is intruded by it. The lower boundary of this domain is the upper surface of the source domain and its upper boundary is the surface or seabed and the base of any overlying extrusive edifice (Fig. 2.1). The exact anatomy and fluid flow processes of these feeder complexes are still the most poorly understood component of the mud volcano system. This is mainly because:

1) There are only a few modern or ancient mud volcano systems that have been studied which are eroded to a sufficient depth to allow examination of conduits at outcrop (Brown & Orange 1993; Clari *et al.* 2004). These outcrops are rare due to their being particularly vulnerable to weathering processes or the fact that they may not have been identified yet;

2) Physical properties of the material within the conduit and the timescales over which mud volcanoes are constructed are poorly constrained making numerical estimates of conduit shape and diameter difficult (Kopf & Behrmann 2000);

3) Seismic reflection data that image the intrusive domains of mud volcano systems are often poor quality due to inherent difficulties imaging steep or vertical conduits and blanking caused by gas (Judd & Hovland 1992).

These intrusive systems have been imaged on seismic data globally however, the resolution at the centre of the feeder complex is often impossible to interpret. This is thought to be the result of many factors including 'acoustic blanking' which appears beneath the extrusive mud cones and around the feeder complexes. This often takes the form of large blanked out chimneys of seismic data where the

reflections are suddenly faint or absent. In many examples chimneys are characterised by loss of the seismic signal, i.e. by low seismic amplitudes and low seismic coherency. The exact causes of these changes in seismic response are not always obvious and explanations depend on local circumstances. In many cases however, this may result from the deposition of thick series of unconsolidated muds absorbing or scattering the acoustic energy in underlying, locally fluid charged sediments (Judd & Hovland 1992). Seismic chimneys are also anomalies usually associated with the upward movement of fluids or free gas (Schroot *et al.* 2005). An alternative explanation for the loss of seismic signal would be the actual break up of layering resulting from fluid escape processes. The latter is only likely to occur in a 'high energy' environment, which implies active seepage (Schroot *et al.* 2005). Seismic imaging of intrusive domains is generally poor (Dimitrov 2002), although modern 3-D seismic data commonly reveal a much narrower vent geometry than commonly apparent on two-dimensional (2-D) seismic data (Van Rensbergen & Morley 2003). Pre-stack depth migration is commonly required to obtain the best imaging results (Davies & Stewart 2005).

In most mud volcano systems these seismic discontinuities are circular in plan view showing that they are pipe-like in 3-D (Fig. 2.4; Fowler *et al.* 2000; Graue 2000; Stewart & Davies 2006). These discontinuities are tall, narrow zones of low signal-to-noise ratios that might be misinterpreted as geological features produced below an energy-absorbing feature, so it is not known to what extent these pipes are geophysical imaging artefacts. This effect could be reduced by altering the streamer length of the seismic acquisition apparatus so that volcanoes with a diameter significantly less than the streamer length (4 km; 2.5 mi) will not be undershot (Stewart & Davies 2006).

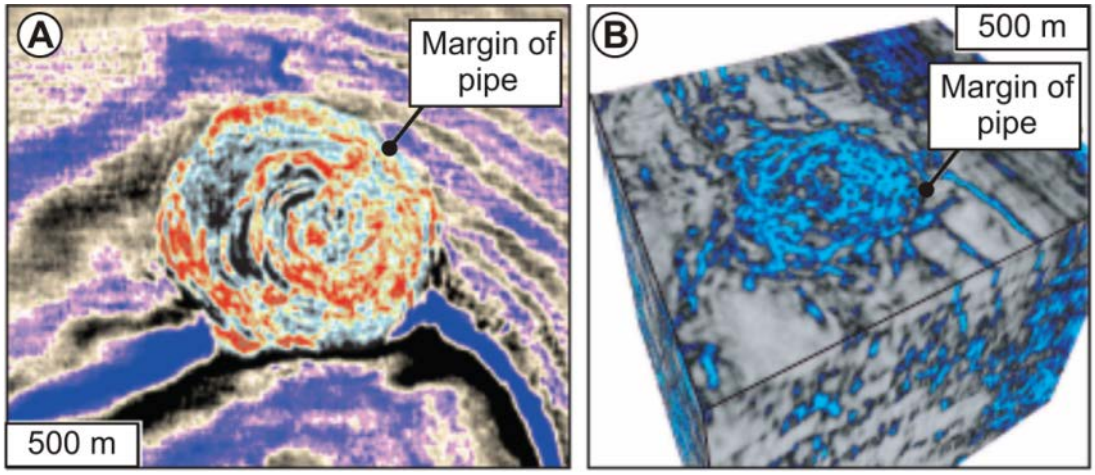

Fig. 2.4: A) Horizontal seismic section (depth slice) through a downward-tapering cone, showing an abrupt change from regional structure to faulting and folding of strata in the downward-tapering cone. B) Seismic coherency data emphasising stratal discontinuities in a mud volcano system. The cube is located below the mud volcano and contains a downward-tapering cone. Discontinuities (bright blue) can be interpreted as faults and fracture zones. This visualisation of structural complexity can be useful in well planning through or around mud volcano substructure. Modified from Stewart & Davies (2006).

Various architectures of feeder system have been suggested as connecting extrusive mud volcanic cones to their underlying parent bed, ranging from bulbous diapirs (Brown 1990; Van Rensbergen *et al.* 1999) to steep diatremes (Brown 1990; Robertson & Kopf 1998) and narrow vertical pipes (Graue 2000; Løseth *et al.* 2001). It is unclear whether current generic models for the structural roots of mud volcanoes are accurate or their relative simplicity reflects insufficient image resolution. Currently the two most popular intrusive systems are believed to be mud diapirism and/or linked mud dyke/sill intrusive complexes similar to igneous volcanic systems. These two processes are now described in detail below.

2.3.1 Mud Diapirism

Mud diapirs form when a kilometre-scale layer of plastic mud moves 'en-masse' and is driven upwards by its internal overpressure and buoyancy as discussed earlier in section 2.2.1 (Barber *et al.* 1986; Brown 1990; Hovland 1990; Morley & Guerin 1996; Kopf 2002). Hovland *et al.* (1998) define a piercement shale diapir as a positive topographical feature constructed mainly of clay sized sediments that

periodically or continuously move from the sub-surface upwards towards and through the sea floor. How such conduits penetrate the crust and how fluid-sediment mixes utilise the conduit systems is largely unknown (Fig. 2.5). The exact mechanism and physical properties of mud involved in diapirism has eluded scientists for decades and recently, it has been questioned whether mud diapirs can physically exist at depth (Davies & Stewart 2005; Deville *et al.* 2006, 2010) and whether they are necessary in order to explain seismic observations (Van Rensbergen & Morley 2003; Calvès *et al.* 2010). Diapirs form bulbous intrusions when viewed in cross section and have diameters that range from tens of metres to kilometre-scale. Various mud diapirs have been described at outcrop (Barber *et al.* 1986; Brown & Orange 1993; Clari *et al.* 2004) and from seismic data worldwide including areas of the Niger Delta, the North Sea and the Alboran Sea (Hovland 1990; Morley 2003; Morley & Guerin 1996). Large parabolic disturbances in seismic data are often interpreted as mud diapirs due to their columnar shape and lack of internal reflectivity (Barber *et al.* 1986). These conduits must narrow considerably otherwise, exceptionally large flow rates would result even when small density contrasts (not to mention an excess hydrostatic head) exist as a driving force. Several different types of mud diapir have been classified depending on the phase of growth by analysing the deformation and thickness distribution of surrounding sediments (Vendeville & Jackson 1992), phases include;

1) Reactive diapirism

This occurs during the initial stages of growth where relief on the top of the mobile mass is caused by the movement on extensional faults (Morley & Guerin 1996). The diapir rises without piercement of the overburden (Vendeville & Jackson 1992). Thickening of surrounding sediments towards the diapir is therefore seen as evidence for a phase of reactive diapir growth (Fig. 2.5).

2) Active diapirism

This stage occurs when a diapir pierces through the overburden due to fluid pressure drive and/or buoyancy forces in the crest of the diapir (Fig. 2.5; Vendeville & Jackson 1992). Thinning of sediment onto the crest of the diapir is characteristic

of this phase as is the presence of laterally adjacent synformal basins that form as a result of mud withdrawal from depth.

3) Passive diapirism

This phase begins when the diapir reaches the surface. If sedimentation is not coeval then the diapir cannot rise but instead widens (Vendeville & Jackson 1992). It is fairly uncommon as most mud diapirs are terminated before reaching the surface due to fluid loss (Morley & Guerin 1996). Indeed, sufficient fluid loss at any stage of diapir growth can lead to shrinkage of the mud mass and diapir collapse. Evidence for this can take the form of circular or radial extensional fault zones in the areas directly above the head of diapir (Morley 2003; Stewart 1999, 2006).

Sediments within a mud diapir can undergo deformation in a variety of mechanical states depending on where they are positioned within the diapir (Brown 1990; Maltman & Bolton 2003). Large exposed mud mélanges (chaotic masses of sediment) are generally 100's of metres thick and thus tend to be described as diapirs (Brown & Orange 1993). Diapirism is believed to be primarily driven by excessive pore fluid pressures (Maltman & Bolton 2003). As discussed in section 2.2.1.1, overpressure is also able to liquidise sediments and so liquid mud flows may erupt if there is extrusion however, in the same diapir there could also be other regions that are experiencing shearing under critical state conditions (Brown 1990; Brown & Orange 1993; Maltman & Bolton 2003). Plastic flow and critical state deformation are most pervasive, producing shear fabrics and marginal 'scaly clays' (Brown 1990; Brown & Orange 1993; Maltman & Bolton 2003).

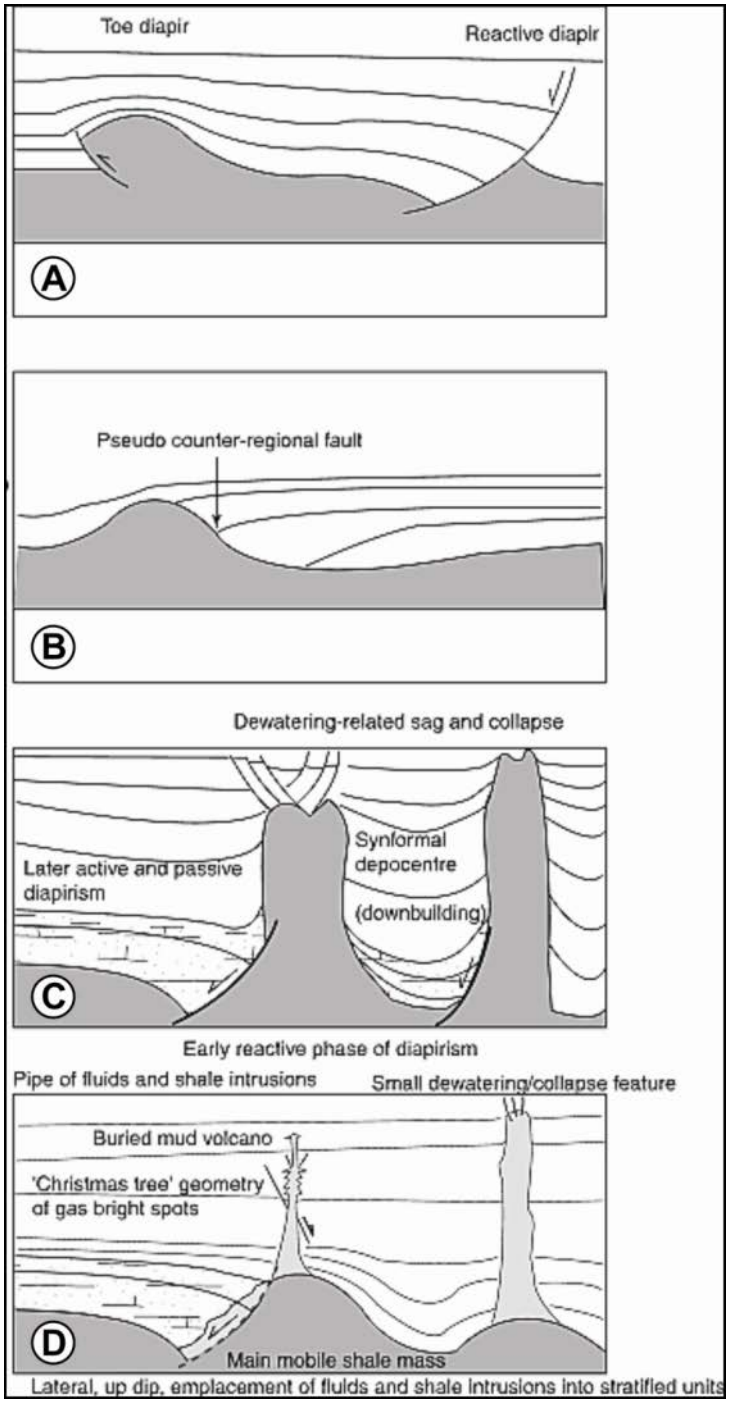

Fig. 2.5: Schematic cross sections illustrating some of the characteristics of shale diapirs and pipes (A and B). Variations on shale bulges developing in response to sedimentary loading by deposition in the hanging wall of a reactive diapir (Fig. 2.5A), and in a withdrawal syncline (Fig. 2.5B); C) development of shale diapirs similar to classic salt diapirs with reactive, active, and passive phases and D) shale diapirs commonly do not develop like Fig. 2.5C but may superficially resemble them. Instead a complex of gas rich fluids and shale intrusions may intrude laterally and vertically (pipes) into the country rock from mobile shale masses at depth. The well developed synformal depocentres in Fig. 2.5C are not seen in Fig. 2.5D. Modified from Morley *et al.* (1998).

The type of deformation that will occur will largely depend on the lithology and physical conditions. The diapir margins with be subjected to increased shear due to contact with the country rock resulting in increased scaly clay formation (Brown 1990). These regions will also drain more efficiently and so re-gain some residual strength (Maltman & Bolton 2003). Maltman & Bolton (2003) also suggested that with decreasing burial depth (i.e. during diapir ascent) liquidisation becomes more pervasive as the confining stress reduces. Brown (1990) commented on how methane exsolution at depths of 2 km or less can locally induce liquidisation within parts of a diapir and lead to the formation of mud pipes rooted in the upper parts of diapirs and on the margins producing conduits to the surface. One of the major problems of how a shale diapir ascends is what happens to the sediments above it as it pierces through them as well as how clasts of country rock get included within the diapir. Fig. 2.6 shows the different ways in which salt diapirs are able to pierce through the overburden which may be analogous to shale diapirs.

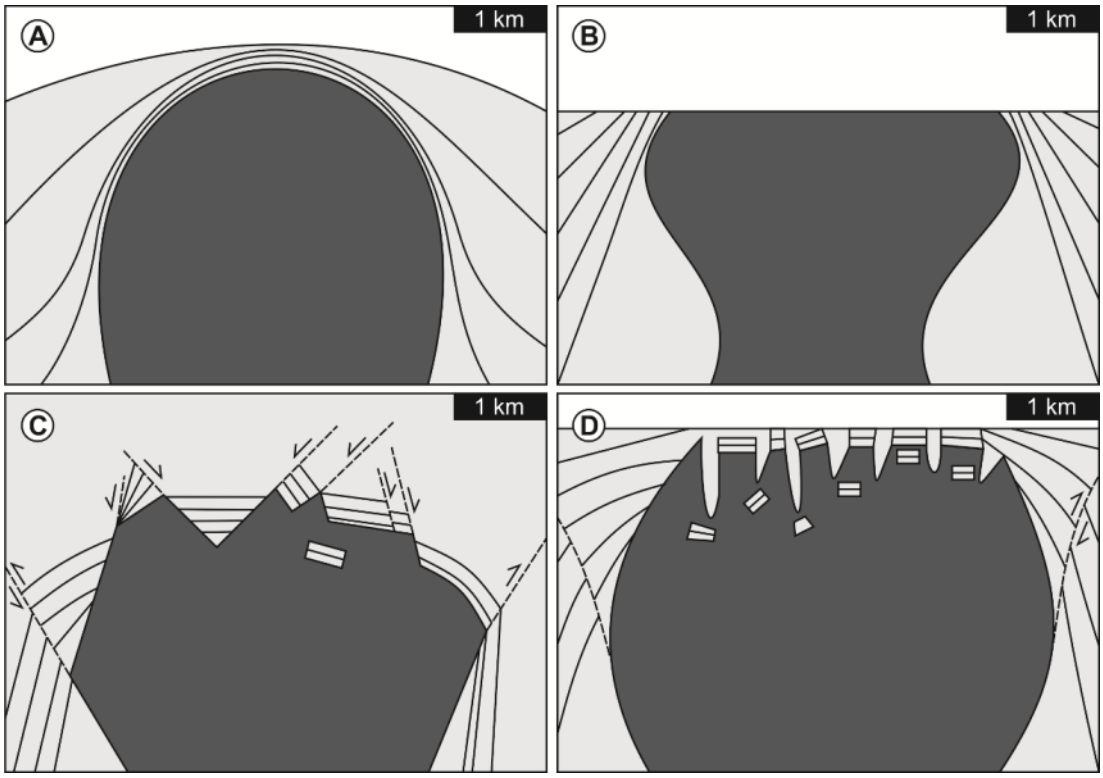

Fig. 2.6: Summary of how diapirs can 'apparently pierce' overburden sediments on seismic reflection profiles. A) Condensed sequence and/or attenuation by ductile creep. B) Non-deposition of sediment and active erosion/dissolution at the sea-bed. C) Extensional faulting and condensed

sequence. D) Dissolution above sea-level with surface run-off creates pot-holes crevasse system with stoping of sediments into dissolved channels and caverns. Modified from Davison *et al.* (1996).

2.3.2 Mud Sill/Dyke Igneous Style Intrusive Complex

Another possibility, determined from analysis of seismic data (Stewart & Davies 2006) is that transport takes place through intricate mud pipe, dyke and sill complexes (Fig. 2.7; Morley 2002), perhaps with similarities with igneous centres (Holmes 1998; Davies & Stewart 2005; Stewart & Davies 2006). Mud pipes are often referred to as diatremes due to their close similarity to these igneous features (Fig. 2.5D; Brown 1990; Morley 2003). Seismic reflection data from the South Caspian Basin are consistent with movement by fluidised mud flows through fractures (e.g. Morley 2003) as there is no evidence for kilometre-scale mud diapirism (Yusifov & Rabinowitz 2004; Davies & Stewart 2005). 'Mud pipes' when viewed on seismic data have been interpreted as broad to very narrow areas of image distortion ranging from < 1 metre to many 100s of metres wide (Løseth *et al.* 2001; Morley 2003). Rare field examples of mud volcano conduits indicate that a large degree of fracture propagation and stoping is required for the ascent process (Pickering *et al.* 1988; Morley 2003). Outcrop examples are described by Morley (2003) as long, narrow forcefully intrusive bodies or networks of intrusions filled with overpressured fluid. Where exposed, mud intrusions tend to be tabular rather than pipe-like (Pickering *et al.* 1988; Morley 2003). Clastic dykes have been identified globally and are fairly well documented however, not in association with extrusive mud edifices (Winslow 1983; Jolly *et al.* 1998; Parize & Friès 2003; Jonk *et al.* 2005).

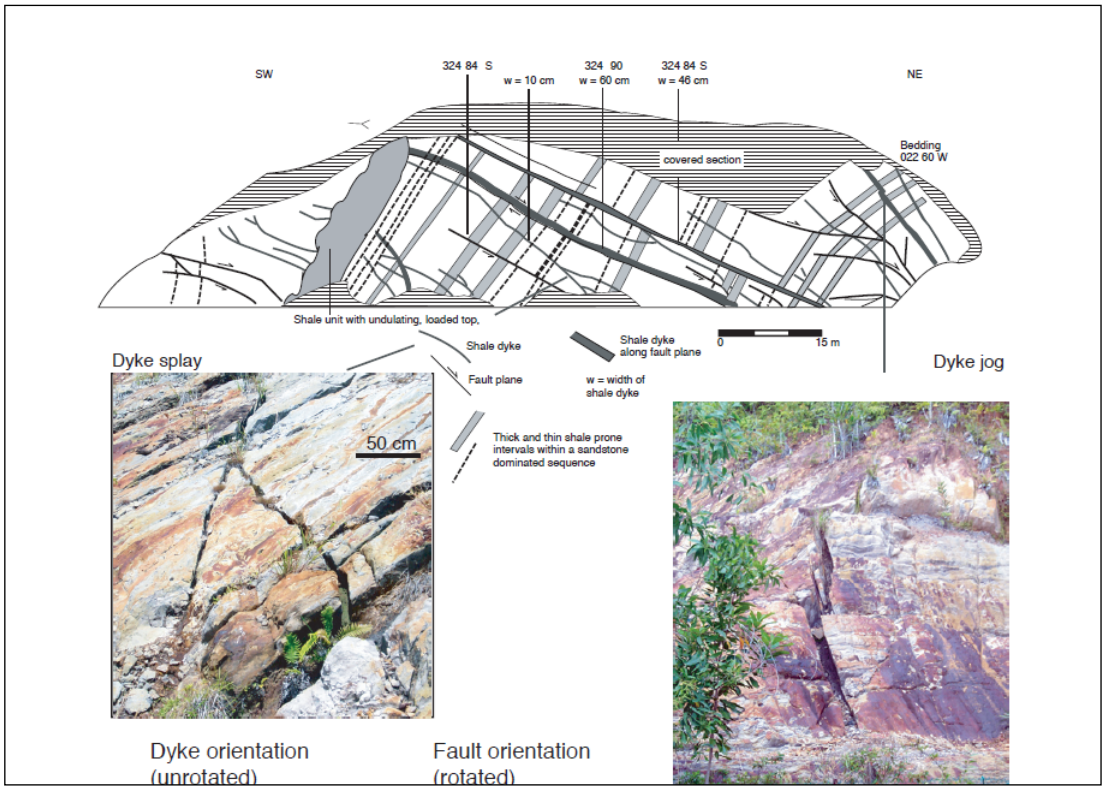

Fig. 2.7: Sketch of an outcrop in Jerudong (Brunei) cut by numerous dykes. Some of the dykes follow older normal faults, but most dykes are independent of the normal faults. The dykes have steep dips in their present orientation. Upon rotation of bedding to horizontal, dyke dips become much lower. Hence assuming dykes were intruded sub-vertically, dyke emplacement is inferred to be post folding. Photographs show jogs and splays in mudstone dykes in sandstones, these dykes are natural hydraulic fractures and do not follow pre-existing faults. Modified from Morley (2003).

Surface conduit widths range from 1 cm to 100 m onshore in Azerbaijan and conduits of 1.5–3.5 km width have been proposed for the Black Sea area and Azerbaijan on seismic data (Stewart & Davies 2006). One opposing theory was proposed by Gorkun & Siryk (1968) who suggested that 30 cm wide conduits formed at depth, which then widened to 2 m surface diameter at the various gryphons of Sakhalin mud volcanoes. The country rock that is replaced by the mud-filled pipe is most likely lost to the surface by wall-rock erosion indicated by mud flows at outcrop often being rich in wall-rock breccias (Kopf *et al.* 2003). This may be enhanced if subsequent pipe intrusions follow similar pathways, but onshore outcrops often show a scattered array of vents indicating that there must be a network of fluid flow pathways at depth rather than a single one, within a kilometre-scale mud volcano (Hovland *et al.* 1997; Planke *et al.* 2003). Evans *et al.*

(2007) suggested that numerous pipes repeatedly intruded the overburden at approximately the same location to feed the constructional edifice. This pipe system would represent a cylindrical zone of heavily intruded country rock or entirely of amalgamated mud pipes. Stewart & Davies (2006) postulated that this cylindrical zone had a low mechanical strength in relation to the surrounding un-intruded country rock and so underwent differential compaction, resulting in what they term a 'downward tapering conical collapse'. The internal structure of this downward tapering cone is a complex zone of faults; mud dykes and pipes feeding the volcanic edifice (Stewart & Davies 2006). The level of seismic resolution found by Stewart & Davies (2006) is rare indicating that either the feeder pipes are below seismic resolution at this structural level, or that they are concentrated on caldera margins.

2.3.2.1 Intrusion and Propagation

Mud pipes unlike diapirs, are formed in response to the rapid flow of pore fluids up through a sedimentary mass which becomes fluidised and entrained into the flow (see section 2.2.1.3; Brown 1990; Morley 2003). Mud volcano fluid fluxes and eruptions are clearly episodic (see Appendix I; Dimitrov 2002), which implies that the underlying mud intrusions are also transient. The most likely mechanism for fluids to intrude into the country rock is by hydrofracturing. A clastic sill or dyke can be considered as a natural hydrofracture (Cosgrove 2001; Jolly & Lonergan 2002). For a hydrofracture to form and propagate, fluid pressure must exceed horizontal stress plus the tensile strength of the overburden (Delaney *et al.* 1986). The pressure at which a formation can be fractured is known as the fracture pressure or P_{Frac} and can be expressed as;

$$P_{Frac} = \sigma'_h + T \qquad \textbf{Eq. 2.3}$$

Where σ'_h is the effective horizontal stress and T is the tensile strength of the formation. Once the effective stress and the tensile strength of a rock have been overcome fracturing can occur and as the fluid rises within the fracture into a lower

pressure environment the fractures increase in volume and become able to entrain and transport considerable amounts of fluid (Judd & Hovland 2007). Intrusion of a high pressured fluid with entrained parent bed particles into the surrounding sediment is needed in order to dilate the fracture (Jolly & Lonergan 2002). In mud volcano systems this excess pressure is most likely caused by overpressure as discussed in section 2.2.1.1. Once a hydrofracture has formed the velocity of upward moving pore fluids can fluidise the sediment and cause it to flow. At any specified depth, the fracture pressure of the rock is generally lower than the lithostatic (overburden) pressure, typically about 70–90% of the overburden, but may be higher at great depths (Osborne & Swarbrick 1997).

A propagating mud dyke is an example of a mode 1 or 'opening fracture' that propagates as a tensile crack in a plane normal to the least compressive stress direction (Delaney *et al.* 1986: Jolly & Lonergan 2002). Jolly & Lonergan discuss three ways in which a host sediment might fail;

1) If the pore pressure (P_f) within the parent bed exceeds the maximum principal stress (σ_1) and the tensile strength (T) of the overlying material in the intrusive domain, brittle failure will occur;

$$P_f > \sigma_1 + T \qquad \textbf{Eq. 2.4}$$

If the sedimentary basin in which this was true had no imposed tectonic stresses then the maximum principle stress would be vertical due to gravitational loading and the minimum principal stress would be horizontal therefore allowing vertical dykes to form.

2) If there are pre-existing faults or fractures within the host sediment with little or no tensile strength, the pore fluid pressure only needs to exceed the normal stress (σ_n) across the older fracture for dilation of that fracture to occur;

$$P_f > \sigma_n \quad \textbf{Eq. 2.5}$$

If the fluid pressure increases a larger range in fracture orientations can be formed and intruded (Delaney *et al.* 1986; Jolly & Lonergan 2002).

3) An increase in fluid pressure can cause pre-existing faults and fractures to shear (Jolly & Lonergan 2002). This can form geometries that are more reminiscent of dyke and sill complexes.

Different conditions are necessary in order to propagate dykes or sills in a sedimentary sequence. In order for a dyke to propagate the fluid pressure must be great enough to overcome the horizontal stress (σ_h) and the tensile strength of the host sediment parallel to bedding (T_h);

$$P_f > \sigma_h + T_h \quad \textbf{Eq. 2.6}$$

For a sill to form the fluid pressure must exceed the vertical stress (σ_v) and the tensile strength perpendicular to the bedding (T_v);

$$P_f > \sigma_v + T_v \quad \textbf{Eq. 2.7}$$

Fluid velocities within intrusive complexes are believed to exceed the minimum values needed in order to mobilise the metre-scale blocks embedded within ancient intrusive structures, both sand and mud filled (Huuse *et al.* 2005). Indeed it is likely that fluid velocities in some sediment pipes are great enough to significantly erode the wall rock in a similar way proposed for igneous conduit systems (Pickering *et al.* 1988; Macedonio *et al.* 1994; Huuse *et al.* 2005).

2.3.3 Faulting

Faulting in the intrusive domain often consists of concentric extensional fault sets that are almost perfectly circular in plan view or radial (Fig. 2.8; Corthay & Aliyev

2000; Graue 2000; Murton & Biggs 2003; Hansen *et al.* 2005; Stewart 2006; Stewart & Davies 2006). Several studies have recognised fault systems around mud volcano systems globally and some examples of these can be seen in Fig. 2.8. Stewart & Davies (2006) mapped fourteen minor extensional ring faults around a mud volcano in the South Caspian Basin. These faults extended to a radial distance of 0.5-10 km from the caldera walls. They observed that the faults were planar in cross section with dips of 45° relative to the bedding. Stewart & Davies (2006) attributed this faulting to representing shear at the base of the bicone towards its central axis, accommodating lateral compaction of the edifice mud i.e. 'gravity contraction'. Mud volcano caldera faulting has also been studied in great detail by Evans *et al.* (2008). Radial faults are commonly associated with doming and extensional faults with basin subsidence (Stewart 2006). Radial extensional faulting may also occur where doming has influenced the orientation of polygonal fault sets (Davison *et al.* 2000) and concentric reverse faults form during uplift due to rapid, forceful intrusion (Stewart 2006). Extensional faults within and surrounding the cone would act as inherent weaknesses localising later fluidised flows, resulting in a geometry reminiscent of 'cone sheets' as described by Anderson (1936).

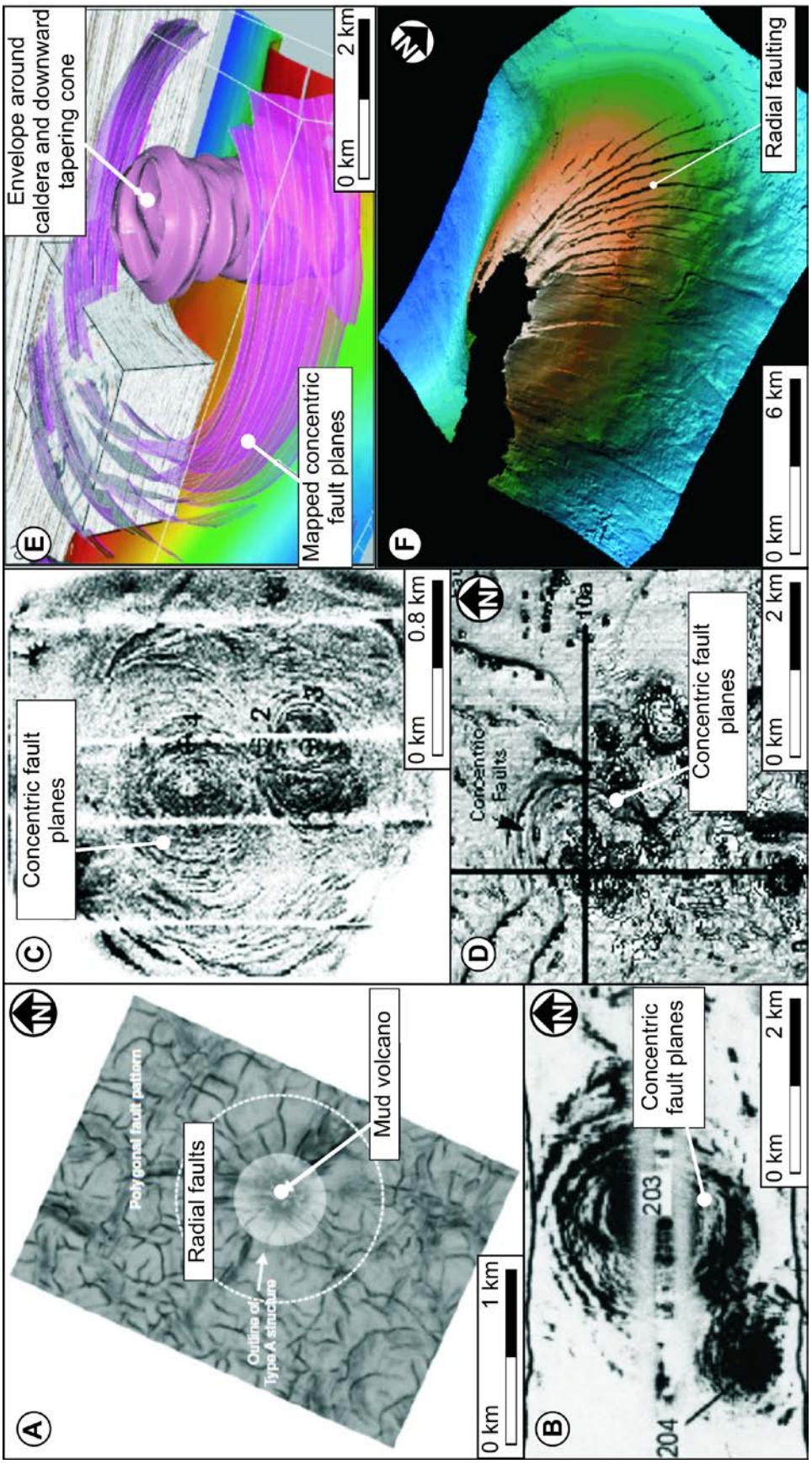
A
Polygonal fault pattern
Radial faults
Outline of type A structure
Mud volcano
0 km 1 km
B
203
204
Concentric fault planes
0 km 2 km
C
Concentric fault planes
0 km 0.8 km
D
Concentric Faults
Concentric fault planes
0 km 2 km
E
Envelope around caldera and downward tapering cone
Mapped concentric fault planes
0 km 2 km
F
Radial faulting
0 km 6 km

Fig. 2.8: A) 'Variance Cube' slice illustrating a change in fault pattern around a 'mud pillow' structure from the Gjallar Ridge, offshore mid-Norway. The variance cube highlights lateral discontinuities such as faults in the seismic data. It was calculated by cross correlating adjacent traces over a 100-ms window and assigning a value from 0 (perfect match) to 1 (no match). The radial pattern in the proximity of the structure and the polygonal pattern away from the structure suggest that the polygonal faults developed when the structure either had formed or was forming. Modified from Hansen *et al.* (2005). B) Sidescan sonar image of a mud volcano from Nigeria. Modified from Graue (2000). C) 30-kHz side-scan sonar image of the mud volcano Yuma (dark tones indicate high acoustic back-scatter), shown with the same horizontal scale, in the Gulf of Cadiz. Note the concentric ring-like structures that are centred on the main summit with the small dome to its left. Modified from Murton & Biggs (2003). D) Seabed dip map in Nigeria. Mud volcanoes are seen as 1–2 km circular features. Note the cuspate faults and numerous pockmarks. Modified from Graue (2000). E) 3-D view of the concentric fault system and margins of the caldera with downward-tapering cone in ACG field, SCB. Elements of the seismic reflection cube are left to indicate the quality of seismic data on which the interpretation is based. Modified from Stewart & Davies (2006). F) Artificially illuminated rendering of the Akchagyl structure map viewed from the northeast to southwest. The rendering illustrates the radial fault pattern and associated fault blocks that offset the Akchagyl horizon, and subtle erosional channels on the eastern (facing) flank of the anticline (vertical exaggeration – 50:1) modified from Corthay & Aliyev (2000).

Stewart (2006) gives a detailed account of how these fault systems could form in relation to the growth phases of both salt and shale diapirism (Fig. 2.9). In addition, use of seismic coherency attributes and mapping the fault pattern illustrate that mud volcanoes in the South Caspian Basin occur strictly in areas of local tension and within regional compressive fields (Cooper 2001). These fault systems are usually connected to the mud volcano systems in some way suggesting that they play some role in their formation. However, there is still a question as to whether the mud volcanoes are triggered by the activity of these faults, or conversely is there any connection at all.

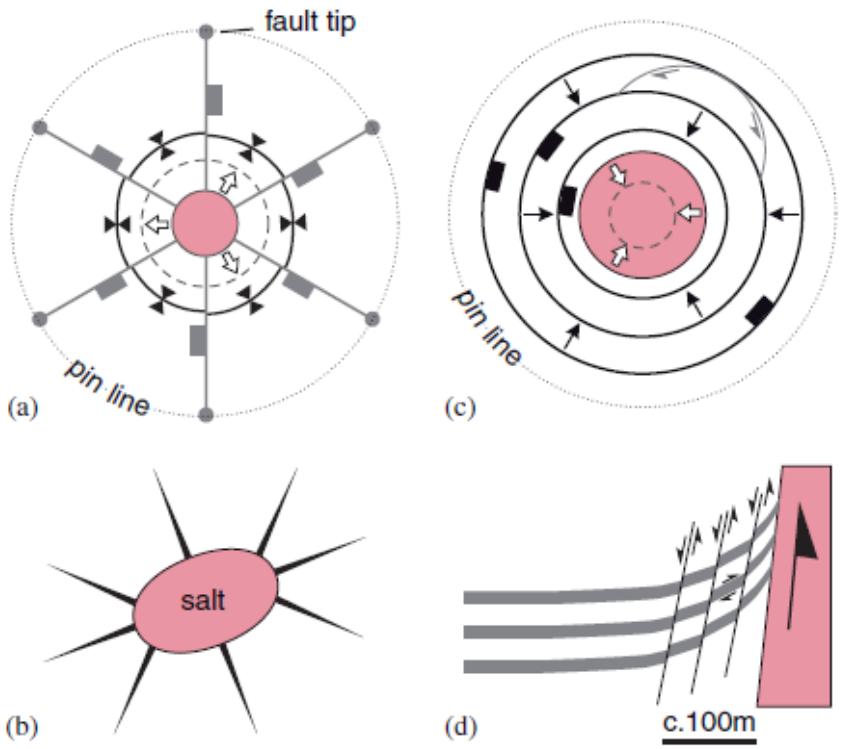

Fig. 2.9: Sketches of radial and concentric fault patterns and kinematics. Driving mechanism is salt flow and volume change of central cylinder. Volume and line length balance assumed. All sketches are plan views except D. Salt is pink. A) Expansion of central zone forces fold with circumferential trend, and circumferential extension accommodated by radial faults. B) Radial fault clustering at each end of elliptical hole or intrusion. C) Contraction of central zone allows concentric, inward-facing extensional faults. Secondary structures accommodate circumferential contraction. D) Sheared sediments close to diapir margin (vertical section). These faults are parallel to the salt sediment interface, i.e. concentric in plan view. From Stewart (2006).

2.4 The Extrusive Domain

The 'extrusive domain' lies on top of the intrusive domain and below the roof domain, if present. This domain has been studied extensively in many locations globally both onshore and offshore (Hovland *et al.* 1997; Kopf 2002; Planke *et al.* 2003; Yusifov & Rabinowitz 2004; Evans *et al.* 2008) and it is probably the most well defined domain within the mud volcano system.

2.4.1 Edifice

In the literature, the term 'mud volcano' commonly refers to a constructional edifice, whether outcropping or buried (Milkov 2000; Stewart & Davies 2006). The 'classic' mud volcano shape is similar to a composite igneous volcano i.e. a conical edifice with a summit crater (Judd & Hovland 2007). Davies & Stewart (2005) termed this the 'extrusive bicone' which can be composed of several separate stacked mud cones forming the classic 'Christmas tree' configuration, first noted in salt structures in the Gulf of Mexico (Stewart & Davies 2006). The first of these eruptive mud cones they termed the 'pioneer cone' (Davies & Stewart 2005). The morphology of the edifice largely depends on the viscosity, density, grain size of the fluids erupted (Kopf 2002), the frequency of eruptions and the volumes of fluids erupted (Judd & Hovland 2007). If there are more frequent eruptions the edifice can accrete relatively quickly and produce a large edifice and vice versa. If the mud erupted has a high viscosity it will form a steep sided conical edifice, however, if it has a low viscosity it will form a 'mud pie' (Kopf 2002). The dependency on these factors results in a wide range of morphologies being produced from calderas to flat plateaus (Fig. 2.10). In Azerbaijan the largest submarine mud volcanoes can reach 7 km diameter and 300-400 m in height whereas onshore they tend to be slightly smaller around with a maximum diameter of 4 km and 200-300 m height. Globally size ranges dramatically (Fig. 2.10) and the edifices can even be as small as < 1 m in height with only a single vent.

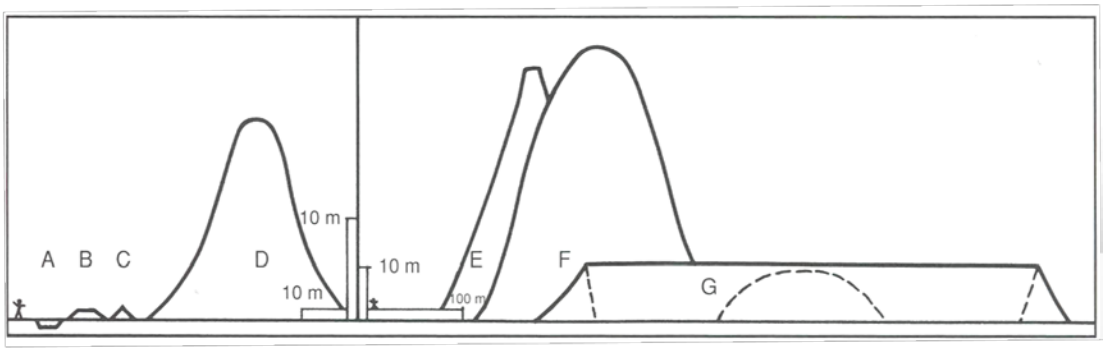

Fig. 2.10: Sizes and shapes of various terrestrial mud volcanoes (note the figure of a man in both frames). Locations: A= Maghaehu Stream, New Zealand; B= Volcanito, near Cartegena, Colombia; C= Moruga Bouff, Trinidad; D= El Totumo, near Cartegena, Colombia; E= Chandragup,

Makran Coast, Pakistan; F= Napag, Makran Coast, Pakistan; G= Gharniarigh-Tapeh, Goran region, northern Iran. From Judd & Hovland (2007).

2.4.2 Classification Schemes

There are several different classification schemes for the differing edifice morphologies and for different eruptive types. The most simple, described by Kopf (2002), in which edifices take the one form of 'mud domes' that consist of a roughly conical edifice with smaller vents i.e. gryphons and salses on its flanks and a crater or 'caldera' at the peak or 'crest' (Fig. 2.11A). The conduit usually intrudes through the centre of the conical edifice and 'builds' the edifice from this point source. The second type is a 'mud pie' otherwise known as 'mud pool', 'mud spring' or 'tassik' (Kopf 2002). The difference between these two morphologies is based on the slope angle i.e. mud pies have slopes of <5° and mud domes with angles >5°. The 'feeder' or 'conduit' of the mud volcano system is found at the centre of the edifice and outcrops as either a caldera or as a fissure i.e. faults and fractures (Kopf 2002).

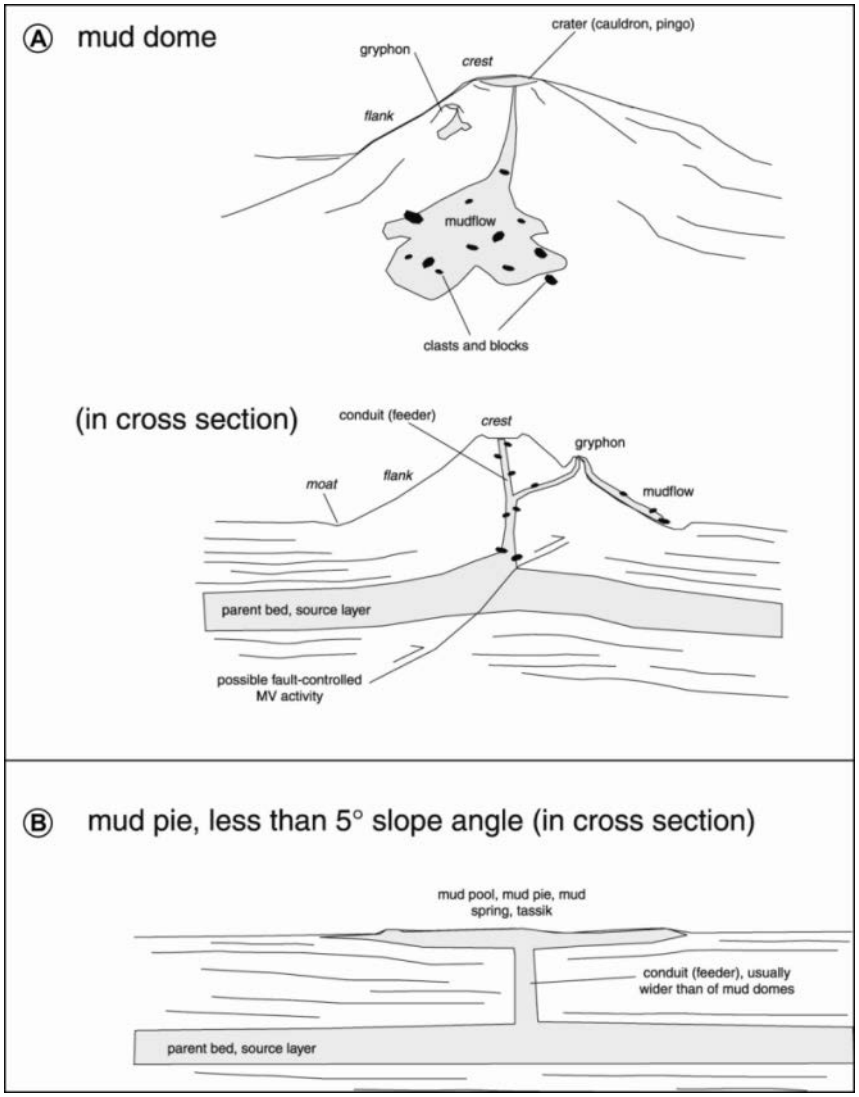

Fig. 2.11: Schematic diagrams of A) cone-shaped and B) pie-shaped mud feature with main applicable terms from Kopf (2002).

Yusifov (2004) distinguished between different mud volcano morphologies using seismic reflection profiles in the South Caspian Basin. This classification consists of four types of mud volcanoes based on their general shape; A) concave, B) convex, C) flat and D) buried. Yusifov (2004) also describes how the viscosity of erupted mud from marine mud volcanoes is lower than that onshore, making their flow lengths longer and their profiles slightly different (Fig. 2.12). However, the main influence on flow length both on and offshore is slope angle.

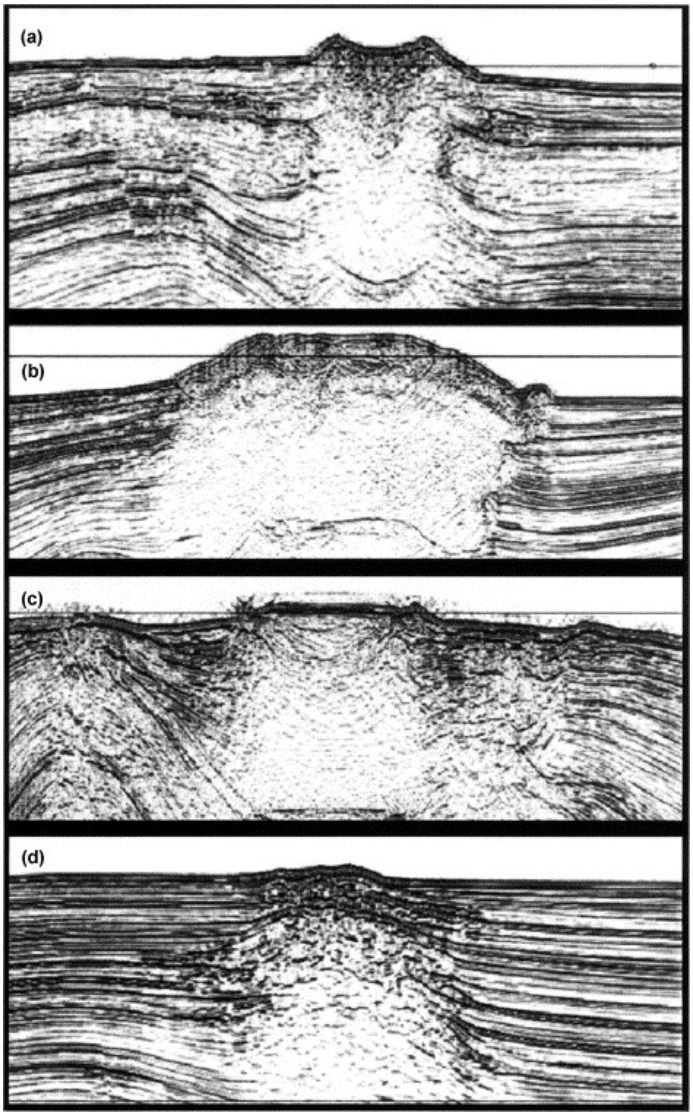

Fig. 2.12: Types of mud volcanoes based on the shape and appearance on the seismic line. A) Concave; B) Convex; C) Flat; D) Buried. From Yusifov (2004).

The State Oil Company of Azerbaijan Republic (SOCAR) define four basic groups of mud volcanoes based on their eruptive style:

1. Explosive - powerful flow of mud and gas that spontaneously ignites.
2. Effusive - ejection of large amount of mud breccia with non-ignited gas emission.
3. Effusive - flow of low viscosity of mud without intense gas emissions.
4. Extrusive - slow extrusion of viscous mud with very insufficient amount of gas (Fowler *et al.* 2000).

Among these types of mud volcano eruptions, the first two can be very hazardous. Others have less destructive power and might be considerably predictable. This

classification system is not very comprehensive and would not suit all mud volcanoes as some display several eruptive types during one event. Dimitrov (2002) refined this scheme by providing descriptions based on their morphology and eruptive type (Table 2.2). Dimitrov (2002) also noted that there is no relationship between type and geographical position i.e. all three types of mud volcano can be found in mud volcanic regions globally depending on the lithology of the local sediments and the regional tectonics. There is no general consensus on which classification scheme to use when describing mud volcano systems something that must be rectified in order to better understand their processes and distributions.

Mud Volcano Type	Description
I class—Lökbatan type	Activity has an explosive character commonly with ignition of the emitted gases. Short periods of explosive activity are separated by long passive periods. Lökbatan mud volcano on the Apsheron Peninsula, Azerbaijan, Caspian Sea is a typical example. Usually, the extruded mud breccia is characterised by low viscosity. This determines the well-formed steep conical shape of mud volcanoes of this type. Blockages of the feeder channel by mud 'corks' and the explosive breaking of these corks when the pore-fluid pressure exceeds the retention force, explain the activity regime of this mud volcano type.
II class—Chikishlyar type	Characterised by calm, relatively weak and continuous activity. Gas is vented continuously in approximately uniform quantities. Numerous vents spit out small amounts of gassy mud and water, a very common feature of this class. This type of mud volcano is strongly affected by the presence of water saturated layers in the upper part of the sedimentary sequence. They form very low, bulged or flat domes, which merge with the surrounding plane, or plate-shaped depressions that are often filled up with water. This type of mud volcano is very common on the Kerch Peninsula, Ukraine.
III class—Schugin type	The eruptive periods are replaced by weak activity. This type of mud volcanoes may have the greatest distribution worldwide. It is characterised by a great variety of forms, but most commonly they build composite craters.

Table 2.2: Classification system based on the character of mud volcano activity with respect to morphological expression, distinguishing three types of mud volcanoes. After Dimitrov (2002).

2.4.3 Mud Volcano Activity

The majority of material forming the kilometre-scale mud volcano edifices is erupted during infrequent violent mud breccia eruptions however, for the majority of their life they are in their dormant state only erupting small amounts of fluid

from metre-scale vents. Mud volcanoes therefore have a relatively simple life cycle which includes (Fowler *et al.* 2000; Yusifov & Rabinowitz 2004);

Stage 1- Eruption: Hydraulic failure of the strata with the overpressured stratigraphic section.

Stage 2- Depletion: Migration of gas, oil and water to the surface from fractures, mud flows and adjacent porous strata.

Stage 3- Quiescence and build-up: Accumulation of primary and/or secondary overpressure.

This life cycle can occur over tens to thousands of years and will vary greatly at different edifices (Judd & Hovland 2007). This means that mud volcanoes can be classified according to the 'eruption type' or stage of life cycle that it is currently in. Mud volcanoes can evolve from one eruptive type to another over a certain period of time. Some violent eruptions have resulted in flames 500 m high erupting from edifices usually accompanied by extrusion of viscous mud breccia (Aliyev *et al.* 2002; see Appendix I). Such an eruption occurred at Lökbatan mud volcano in 2001 with the main eruption lasting 2-4 hours but a smaller flame continued to burn for months after the initial eruption (Aliyev *et al.* 2002). Only 25% of the mud volcanoes in Azerbaijan erupt and only a third of these have been known to ignite (Judd & Hovland 2007). Ignition of erupting gases is thought to occur because of the supersonic velocity at which the erupting gas jets escape, this has also been noted for submarine mud volcanoes (Judd & Hovland 2007). During a mud volcanoes 'dormant' stage of life varying vent types can form on their crests depending on the nature of fluids being erupted. These 'dormant' phases comprise approximately 95% of a mud volcanoes life cycle with the remaining 5% being violent eruptions (Judd & Hovland 2007). Vent types include; gryphons, salses, pools, breccia pipes, mud plugs and cinder mounds (Table 2.3; Hovland *et al.* 1997; Guliyev *et al.* 2000; Planke *et al.*2003*;* Mazzini *et al.* 2009). Many 'dormant' mud volcanoes show no sign of active fluid venting however, do have kilometre-scale

mud flows on their flanks which are testament to mass mud and fluid venting in the past.

Sub-areal mud edifices get heavily eroded by weathering processes, but submarine edifices build aggradational structures whose overall shape and lateral margins reflect relative rates of extrusion and background sedimentation (Evans 2008). In due course these extrusions get buried and can alias as intrusive chambers (Stewart & Davies 2006). Depending on the eruption rate, different extrusive events may become 'inter-fingered' with background sedimentation forming the typical 'Christmas tree' structures seen on seismic reflection data (Fig. 2.13; Stewart & Davies 2006). Unlike salt the mobility of mud decreases with time via fluid loss so extrusive edifices generally become integrated into basin tectono-stratigraphy as mechanically stable units (Stewart & Davies 2006).

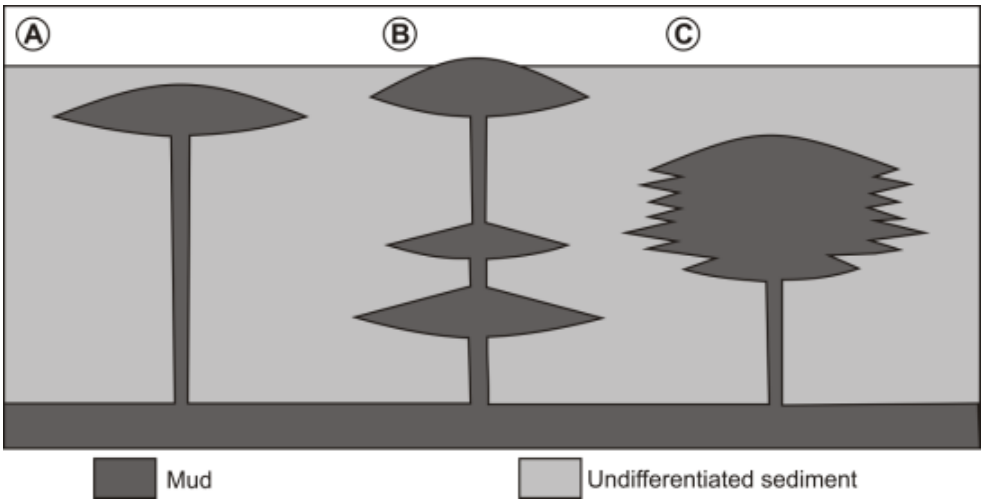

Fig. 2.13: Schematic showing end-member geometries of stacked mud volcanoes in a subsiding basin. Volcanoes are kilometre-scale. No sub-volcanic structure is implied. A) A single mud volcano bicone at a shallow structural level, connected by a long feeder to the mud source. B) Episodic reactivation, edifice building and burial create a stack of bicones of various sizes, the youngest shown here yet to be fully buried. C) A single episode of pulsed extrusion, punctuated by brief periods of relatively high rates of background sedimentation, creates an interdigitating margin and 'Christmas tree' appearance. Geometries A or C could be misinterpreted as plutonic intrusions. Modified from Stewart & Davies (2006).

Vent Type	Picture of Vent	Description	Composition	Height (m)	Width (m)	Erupts clasts? (Yes/No)	Fluid Type
Gryphons		'Cones' of mud breccias with bubbling pools of mud in their crater.	>30-90% Mud: <30% Fluids	0.02-10	0.05-360	Yes	Shear thinning or thixotropic
Salses		Shallow sided 'cones' of mud breccias with a large pool of watery mud at the summit and several bubbling centres.	<30% Mud: >70-100% Fluids	0.02-2	0.05-80	No	Mud suspensions
Pools	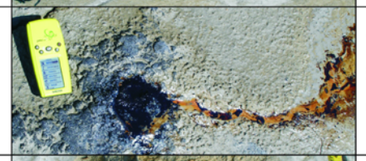	Small vents that cluster round gryphons and salses only erupting water and/or gas.	100% Fluids	0.01	<0.05	No	-
Dormant or Extinct		Vents that are no longer actively venting fluids.	-	0.02-10	0.05-360	-	-
Cinder Mounds		Mounds of red/ orange/ brown glassy mud breccia.	100% Gaseous	0-3	1-50	Yes	Gaseous
Mud Plugs	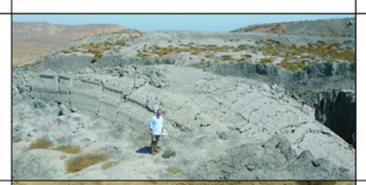	Large flows of mud breccia emanating from one vent.	90-100% Mud	4	30-100	Yes	Bingham
Breccia Pipes	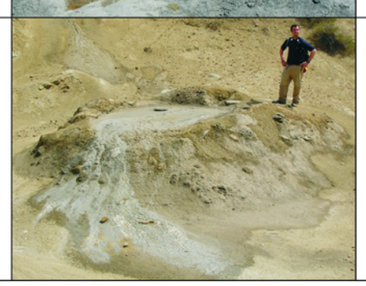	Clusters of salses surrounded by damp mud containing clasts of country rock.	>30-90% Mud: <30% Fluids	0.5-1.5	0.5-10	Yes	Mud suspensions

Table 2.3: Different vent types found on mud volcanoes.

2.4.4 Calderas

These structures have been the subject of an increasing number of recent publications especially in reference to their identification in seismic reflection data (Fowler *et al.* 2000; Graue 2000; Kopf 2002; Somoza *et al.* 2003; Davies & Stewart 2005; Stewart & Davies 2006; Evans *et al.* 2008). Calderas are a structural feature that can be found on both igneous and mud volcanoes globally. They form after fluids and sediment from depth has been erupted onto the surface allowing collapse into the conduit during evacuation. This void is later infilled by the collapse of the strata above resulting in a collapse structure at the surface i.e. a caldera. They take the form of circular or elliptical depressions on the summit of the edifices (Fig. 2.14). Some studies have utilised caldera elongation as regional stress indicators (Bonini 2008; Bonini & Mazzarini 2010). The depressions are often bounded by inward-facing faults at the terminations of kilometre-scale mud volcano systems (Evans *et al.* 2008). The largest mud volcano caldera collapse structure identified by Evans *et al.* (2008) is 2.5 km in diameter. Using data from both on- and offshore Evans *et al.* (2008) noted that the morphology of these structures briefly consists of a 'rim' that defines the topographic boundary of the caldera, a 'caldera fault system' usually consisting of concentric faults (see section 2.3.3), a 'moat' and a series of mud breccia deposits that built up to form a 'pedestal' (Fig. 2.14). These features can occur at a range of scales with both on- and offshore examples sharing a common form globally.

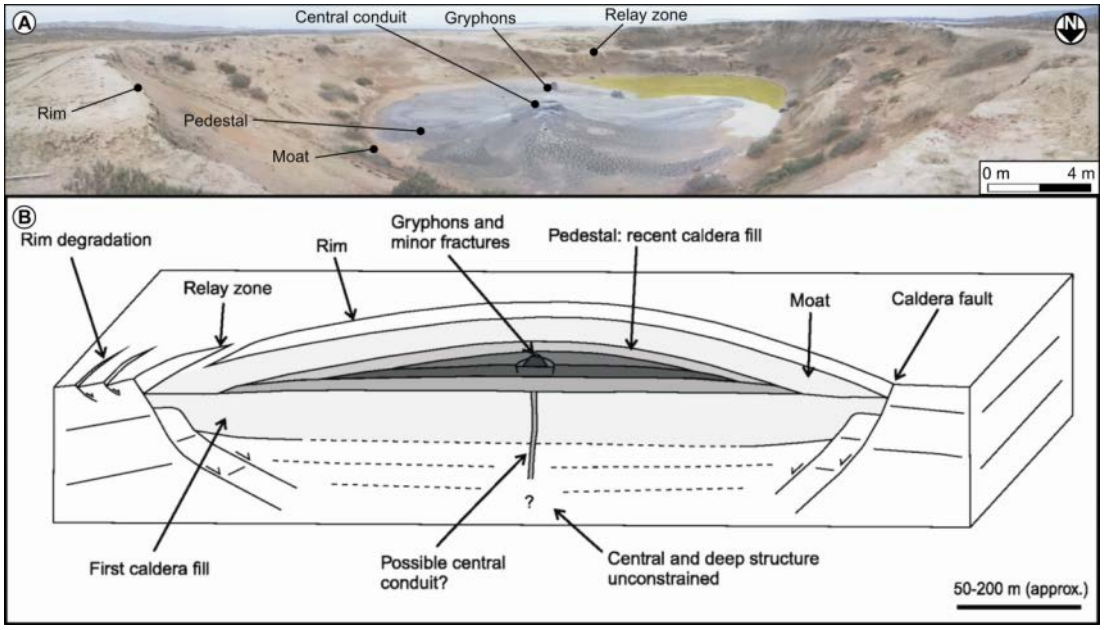

Fig. 2.14: Mud volcano calderas. A) Photograph of a small caldera to the west of Bahar mud volcano, Azerbaijan. B) Schematic block diagram illustrating the principal structural and morphological elements of a typical circular mud volcano summit caldera identified. Dashed lines indicate areas of tentative interpretation. From Evans *et al.* (2008).

2.4.5 Flows

Mud flows are an extremely common structure found on the edifice flanks of mud volcano systems. Their morphology is heavily influenced by rheology, slope angle, grain size and fluid content. Flows can often resemble those from igneous volcanoes or even glaciers (Planke *et al.* 2003; Judd & Hovland 2007). These flows will always flow down the steepest flank of the edifice unless confined by some other topographic features i.e. a caldera or a gulley. If the flow is composed of viscous mud if may erode into the flanks of the volcano becoming highly channelised (Planke *et al.* 2003). Less viscous mud forms levees at the periphery of the flows with a faster moving region at the centre of the flow. On high slope angles (>10°) flows are relatively thin i.e. <100 m wide, however, once slope angle decreases or the flow reaches a plain it will become more lobate and spread out. If slope angle decreases, the flow encounters an obstacle or reaching the termination of a flow compressional ridges will form similar to those in 'ropey' lava flows. Mud flows can look similar on several scales indicating that they may be self similar in nature (Fig. 2.15). Kilometre-scale mud flows are able to carry clasts up to 1.5 m in

length but this may largely be dependent on the rheology of the mud and energy of the eruption.

These individual mud flows eventually aggrade to form one edifice, which is actually composed of a series of pulsed eruptive events which control the morphology of the edifice over time. The duration and frequency of each 'pulse' is key to controlling the internal architecture of the edifices (Evans *et al.* 2006). Evans *et al.* (2007) used seabed phase reversals on seismic reflection data to identify fluid rich, mud flows in the South Caspian Basin. Chow *et al.* (2006) used ground penetrating radar (GPR) in south-western Taiwan in order to construct high-resolution imaging of subsurface structures in mud volcano sediments and flows. They found that the key controls on flow morphology are rainfall, viscosity of mud and the gradient.

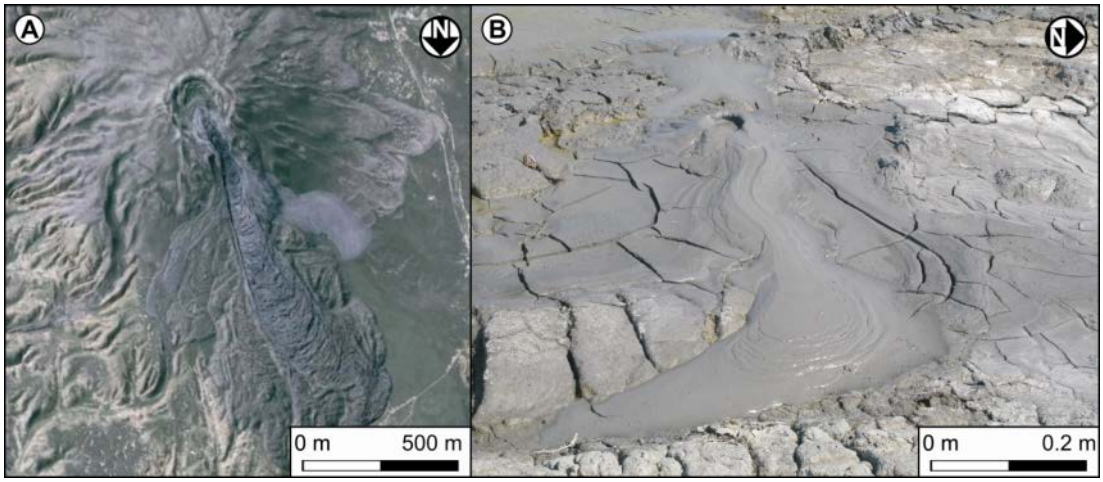

Fig. 2.15: Different scales of mud flow from mud volcanoes. A) Koturdag mud volcano with a 1.3 km long mud flow emanating from its caldera. Image © 2010 GeoEye, © 2010 Google. B) Photograph of a gryphon with a centimetre-scale mud flow flowing from a small depression at its crest. Note in both pictures the compressional ridges at the base of each flow and the levees building up on either side of the flows in their lower reaches.

2.4.6 Deposits

Mud volcano systems generally emit mixes of gas, water, oil and solid sediment a feature that is common to all globally. It is these deposits which govern how the edifice itself accretes as discussed earlier in this section. There is no accepted

terminology for the sediments deposits or erupted by mud volcano systems (Kopf 2002). The 'liquid mud' that is erupted often contains clasts ranging from <1 cm to ~1.5 m (Fig. 2.16B; Judd & Hovland 2007) and these can vary from rounded to angular. These clasts may have been part of the original source domain or they may have been plucked from the strata that compose the sides of the intrusive conduit.

Fluids that erupt from mud volcano edifices may have a number of sources as discussed earlier in section 2.1. Chemical analysis of fluids in Azerbaijan show that mud volcanoes can erupt four different mixes of dissolved components including; a) hydrocarbons and sodium, b) chlorine and magnesium, c) chlorine and calcium and d) sulphur and sodium (Aliyev *et al.* 2002). These different components result in a range of crystalline deposits forming at the surface around vents (Fig. 2.16A, D and E). Gases emitted by mud volcanoes are predominantly hydrocarbon based i.e. methane however, some mud volcanoes have been known to emit carbon dioxide or nitrogen (Judd & Hovland 2007). These gases can ignite leaving the mud surrounding the seep vitrified and burned producing cinder mounds (Fig. 2.16C). The study of methane flux to the atmosphere from mud volcanoes has been of significant interest in the recent literature (Hedberg 1974; Milkov 2000; Kopf 2002; Dimitrov 2002; Etiope *et al.* 2002; Milkov *et al.* 2003; Etiope & Milkov 2004).

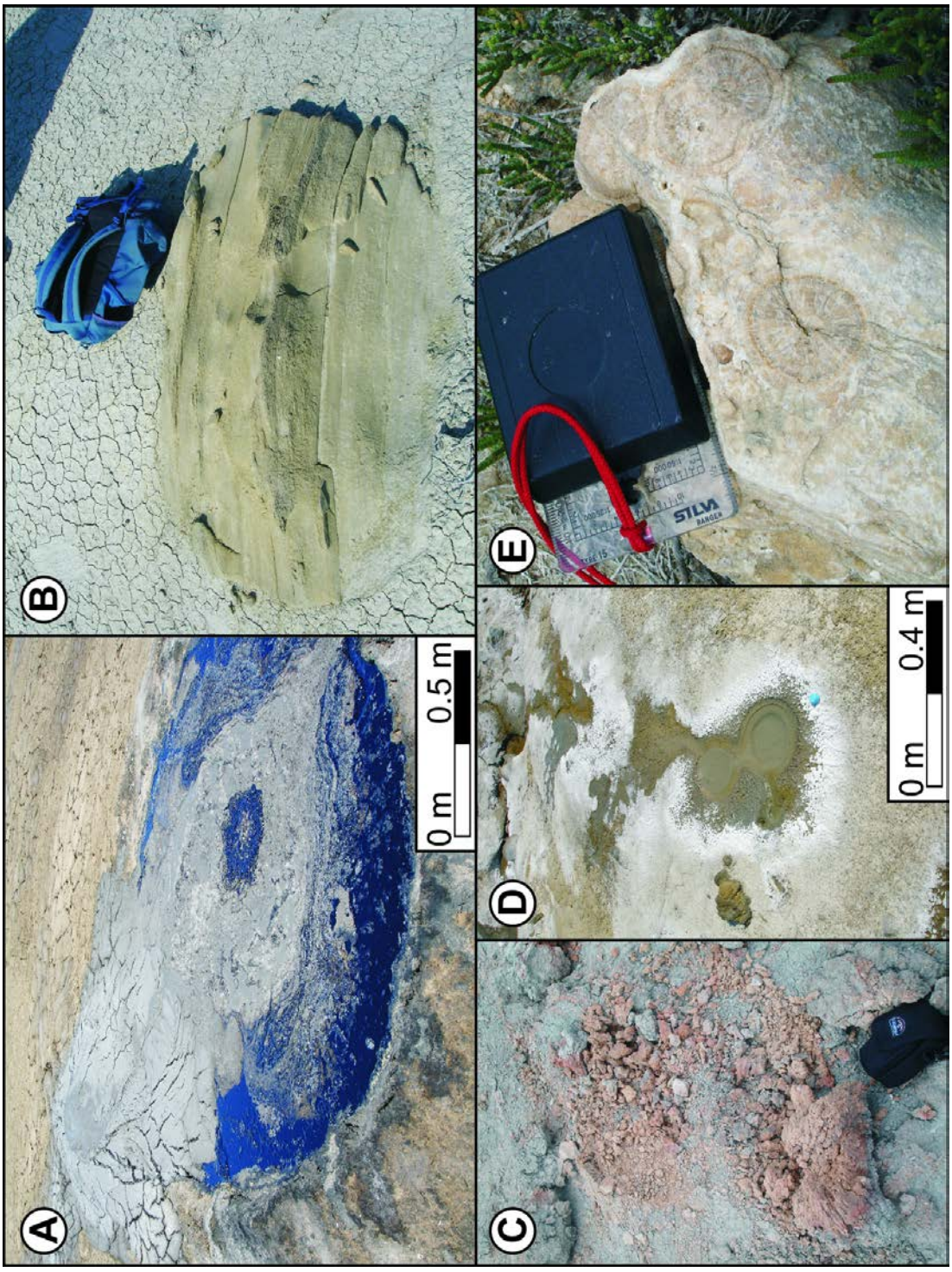
A
B
C
D
E
0 m
0.5 m
0 m
0.4 m
STILVA
RANGER

Fig. 2.16: Photographs of eruptive deposits on mud volcanoes in Azerbaijan. A) A salse erupting oil with a gryphon erupting mud into it at Pirsaatadag mud volcano. B) A sandstone clast within the kilometre-scale mud flow on Kichik Kharami mud volcano. Note the rucksack for scale. C) Cinder mound marking the location of the gaseous eruption of Lökbatan mud volcano in 2001. Note the camera case for scale. D) Salt deposits around a salse on Kichik Kharami mud volcano. E) Nodular concretions found on top of Kichik Kharami, Koturdag C and Pirsaatadag mud volcanoes.

2.5 The Roof Domain

The roof domain is the shallowest structural domain of the mud volcano system. Its base is defined by the top of the extrusive domain and any extrusive edifice that has formed (Fig. 2.1). Its top is defined by the surface of sediment that has buried the system and covered the extrusive domain. The roof domain therefore is only present in systems that have undergone burial and it can only be identified if a cross-section through the system is available (i.e. a seismic profile). It is not possible to determine whether a system has a roof domain through surface analysis alone therefore for the purpose of this study it is not important. Principally the roof domain consists of sediments that bury the system, any through-going minor intrusive systems that connect the buried portion of the system to the surface and any surface expression that results i.e. seeps. The roof domain includes a variety of differential compaction structures including a zone of fluid escape structures above the apex of the buried, compacting mud volcano. On shore these occur as swarms of metre-scale gryphons, offshore large mud pools occur on the sea bed (Evans 2008).

3 Structure of Exhumed Mud Volcano Feeder Complexes, Azerbaijan[1]

Abstract

This study documents the first structural field mapping of exhumed mud volcano feeder complexes. Three mud volcanoes outcropping onshore in Azerbaijan were selected on the basis of outcrop quality and scale. These examples are all located within 1 km of the axes of NW-SE trending folds associated with the southern margin of the Greater Caucasus mountain belt. The mapping shows that the intrusive complexes are 200 m to 800 m wide and roughly circular. These feeder complexes consist of a mega-breccia of country rock blocks at a scale of tens of metres, enclosed in a matrix of intrusive mud. Minor structures include grid like or conjugate fractures sets, sinuous fractures, mud plugs and breccia pipes. The country rock blocks are deformed and rotated relative to surrounding sedimentary strata. Alternative mechanisms to explain the strain history of these large blocks in the feeder complexes are: a) stoping, b) flow rotation and c) caldera collapse. The mapping indicates that the most likely mechanism involves stoping processes, similar to those identified in igneous systems. This chapter provides a basis for reservoir distribution in commercial geological models that contain the feeder complexes of mud volcano systems, and also constrains conduit geometry for modelling studies of evolution and flow dynamics.

[1] This chapter is based on a paper that has been published in the journal 'Basin Research' as part of a thematic set. Referenced as 'Roberts, K.S., Davies, R.J. & Stewart, S.A. (2010). Structure of exhumed mud volcano feeder complexes, Azerbaijan. *Basin Research*, **22**, 439-451, DOI: 10.1111/j.1365-2117.2009.00441.x', see Appendix V.

3.1 Introduction

Mud volcanoes are a widespread type of piercement structure that allow for focussed fluid escape from sedimentary basins. Little is known, however, about the geometry of the sub-volcanic feeder complexes that constitute the intrusive domains (Davies & Stewart 2005). Even less is known about the small scale structure of these feeder systems and their effect on the country rock that they intrude (Davies & Stewart 2005). The term 'mud volcano system' was coined by Stewart & Davies (2006) to describe the set of structures associated with a constructional, extrusive edifice (mud volcano) and underlying plumbing of the volcano, which connects it to its stratigraphic source unit (Stewart & Davies 2006). Previous studies have described various architectures connecting extrusive mud cones to their underlying source layer, ranging from bulbous diapirs (Brown 1990) to steep diatremes (Robertson & Kopf 1998) and narrow vertical pipes (Graue 2000). Currently, the two most widely-publicised alternative models for the sub-volcanic plumbing system are kilometre-scale mud diapirs (Morley & Guerin 1996) or intricate mud pipe, dyke and sill complexes (Morley 2002; Stewart & Davies 2006).

Detailed mapping of the intrusive domains of mud volcanoes will enable better understanding of the processes governing the fluid transport through the shallow crust and how the surrounding country rock is influenced. Comparisons can be made with igneous systems that appear to share many common features with mud volcanoes (Stewart & Davies 2006). Guliyev *et al.* (2000) commented on the spatial and genetic relationship of mud volcanoes with oil and gas fields, an affiliation that impacts drilling operations, rig installations and pipeline routings. Problems occur as a result of mud eruptions and instability of the surrounding sediments (Yusifov & Rabinowitz 2004). There are further instances of commercial significance where reservoirs are intersected by the intrusive domain of mud volcano systems. In these cases the size, shape and internal structure of feeder systems is a local control on both hydrocarbons in place and reserves (Stewart & Davies 2006).

This study investigates outcrop-scale features seen within intrusive systems of kilometre-scale mud volcano systems exposed onshore in Azerbaijan (Fig. 3.1). Field mapping focussed on the size, shape and internal structure of country rock outcrops within the feeder complexes, an aspect poorly described in previous studies. These conduits are interpreted as mature, long-lived systems where episodic activity has continued throughout recent exhumation of the onshore area (Fig. 3.2). Although the majority of onshore mud volcano outcrops are recent extrusive edifices, there are occasional examples where lack of recent voluminous eruptions means that exhumed intrusive domains are as yet-unburied (Fig. 3.2). Three of these exposed intrusive domains were identified for mapping in this study.

3.2 Geological Setting

The South Caspian Basin is known for its abundant large mud volcano systems (Guliyev *et al.* 2000; Milkov 2000; Aliyev *et al.* 2002). This concentration of mud volcano systems occurs due to the presence of a thick deposit of the argillaceous Maykop Formation of Oligocene to Miocene age (Hudson *et al.* 2008). The formation is approximately 1 km thick and is buried to a depth 3.5-5 km in the area of this study (Allen *et al.* 2002). The Maykop Formation is thought to be overpressured and therefore under-compacted, fluids from deeper sources (Kopf 2002) probably entrain the mud during their ascent and erupt at the surface. A compressional tectonic regime has been maintained since the Late Pliocene (Allen *et al.* 2002, 2003; Jackson *et al.* 2002) resulting in the formation of a large number of fold structures within the basin. The anticlinal crests contain some of the largest hydrocarbon accumulations in the world and many large mud volcanoes (Devlin *et al.* 1999).

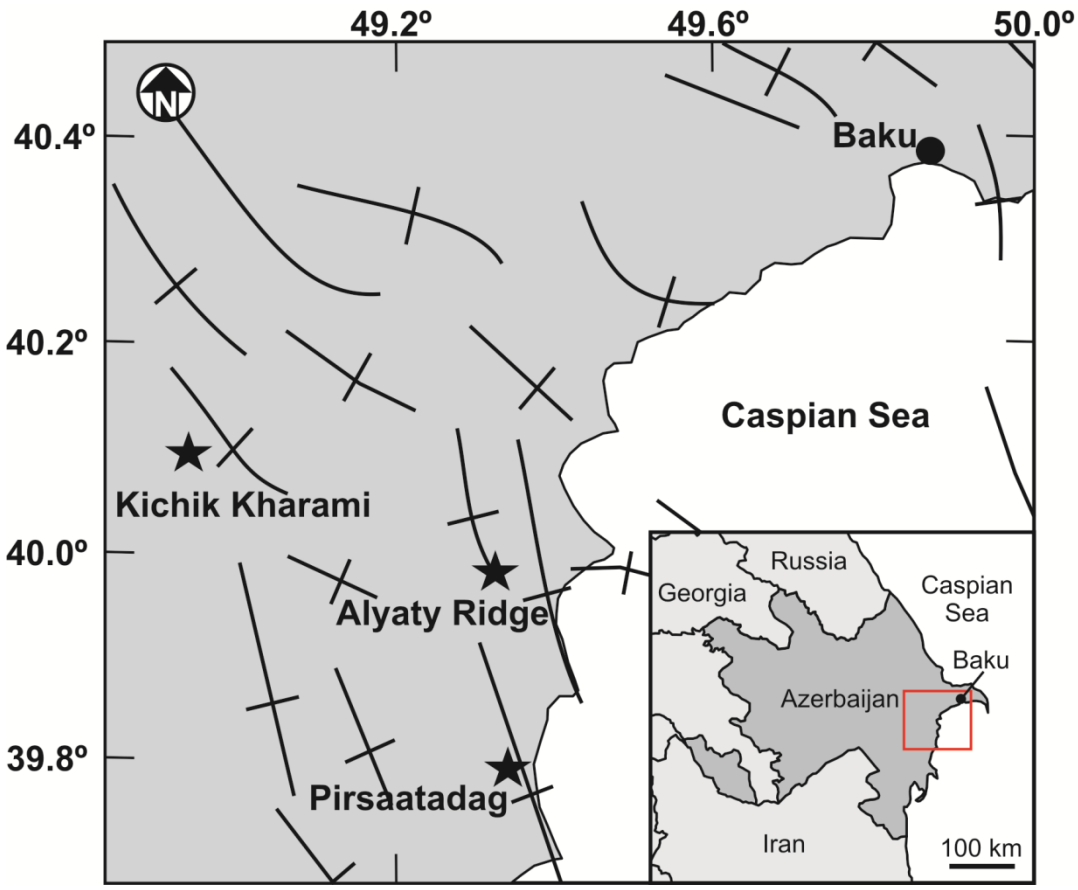

Fig. 3.1: Map of the Caspian coastline in Azerbaijan showing the location of the study areas (localities marked with stars) and the trends of anticlines axes (indicated by black line with dash across). Inset map of Azerbaijan shows map location as red box.

Allen *et al.* (2002) backstripped a stratigraphic column from the northwest of the South Caspian Basin and found that 2.4 km of tectonic subsidence had occurred since *c*. 5.5 Ma which they attributed to basement subduction. Several kilometres of sediment has accumulated in this time, while the upper part of the succession has begun to deform by buckle folding (Allen *et al.* 2002). Allen *et al.* (2002) proposed that basement subduction began *c.* 5.5 Ma to create the major Pliocene-Quaternary subsidence. Buckle folds have now been exhumed onshore and the crests of the anticlines have been eroded. The present day mud volcanoes seen onshore therefore extrude through partially eroded anticlinal crests. The mud volcano systems, studied here, pierce through strata up to and including the Absheronian (Early Pleistocene; Fig. 3.2; Reynolds *et al.* 1998; Abdullayev 2000). Since the uppermost parts of the feeder systems have been eroded, the onshore exposures do not provide a complete replica of subsurface structures imaged on

seismic reflection data (Fig. 3.2). On the other hand this does provide the opportunity, in those cases where the feeder complex is exposed, to directly map the intrusive domains that are imaged as part of mud volcano systems offshore. This exhumation has not occurred to the offshore structures of the Caspian Sea where complete mud volcano systems are imaged on seismic reflection data (Fig. 3.2; Stewart & Davies 2006).

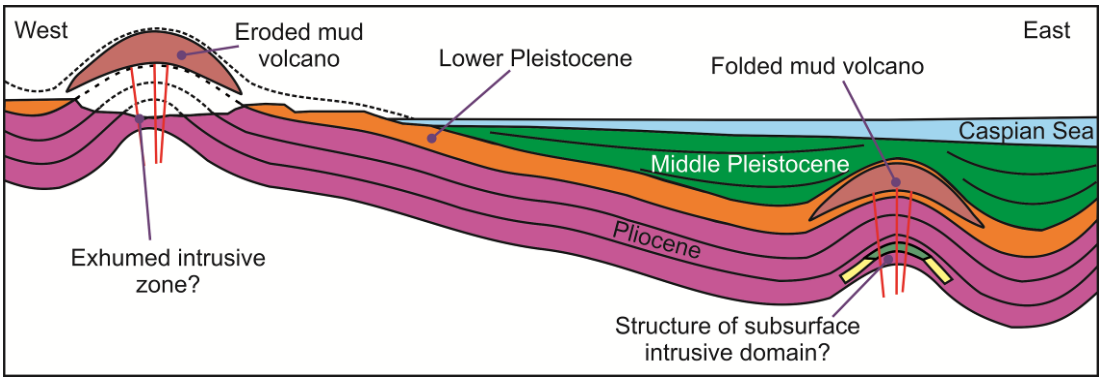

Fig. 3.2: Schematic regional seismic section depicting the relationship between exhumed intrusive domains onshore to the deeply buried, folded mud volcanoes offshore. Yellow and green marker in the Pliocene offshore strata represent hydrocarbon reserves.

3.3 Methods and Datasets

Three separate mud volcano systems were chosen on the basis of the extrusive domain being partially or completely eroded, exposing the underlying feeder complex. Kichik Kharami, Alyaty Ridge and Pirsaatadag mud volcanoes along the west coast of the Caspian Sea were selected on this basis (Fig. 3.1). Mapping of these onshore mud volcano systems was carried out using a handheld global positioning system (GPS) receiver, with a positional accuracy of 5 m. Structural readings such as bedding, fracture and fold orientations were measured using a compass clinometer (see electronic Appendix II for raw data) then loaded into GEOrient software to plot stereographic projections. Fracture density was measured by placing a metre rule parallel to bedding and counting the number of fractures that crossed the rule over one metre length. The GPS co-ordinates with their corresponding structural datasets were integrated as layers in ArcMap

software. The coordinate system for the data was input using spheroid WGS 1984. This automated transcription produced the basic structural maps reproduced in this chapter.

3.4 Observations

3.4.1 Kichik Kharami Mud Volcano

This is located 87 km southwest of Baku (Fig. 3.1) and outcrops 0.6 km to the south of an anticline axis (Fig. 3.3A). The plan-view shape of the volcano system is broadly circular and measures *c.* 0.9 km by 0.6 km in aerial extent. The boundary of this area is defined by the edge of the peripheral faulted/fractured zone within the feeder complex where both sinuous and conjugate fracture types are found. Of the total feeder complex area, some 20% is exposed while the remaining 80% is covered by very recently erupted mud, indeed mud is still extruding in small quantities at present. The volcano is surrounded by well-exposed country rock forming the anticline through which the feeder complex intrudes (Fig. 3.3C).

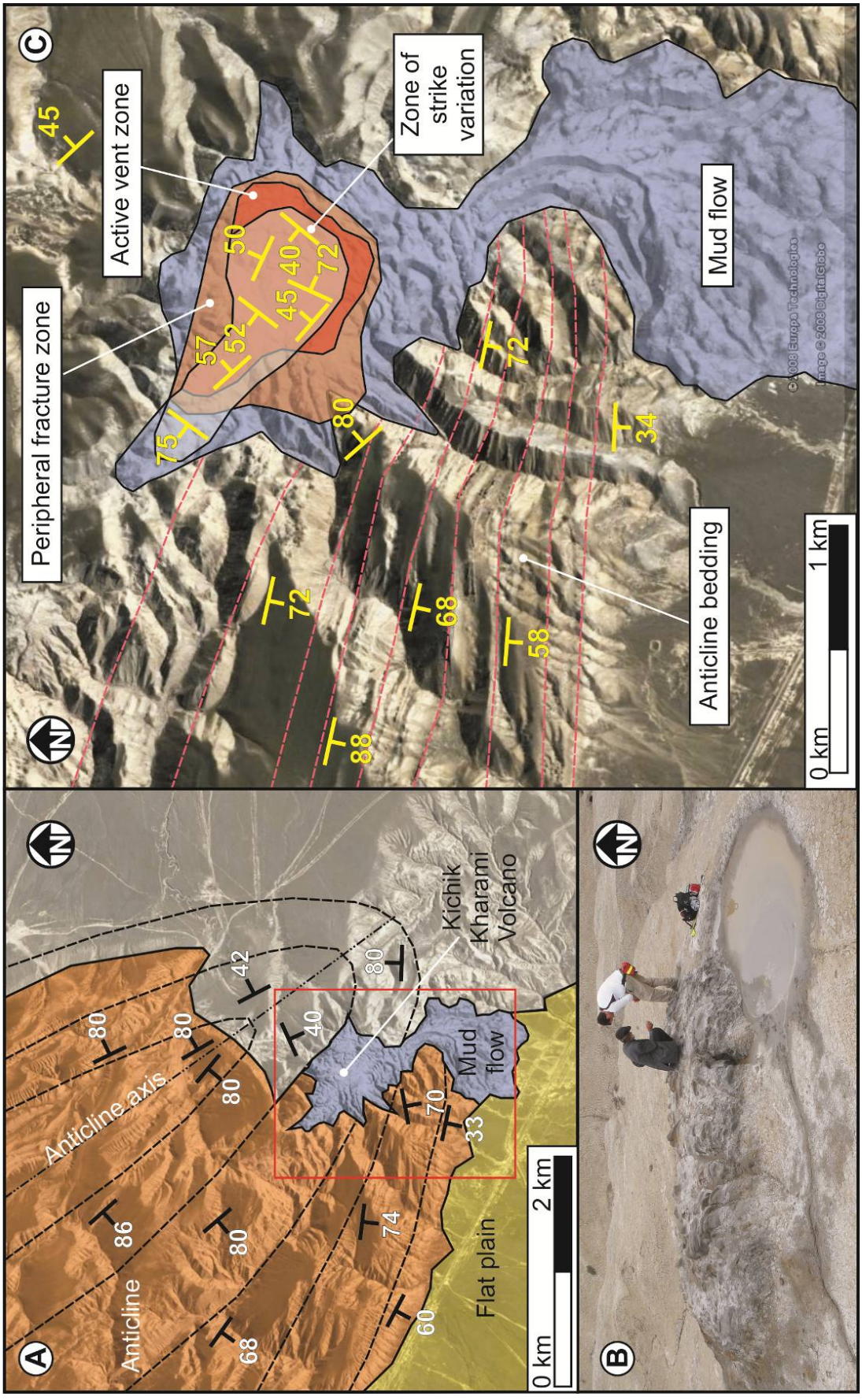
A
Anticline
Anticline axis
Flat plain
Mud flow
Kichik Kharami Volcano
0 km 2 km
B
C
Peripheral fracture zone
Active vent zone
Zone of strike variation
Mud flow
Anticline bedding
0 km 1 km

Fig. 3.3: Case Study 1- Kichik Kharami Mud Volcano. A) Location of Kichik Kharami to the south of an anticline axis. Red rectangle marks the area seen in Fig. 3.3C. Image © 2010 DigitalGlobe, © 2010 Google. B) Outcrop at centre of Kichik Kharami volcano showing a large 'block' of highly fractured sandstone surrounded by a mud matrix. C) Structural map of Kichik Kharami. The central red area marks the zone where fluid is currently being extruded (i.e. the 'active vent zone'). The orange area outlines the zone where both sinuous and conjugate fracture systems are found (i.e. the 'peripheral fracture zone'). The grey transparent zone represents the area where bedding strike measurements vary greatly from the surrounding anticlinal bedding (i.e. the 'central zone of block rotation'). Any other areas that do not fall into these coloured zones are part of the 'un-intruded zone' which contains only conjugate faulting/fracturing. Purple areas mark areas where old mud flows cover outcrop. Image © 2010 DigitalGlobe, © 2010 Google.

The 'feeder complex' of all three case studies is defined as the area delimited by the peripheral fracture zone (highlighted in orange in Fig. 3.3C, Fig. 3.7B and D). Fracturing of the country rock increases in intensity towards the centre of the feeder complex, with the most common fractures being regular, grid-like fractures 2-3 m in length (Fig. 3.4A; see Appendix II for more pictures of fractures). These are present in both the surrounding country rock and the intrusive domain. Conjugate fractures (0.5-1 m in length) become increasingly infilled closer to centre of the complex. Finally, sinuous fractures (0.5-1 m in length) appear to be restricted to a 200 m radius from the centre of the feeder complex (Fig. 3.3C). Fracture density ranges from twenty-eight per metre at the centre of the feeder complex to two per metre within the anticline bedding at the edge of the peripheral faulted/fractured zone (Fig. 3.5A).

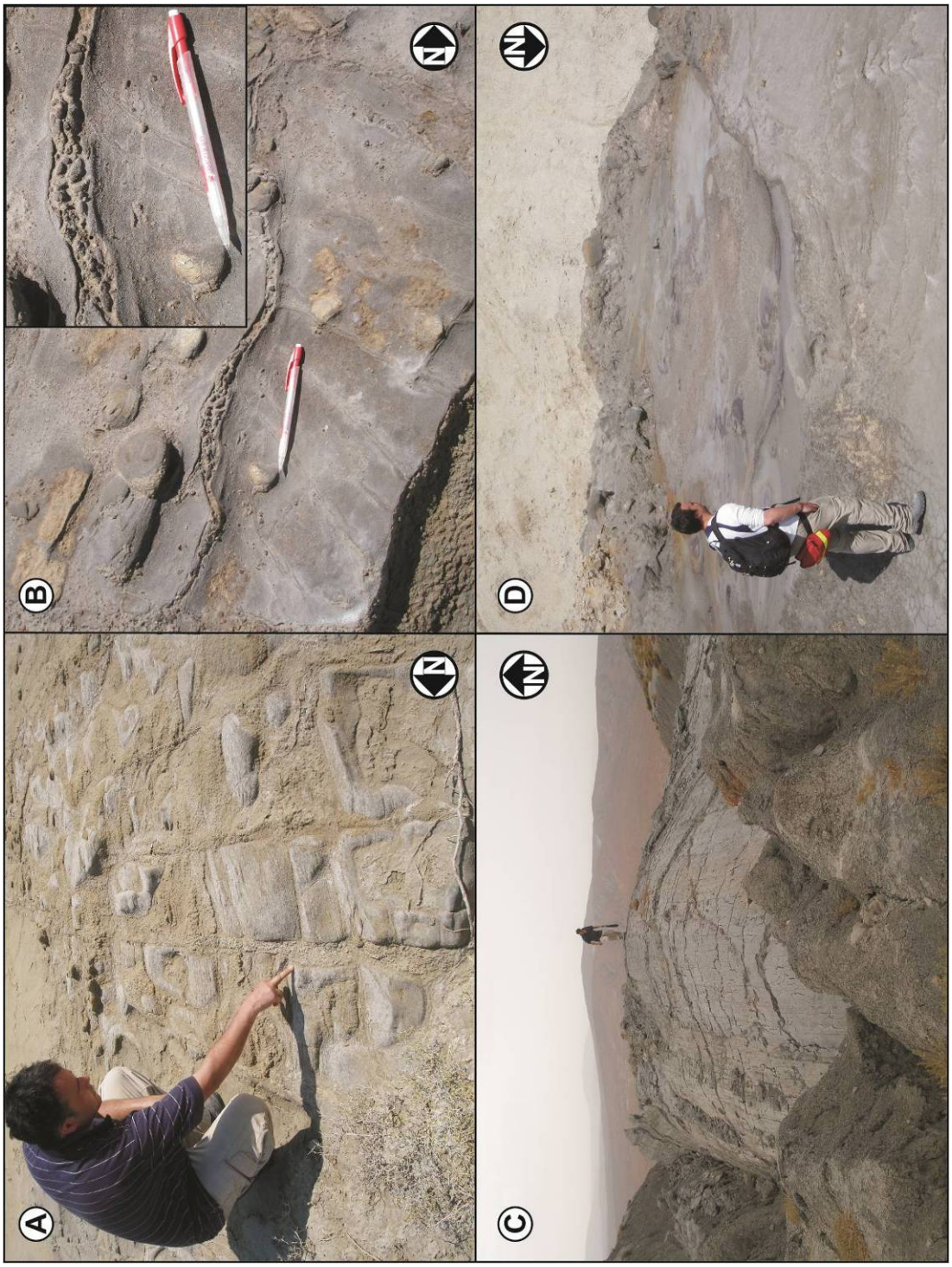
A
B
C
D
N
N
N
N

Fig. 3.4: A) Mud infilling pre-existing joints and fractures within the country rock, found in both the peripheral fracture zone and the un-intruded zone. B) Sinuous fractures only found in the peripheral fractured zone, often contain small clasts of country rock as seen in the inset picture. Pen for scale. C) Mud plugs consisting of dense mud breccia flows and D) Breccia pipes where country rock clasts have been incorporated into the vent walls to form a breccia.

Minor amounts of mud are currently being expelled from this feeder system in the form of watery-mud salses (Hovland *et al.* 1997), although a large, relatively fresh mud flow to the south of the mapped area is testament to significant reactivation within the past few hundred years or so. The structural map (Fig. 3.3C) shows that the country rock comprising the southern limb of the anticline dip uniformly to the south, while blocks within the feeder complex have dip and strike directions that vary un-systematically. The strike directions of the blocks vary up to 90° away from the regional anticline bedding strike orientations (Fig. 3.3C). A slight concentric alignment can be discerned from the dip data of beds which dip in towards the centre of the feeder complex. Moving outwards, the beds dip away from the centre of the feeder complex and return back to the regional trend of the host anticline by a radial distance of 180 m from the centre of the feeder complex. Stereonets reveal that the anticline intruded by Kichik Kharami has a moderate curvature and interlimb angle (Fig. 3.6A). All the bedding measurements lie roughly along the same plane, apart from bedding readings taken at the centre of the volcano which have a large spread with no clear alignment (Fig. 3.6B).

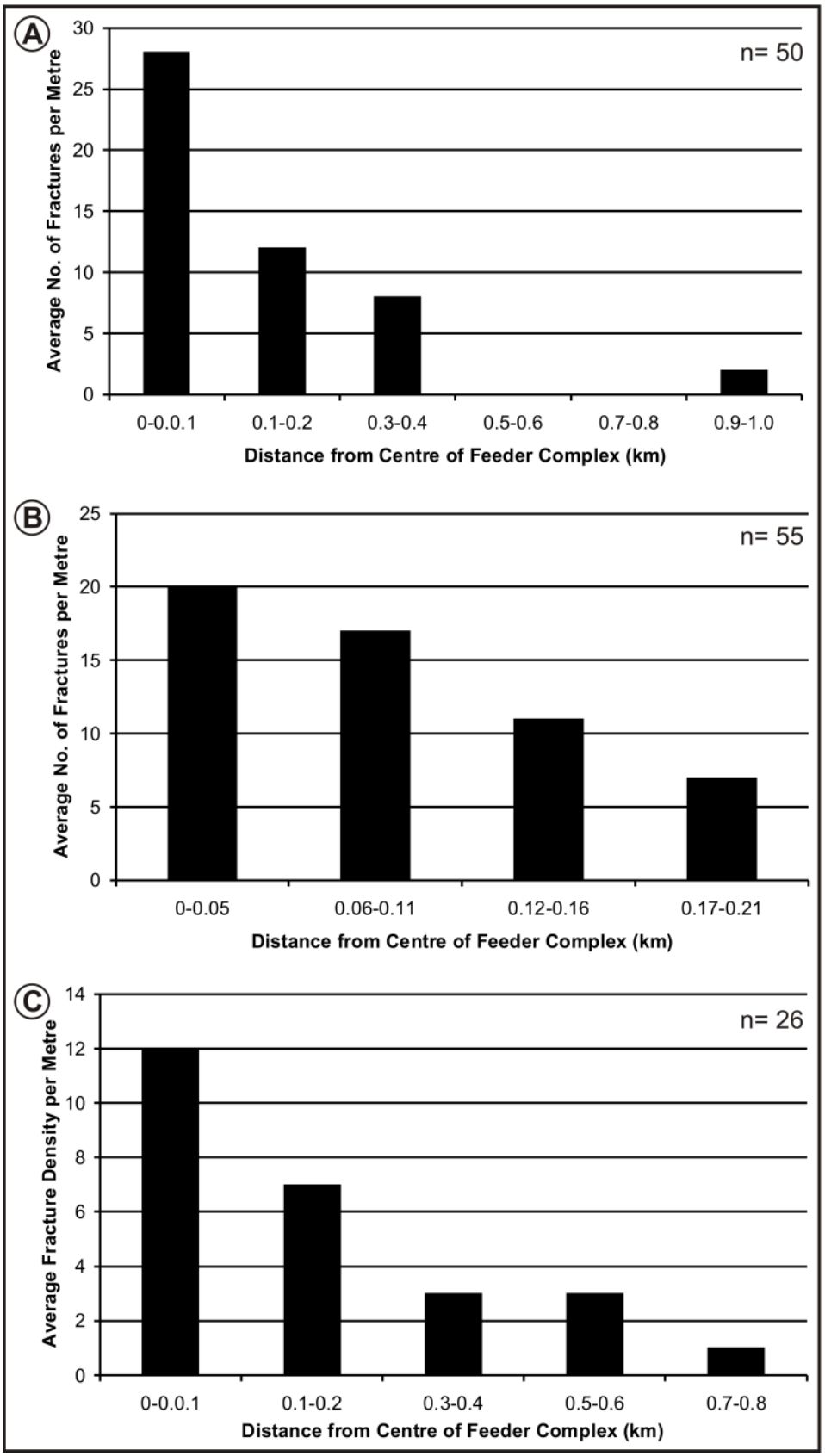

Fig. 3.5: Histograms showing the change in fracture densities per metre with distance from the centre of the mud volcano feeder complexes. A) Kichik Kharami mud volcano, B) Pirsaatadag Mud Volcano and C) Alyaty Ridge.

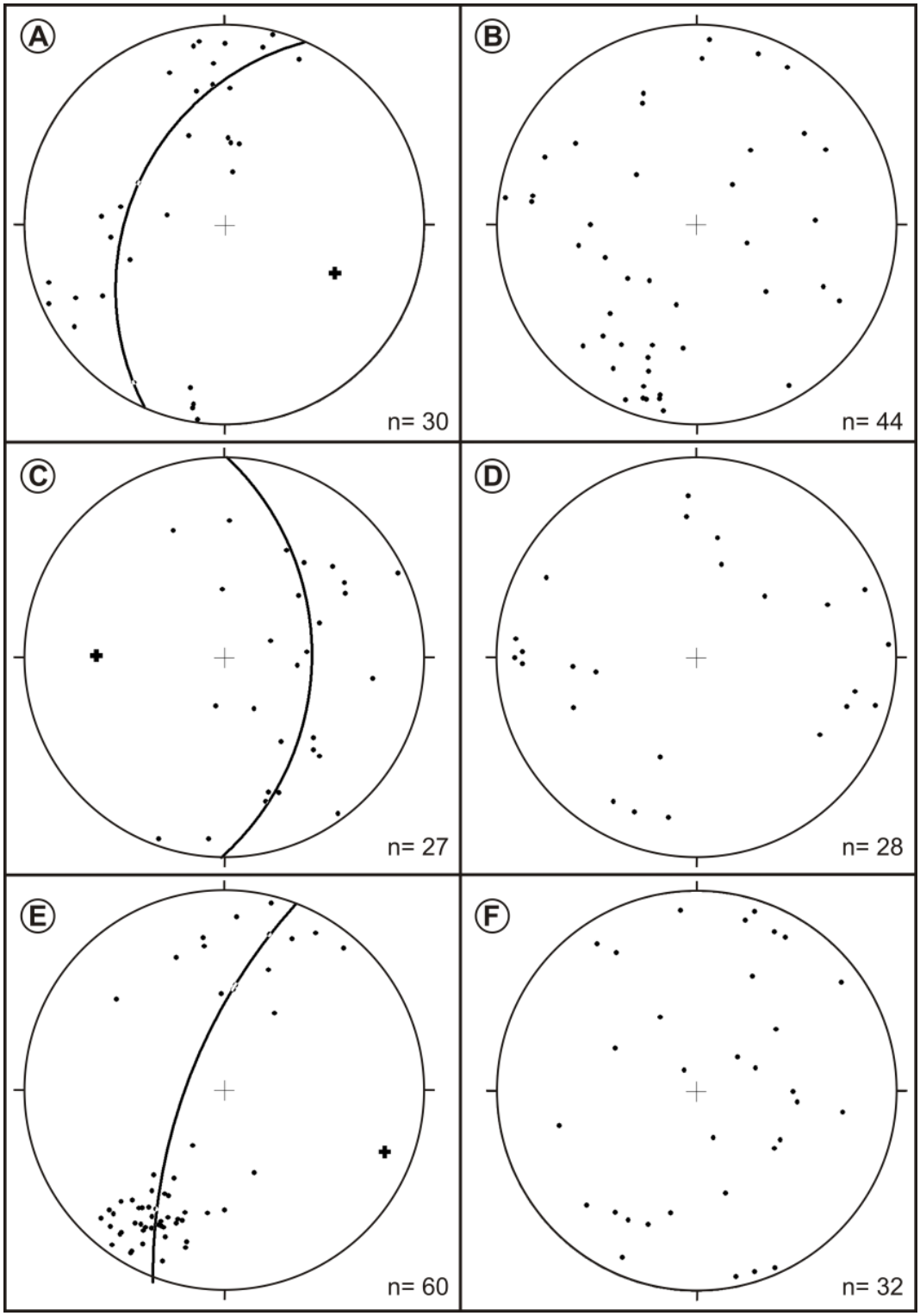

Fig. 3.6: A) Stereonet showing anticline bedding around Kichik Kharami mud volcano. B) Stereonet showing the varying bedding measurements found at the centre of Kichik Kharami mud volcano. C) Stereonet showing anticline bedding around Pirsaatadag mud volcano. D) Stereonet showing the varying bedding measurements found at the centre of Pirsaatadag mud volcano. E) Stereonet showing anticline bedding around Alyaty Ridge. F) Stereonet showing the varying bedding measurements found at the centre of Alyaty Ridge.

3.4.2 Pirsaatadag Mud Volcano

This is located on the southern coast of the Caspian, 81 km south of Baku (Fig. 3.1) and is positioned on the hinge of an anticline (Fig. 3.7B). The exposure of the volcano system is in low-lying topography adjacent to the present Caspian shoreline and measures *c.* 0.37 km by 0.4 km in aerial extent. The location has excellent exposures of the mud volcano feeder complex, however, little of the surrounding strata is exposed making it difficult to map the margin of the intrusion. The proximity to the present shoreline suggests that this mud volcano system is particularly prone to erosion due to its exposure to the Caspian Sea.

Again, three fracture types (sinuous, conjugate and grid-like) are present in this mapping area. The sinuous fractures are wider (1-4 cm wide) than those seen in the other case studies and sometimes contain small sandstone clasts within a mud matrix (Fig. 3.4B; see Appendix II for more pictures of fractures). Fracture density ranges from twenty fractures per metre at the centre of the feeder complex to seven per metre 0.17-0.21 km from the centre (Fig. 3.5B). The structural map (Fig. 3.7B) shows a similar layout to that seen at Kichik Kharami mud volcano system, except that the zone of rotated blocks is offset to the southeast of the active vent zone. The extrusive features are dominantly active salses inferring that at present more fluid is flowing up the Pirsaatadag feeder complex compared with Kichik Kharami. Many structural elements within this feeder complex are exposed as positive topographic features consisting of brecciated country rock, mainly sandstone (Fig. 3.7A).

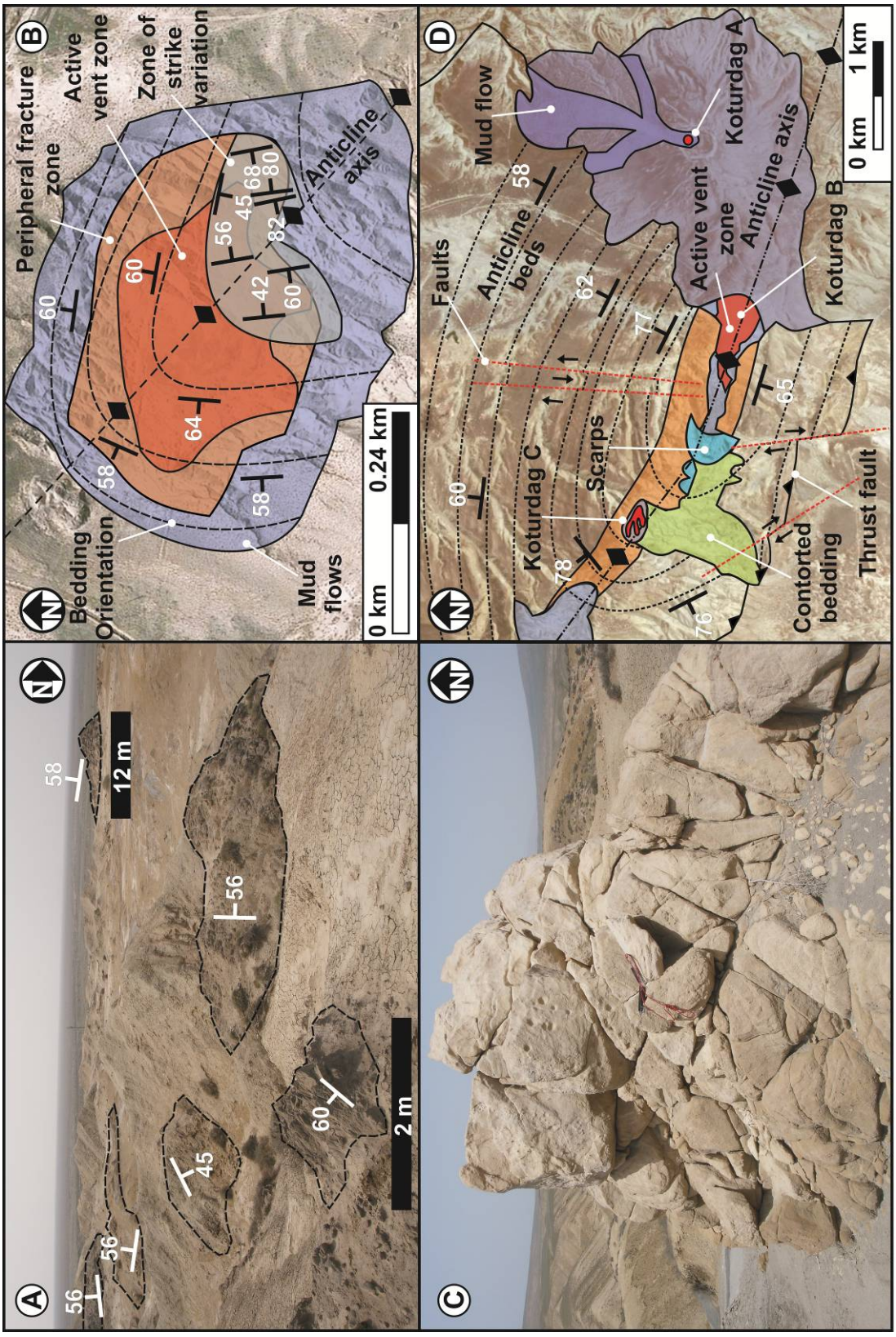
A
N
56
56
58
12 m
56
45
60
2 m
B
N
Peripheral fracture zone
Active vent zone
Zone of strike variation
Anticline axis
Bedding Orientation
Mud flows
60
58
64
58
60
56
45
68
80
82
42
60
0 km
0.24 km
C
N
D
N
Faults
Anticline beds
Mud flow
Koturdag A
Anticline axis
Active vent zone
Koturdag B
Koturdag C
Scarps
Contorted bedding
Thrust fault
60
58
62
77
65
78
76
0 km
1 km

Fig. 3.7: A) Case Study 2: Outcrop at centre of Pirsaatadag volcano with rotated bedding strike orientation. B) Structural map of Pirsaatadag Mud Volcano. The central red area marks the zone where fluid is currently being extruded (i.e. the 'active vent zone'). The orange area outlines the zone where both sinuous and conjugate fracture systems are found (i.e. the 'peripheral fracture zone'). The grey transparent zone represents the area where bedding strike measurements vary greatly from the surrounding anticlinal bedding (i.e. the 'central zone of block rotation). Any other areas that do not fall into these coloured zones are part of the 'un-intruded zone' which contains only conjugate faulting/fracturing. Image ©2010 GeoEye, ©2010 Google. C) Case Study 3: Outcrop at the centre of Alyaty Ridge (compass clinometer at centre of picture for scale). D) Structural map of Alyaty Ridge. The central red areas at the centre of Koturdag A, B and C volcanoes mark the zones where fluid is currently being extruded (i.e. the 'active vent zone'). The orange area outlines the zone where both sinuous and conjugate fracture systems are found (i.e. the 'peripheral fracture zone'). Any other areas that do not fall into these coloured zones are part of the 'un-intruded zone' which contains only conjugate faulting/fracturing. The green area represents an area of contorted bedding and the blue areas indicate areas where scarps have formed due to slope failures down the flank of the anticline. Purple areas mark areas where old mud flows cover outcrop. Image ©2010 GeoEye, ©2010 Google.

3.4.3 Alyaty Ridge

Within this area there are three mud volcanoes termed here Koturdag A, Koturdag B and Koturdag C (Fig. 3.7D and Table 3.1). This area was chosen as it has a structurally complex, exposed anticlinal core with several mud volcanoes extruding along its axis (Table 3.1 and Fig. 3.7D). This provides a comparison to the two less structurally complex case studies.

Mud Volcano	Long Axis (km)	Short Axis (km)
Koturdag A	1.4	1.35
Koturdag B	1.0	0.45
Koturdag C	0.35	0.2

Table 3.1: Dimensions of mud volcanoes (A, B and C), that extrude along Alyaty Ridge.

Once more the sinuous, grid-like and conjugate fractures can be seen with the sinuous fracturing becoming more intense towards the central axes of the mud volcanoes (Fig. 3.5C; see Appendix II for more pictures of fractures). Fracture

density rises from one per metre at a radial distance of 0.75 km, and rises to twelve per metre within the feeder complex (Fig. 3.5C). The core of this anticline consists of a structurally complex zone of disharmonic folds and contorted bedding (Fig. 3.7D). This structural complexity appears to be genetically separate from the mud volcano systems, a product of the relative tightness of the folding.

Fig. 3.4C and D shows the extrusive features seen at two of the volcanoes. Koturdag A produces a kilometre-scale Bingham body style mud flow (Iverson 1997) that has been moving for the past fifty years at a rate of 2-6cm/day (Fig. 3.4C; Aliyev *et al.* 2002). This contrasts with the extrusive features seen at Koturdag B and C at which only gryphons, salses and breccia pipes (Fig. 3.4D) are visible. Multiple oil seeps are also visible along the stream section of the anticline following a fault which lies at right angles to the anticline axis.

The common structural features seen in all three field examples are summarised in Table 3.2.

Mud Volcano	Features							
	Sinuous Fractures	Pre-Existing Fractures with Mud Fill	Breccia Pipes	Mud Plugs	Zone of Random Strike Orientations	Distance from Anticline Axis (km)	Block Size (m)	Dip Angles (°)
Kichik Kharami	Yes	Yes	Yes	No	Yes	0.6	2-20	>42
Alyaty Ridge	Yes	Yes	Yes	Yes	No	0.1	1-5	>52
Pirsaatadag	Yes	Yes	Yes	No	Yes	0.01	1-20	>42

Table 3.2: Table of structural features present in each field area.

3.4.4 Structural Sub-Domains Associated with Feeder Complexes

The mapping revealed zones of similar structural elements common to all three feeder complexes. These are the 'active vent zone', 'peripheral fracture zone', and 'central zone of block rotation', which together comprise the feeder complex itself, and finally the 'un-intruded zone' which lies outside the feeder complex. In all three field examples mapped in this study, the structural zones can overlap. Following the general nomenclature set up by Stewart & Davies (2006), here these zones are termed structural sub-domains associated with the intrusive domain of mud volcano systems (Fig. 3.8). These sub-domains are defined here in the context of mud volcanism for the first time. The mud volcano feeder complex can be defined as the area which has undergone any change in physical characteristics due to the intrusion of mud and fluids from the intrusive mud system. The boundary of this complex usually corresponds with that of the peripheral fracture zone, however, lateral intrusions extending locally beyond the peripheral fracture zone are possible. The criteria by which the sub-domains are identified are defined first, starting with that closest to the centre of the feeder complex, moving outwards and then illustrate their extent in the field examples.

3.4.4.1 Active Vent Zone (red area on structural maps)

This zone is recognised as the area in which mud and fluids are actively being extruded within the mapped exhumed intrusive domains. A range of extrusive features were observed including gryphons, salses and cinder mounds as described by Hovland *et al.* (1997). These structural elements were centimetres to metres in scale.

3.4.4.2 Central Zone of Block Rotation (grey area on structural maps)

This region characterises the centre of the feeder complex. It consists of a region of large blocks of country rock (1-20 m in length; see Appendix II for more pictures of clasts) which have strike orientations varying up to 90° to that of the surrounding sedimentary strata. The blocks are separated by a matrix of mud breccia.

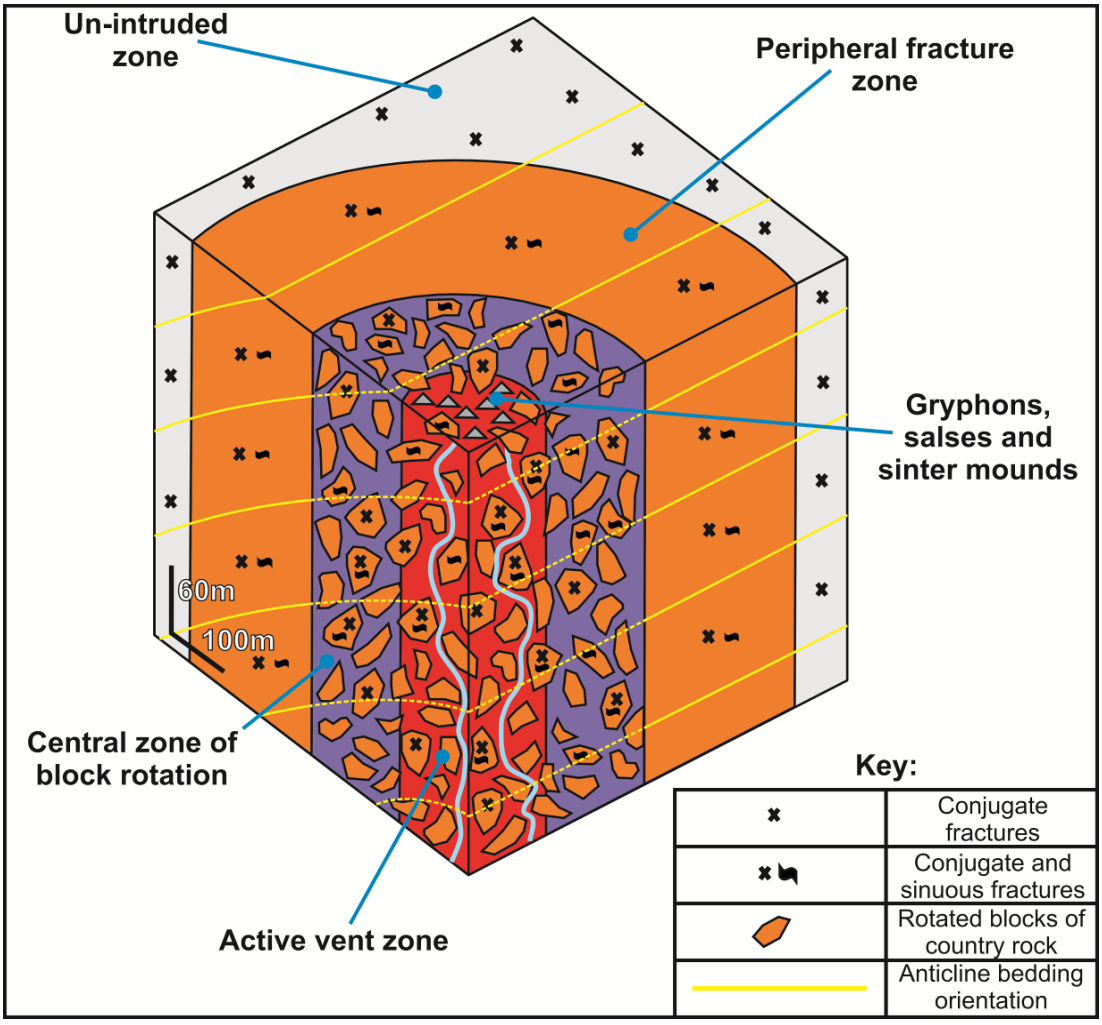

Fig. 3.8: Schematic of the mud volcano 'feeder complex'. The 'active vent zone' is highlighted in red, this represents the area of the mud volcano that is currently erupting fluid. The 'peripheral fractured zone', in orange, marks the region where both sinuous and conjugate fracture sets are present in the country rock. The 'central zone of block rotation', in purple, indicates the area where blocks of country rock with bedding strike measurements vary from the normal bedding orientations seen in the un-intruded anticlinal bedding. The 'un-intruded zone', in grey, denotes the region that has been unaffected by the intrusion of the mud volcano system. Here only conjugate fractures that contain no fill are found. The full yellow lines represent areas of bedding that follow the general anticlinal trend, whereas dashed yellow lines indicate areas where bedding strikes could be rotated away from the regional trend. Sinuous blue lines indicate active fluid flow to the vents erupting at the surface.

3.4.4.3 Peripheral Faulted/Fractured Zone (orange area on structural maps)

This region is characterised by country rock that contains fracture sets only seen in proximity to the mud volcano system, as opposed to regional fracture sets. These fractures are often sinuous and infilled with mud and small clasts of country rock, with typical widths of 1-2 cm and lengths of 2-4 m.

3.4.4.4 Un-Intruded Zone

This zone contains strata that has been un-affected by the intrusion of the mud. It is usually composed of country rock with open, un-filled, conjugate fractures and jointing produced by folding. The fractures do not contain any mud infill.

3.4.4.5 Fracturing

Sinuous fractures and conjugate fractures are present in all three case studies. The grid-like fractures occur throughout every region of the mapping areas. These are interpreted as being typical of fold-related fractures (Ramsay & Huber 1987) on the basis that these fractures are present in areas at some distance from mud volcano feeder complexes. Fractures within the feeder complexes are infilled by mud; those in un-affected country rock tend to be open. The sinuous fracture systems are only found within the feeder complexes and are usually infilled by mud. In cross section these fractures appear to be sinuous in form, however, it is important to note that in three dimensions the fracture plane would also have a sinuous morphology. At Kichik Kharami they are found within a 250 m radius of the centre of the feeder complex and at Pirsaatadag they are 180 m radius from the centre (Fig. 3.5B).

3.4.4.6 Blocks of Country Rock in the Feeder Complexes

Large blocks of country rock are present at outcrop within all the feeder complexes mapped in this study. These blocks are up to 20 m in length and clearly preserve original sedimentary architecture. However, they are heavily fractured with the majority of these fractures being infilled by mud. The blocks consist of sands and

shales, as does the country rock but due to the monotonous nature of the regional stratigraphy it was difficult to determine whether the blocks had moved vertically within the feeder complex, or whether they correlate laterally with strata that currently outcrop adjacent to the feeder complex.

In Kichik Kharami and Pirsaatadag mud volcanoes the blocks are rotated relative to the surrounding country rock. The degree of rotation generally increases towards the centre of the feeder complexes.

3.5 Interpretation

This discussion focuses on three key features apparent from the mapping a) the varying degree of fracturing, b) the presence of large blocks of country rock in the feeder complexes and c) deformation of these blocks.

3.5.1 Degree of Fracturing

In each case study fracture density increases from the far field to the centre of the feeder complexes (Fig. 3.5). At Pirsaatadag the fracture density increase towards the centre of the edifice which may also have a component of fracture density variation due to the position of the mud volcano system on the regional fold axis (Fig. 3.6C). Kichik Kharami intrudes to the south of the anticline axis, an area which would not be as highly fractured, however, still maintains a fourteen fold increase in fracture density at the centre of the mud volcano (Fig. 3.5A). It is only the sinuous fracture set that dramatically increases in fracture density towards the centre of the feeder complexes in all three case studies. This suggests that the intrusion itself, rather than the folding, is the principal control on fracture distribution in the feeder complex.

The non-tectonic fractures can be explained by the mud intrusion process. Overpressured mud produces a sustained pressure differential between the fluid in

the propagating fractures and the fluid in the pores of the country rock. This exceeds the minimum principal stress, causing fracture dilation and enabling the fluid mixture to flow through the fracture (Morley *et al.* 1998; Jolly & Lonergan 2002). This may be enhanced by an impermeable 'mud cake' being deposited on the fracture walls which would prevent fluid leakage out of the fracture and help sustain the fluid pressure within the fracture (Morley 2003). These processes facilitate fracturing at depth and eventual propagation towards the surface. As fracture size and density increases, more mud intrusion occurs and eventually forms one large feeder complex (Abidin *et al.* 2008).

3.5.2 Blocks of Country Rock within the Feeder Complex

Up to 20 m in length, these are prominent features at outcrop but would be un-detectable at the resolution of seismic reflection data employed in commercial hydrocarbon exploration. The varying strike orientations imply that the blocks are rotated. These blocks are interpreted as 'megaclasts' of country rock. The large proportion of mud outcropping in the feeder complexes indicates the amount of country rock that has now been removed. It is not obvious from the mapping whether the missing volume of country rock has risen upwards towards the extrusive domain, or sunk downwards towards the mud source.

A feature of the country rock blocks within the feeder complexes is that they become increasingly rotated with proximity to the central (vertical) axis of the feeder complex. The dips of the blocks still remain in the range of 40-88°, similar to dip magnitudes observed in the surrounding country rock. The bedding at the core of Kichik Kharami dips towards the centre of the feeder complex (Fig. 3.3C). This is interpreted as indicating that the cause of the block rotation is a process related to the mechanics of the feeder system. At Pirsaatadag the central zone of block rotation is offset to the southeast of the centre of the active vent zone (Fig. 3.7B). It is likely that the area of current extrusion has migrated to the northwest from the southeast resulting in exposure of the extinct zone of intrusion. The map of

bedding in Fig. 3.7B shows a similar layout to that seen at Kichik Kharami mud volcano suggesting that this is a common occurrence in the intruded strata.

3.6 Discussion: Block Rotation Processes

This study has shown the occurrence of discrete sub-domains within mud volcano feeder complexes (active vent zone; peripheral faulted/fractured zone; etc.). These have only been mapped in 2-D (map view) in the examples studied here– but given the arbitrary structural level of exhumation in the field area, it can be suggested that the zonation mapped in this study is representative of the structure of feeder complexes in the subsurface. The form and dimension of a feeder complex could change relative to the proximity to either the extruded edifice or whether it is just above the source domain. The observations made therefore might only be applicable to a certain part of the mud volcano system and this should be taken into consideration. Because of the small (metre) scale of these features, such a subdivision, has not been possible using the seismic reflection method previously applied to subsurface examples offshore Azerbaijan (Davies & Stewart 2005; Stewart & Davies 2006). However, it has been possible to witness the development of potentially similar zones at the Lusi mud volcano system which is currently forming in East Java. The Lusi mud volcano has a central zone which is coincident with the main active vent. Surrounding this is evidence for faulting and fracturing (peripheral fault and fracture zone), that has led to the establishment of approximately 169 new vent sites (Mazzini *et al.* 2007).

Alternative models are now considered to account for the observed distribution and deformation of blocks within the mapped feeder complexes, and identify the most likely mechanism for these examples.

3.6.1 Flow Rotation

Flow rotation is a common mechanism of rotation found in several geological environments (Reading 1996). It is most commonly seen within debris flows that are gravity-driven surges of roughly equal volumes of water and poorly sorted sediment, with the largest flows transporting boulders in the order of 10 m in diameter (Iverson 1997). Intrusive mud has to overcome the gravitational force, nonetheless the process may be applicable. Another analogue could be fluvial imbrication where a shear force is exerted on pebbles in a stream bed causing the pebbles to rotate and stack on top of one another with their long axes pointing in the direction of flow (Reading 1996). Application of this mechanism would involve long-lived, multiple intrusive events of mud intruding upwards through pre-existing and new fractures. Shear forces on the fracture walls are the mechanism driving block rotation – it seems reasonable to assume that variation in amount of shear stress around the margins of a block (a necessity for rotation) would occur as a result of variations in mud flow rates through the fracture network (Fig. 3.9C). In order to conserve volume, the addition of mud to the system must also result in expulsion of the country rock that the mud now replaces. The smaller blocks could be carried upwards by intruding mud, ultimately to be expelled in the constructional edifice of the extrusive domain. Evidence to support this is the common presence of deep-sourced clasts in extruded mud flows (Guliyev *et al.* 2000).

Flow rotation is probably an unlikely mechanism due to the magnitude of forces needed to rotate such large blocks of country rock (Kopf & Behrmann 2000). The density of the mud-fluid mix required to exert a shear force on 20 m long blocks of country rock would be extremely large. Even in the largest mud flows emanating from mud volcanoes, no blocks greater than 1 m in length were observed in the study or reported in the literature (Guliyev *et al.* 2000). This suggests that the force of the flowing mud is not capable of moving blocks of the largest scale (20 m) observed in the feeder complexes.

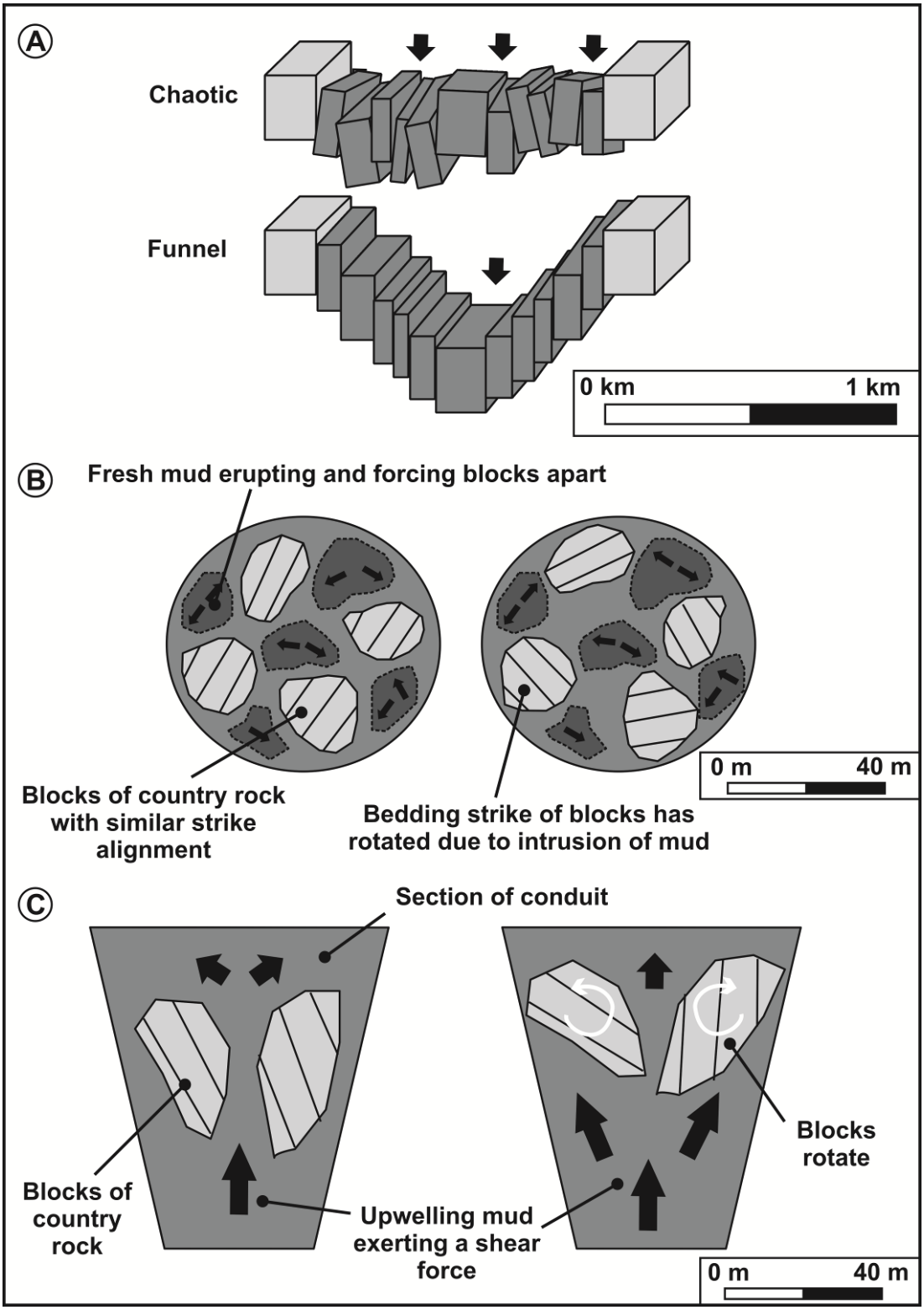

Fig. 3.9: Mechanisms. A) Schematic of the 'caldera collapse', mechanism modified from Cole *et al.* (2005), B) schematic map view of the intrusive mud rotation and C) schematic cross section of the 'flow rotation' mechanism.

3.6.2 Stoping

Stoping in its igneous context is the mechanical disintegration of the country rock surrounding an intrusion, typically through fracturing due to pressure increases associated with thermal expansion of the host rock in proximity of the interface with the melt (Pinotti *et al.* 2002). Fracture networks begin to propagate through the country rock closest to the intrusion. Once fractures are formed, melt and volatiles typically invade, widening the fracture and promoting the foundering of host rock blocks (Marsh 1982). When suspended in the melt, 'stoped' blocks may either sink or float depending upon the density of the block relative to that of the melt (Marsh 1982; Kopf & Behrmann 2000).

This process is not directly applicable to mud volcano systems as the upwelling fluids are not hot (Guliyev *et al.* 2000) and so would have no significant effect on the thermal expansion of the surrounding country rock. However, upwards-propagation of a fracture network driven by overpressured mud and fluids could set up a similar situation to igneous stoping (Morley *et al.* 1998; Kopf & Behrmann 2000; Morley 2003). Blocks isolated by this means would become suspended in the mud and allowed to rotate freely.

Once the initial failure of the rock occurs at depth more mud can intrude along the fractures and the stoping process slowly propagates to the surface of the edifice, with the majority of the fracture network being produced by hydrofracturing (Jolly & Lonergan 2002). This highly intruded zone of country rock now forms a 'stoping column' (Fig. 3.10C; Geshi *et al.* 2002). Breaching the surface would release fluids and with it some of the overpressure from the chamber (Geshi *et al.* 2002). The evacuation of material would cause a void to form at depth resulting in lack of support for the country rock above (Fig. 3.10D). As more fluids are expelled, the overburden would increase and may induce piecemeal caldera collapse into the void left in the vent (Fig. 3.10D; Cole *et al*. 2005).

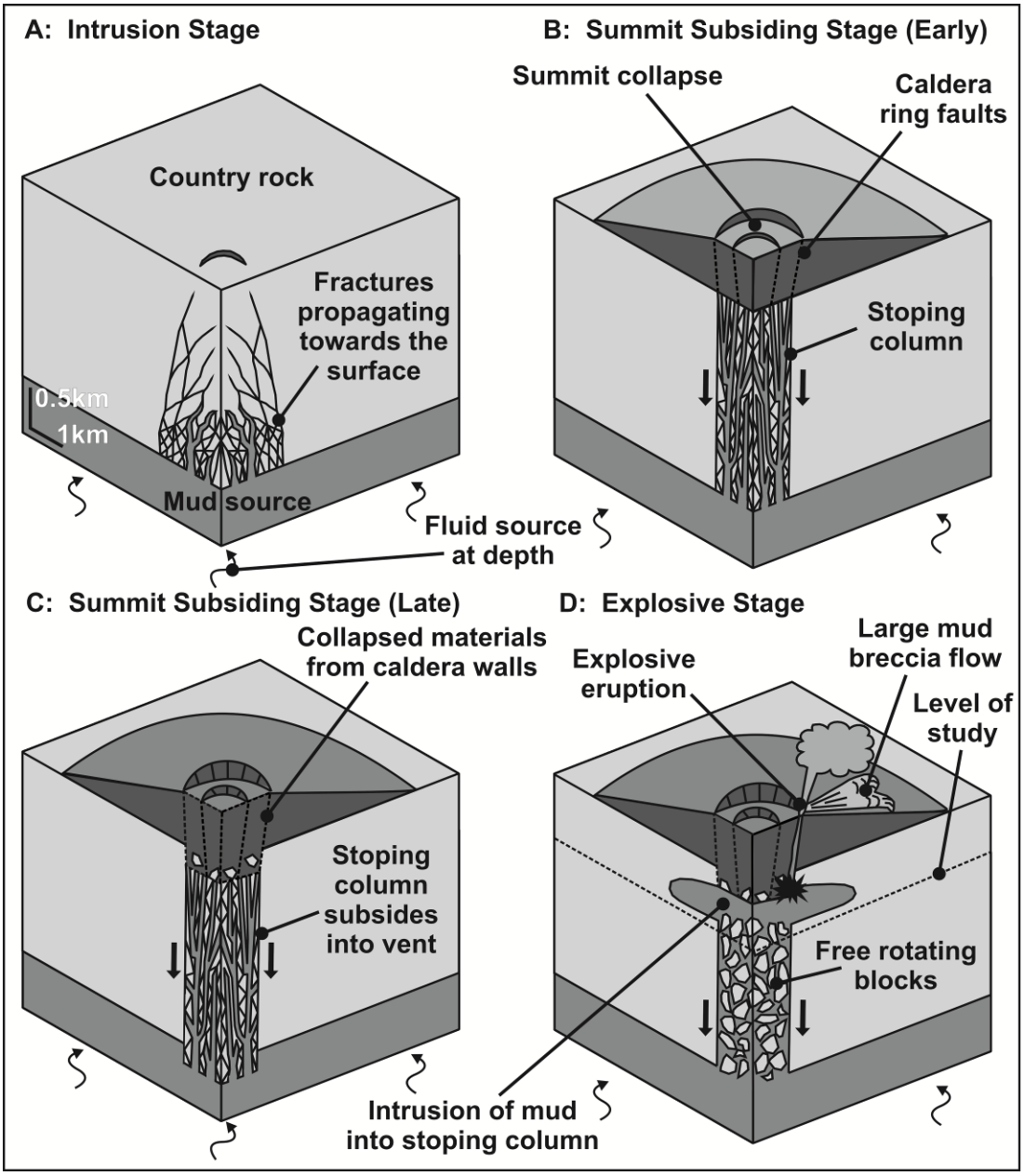

Fig. 3.10: Schematic of the 'hybrid stoping' mechanism modified from Geshi *et al.* (2002). A) Intrusion stage before the surface collapse. Evacuation of mud from the reservoir caused stoping of the roof rock of the reservoir. Underground stoping formed a cavity at the top of the stoping column. B) The early stage of summit subsidence. The roof rocks of the cavity cannot carry their own weight and collapse into the cavity. Release of mud and fluids fills the cavity. C) The late stage of the summit subsidence. Continuous evacuation of mud from the reservoir caused the subsidence of the roof of the reservoir. The top of the stoping column was filled with the collapsed materials from the outward migrating caldera wall. D) Explosive stage. Invasion of fluids to the stoping column causes eruption and conduit consists of large blocks of country rock rotating freely within it.

The stoping hypothesis assumes a general downwards movement of stoped blocks, a feature that is not demonstrable in the case studies. Stoping models also, often, contain an element of block melting and mixing to preserve the volume of the system. This is not an option in mud volcano systems due to the low temperature of the intruding mud.

3.6.3 Rotation Due to Multiple Intrusive Episodes

After the major stoping event the intrusion of mud, occurring as a result of the stoping process, would also exert forces on the blocks of 'stoped' country rock. As mud forces its way between the stoped blocks it pushes them away from the flow (Fig. 3.9B). Each time a new intrusion of mud occurs up the conduits more force is exerted rotating the blocks further. This is a similar process found in dyke swarms in ophiolites and spreading centres (Moores & Vine 1971). Igneous dykes intrude up the centre of pre-existing dykes, forcing each half of the intruded dyke to opposite sides of the new dyke (Moores & Vine 1971). If one area of the mud volcano has a higher rate of intrusion than others then the blocks will be pushed and rotated towards areas that are more quiescent.

3.6.4 Caldera Collapse

Both trap-door and piston caldera collapses have been identified on the underwater mud volcanoes in the Caspian Sea (Cole *et al.* 2005; Stewart & Davies 2006; Evans *et al.* 2008). In these onshore examples the dominant morphology is the piecemeal collapse (Fig. 3.9A). The evacuation of the mud from a chamber at a shallow depth would cause a void to be formed. This would enable the strata above to collapse into the chamber. The effect of this would be enhanced by the increased overburden of erupted mud on top of the country rock causing more subsidence. This collapse would not have occurred as one event, instead a piecemeal collapse results in the country rock collapsing at different rates and times. This varying collapse rate would enable different blocks of rock to collapse and rotate at different times and to varying degrees of rotation.

The discrepancy with the piecemeal caldera collapse arises with the large differences in strike angles within such a small area. Piecemeal collapses usually only allow bedding rotations of a few degrees (0-20°) rather than the observed rotations (0-90°; Cole *et al.* 2005). This suggests that caldera collapse cannot be the singular cause of the block rotations seen at the centre of the feeder complexes.

3.6.5 Diapirs

Hovland *et al.* (1998) define a piercement shale diapir as a positive topographical feature constructed mainly of clay-sized sediments that periodically or continuously move from the sub-surface and upwards towards and through the sea floor. This is on a scale of 100's to 1000's of metres in depth and width. The diapir itself would be composed almost entirely of mud or shale on a ratio of 80:20 (mud : xenoliths). This study follows Cooper (2001) and Davies & Stewart (2005) in discounting large-scale mud diapirism on the basis of there being no observations of that phenomenon in the basin.

3.7 Implications

The identification of structural sub-domains is expected to be of utility for the study of other exhumed intrusive domains. Similar and additional sub-domains could be identified in other exhumed feeder complexes and with improved seismic reflection technology it is conceivable that similar zones may be detectable in the subsurface. The blocks of country rock within these complexes are heavily fractured and cut by dense networks of mud intrusions. This dramatically reduces the reservoir potential of these segments within the vent as the country rock has become extremely compartmentalised. Commercially the compartmentalisation of the country rock will be significantly increased by the intrusion of the mud dyke systems. Although these segments of country rock are not economic the observation that they are present and can be recognised by their change in strike compared to the surrounding country rock will improve identification of mud

volcano systems when drilling. The evolution of this system over time should be considered when planning wells because old feeder dykes may be encountered when drilling. The reservoir surrounding mud volcano intrusive domains are commercially viable, however, large, seismic scale faults, seen during the mapping of Alyaty Ridge, may pose problems away from the intrusive domain within tight regional fold structures.

These interpretations will enable a better understanding of the processes governing fluid transport through the shallow crust and how the processes affect the surrounding country rock. Comparisons with igneous vent systems could be fruitful as they share some common morphological and mechanical process with mud volcanoes and there may be parallels with the mechanisms by which fluids travel to the surface. Further studies of piercement structures will help establish the common processes and products.

3.8 Conclusions

On the basis of field mapping, including collection of bedding orientations, fracture types and densities, sub-domains have been identified within mud volcano feeder complexes. This represents the first study on mud volcano systems of its kind. These sub-domains consist of the 'active vent zone' where fluids are currently being extruded, the 'peripheral fracture zone' where both infilled sinuous and conjugate fracture systems are found, the 'central zone of block rotation' where bedding strike measurements vary greatly from the surrounding anticlinal bedding and the 'un-intruded zone' which contains only un-filled conjugate faulting/fracturing. The 'active vent zone', 'peripheral fracture zone', and 'central zone of block rotation', together comprise the mud volcano feeder complex itself, with the 'un-intruded zone' lying outside the feeder complex. Further research could establish the existence of these sub-domains elsewhere, refine the characteristics for their identification and lead to the identification of new examples. Their delineation

should also provide an objective method for the comparison of other mud volcano feeder complexes.

Overall findings suggest the feeder complexes consist of a megabreccia of country rock surrounded by intruded mud and some long-lived fluid conduits. The preferred model consists of a propagating fracture network that isolates blocks which then become free to move as the smaller clasts become eroded by the mud-water-gas mix through time. This process has similarities with the better-known stoping process in igneous volcanic complexes. The initial stoping mechanism allows an upward-propagating fracture network to isolate a megabreccia of blocks up to 20 m in scale. Once the fracture system breaches the surface and becomes an anastomosing flow pathway, the smaller blocks within the breccia are eroded and extruded, creating space for widening of the flow conduits and settlement and rotation of the larger blocks whose size and weight prevent them from being carried upwards. During periods of low mud flow rates, gravity driven compaction of the system may account for relatively low levels of water and gas eruption observed during 'quiescent' periods.

Furthermore in addition to supplying parameters for lithology and 3-D porosity and permeability distribution in feeder complexes, the observations also provide a starting assumption for the dimensions of these structures in areas where seismic imaging does not clearly resolve their extent. These parameters will be useful in the cases of reserves assessment and drilling planning in the deeper parts of mud volcano systems.

4 Structural Controls on Mud Volcano Vent Distributions: Examples from Azerbaijan and Lusi, East Java[1]

Abstract

Structural mapping, nearest neighbour and 2-point azimuth statistical analysis of vent distributions are described from nine mud volcanoes in Azerbaijan and Lusi mud volcano, East Java. Spatial distributions are significantly non-random, clustering to form alignments with: 1) anticline crestal faulting, 2) ring faults, 3) conjugate faults and 4) detachment faults. Clustering of vent fluid types also suggests separation within the intrusive system. The influences on distribution of vents erupting in Azerbaijan are used to identify the structural controls on vent distributions at Lusi mud volcano which shows changes in vent alignment through time. There is an early NE-SW trend corresponding to the trend of the Watukosek fault, changing to an east-west trend, parallel to local fold axes and faulting. Fractures are important elements of feeder system architecture and their orientation is related to regional-scale structural elements e.g. anticlines, and the in-situ stress state, opening the possibility of predictive modelling. Changes in active fracture orientation through time, as at the Lusi mud volcano, are important for managing the disaster by predicting which populated areas will be most affected by the eruptions. Results indicate regions east and west of the main vent are more likely to be impacted by new vents than those to the north and south due to probable onset of elongate caldera collapse within 10 km diameter of the central vent.

[1] This chapter is based on a paper that has been accepted for publication in the journal 'Journal of the Geological Society, London'. Referenced as 'Roberts, K.S., R.J. Davies, Stewart, S.A. & Tingay, M. (2011). Structural controls on mud volcano vent distributions: Examples from Azerbaijan and Lusi, East Java. *Journal of the Geological Society, London*, DOI: 10.1144/0016-76492010-158', see Appendix V.

4.1 Introduction

Mud volcano systems are integral elements in many sedimentary basins globally (e.g. Kopf 2002). However, because of the ephemeral nature of the fluid flow the structural pathways exploited during their intrusion are poorly defined. Sediment, fluid and minerals can be transported through these structural pathways, from depths exceeding 8 km (Kopf 2002) resulting in eruption at the surface as edifices reaching volumes in excess of 25 km^3 (Davies & Stewart 2005). Faults and fractures are probably one of the dominant controls on fluid migration pathways during the intrusion of mud volcano systems (*cf.* Morley 2003; Roberts *et al.* 2010; see Chapter 3).

Vent populations for igneous volcanoes have been widely studied on Earth (Lutz 1986; Wadge & Cross 1988; Connor 1990; Hammer 2009; Paulsen & Wilson 2010a) and on extraterrestrial bodies (Bleacher *et al.* 2009) but little is known about the fluid flow pathways or organisation of eruptive vent populations for mud volcano systems. It has been proposed that alignment of point-like geological features such as volcanic cones, hydrothermal vents, fluid expulsion pipes and springs may reflect underlying features, particularly subsurface dyke orientation, faults and joints (e.g. Hovland *et al.* 2006; Hammer 2009; Moss & Cartwright 2010; Paulsen & Wilson 2010a). Time dependent changes in vent distributions in igneous or sediment-fluid venting has never been considered (Paulsen & Wilson 2010a). Well exposed sub-aerial mud volcanoes in Azerbaijan provide examples where the distribution of vents can be related to mapped structural features (Hovland *et al.* 1997; Guliyev *et al.* 2000; Planke *et al.* 2003). This provides confidence in assessing the controls on vent distributions which have changed from 2006-2010 at Lusi mud volcano, East Java. This mud volcano first erupted in May 2006 and now covers an area of 7 km^2, it has displaced *c.* 40,000 people and currently has 169 vents erupting and igniting without any warning in the surrounding densely populated areas (Tingay 2010). This makes the evolution and prediction of fluid flow pathways particularly important.

The aim of this chapter is to investigate the distribution of a variety of vents erupting variable compositions of water, mud and gas within kilometre-scale mud volcano edifices in Azerbaijan and at Lusi (Fig. 4.1) and to use the observations to identify the structural controls on their distribution. The field mapping focuses on the geographical position and general composition of vents at eight field examples. The spatial distributions of vent populations are statistically analysed allowing for an assessment of the geometry of the subsurface feeder systems.

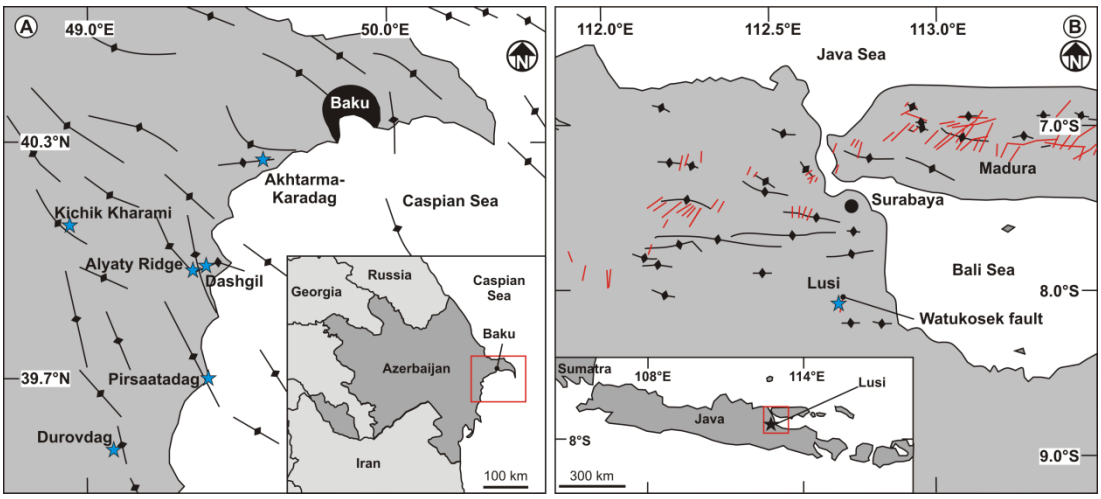

Fig. 4.1: A) Major structural elements of eastern Azerbaijan after Jackson *et al.* (2002), showing the location of the mud volcanoes in this study (localities marked with blue stars; see inset for global location). B) Major structural elements of the East Java Basin, after The Geological Survey of Indonesia (1963), showing the location of Lusi mud volcano (marked with a star) and main faults marked in red (see inset for global location).

4.1.1 Mud Volcanoes and Vent Complexes

A mud volcano system refers to the intrusive domain, which contains the feeder complex; the source domain and extrusive domain, which is generally comprised of an eruptive edifice (Stewart & Davies 2006; Roberts *et al.* 2010; see Chapter 3). Mud volcano eruptions can be violent with quiescent inactive stages where eruption from multiple, small vents is the dominant process (Guliyev *et al.* 2000). Dormant mud volcano edifices can have anything from one to thousands of vents of differing types. Herein the pattern of vents on edifices, are termed 'vent populations'. There are a variety of vent types with a range of mud-water-gas

compositions (Table 4.1; Fig. 4.2). Cinder mounds are suggested to be caused by close to 100% gaseous phase eruptions. Mud breccia flows consist of *c.* 90-100% mud that has the rheology of a Bingham body (Iverson 1997). Salses contain suspensions of <30% mud particles in water and gryphons have a composition of 30-90% mud particles in water that are either thixotrophic or shear thinning (Yassir 1990, 2003; Mueller *et al.* 2010). The area that is most densely populated with vents is termed the active vent zone (see Chapter 3; Roberts *et al.* 2010).

Vent Type	Composition	Height (m)	Width (m)	Clasts? (Y/N)	Morphology	Fluid Type
Gryphons	>30-90% mud: <30% fluids	0.02-10	0.05-360	Y	'Cones' of mud breccias with bubbling pools of mud in their crater	Shear thinning or thixotropic
Salses	<30% mud: >70-100% fluids	0.02-2	0.05-80	N	Shallow sided 'cones' of mud breccias with a large pool of watery mud at the summit and several bubbling centres	Mud suspensions
Cinder Mounds	100% gaseous	0-3	1-50	Y	Mounds of red/ orange/ brown glassy mud breccia	Gaseous
Breccia Pipes	>30-90% mud: <30% fluids	0.5-1.5	0.5-10	Y	Clusters of salses surrounded by damp mud containing clasts of country rock	-
Mud Plugs	90-100% mud	4	30-100	Y	Large flows of mud breccia emanating from one vent	Bingham
Pools	100% water	0.01	<0.05	N	Small vents that cluster round gryphons and salses only erupting water and/or gas	-

Table 4.1: Classification of vents mapped during the study.

4.2 Geological Settings

4.2.1 Azerbaijan

Azerbaijan's mud volcanoes form due to a combination of factors, including rapid sedimentation during the last 5.5 Ma, tectonic compression, the presence of a thick overpressured mudstone (Maykop Formation) at 5-8 km depth and hydrocarbon maturation (Davies & Stewart 2005; Evans *et al.* 2008). All the mud volcanoes are located along or near the crests of anticlines and most are thought to have initiated in the Pliocene (*c.* 3.5 Ma; Narimanov 1993; Yusifov & Rabinowitz 2004). The mud volcano systems may also incorporate fluids rising from below the Maykop Formation (Kopf 2002; Hovland *et al.* 2006).

The region has undergone 2.4 km of tectonic subsidence since *c.* 5.5 Ma (Allen *et al.* 2003). Several kilometres of sediment accumulated during the Pliocene and have subsequently been folded, with these structures having a dominant NW-SE fold axis orientation (Allen *et al.* 2003, Yusifov & Rabinowitz 2004).

4.2.2 Lusi, Sidoarjo, East Java

This mud volcano erupted in the East Java basin in May 2006 (Davies *et al.* 2007; Mazzini *et al.* 2007). During the Eocene NE-SW–oriented rift basins formed and filled with continental clastics that host both source rock and productive reservoirs (Kusumastuti *et al.* 2002). In the Oligocene to early Miocene east-west trending normal faults formed (Kusumastuti *et al.* 2002; Istadi *et al.* 2009). Carbonate platforms developed on some palaeo-basement highs. The Porong-1 carbonate reef is located beneath the Lusi mud volcano and has an E-W orientation (Kusumastuti *et al.* 2002). Compression during the late Miocene-Pleistocene resulted in inversion associated with E-W trending fault movement (Istadi *et al.* 2009). This produced the E-W orientation of the anticline structures (Istadi *et al.* 2009). Subsequent Pliocene-Pleistocene sedimentation consisted of an eastward-prograding mudstone-dominated volcaniclastic wedge derived from the Java volcanic arc (Istadi *et al.* 2009). The mudstone of the Pleistocene Kalibeng

Formation is overpressured at 900-1870 m depth at Lusi (Istadi *et al.* 2009). This is the source of the mud that makes up the solid fraction of the mud erupted at Lusi (Mazzini *et al.* 2007). The water has an unknown source estimated to be from >1700 m depth by its temperature, isotopic composition and chemical composition (Davies *et al.* 2007, Mazzini *et al.* 2007), but is considered here to be primarily from the Miocene carbonates (2833-3500 m; Tingay 2010) with a contribution from the remobilisation of the Upper Kalibeng Formation (Davies *et al.* 2007). Some fluids may also be sourced from shallow aquifers in the Pleistocene Pucangan Formation at 280-900 m depth (Tingay *et al.* 2008).

New vents form frequently, and are a safety concern, for example a vent eruption in April, 2010 was in close proximity to railway tracks and contained flammable gas. The Porong highway near Lusi had developed metre long cracks leaking methane on 2nd July, 2010, with the highway surface increasingly sloping toward the mud embankments. New vents and increased subsidence are still developing and the eruptions could continue for decades which will have an important impact on the structural evolution of the region (Davies *et al.* 2008; Istadi *et al.* 2009).

4.3 Database and Methodology

4.3.1 Structural Mapping

Eight of the mud volcanoes in this study lie along the Caspian Sea coastline in Azerbaijan; Koturdag A, B and C (Alyaty Ridge), Kichik Kharami, Pirsaatadag, Dashgil, Durovdag, and Akhtarma-Karadag, the ninth is Lusi (Fig. 4.1; for more field examples from Azerbaijan see Appendix III). Mapping was carried out using a handheld global positioning system (GPS) receiver, with a positional accuracy of 5 m (Azerbaijan) and 5-12 m (Lusi data, courtesy of Badan Penanggulangan Lumpur Sidoarjo (BPLS); see electronic version of Appendix III). Bedding, fracture and fold orientations were plotted using GEOrient software onto stereographic and rose projections (see electronic Appendix III for structural field data and vent location data). The GPS co-ordinates and corresponding structural data were integrated in

ArcMap software. The coordinate system for these data were input using spheroid WGS 1984.

Vent types are classified as either: gryphons, salses, cinder mounds, mud plugs or pools (Fig. 4.2; Table 4.1; Hovland *et al.* 1997; Guliyev *et al.* 2000; Mazzini *et al.* 2009). Each is marked onto satellite imagery with different symbols (Fig. 4.2). The relationship between faulting, folding and regional structure of the mud volcanoes in Azerbaijan is clear as the area has been exhumed and exposure of country rock is >60% in the cases of Alyaty Ridge, Kichik Kharami and Pirsaatadag volcanoes. Structural data from outcrop and 2-D seismic coverage for Lusi mud volcano are limited. Therefore the Azerbaijan mud volcanoes are used to develop confidence about the relationships between structures and vent populations and also aid interpretation of the vent trends at Lusi.

4.3.2 Statistical Analyses

Two statistical approaches, adapted from igneous vent systems, are used to characterise spatial patterns within vent populations (see Chapter 1 for a more detailed account of the statistical techniques). At igneous vent systems these techniques have revealed that magmatic volcanic vents often form clusters and define alignments at several scales from 10 m's to over 1000 km's (Bleacher *et al.* 2009; Paulsen & Wilson 2010a). As the GPS accuracy is 5 m, vent alignments have 5 m accuracy. The goal of these spatial studies is to provide insights into the links between the distribution of vents, causal processes and controls on fluid flow pathways.

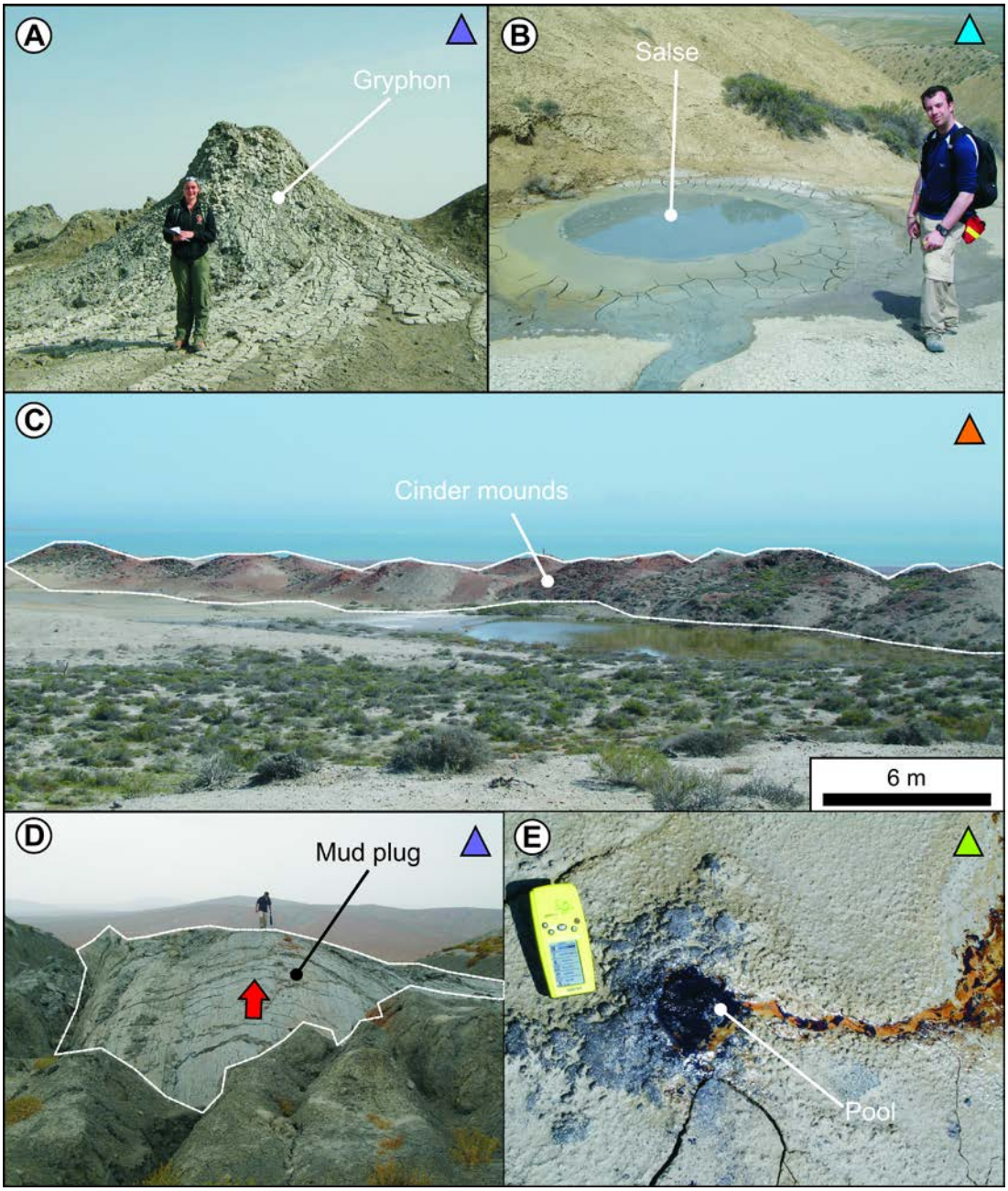

Fig. 4.2: A) Gryphons (purple triangles on Fig. 4.3, Fig. 4.5, Fig. 4.6 and Fig. 4.7). Conical vents erupting mud, a few centimetres to 4 m high. B) Salses (blue triangles on Fig. 4.3, Fig. 4.5, Fig. 4.6 and Fig. 4.7). 'Lakes' of muddy water, with cones 1-2 m high and diameters of a few centimetres to over 50 m (Guliyev *et al.* 2000). C) Cinder mounds (orange triangles on Fig. 4.3, Fig. 4.5, Fig. 4.6 and Fig. 4.7). Erupt only gaseous phases. Resemble heaps of fired clay, up to 4 m high and 10-20 m long displaying an orangey-red ceramic appearance (Hovland *et al.* 1997; Planke *et al.* 2003). D) Mud plugs (purple triangle labelled in Fig. 4.3A). Breccia with a putty-like malleable consistency extruding from craters like 'paste from a tube', on Koturdag A mud volcano (Guliyev *et al.* 2000; Planke *et al.* 2003). E) Pools (green triangles on Fig. 4.3, Fig. 4.5, Fig. 4.6 and Fig. 4.7). Bubbling pools of fluid, less than 2 cm in diameter (Mazzini *et al.* 2009). Extinct or dormant vents (black triangles on Fig. 4.3,

Fig. 4.5, Fig. 4.6 and Fig. 4.7). Vents that were once actively extruding fluids but have since dried up and are no longer active.

The nearest neighbour technique (Clark & Evans 1954) tests randomness in spatial distributions by calculating the ratio of the observed mean distance to the expected mean distance for a hypothetical random distribution to determine whether the points are clustered. A ratio of 1 indicates a random distribution and a ratio of <1 is clustered, the nearer to 0 the more clustered the distribution. This was carried out using ArcGIS which measures the distance from every vent point to its nearest neighbouring vent point (see Chapter 1 for a more detailed account).

The 2-point azimuth technique (Lutz 1986; Bleacher *et al.* 2009) was used as a measure of the significance of alignments between vents. The technique quantitatively identifies trends within vent populations and has been widely used in literature dealing with the structural geology of igneous volcanoes (Wadge & Cross 1988; Connor 1990; Bleacher *et al.* 2009). The azimuth of line segments that connect each vent to all other vents east of its location were calculated (Bleacher *et al.* 2009; see Appendix III for Matlab script). Only points to the east of each vent were measured so as not to duplicate any measurements. Histograms of azimuth values (0°=north, 90°=east, 180°=south) were produced with 10° bins. Peaks in the frequency distribution of the azimuths result from preferred formation of vents in response to structural controls (Bleacher *et al.* 2009; see electronic Appendix III for azimuth data). In this study the 'dominant' alignment refers to the azimuthal trend with the highest frequency of azimuths. 'Sub-alignments' include smaller peaks in azimuth frequency less significant than that of the 'dominant' alignment. Different vent types are separated and the individual azimuth alignments of different vent fluid types displayed (i.e. mud, water and gas) are analysed. The 'overall' azimuth alignments including all vent types are also plotted to identify larger scale influences on vent alignments of the whole edifice. On each of the graphs the 'Y' indicates the orientation of the anticline axis in the region, 'X' the orientation of any faulting measured during mapping and 'A' any anomalous values that may be the

result of external factors, such as human influences i.e. loading induced fluid flow around man made dams (e.g. Londe 1987).

4.4 Observations

4.4.1 Alyaty Ridge

Alyaty Ridge hosts twelve mud volcano systems, three of which were selected to study (Koturdag A, B and C; Fig. 4.1A and Fig. 4.3A). Koturdag A has a single, 240 m diameter caldera on its summit that is extruding 500 m to the north of the anticline axis (Fig. 4.3A). The most recent mud breccia flow has been ongoing for approximately fifty years and is currently extruding mud breccia from a 20 m wide vent at a rate of 2-6 cm length per day. The flow has areas of oxidised mud breccia and cinder which are the result of escaping gases igniting mud during eruptions (Fig. 4.2C; Hovland *et al.* 1997; Guliyev *et al.* 2000). The 20 m wide vent has a 1 m high gryphon 5 m away from it. This contrasts with the extrusive features seen at Koturdag B and C at which gryphons, salses and breccia pipes are present (Fig. 4.2A and B). Koturdag B has a high concentration of salses, 0.2-5 m in diameter, compared to the increased concentration of 1-2 m high gryphons found at Koturdag C (Fig. 4.3A). Another difference seen along Alyaty Ridge anticline is the change in dominant vent types at each volcano. Koturdag C is located at 100 m higher elevation than Koturdag B and has twice as many gryphons. In contrast, Koturdag B has twice as many salses as Koturdag C. Both Koturdag B and C edifices have long axes which align with the anticline axis at 130°N (Fig. 4.3A).

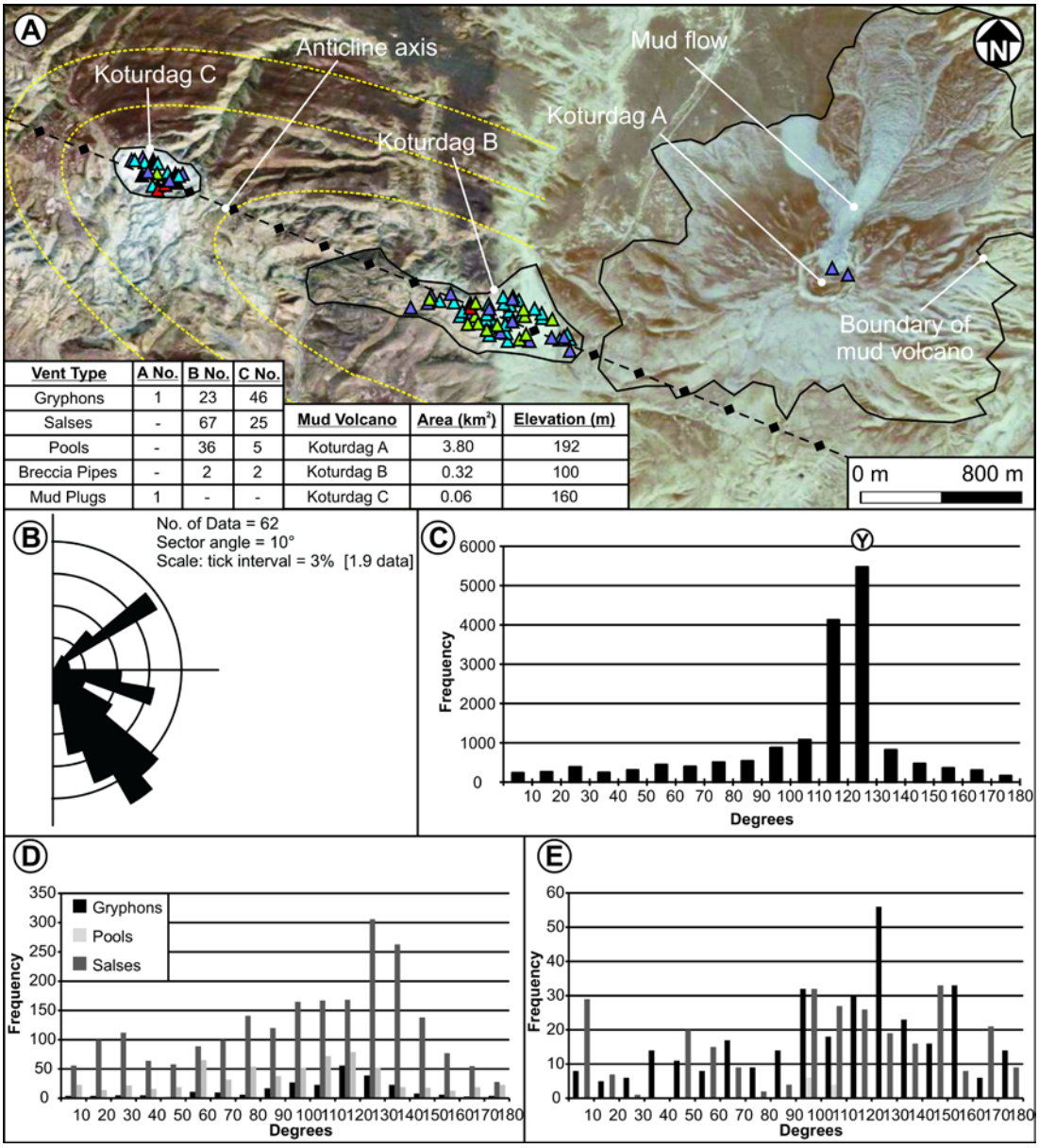

Vent Type	A No.	B No.	C No.
Gryphons	1	23	46
Salses	-	67	25
Pools	-	36	5
Breccia Pipes	-	2	2
Mud Plugs	1	-	-

Mud Volcano	Area (km²)	Elevation (m)
Koturdag A	3.80	192
Koturdag B	0.32	100
Koturdag C	0.06	160

Fig. 4.3: A) Part of Alyaty Ridge with three mud volcanoes intruded along its axis. Koturdag A is located to the 0.6 km north of the fold axis. Yellow dashed lines represent the bedding orientation. Triangles: Purple- gryphons, orange- cinder mounds, black- extinct vents, blue- salses and green- pools. Image © 2010 DigitalGlobe, © 2010 GeoEye and © 2010 Geocentre Consulting, © 2010 Google. B) Rose diagram of fault and fracture orientations measured along Alyaty Ridge. C) Histogram of frequencies of azimuthal direction for 2-point azimuth technique of all vent types grouped together for Koturdag A, B and C. D) Histogram of frequencies of azimuthal direction for 2-point azimuth technique of individual vent types separated into their different distributions for Koturdag B. E) Histogram of frequencies of azimuthal direction for 2-point azimuth technique of individual vent types separated into their different distributions for Koturdag C.

The orientations of fractures in the area are sub-parallel to the anticline axis at 130-140°N with another peak at 90° to this, at around 050°N (Fig. 4.3B). When including all the vent positions along Alyaty Ridge as a whole the observed frequencies of azimuths derived from the 2-point azimuth technique show preferential alignment in the direction of 120-130°N (Fig. 4.3C). When examining Koturdag B (Fig. 4.3D) and C (Fig. 4.3E) individually, both share this dominant 130°N trend. Koturdag B also shows a peak in salse alignment at this orientation whereas Koturdag C shows a peak in gryphon alignment (Fig. 4.3D and E).

4.4.2 Kichik Kharami Mud Volcano

This mud volcano edifice is 1 km to the south of a NW-SE trending anticline axis and is roughly circular in plan view (Fig. 4.1A and Fig. 4.4A and B). Minor amounts of mud are being expelled in the form of salses, although a 1.2 km long mud flow to the south of the feeder complex is testament to significant eruption of mud breccia within the past few hundred years (Fig. 4.4A). The salses have a circular arrangement at the centre of the volcano (Fig. 4.4B). 100 m from the centre of the volcano the salses orient themselves in NW-SE and NE-SW linear trends (Fig. 4.4B).

At Kichik Kharami fractures are dominantly arranged sub-parallel to the anticline axis at 120-130°N with a set perpendicular to this at 030°N. There are also smaller fracture alignments at 100°N and 160°N which form two planes, each roughly 30° to the fold axis (Fig. 4.4C). The dominant azimuthal frequency at Kichik Kharami is 130-140°N (Fig. 4.4). There are also secondary alignments, for example at 090°N (Fig. 4.4) which don't share a common orientation with any structures in the area. The salses show a dominant azimuth sub-parallel to that of the strongest fracture orientation at 130°N.

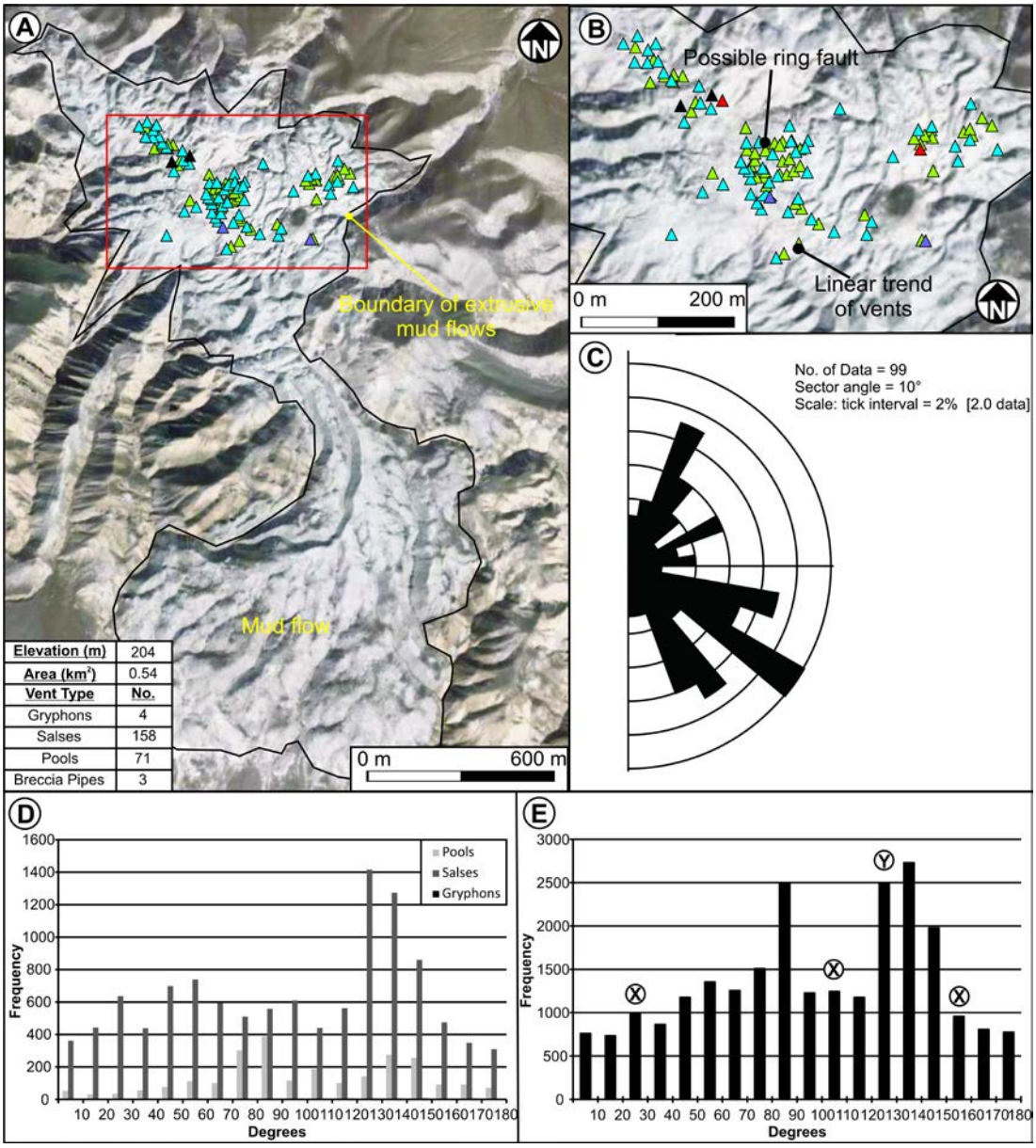

Fig. 4.4: A) Kichik Kharami mud volcano. B) Zoomed in image of the centre of the mud volcano seen in Fig. 4.4A. Vents can be seen clustering in concentric rings at the centre of the volcano whereas they form along lines orientated in NW-SE and NE-SW directions further out from the centre of the volcano. Triangles: Purple- gryphons, orange- cinder mounds, black- extinct vents, blue- salses and green- pools. Images © 2010 DigitalGlobe and © 2010 Geocentre Consulting, © 2010 Google. C) Rose diagram of fault and fracture orientations from country rock in and around Kichik Kharami. D) Histogram of frequencies of azimuthal direction for 2-point azimuth technique of individual vent types separated into their different distributions. E) Histogram of frequencies of azimuthal direction for 2-point azimuth technique of all vent types grouped together.

4.4.3 Pirsaatadag Mud Volcano

This mud volcano is located on the axis of a NW-SE trending anticline and has an elliptical shape, the long axis of which is aligned with the anticline axis at 150°N (Fig. 4.1A and Fig. 4.5). Minor amounts of mud are being expelled in the form of salses and pools. The mud volcano is heavily eroded and so exposure of country rock at its centre allows easy measurement of structure. The active vent zone of the volcano is offset to the north-western end of the edifice and displays a slight circular arrangement of vents at its centre (Fig. 4.5A).

The dominant orientation of fractures is at 030°N with the second most prevalent fracture orientation being sub-parallel to the fold axis at 150°N (Fig. 4.5B). The dominant azimuthal frequency at Pirsaatadag is 180°N (Fig. 4.5C and D) however, there is also a high azimuth frequency sub-parallel to the anticline axis at 150°N. There is a distinct lack of azimuths around 090°N.

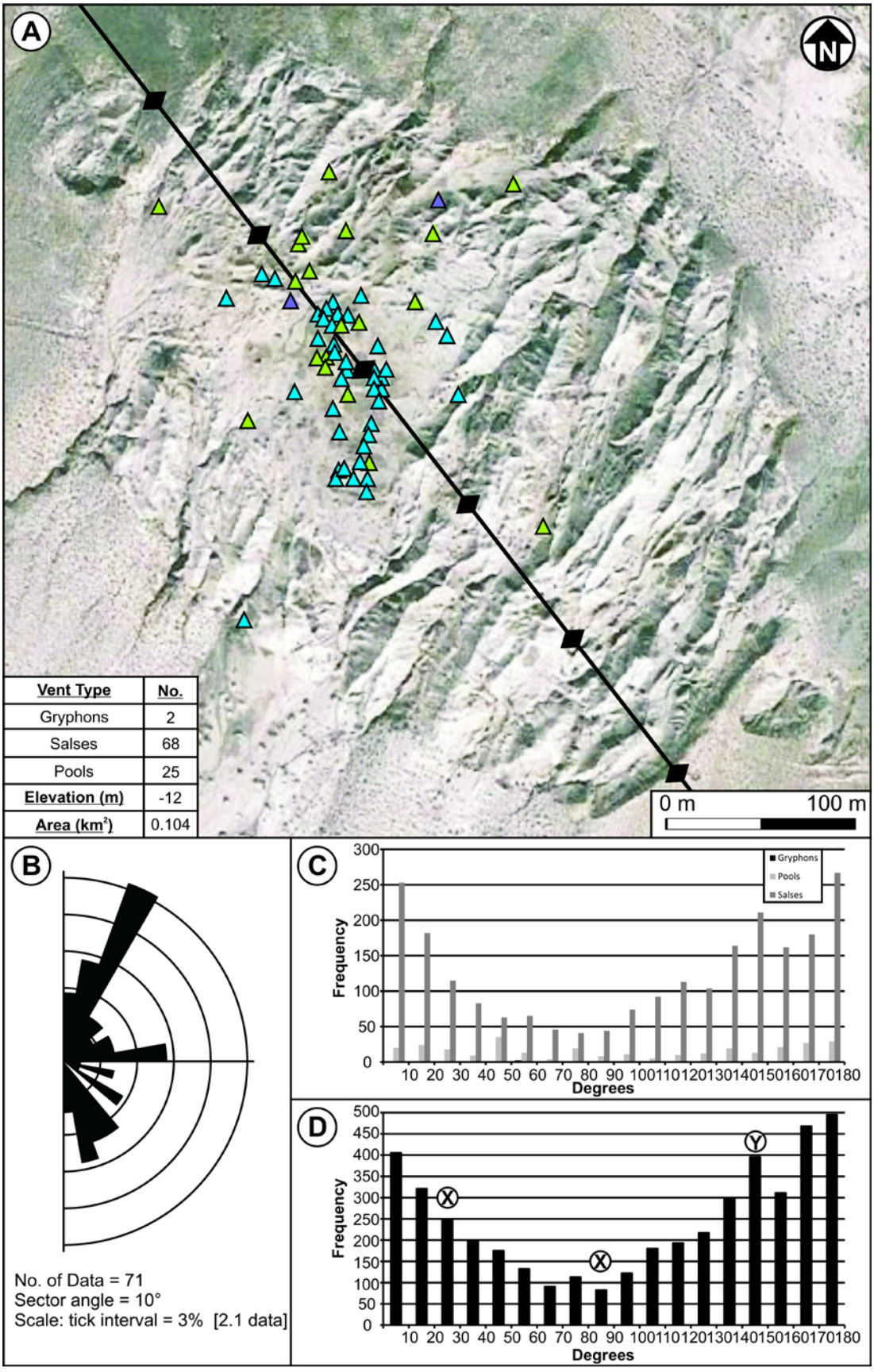

Fig. 4.5: A) Pirsaatadag mud volcano. Triangles: Purple- gryphons, orange- cinder mounds, black- extinct vents, blue- salses and green- pools. Image © 2010 GeoEye and © 2010 Geocentre

Consulting, © 2010 Google. B) Rose diagram of fault and fracture orientations from country rock in and around Pirsaatadag. C) Histogram of frequencies of azimuthal direction for 2-point azimuth technique of individual vent types separated into their different distributions. D) Histogram of frequencies of azimuthal direction for 2-point azimuth technique of all vent types grouped together.

4.4.4 Akhtarma-Karadag Mud Volcano

Akhtarma-Karadag outcrops along an ENE-WSW trending anticline axis and is also elongate parallel to this anticline axis (Fig. 4.1A and Fig. 4.6A). The active vent zone on the summit is found at the western end of the edifice (Fig. 4.6A). It has three eruptive compositions: cinder mounds, salses and gryphons.

There are three cinder mounds at the western edge of the mud volcano (Fig. 4.6A), only 1 m in height and diameter. The salses are found further towards the centre of the edifice and have a maximum diameter of 10 m. The main concentration of gryphons is closer (6 m) to the cinder mounds. There are also numerous dormant gryphons (Fig. 4.6A). The 2-point azimuth technique for Akhtarma-Karadag with vent types separated on the basis of fluid type shows a dominant azimuth frequency for gryphons and salses at 030°N whereas the pools tend to align at 120°N (Fig. 4.6B). When including all vent types in the 2-point azimuth analysis the dominant alignment can be seen to be at 070°N which does not align with the anticline axis oriented at 090°N (Fig. 4.6).

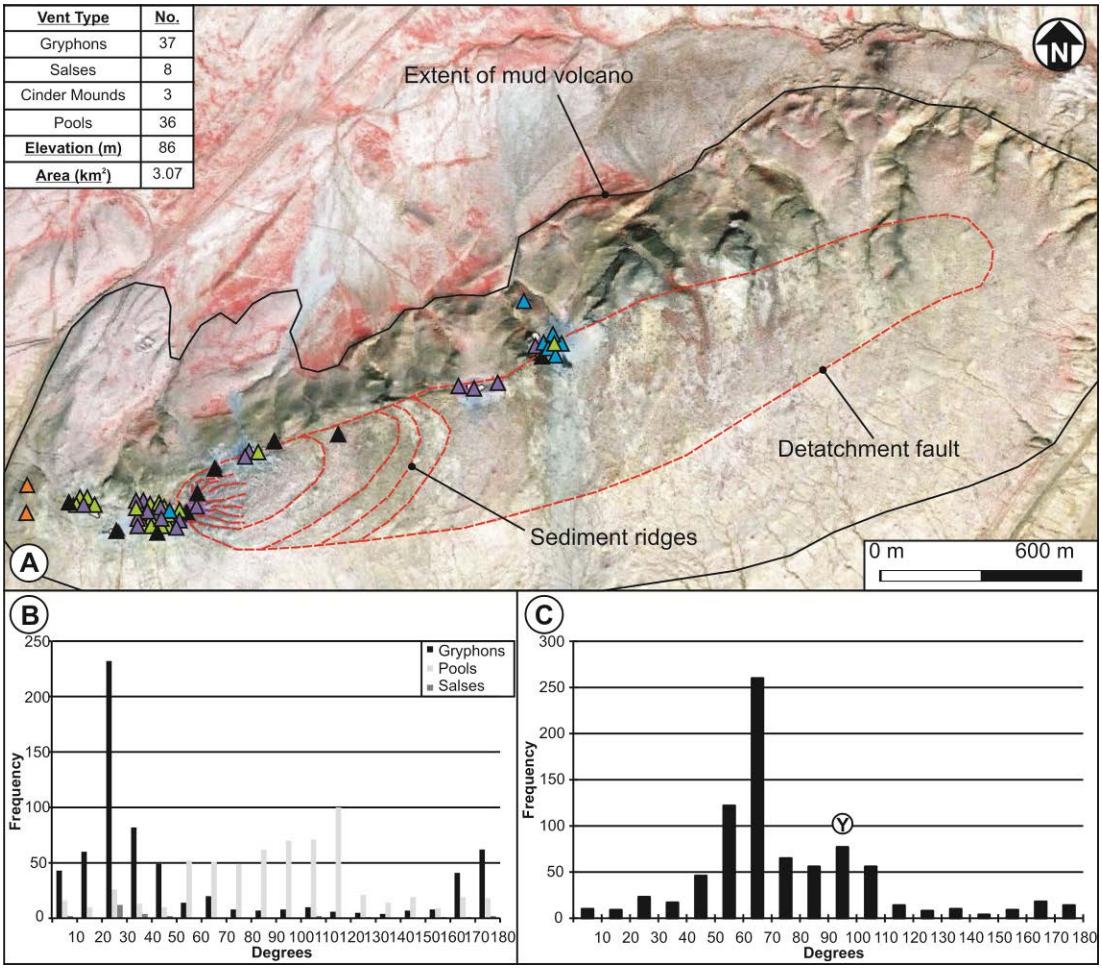

Fig. 4.6: A) Akhtarma-Karadag mud volcano. This volcano is dominated by gryphons at its western edge next to two small cinder mounds. The majority of the salses and larger gryphons extrude along an elongate ring detachment fault found along the length of the edifice (see Chapter 5; Roberts *et al.* 2011). The salses are found furthest away from the main centre of eruption further to the east of the volcano. Triangles: Purple- gryphons, orange- cinder mounds, black- extinct vents, blue- salses and green- pools. Image © 2010 GeoEye. B) Histogram of frequencies of azimuthal direction for 2-point azimuth technique of individual vent types separated into their different distributions. C) Histogram of frequencies of azimuthal direction for 2-point azimuth technique of all vent types grouped together.

4.4.5 Dashgil Mud Volcano

Dashgil outcrops on the crest of the Dashgil fold (Fig. 4.1A) which is 6-8 km long, 3.5-4 km wide and trends in an E-W direction. The entire mud volcano can be seen with the active vent zone offset to the western end of the edifice (Fig. 4.7A).

There is a concentration of gryphons, 2-3 m in height, clustering at the centre of 200 m diameter crater to the west of the volcano (Fig. 4.7A). A 200 m long row of 2-3 m high, 4-5 m wide cinder mounds trends in an E-W direction. These are only found in the south-eastern section of the volcano and form a sharp, straight boundary to the edge of the active vent zone. Dashgil also has two salses 20-30 m in diameter on its summit in the eastern portion of the mud volcano. These are comprised of several bubbling centres. There is also a small cluster of dormant gryphons in the northern section of the volcano.

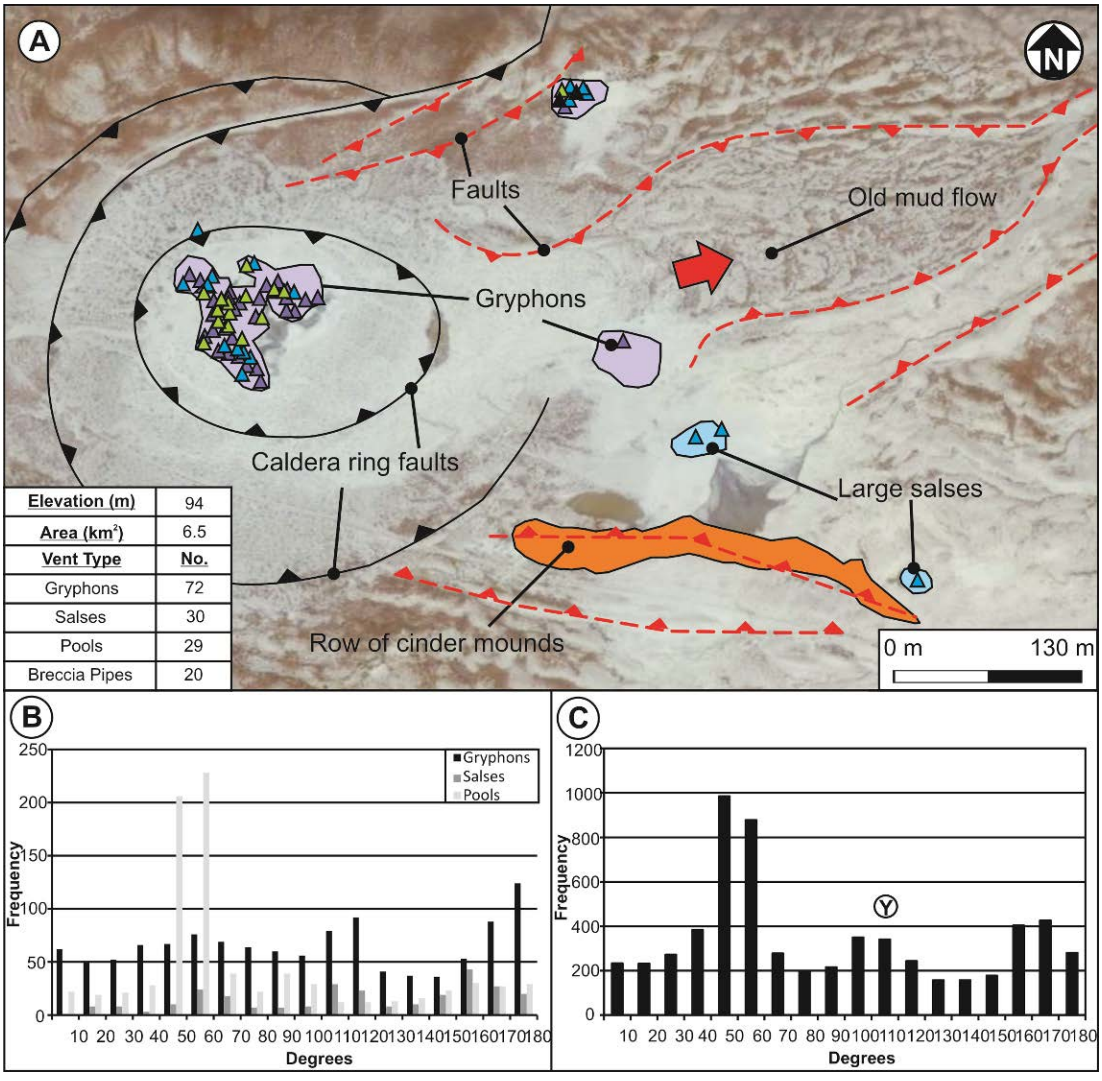

Fig. 4.7: A) Dashgil mud volcano zoomed in on the active vent zone. Gryphons can be seen clustering in the western section of the volcano. Cinder mounds form an elongate ridge at the southern limit of the active vent zone and two large salses are found at the southeast end of the volcano. Triangles: Purple- gryphons, orange- cinder mounds, black- extinct vents, blue- salses and green- pools. Red lines show faults and black lines show breaks in slope, with triangles pointing

towards the downthrown side. Image © 2010 GeoEye and © 2010 Geocentre Consulting, © 2010 Google. B) Histogram of frequencies of azimuthal direction for 2-point azimuth technique of individual vent types separated into their different distributions. C) Histogram of frequencies of azimuthal direction for 2-point azimuth technique of all vent types grouped together.

Both the combined and separate vent type 2-point azimuth results show that the dominant orientation in this system is at 050°N with sub-orientations at 100°N and 170°N (Fig. 4.7C). When separating different vent types from each other three 'peaks' in azimuth frequency can be seen for both gryphons and salses at 060°N, 110°N and 170°N whereas pools only have one dominant trend at 060°N (Fig. 4.7B).

4.4.6 Durovdag Mud Volcano

The crest of the volcano is dominated by gryphons and salses which are <2 m in height (Fig. 4.1A and Fig. 4.8A). There is a concentration of gryphons at the northern end of the volcano, with an average vent spacing of 5 m. Due to the un-stable nature of this region separate readings could not be taken and so the area has been considered as one large vent in the statistical analysis. The majority (~92%) of the remaining vents on the summit are found around the outer edge of the mud volcano forming an 800 m diameter 'ring' (Fig. 4.8A). The vents also align at tens of metre-scale, along linear conjugate paths within this 'ring' zone.

Durovdag volcano has a wide spread of vent azimuth frequencies which is also seen on a smaller scale at the centre of Kichik Kharami volcano (Fig. 4.4). The dominant orientation in this system is at 160°N with sub-orientations at 100°N and 020°N (Fig. 4.4).

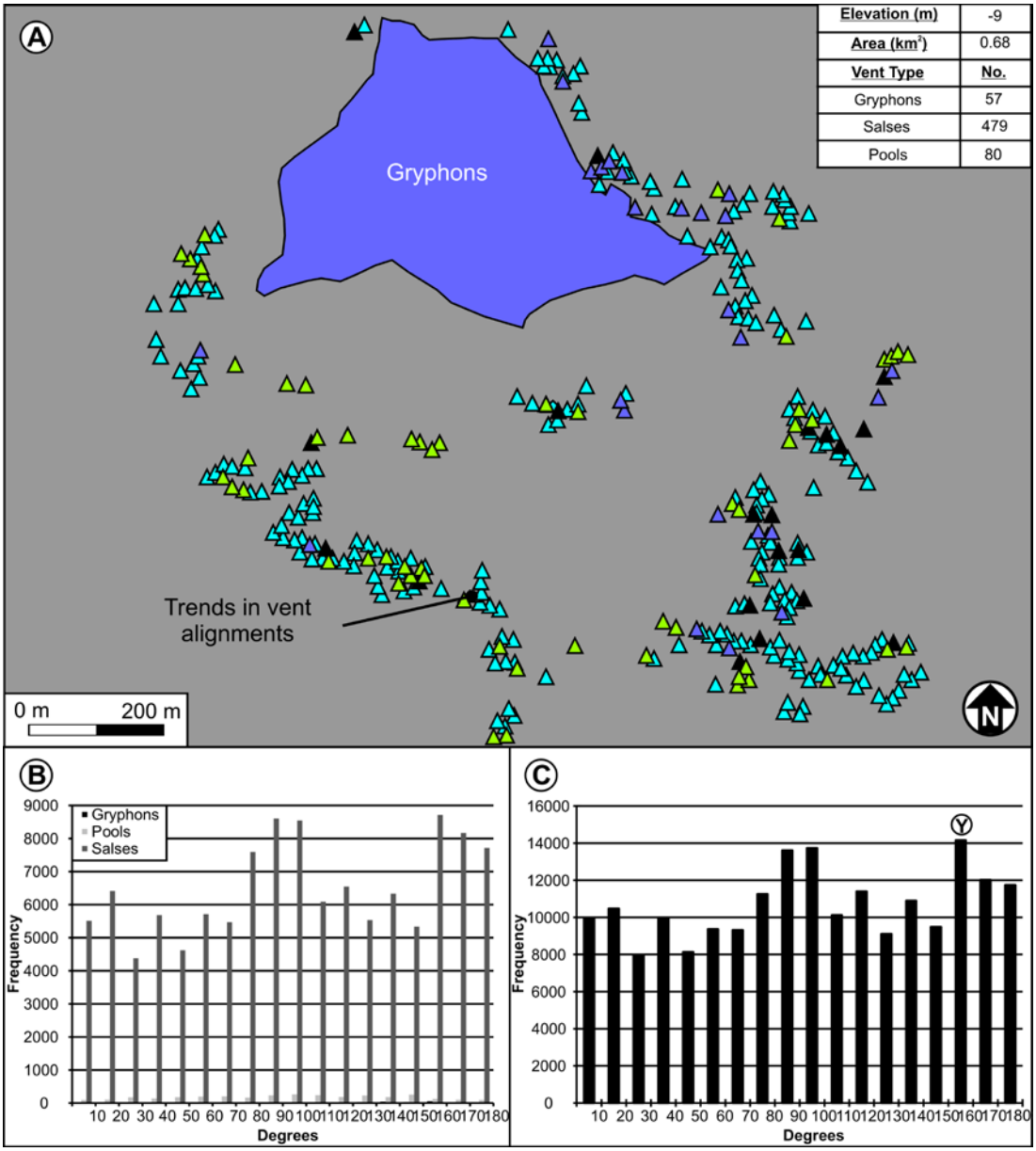

Fig. 4.8: A) Durovdag mud volcano. Showing that this volcano is dominated by gryphons at its northern edge. This purple area had such a large concentration of gryphons that the whole of this area has been coloured purple to represent the intense number of gryphons found in this region, approximately one gryphon every 5 m^2. Due to the un-stable nature of this area separate readings could not be taken and so the area has been considered as one large vent. The majority of the salses cluster in a ring around the outer edge of the mud volcano with only a few small vents and extinct vents at the centre of the edifice. Triangles: Purple- gryphons, orange- cinder mounds, black- extinct vents, blue- salses and green- pools. B) Histogram of frequencies of azimuthal direction for 2-point azimuth technique of individual vent types separated into their different distributions. C) Histogram of frequencies of azimuthal direction for 2-point azimuth technique of all vent types grouped together.

4.4.7 Lusi Mud Volcano, East Java

Lusi mud volcano is 3.4 km by 2.6 km in aerial extent and 7 m elevation (Fig. 4.9). The main active vent is 100 m in diameter and located at the centre of the edifice (Fig. 4.9). The first few vents were originally aligned in a NE-SW direction (Mazzini *et al.* 2007). A fracture hundreds of metres long and tens of centimetres wide was observed a few days after the eruption which also had a NE-SW orientation (Mazzini *et al.* 2007). This was interpreted as being the Watukosek fault which crosses the area (Fig. 4.9; Mazzini *et al.* 2007). Most of the early 'sandy' eruption sites discussed by Mazzini *et al.* (2007) were buried during the second week of June 2006, by the mud erupting from the main vent. New smaller vents started erupting in November 2006 approximately 1 km to the SW of the main crater (Mazzini *et al.* 2007). Currently there are 169 active vents (BPLS) although not all vent occurrences can be documented due to limited access to the majority of the edifice and because some are short lived. The vents near the main central vent had a roughly concentric pattern (Fig. 4.9A) whereas vents further away are closer to the observed faults in the region (Fig. 4.9A). Newer vents occur further away from the central vent and are now clustering close to the Kendensari River to the west of Lusi (Fig. 4.9B and C). These eruption sites erupt gas or suspensions of <20% mud in water.

The 2-point azimuth data for Lusi mud volcano (Fig. 4.9) show the vent distribution in 2006 a few months after it first erupted compared to the vent distributions seen in 2009 and 2010. In 2006 the dominant azimuth frequency is WNW-ESE (100°N), with two smaller trends at 060°N in a NE-SW orientation and 120°N in a NW-SE orientation (Fig. 4.9A). There is also a fairly large spread in azimuth frequencies apart from the dominant trends (Fig. 4.9A). In 2009 there are two dominant azimuthal trends at 010°N and 180°N with two less dominant trends at 100°N and 120°N (Fig. 4.9B). The dominant azimuthal orientation of vents in 2006 has now decreased in frequency. In 2010 this trend continues with the decreasing influence of the 060°N and 120°N alignments and increasing frequency of alignments at 010°N, 180°N (which are essentially the same trend) and 100°N (Fig. 4.9C)

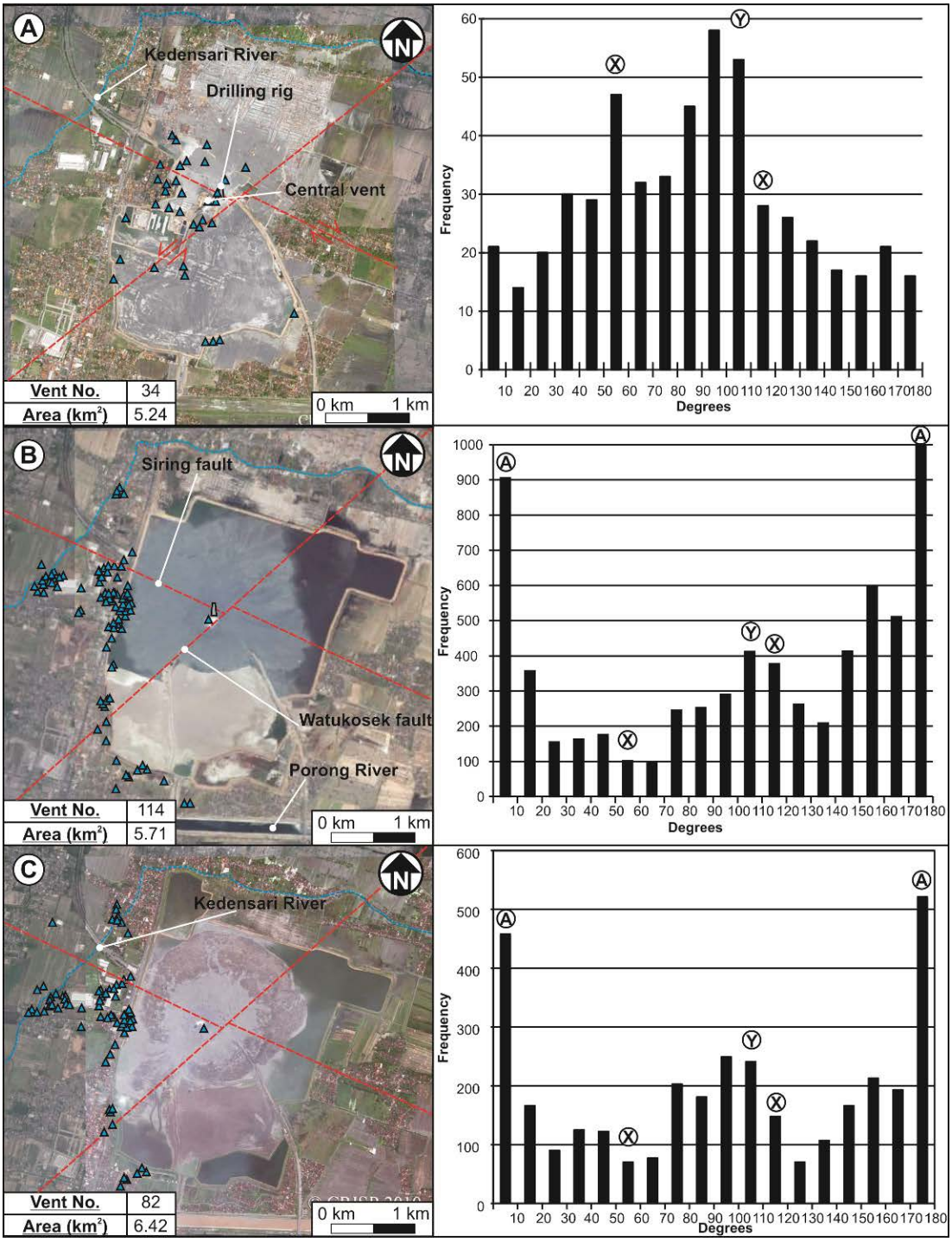

Fig. 4.9: Lusi mud volcano, East Java. A) November, 2006. Histogram of frequencies of azimuthal direction for 2-point azimuth technique of active vents in 2006. B) 30th September 2009. Histogram of frequencies of azimuthal direction for 2-point azimuth technique of active vents in 2009. C) January, 2010. Histogram of frequencies of azimuthal direction for 2-point azimuth technique of active vents in 2010. Blue dashed line shows trace of Kendensari River. The blue triangles represent 'bubbles' that are or were currently active at that time. Red dashed lines indicate faults described by Istadi *et al.* (2009). Images courtesy of CRISP.

4.4.8 Nearest Neighbour Analysis

It can be seen that all of the mud volcano vent systems nearest neighbour analyses are statistically 'clustered' to a significant value of <0.05 (Table 4.2). This clustering occurs around structural features. The 2-point azimuth results also indicate that there is a significant alignment of vents along mapped structural features. These statistical analyses indicate that fluid flow along structural features (faults, fractures and anticlines) may be enhanced in certain regions causing regions of vent clustering along the structures. It should be kept in mind that where vent spacing is <5 m the alignments identified will be less reliable. However there are clear visual and statistical alignments in vents that are consistent and geological sensible in areas where the vent spacing drops below 5 m.

Volcano	Observed Mean Distance (km)	Clustered/Dispersed	Significance Value	Critical Value	Z Score	Nearest Neighbour Observed Mean Distance (km)	Expected Mean Distance (km)	Nearest Neighbour Index
Dashgil	0.29	Clustered	0.01	-2.58	-14.34	0.000047	0.000161	0.291484
Durovdag	0.34	Clustered	0.01	-2.58	-31.44	0.000025	0.000072	0.34203
Akhtarma-Karadag	0.82	Clustered	0.05	-1.96	-2.22	0.000237	0.00029	0.818488
Kichik Kharami	0.55	Clustered	0.01	-2.58	-12.92	0.00007	0.000128	0.546609
Koturdag B	0.71	Clustered	0.01	-2.58	-6.18	0.000106	0.000149	0.714539
Koturdag C	0.51	Clustered	0.01	-2.58	-6.95	0.000047	0.000091	0.514191
Lusi	0.39	Clustered	0.01	-2.58	-12.39	0.003464	0.008802	0.393561

Table 4.2: Showing different mud volcanoes nearest neighbour statistical analysis results.

4.5 Discussion

These data reveal a significant degree of clustering and alignments of vents on mud volcanoes. The structural controls on permeability are now considered and this interpretation used to make a qualitative assessment of vent populations likely to form at Lusi.

4.5.1 Alignments

1) Alignment along anticline crests

It has previously been noted that kilometre-scale mud volcano systems align along the crest and hinges of anticlines (Fig. 4.10D; Devlin *et al.* 1999; Planke *et al.* 2003; Bonini 2007, 2008) and this observation is also made here. However, the 2-point azimuth technique also identifies a clear trend of both the kilometre-scale mud volcano systems and the metre-scale vents aligning on crests, and an alignment sub-parallel to the anticlinal trend evident in all mud volcano systems in this study (Fig. 4.3, Fig. 4.4, Fig. 4.5, Fig. 4.6, Fig. 4.7 and Fig. 4.8).

Koturdag B and C align along the axis of an anticlinal structure that forms the Alyaty Ridge at 130°N (Fig. 4.3A). Dominant trends at each of these volcanoes individually is also at 130°N showing that both the mud volcano systems as a whole and the metre-scale vent populations align in the same orientation as anticline axes. Fluids are most likely taking advantage of pathways produced by increased compressive shear failure in the anticlinal cores, and outer arc crestal faulting along the anticlines (Ramsay & Huber 1987). The folding has brought the overpressured Maykop Formation to a shallower depth in the subsurface and allowed thickening of these strata in the anticlinal hinges (Allen *et al.* 2003). This as well as the unloading of the anticlines during exhumation onshore and decreased overburden load on the anticlinal fold hinge compared to that on the limbs would decrease the force needed for the overpressured Maykop Formation to overcome the vertical stress and the tensile strength of the overburden (Magara 1981; Yassir & Bell 1996). These factors significantly increase the potential for the mud-water-gas mix to travel to the surface and erupt along these planes of weakness (Yusifov & Rabinowitz 2004).

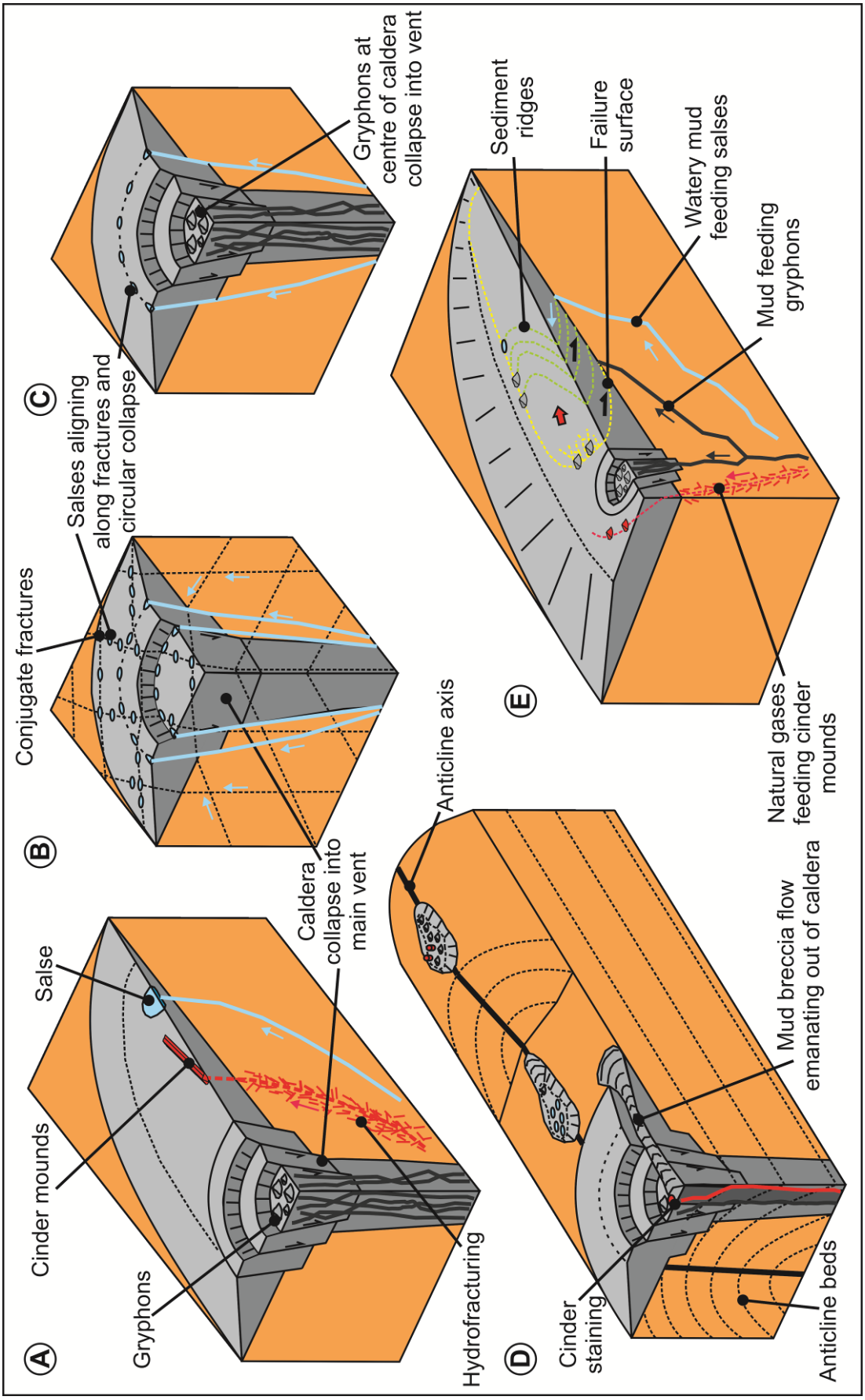
A
Salse
Cinder mounds
Gryphons
B
Conjugate fractures
Salses aligning along fractures and circular collapse
Caldera collapse into main vent
C
Gryphons at centre of caldera collapse into vent
D
Anticline axis
Hydrofracturing
Mud breccia flow emanating out of caldera
Cinder staining
Anticline beds
E
Sediment ridges
Failure surface
Watery mud feeding salses
Mud feeding gryphons
Natural gases feeding cinder mounds
1
1

Fig. 4.10: Schematics of the structures that may cause the varying vent distributions. A) Dashgil type, some form of phase segregation is occurring at depth allowing the gryphons to erupt in the area of caldera collapse, the cinder mounds to follow a linear area of weakness and so erupt in a line and the watery salses erupt further away from the main vent zone. B) Kichik Kharami type, where small salses line up along pre-existing conjugate fractures and also concentrically at the centre of the edifice where caldera collapse may be initiating. C) Durovdag type, where some form of phase segregation is occurring at depth allowing the gryphons to erupt in the central zone of caldera collapse beneath the main vent, with the watery salses erupting further away from the main vent zone along concentric ring faults produced during caldera collapse. D) Koturdag type, where mud volcanoes can be seen aligning along anticline axes but have varying vent fluid compositions along the length of the anticline. E) Akhtarma-Karadag type, some form of phase segregation is occurring at depth allowing the gryphons to erupt in the area of caldera collapse, the cinder mounds to follow a linear area of weakness and so erupt in a line and the watery salses to erupt further away from the main vent zone along the detachment fault.

Mud volcanoes also tend to become elongate in the direction of the anticline axis as seen by many of the examples in this chapter (Fig. 4.3, Fig. 4.4, Fig. 4.5, Fig. 4.6, Fig. 4.7 and Fig. 4.8). Elongation of edifices is also seen in igneous volcanoes and is generally parallel to the maximum horizontal stress (Nakamura 1977; Paulsen & Wilson 2010a). This is attributed to formation of vents along feeder dykes which orient parallel to the maximum stress and open perpendicular to the minimum horizontal stress (σ_{Hmin}; Paulsen & Wilson 2010a). In mud volcano systems and their vent populations this is not the case as they all extrude along or sub-parallel to anticline axes which form perpendicular to the maximum horizontal stress (σ_{Hmax}; Fig. 4.11). This is to be expected as the 'source' of the fluids and any mud chambers feeding the edifices would also become elongate perpendicular to the maximum horizontal stress (Fig. 4.11). The result of this being that vent populations on mud volcano edifices provide a good indicator of both palaeo- and current regional stress regimes.

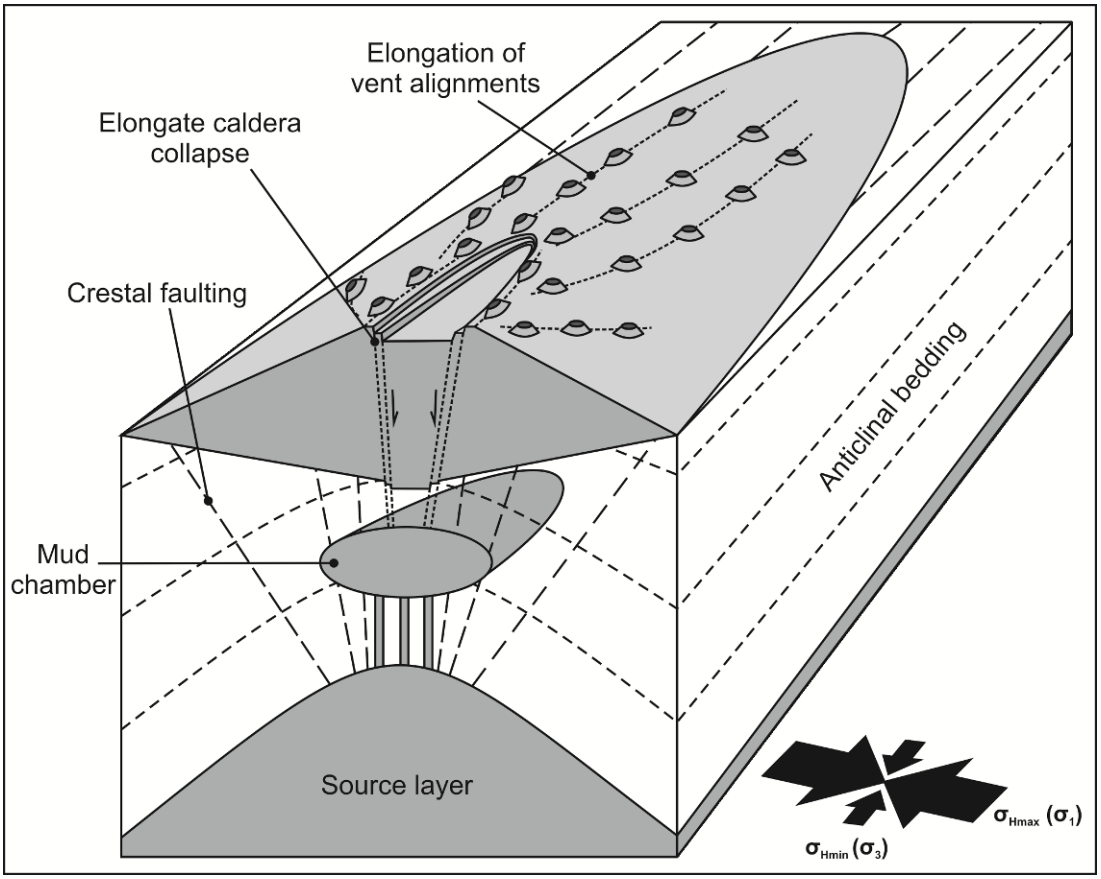

Fig. 4.11: Schematic model depicting mud volcano elongation, elongated vent distributions, mud chamber elongation and summit caldera elongation patterns. Mud dykes preferentially trend perpendicular to σ_{Hmax} taking advantage of the crestal faulting along the anticline. Summit calderas and mud chambers also become elongate perpendicular to σ_{Hmax}. After Paulsen & Wilson (2010a).

2) Alignment with fractures

Fault and fracture networks can act to either enhance or prevent fluid flow depending on their relative permeability to that of the surrounding country rock (Aydin 2000; Eichhubl & Boles 2000; Faulkner *et al.* 2010). When faults and fractures have high permeabilities they are able to act as pathways allowing fluids to utilise them as a conduit to the surface (e.g. Sibson 1996; Faulkner *et al.* 2010). A prominent characteristic of mud volcano systems are high fluid pressures, which may result in the formation of hydrofractures and shearing producing open fractures and dilatant faults (e.g. Aydin 2000). By comparing vent alignment orientations to structures mapped in close proximity it is possible to identify which fault and fracture systems have the highest permeability in a certain region. The cinder mounds on Dashgil are only found in a discrete elongate zone and so

probably form when gas venting from the mud volcano feeder complex travels along a pre-existing fault line (Fig. 4.10A). This faulted zone may intersect a mud chamber that has separated phases of gas, water and mud within it. Periodically the pressure in this chamber would become high enough to overcome the tensile strength and minimum horizontal stress producing new hydrofractures in a similar way to fault-valve behaviour allowing fluids to erupt at the surface as discrete events (Sibson 1990, 1992). This fault may even be an anticline crestal fault as the cinder mounds can be seen oriented in an E-W direction similar to that of the Dashgil Fold (Fig. 4.7A).

Kichik Kharami mud volcano is similar to Durovdag at its centre, with a 10 m diameter ring of salses forming along a circular collapse structure. However, 100 m out from the centre, the salses are aligned in rows in NW-SE (160°N) and NE-SW (100°N) directions (Fig. 4.4D and E). These orientations are coincident with the orientation of shear fractures (Fig. 4.4C) found on anticline flanks (Ramsay & Huber 1987) and both occur at 30° from the anticline axis orientation of 130°N. This implies that these have the highest permeability compared to other structures in the region (Fig. 4.10B). Dashgil also displays these fault arrangements (Fig. 4.7) with 'peaks' in both gryphon and salse azimuths occurring at 060°N and 170°N fracture orientations occurring at 60° to the anticline axis orientation (110°N).

3) Detachment fault alignment

Both active and extinct gryphons and salses on the Akhtarma-Karadag mud volcano align along a linear offset that can be traced around the summit of the volcano which is interpreted here as a detachment fault (Fig. 4.6 and Fig. 4.10E; see Chapter 5; Roberts *et al.* 2011). Pressure ridges of sediment can be seen at the centre of the detachment fault, suggesting that the mud volcano appears to be failing to the northeast (Fig. 4.6A). This movement is confirmed by the presence of plants being torn across the head of the detachment fault and en-echelon fracturing. This is again supported by the 2-point azimuth statistics which show the vents have a dominant orientation similar to that of the detachment fault at 070°N (Fig. 4.6C).

4) Ring fault alignment

Durovdag displays clear alignment of its vents with 92% of the gryphons and salses erupting around the periphery of the edifice (Fig. 4.8). This alignment is to be expected for a caldera collapse system (Stewart & Davies 2006; Evans *et al.* 2008) with the majority of the vents forming a 'ring' around the outer edge of the mud volcano (Fig. 4.10C). These fluids are taking advantage of ring faulting that is forming as a result of the gravitational collapse of the mud volcano. This distribution is displayed as a large spread of alignments on the 2-point azimuth histograms, as well as showing the slightly more dominant anticline axis alignment (160°N) and less dominant alignments that may be caused by fracture alignments (100°N and 020°N; Fig. 4.10C). On a metre-scale vents align in a conjugate pattern similar to shear fracturing on anticline limbs (Ramsay & Huber 1987). These metre-scale alignments occur around the trace of the kilometre-scale 'ring' fault itself (Fig. 4.8A). It is likely that these metre-scale conjugate vent alignments formed first aligning with the pre-existing anticline fractures. After this caldera collapse initiated and formed the more recent ring fault alignments which then overprinted the conjugate alignments to produce the dominant azimuth frequency. The concentration of gryphons to the north of the volcano indicates that there may be a large mud chamber beneath this area.

4.5.2 Distributions - Fractionation of Vent Eruptive Phases

Dashgil and Akhtarma-Karadag both produce three eruptive compositions, gaseous (cinder mounds), watery mud (salses) and viscous mud-water mix (gryphons). They also show a similar spatial distribution of erupting fluid types. Dashgil is dominated by gryphons on its westerly side, salses to the east and cinder mounds to the south of the active zone of the edifice (Fig. 4.7A). Akhtarma-Karadag has cinder mounds in the most westerly section, 5-10 m from an area of gryphons at the centre of the active zone and then salses at the easterly end of the volcano (Fig. 4.6A). From these observations it is possible to ascertain that these three phases must be separating some areas within the conduit and travelling to their points of eruption via different pathways. This has been noted by others in past studies at Dashgil

mud volcano (Mazzini *et al.* 2009). Mazzini *et al.* (2009) found that the water geochemistry highlights different water sources and reactions that occur at gryphons, pools, and salses. Gryphons have a signature of deep-rising fluids, while pools and salses show the imprint of meteoric fluids and a solute content increased by in situ evaporation (Mazzini *et al.* 2009). When integrating this with the observations it can be assumed that gryphons may be fed directly from a mud chamber in the main feeder complex of the mud volcano from depth whereas salses and cinder mounds are most likely sourced from shallow, smaller chambers that remain 'stagnant' for periods of time allowing them to interact with the surrounding meteoric fluids. When looking at vent type azimuth frequencies individually they show that gryphons and salses often display common orientations indicating that they may share similar fluid flow pathways in the subsurface (Fig. 4.3, Fig. 4.6 and Fig. 4.7). Pools show no correlation with other vent types agreeing with Mazzini *et al.* (2009) who suggested that these are only shallow fluid flow pathways that are not influenced by regional structure (Fig. 4.3, Fig. 4.6 and Fig. 4.7).

4.5.3 Time Dependent Changes – Lusi Mud Volcano

It has been noted that when Lusi initially erupted in 2006 its first few vents aligned in a NE-SW orientation (Fig. 4.9A) similar to the NE-SW trending faulting. This resulted in suggestions of a major fault (termed the Watukosek Fault Zone) passing through the Lusi eruption site and being a dominant control on fluid flow (Mazzini *et al.* 2007, 2009). In 2009, however, the dominant azimuth frequencies at 010°N and 180°N are most likely the result of the majority of vents being covered by mud and others occurring in populated areas where they are more likely to be identified. This could account for the high proportion of vents located near roads, dam walls and high density urban areas. This may also be the result of loading in this region allowing focused fluid flow in this orientation (e.g. Londe 1987). Because of this possible influence this study now focuses on the second most dominant alignments in 2009 and 2010.

The NE-SW trend evolved to have a dominant vent azimuthal direction of E-W (100°N) in 2009 (Fig. 4.9B), becoming even more prominent in 2010 (Fig. 4.9C). This evolution of the vent alignments has occurred in only 9 months and implies that the fluid pathways themselves are developing during a similar time period. It also suggests that an important E-W trending, regional scale anticlinal structure influences the feeder system architecture, reducing the influence of the local NE-SW faults. Also in the 2009 and 2010 data (Fig. 4.9) there is a 120°N trend which is sub-parallel with the NW-SE Siring fault that cross-cuts the region. From the aerial mapping it can be seen that some of the new vents are aligning with the Kendensari River (Fig. 4.9; see Appendix III for a figure illustrating the growth of Lusi mud volcano). The river in the region where the vents are erupting is very straight and has the same orientation of the major fault trends in the area. From these observations it can be inferred that there may be a fault in this area which is being exploited by the river and is now a locus for eruptions.

The present day orientation of the maximum horizontal stress (σ_{Hmax}) is NNE-SSW and has not changed during the formation of Lusi (Tingay *et al.* 2010). Lusi erupted along the crest of an anticlinal structure which trends in an E-W direction sub-perpendicular to the main stress field, a typical path exploited by mud volcanoes globally (Devlin *et al.* 1999), and indicates very deep fault trends. In 2009, E-W was also the dominant orientation of vents in the region (Fig. 4.9). Another control are the Miocene carbonates (2833-3500 m) that have been suggested as a possible source of the erupted fluids at depth (Davies *et al.* 2007). These carbonates were deposited on the structural 'highs' in an ENE-WSW orientation (Istadi *et al.* 2009). The evacuation of such large volumes of fluid and mud has induced subsidence (Abidin *et al.* 2008; Istadi *et al.* 2009) which in turn has probably resulted in faulting that could be being used as a conduit for fluid flow. The orientation of the Miocene carbonate build-ups and the anticlinal structure are intimately linked and share a common orientation indicating that these are most likely to be the dominant controls on the evolution of Lusi's fluid flow pathways. The fact that so few vents are erupting the same fluid as the main Lusi vent, and most are thought to be very shallow rooted, suggests that the fluid pathways and source for the main vent and

the smaller vents may differ. One preferred interpretation is that many of the water eruptions are coming from *c.* 290-900 m deep aquifers (Tingay *et al.* 2008) that have become faulted due to the subsidence resulting in seal breakage and fluid flow.

A ring-like arrangement of vents is observed around the main central vent at Lusi (Fig. 4.9), similar to the pattern seen at Durovdag (Fig. 4.8). This could indicate that a ring fault has formed as a result of subsidence in the region due to the evacuation of large volumes of fluid from depth (Fukushima *et al.* 2009). Abidin *et al.* (2008) and Fukushima *et al.* (2009) both used time-lapse SAR interferograms from one year after the birth of the Lusi mud eruption in May 2006 to show subsidence over an ellipsoidal area of 12 km^2 centred on the main eruptive vent. Depletion of material and decrease of fluid pressure at depth were described as being the dominant cause of the subsidence. Fukushima *et al.* (2009) found that deflation of an oblate spheroid lying shallower than 1 km explains the observed displacements. This observation is supported by the 2010 azimuth data (Fig. 4.9C) that show a wider spread of azimuth trends than seen in 2009.

4.5.3.1 Mode of Formation

The first of Lusi's vent eruptions (seven vents forming a lineation oriented NE-SW during the first week of eruption (29th May; Mazzini *et al.* 2007) and increasing to 34 in November (BPLS)) in 2006 occurred in a NE-SW orientation, roughly 30° to the present day maximum horizontal stress ($\sigma1$, σ_{Hmax}) orientation of NNE-SSW (Mazzini *et al.* 2009; Sawolo *et al.* 2009; Tingay *et al.* 2010). This indicates that fluids first travelled up the highest permeability paths that were optimally oriented for sinistral shear failure in a strike-slip faulting stress regime (Fig. 4.12A) from the Miocene carbonates at >2800 m depth (Fig. 4.12A; Davies *et al.* 2008; Tingay 2010). This is analogous to the formation of Miocene shale dykes along faults in the Jerudong Anticline of Brunei (Tingay *et al.* 2005). It is well documented that faults can transmit significant volumes of fluids when active (Barton *et al.* 1995; Sibson 1996) especially if they have a higher permeability than the surrounding country

rock (Reitsma & Kueper 1994). Initial eruptions of mud near Lusi are consistent with fluid flow up a reactivated NE-SW trending strike-slip fault although this in no way indicates that the fault triggered the initial eruption (see Davies *et al.* 2008). The propagation of overpressured fluids is also thought to have increased the pore pressure so that it exceeded the minimum principal stress (σ3, σ_{Hmin}) and tensile strength of the surrounding rock resulting in hydrofracturing of the country rock around the vent and new eruptions (e.g. Jolly & Lonergan 2002). It should be noted however, that the alignments seen at Lusi may differ from those in Azerbaijan as it is not necessarily a naturally occurring mud volcano. The temperature of the fluids erupting at Lusi are around 70-100°C (Tingay 2010) whereas mud volcano fluids in Azerbaijan are classically around 10-20°C (Guliyev *et al.* 1994). This may be due to relatively rapid fluid ascent rates at Lusi compared to those in Azerbaijan where fluid flow pathways have been present for thousands of years. Lusi had an average mud and fluid flow rate of approximately 64,000 m^3/day over the first three years (Istadi *et al.* 2009; Tingay 2010) differing dramatically from most naturally occurring mud volcano systems. In Azerbaijan flow rates of only a few tens to hundreds of cubic metres per day occur, but can occasionally have eruptions that are short-lived (1-14 days) and extremely violent (100,000-1,000,000 m^3/day; Tingay 2010). When compared to mud volcanoes in Azerbaijan, Lusi is an extremely rapidly evolving system but this does not mean that the structural influences will differ and ultimately regional structure will govern both areas.

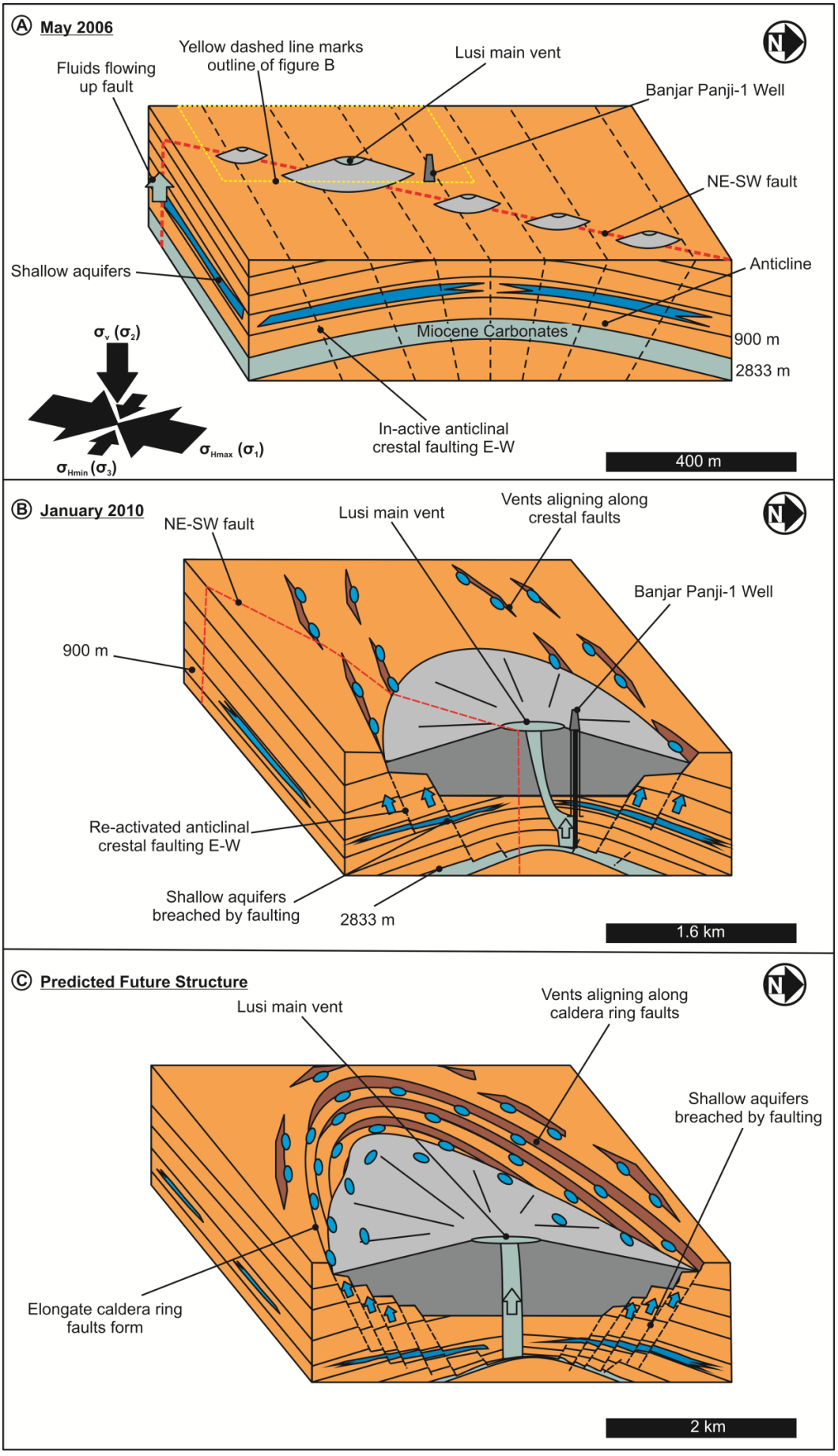
Ⓐ May 2006
Yellow dashed line marks outline of figure B
Fluids flowing up fault
Lusi main vent
Banjar Panji-1 Well
NE-SW fault
Shallow aquifers
Anticline
Miocene Carbonates
900 m
2833 m
In-active anticlinal crestal faulting E-W
400 m
σv (σ2)
σHmax (σ1)
σHmin (σ3)
Ⓑ January 2010
NE-SW fault
Lusi main vent
Vents aligning along crestal faults
Banjar Panji-1 Well
900 m
Re-activated anticlinal crestal faulting E-W
Shallow aquifers breached by faulting
2833 m
1.6 km
Ⓒ Predicted Future Structure
Lusi main vent
Vents aligning along caldera ring faults
Shallow aquifers breached by faulting
Elongate caldera ring faults form
2 km

Fig. 4.12: Schematic diagram of the mode of formation of Lusi mud volcano and how its vent systems have evolved through time. A) November 2006 with its initial NE-SW vent alignment. B) January 2010 with the initiation of caldera collapse with vents aligning along re-activated E-W trending anticline crestal faulting. C) Predicted future development including elongate caldera collapse structure with vents aligning along caldera ring faults.

As the feeder system evolved through time, the vent populations changed to an E-W orientation in 2009 and 2010 with a possible increase in vent formation along the confining dams due to the load they impose in N-S orientation (Londe 1987). From studies of mud volcanoes in Azerbaijan it is possible to make the assumption that older feeder systems naturally take advantage of pre-existing structures in the region (Fig. 4.12B). It is proposed that this change in orientation occurred due to a drop in pore fluid pressure in the system once the main source of overpressured fluid had been erupted. The decreased pore fluid pressure was lower than the tensile strength and minimum principle stress required to keep the original hydrofractures open resulting in closure of these pathways and decreasing their permeability (e.g. Jolly & Lonergan 2002).

In 2008 Lusi had erupted mud and fluids at an average rate of 64,000 m^3 per day producing subsidence up to 10 km away from the main vent (Abidin *et al.* 2008). This subsidence would be accommodated by the re-activation of the E-W trending crestal faulting along the anticline. During reactivation these faults would have breached aquifers located in the Pucangan Formation (280-900 m depth; Fig. 4.12B; Tingay *et al.* 2008). Overpressured fluids from these aquifers would use these high permeability re-activated faults as conduits to the surface. This is supported by the relatively low height of eruptions (1-3 m) indicating modest overpressure and that the pore fluid is not hydraulically connected to the source of the fluid for the main vent, where eruptions can be tens of metres in height. Almost none of the vents are erupting mud, indeed, a very large number are erupting fluids comprised of methane, CO^2, alkanes and a mix of both thermogenic and biogenic hydrocarbons (Mazzini *et al.* 2007; Sawolo *et al.* 2009). In this study the Miocene carbonates are proposed as the primary source of the fluids driving the eruption from the main

vent (Davies *et al.* 2008), because of the absence of other lithologies that could deliver fluid at the rates observed. However, other studies have suggested that the shallower Upper Kalibeng clays are the source of the majority of the fluids (Mazzini *et al.* 2007). These deposits also trend in an E-W orientation (Carter *et al.* 2005) and so subsequent subsidence in the vicinity of the reefal mounds could result in localised reactivation of pre-existing E-W faults. As the main vent continues to remobilise mud from the Kalibeng Formation (900-1870 m), this will load the surface and more subsidence will occur resulting in more faulting, aquifer breaches and new vent formation. When the system evolves further an elongate caldera collapse could develop, similar to the Porong collapse identified 8 km to the northeast of Lusi (Fig. 4.12C; Istadi *et al.* 2009). This will produce a vent azimuth distribution similar to that seen at Durovdag mud volcano, indeed the 2010 vent azimuth histogram is already exhibiting ring fault distribution more so than previous years.

4.6 Conclusions

The orientation of regional folds, faults and local metre- to kilometre-scale fractures, detachment and ring faults are the key control to the vent patterns in the mud volcanoes studied here. The most dominant vent orientations occur sub-parallel to anticline axes causing elongation of the volcanic edifice perpendicular to the regional maximum horizontal stress. If later detachment or ring faulting form this will then overprint the original sub-parallel anticline crestal faulting. Zonation of eruptive phase types also occurs implying that there is some form of fractionation beneath the edifices in either one large chamber or a network of smaller linked chambers.

The composition of the fluids being erupted and alignment of vents along anticline axes is significant as it will dictate how the edifice itself will accrete over time causing volcano edifices becoming elongate sub-parallel to anticline axes. Mud volcano alignments can occur on a range of scales from metre-scale vents that

erupt along crestal fractures to the 1-4 km systems that align along anticline axes. Lusi mud volcano is an example of how fluid flow pathways evolve through time from a localised kilometre-scale fault zone and hydrofracture system in 2006 to exploiting pre-existing pathways on the larger regional anticlinal structural control in 2009 and 2010. This evolution is likely to continue along this trend and in a similar ring fault style to that seen in Azerbaijan which could have major implications for the local population. It can be predicted that the flux of fluid flow up E-W orientated structures at Lusi will be more important than NE-SW and that as more subsidence occurs in the region more hazardous vents will form eventually producing multiple ring fault alignments and ultimately elongate caldera collapse up to 10 km away from the main vent as seen in palaeo-collapse structures in the region.

5 Sector Collapse of Mud Volcanoes, Azerbaijan[1]

Abstract

Field data collected from mud volcanoes in Azerbaijan are used to describe a process in mud volcano development that involves portions of the constructional edifices collapsing outwards in 'thin-skinned' slides. These events create kilometre-scale scarps that are tens of metres in height, arcuate in plan view, elongate and facing downdip. Similar morphological features occur on igneous volcanoes and have been described as 'sector collapse' structures. The largest sector collapses in igneous volcanoes involve some 10^{12} tons of mobilised material; equivalent structures in mud volcanoes are several orders of magnitude smaller. A shape parameter is employed that can be utilised in field and satellite-based mapping, to distinguish between slope failure and eruptive deposits. Three mud volcanoes with kilometre-scale sector collapses are described and controlling mechanisms are reviewed. The updip domains of these collapses are characterised by fluid escape showing there is also linkage to deeper mud volcano structure. The observations are reconciled in a model consisting of a deflating mud chamber that triggers thin-skinned sector collapse. The updip domain of the sector collapse is localised above a deep-seated zone of volume loss and the downdip domain of the collapse runs down the edifice flank on to the surrounding plain.

[1] This chapter is based on a paper that is in press in the journal 'Journal of the Geological Society, London'. Referenced as 'Roberts, K.S., Stewart, S.A., Davies, R.J. & Evans, R.J. (2011). Sector Collapse of Mud Volcanoes, Azerbaijan. *Journal of the Geological Society, London,* **168**, DOI: 10.1144/0016-76492010-115', see Appendix V.

5.1 Introduction

Mud volcanoes range in size from 0.01-5 km in diameter and occur in a range of tectonic settings, yet there are relatively few detailed descriptions of the morphology of kilometre-scale edifices (Milkov 2000; Kopf 2002; Planke *et al.* 2003; Yusifov & Rabinowitz 2004). Mud volcanoes are similar to igneous volcanoes in that they both form constructional edifices when erupting at the surface and can develop structural elements such as calderas and ring faulting (Evans *et al.* 2008). The structural development of mud volcano edifices has received some attention (Hovland *et al*. 1997; Davies & Stewart 2005; Mazzini *et al.* 2007; Evans *et al*. 2008; Mazzini *et al.* 2009; Roberts *et al.* 2010; see Chapter 3) but has been studied far less than their igneous equivalents (Fisher 1990; Kokelaar & Romagnoli 1995; Lipman 1997; Leyrit 2000; Geshi *et al.* 2002; Masson *et al.* 2002; Kennedy *et al.* 2004; Cole *et al.* 2005).

The aim of this chapter is to describe kilometre-scale collapse phenomena and related morphological features seen on mud volcano edifices based on field mapping in Azerbaijan, and to identify the most likely trigger mechanisms for collapse events. A particular difficulty in the study of mud volcanoes is distinguishing between features that are dominantly due to slope failure versus features that are largely the product of incision and erosion of the flanks during an eruptive event. These processes are distinguished between on the basis of geomorphological criteria and the overall dimensions of the deposits.

5.2 Geological Setting

The South Caspian Basin is known for its abundant kilometre-scale mud volcano systems (Guliyev *et al.* 2000; Milkov 2000; Aliyev *et al.* 2002). This concentration of mud volcano systems occurs due to the presence of the argillaceous Maykop Formation of Oligocene to Miocene age (Hudson *et al.* 2008) which has become overpressured due to disequilibrium compaction and mobilised by the addition of

fluids from depth (Kopf *et al.* 2003). The Maykop Formation is approximately 1 km thick and is buried to a depth 3.5-5 km in the area of this study (Allen *et al.* 2003). Mud volcano edifices are the extrusive termination of steep intrusive feeder complexes that are created by pressure at depth exceeding the lithostatic pressure resulting in hydrofracturing. This leads to intrusion of fluids and mud resulting in eventual stoping of the surrounding country rock (Stewart & Davies 2006; Deville & Guerlais 2009; Roberts *et al.* 2010; see Chapter 3).

5.3 Methods and Datasets

The edifices studied were Akhtarma-Karadag, Pilpilya and Lökbatan mud volcanoes, all located in Azerbaijan along the west coast of the Caspian Sea (Fig. 5.1). Mapping was carried out using a handheld global positioning system (GPS) receiver, with a positional accuracy of 5 m. Structural readings such as bedding and fracture and fold orientations were measured using a compass clinometer. The GPS co-ordinates with their corresponding structural datasets were integrated as layers in ArcMap software. The coordinate system for the data was input using spheroid WGS 1984. Areal imagery is from Digital Globe and IKONOS via Google Earth, all areal imagery has a resolution of 6.5-23 m. The volumes of scarps were calculated by splitting the scarp into smaller wedges, calculating their individual volumes and then summing them as a whole volume. The thickness of the wedges were considered to be the maximum height of the scarp at the head and then tapered to the height of the scarp at the base of the edifices, therefore making the volume calculations dependent on the chosen value of scarp height. Errors in these measurements may arise as volume calculations were based on scarp heights that may have been affected by erosive processes.

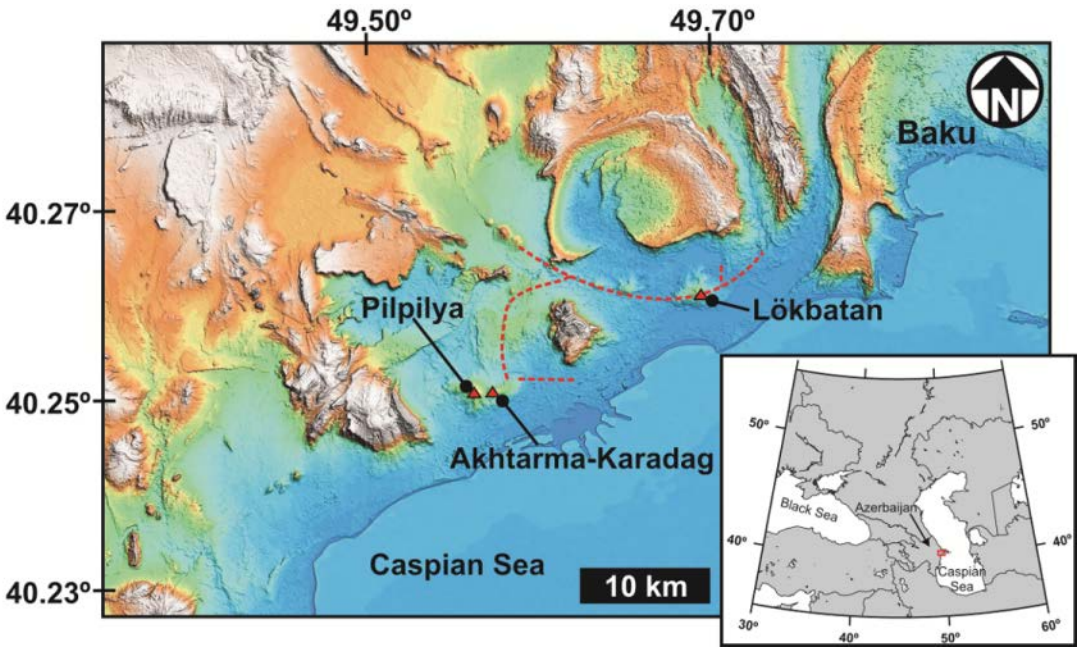

Fig. 5.1: Digital elevation map of the Caspian coastline in Azerbaijan showing the location of the study areas (localities marked with red triangles). Red dashed lines indicate presence of faults. Inset map of Azerbaijan shows map location as red box. White colouring indicates highest topographic areas with blue representing the lowest topographic areas.

5.4 Observations

A number of mud volcano edifices from the South Caspian Basin feature elongate collapse scars on their flanks. A detailed description of two representative collapse structures and their associated deposits is now provided, plus one feature interpreted as an incipient collapse structure. Locations are shown in Fig. 5.1.

5.4.1 Lökbatan Mud Volcano

Lökbatan is one of Azerbaijan's most active mud volcanoes, with twenty-two major eruptions from 1810-2010 (Aliyev *et al*. 2002; see Appendix I); it is located 15 km southwest of Baku (Fig. 5.1). Lökbatan is situated on the crest of an anticline of the same name which trends in an east-west orientation. The fold has a steeper northern limb (55-60°) than its relatively gentle southern limb (30-35°), and its crest is faulted. The plan-view shape of the mud volcano edifice is elongate, in contrast with many other examples documented in the area (Evans *et al.* 2008). Its plan-

view dimensions are *c.* 1.6 km by 0.9 km (Fig. 5.2) and its crest is 130 m above the level of the Caspian Sea.

The western flank of Lökbatan is characterised by an arcuate, elongate failure scarp measuring 1.62 km long in the dip direction. This feature was first described by Planke *et al.* (2003) as a 'western trending graben collapse structure'. The failure has a maximum width of 0.48 km and is 6 m high at the crest of the edifice (Fig. 5.2). The failure is orientated coaxially with the mud volcano edifice. Where the fault scarp is exposed it dips at 60-80° towards the collapse structure. There is no scarp at the downdip limit of the collapse structure. At the base of the scarp, 1-2 m high elongate mounds of mud breccias demarcate the sides of the failure.

Freshly erupted mud breccias occupy an area of *c.* 0.096 km^2 in the upper reaches of the area enclosed by this scarp. The contrast in colour and texture of the mud breccias, and their field relationships with the scarp, indicate that these were erupted some time after the main collapse structure developed (Fig. 5.2). Scholte *et al.* (2003) refer to this as a 'breccia field'. 'Megablocks' (Siebert 1984) occur within the main flow measuring up to 110 m in length (Fig. 5.2). The megablocks display a similar light grey colour to those of the flanks of the volcano when compared to the darker grey flow deposit within the collapse structure and the blue-grey of the younger mud breccia flows (Fig. 5.2). One indicator that these megablocks are not in-situ is that they rise from 2-5 m above the height of the flanks in their present location, suggesting that they came from a location further updip, where the fault scarp is higher. Also- in Fig. 5.2A, a wedge shaped megablock ('megablock A') can be 'fitted' back to where its height corresponds to the volcano flanks. The 'long axis' of this block is determined on the basis of variations in thickness of the block, with a view to establish whether the block has rotated about a steep or vertical axis (Fig. 5.2A). This method suggests that the block has moved 160 m down the flank and has been rotated 26° from its original long axis orientation (Fig. 5.2A).

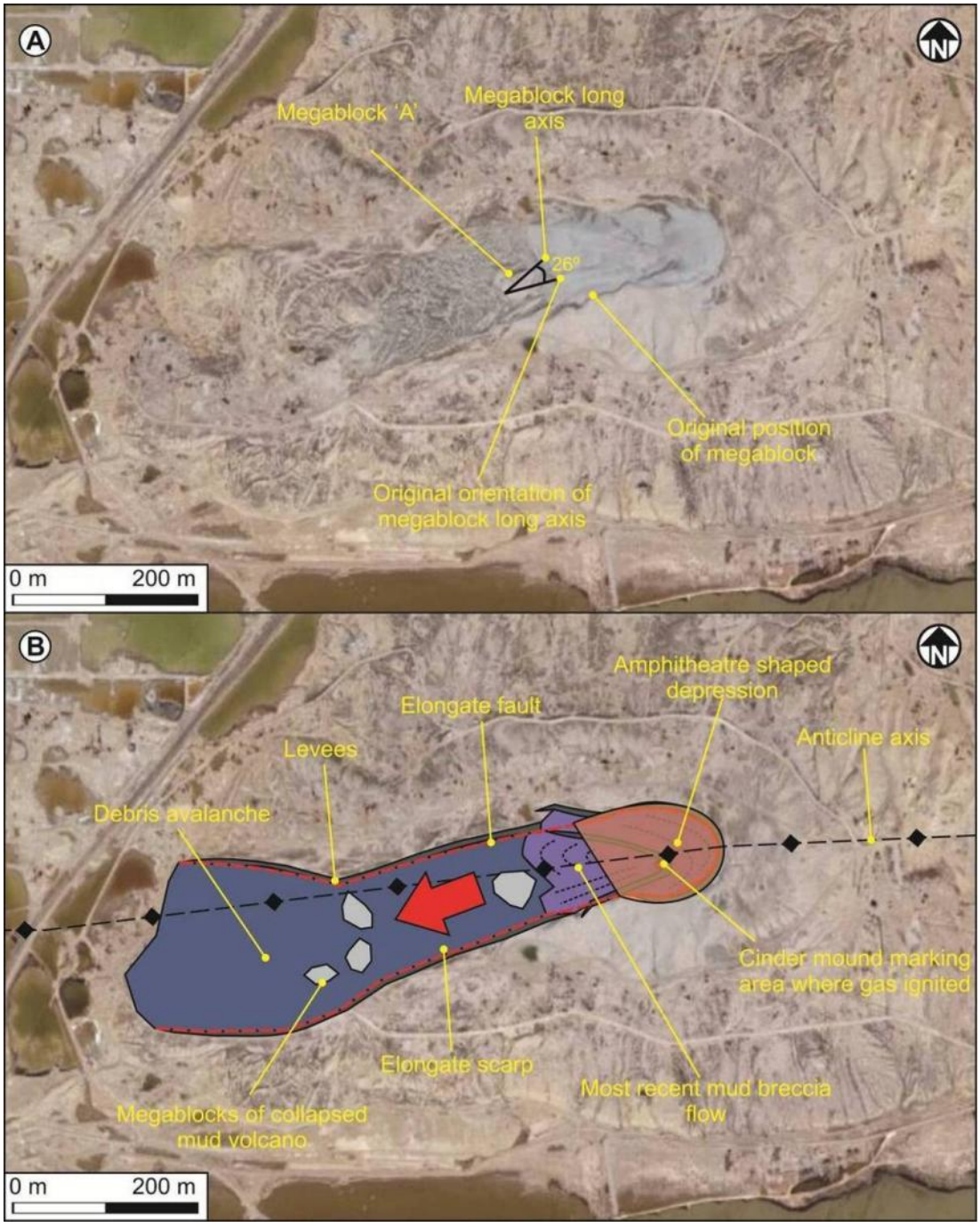

Fig. 5.2: A) Lökbatan mud volcano, Baku, Azerbaijan. B) The western flank of this volcano collapsed in 2001 during an eruption. Red arrow indicates the direction of the main failure. Amphitheatre shaped depression is shaded in orange. Old mud breccia flows are coloured in purple. Levees are dark brown. Edges of collapse structure are marked by the dashed red line. Image © 2010 DigitalGlobe, © 2010 Google.

5.4.2 Akhtarma-Karadag and Pilpilya Mud Volcanoes

These volcanoes are located on an east-west trending anticlinal structure 87 km southwest of Baku. Akhtarma-Karadag and Pilpilya are essentially two summits of a single elongate mud volcano (Fig. 5.3A), the summits being separated by a col tens of metres below the elevation of the adjacent highs. Each elongate summit area is characterised by kilometre-scale failure – that face in opposite directions to one another and are a few hundred metres apart at their closest approach.

Pilpilya, the westerly half of the mud volcano, has an almost circular plan-view shape measuring *c.* 2.06 by 1.90 km (Fig. 5.3B). The main active vent zone on the summit is found at the eastern end of the edifice. Although no vents are currently active on the volcano itself, a single, 200 m diameter active gryphon is located 500 m west of the mud volcano (Fig. 5.3B). Pilpilya has a failure structure *c.* 1.58 km in length and *c.* 240 m wide that has failed in a westerly direction (Fig. 5.3B).

The head-scarp at the top of the edifice is arcuate and *c.* 170 m wide. At the top of the edifice the scarp is 5.5 m high reducing to 20 cm at the base of the mud volcano flanks. The sides of the scarp dip steeply at 30-40° towards the collapse structure on all sides of the failure. At the base of the scarp 1-2 m high elongate mounds of breccias mark the sides of the failure. A major mud breccia eruption has occurred subsequent to the failure as a large breccia flow oversteps the debris avalanche (Fig. 5.3B).

A
N
0 km 1 km
B
N
Amphitheatre shaped depression
Old oil wells
Cinder mounds
Gryphons
Circular fault
Akhtarma-Karadag
Pilpilya
Elongate fault
Levees
Elongate scarp
Most recent mud breccia flow
Satellite gryphon
0 km 1 km
C
N
0 m 800 m
D
N
Gryphons
Smaller faults at highest point of ring fault
Fault forming around mud volcano
Sediment 'ridges'
Cinder mounds
0 m 800 m

Fig. 5.3: A) Akhtarma-Karadag mud volcano and west of it Pilpilya mud volcano with a collapse structure. Image © 2010 GeoEye, © 2010 Google. B) Interpretation of Fig. 5.3A. Red arrow indicates the direction the main slope failure has/could occur in. On Pilpilya the collapse and most recent flow can be seen to fail down the volcanoes western flank. C) IKONOS image of Akhtarma-Karadag mud volcano. D) Interpretation of Fig. 5.3C. Dotted black line shows fault trace. Purple areas represent gryphons and orange areas indicate regions where cinder mounds are present. Image © 2010 GeoEye.

Akhtarma-Karadag volcano is elongate and measures *c.* 2.15 km by 0.8 km in areal extent and 96 m elevation (Fig. 5.3C). The main active vent zone on the summit occurs at the western end of the edifice (Fig. 5.3C). This feature was first observed using satellite imagery that identified a closed, kilometre-scale elongate structure (Fig. 5.3C). Field mapping demonstrated the western end of this feature to be an arcuate fault (Fig. 5.3D). Displacement decreases from *c.* 1.5 m at the west end of the structure, to a centimetre-scale fracture zone at the eastern end, barely perceptible in the prevailing outcrop conditions (Fig. 5.4). The head of the break in slope at the western end of the volcano is arcuate and has several smaller fractures radiating from it in east-west orientations (Fig. 5.3D). There are several centimetre-to metre-scale kinematic shear sense indicators that have been identified from the incipient fault. The most prominent of these shear indicators being en-echelon fractures (Fig. 5.4B, inset) showing lateral movement towards the northeast. Freshly-exposed plant root systems span the main open fracture, and many gryphons and salses are coincident with the fracture zone (Fig. 5.4A and B). Another kinematic indicator are the 'sediment ridges' that occur within the structure, similar in form to pressure ridges seen in lava flows (Fig. 5.3; Sigurdsson *et al.* 2000). These also indicate movement to the northeast.

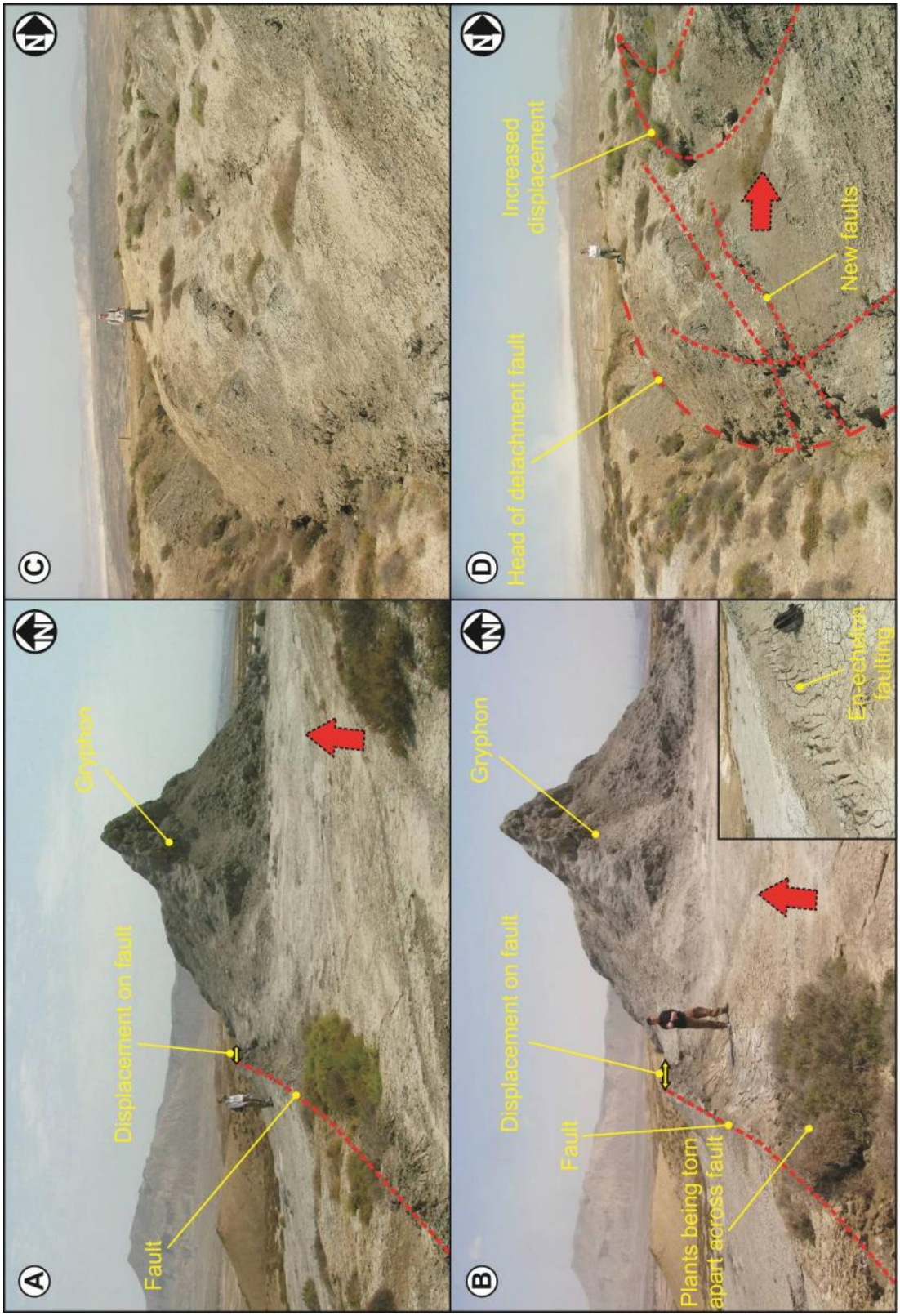
A
Gryphon
Displacement on fault
Fault
B
Gryphon
Displacement on fault
Fault
Plants being torn apart across fault
En-echelon faulting
C
D
Increased displacement
Head of detachment fault
New faults

Fig. 5.4: Photos of the Akhtarma-Karadag mud volcano, Azerbaijan. A) At northern side of ring fault, June, 2006 and B) April, 2009 with an inset photo of en-echelon faulting seen along the main ring fault. Rucksack for scale. The photos show a section of the ring fault (marked by the dashed red line) that has an offset on it. There is also a large gryphon that is erupting along this fault line. C) Photo taken at the head of the ring fault in June, 2005 and D) Photo taken at the head of the ring fault in June, 2006.

5.5 Interpretation

The main features described are elongate scarps on the flanks of mud volcanoes, mud breccia levees; arcuate-amphitheatre shaped craters and allochthonous megablocks. All of these features are consistent with thin-skinned failure of the margins of the mud volcano flanks (as opposed to deep-rooted caldera collapse) all of which are now described drawing parallels with equivalent structures documented on igneous volcanoes. Where possible, nomenclature used in igneous context by Ui *et al.* (2000) is followed.

5.5.1 Amphitheatre

The volume encompassed by an arcuate, updip part of a scarp that delimits a sector collapse is termed the 'amphitheatre' as the scarp forms a 'horseshoe' shape (Fig. 5.5; Leyrit 2000). This morphology is accentuated when the collapse is accompanied or overprinted by eruptive activity (Leyrit 2000). The walls of the amphitheatre are steep and reach several hundreds of metres height in igneous volcanoes. At Lökbatan and Pilpilya mud volcanoes these walls are steep but only reach 2-10 m in height.

The edge of the amphitheatre is defined by the footwall high of the sector collapse fault. Its height is controlled by the amount of fault displacement and the amount of material removed by the debris avalanche. The examples suggest that amphitheatre height in mud volcanoes is restricted to a maximum of *c.* 10 m.

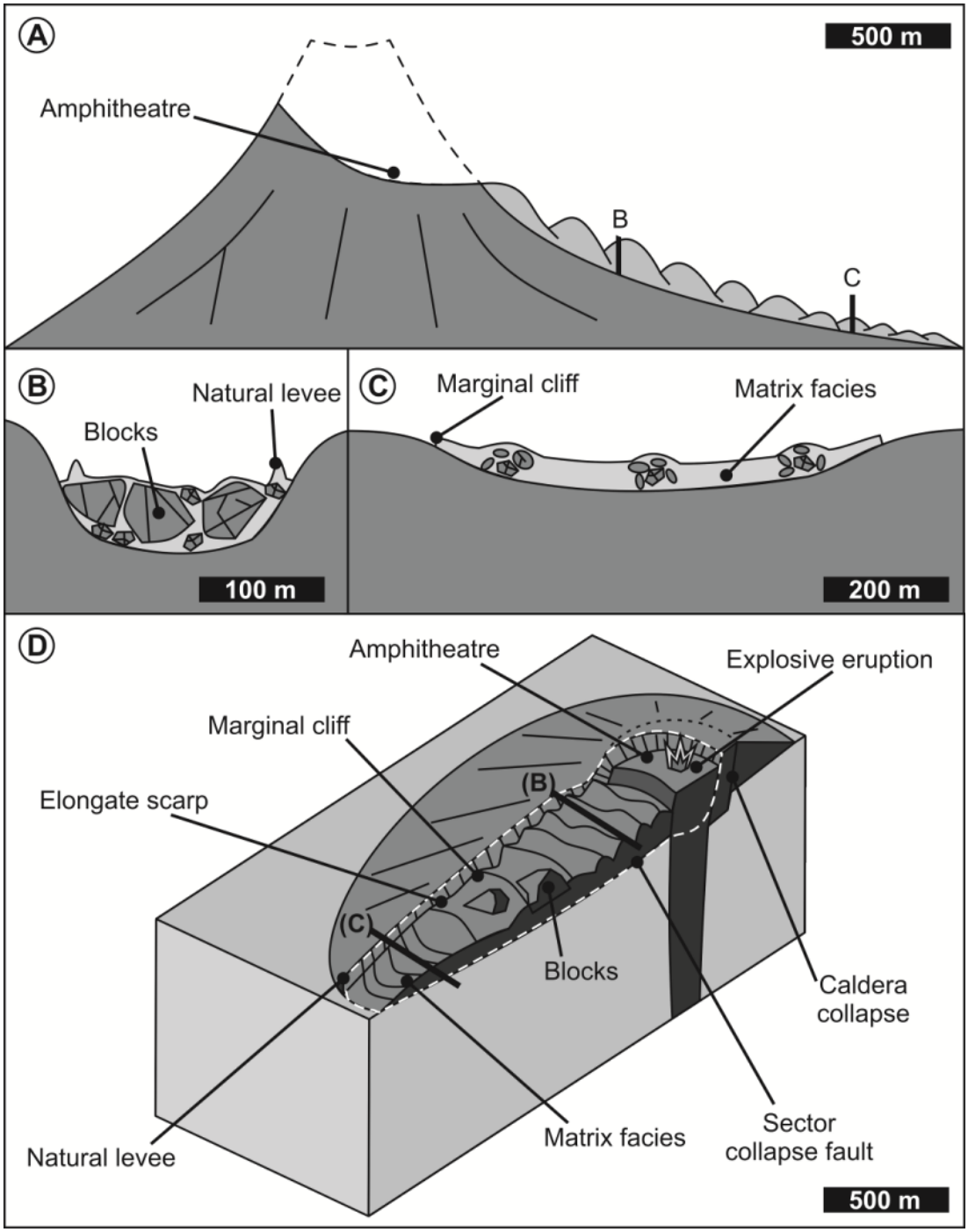

Fig. 5.5: Schematic of sector collapse of an igneous volcano after Ui *et al.* (2000). A) Longitudinal section of a sector collapse. The dashed line indicates the previous morphology of the volcano before the collapse took place. B) Cross section across the debris avalanche high on the flanks of the volcano- 'debris avalanche block facies', location (B). C) Cross section across the debris avalanche low down on the flanks of the volcano- 'debris avalanche matrix facies', location (C). D) 3-D schematic of mud volcano sector collapse with localities of cross sections B and C drawn on. White dashed line marks sector collapse fault.

5.5.2 Sector Collapse Fault

The margin of the amphitheatre is marked either by an inward-dipping scarp or a slope with a pronounced break at its base. This defines the 'elongate scarp' marking the limits of failure. This scarp varies in height from *c.* 10 m in the amphitheatre to less than 1 m at the downdip limit.

At Akhtarma-Karadag this fault is interpreted to be in an incipient stage at present. The elongate shape of this ring fault is similar in plan-view form to the failure at Lökbatan mud volcano. The dimensions of this structure are *c.* 1.2 km in length and *c.* 400 m wide, similar to the collapses mapped at Lökbatan and Pilpilya. The fault is currently active on the basis that exposed and broken plant root systems can be found spanning open fractures, en-echelon fracturing and sediment ridges (Fig. 5.4B, inset). Gryphons and salses coincident with this fault demonstrate active fluid flow preferentially localising on to the fault surface. This link between fluid flow and faulting argues against a purely thin-skinned interpretation along the whole length of the sector collapse fault (Fig. 5.4A and B).

Caldera collapse and sector collapse can be distinguished in terms of their bounding fault geometry. The lower tips of faults associated with calderas and ring complexes occur at depth in the subsurface below or within a volcanic edifice and could be described as 'thick-skinned collapse' (Fig. 5.6A). On the other hand the lower tip line of a fault or shear zone bounding a sector collapse outcrops at the surface on the volcano flank and can be considered as 'thin-skinned' failure (Fig. 5.6B). So in terms of peripheral, bounding structures (as opposed to internal structures), sector collapse structures should have a downdip domain characterised by surface expression of compression (which may be an overthrust or flow over laterally equivalent units), whereas caldera structures do not.

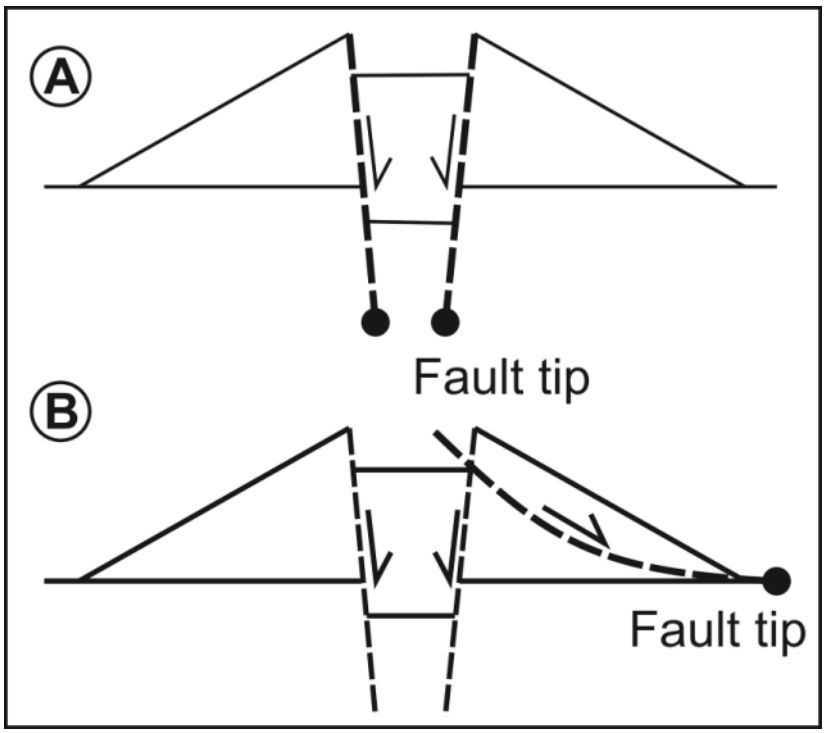

Fig. 5.6: A) Schematic diagram showing the positions of fault tips during caldera collapse and B) fault forming due to sector collapse of mud volcanoes.

Planke *et al.* (2003) describe the elongate portion of the sector collapse fault at Lökbatan as a 'graben collapse structure'. They suggest that this was caused by the presence of an elongated, shallow mud chamber within the crest of the anticline and that during an eruption mud was drained from the chamber resulting in subsidence and collapse of the roof, essentially viewing the whole structure as an elongate caldera. This study proposes an alternative interpretation, that the scarp was produced by a process of 'thin-skinned', detached collapse only indirectly linked to a deeper-seated deflating chamber. A critical piece of evidence supporting this interpretation is the presence of hummocky terrain, enclosed by the downdip portion of the elongate ring fault.

5.5.3 Levees

These morphological features form on the downthrown side of the elongate scarp and mark the edges of the debris avalanche field. They can be seen at both Lökbatan and Pilpilya. At the updip (headscarp) end of the collapse, the levees are between 2-4 m in height and towards the foot of the edifice they decrease to less

than 1 m in height. In cross section they have a wedge shape and in 3-D this wedge is sinuous, defining the edges of the debris avalanche deposit. This morphology is similar to debris avalanche levees common on igneous volcano sector collapse deposits (Siebert 1984), and also fluvial/alluvial levees (Adams *et al.* 2004). This similarity suggests that these processes share a common mode of formation. Levees form on mud volcano sector collapse flows as opposed to eruptive flows because sector collapse flows are geologically instantaneous, catastrophic events involving very poorly sorted material. As this debris avalanche moves downslope and outwards the levees build up in areas where flow boundary conditions are markedly non-uniform as flow energy decreases towards the outer edges of the avalanche. This process does not occur in eruptive flows as they often flow at an average rate of 0.5-2 m per year and are composed of a mass of mud breccia that flows downhill almost as a coherent block.

5.5.4 Debris Avalanche Deposit

These produce hummocky deposits of fragmented debris towards the base of volcanoes (Fig. 5.5D and Fig. 5.7B). Early igneous workers variously interpreted these hummocks as glacial moraines, phreatic blisters on the surface of gas-rich lava flows, small independent volcanic vents, lahars, or man-made features (Siebert 1984). Debris avalanche deposits in the case studies considered here consist primarily of the mud breccia that originally comprised the mud volcano edifice. Table 5.1 shows that the volumes of debris avalanches are comparable to those of the missing sectors of the cone, indicating that the dominant process is not input of new, erupted material, but slope failure of a pre-existing portion of the volcanic edifice.

Mud Volcano	Angle of Sector (°)	Length of Elongate Scarp (km)	Volume of Debris Avalances (m^3)	Volume of Scarp (m^3)	Angle of Repose (°)	Width of Elongate Scarp (km)	Area of Volcano (km^2)
Akhtarma-Karadag	35	1.6	-	-	6	0.9	5.8
Pilpilya	29	1.8	~$7.4*10^6$	~$7.3*10^6$	10	0.8	6.8
Lökbatan	28	1.7	~$7.4*10^6$	~$6.3*10^6$	10	0.8	5.8
Mount St Helens	36	15.4	$2.3*10^9$	-	15	3.5	70.4

Table 5.1: Dimensions of sector collapse structures discussed in the text. The 'angle of repose' is measured from the slope angle of the sector failure.

Debris avalanche deposits are poorly sorted and the dominant constituent is material of the volcanic edifice. Some freshly erupted material may be present, though this is hard to distinguish in mud volcanic eruptions if the deposits are old. Large fragments of the volcanic edifice, tens of metres in size or larger, termed 'megablocks' (Siebert 1984), can be incorporated in debris avalanches, for example at Lökbatan. Debris avalanche deposits display surface morphology with textural and morphological features characteristic of landslide deposits (Fig. 5.5; Siebert 1984). In particular, hummocky topography with numerous hills, closed depressions, and longitudinal and transverse ridges occur at both Lökbatan and Pilpilya (Fig. 5.5D and Fig. 5.7B). Mud volcano debris avalanches are more easily eroded than those at igneous volcanoes and so are relatively inconspicuous.

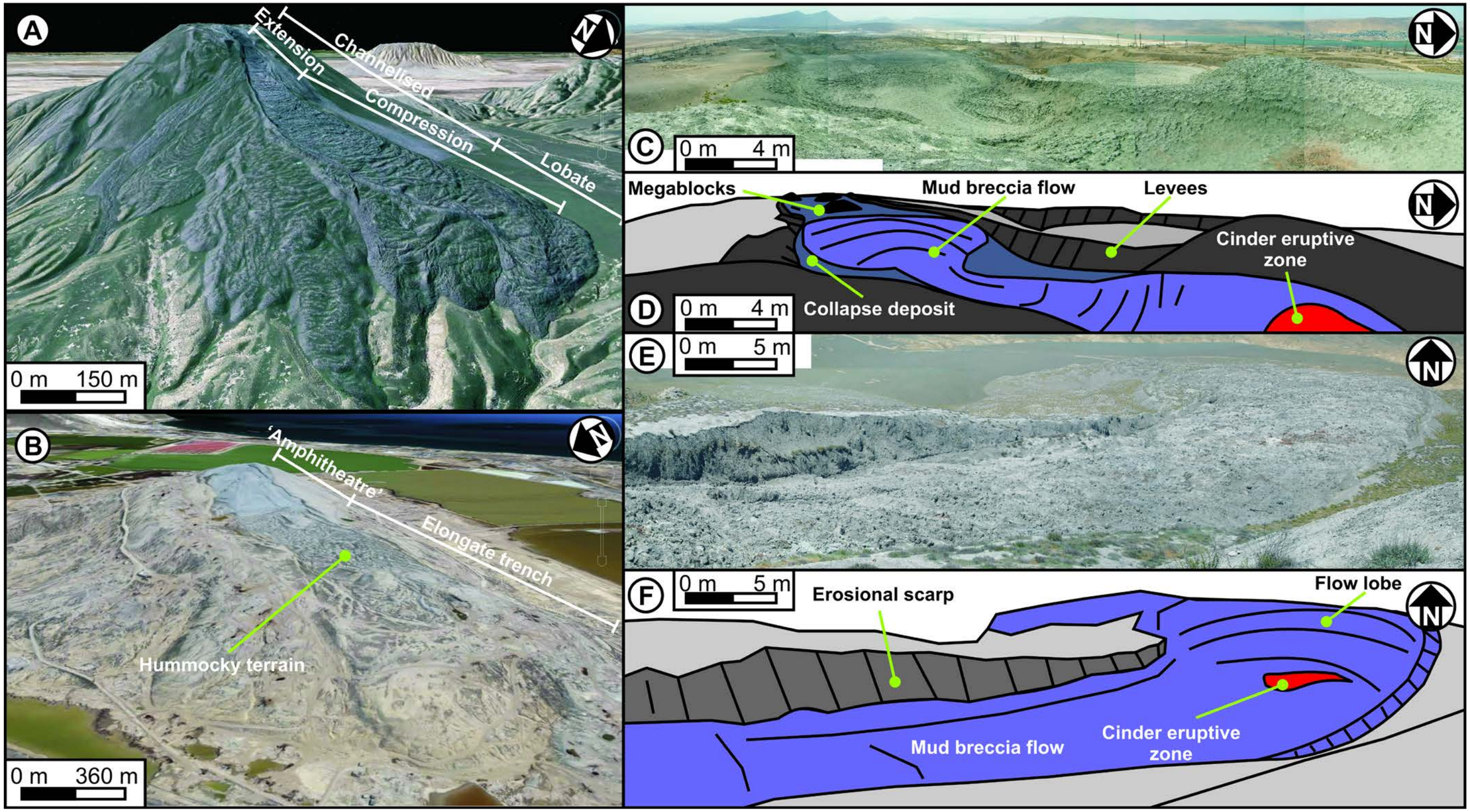

Fig. 5.7: Structure of mud breccia flows compared to collapse deposits. A) Mud breccia flow emanating from Koturdag crater (3 times vertical exaggeration). Image © 2010 GeoEye, © 2010 Google. Koturdag mud volcano is located 30 km southwest of Pilpilya. B) Elongate collapse structure on Lökbatan (3 times vertical exaggeration). Image © 2010 DigitalGlobe, © 2010 Google. C) Photograph of the elongate collapse structure on Lökbatan. D) Schematic of structural features seen in Fig. 5.7C. E) Photograph of the mud breccia flow emanating from Koturdag crater. F) Schematic of the structural features seen in Fig. 5.7E.

5.5.5 Eruptive Flow Versus Sector Collapse

It is not necessarily straightforward to distinguish between scarps produced by sector collapse and those excavated by erosive flow of erupted mud. However, there appear to be morphological differences between the kilometre-scale structures produced by these processes (Fig. 5.7). Mud breccia flows tend to be narrow, point-sourced phenomena originating near the top of the mud volcano edifice (Fig. 5.7A, E and F; Chow *et al.* 2006; see Appendix II for more examples of mud breccia flows). As they reach lower lying, gentler slopes they spread out into wider, lobate deposits. By contrast, sector collapses involve a whole segment of the flank moving down slope (Fig. 5.5, Fig. 5.7B, C and D; see Appendix II for more examples of sector collapses). The dimensions of eight sector collapses and twenty-one mud breccia flows were measured from areal imagery and are plotted on Fig. 5.8 (see Appendix II for raw data). Flows in this dataset were characterised on the basis of field work and/or diagnostic features recognised on areal imagery (levees, megablocks, sinuosity and colour (Fig. 5.7). The results show that the ratio of 'Bottom Width' (width at the most distal termination of the structure) to 'Average Width' (an average of the widths of the top and halfway down the structure) of the structures effectively distinguishes between the two failure modes with sector collapse ratio being ~1 and flows being greater than 1 (typically 2 or more; Fig. 5.8).

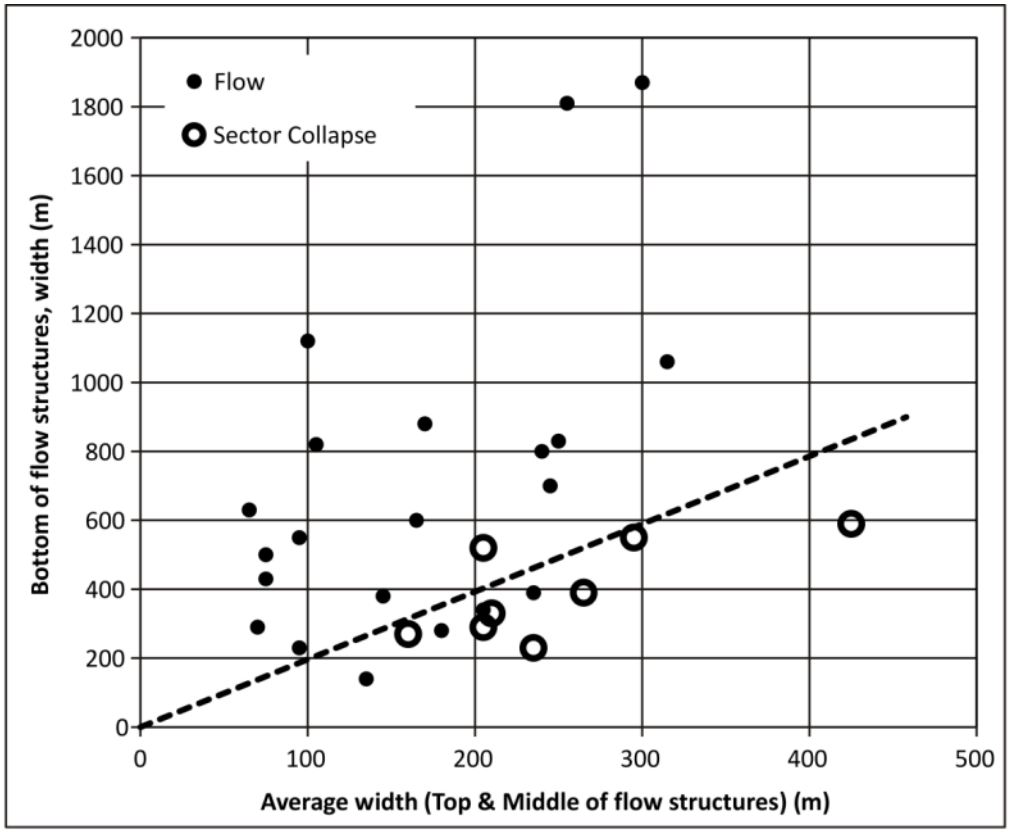

Fig. 5.8: Graph showing the relationship between length and widths of various structures on mud volcano edifices. Dashed line represents the transition zone between mud breccia flows and sector collapse geometries (depicting a 2:1 ratio).

Three end members of failure and resulting deposits on mud volcano flanks are identified here based on scale, and relative importance of slope failure versus eruptive processes (Fig. 5.9). Erosive flow of a mud breccia deposit can involve relatively long, meandering tongues of mud breccia that cut into the flanks of the volcano from which they emanate. They tend to spread out once they meet the plain on which the edifice is building (Fig. 5.7 and Fig. 5.8). At the foot of the flows pressure ridges build up giving them an appearance similar to 'ropey' lava flows (Fig. 5.7A; Sigurdsson *et al.* 2000).

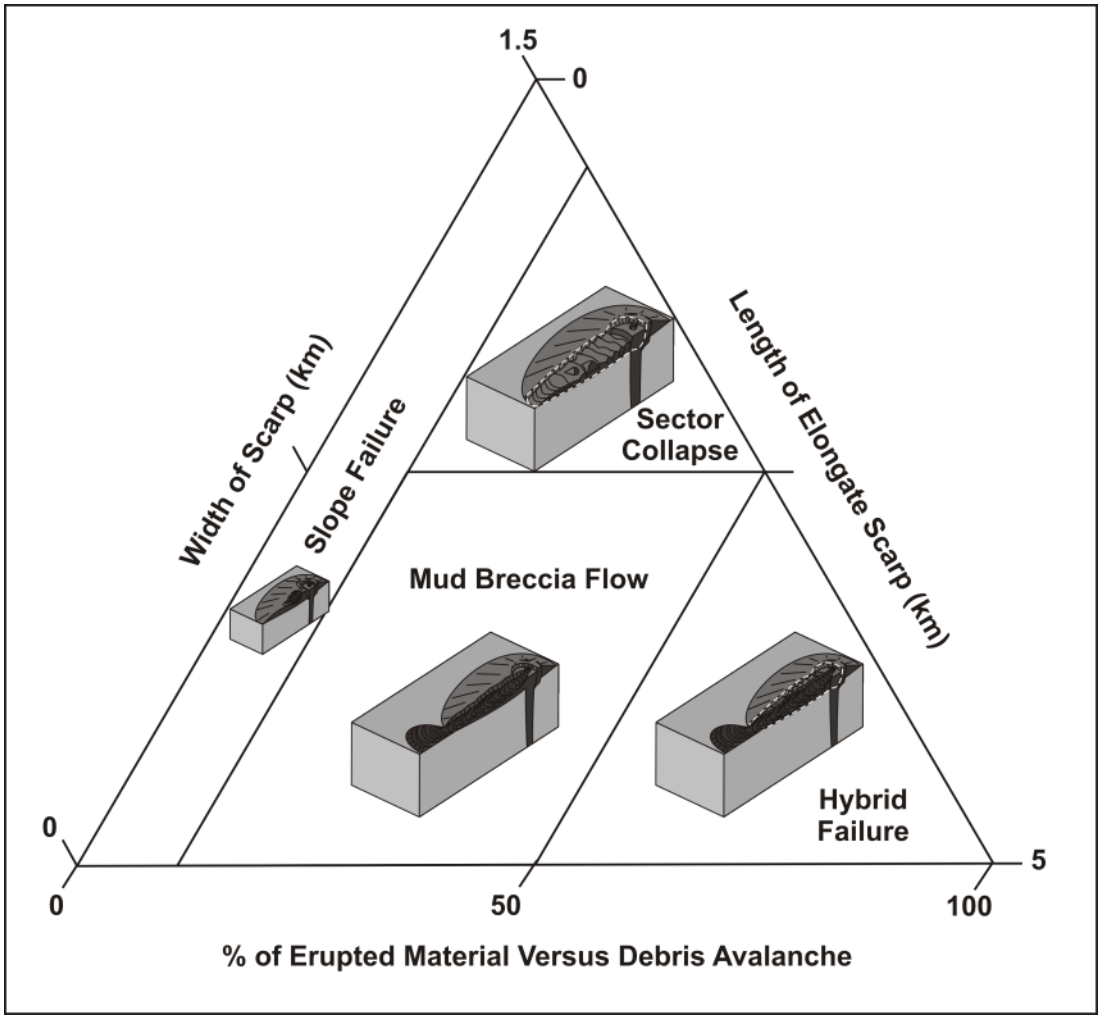

Fig. 5.9: Schematic ternary diagram showing the positions of mud breccia flows, sector collapses, slope failures and hybrid failures occurring on mud volcanoes in relation to the scarp length and width and the size of the feature. The internal structure of each deposit can also be seen in the block diagrams.

Sector collapse deposits have a low to moderate length and a uniform width throughout their length. Their internal structure resembles that of a debris avalanche with an extensional zone at the top and a compressional zone at the bottom of the deposit. Surface morphology of sector collapse deposits includes hummocky terrain and megablocks of the flanks of the volcano. Small slope failures (5-30 m length) also occur on the flanks of these volcanoes and structurally resemble the larger sector collapse deposits. They have short downslope length and relatively wide compared to their length.

5.6 Discussion: Mechanisms for Mud Volcano Sector Collapse

Sector collapses are well documented in the context of igneous volcanoes (Siebert *et al.* 1987; Van Wyk de Vries *et al.* 2000; Lundgren *et al.* 2003). In relation to igneous volcanoes these structures are in excess of tens of kilometres in extent, some of the largest examples involve approximately 10^{12} tons of mobilised material (Masson *et al.* 2002). Mud volcanoes are generally smaller than igneous volcanoes, so sector collapse of mud volcano edifices occupy a different scale range. The lower cut-off for length scale of sector collapse in mud volcanoes employed here is 1 km on the basis that these are substantial structures that are relatively easy to identify in the field and on seismic reflection data, and are of a scale to pose significant risk to subsea infrastructure.

A range of possible mechanisms may be involved in triggering sector collapse in mud volcanoes; it may be that actual events result from combinations of such factors. A brief review is presented here based in part on processes that have been discussed in relation to sector collapse in igneous settings (Fig. 5.10; Voight & Elsworth 1997). Most likely mechanisms for mud volcano sector collapse are highlighted;

Oversteepening of summit region of the volcano, for example tumescence due to mud injection could produce gravitational instability (Fig. 5.10A). Slope angles in the case studies reported here range from 6-10° (Table 5.1). On igneous volcanoes the majority of collapses occur on slopes of 28-30° (Voight & Elsworth 1997). The slope failures reported here from Azerbaijan do not, however, occur on the steepest parts of the edifice.

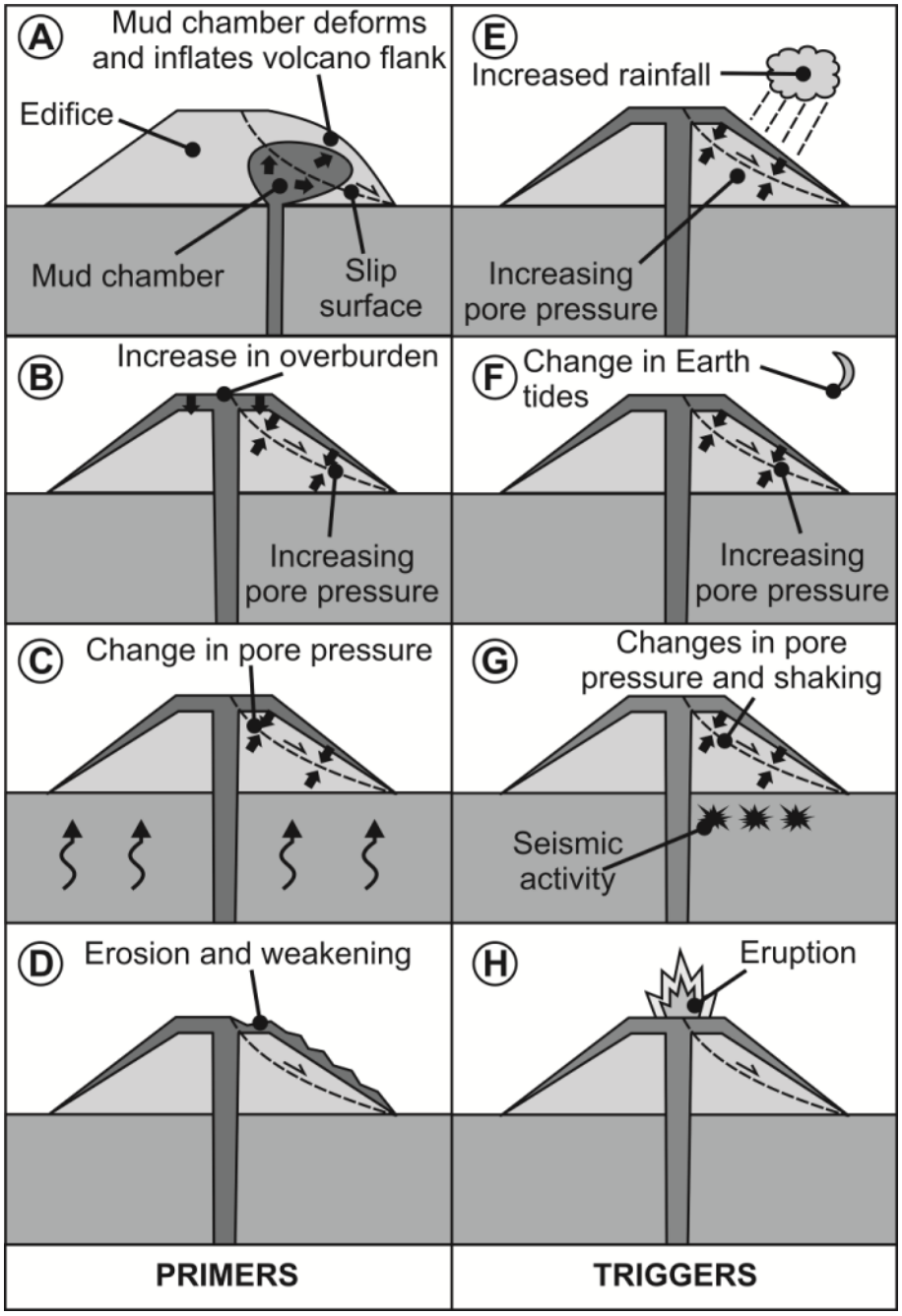

Fig. 5.10: Schematic diagrams showing primers and triggers of mud volcano sector collapse events. A) Inflation of mud chamber and volcano causing instability. B) Addition of overburden when mud breccia is erupted onto the volcano flanks. C) Change in pore pressure within the mud volcano. D) Erosion and removal of support. E) Precipitation increasing pore fluid and loading and therefore pore pressures. F) Earth tides exerting different gravitational forces on the mud source causing more or less violent eruptions. G) Seismicity shaking the ground and changing pore pressure in the mud volcanoes. H) Eruption of mud volcano.

Regional Stress Siebert *et al.* (1987) stated that the location of sector collapses within the igneous volcanic edifice can be influenced by local and regional stress

regimes. Swarms of mud volcano vents often occur parallel to the regional maximum horizontal compression (see Chapter 4; Roberts *et al.* 2010), resulting in the elongation of the volcanic edifice in that direction. In the Azerbaijani examples mud breccia flows show weak clustering in a northeast or southwest direction, generally flowing down the steepest topography (Fig. 5.11B; see Appendix II for more examples). By contrast, the sector collapse failures occur parallel to the direction of mud volcano edifice elongation, generally an east-west trend that is also parallel to the anticline axis at each location (Fig. 5.11C; see Appendix II for more examples). This relationship suggests that, while the sector collapses may be related to some aspect of mud volcano edifice geometry, they are not directly related to regional stress.

Loading of the volcano flanks by erupted mud breccia may cause increase in pore pressure resulting in collapse (Fig. 5.10B). Rainfall could be another significant loading factor in the onshore mud volcanoes in Azerbaijan. The climate is arid for much of the year and the mud flows become heavily fractured as they dry out - appreciable water load is absorbed in the wet season.

Overpressure of pore fluids in and around the mud volcano edifice may cause failure (Fig. 5.10C). If the sediments are sealed, pore pressure within them will increase, reducing the effective normal stress as well as shear strength of the sediment. No additional trigger is necessarily required; pore pressure can simply increase until the down-slope component of the gravitational force is greater than the shear strength of the sediment and its cohesion, at which point failure occurs.

Erosion can create steeper zones that are susceptible to de-stabilisation (Fig. 5.10D). It may also remove lateral support to slopes and so induce collapse.

Hydrothermal alteration along regional fracture sets also may be an important process in the localisation of sector collapse features (Lopez & Williams 1993; Reid *et al.* 2001; Reid 2004). Circulation of fluids (meteoric and hydrothermal) can result in an increase in pore water pressure.

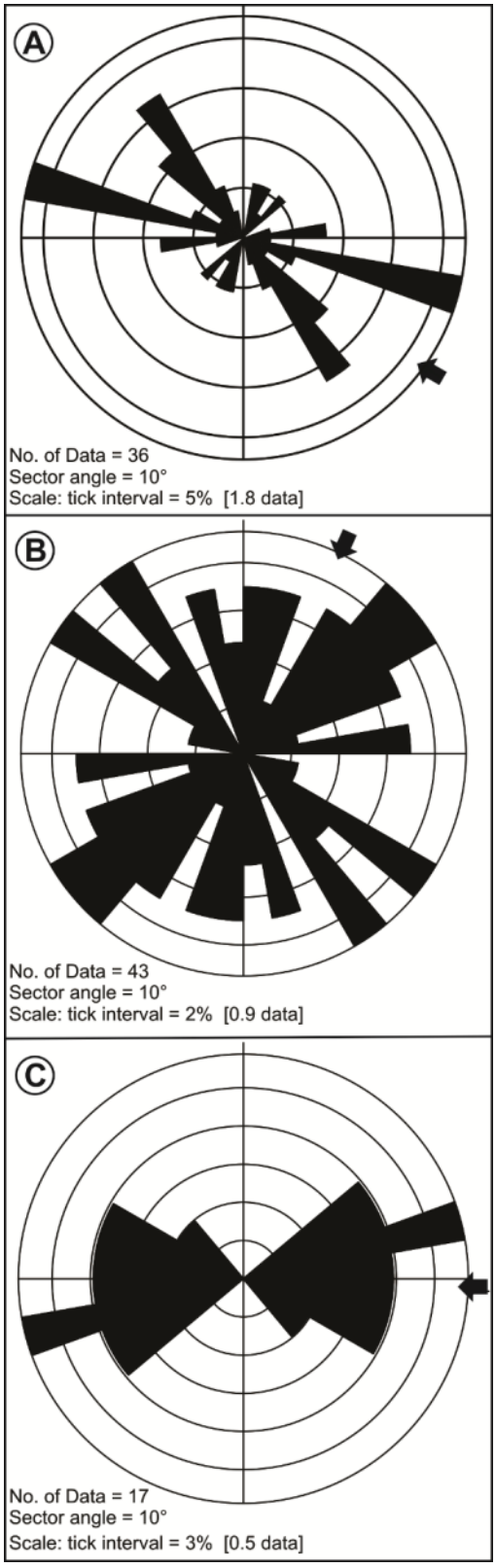

Fig. 5.11: Rose diagrams of orientations of A) long axes of mud volcano calderas, B) mud breccia flows and C) sector collapse troughs.

Seismic activity is a documented triggering factor of both igneous and mud volcano eruptions and collapses (Fig. 5.10G; Manga 2007; Manga *et al.* 2009). Continuous monitoring of Lökbatan mud volcano has indicated the occurrence of weak earthquakes during eruptions but it is not clear is these are a cause or effect of the eruption process.

Earth tides have been linked with both mud volcano and igneous volcano eruptive periodicity (Fig. 5.10F; Mauk & Johnston 1973; Aliyev *et al.* 2002).

Eruptions and fluid activity are involved in some 50% of all igneous sector collapses (Leyrit 2000). Lökbatan's first recorded eruption took place in 1864 (Aliyev *et al*. 2002; see Appendix I for eruption histories). The 2001 eruption involved ignited gas jets 50-60 m in height (Aliyev *et al*. 2002; Kadirov & Mukhtarov 2004) and 304 m^3 of erupted mud breccia (Aliyev *et al*. 2002). Sector collapse at Lökbatan may have coincided with the eruption on February 23, 1935. Aliyev *et al.* (2002) document this eruption as 'taking place without noise, gas and breccia emanation'. Aliyev *et al.* (2002) noted that step like subsidence occurred with landslides which were most likely the result of a collapse of the western portion of the volcano. The centre of the volcano then subsided up to 22 m and numerous fractures formed that then began to emit gas and breccia that covered up to 25,000 m^2 (Aliyev *et al*. 2002).

A broader summary of factors that may relate to sector collapse are tabulated in Table 5.2.

Inherent causes	Initial composition	
	Texture- loose, porous, weak materials are slide prone	
	Bedding attitude relative to slope face	
	Layering sequences in relation to strength, permeability	
	Discontinuity systems- faults, joints, bedding planes	
	Slope forming process history, movement history; bedding slip and fault slip history and orientation of movement	
	Initial physiochemical setting; conditions of weathering and alteration	
	History of seismicity and seismic damage	
	Ambient (seasonal) groundwater conditions	
Causes of increased shear stress	Removal of lateral or underlying support of slopes	Erosional processes producing, steepening, or undercutting natural slopes
		Prior mass movements
		Eruptions near base of slope
	Static Loading	Natural deposition- slope or river sedimentation
		Weight of water added by natural precipitation or by exolved volatiles
		Seepage pressures and joint water pressures
		Mud/fluid pressure
		Swelling pressures in expansions clays
	Dynamic loading	Regional or local tectonic earthquakes
		Vibrations from volcanic earthquakes, explosion and eruptive processes
		Vibrations from adjacent, rapidly moving landslides
	Increase of surface slope	Mud/fluid intrusion related deformation
		Regional tectonics
		Slope changes due to depositional processes
Causes that reduce shear strength	Physiochemical Factors	Hydrothermal alteration
		Softening of clays
		Hydration of clay minerals
		Ion exchange of clays
		Weathering
		Solution of grain cement
		Decomposition of organic materials
		Physiochemical fracturing
	Pore fluid pressure enhancement	Heavy rainfall or rapid snowmelt
		Changes in groundwater flow regime
		Pore pressure changes due to hydrothermal processes
		Thermal expansion of pore fluid due to frictional slip
		Vibration induced pore fluid pressure rise
		Shear deformation induced pressure rise
		Consolation seepage induced by surcharge
		Base level changes in reservoirs, lakes or oceans
		Flow boundary condition changes
	Changes in structure	Disturbance
		Particle reorientation due to slip or dynamic loading; peak to residual strength loss
		Grain collapse in altered deposits
		Fracturing and loosening of valley walls, stress relief
		Deep seated fracturing associated with fluid intrusion, stress relief, physiochemical alteration
		Adjustments to groundwater flow paths; slope drainage enhanced or impeded

Table 5.2: Causes of mud volcano collapse adapted from Voight & Elsworth (1997).

Mapping in this study has revealed apparently conflicting structural evidence in relation to mechanism of the kilometre-scale elongate collapse structures on mud volcanoes in Azerbaijan. On one hand, there is good morphological evidence of mass flow on shallow detachment with many similarities to sector collapse structures in igneous volcanoes. On the other hand alignments of fluid expulsion features are observed along the bounding faults, particularly in the updip domains, of these structures (see Chapter 4). Reconciling these observations leads us to a preferred model that is essentially a development of that previously published by Planke *et al.* (2003). This study adopts their idea of an elongate mud chamber at relatively shallow (<1 km) level. But rather than the elongate fault-bound structures at the surface directly representing a collapsing roof of a deflating mud chamber, these findings suggest that the observed sector collapse structures are 'thin-skinned' sector collapses triggered and localised by mud chamber deflation during eruptions, as shown in Fig. 5.12. This ring fault provides a pathway for fluids and so results in vents aligning along the fault itself (Fig. 5.12B; see Chapter 4). Ring fault formation may be enhanced by fluid flow up crestal faulting parallel to the anticline axis which would explain why failure sometimes occurs on the shallowest slopes.

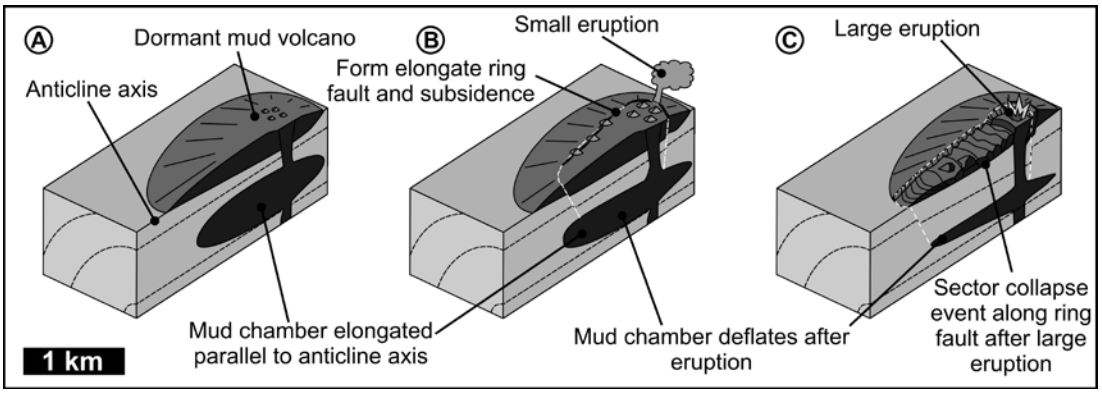

Fig. 5.12: Schematic sector collapse formation. A) Dormant mud volcano edifice. B) Ring fault forms after small eruption and evacuation of material from depth. C) Large eruption causes subsidence to occur due to expulsion of fluids at the surface resulting in sector collapse along ring fault. Green dashed line represents position of anticline axis.

Subsea examples of igneous sector collapse have also been identified in both seismic reflection and multibeam (swath) bathymetric sonar data (Mattioli *et al.*

1995; Leat *et al.* 2010) as well as possible un-identified sector collapse structures on mud volcanoes in subsea seismic reflection data from the South Caspian Basin e.g. Corthay & Aliyev (2000). These structures also share the same 'shape parameters' that this study identifies as being characteristic of sector collapse. Using this study to identify similar subsurface structures could aid a better understanding of the processes at depth as well as determining areas that may be at risk to these potential geohazards (Corthay & Aliyev 2000; Leat *et al.* 2010).

5.7 Conclusions

Elongate trench like depressions bounded by shallow inward-facing faults trending from the summit to the base of some mud volcanoes in Azerbaijan, and displaying evidence of downdip lateral movement, are termed 'mud volcano sector collapses'. Examples mapped in the field range in size from ~180 m to ~200 m width and 1-2 km in length, each representing up to 10^6 tons of mobilised material assuming depth to detachment averaging 10-20 m. Field observations include an elongate trough that is fault-bounded, on three sides (open downdip), with an updip 'amphitheatre' depression, levees, and a downdip domain with hummocky morphology. The bounding fault system shows kinematic evidence of lateral movement. However the presence of fluid escape structures in the updip parts of these collapses also indicate a relationship with the deeper-seated structure of the mud volcano. The observations made here are reconciled in a model where a deflating, perhaps elongate, shallow mud chamber (<1 km) triggers detached sector collapse. This model could account for the range of observations plus the curious spatial relationship of the sector collapses, namely they occur on the gentler slopes (i.e. elongate crest) of the mapped mud volcano edifices. The model also allows the sector collapse to be more extensive than any underlying mud chamber, potentially running out to, and beyond the edifice on to the surrounding plain.

A by-product of this study is recognition that sector collapse flows tend to have a different planform shape relative to eruptive flows, the latter having a pronounced

lobe at the base of slope. This criterion enables these structures to be distinguished on remote-sensed data. The observations of sector collapse made herein can also be applied in risk assessments, for instance it should not be assumed that mud flow hazard is restricted to areas downdip of the steepest sides of mud volcanoes. This can equally be applied in submarine settings.

6 Discussions and Conclusions

6.1 Introduction

In this chapter the primary findings of the thesis are brought together to provide an overview of the mud volcano system as well as any limitations that the structural model developed may exhibit. The results of each chapter are compared with the questions and thesis aims posed in Chapter 1. Finally, suggestions are made for further work and other studies that may enhance the understanding of mud volcano systems.

6.2 Discussion

This thesis has used field mapping, statistical methods and high resolution satellite imagery to perform a detailed analysis of the structure, evolution and processes of the intrusive and extrusive domains of mud volcano systems from Azerbaijan and East Java. The use of multiple data types has produced a detailed evaluation of the structure and geometry of the fluid flow pathways utilised and the various structural features (faults, fractures and anticline axes) found within these systems. This section in conjunction with the discussions sections in Chapters 3, 4 and 5 relates the key scientific results of each core research chapter and draws them together into a generalised structural model of large mud volcano systems from the South Caspian Basin. Each chapter is now discussed in reference to the key linking factors including the similarity between igneous and sedimentary volcanism, structural influences (i.e. faults, fractures and anticline axes that may control fluid flow within the crust), fluid flow within the mud volcano system, geo-hazard prediction and the mud volcano system as a whole. These are presented in sub-sections 6.2.1-6.2.5.

6.2.1 Comparison to Igneous Volcanic Systems

One of the most significant observations about mud volcano systems over the past decade is that they bear a striking resemblance to igneous volcanic systems in various ways (Davies & Stewart 2005; Stewart & Davies 2006; Evans *et al.* 2008; Bonini & Mazzarini 2010). Table 6.1 shows a comparison between igneous volcanoes and mud volcanoes made during this study. Similarities addressed are between; calderas, sector collapses, flows, edifices, vent alignments and processes of intrusion. Obviously they differ in some aspects being that igneous volcanic activity is primarily driven by hot, molten rock and mud volcanoes are mostly cool, fluidised sediments, however both produce morphologically and geometrically similar products and are driven by pressure differentials. Both types of volcanism form steep-sided cones with vent populations on their crests which emit fluids (Kopf 2002; Table 6.1). As discussed in Chapter 2 mud volcano activity can by characterised by explosive or effusive eruptions, in which the mud flows produced resemble lava flows from igneous volcanoes (Table 6.1). Many explosive eruptions of igneous volcanoes have been triggered by earthquakes of a threshold magnitude, which occur several days before (Manga & Brodsky 2006). The same relationship has been seen with mud volcanoes with the physical processes that initiate eruptions still not being fully understood (Delisle *et al.* 2001; Mellors *et al.* 2007; Manga *et al.* 2009).

Several studies have focused on the largest known mud volcano system, Chirag mud volcano in the South Caspian Basin (Davies & Stewart 2005; Stewart & Davies 2006; Evans *et al.* 2008). This mud volcano is ~600 m thick, with a 4 km wide caldera collapse structure and downward tapering cone complex beneath it (Davies & Stewart 2005; Stewart & Davies 2006; Evans *et al.* 2008). The dimensions of these structures make them comparable in size to their igneous equivalents (Hansen 2006). Evans *et al.* (2008) also discussed the similarity between igneous and mud volcanic caldera formation, structure and geometry and Bonini (2008) related mud volcano caldera elongation to the direction of regional stress in a similar fashion to that used on igneous volcano calderas (Lipman 2000).

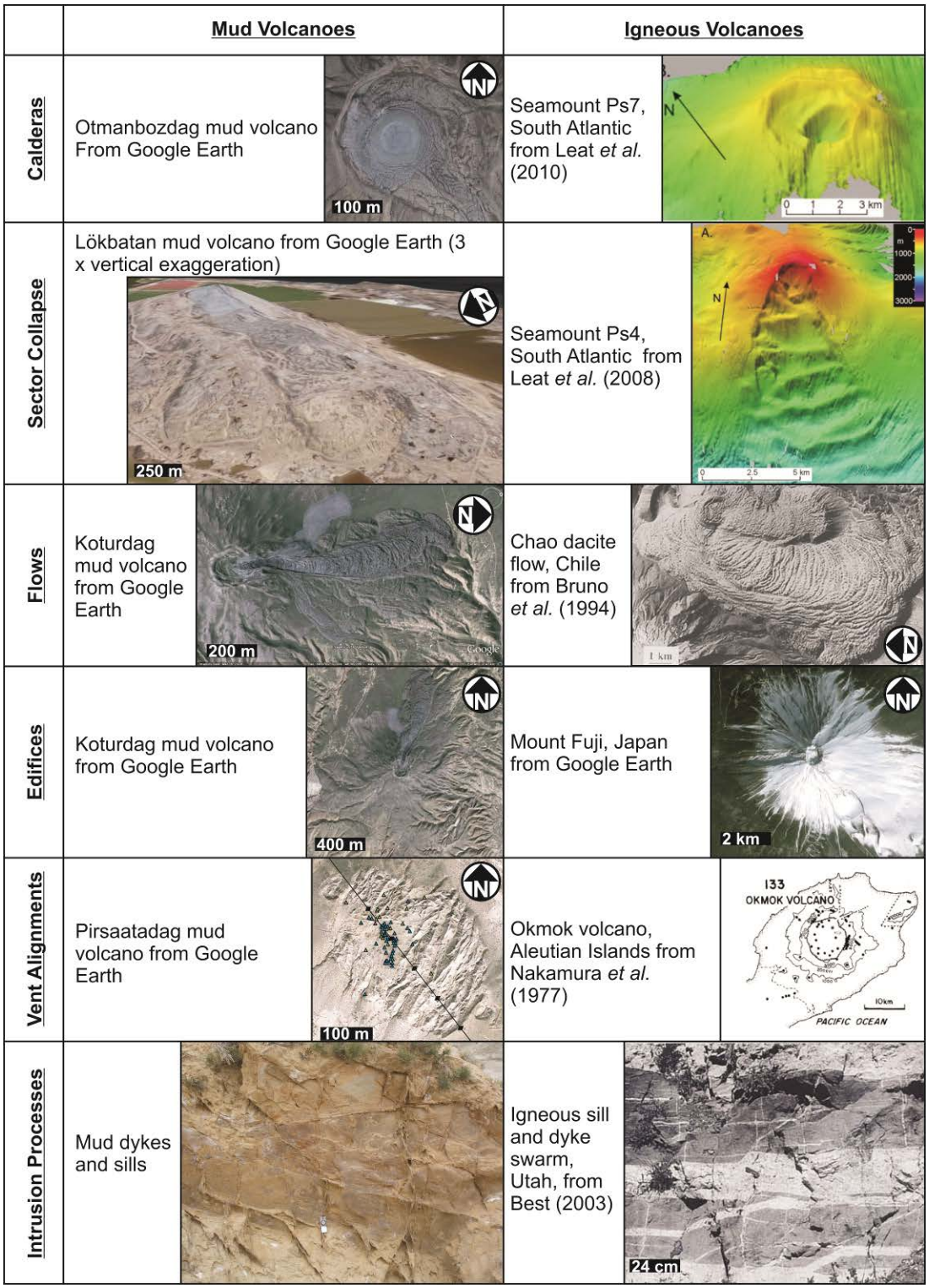

Table 6.1: Comparison of igneous and mud volcanic systems. Google Earth Images © 2010 DigitalGlobe and © 2010 GeoEye, © 2010 Google.

One of the best examples of the parity between igneous and mud volcano systems in this thesis is shown in Chapter 5 where elongate depressions, bounded by shallow inward-facing faults, are classified as 'mud volcano sector collapses', as

they show similarities with igneous sector collapse structures. These collapses trend from the summit to the base of some mud volcanoes in Azerbaijan, and display evidence of downdip lateral movement in a similar fashion to those displayed by igneous volcanoes. Examples from mud volcanoes range in size from ~180 m to ~200 m width and 1-2 km in length, each representing up to 10^6 tons of mobilised material assuming depth to detachment averaging 10-20 m. Field observations included an updip 'amphitheatre' depression, levees, and a downdip domain with hummocky morphology. These collapses are triggered by violent eruptions on both igneous and sedimentary volcanoes. Structurally and morphologically the two types of collapses are identical however, the difference arises with scale as igneous sector collapses are several orders of magnitude above the volume of mud volcano collapses. This may be due to the rheology and temperature of the material being erupted. Igneous material is more viscous and when it cools can form steep conical edifices that usually fail at an angle of repose of around 30° (Siebert 1984). Mud volcanoes often fail at a shallower angle than this of around 10° probably due to the relative weakness of the mud that the edifice is composed of.

Vent alignments on igneous volcanoes have been studied in great detail and have had numerous statistical techniques carried out on them to determine what processes might control these arrangements (Wadge & Cross 1988; Connor 1990; Bleacher *et al.* 2009). In Chapter 4 it can be seen that this is also useful for analysis of mud volcano vent populations. These statistical techniques prove that like igneous volcano vent populations those on mud volcano edifices also reveal what the structure of the intrusive domain is like. This will be discussed in more detail in section 6.2.2. Venting only occurs in the 'active vent zone' of the intrusive domain as discussed in Chapter 3. This distribution of vents will determine the overall morphology of the edifice itself and if there is an elongate vent distribution it will also be likely that the edifice will become elongate as it accretes which is also true of igneous edifices (Bonini & Mazzarini 2010).

The observation that igneous and mud volcanoes are akin is also true of the intrusive domain as discussed in Chapter 3. Davies & Stewart (2005) determined that the intrusive domain was composed of feeder pipes and dykes that connected to a deeper source layer several kilometres below. They described this conduit system as being a steep cylindrical zone of densely intruded country rock comprised of mud pipes and exhibiting low mechanical strength in comparison to the surrounding un-intruded country rock (Davies & Stewart 2005). This intrusive domain underwent differential compaction and resulted in the caldera collapse structure which overlies the downward tapering cone (Davies & Stewart 2005). These characteristics are similar to those found for igneous volcanoes, which share the same structure (Lorenz 1986; Hansen 2006). Ring faulting in mud volcano systems, as discussed in Chapter 2, also closely matches the form of 'ring dykes' and 'cone sheets' in igneous intrusive systems (Anderson 1936, 1937). In Chapter 3 mud volcano system feeder complexes were found to consist of megabreccia of country rock surrounded by intruded mud and some long-lived fluid conduits. This is a description that would also fit that of an igneous diatreme complex, these are cone shaped areas of brecciated country rock and juvenile material that extend down to igneous dykes and sills at depth (Lorenz 1986). The model of intrusion discussed in Chapter 3 consists of a propagating fracture network that isolates blocks and eventually allowing them to move freely as the smaller clasts become eroded by the mud-water-gas mix through time. This process has similarities with the better-known 'stoping' process in igneous volcanic complexes where an upward-propagating fracture network isolates a megabreccia of blocks. Once the fracture system breaches the surface and becomes an anastomosing flow pathway, the smaller blocks within the breccia are eroded and extruded, creating space for widening of the flow conduits and settlement and rotation of the larger blocks whose size and weight prevent them from being carried upwards.

Another analogue is that of sand injectites where intrusions may be filled by sand- or mud-sized grains and form by the hydrofracturing of the interface between liquidised sediment and stronger surrounding sediments or the forceful intrusion of existing fractures (Jolly & Lonergan 2002; Hurst *et al.* 2003a, b). If overpressured

fluids passing into the opening fracture do so at a sufficient velocity, the fluid shear stress will balance or exceed the weight of a sediment grain and the grain will become entrained into the flow through fluidisation (Lowe 1975). These structures can form networks of cross-cutting or merged intrusions, of both dykes and sills (Hurst *et al.* 2003a, b). Individual examples can reach sizes of up to 3 km in length and 20 m thickness (Huuse *et al.* 2005). Their scale means they are can be observed on seismic reflection profiles, typically as 'v' or 'w' shaped amplitude anomalies in cross-section (Hurst *et al.* 2003a). The orientation of the intrusions is controlled by the orientation of the regional stresses and the tensile strength of the surrounding sediments (Jolly & Lonergan 2002). This results in sand injectites being a useful palaeostress indicator in a similar way to igneous dykes (Nakamura 1977; Boehm & Moore 2002).

The intrusion size and fill is controlled by volume and type of sediment within the source body and the duration of sufficient pressure drive. Consolidated clay particles have a greater degree of cohesion than sand grains and are not as easily fluidised (Brown 1990). A combination of liquidisation, plastic flow and critical state deformation may therefore be important in the formation of shallow mud injectites (Brown & Orange 1993) as noted by Morley (2003) in Brunei. The scale, orientation relative to regional stresses, volume of source and type of sediment, are also dominant controls on igneous dyke and sill intrusive complexes (Petford 1996). Sand injectites, mud volcano intrusive domains and igneous intrusive complexes all propagate via hydrofracturing (Petford 1996; Jolly & Lonergan 2002; Morley 2003) making the scale of these features all largely dependent on the volume of the fluid source, the velocity and the pressure differentials. This indicates that all three of these intrusive structures share more in common than previously thought especially their modes of formation and driving mechanisms.

The similarities between mud and igneous volcanic systems in relation to their morphology, internal structure, plumbing systems, vent distributions and eruptive activity show that these systems may share similar processes and driving forces. The processes controlling the two types of volcanism are fundamentally driven by

pressurised fluids at depth. Conversely if these systems do not share causal mechanisms then the question has to be asked, why do they still form such similar constructions?

6.2.2 Influence of Regional and Local Structure and Stresses

The influence of regional structure and stress regimes is extremely important in igneous volcanic systems with a number of studies being carried out in relation to the topic (Nakamura 1977; McGuire & Pullen 1989; Voight & Elsworth 1997; Day *et al.* 1999; Acocella *et al.* 2003; Bosworth *et al.* 2003; Holohan *et al.* 2005; Paulsen & Wilson 2010a, b) however, there are far less that focus on mud volcano systems (Morley 2003; Bonini 2007, 2008; Bonini & Mazzarini 2010). Chapter 3 evaluates the structure of the intrusive domain of a mud volcano system for the first time. The study splits the intrusive domain into sub-domains comprised of; the 'active vent zone' where fluids are currently being extruded; the 'peripheral fracture zone' where both sinuous and conjugate fracture systems are found with infill; the 'central zone of block rotation' where bedding strike measurements vary greatly from the surrounding anticlinal bedding and the 'un-intruded zone' which contains only open conjugate faulting/fracturing that has not been infilled or intruded. This model for the intrusive domain shows how important the pre-existing structure within the country rock is to the intrusive process with the majority of intrusions occurring along pre-existing fracture systems and some along sinuous hydrofractures. This would be of particular interest to hydrocarbon production as the effects of intrusion on the country rock can be evaluated in order to assess how much of the reservoir has been compartmentalised. The internal structure of this intrusive domain model could be what comprises the centre of the 'downward tapering cone' structures that were first noted by Stewart & Davies (2006). If this is the case then the intrusive domain of mud volcanoes bear more in common with igneous diatremes (Lorenz 1986; Hansen 2006) than first thought however, it is only by improving seismic imaging techniques that the structure will truly be determined.

The most critical information that this mapping uncovered was that there are megablocks of country rock within the centre of these intrusive domains that at some point have been rotated in order to give them strike orientations that vary by up to 90° from the surrounding country rock. One analogy might be the smaller scale 'blow out pipes' seen on the island of Rhodes (Fig. 6.1; Løseth *et al.* 2001). These pipes are most likely formed by explosive eruptions of gas forming the circular structures that are linked by 3-4 m high and 0.2 m wide vertically oriented fractures (Løseth *et al.* 2001). The fractures and circular structures are both filled with clay clasts and slurry from the overlying units. All pipes have a wide, sub-concentric deformation zone up to 10 m away from the core (Løseth *et al.* 2001). This raises the question of if the intrusive domain can be described as being 'self-similar'. If the structure of a metre-scale blow-out pipe resembles that of a kilometre-scale mud volcano intrusive domain then this surely implies some scale-dependence. This self-similar nature is seen in other parts of mud volcano systems such as the kilometre-scale edifices and metre-scale vents; kilometre-scale breccia flows with metre-scale mud flows from gryphons; and also in vent and mud volcano edifice alignments as seen in Chapter 4. Why could the same not be true of the intrusive domain? If this self-similar scaling is valid it would increase the potential to produce valid models of these systems.

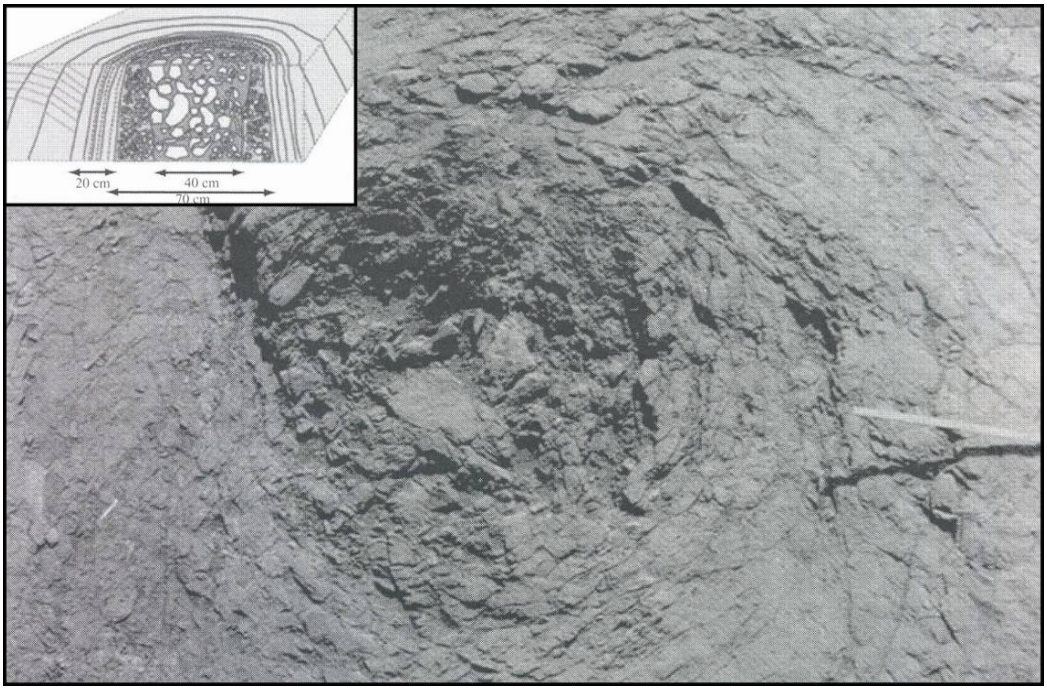

Fig. 6.1: Photograph showing a horizontal cross section through a sedimentary blowout pipe of late-Pleistocene age on the Greek island of Rhodes; the inset sketch illustrates the feature in three-dimensions. The inner central zone comprises relatively large (<5-10 cm) angular mud clasts floating in a muddy matrix; the outer zone has smaller (<5 cm) clasts. These zones are surrounded by 20 cm of heavily fractured country rock (limestone) and a further 4 m of less fractured rock. From Judd & Hovland (2007).

In igneous volcanic systems structural concepts usually assume that the geometric characteristics of volcanic features i.e. elongation of edifices or calderas and alignment of vents or edifices, reflect the regional stress axis orientation. Nakamura (1977) inferred that the rows of aligned volcanic vents frequently form above subsurface feeder dykes. Therefore, vent alignments have been used to infer the direction of the minimum horizontal stress (σ_{Hmin}) or the maximum horizontal stress (σ_{Hmax}; Nakamura 1977; Lutz 1986; Wadge & Cross 1988). Pre-existing faults and fractures may influence dyke trajectory, but in general the stress field in the country rock is thought to exert the primary control on dyke orientation in igneous systems (Delaney *et al.* 1986). In Chapter 4 these techniques are used on the vent distributions at the surface of mud volcano systems in order to reveal intricate detail about the subsurface pathways that have been exploited by the migrating fluids and how these pathways can change with time. It is most likely that the orientation of regional stress regimes and local metre- to kilometre-scale structures are the key control to the vent arrangement proving that fluid often flows up conjugate fractures, anticline crestal faults, detachment faults, ring faults and parallel to anticline axes. Interestingly a similar study carried out by Bonini (2008) showed that the majority of vents on Napoli mud volcano in Italy aligned with jointing at 90° to the anticline axis and parallel to the maximum horizontal stress (Fig. 6.2B). This was also found by Winslow (1983) who looked at the orientation of clastic dykes intruding at 90° to the anticline axis (Fig. 6.2C). This contradicts the findings of Chapter 4 with the volcanoes in Azerbaijan and may show that intrusion is controlled on an even smaller scale than previously thought. Vent alignments on igneous volcanoes also usually occur parallel to the maximum horizontal stress as the dykes dilate perpendicular to the maximum horizontal stress (Fig. 6.2A).

Chapter 4 shows that the dominant orientation for mud volcano vent populations is nearly always parallel to the anticline axes on which they erupt. This means that if you infer the vents form at the termination of a linear 'mud dyke' at the surface, that the orientation of that dyke is also perpendicular to the regional maximum horizontal stress and so the opposite to what is seen on igneous vent populations and dyke swarms. One explanation for this is that mud volcano systems are largely controlled by the anticlinal structures through which they intrude unlike igneous volcanoes which, due to their scale and the energy involved, would not be influenced by local structure. Anticline axes will always be oriented at 90° to the maximum horizontal stress as the anticline forms as a result of this compressive stress, as will their crestal faulting. As a result of this, mud volcano alignments can occur on a range of scales from the 1-4 km systems that align along anticline axes to metre-scale vents that erupt along anticline crestal faulting. If there are mud chambers within the intrusive domain then they may also become elongated perpendicular to the maximum horizontal stress as has been inferred in igneous systems (Paulsen & Wilson 2010a). This alignment of vents and mud chambers also allows the edifice itself to become elongate due to the sources of fluids accreting along anticline axes, another feature which has been noted in igneous volcanic systems (Paulsen & Wilson 2010a).

The opening direction of igneous volcanic amphitheatre craters or orientation of sector collapse structures of igneous volcano systems has been found to occur consistently sub-parallel to the direction of regional minimum horizontal stress. Some studies of igneous volcanoes have linked vent alignments with the orientation of sector collapse structures suggesting that failure is more likely to occur along lines of weakness i.e. dykes and so fail perpendicular to the maximum horizontal stress (Fig. 6.2A; Siebert 1984). However, these relations are apparently more complex (for an overview see Lagmay & Valdivia 2006). For instance, in regions dominated by trans-tensional tectonics, crater breaching is most commonly parallel to the fault strike (Tibaldi 1995) or it forms an acute angle to the σ_{Hmax} direction (Lagmay & Valdivia 2006). In extensional settings, cone breaching is perpendicular to normal fault strike and the σ_{Hmax} (Tibaldi 1995). In volcanoes developed under

compressional settings, crater opening and debris avalanches tend to develop roughly orthogonal to the regional trend of thrusts, as inferred for the Central Andes (Francis & Wells 1988), and thus roughly parallel to the direction of regional σ_{Hmax}. In Chapter 5 it can be seen that all mud volcano sector collapses in Azerbaijan occur parallel to the local anticline axis orientation and so perpendicular to the maximum horizontal stress similar to their igneous equivalents (Siebert 1984). In Chapter 5 sector collapse parallel to the anticline axis is explained with a model where a deflating, perhaps elongate, shallow mud chamber (<1 km) triggers detached sector collapse. This model accounts for the orientation observations plus the occurrence of collapses on the gentler slopes (i.e. elongate crest) of the mapped mud volcano edifices.

Igneous volcanic calderas form as a result of the removal of magma from an underlying magma chamber or reservoir, the roof of which subsequently collapses (Anderson 1936; Lipman 1997; Cole *et al.* 2005). Caldera collapse depressions are often elongated in plan view, and elongation is usually taken as a reliable indicator of regional stress orientation. Elliptical igneous calderas normally become elongate parallel to the direction of the minimum horizontal stress, this is also true of mud volcano calderas as seen in Chapter 5 and Appendix IV. Different models have been proposed to explain the ellipticity (ratio of the long axis/short axis) of igneous calderas (Acocella 2007). It has been suggested that at some igneous volcanoes the magma chamber underlying the caldera grows along brittle discontinuities that formed prior to the emplacement of the magma, making caldera elongation dependent upon the local structural setting (Acocella 2007). It has also been proposed that the growth of the magma chamber may occur in the direction of the σ_{Hmin} as the fluid chamber walls change shape due to stress concentrations and resulting brittle failure of the wall rock, analogous to the breakouts in a wellbore (Bosworth *et al.* 2003). Bonini (2008) suggested that growth of a fluid-mud chamber in the σ_{Hmin} direction is appropriate to explain the presence of elliptical mud calderas elongating sub-parallel to the axis of anticlines over which they usually develop. It has been proposed that elliptical calderas may reflect the shape of the underlying magma/fluid-mud mix reservoir, and that the caldera long axis

could reveal the shallow σ_{Hmin} orientation (Bosworth *et al.* 2003) a similar finding to the model proposed in Chapter 5 of elongate sector collapse orientation.

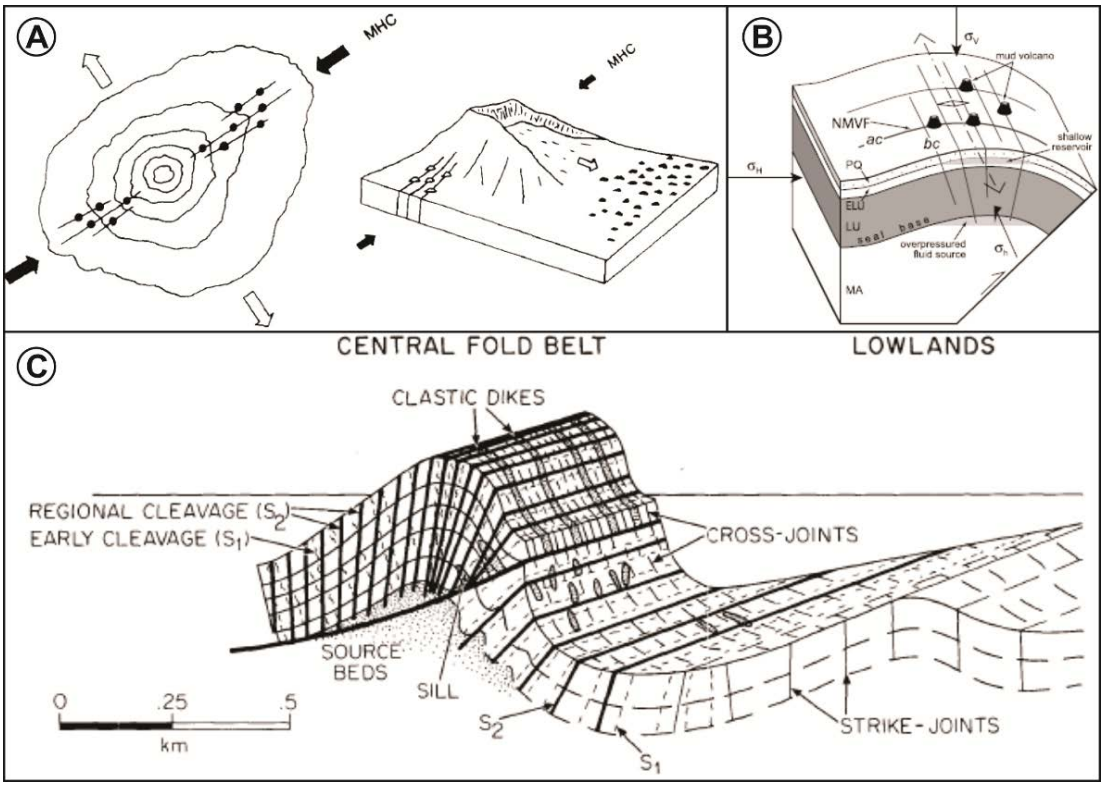

Fig. 6.2: A) Sketch illustrating emplacement of radial dykes and parasitic vents in a direction parallel to the maximum horizontal compression (MHC), producing elongation of the edifice and a dilatational stress within the volcano, promoting collapse in a direction normal to the MHC. The sketch on the right-hand side illustrates typical morphology of sector collapses. From Siebert (1984). B) Schematic block diagram showing the relations between the orientation of the principal stress axes and the main fracture sets in a sealed-type thrust fold. The steep brittle discontinuities may potentially operate as conduits transferring fluids from depth up to surface. Notably, the intersection of 'ac' and 'bc' fracture families may represent a locus potentially very favourable for localising fluidising pipes feeding mud volcanoes. The thick 'ac' joint indicates the setting at Nirano mud volcano field, Italy (NMVF), where this joint family is controlling mud volcanism. 'H' - maximum horizontal stress; 'h' - minimum horizontal stress; 'V' - maximum vertical stress. MA, Marnoso Arenacea; LU, Ligurian units; ELU, Epi- Ligurian units; PQ, Pliocene-Quaternary deposits. From Bonini (2007). C) Schematic fold and its major and minor structures from relationships seen in the clastic dyke swarm in Western Isla Grande, Southern Andes. From Winslow (1983).

6.2.3 Fluid Flow Pathways within Mud Volcano Systems

Chapters 3 and 4 in conjunction provide intricate detail about the subsurface pathways that have been exploited by the migrating fluids and how these pathways can change with time within mud volcano systems. One of the major findings of this study is that no kilometre-scale mud diapirs have been found. In other locations globally structures previously interpreted as diapirs have frequently turned out to be poorly imaged thrust cored anticlines associated with gas charge and mud volcanoes piercing their culminations, giving an impression of a large mud-cored anticline (Huuse *et al.* 2010). This study, particularly in Chapter 3 has found that fluid flow only occurs in certain parts of the intrusive domain namely the 'active vent zone', 'central zone of block rotation' and the 'peripheral fracture zone'. Intrusion of fluids dominantly occurs via pre-existing faults and fractures which are conjugate or form a 'grid' like mesh. This is inline with other studies which have noted intrusion in pre-existing structures (Bonini 2008). A second type of fracture was also seen, these were described as 'sinuous fractures' and were formed as a result of fluid intrusion most likely by hydrofracturing. This kind of fluid flow pathway was also noted by Morley (2003) in Brunei. These findings were also backed up in Chapter 4 as mapped vent distributions also revealed alignment with pre-existing structures in country rock as well as with anticline axes, ring faulting and detachment faults. Alignment of vents along ring faults have also been noted in igneous volcanic systems (Nakamura 1977).

Chapter 4 shows that on some mud volcanoes zonation of eruptive phase types is also occurring implying that there is some form of fractionation at depth in either one large chamber or a network of smaller linked chambers. Unfortunately the precise mechanisms causing this to occur have not been identified but it does show that certain fluid types travel through different fluid flow pathways. From the 2-point azimuth statistics in Chapter 4 it is usually the case that both mud (gryphon) and water (salse) fluid types display the same azimuth alignments and so may share similar fluid flow pathways. Cinder mounds (gaseous) tend to form in discrete zones and so are probably controlled by metre-scale fault valve behaviour (Sibson

1990). Pool vent types bear no orientation relationship to any other vent type indicating that they are probably only very shallow features that form as a result of dewatering of the surrounding mud edifice (Mazzini *et al.* 2009).

The composition of the fluids being erupted at each volcano is significant as it will dictate how the edifice itself will accrete over time. Fluid flow pathways may also be a precursor to edifice collapse or indeed may prime it for failure as shown in Chapter 5. The presence of vents in the updip parts and margins of the incipient collapse structures in Chapter 5 also indicate a relationship with the deeper-seated structure of the mud volcano. It is most likely that intrusion initially occurs through pre-existing fracture networks and along crestal faulting and then subsequently influenced by formation of detachment and ring faulting. This obviously suggests that fluid flow pathways can change over time depending on what structures may be present within the edifice itself. In Chapter 4 the Lusi mud volcano is also given as an example of how fluid flow pathways evolve through time from a localised kilometre-scale fault zone and hydrofacture system in 2006 to a larger regional anticlinal structural control in 2009 and 2010. This evolution is likely to continue along this trend and in a similar ring fault style to that seen in Azerbaijan as subsidence increases more faulting will probably occur up to 10 km away from the central vent which could have major implications for the local population. In order to better understand mud volcano fluid flow pathways time-dependant studies must be carried out on Lusi and mud volcanoes globally to determine exactly how these pathways evolve.

6.2.4 Geo-Hazard Prediction

Mud volcano systems globally pose a significant hazard to economic drilling and engineering operations as well as local infrastructure. Most importantly Chapters 3 and 4 introduce the Lusi mud volcano which may have been triggered by the drilling of a gas exploration borehole 200 m away from the central vent (Davies *et al.* 2008). Events like this make predicting the evolution of a mud volcano system even more important in reducing the possible occurrence of such blow-outs. Mud

volcano systems in Azerbaijan are typically located on the crest of anticlines which usually host hydrocarbon accumulations likely to be located in close proximity to their feeder conduits. Mud volcanoes can have a significant impact on the petroleum plays through which they penetrate and may act to either help or hinder the migration of hydrocarbons in a region. In many cases an impermeable clay 'cake' builds-up on the walls of the intruding mud pipes or dykes in a similar fashion to mud cake formation in drilled wells (Morley 2003). This build-up prevents fluid loss into permeable lithologies within the overburden and seals shallow reservoirs from the effects of short-term fluctuations in fluid content and pressure in mud feeders (Morley 2003). Fresh permeable lithologies will be exposed to the mud feeder system during the propagation of new pipes and faulting associated with the collapse of a downward-tapering cone (Stewart & Davies 2006). As shown in Chapters 3 and 4 the feeder complex is intensely fractured, intruded by mud and fluids, contains megablocks and may experience large pressure variations all of which are potential problems that may be encountered within and around this area of the system. In order to avoid these regions reservoir models must be designed to predict potential hazards. The overall model presented in this thesis can be integrated into these models especially taking into account the regional stress orientation and any local scale structures.

Sector collapse of mud volcano edifices presents a hazard to infrastructure both on and offshore and warning signs of incipient collapse can now be noted due to the observations made in Chapter 5. This study has provided a detailed account of the internal structure of the intrusive and extrusive domains of mud volcano systems and has helped to better understand and identify some of the potential hazards posed by these systems. The observations of sector collapses, can also be applied in risk assessments, for instance it should not be assumed that mud flow hazards are restricted to areas downdip of the steepest sides of mud volcanoes. This can equally be applied in submarine settings.

6.2.5 Mud Volcano System Model

By integrating the findings of Chapters 3, 4 and 5 a comprehensive structural model can be produced which schematically depicts the configuration of the extrusive and intrusive domains of a typical mud volcano system (Fig. 6.3). Chapter 5 has recognised that sector collapses tend to have a different planform shape relative to eruptive flows, the latter having a pronounced lobe at the base of slope. This criterion enables these structures to be distinguished on remote-sensed data and seismic reflection data and so these structures have also been added in to the structural model. In order for this model to be of further use for predictive modelling several more parameters must be supplied including lithology, pressure measurements and 3-D porosity and permeability distribution in feeder complexes. This model provides a starting assumption for the dimensions of these structures in areas were seismic imaging does not clearly resolve their extent. These parameters will be useful in the cases of reserves assessment and drilling planning in the deeper parts of mud volcano systems.

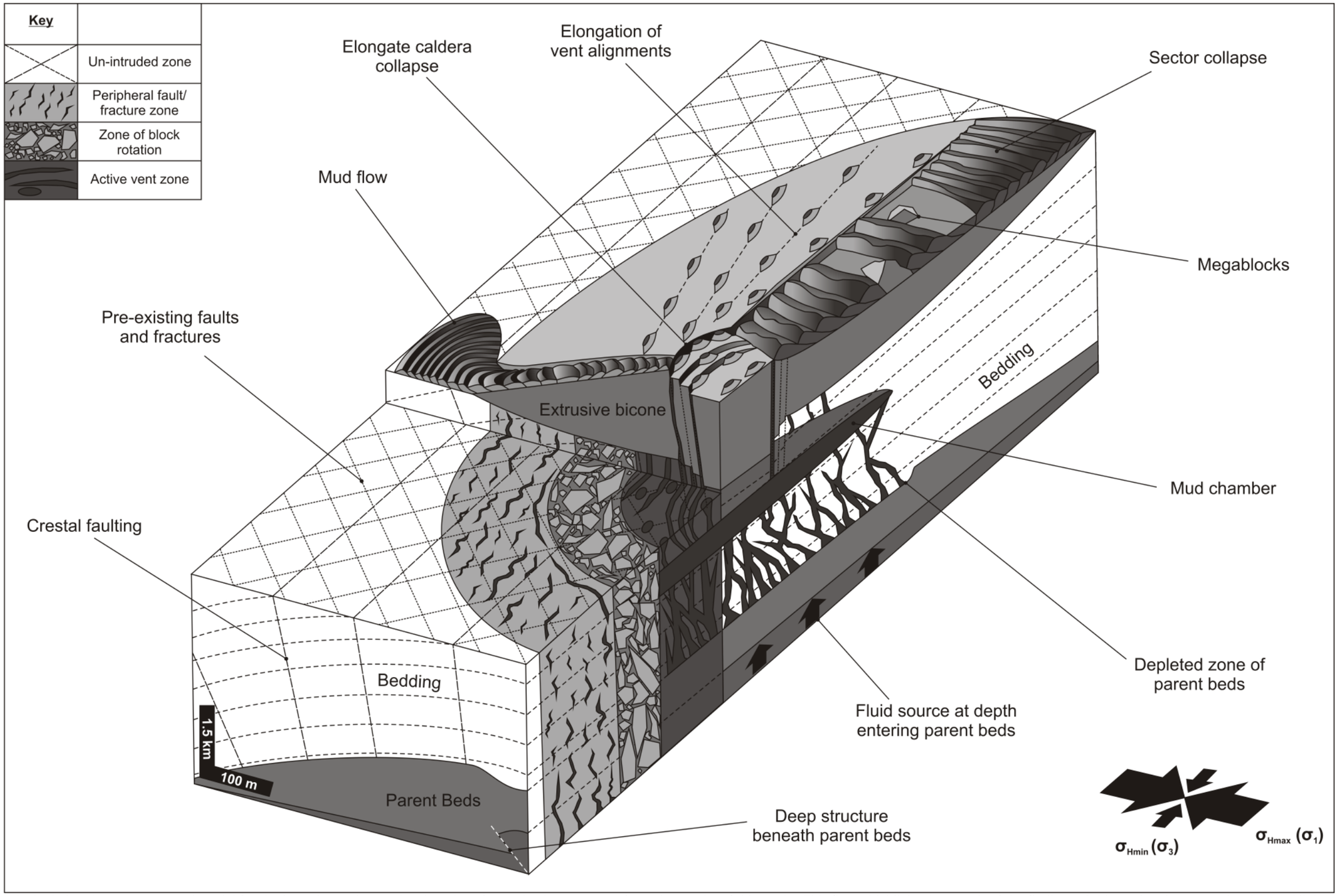

Fig. 6.3: Schematic depicting the new structural model for the intrusive and extrusive domains of a mud volcano system from the results of this study. This figure highlights how each of the findings of this study relate to each other and link together to form one complete system.

6.2.6 Limitations

One of the main discrepancies of the study in Chapter 3 is that the position of the 'rotated blocks' at the centre of the feeder complex have not been correlated to the surrounding country rock. This means that it is not possible to determine whether these blocks have moved up, down or stayed in the same position within the intrusive domain. A second point about this study is that it is not possible to know at what structural level the intrusive system is being mapped. So although mud volcanoes that had the largest amount of country rock visible were mapped, it is still not known how much of this feeder complex had been eroded in the past. It also means that it is only possible to see a single 2-D 'slice' of the intrusive system at any one mud volcano.

Limitations faced in Chapter 4 are that only a limited number of the mud volcanoes had structural data available as the majority of the country rock is usually covered with mud flows. This meant that exact correlation of the vent alignments with structural features could not be carried out at every mud volcano. The accuracy of GPS measurements may also influence the vent positioning and the statistical analysis presented here would be enhanced if accuracies could be decreased to the sub-metre scale. Another consideration when looking at the Lusi mud volcano alignments is that because the volcano may be subjected to different structural influences than those in Azerbaijan it may not be directly applicable. Some uncertainties may arise when mapping vents at Lusi as it is unknown how many of these vents are either linked to a deeper feeder system or simply shallow eruptions linked to the massive and rapid subsidence occurring in the area. Some large areas covered in mud meant vent locations could not be mapped which possibly accounts for the high proportion of bubbles located near roads, dam walls and high density urban areas.

Chapter 5 presents limitations in the way that the exact depth to the detachment of the sector collapse is not known and can only be estimated. If a fresh sector collapse occurred that hadn't been subjected to erosion and subsequent mud

breccia flows infilling the depression then a more accurate depth could be determined. Identification of more sector collapse structures using seismic reflection data would also have been useful in assessing how deep this detachment occurs and has been carried out to some degree by Corthay & Aliyev (2000). In order to overcome some of these problems more future work could be done to address them as discussed in the section 6.4.

6.3 Conclusions

The investigations presented in this thesis provide a detailed study on the structure, evolution and geometry of the intrusive and extrusive domains of kilometre-scale mud volcano systems from the South Caspian Basin and East Java. The structural field mapping, aerial image analysis and statistical techniques carried out during this study have significantly enhanced the understanding of fluid flow through the crust and how large volumes of sediment can be mobilised and erupted at the earth's surface. This relationship of fluid flow and its influence upon surrounding country rock and structures on the mud volcano edifice itself have been determined. Whilst the study is focussed on only two geographic regions it is anticipated that the results are relevant to mud volcano systems globally. The following sections list a number of statements that summarise the conclusions of this project in reference to the hypotheses posed at the beginning of the thesis.

1) **Mud transport is through linked mud dykes and sills that have dimensions similar to their igneous counterparts (a few metres to tens of metres wide) and that these collectively form highly efficient conduit systems capable of transporting and re-cycling tens of cubic kilometres of mud and fluid. If the hypothesis is correct it would counter the common conception of kilometre-wide mud diapir systems.**

During this study no field evidence for kilometre-scale mud diapirism was found. The structure of the intrusive domain of mud volcano systems in Azerbaijan was found to be composed of sinuous hydrofractures and pre-existing fracture systems that were infilled with mud or mineral precipitations. Country rock was largely

intact apart from in the 'central zone of block rotation' which was composed of a megabreccia of country rock containing blocks of up to 20 m in length and with bedding strike rotations that differed from the surrounding country rock by up to 90°. Fracture density towards the centre of these intrusive domains also increased dramatically as did mud intrusions. This megabreccia, increased fracturing and intrusion, result in the reservoir potential of the country rock through which they pass being severely reduced as compartmentalisation increases.

Sub-domains of the intrusive domain have been defined as; the 'active vent zone' where fluids are currently being extruded, the 'peripheral fracture zone' where both infilled sinuous and conjugate fracture systems are found, the 'central zone of block rotation' where bedding strike measurements vary greatly from the surrounding anticlinal bedding and the 'un-intruded zone' which contains only open conjugate faulting/fracturing. The 'active vent zone', 'peripheral fracture zone', and 'central intrusive zone', together comprise the mud volcano feeder complex itself, with the 'un-intruded zone' lying outside the feeder complex. Formation of the intrusive domain is likely to be similar to stoping processes in igneous volcanic complexes where an upward-propagating fracture network isolates a megabreccia of blocks via mechanical breakdown of the country rock. Once the fracture system breaches the surface and becomes an anastomosing flow pathway, the smaller blocks within the breccia are eroded and extruded, creating space for widening of the flow conduits and settlement and rotation of the larger blocks whose size and weight prevent them from being carried upwards however, relative positioning of blocks has still to be determined.

2) Identify evidence for faults and fluid flow at the surface and relate these to sub-surface fluid flow. Investigate mud volcano vent distributions on several edifices in order to determine which fluid flow pathways are exploited.

2-point azimuth and nearest neighbour statistical analyses of mud volcano vent populations in Azerbaijan and East Java picked out dominant vent alignments and their orientations. The principle fluid flow pathways exploited nearly always shared the same orientation of regional folds axes, local metre- to kilometre-scale

fractures, detachment faults and ring faults suggesting that these are the key controls of the vent patterns. The dominant vent orientations are located sub-parallel to anticline axes causing elongation of the volcanic edifice perpendicular to the regional maximum horizontal stress. If later detachment or ring faulting form this will then overprint the original sub-parallel anticline crestal faulting. Zonation of eruptive phase types also occurs implying that there is some form of fractionation beneath the edifices in either one large chamber or a network of smaller linked chambers.

The observations in Azerbaijan were used to assess how the fluid flow pathways at Lusi mud volcano are evolving through time, from a localised kilometre-scale fault zone and hydrofracture system in 2006 to exploiting pre-existing pathways on the larger regional anticlinal structural control in 2009 and 2010. Predicted evolution is likely to continue along this trend and in a similar ring fault style to that seen in Azerbaijan, with the fluid flow up E-W orientated structures becoming increasingly more dominant than NE-SW and that as more subsidence occurs in the region more hazardous vents will occur, eventually producing multiple ring fault alignments and elongate caldera collapse up to 10 km away from the main vent. Mud volcano alignments can occur on a range of scales from metre-scale vents that erupt along crestal fractures to the 1-4 km systems that align along anticline axes.

3) Characterise the morphology and structures on edifices at the upper terminations of mud volcano systems that may be influenced by the intrusive domain i.e. sector collapse scarps.

Field observations identified elongate troughs that are fault-bounded, on three sides (open downdip), with an updip 'amphitheatre' depression, levees, and a downdip domain with hummocky morphology on some mud volcanoes in Azerbaijan. Examples mapped in the field range in size from ~180 m to ~200 m width and 1-2 km in length, each representing up to 10^6 tons of mobilised material assuming depth to detachment averaging 10-20 m and display evidence of downdip lateral movement. These structures have been identified as 'mud volcano sector collapses' similar to their igneous equivalents. The presence of fluid escape

structures in the updip parts of these collapses also indicate a relationship with the deeper-seated structure of the mud volcano.

The observations made here are reconciled in a model where a deflating, perhaps elongate, shallow mud chamber (<1 km) triggers detached sector collapse. This model could account for the range of observations plus the curious spatial relationship of the sector collapses namely they occur on the gentler slopes (i.e. elongate crest) of the mapped mud volcano edifices. The model also allows the sector collapse to be more extensive than any underlying mud chamber, potentially running out to, and beyond the edifice on to the surrounding plain. The differences between sector collapse flows and eruptive flows has also been identified as they each have a different planform shape, with eruptive flows displaying a more pronounced lobe at their base. This criterion enables these structures to be distinguished on remote-sensed data and possible seismic reflection data. The observations of sector collapse made herein can also be applied in risk assessments, for instance it should not be assumed that mud flow hazard is restricted to areas downdip of the steepest sides of mud volcanoes.

6.3.1 General Conclusions

This project has shown that mud volcano systems share more in common with igneous volcanic systems than previously thought, with similarities between intrusive domain structures, i.e. dykes and sill complexes and stoping; edifice evolution and morphology, i.e. sector collapse, calderas, flows and vents; structural influences, i.e. caldera ellipticity, vent alignments and sector collapse orientation; and both present potential geo-hazards. In order to fully understand mud volcano systems their link to their igneous equivalents must be studied to gain a better understanding of the intrusive processes.

Both regional and local structure have a significant influence on how mud volcano intrusive systems penetrate the crust on several scales from the sub-metre-scale fractures to kilometre-scale feeder complexes. Regional stress regimes dictate how

a mud volcano edifice will accrete over time as well as determining which structural pathways will act as potential conduits. Regional stress will also control what orientation a mud volcano caldera is likely to breach and so will dictate where a sector collapse structure will form.

The fluid flow pathways that compose the intrusive domain in mud volcano systems govern the evolution of the extrusive domain, with fractures forming planes of weakness for failures to occur along and for vents to erupt along producing alignments. Mud volcano systems, unlike igneous volcanic systems are strongly influenced by the local anticlinal structures through which they intrude and it seems that it is these that ultimately control the evolution, position and structure of the intrusive domain.

6.4 Future Work

The range of data types and varying scales of investigation in this project have led to a thorough investigation of the intrusive and extrusive domains of mud volcano systems. However, whilst the project represents a considerable advancement of the knowledge and understanding of these aspects of mud volcanism, certain limitations have been imposed by limited data availability, data quality gaps and the relatively small number of examples available for study. The remainder of this section now provides a discussion of the project limitations together with a number of suggestions as to how further work may be of use in overcoming them.

6.4.1 Field Studies

- The main outstanding question that is raised by this thesis is whether these intrusive domains have the same geometry globally. More studies should aim to identify outcrop analogues of mud volcano feeders and pipes as in Chapter 3 so that a wider comparison can be drawn between intrusive domains on a global scale. Studies of ancient mud volcanoes and their feeder systems have the potential to elucidate what the feeder system looks like and how they may

be influenced by regional and local structures. One particular area that would be of use identified during this study is that of the mud volcanoes in south-western Pakistan (Snead 1964; Von Rad *et al.* 2000; Delisle *et al.* 2001; Wiedicke *et al.* 2001). These mud volcanoes erupt in areas where structural features can be easily mapped in relation to the intruding system, even via Google Earth. The structural detail in this region along with its close proximity to the edifices would greatly enhance our understanding of mud volcano systems especially their feeder systems.

- One of the main unknowns in the feeder complex study detailed in Chapter 3 is that it was difficult to determine whether 'blocks' within the central zone of block rotation had been moved up, down or stayed at the same stratigraphic level within the intrusive complex. If this could be determined it would help to better constrain the fluid flow regimes within the intrusive system. It would reveal information about the rheology, velocity, density and viscosity of the mud erupted and energy of eruptions themselves that would be required in order to cause these blocks to move. This could be achieved if stratigraphic correlation between the blocks and the surrounding country rock could be determined most likely using biomarkers.

- Structural mapping around mud volcano systems would also increase understanding about how these structures pierce the country rock. Of particular interest would be how the intrusion of mud volcano systems may affect the growth of the anticlines through which they penetrate, particularly in Azerbaijan. This would be of use for the hydrocarbon industry as it may have an impact upon how their petroleum systems evolve through time.

- How intrusion of mud volcano systems affects the country rock through which it intrudes on a micro-scale should also be addressed. During this study a small grain crushing analysis was carried out on six transects across three mud volcano systems. This was carried out in order to assess the amount of grain crushing that was caused by the intrusion of the mud volcano systems.

Transects were carried out perpendicular and parallel to anticline axes across the different mud volcanoes. Thin sections of each hand specimen were made and stained with blue dye. Although no significant grain crushing was found in relation to proximity to the mud volcano systems micro-scale fracturing was observed. This fracturing contained clay infills suggesting that mud may invade on a variety of scales. A study that focuses primarily on this micro-scale intrusion would be useful in gaining insight into how far this fracturing occurs from the centre of the intrusive complex, what orientation these formed at and what impact this may have on the surrounding country rock.

- Mud volcano edifices and structures on their crests display a degree of statistical 'self-similarity', they are geometrically similar at a range of scales, for example gryphons on the crest of a large mud volcano resemble the kilometre-scale edifices on which they sit (Bonini & Mazzarini 2010). The schematic model of the intrusive domain in Chapter 3 bears a striking resemblance to the blow-out pipe in Fig. 6.1 indicating that the intrusive domain of kilometre-scale mud volcanoes share similar structure to metre-scale pipes. If this is true of the mud volcano system as a whole a study focusing on this aspect might be able to shed some light on the geometry of the intrusive system at depth and may enable predictive modelling of these systems.

- How different fluid types erupt along different parts of the same anticline could also be investigated. In Chapter 4 it can be seen that different fluid types erupt along separate sections of the same anticline, with one part erupting a mud plug, another dominantly salses and another dominantly gryphons. Does the location along the anticline or the tilt of the anticline hinge affect which types of fluids are able to erupt?

- During this study mud particle size analysis and rheological experiments on erupted mud from various different mud volcanoes in Azerbaijan were carried out. These data in conjunction with particle shape analysis could be used to determine how these parameters influence mud flow through the crust. Future

research in this area should be cross-disciplinary, focusing on the coupling between stress, pressure, particles size, shape, fluid and mass transport, and will involve geologists, geochemists, mathematicians and physicists.

- How does the structure of the intrusive domain evolve through time? In Chapter 4 the analysis of the Lusi mud volcano revealed an evolution of its fluid flow pathways within only a few years of its birth. This highlights the importance of time-lapse monitoring of mud volcano systems globally in order to better understand their evolution. If this could be done it would greatly enhance hazard prediction during well planning.

6.4.2 Modelling

- Further data-driven research would be significantly boosted by numerical and analogue modelling to constrain the mechanics of deep subsurface sediment remobilisation as these processes cannot be readily observed, unlike many conventional sediment transport phenomena.

- Incorporation of focused fluid flow conduits in basin and fluid flow modelling to ascertain impacts on migration and storage of fluids, compaction, heat flow, both during and following the emplacement of such conduits (transient vs. steady- state modelling).

6.4.3 Seismic Imaging Techniques

- It is only recently that good quality 3-D seismic data that cover mud volcano systems have become available. Despite the large volume and high quality of seismic data available to this project no intrusive domains are imaged in enough detail to allow for meaningful seismic interpretation to take place. Whilst analysis of these examples has proved successful, the inclusion of more 3-D seismic data and more well-imaged examples would allow for a more informed comparison of systems globally. Significant advancements are also likely to take

place in this field as better quality seismic data becomes available. In particular there are ongoing projects focussed on producing high quality converted wave seismic data in the South Caspian Sea (Bouska & Johnston 2005). These new data are likely to lead to improved imaging of the intrusive elements of mud volcano systems since they are not subject to the gas-related imaging problems that hamper normal P-wave data acquisition. In order to really determine the structure of subsurface fluid flow pathways especially in mud volcano systems seismic reflection data must improve its resolution in order to image metre-scale structures and features that contain or exist beneath gas accumulations or large quantities of fluid that distort any images produced.

- In the case of the source domain there is a large gap in the knowledge of its physical properties and the structures which control the location of large mud volcano systems. This is partly due to a lack of any boreholes that penetrate the source domain. It is also a result of the fact that most commercially acquired seismic surveys become very poorly quality at the typical depth of mud volcano parent beds

Many of these suggestions are far beyond the scope of this thesis however, all would lead to a more comprehensive understanding of mud volcano systems as a whole. The rewards of such studies should be an improved understanding of dynamic basin processes, fluid flow within the crust, hazard distributions and understanding the impacts of these natural processes on the environment in the near and long term.

Appendix I: Azerbaijan Locations, Structural Maps and Eruption History

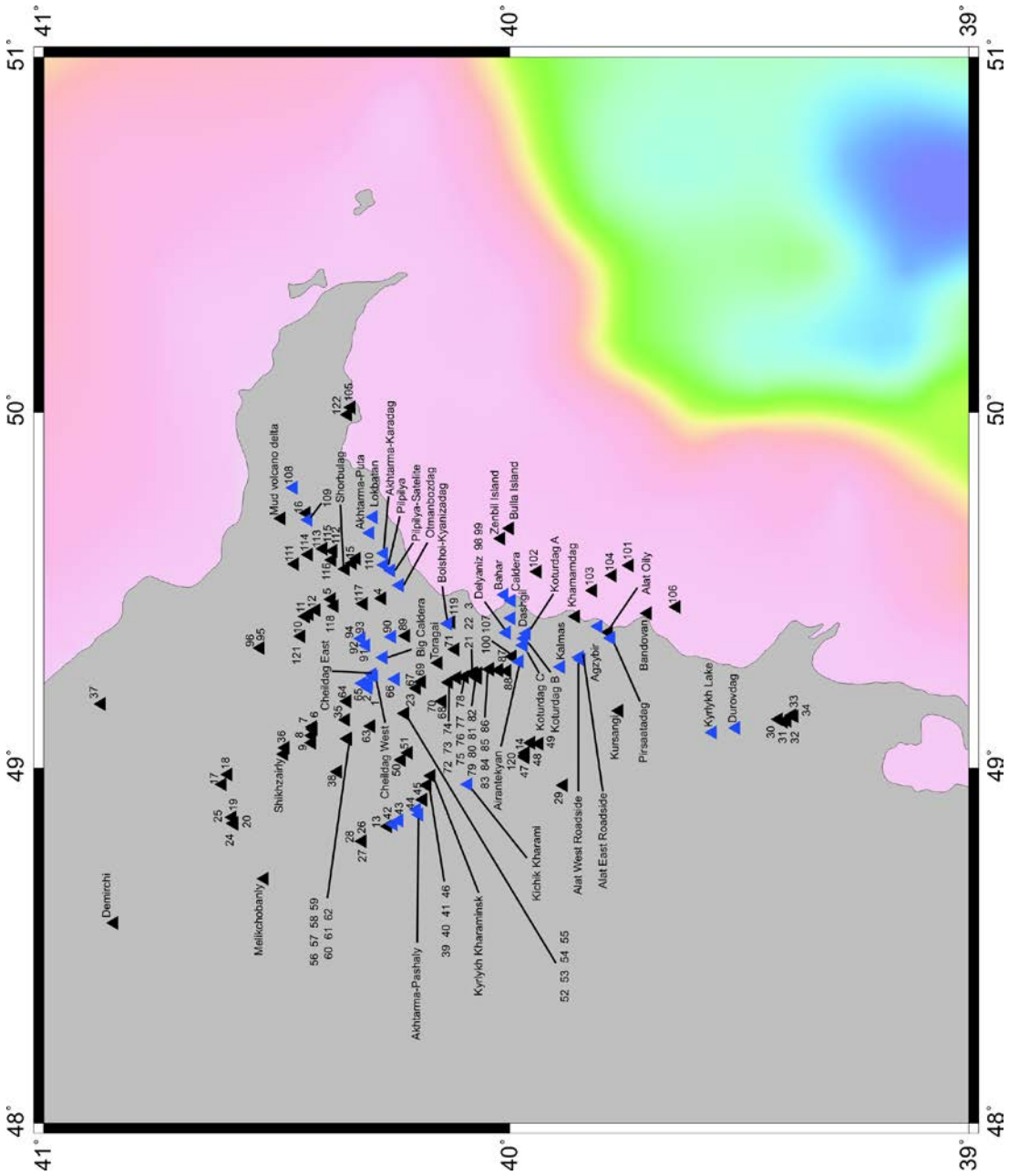

Mud volcano location map. Mud volcanoes marked by blue triangles were visited during the study. Mud volcanoes marked with black stars were mapped on Google Earth.

Structural Map of the Lökbatan Area (Courtesy of Geospatial Research Ltd (GRL))

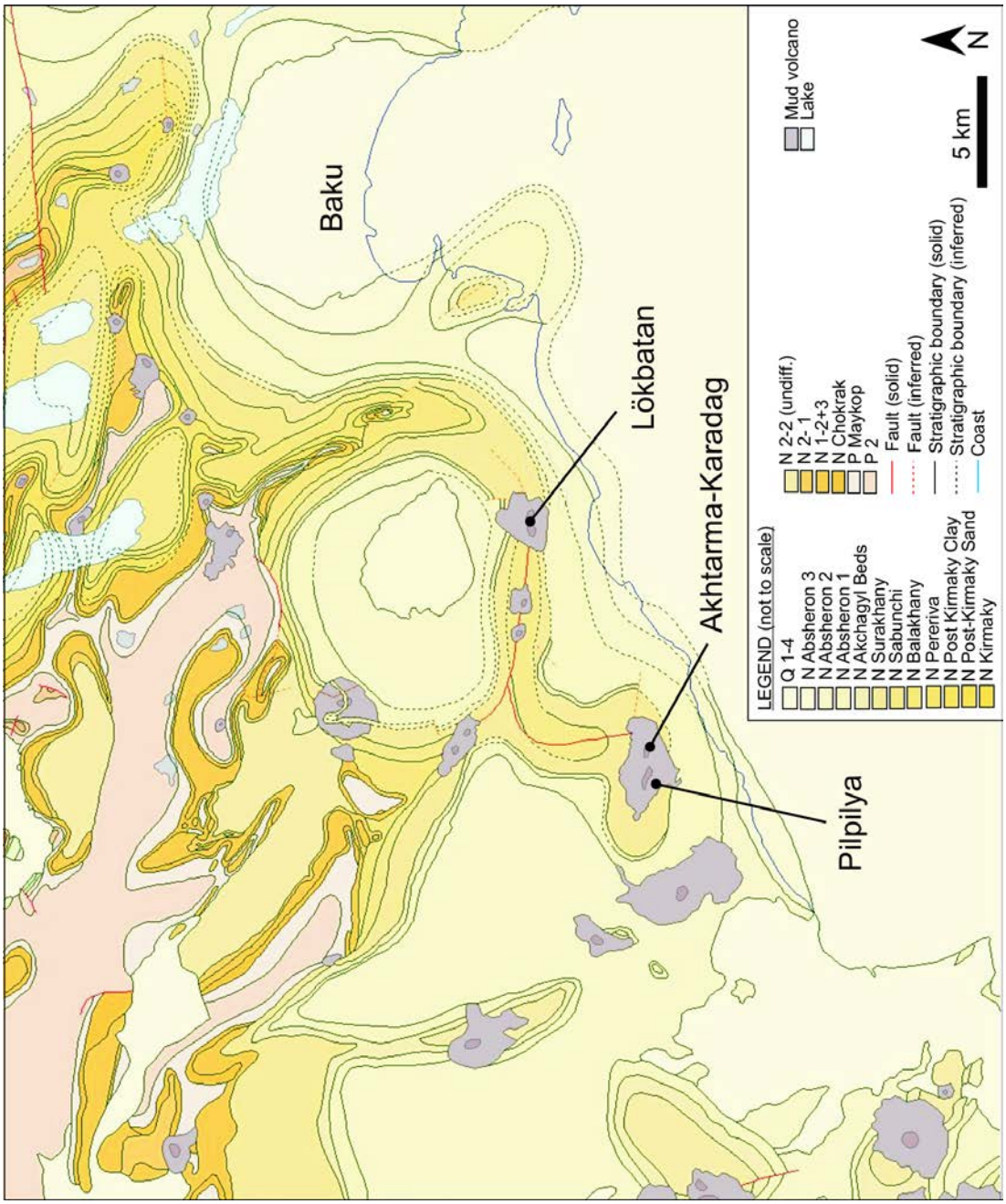

Azerbaijan Mud Volcano Eruption Records: 1810-2001 (Aliyev *et al.* 2002)

Volcano	Date of Eruption	Time	Duration (hrs)	
			Hours	Minutes
Gil Island	1810			
Khare-Zire Island	1810			
Yanan-Tava				
Keyreki	1824			
Yanan-Tava	1825			
Bozag-Gobu	09/12/1827	18:00:00	3	
Lokbatan	06/01/1829			
Keyreki	03/06/1830	19:30:00	1	30
Bozag-Gezdek	10/02/1839	13:00:00	20	
Toragai	1841			
Yanan-Tava	1841			
37 km from Shamakhi City	21/06/1844	19:00:00		45
Pirsagat River Valley	21/07/1845	19:00:00		
Shikhzairli	20/07/1848	Night		
Marazy	24/11/1848	12:00:00		
Jengi	24/03/1851	20:00:00		
Bakhar	1853			
Otmanbozdag	03/02/1854	21:00:00	3	
Khare-Zire Island	22/03/1857	05:30:00		45
Gil Island	05/07/1859	20:00:00		
Khare-Zire Island	1859	23:00:00		20
Bakhar	1859			
Gil Island	24/06/1860	12:00:00		25
Chigil-deniz	19/05/1861			
Lokbatan	1864			
Keyreki	1865			
Degne	09/08/1866	14:45:00		
Bozdag-Gezdek	17/11/1867	16:00:00		4
Yanan-Tava	24/04/1868	19:00:00		
Shikhzairli	27/05/1868	Night	3	
Aran-deniz	1868			
Cheildag	01/12/1870	Afternoon		
Kalamaddyn	26/01/1872	11:00:00		
Shikhzairli	26/01/1872	11:00:00		
Jengi	23/08/1873			
Bakhar-deniz	1876			
Garasu Island	29/02/1876	Morning		
Garasu Island	21/03/1876	Evening		
Dashgil	30/06/1882			
Near Salyan City	1882		2	
Keyreki	1885			
Bakhar	30/07/1886			
Lokbatan	17/01/1887	12:00:00		10
Abseron Kyupesi	1888			
Lokbatan	1890			
Buzovna Sopkasi	02/05/1890			
Bozdag-Gobu	1894			
Lokbatan	1900			

Toragai	1901			
Bozakhtarma	13/02/1902			
Shikhzairli	13/02/1902			
Bozdag-Gezdek	1902			
Keyreki	1902			
Dashgil	1902			
Lokbatan	1904			
Otmanbozdag	22/11/1904			
Bank	03/10/1906			
Sabail	1907			
Dashgil	04/07/1908			
Bakhar	14/03/1909		216	
Bakhar	1911			
Delyaniz	19/04/1912	18:00:00		20
Bakhar-deniz	1912			
Kichik Kharami	1912			
Gushchi	05/01/1913			
Gil Island	27/08/1913	Night		15
Aran-deniz	1913			
Giziltepe	03/01/1914			
Giziltepe	10/04/1914			
Lokbatan	03/02/1915	23:10:00	1	
Keyreki	17/02/1915	20:00:00		5
Sabail	27/07/1915			
Buzovna Sopkasi	27/07/1915		2	
Gushchi	13/11/1917			
Lokbatan	14/03/1918			
Dashly Island	07/10/1920			
Bakhar-deniz	1921			
Beyukdag	1921			
Beyukdag	1921			
Otmanbozdag	31/01/1922	18:25:00		25
Lokbatan	07/01/1923	Evening	1	30
Garasu Island	08/02/1923	17:37:00		40
Sangi-Mugan Island	29/03/1923			
Buzovna Sopkasi	08/10/1923	00:00:00	2	
Akhtarma-Puta	1923			
Toragai	13/03/1924	19:33:00		22
Gushchi	1924			
Between Stations Alyat and Navagi	24/03/1924			25
Bakhar-deniz	07/07/1925	Night		
Basgal	1926			
Ayazakhtarma	1926			5
Bozdag-Gekmaly	17/05/1926	06:00:00		30
Dashgil	08/06/1926			
Lokbatan	14/08/1926	20:00:00	3	30
Bakhar	11/10/1926	14:05:00		
Gil Island	13/11/1926	21:25:00		40
Chigil-deniz	01/05/1927	02:15:00		
Shikhzairli	14/08/1927			
Chigil-deniz	13/11/1927			
Garakure	1928			

Chigil-deniz	05/11/1928	14:15:00	45	
Chapylmish	01/06/1929			
Shikhzairli	24/11/1929	11:35:00	1	30
Sangi-Mugan Island	11/04/1932	19:30:00	9	
Bandovan	1932			
Toragai	20/04/1932	02:25:00		
Lokbatan	05/03/1933			
Sangi-Mugan Island	22/05/1933	21:35:00		4
Chapylmish	28/05/1933	11:30:00		
Akhtarma-Puta	01/11/1933			
Near Bakhar-deniz	1933			
Lokbatan	23/02/1935	21:00:00		
Saryncha	15/06/1936	Morning		
Gil Island	28/09/1937	08:45:00		15
Lokbatan	18/01/1938	22:00:00		
Shikhzairli	1939			
Chigil-deniz	08/11/1939	17:45:00		30
Khare-Zire Island	11/08/1940	10:20:00		48
Agnour	21/09/1940	Night		15
Lokbatan	01/03/1941	08:20:00		
Bakhar-deniz	1941			
Gushchi	1941			
Duzdag	07/09/1941			15
Near Marazy Village	05/07/1944		11	
"Dead Valley"	01/12/1945			
Shikhzairli	03/07/1946	10:30:00		
Neftchala Sopkalari	1947			
Neftchala Sopkalari	14/07/1947			
Khare-Zire Island	1947			
Khamamdag	01/09/1947			
Toragai	13/11/1947	19:20:00		30
Agnour	1948			
Nardaranakhtarma	25/11/1948			
Akhtarma-Puta	25/11/1948	14:00:00		
Shikhzairli	03/04/1949			
Solakhai	23/09/1949	04:00:00		
Neft Dashlari	01/10/1949			
Beyuk Kanizadag	12/05/1950	06:00:00	4	
Toragai	1950			
Buzovna Sopkasi	18/07/1950			
Akhtarma-Puta	1950	18:40:00		30
Chigil-deniz	04/12/1950			
Jairli	1951			
Dalyaniz	01/06/1951			
Garakyure	18/07/1951	18:00:00		35
Otmanbozdag	1951			
Neft Dashlari	1952			
Gushchi	1952			
Keyreki	01/08/1952	11:30:00	4	30
Buzovna Sopkasi	26/02/1953	20:00:00		
North East from Amiya cape, 13 km off-shore	20/07/1953	11:00:00		
Bozdag-Gobu	23/08/1953	10:30:00		

Buzovna Sopkasi	10/09/1953	Afternoon		
Durovdag	1953			
Lokbatan	30/07/1954	22:22:00		15
Gushchi	1954			
Dashmardan	21/11/1954	14:30:00	1	15
Shikhzairli	30/01/1955			
Mugan-deniz	1957			
Bozdag-Gobu	27/08/1957	22:00:00		30
Neft Dashlari	01/12/1957			30
Keyreki	1957			
Dashgil	20/03/1958	12:20:00		
Bakhar-deniz	15/10/1958	21:50:00		35
Demirchi	1958			
Gushchi	1958			
Khare-Zire Island	21/10/1959			
Lokbatan	17/12/1959	18:10:00		10
Chigil-deniz	25/12/1959	08:45:00		18
300m eastward from Gil Island	08/05/1960	00:00:00		
Durandag	18/06/1960	Evening		
Khare-Zire Island	23/07/1960	22:00:00	4	
Gushchi	01/08/1960			
	01/05/1961			
Bank	1960			
Zenbil Island	04/09/1961	08:45:00		35
Khare-Zire Island	23/03/1962			
Gil Island	04/09/1962			
Kelany	15/09/1962		3	
Bakhar-deniz	01/02/1963			30
Ajiveli	01/03/1963	14:30:00	1	30
Lokbatan	1963			
Agzybir	17/06/1964	21:15:00		10
Airanteken	07/10/1964	00:30:00	3	
Keyreki	1964			
Kursangi	03/01/1965	20:45:00		
Gushchi	11/09/1965	02:00:00	2	
Otmanbozdag	01/10/1965	13:00:00	2	30
Keyreki	01/07/1966		2	
Goturdag	15/10/1966			
Kelany	01/12/1966	16:00:00	4	
Bakhar	20/03/1967	20:45:00		
Melikchobanli	03/10/1967	15:00:00	1	
Keyreki	14/04/1968	16:00:00	3	
Bozakhtarma	1969			
K.Maraza	1969			
Airanteken	10/06/1969	17:15:00		
Shikhzairli	1969			
Akhtarma-Pashaly	07/07/1969			
Kelany	12/12/1969	20:40:00	3	
Kalajalar	1970			
Bozakhtarma	1970			
K.Maraza	1970			
Cheildag	04/06/1970	16:30:00		

Sabail	25/06/1970	22:00:00		
Goturdag	1970			
Kurdamir	1970			
Cheildag	01/12/1970	Night		
Kurdamir	1971			
Demirchi	12/11/1971	Evening		
Two groups of Nardaranakhtarme	1971-1972			
Lokbatan	01/10/1972	05:47:00	1	
Ayazakhtarma	01/06/1973			
Ayazakhtarma	1973			
Bozdag-Gobu	09/05/1974	11:10:00		20
Shikhzairli	1974			
Davalidag	01/04/1975			
Sheytanud	1975			
Agnour	01/05/1976	07:40:00		15
Dashmardan	26/09/1976	13:26:00		35
Saryncha	10/10/1976			
Garasu Island	28/03/1977	23:34:00	168	
Airanteken	18/09/1977	13:57:00		
Lokbatan	06/10/1977	14:30:00	2	30
Goturdag	01/12/1977			
Melikchobanli	1977			10
Agzybir	1978			
Lokbatan	31/03/1980	01:26:00		19
Shikhzairli	02/11/1980	19:15:00	2	
Akhtarma-Pashaly	1982			
Nardaranakhtarma	1982			
Jagirli	1983			
Nardaranakhtarma	1984			
Chapylmish	1984			
Khamamdag	25/05/1984			
Bakhar-deniz	01/06/1984			
Toragai	1985			
Ayazakhtarma	1985			
Akhtimer	1985			
Otmanbozdag	1985			
Shikhzairli	1986			
Kichik Maraza	1986			
Bozdag-Gezdek	1986			
Bozdag-Gobu	1986			
Dashmardan	1986			
Akhtarma-Pashaly	1986			
Nardaranakhtarma	1986			
Gushchu	01/08/1986			
Shorsulu	1986			
Shikhzairli	01/04/1987			
Bozdag-Gobu	24/06/1987			
Kalajalar	1987			
Astrakhanka	1987			
Bozakhtarma	1987			
Bozdag-Gezdek	1988			
Toragai	1988			

Solakhai	1988			
Shekikhan	1988			
Airanteken	1988			
Akhtimer	1988			
Keyreki	26/02/1989	08:30:00		20
Akhtimer	1989			
Solakhai	1989			
Shekikhan	1989			
Gotur	1989			
Lokbatan	23/03/1990			
Airanteken	22/07/1990			
Akhtarmaardi	27/06/1990	23:00:00		
Keyreki	23/01/1991			
Shikhzairli	1991			
Shikhzairli	30/09/1991			
Gushchi	12/10/1992			
Bakhar	03/10/1992	18:00:00	7	
Gasimkend	29/11/1993	Evening		
Garasu Island	1993			
Khare-Zire Island	1993			
Otmanbozdag	12/12/1994	17:00:00		
Zenbil Island	20/08/1995	17:50:00		
Bozdag-Gezdek	01/05/1995			
Nardaranakhtarma	01/10/1996			
Beyuk Kanizadag	01/10/1996			
Khamamdag	01/10/1996			
Shikhzairli	01/06/1997			
Khare-Zire Island	20/10/1997			
Bozdag-Gobu	01/07/1999			
Kechaldag	10/10/2000			
Akhtimer	01/12/2000			
Durandag	01/01/2001			
Garabujag	2001			
Shekikhan	2001			
Gotur	2001			
Ayazakhtarma	2001			
Nardaranakhtarma	2001			
Chapylmish	2001			
Solakhai	2001			
Buzovna Sopkasi	21/03/2001			
Dashgil	01/05/2001			
Chigil-deniz	30/05/2001			
Keyreki	26/06/2001	20:42:00	2	30
Lokbatan	24/10/2001	14:45:00		28
Bozdag-Gekmaly	24/11/2001			

Appendix II: Supporting Material for Chapter 3

Alyaty Ridge, Azerbaijan

Field photographs from Alyaty Ridge. A) Weathered clast on the top of Koturdag B mud volcano. B) Fractured sandstone clast on top of Koturdag B mud volcano. C) Pre-intrusion fracturing in sandstone country rock along stream section in between Koturdag B and C. D) Pre-intrusion fractures in sandstone country rock along stream section in between Koturdag B and C. E) Sinuous fractures with clay infill in sandstone country rock along stream section in between Koturdag B and C. F) Pre-intrusion fractures infilled with gypsum in sandstone country rock along stream section in between Koturdag B and C.

Kichik Kharami Mud Volcano, Azerbaijan

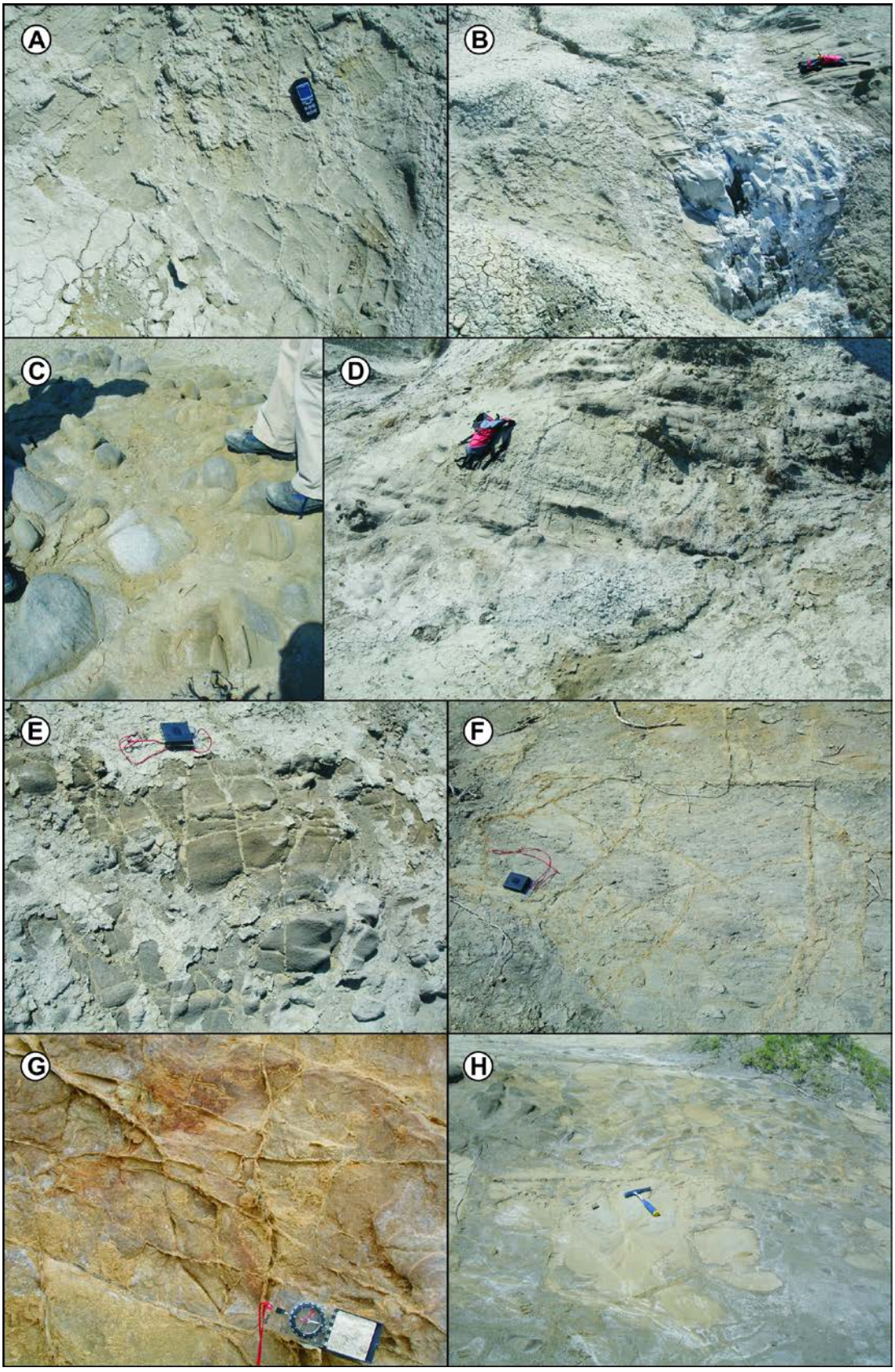

Field photographs of mud intrusions from Kichik Kharami mud volcano. A) Sinuous fracturing with a clay infill, in sandstone. B) Pre-intrusion fractures in sandstone country rock with clay infill. C) Pre-intrusion fractures in sandstone country rock. D) Sinuous fracturing with a clay infill, in sandstone. E) Sinuous fracturing with a clay infill, in sandstone. F) Sinuous fracturing with a clay infill, in sandstone. G) Pre-intrusion fractures in sandstone country rock with clay infill.

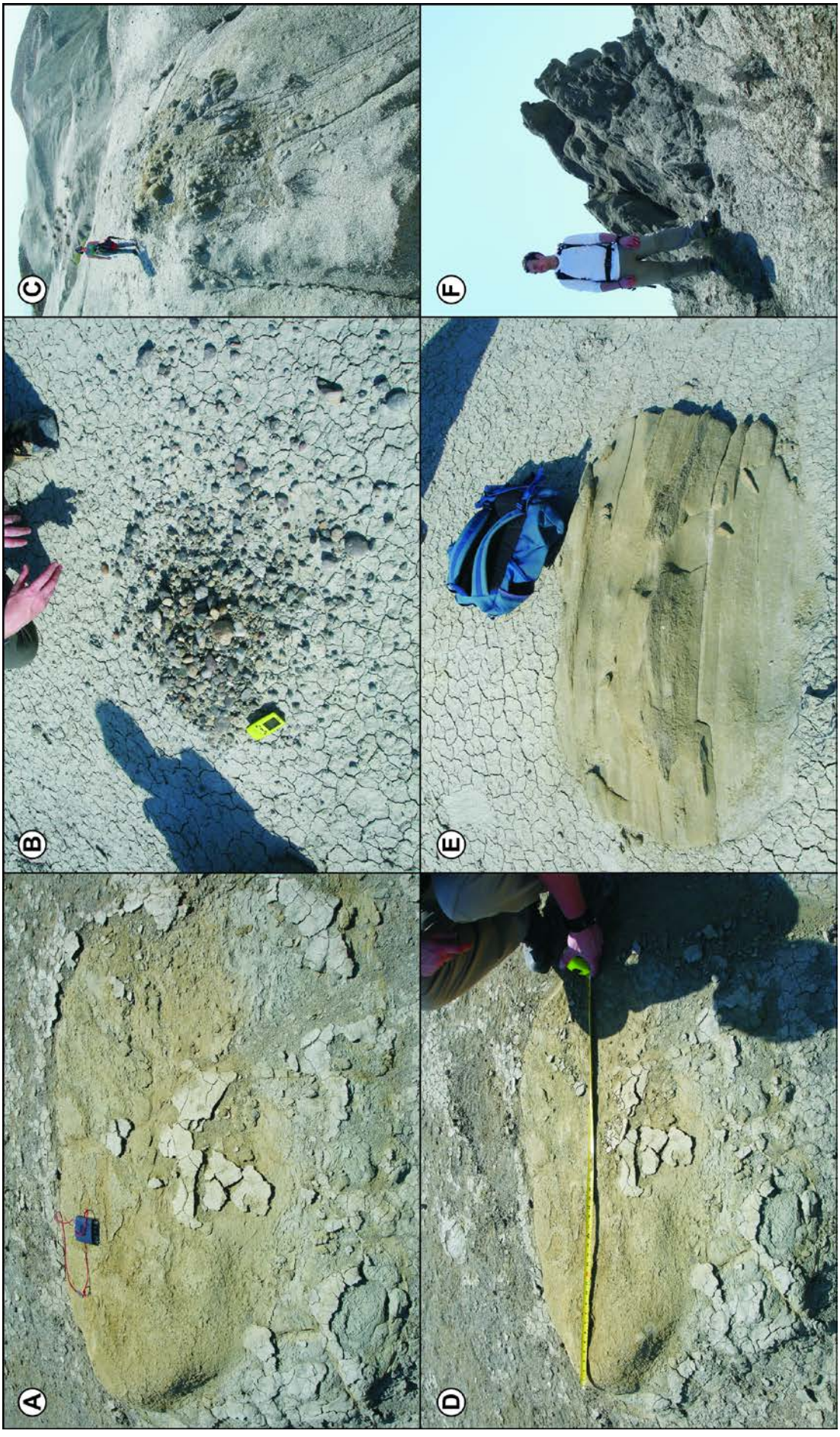
C
F
B
E
A
D

Field photographs of clasts and megablocks from Kichik Kharami mud volcano. A) Sandstone clast, compass clinometer for scale. B) Eroded conglomerate clast, Garmin Geko GPS for scale. C) Highly fractured sandstone clast. D) Sandstone clast. E) Sandstone clast, rucksack for scale. F) Fractured sandstone clast.

Pirsaatadag mud volcano, Azerbaijan

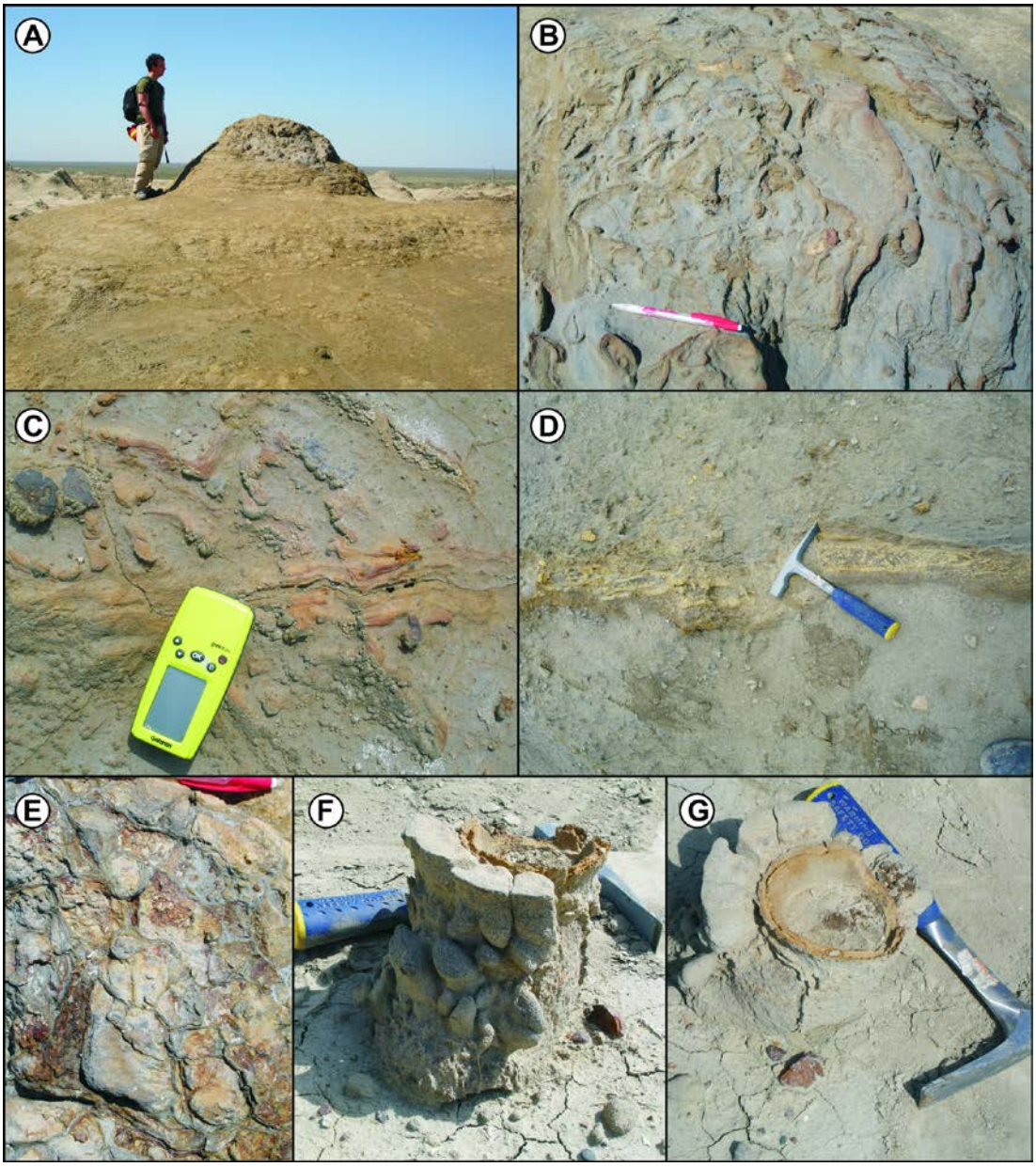

Field photographs of intrusions from Pirsaatadag mud volcano. A) Dead vent complex with feeder pipes forming a mound due to increased resistance to weathering compared to the erupted mud. B) Dead feeder pipe complex, pipes have red/brown staining where fluids have been flowing, pen for scale. C) Dead feeder pipe complex, pipes have red/brown staining where fluids have been flowing, Garmin Geko GPS for scale. D) Yellow mineralisation along a faulted fracture, hammer for scale. E) Fractures infilled by clay and 'tar', pen top for scale. F) Pipe structure with sandstone clasts attached to its side, pipe is more resistant to weathering standing proud of erupted mud, hammer for scale. G) Different view of F) note the red/brown staining on the edges and at the core of the pipe.

Appendix III: Supporting Material for Chapter 4

Mud Volcano Vent Distribution Maps and Statistics

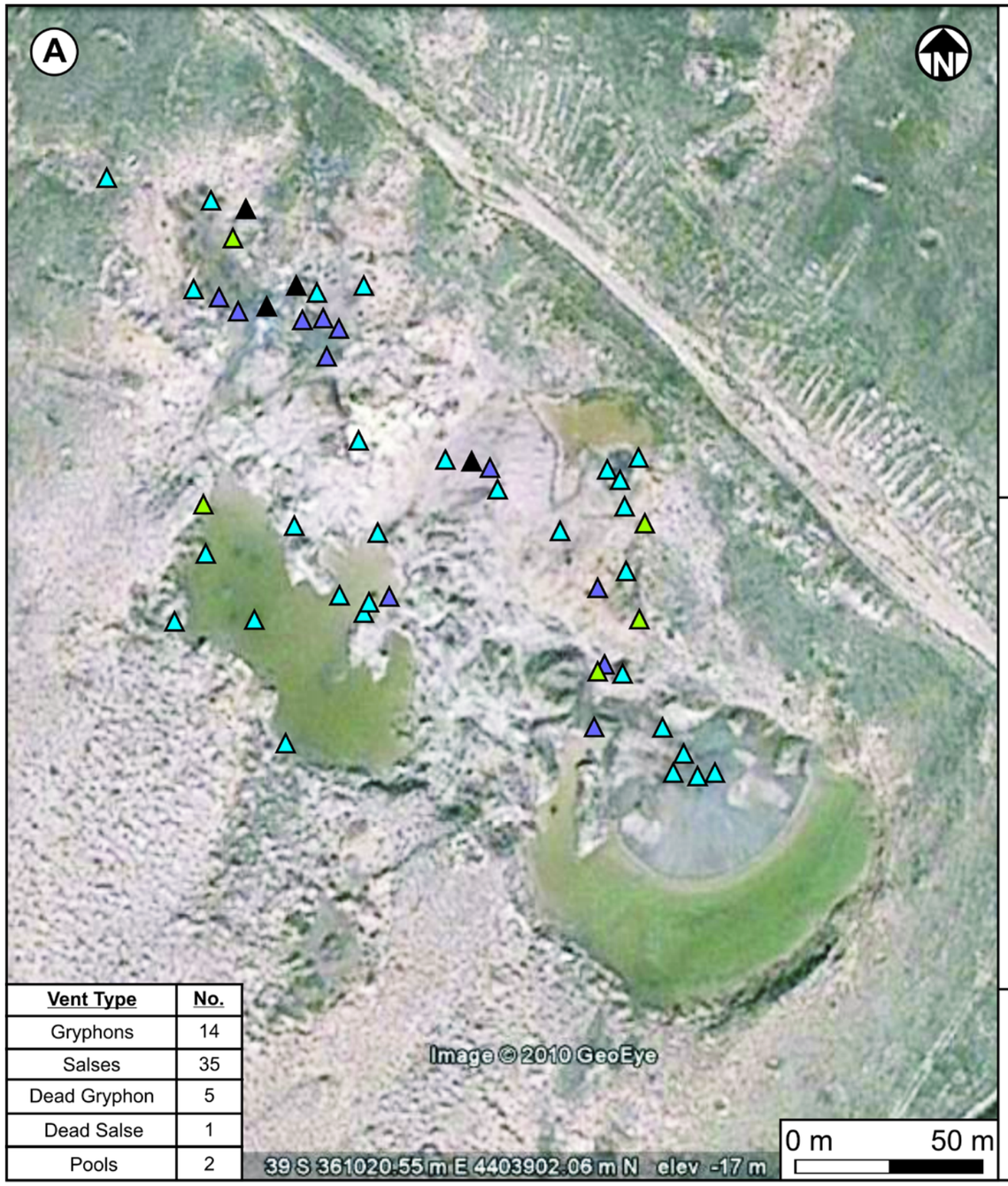

Vent Type	No.
Gryphons	14
Salses	35
Dead Gryphon	5
Dead Salse	1
Pools	2

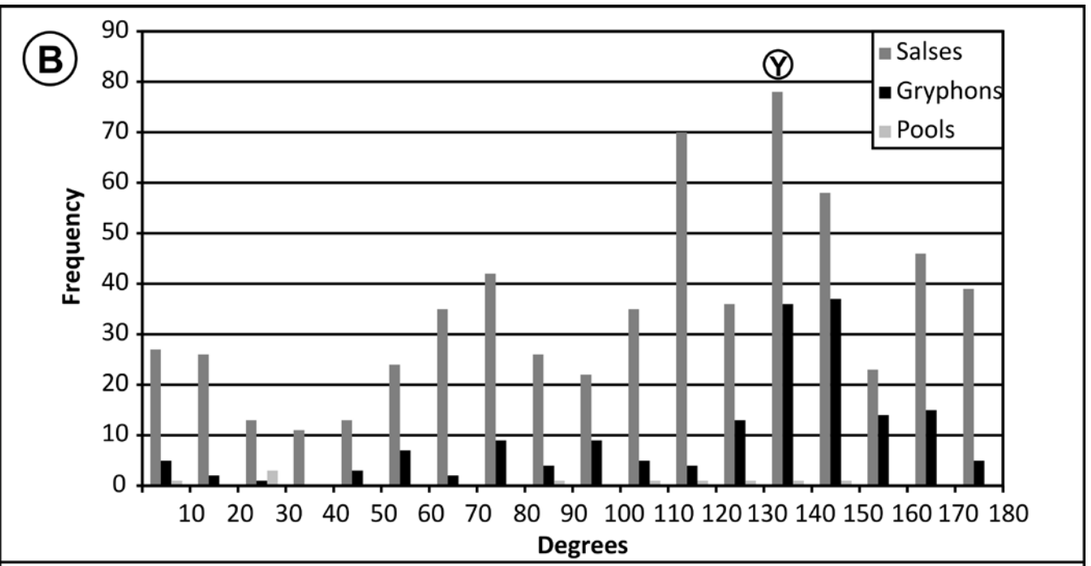

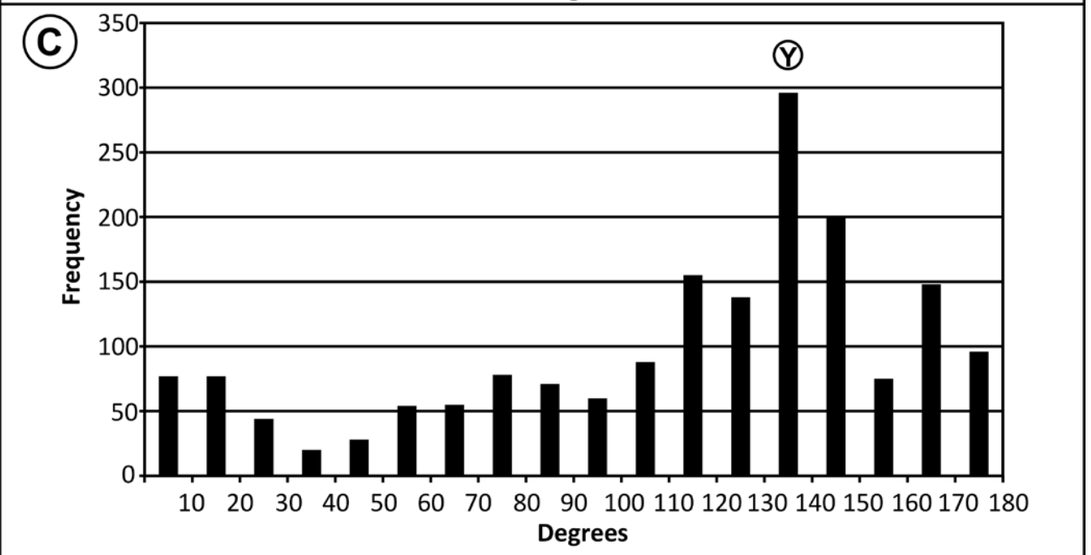

D

Volcano	Observed Mean Dist./ Expected Mean Dist.	Clustered/ Dispersed	Significance Value	Critical Value	Z Score	Nearest Neighbour Observed Mean Dist. (km)	Expected Mean Distance (km)	Nearest Neighbour Ratio
Alat Oily	0.64	Clustered	0.01	-2.58	-5.32	0.000063	0.000098	0.641102

Alat Oily mud volcano. A) Vent distribution map. Triangles: Purple- gryphons, orange- cinder mounds, black- extinct vents, blue- salses and green- pools. Image © 2010 GeoEye, © 2010 Google. B) Histogram of frequencies of azimuthal direction for 2-point azimuth method of individual vent types separated into their different distributions. C) Histogram of frequencies of azimuthal direction for 2-point azimuth method of all vent types grouped together. D) Nearest neighbour statistical analysis results.

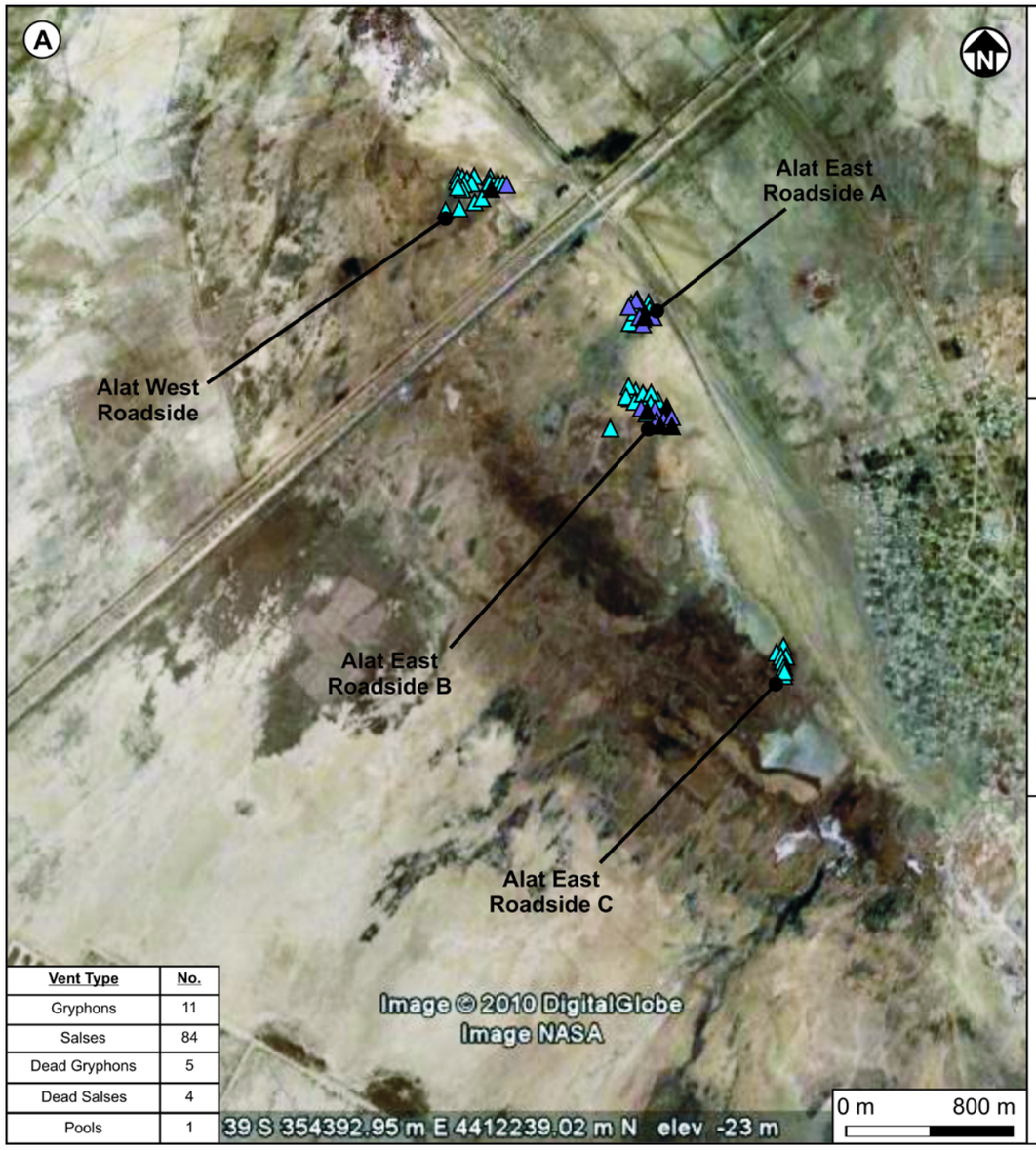

Vent Type	No.
Gryphons	11
Salses	84
Dead Gryphons	5
Dead Salses	4
Pools	1

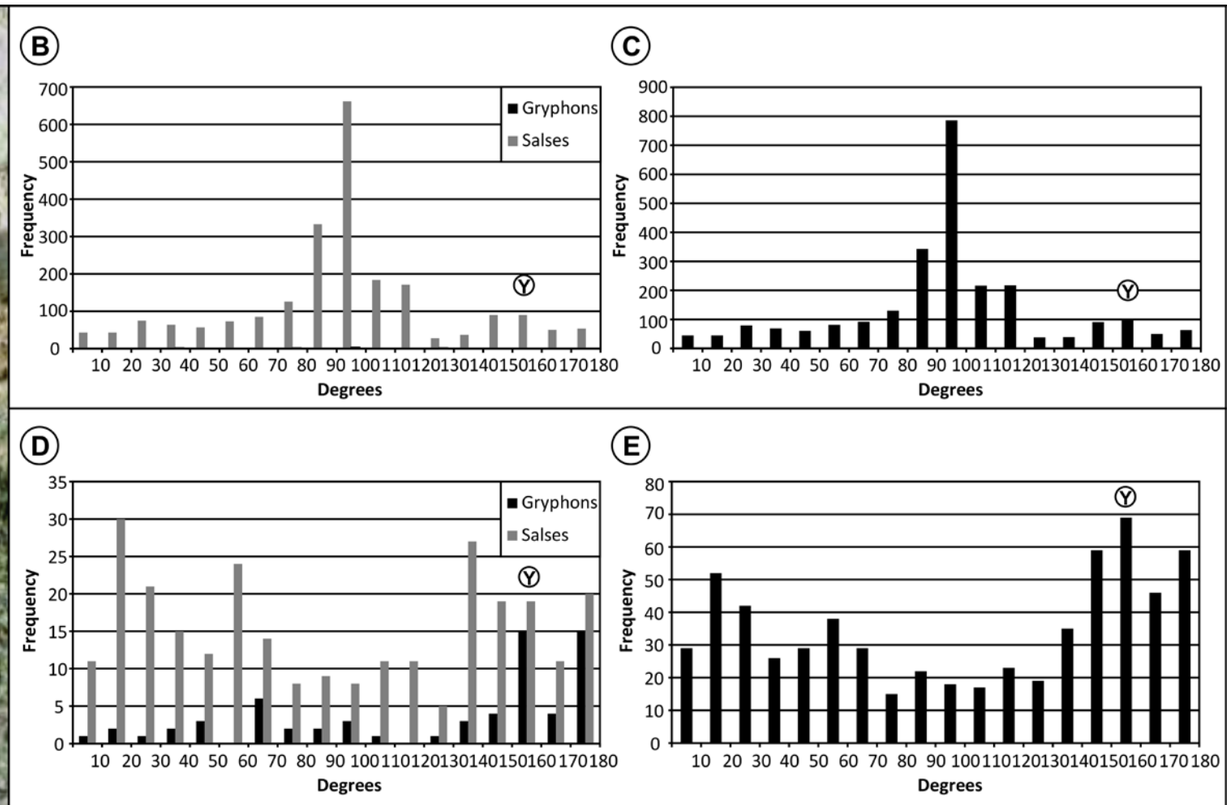

F

Volcano	Observed Mean Dist./ Expected Mean Dist.	Clustered/ Dispersed	Significance Value	Critical Value	Z Score	Nearest Neighbour Observed Mean Dist. (km)	Expected Mean Distance (km)	Nearest Neighbour Ratio
Alat West	0.44	Clustered	0.01	-2.58	-9.02	0.000066	0.000149	0.444584
Alat East A	0.83	Clustered	010	-1.65	-1.92	0.000090	0.000108	0.832818
Alat East B	0.41	Clustered	0.01	-2.58	-15.36	0.000038	0.000091	0.412995
Alat East C	0.29	Clustered	0.01	-2.58	-16.75	0.000009	0.000030	0.294254

Alat East and West mud volcanoes. A) Vent distribution map. Triangles: Purple- gryphons, orange- cinder mounds, black- extinct vents, blue- salses and green- pools. Image © 2010 DigitalGlobe, © 2010 Google. B) Histogram of frequencies of azimuthal direction for 2-point azimuth method of individual vent types separated into their different distributions for Alat West Mud Volcano. C) Histogram of frequencies of azimuthal direction for 2-point azimuth method of all vent types grouped together for Alat West Mud Volcano. D) Histogram of frequencies of azimuthal direction for 2-point azimuth method of individual vent types separated into their different distributions for Alat East Mud Volcano. E) Histogram of frequencies of azimuthal direction for 2-point azimuth method of all vent types grouped together for Alat East Mud Volcano. F) Nearest neighbour statistical analysis results.

Vent Type	No.
Gryphons	33
Salses	26
Dead Gryphons	4
Pools	36

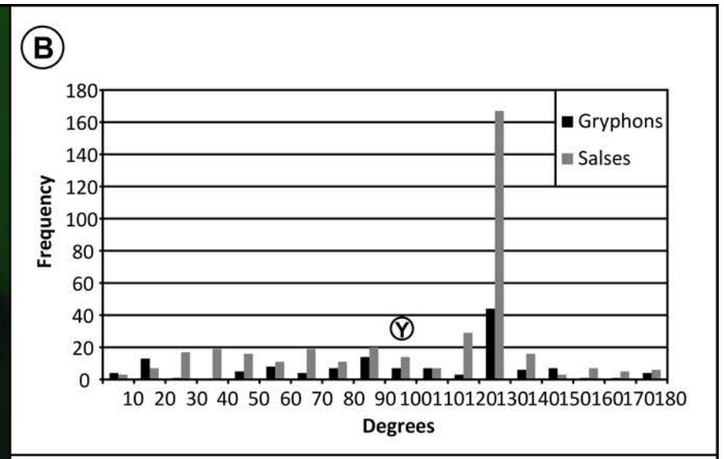

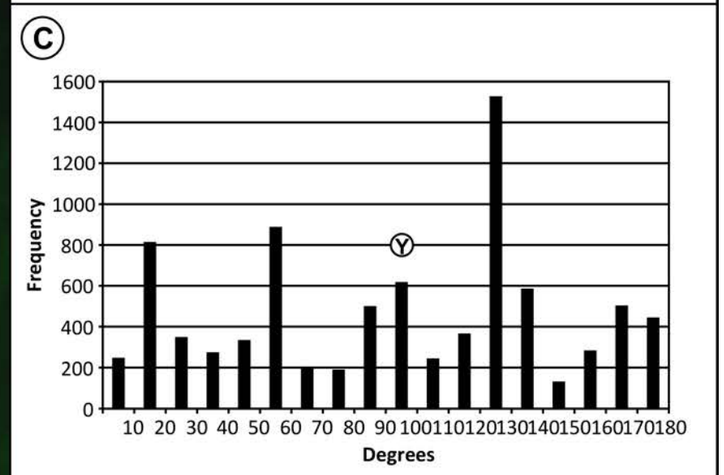

D

Volcano	Observed Mean Dist./ Expected Mean Dist.	Clustered/ Dispersed	Significance Value	Critical Value	Z Score	Nearest Neighbour Observed Mean Dist. (km)	Expected Mean Distance (km)	Nearest Neighbour Ratio
Bahar	0.47	Clustered	0.01	-2.58	-7.33	0.000185	0.000394	0.468677

Bahar mud volcano. A) Vent distribution map. Triangles: Purple- gryphons, orange- cinder mounds, black- extinct vents, blue- salses and green- pools. Image © 2010 GeoEye, © 2010 Google. B) Histogram of frequencies of azimuthal direction for 2-point azimuth method of individual vent types separated into their different distributions. C) Histogram of frequencies of azimuthal direction for 2-point azimuth method of all vent types grouped together. D) Nearest neighbour statistical analysis results.

Vent Type	No.
Gryphons	6
Salses	31

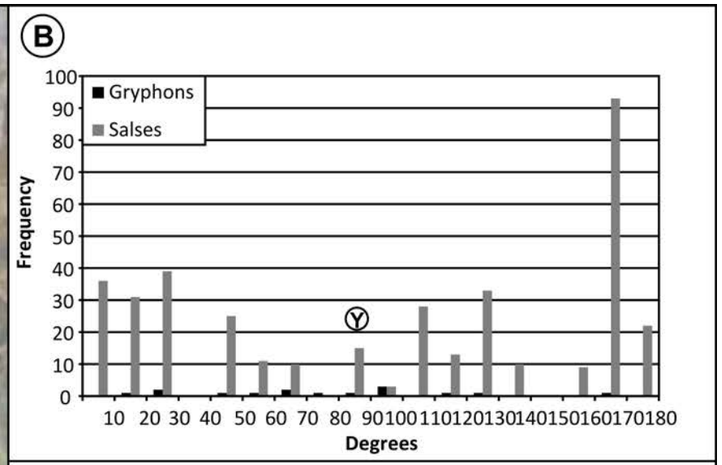

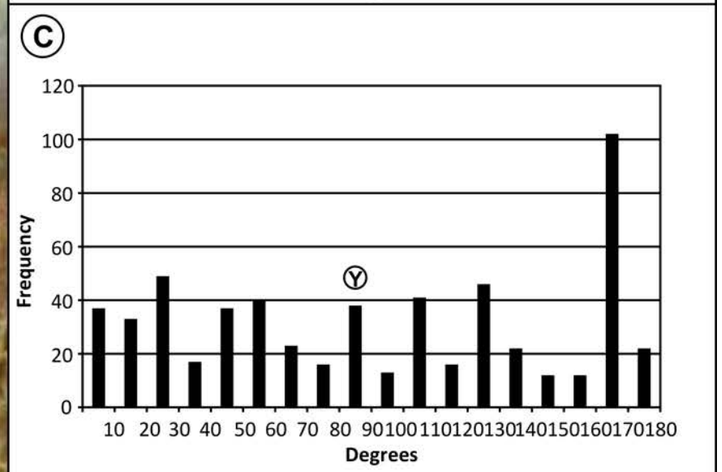

D

Volcano	Observed Mean Dist./ Expected Mean Dist.	Clustered/ Dispersed	Significance Value	Critical Value	Z Score	Nearest Neighbour Observed Mean Dist. (km)	Expected Mean Distance (km)	Nearest Neighbour Ratio
Caldera	0.55	Clustered	0.01	-2.58	-5.21	0.000007	0.000013	0.552016

Caldera mud volcano. A) Vent distribution map. Triangles: Purple- gryphons, orange- cinder mounds, black- extinct vents, blue- salses and green- pools. Image © 2010 GeoEye, © 2010 Google. B) Histogram of frequencies of azimuthal direction for 2-point azimuth method of individual vent types separated into their different distributions. C) Histogram of frequencies of azimuthal direction for 2-point azimuth method of all vent types grouped together. D) Nearest neighbour statistical analysis results

BPLS Lusi Map 2006

CRISP Aerial Imagery Showing the Evolution of Lusi Mud Volcano: 2006-2010: Image © 2010 DigitalGlobe and © 2010 DigitalGlobe, © 2010 Google

	January	February	April	May	June	July	August	September	October	December
2005										
2006									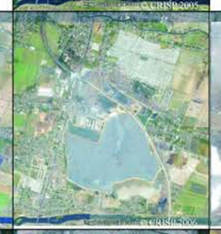	
2007	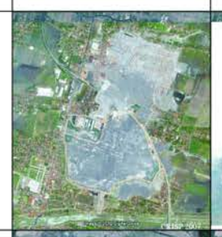	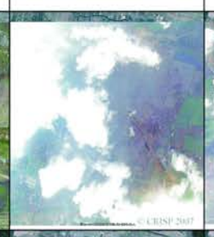	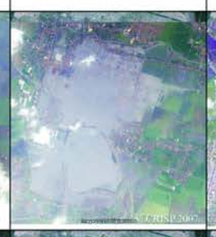							
2008										
2009		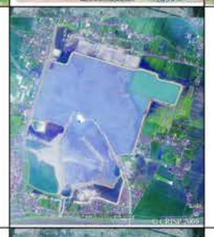						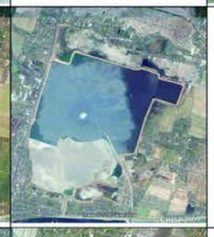		
2010										

Matlab Script for 2-Point Azimuth Technique

```
function Azimuth

[nums,text,raw] = xlsread('File_name.xls')

Northings = nums(:,1)

Eastings = nums(:,2)


i=0;

for index = 1:length(Northings)
   N1 = Northings(index,1);
   E1 = Eastings(index,1);
   for index2 = 1:length(Northings);
      N2 = Northings(index2,1);
      E2 = Eastings(index2,1);
      DiffE = E2-E1;
      DiffN = N2-N1;
      Azimuth2 = atan2(DiffE,DiffN);
      AzimuthDeg2(index,index2) = Azimuth2*(180/pi);

      if (AzimuthDeg2(index,index2) >= 0);
         i=i+1;
         Azdegpos(i)=AzimuthDeg2(index,index2);
        % AzimuthDeg2(index,index2) = NaN;
      end
   end
end



az = Azdegpos
%az = reshape(AzimuthDeg2,Northings*Northings,1);
N = hist(az,18)
bar(N)

az = az'
dlmwrite('New_File_Name.txt',az)
```

Appendix IV: Supporting Material for Chapter 5

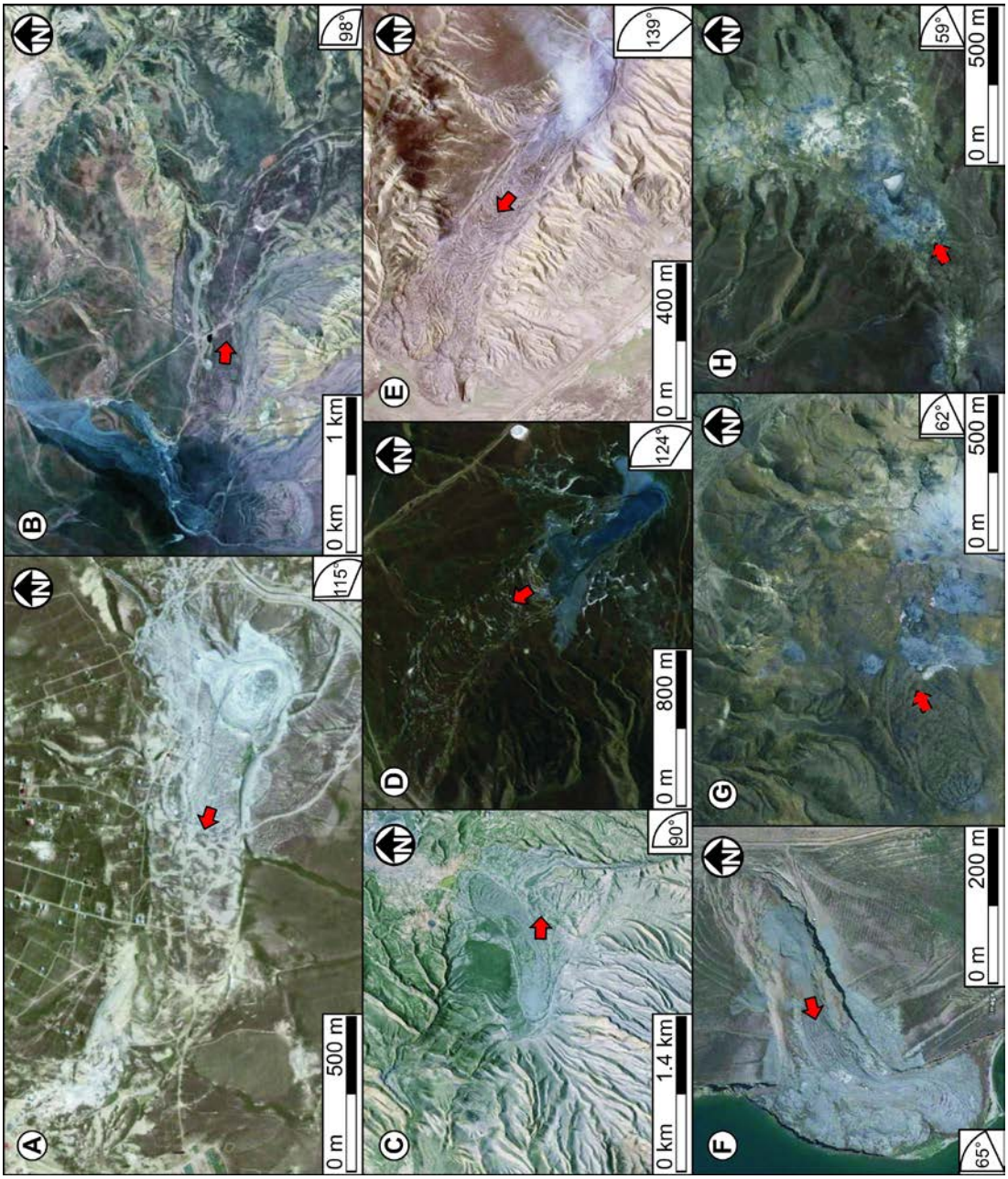

Mud volcano sector collapse structures. A) 109. Image © 2010 GeoEye, © 2010 Google. B) 51. Image © 2010 GeoEye and © 2010 DigitalGlobe, © 2010 Google. C) 88. Image © 2010 GeoEye, © 2010 Google. D) 63. Image © 2010 GeoEye, © 2010 Google. E) 70. Image © 2010 GeoEye and © 2010 DigitalGlobe, © 2010 Google. F) Mud volcano delta. Image © 2010 GeoEye, © 2010 Google. G) 93. Image © 2010 GeoEye, © 2010 Google. H) 66. Image © 2010 GeoEye, © 2010 Google. Red arrows point in direction that failure has occurred in. Angles show orientation of failure relative to North. Numbers and names can be used to identify mud volcano locations in the figure above and in the 'Mud volcano locations' table in the digital version of this section.

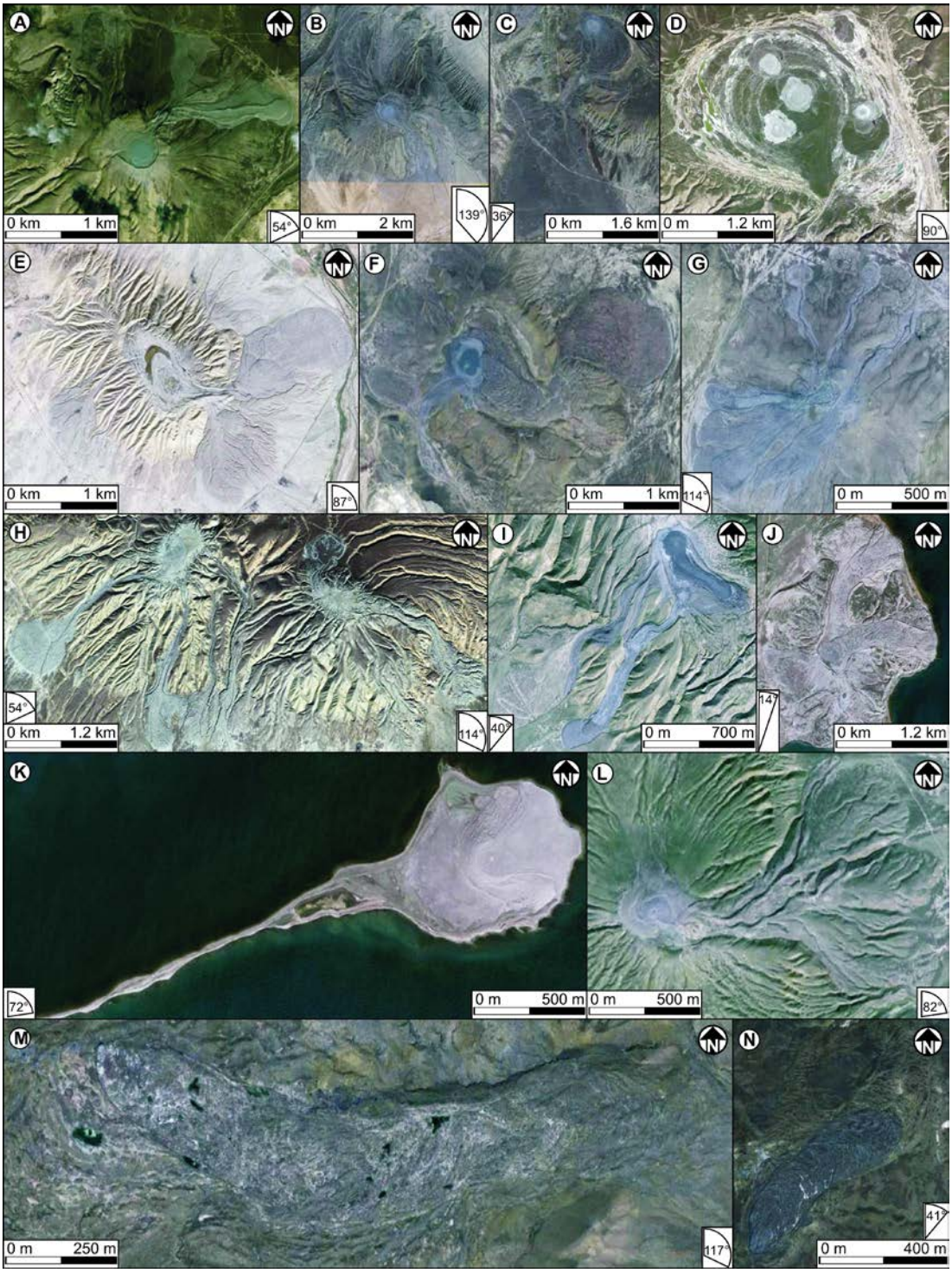

Mud volcano flows. A) 112. Image © 2010 GeoEye, © 2010 Google. B) Otmanbozdag. Image © 2010 GeoEye and © 2010 Terrametrics, © 2010 Google. C) 90. Image © 2010 GeoEye, © 2010 Google. D) Akhtarma-Pashly. Image © 2010 Terrametrics and © 2010 DigitalGlobe, © 2010 Google. E) Kalmas. Image © 2010 GeoEye and © 2010 Geocentre Consulting, © 2010 Google. F) 117. Image © 2010 GeoEye and © 2010 Geocentre Consulting, © 2010 Google. G) 110. Image © 2010 GeoEye and © 2010 Geocentre Consulting, © 2010 Google. H) 49 and 48. Image © 2010 GeoEye and © 2010 Geocentre Consulting, © 2010 Google. I) Airantekyan. Image © 2010 GeoEye and ©

2010 Geocentre Consulting, © 2010 Google. J) Khamamdag. Image © 2010 GeoEye and © 2010 Geocentre Consulting, © 2010 Google. K) 102. Image © 2010 GeoEye and © 2010 Geocentre Consulting, © 2010 Google. L) 98. Image © 2010 GeoEye and © 2010 Geocentre Consulting, © 2010 Google. M) Cheildag East. Image © 2010 GeoEye and © 2010 Geocentre Consulting, © 2010 Google. N) Cheildag West. Image © 2010 GeoEye and © 2010 Geocentre Consulting, © 2010 Google. Angles show orientation of mud flows relative to North. Numbers and names can be used to identify mud volcano locations in the figure above and in the 'Mud volcano locations' table in the digital version of this section.

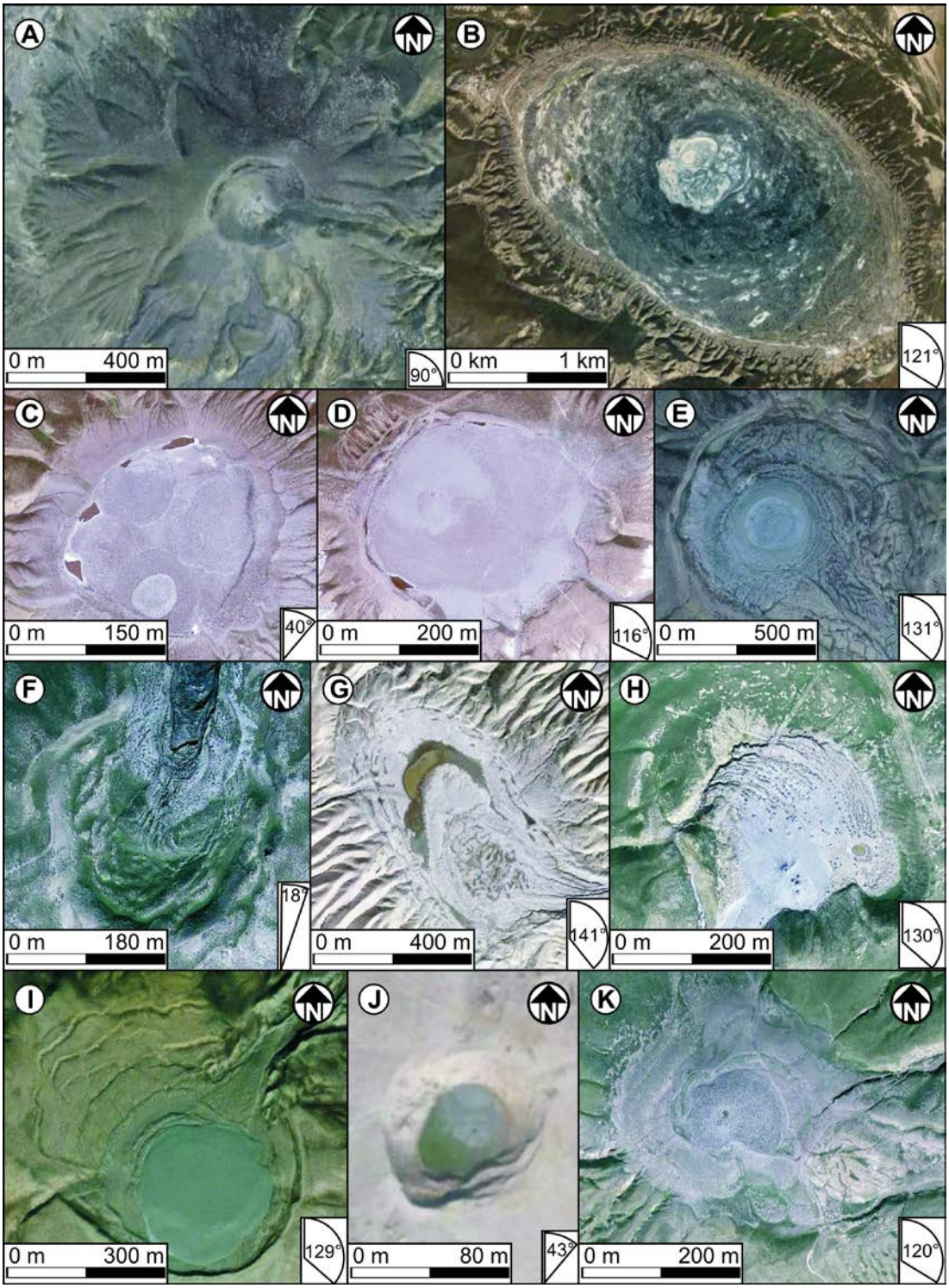

Mud volcano calderas. A) Big caldera. Image © 2010 GeoEye and © 2010 Geocentre Consulting, © 2010 Google. B) 38. Image © 2010 GeoEye © 2010 DigitalGlobe and © 2010 Geocentre Consulting, © 2010 Google. C) Toragai. Image © 2010 GeoEye and © 2010 Geocentre Consulting, © 2010 Google. D) Bolshoi-Kyanizadag. Image © 2010 GeoEye and © 2010 Geocentre Consulting, © 2010 Google. E) Otmanbozdag. Image © 2010 GeoEye and © 2010 Geocentre Consulting, © 2010 Google. F) Koturdag A. Image © 2010 GeoEye, © 2010 Google. G) Kalmas. Image © 2010 GeoEye

and © 2010 Geocentre Consulting, © 2010 Google. H) 99. Image © 2010 GeoEye and © 2010 Geocentre Consulting, © 2010 Google. I) 112. Image © 2010 GeoEye and © 2010 Geocentre Consulting, © 2010 Google. J) Caldera. Image © 2010 GeoEye © 2010 DigitalGlobe and © 2010 Geocentre Consulting, © 2010 Google. K) 98. Image © 2010 GeoEye and © 2010 Geocentre Consulting, © 2010 Google. Angles show orientation of caldera long axes relative to North. Numbers and names can be used to identify mud volcano locations in the figure above and in the 'Mud volcano locations' table in the digital version of this section.

Length – Width Profiles for Sector Collapses, Flows and Calderas

Structure	Length (m)	Top Width (m)	Middle Width (m)	Bottom Width (m)	Average Width (m)	Ratio	Middle/Bottom
Flow	840	290	180	390	286.67	2.930232558	0.461538462
Flow	1390	230	270	830	443.33	3.135338346	0.325301205
Flow	1090	210	280	700	396.67	2.74789916	0.4
Flow	1940	70	140	820	343.33	5.650485437	0.170731707
Flow	1380	70	130	1120	440.00	3.136363636	0.116071429
Flow	1250	40	90	630	253.33	4.934210526	0.142857143
Flow	1930	70	80	430	193.33	9.982758621	0.186046512
Flow	1570	60	130	230	140.00	11.21428571	0.565217391
Flow	440	50	240	380	223.33	1.970149254	0.631578947
Flow	1830	130	280	340	250.00	7.32	0.823529412
Flow	2700	170	170	880	406.67	6.639344262	0.193181818
Flow	2700	120	210	600	310.00	8.709677419	0.35
Flow	2450	210	270	800	426.67	5.7421875	0.3375
Flow	1370	70	120	550	246.67	5.554054054	0.218181818
Flow	830	120	150	140	136.67	6.073170732	1.071428571
Flow	1560	110	250	280	213.33	7.3125	0.892857143
Flow	2200	300	330	1060	563.33	3.905325444	0.311320755
Flow	3280	230	280	1810	773.33	4.24137931	0.154696133
Flow	3400	210	390	1870	823.33	4.129554656	0.20855615
Flow	770	40	100	290	143.33	5.372093023	0.344827586
Flow	1490	50	100	500	216.67	6.876923077	0.2
Sector Collapse	1540	300	550	590	480.00	3.208333333	0.93220339
Sector Collapse	3240	240	350	550	380.00	8.526315789	0.636363636
Sector Collapse	810	200	330	390	306.67	2.641304348	0.846153846
Sector Collapse	1610	140	280	330	250.00	6.44	0.848484848
Sector Collapse	1650	120	200	270	196.67	8.389830508	0.740740741
Sector Collapse	1420	180	290	230	233.33	6.085714286	1.260869565
Sector Collapse	1600	160	250	520	310.00	5.161290323	0.480769231
Sector Collapse	1120	130	280	290	233.33	4.8	0.965517241

Sector Collapse, Flow and Caldera Long Axis Orientations

Long Axis Orientation (˚)		
Calderas	**Sector Collapse**	**Flows**
150	120	60
290	70	70
155	125	30
135	290	260
145	90	240
110	75	10
260	300	50
90	320	350
110	100	145
20	70	130
110	280	50
150	55	150
145	90	190
295	260	150
270	290	110
350	240	40
20	75	355
300		40
280		150
290		180
270		140
110		240
110		350
145		90
110		180
220		200
140		310
50		120
150		200
140		90
155		130
210		230
310		10
45		70
210		15
320		50
		170
		220
		310
		320
		70
		90
		60

Appendix V: Published Journal Articles

Basin Research

IAS EAGE

Basin Research (2010) **22**, 439–451, doi: 10.1111/j.1365-2117.2009.00441.x

Structure of exhumed mud volcano feeder complexes, Azerbaijan

K. S. Roberts*, R. J. Davies* and S. A. Stewart†

*Science Laboratories, Department of Earth Sciences, Centre for Research into Earth Energy Systems (CeREES), Durham University, Durham, UK

†Institute of Petroleum Engineering, Heriot-Watt University, Edinburgh, UK

ABSTRACT

We report the first structural field mapping of exhumed mud volcano feeder complexes. Three mud volcanoes outcropping onshore in Azerbaijan were selected on the basis of outcrop quality and scale. These examples are all located within 1 km of the axes of NW–SE-trending folds associated with the southern margin of the Greater Caucasus mountain belt. The mapping shows that the intrusive complexes are 200–800 m wide and roughly circular. These feeder complexes consist of a megabreccia of country rock blocks at a scale of tens of metres, enclosed in a matrix of intrusive mud. Minor structures include grid like fractures sets, sinuous fractures, mud plugs and breccia pipes. The country rock blocks are deformed and rotated relative to surrounding sedimentary strata. Alternative mechanisms to explain the strain history of these large blocks in the feeder complexes are: a. stoping, b. flow rotation and c. caldera collapse. Our mapping indicates that the most likely mechanism involves stoping processes, similar to those identified in igneous systems. This study provides a basis for reservoir distribution in commercial geological models that contain the feeder complexes of mud volcano systems, and also constrains conduit geometry for modelling studies of evolution and flow dynamics.

INTRODUCTION

Mud volcanoes are a widespread type of piercement structure that allow for focussed fluid escape from sedimentary basins. Little is known, however, about the geometry of the sub-volcanic feeder complexes that constitute the intrusive zones (Davies & Stewart, 2005). Even less is known about the small scale structure of these feeder systems and their effect on the country rock that they intrude (Davies & Stewart, 2005). The term 'mud volcano system' was coined by Stewart & Davies (2006) to describe the set of structures associated with a constructional, extrusive edifice (mud volcano) and underlying plumbing of the volcano, which connects it to its stratigraphic source unit (Stewart & Davies, 2006). Previous studies have described various architectures connecting extrusive mud cones to their underlying source layer, ranging from bulbous diapirs (Brown, 1990) to steep diatremes (Robertson & Kopf, 1998) and narrow vertical pipes (Graue, 2000). Currently, the two most widely publicized alternative models for the sub-volcanic plumbing system are kilometre scale mud diapirs (Morley & Guerin, 1996) or intricate mud pipe, dyke and sill complexes (Morley, 2002; Stewart & Davies, 2006).

Detailed mapping of the intrusive zones of mud volcanoes will enable better understanding of the processes governing the fluid transport through the shallow crust and how the surrounding country rock is influenced. Comparisons can be made with igneous systems that appear to share many common features with mud volcanoes (Stewart & Davies, 2006). Guliyev *et al.* (2000) commented on the spatial and genetic relationship of mud volcanoes with oil and gas fields, an affiliation that impacts drilling operations, rig installations and pipeline routings. Problems occur as a result of mud eruptions and instability of the surrounding sediments (Yusifov & Rabinowitz, 2004). There are further instances of commercial significance where reservoirs are intersected by the intrusive domain of mud volcano systems. In these cases the size, shape and internal structure of feeder systems is a local control on both hydrocarbons in place and reserves (Stewart & Davies, 2006).

This paper investigates outcrop-scale features seen within intrusive systems of kilometre-scale mud volcano systems exposed onshore in Azerbaijan (Fig. 1). Our field mapping focussed on the size, shape and internal structure of country rock outcrops within the feeder complexes, an aspect poorly described in previous studies. These conduits are interpreted as mature, long-lived systems where episodic activity has continued throughout recent exhumation of the onshore area (Fig. 2). Although the majority of onshore mud volcano outcrops are recent, extrusive edifices, there are occasional examples where lack of recent voluminous eruptions means that exhumed intrusive domains are as yet-unburied (Fig. 2). Three of these exposed intrusive zones were identified for mapping in this study.

Correspondence: Katie S. Roberts, University Science Laboratories, Department of Earth Sciences, Durham University, Durham DH1 3LE, UK. E-mail: k.s.roberts@durham.ac.uk

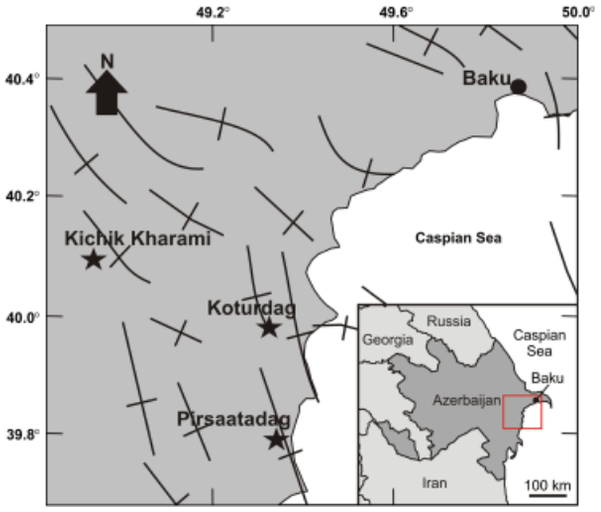

Fig. 1. Map of the Caspian coastline in Azerbaijan showing the location of the study areas (localities marked with stars) and the trends of anticlines axes (indicated by black line with dash across). Inset map of Azerbaijan shows map location as red box.

GEOLOGICAL SETTING

The South Caspian Basin is known for its abundant large mud volcano systems (Guliyev *et al.,* 2000; Milkov, 2000; Aliyev *et al.*, 2002). This concentration of mud volcano systems occurs due to the presence of a thick deposit of the argillaceous Maykop Formation of Oligocene to Miocene age (Hudson *et al.*, 2008). The formation is approximately 1 km thick and is buried to a depth 3.5–5 km in the area of this study (Allen *et al.*, 2002). The Maykop Formation is thought to be overpressured and therefore undercompacted, fluids from deeper sources (Kopf, 2002) probably entrain the mud during their ascent and erupt at the surface. A compressional tectonic regime has been maintained since the Late Pliocene (Allen *et al.*, 2002, 2003; Jackson *et al.*, 2002) resulting in the formation of a large number of fold structures within the basin. The anticlinal crests contain some of the largest hydrocarbon accumulations in the world and many large mud volcanoes (Devlin *et al.*, 1999).

Allen *et al.* (2002) backstripped a stratigraphic column from the NW of the South Caspian Basin and found that 2.4 km of tectonic subsidence had occurred since *ca.* 5.5 Ma which they attributed to basement subduction. Several kilometres of sediment has accumulated in this time, while the upper part of the succession has begun to deform by buckle folding (Allen *et al.,* 2002). Allen *et al.* (2002) proposed that basement subduction began *ca.* 5.5 Ma to create the major Pliocene–Quaternary subsidence. Buckle folds have now been exhumed onshore and the crests of the anticlines have been eroded. The present day mud volcanoes seen onshore therefore extrude through partially eroded anticlinal crests. The mud volcano systems, studied here, pierce through strata up to and including the Absheronian (Early Pleistocene) (Fig. 2) (Abdullayev, 1998; Reynolds *et al.*, 1998). Since the uppermost parts of the feeder systems have been eroded, the onshore exposures do not provide a complete replica of sub-surface structures imaged on reflection seismic data (Fig. 2). On the other hand this does provide the opportunity, in those cases where the feeder complex is exposed, to directly map the intrusive domains that are imaged as part of mud volcano systems offshore. This exhumation has not occurred to the offshore structures of the Caspian Sea where complete mud volcano systems are imaged on reflection seismic data (Stewart & Davies, 2006) (Fig. 2).

METHODS AND DATASETS

Three separate mud volcano systems were chosen on the basis of the extrusive domain being partially or completely eroded, exposing the underlying feeder complex. Kichik Kharami, Koturdag Anticline and Pirsaatadag mud volcanoes along the west coast of the Caspian Sea were selected on this basis (Fig. 1). Mapping of these onshore mud volcano systems was carried out using a handheld global positioning system (GPS) receiver, with a positional accuracy of 5 m. Structural readings such as bedding, fracture and fold orientations were measured using a compass clinometer then loaded into GEOrient software to plot stereographic projections. Fracture density was measured by placing a metre rule parallel to bedding and counting the number of fractures that crossed the rule over 1 m length. The GPS co-ordinates with their corresponding structural datasets were integrated as layers in ArcMap software. The coordinate system for the data was input using spheroid WGS 1984. This automated transcription produced the basic structural maps reproduced in this paper.

OBSERVATIONS

Kichik Kharami Volcano (GR: 40°5′17.25″N, 48°57′7.36″E)

This is located 87 km SW of Baku (Fig. 1) and outcrops 0.6 km to the south of an anticline axis (Fig. 3a). The plan-view shape of the volcano system is broadly circular and measures *ca.* 0.9 km × 0.6 km in aerial extent. The boundary of this area is defined by the edge of the peripheral faulted/fractured zone within the feeder complex where both sinuous and conjugate fracture types are found. Of the total feeder complex area, some 20% is exposed whereas the remaining 80% is covered by very recently erupted mud, indeed mud is still extruding in small quantities at present. The volcano is surrounded by well-exposed country rock forming the anticline through which the feeder complex intrudes (Fig. 3c).

We define the feeder complex of all three case studies as the area delimited by the peripheral fractured zone (highlighted in orange in Figs 3c, 7b and d). Fracturing of the country rock increases in intensity towards the centre of the feeder complex, with the most common fractures being regular, grid-like fractures 2–3 m in length (Fig. 4a).

These are present in both the surrounding country rock and the intrusive zone. Conjugate fractures (0.5–1 m in length) occur closer to centre of the complex. Finally, sinuous fractures (0.5–1 m in length) appear to be restricted to a 200 m radius from the centre of the feeder complex (Fig. 3c). Fracture density ranges from 28 m^{-1} at the centre of the feeder complex to 2 m^{-1} within the anticline bedding at the edge of the peripheral faulted/fractured zone (Fig. 5a).

Minor amounts of mud are currently being expelled from this feeder system in the form of watery-mud salses (Hovland *et al.*, 1997), although a large, relatively fresh mud flow to the south of the mapped area is testament to significant reactivation within the past few hundred years or so. The structural map (Fig. 3c) shows that the country rock comprising the south limb of the anticline dip uniformly to the south, whereas blocks within the feeder complex have dip and strike directions that vary unsystematically. The strike directions of the blocks vary up to 90° away from the regional anticline bedding strike orientations (Fig. 3c). A slight concentric alignment can be discerned from the dip data of beds which dip in towards the centre of the feeder complex. Moving outwards, the beds dip away from the centre of the feeder complex and return back to the regional trend of the host anticline by a radial distance of 180 m from the centre of the feeder complex. Stereonets reveal that the anticline intruded by Kichik Kharami has a moderate curvature and interlimb angle (Fig. 6a). All the bedding measurements lie roughly along the same plane, apart from bedding readings taken at

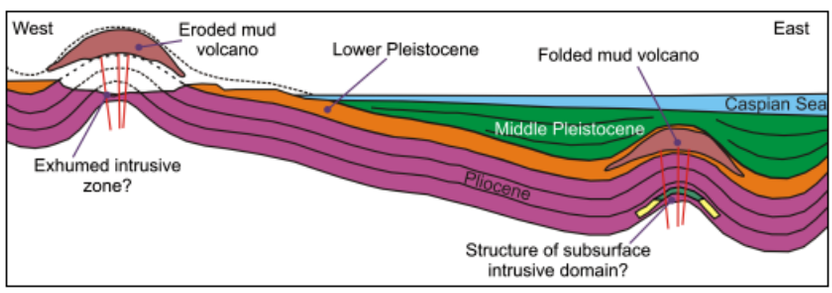

Fig. 2. Schematic regional seismic section depicting the relationship between exhumed intrusive zones onshore to the deeply buried, folded mud volcanoes offshore.

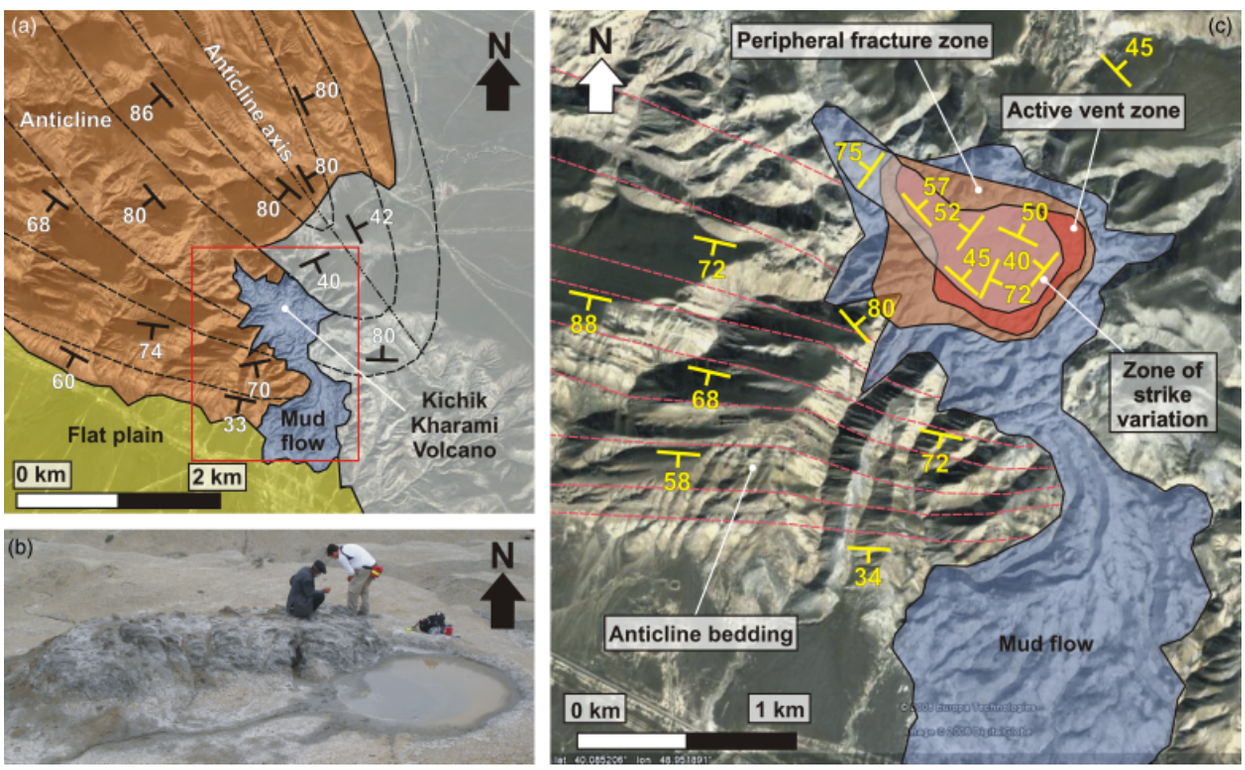

Fig. 3. Case Study 1- Kichik Kharami Mud Volcano. (a) Location of Kichik Kharami to the south of an anticline axis. Red rectangle marks the area seen in (c) (satellite image from Google Earth), (b) Outcrop at centre of Kichik Kharami volcano showing a large 'block' of highly fractured sandstone surrounded by a mud matrix. (c) Structural map of Kichik Kharami (satellite image from Google Earth). The central red area marks the zone where fluid is currently being extruded (i.e. the 'active vent zone'). The orange area outlines the zone where both sinuous and conjugate fracture systems are found (i.e. the 'peripheral fracture zone'). The grey transparent zone represents the area where bedding strike measurements vary greatly from the surrounding anticlinal bedding (i.e. the 'central zone of block rotation'). Any other areas that do not fall into these coloured zones are part of the 'unintruded zone' which contains only conjugate faulting/fracturing. Purple areas mark areas where old mud flows cover outcrop.

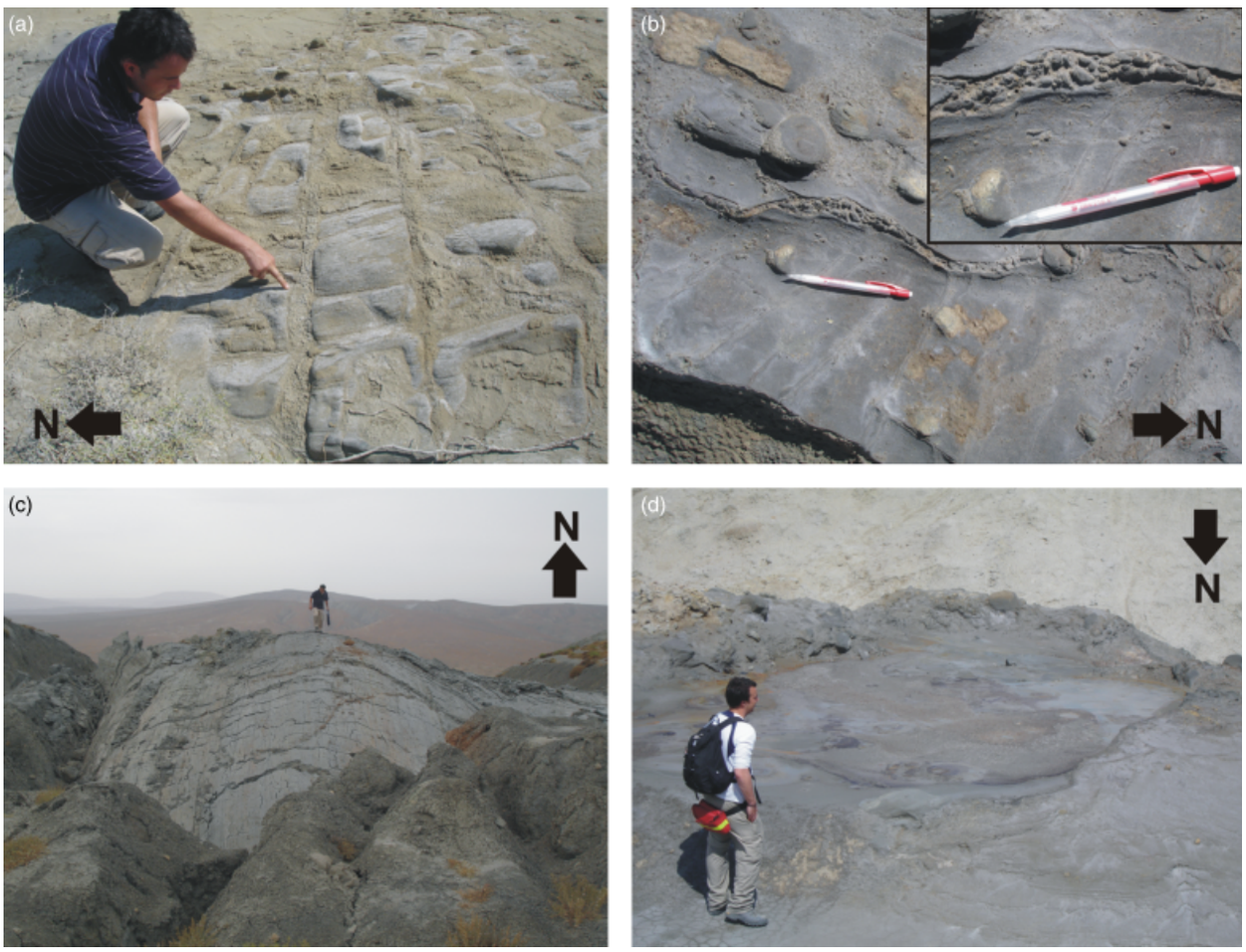

Fig. 4. (a) Mud infilling pre-existing joints and fractures within the country rock, found in both the peripheral fracture zone and the unintruded zone. (b) Sinuous fractures only found in the peripheral fractured zone, often contain small clasts of country rock as seen in the inset picture. (c) Mud plugs consisting of dense mud breccia flows and (d) Breccia pipes where country rock clasts have been incorporated into the vent walls to form a breccia.

the centre of the volcano which have a large spread with no clear alignment (Fig. 6b).

Pirsaatadag Volcano (GR: 39°46′26.20″N, 49°22′38.44″E)

This is located on the southern coast of the Caspian, 81 km south of Baku (Fig. 1) and is positioned on the hinge of an anticline (Fig. 7b). The exposure of the volcano system is in low-lying topography adjacent to the present Caspian shoreline and measures *ca*. 0.37 km × 0.4 km in aerial extent. The location has excellent exposures of the mud volcano feeder complex, however, little of the surrounding strata is exposed making it difficult to map the margin of the intrusion. The proximity to the present shoreline and the recent rapid sea level changes of the Caspian Sea (Kroonenberg *et al*., 2000) suggests that this mud volcano system is particularly prone to erosion.

Again, three fracture types (sinuous, conjugate and grid-like) are present in this mapping area. The sinuous fractures are wider (1–4 cm wide) than those seen in the other case studies and sometimes contain small sandstone clasts within a mud matrix (Fig. 4b). Fracture density ranges from 20 fractures per metre at the centre of the feeder complex to 7 m^{-1}, 0.17–0.21 km from the centre (Fig. 5b). The structural map (Fig. 7b) shows a similar layout to that seen at Kichik Kharami mud volcano system, except that the zone of rotated blocks is offset to the SE of the active vent zone. The extrusive features are dominantly active salses inferring that at present more fluid is flowing up the Pirsaatadag feeder complex compared with Kichik Kharami. Many structural elements within this feeder complex are exposed as positive topographic features consisting of brecciated country rock, mainly sandstone (Fig. 7a).

Koturdag Anticline (GR: 39°58′24.11″N, 49°20′12.55″E)

Within this area there are three mud volcanoes termed here Koturdag A, Koturdag B and Koturdag C (Fig. 7d) (Table 1). This area was chosen as it has a structurally complex, exposed anticlinal core with several mud volcanoes extruding along its axis (Table 1 and Fig. 7d). This

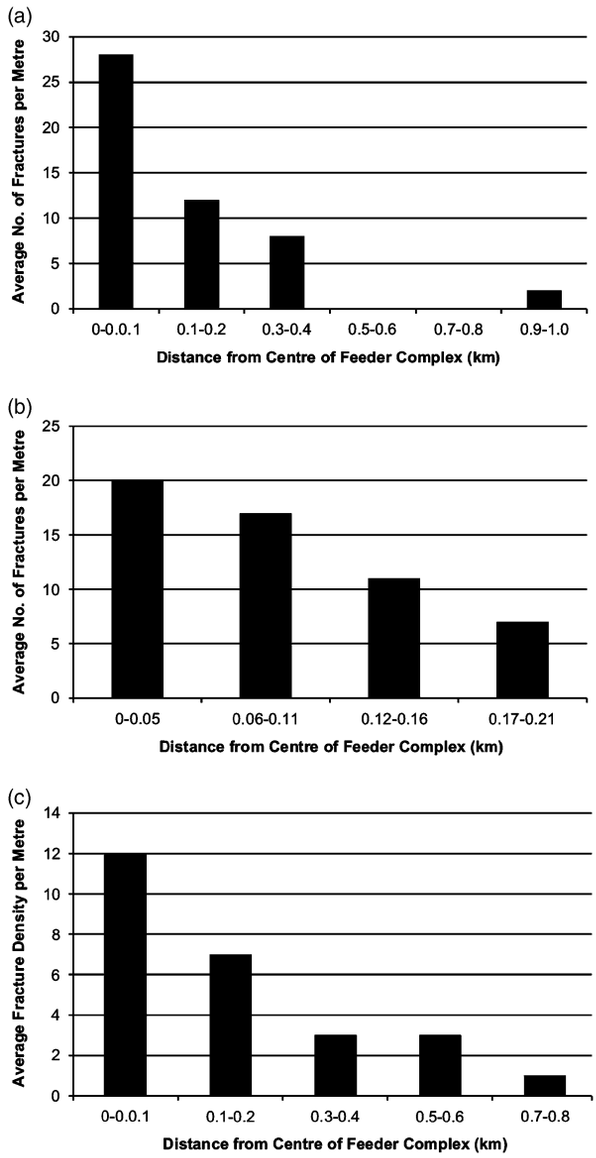

Fig. 5. Histograms showing the change in fracture densities per metre with distance from the centre of the mud volcano feeder complexes. (a) Kichik Kharami mud volcano, (b) Pirsaatadag Mud Volcano and (c) Koturdag Anticline.

provides a comparison to the two less structurally complex case studies.

Once more the sinuous, grid-like and conjugate fractures can be seen with the sinuous fracturing becoming more intense towards the central axes of the mud volcanoes (Fig. 5c). Fracture density rises from 1 m^{-1} at a radial distance of 0.75 km, and rises to 12 m^{-1} within the feeder complex (Fig. 5c). The core of this anticline consists of a structurally complex zone of disharmonic folds and contorted bedding (Fig. 7d). This structural complexity appears to be genetically separate from the mud volcano systems, a product of the relative tightness of the folding.

Figure 4c and d shows the extrusive features seen at two of the volcanoes. Koturdag A produces a kilometre-scale Bingham body style mud flow (Iverson, 1997) that has been moving for the past 50 years at a rate of 2–6 cm day^{-1} (Aliyev *et al.*, 2002) (Fig. 4c). Iverson (1997) describes that Bingham flow is characterized by a material that remains rigid or elastic unless stresses exceed a threshold value, the plastic yield strength. Where stresses exceed the yield strength, the material flows like a viscous fluid (Iverson, 1997). This contrasts with the extrusive features seen at Koturdag B and C at which only gryphons, salses and breccia pipes (Fig. 4d) are visible. Multiple oil seeps are visible along the stream section of the anticline following a fault which lies at right angles to the anticline axis (Fig. 7d).

The common structural features seen in all three field examples are summarized in Table 2.

Structural sub-domains associated with feeder complexes

The mapping revealed zones of similar structural elements common to all three feeder complexes. These are the 'active vent zone','peripheral fracture zone' and 'central intrusive zone', which together comprise the feeder complex itself, and finally the 'unintruded zone' which lies outside the feeder complex. In all three field examples mapped in this study, the structural zones can overlap. Following the general nomenclature set up by Stewart & Davies (2006), we term these zones structural sub-domains associated with the intrusive domain of mud volcano systems (Fig. 8). These sub-domains are defined here in the context of mud volcanism for the first time. The mud volcano feeder complex can be defined as the area which has undergone any change in physical characteristics due to the intrusion of mud and fluids from the intrusive mud system. The boundary of this complex usually corresponds with that of the peripheral fracture zone, however, lateral intrusions extending locally beyond the peripheral fracture zone are possible. We first describe the criteria by which the sub-domains are identified, starting with that closest to the centre of the feeder complex, moving outwards and then illustrate their extent in the field examples.

Active Vent Zone (red area on structural maps)

This zone is recognized as the area in which mud and fluids are actively being extruded within the mapped exhumed intrusive domains. A range of extrusive features were observed including gryphons, salses and sinter cones as described by Hovland *et al.* (1997). These structural elements were centimetre to metre in scale.

Central Zone of Block Rotation (grey area on structural maps)

This region characterises the centre of the feeder complex. It consists of a region of large blocks of country rock (1–20 m in length) which have strike orientations varying up to 90° to that of the surrounding sedimentary strata. The blocks are separated by a matrix of mud breccia.

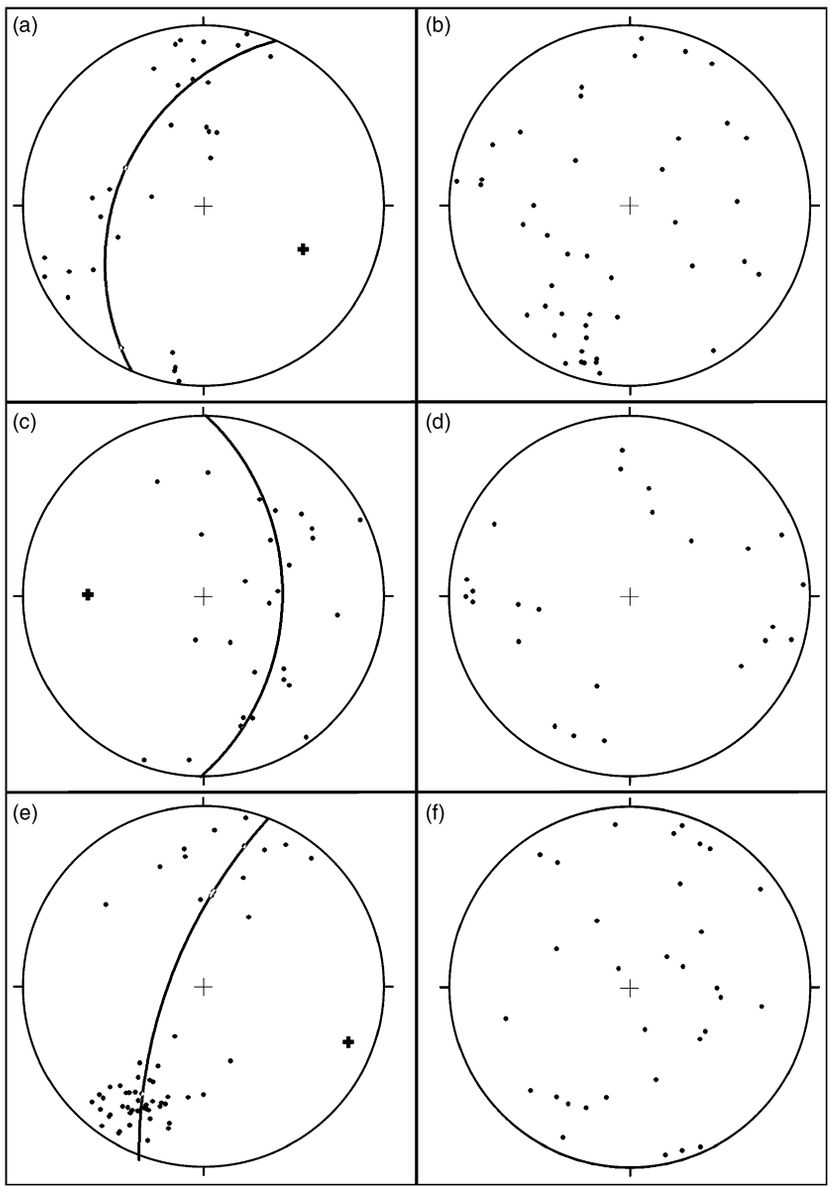

Fig. 6. (a) Stereonet showing anticline bedding around Kichik Kharami mud volcano. (b) Stereonet showing the varying bedding measurements found at the centre of Kichik Kharami mud volcano. (c) Stereonet showing anticline bedding around Pirsaatadag mud volcano. (d) Stereonet showing the varying bedding measurements found at the centre of Pirsaatadag mud volcano. (e) Stereonet showing anticline bedding around Koturdag Anticline. (f) Stereonet showing the varying bedding measurements found at the centre of Koturdag Anticline.

Peripheral faulted/fractured zone (orange area on structural maps)

This region is characterized by country rock that contains fracture sets only seen in proximity to the mud volcano system, as opposed to regional fracture sets. These fractures are often sinuous and infilled with mud and small clasts of country rock, with typical widths of 1–2 cm and lengths of 2–4 m.

Unintruded zone

This zone contains strata that has been unaffected by the intrusion of the mud. It is usually composed of country rock with conjugate fractures and jointing produced by folding. The fractures do not contain any mud infill.

Fracturing

Sinuous fractures and conjugate fractures are present in all three case studies. The grid-like fractures occur throughout every region of the mapping areas. We interpret these as being typical of fold-related fractures (Ramsay *et al.*, 1987) on the basis that these fractures are present in areas at some distance from mud volcano feeder complexes. Fractures within the feeder complexes are infilled by mud; those in unaffected country rock tend to be open. The sinuous fracture systems are only found within the feeder complexes and are usually infilled by mud. In cross-section these fractures appear to be sinuous in form, however, it is important to note that in three dimensions the fracture plane would also have a sinuous morphology. In Kichik Kharami they are found within a 250 m radius of the centre of the feeder complex and at Pirsaatadag they are 180 m radius from the centre (Fig. 5b).

Blocks of country rock in the feeder complexes

Large blocks of country rock are present at outcrop within all the feeder complexes mapped in this study. These

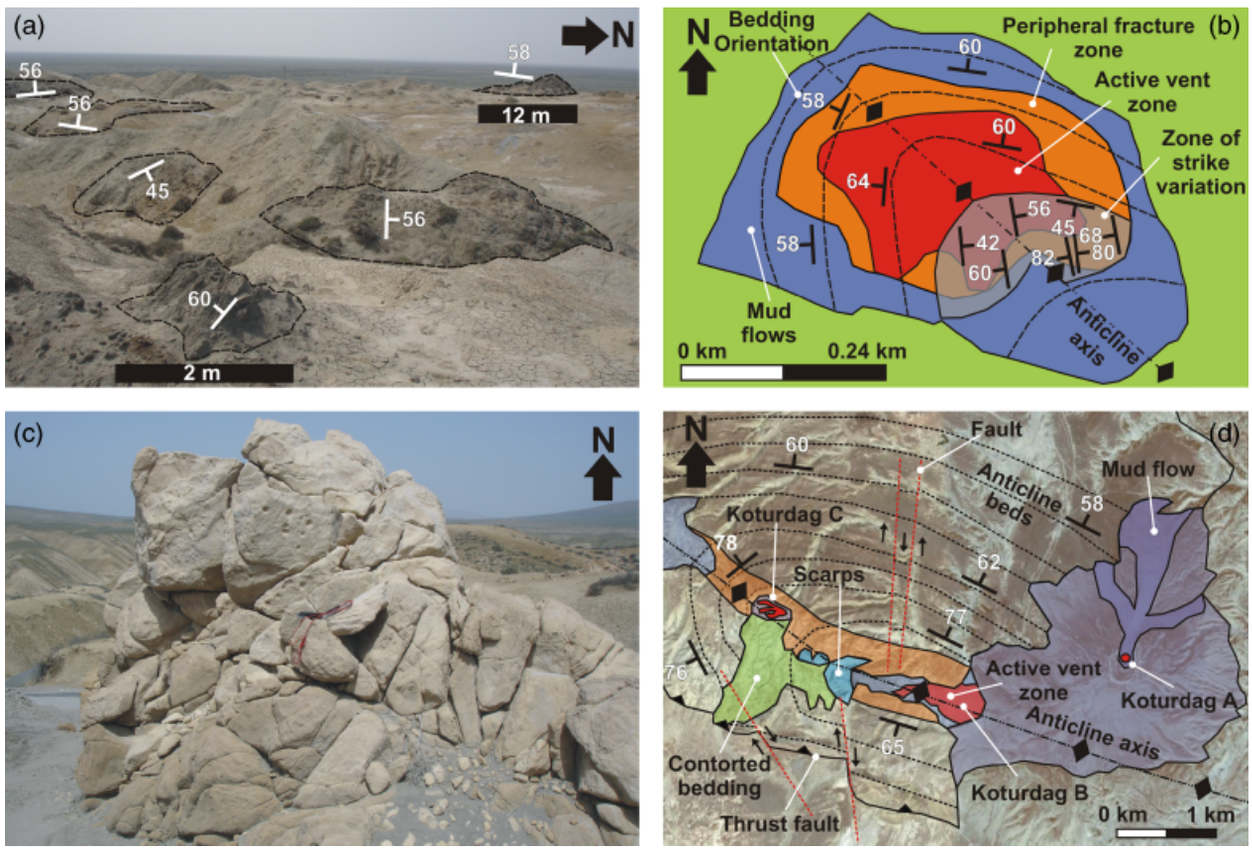

Fig. 7. (a) Case Study 2: Outcrop at centre of Pirscatadag volcano with rotated bedding strike orientation. (b) Structural map of Pirscatadag Mud Volcano (satellite image from Google Earth). The central red area marks the zone where fluid is currently being extruded (i.e. the 'active vent zone'). The orange area outlines the zone where both sinuous and conjugate fracture systems are found (i.e. the 'peripheral fracture zone'). The grey transparent zone represents the area where bedding strike measurements vary greatly from the surrounding anticlinal bedding (i.e. the 'central zone of block rotation). Any other areas that do not fall into these coloured zones are part of the 'unintruded zone' which contains only conjugate faulting/fracturing. (c) Case Study 3: Outcrop at the centre of Koturdag Anticline (compass clinometer at centre of picture for scale). (d) Structural map of Koturdag Anticline (satellite image from Google Earth). The central red areas at the centre of Koturdag A–C volcanoes mark the zones where fluid is currently being extruded (i.e. the 'active vent zone'). The orange area outlines the zone where both sinuous and conjugate fracture systems are found (i.e. the 'peripheral fracture zone'). Any other areas that do not fall into these coloured zones are part of the 'unintruded zone' which contains only conjugate faulting/fracturing. The green area represents an area of contorted bedding and the blue areas indicate areas where scarps have formed due to slope failures down the flank of the anticline. Purple areas mark areas where old mud flows cover outcrop.

Table 1. Dimensions of mud volcanoes (A–C), that extrude in the Koturdag Anticline area

Mud volcano	Long axis (km)	Short axis (km)
Koturdag A	1.4	1.35
Koturdag B	1.0	0.45
Koturdag C	0.35	0.2

blocks are up to 20 m in size and clearly preserve original sedimentary architecture. However, they are heavily fractured with the majority of these fractures being infilled by mud. The blocks consist of sands and shales, as does the country rock but due to the monotonous nature of the regional stratigraphy it was difficult to determine whether the blocks had moved vertically within the feeder complex, or whether they correlate laterally with strata that currently outcrop adjacent to the feeder complex.

In Kichik Kharami and Pirsaatadag mud volcanoes the blocks are rotated relative to the surrounding country rock. The degree of rotation generally increases towards the centre of the feeder complexes.

INTERPRETATION

We focus our discussion on three key features apparent from the mapping (a) the varying degree of fracturing, (b) the presence of large blocks of country rock in the feeder complexes and (c) deformation of these blocks.

Degree of Fracturing

In each case study fracture density increases from the far field to the centre of the feeder complexes (Fig. 5). At Pirsaatadag the fracture density increase towards the centre of

Table 2. Table of structural features present in each field area

Mud volcano	Features							
	Sinuous fractures	Pre-existing fractures with mud fill	Breccia pipes	Mud plugs	Zone of random strike orientations	Distance from anticline axis (km)	Block size (m)	Dip angles
Kichik Kharami	Yes	Yes	Yes	No	Yes	0.6	2–20	$>42^{\circ}$
Koturdag	Yes	Yes	Yes	Yes	No	0.1	1–5	$>52^{\circ}$
Pirsaatadag	Yes	Yes	Yes	No	Yes	0.01	1–20	$>42^{\circ}$

the edifice may also have a component of fracture density variation due to the position of the mud volcano system on the regional fold axis (Fig. 6c). Kichik Kharami intrudes to the south of the anticline axis, an area which would not be as highly fractured, however, still maintains a 14-fold increase in fracture density at the centre of the mud volcano (Fig. 5a). It is only the sinuous fracture set that dramatically increases in fracture density towards the centre of the feeder complexes in all three case studies. This suggests that the intrusion itself, rather than the folding, is the principal control on fracture distribution in the feeder complex.

The non-tectonic fractures can be explained by the mud intrusion process. Overpressured mud produces a sustained pressure differential between the fluid in the propagating fractures and the fluid in the pores of the country rock. This exceeds the minimum principal stress, causing fracture dilation and enabling the fluid mixture to flow through the fracture (Morley *et al.*, 1998; Jolly & Lonergan, 2002). This may be enhanced by an impermeable 'mud cake' being deposited on the fracture walls which would prevent fluid leakage out of the fracture and help sustain the fluid pressure within the fracture (Morley, 2003). These processes facilitate fracturing at depth and eventual propagation towards the surface. As fracture size and density increases, more mud intrusion occurs and eventually forms one large feeder complex (Abidin *et al.*, 2008).

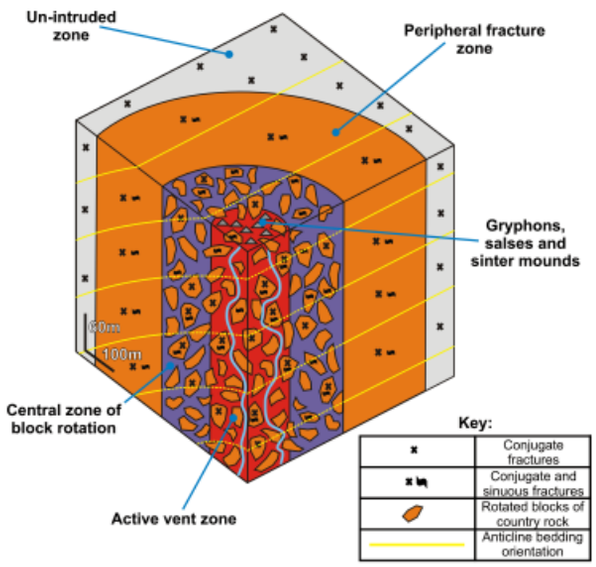

Fig. 8. Schematic of the mud volcano 'feeder complex'. The 'active vent zone' is highlighted in red, this represents the area of the mud volcano that is currently erupting fluid. The 'peripheral fractured zone', in orange, marks the region where both sinuous and conjugate fracture sets are present in the country rock. The 'central zone of block rotation', in grey, indicates the area where blocks of country rock with bedding strike measurements vary from the normal bedding orientations seen in the unintruded anticlinal bedding. The 'unintruded zone', in white, denotes the region that has been unaffected by the intrusion of the mud volcano system. Here, only conjugate fractures that contain no fill are found. The full yellow lines represent bedding areas that follow the general anticlinal trend, whereas dashed yellow lines indicate areas where bedding strikes could be rotated away from the regional trend. Sinuous blue lines indicate active fluid flow to the vents erupting at the surface.

Blocks of country rock within the Feeder Complex

Up to 20 m in length, these are prominent features at outcrop but would be undetectable at the resolution of seismic reflection data employed in commercial hydrocarbon exploration. The varying strike orientations imply that the blocks are rotated. We interpret these blocks as 'megaclasts' of country rock. The large proportion of mud outcropping in the feeder complexes indicates the amount of country rock that has now been removed. It is not obvious from our mapping whether the missing volume of country rock has risen upwards towards the extrusive zone, or sunk downwards towards the mud source.

A feature of the country rock blocks within the feeder complexes is that they become increasingly rotated with proximity to the central (vertical) axis of the feeder complex. The dips of the blocks still remain in the range of 40–88°, similar to dip magnitudes observed in the surrounding country rock. The bedding at the core of Kichik Kharami dips towards the centre of the feeder complex (Fig. 3c). We interpret this as indicating that the cause of the block rotation is a process related to the mechanics of the feeder system. At Pirsaatadag the central zone of block rotation is offset to the SE of the centre of the active vent zone (Fig. 7b). It is likely that the area of current extrusion has migrated to the NW from the SE resulting in exposure of the old zone of intrusion. The map of bedding in Fig. 7b shows a similar layout to that seen at Kichik Kharami mud volcano suggesting that this is a common occurrence in the intruded strata.

DISCUSSION: BLOCK ROTATION PROCESSES

This study has shown the occurrence of discrete sub-domains within mud volcano feeder complexes (active vent zone; peripheral faulted/fractured zone; etc). These have only been mapped in two-dimensional (2D) (map view) in the examples we have studied – but given the arbitrary structural level of exhumation in the field area, we suggest that the zonation mapped in this study is representative of the structure of feeder complexes in the sub-surface. The form and dimension of a feeder complex could change relative to the proximity to either the extruded volcano or whether it is just above the source bed. The observations made therefore might only be applicable to a certain part of the mud volcano system and this should be taken into consideration. Because of the small (metre) scale of these features, such a sub-division, has not been possible using the seismic reflection method previously applied to sub-surface examples offshore Azerbaijan (Davies & Stewart, 2005; Stewart & Davies, 2006). However, it has been possible to witness the development of potentially similar zones in a currently developing mud volcano system in east Java. The Lusi mud volcano has a central zone which is coincident with the active vent. Surrounding this is evidence for faulting and fracturing (fault and fracture zone), that has had led to the establishment of approximately 100 new vent sites (Mazzini *et al.*, 2007).

We now consider alternative models to account for the observed distribution and deformation of blocks within the mapped feeder complexes, and identify the most likely mechanism for these examples.

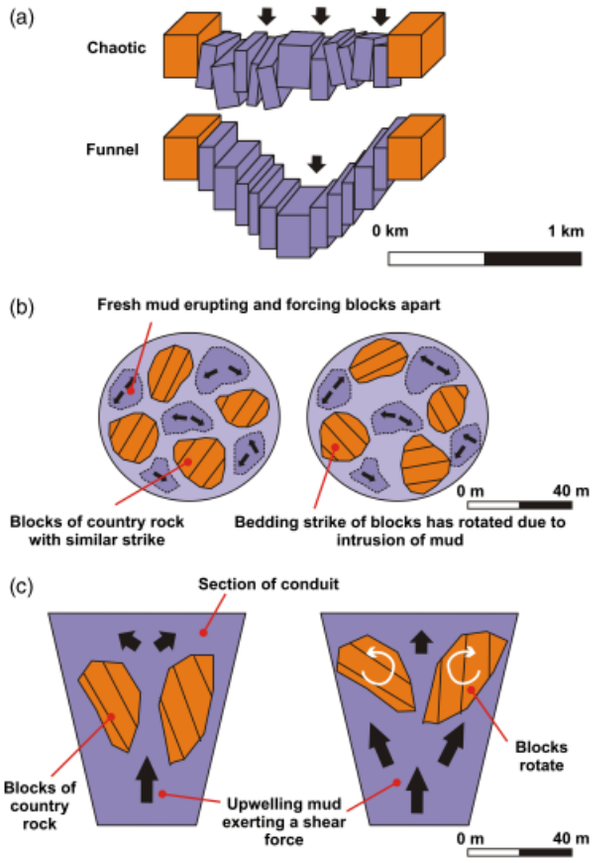

Fig. 9. Mechanisms. (a) Schematic of the 'Caldera Collapse' Mechanism modified from Cole *et al.* (2005), (b) Schematic of the intrusive mud rotation and (c) 'Flow Rotation' Mechanism.

Flow Rotation

Flow rotation is a common mechanism of rotation found in several geological environments (Reading, 1996). It is most commonly seen within debris flows that are gravity-driven surges of roughly equal volumes of water and poorly sorted sediment, the largest flows transporting boulders in the order of 10 m in diameter (Iverson, 1997). Intrusive mud generally works against gravity, nonetheless the process may be applicable. Another analogue could be fluvial imbrication where a shear force is exerted on pebbles in a stream bed causing the pebbles to rotate and stack on top of one another with their long axes point in the direction of flow (Reading, 1996). Application of this mechanism would involve long-lived, multiple intrusive events of mud intruding upwards through pre-existing and new fractures. Shear forces on the fracture walls are the mechanism driving block rotation – it seems reasonable to assume that variation in amount of shear stress around the margins of a block (a necessity for rotation) would occur as a result of variations in mud flow rates through the fracture network (Fig. 9c). In order to conserve volume, the addition of mud to the system must also result in expulsion of the country rock that the mud now replaces. We suggest that smaller blocks are carried upwards by intruding mud, ultimately to be expelled in the constructional edifice of the extrusive zone. Evidence to support this is the common presence of deep-sourced clasts in extruded mud flows (Guliyev *et al.*, 2000).

We suggest that flow rotation is an unlikely mechanism due to the magnitude of forces needed to rotate such large blocks of country rock (Kopf & Behrmann, 2000). The density and viscosity of the mud-fluid mix required to exert a shear force on 20-m-long blocks of country rock would be extremely large. Even in the largest, most dense and viscous mud flows emanating from mud volcanoes no blocks >1 m in length were observed in the study or reported in the literature (Guliyev *et al.*, 2000). The flow at Koturdag mud volcano only extrudes its large mud plug flow at a rate of 2 cm day^{-1} from a 20 m wide vent. This indicates that even if two contributing influences were at a maximum the velocity of the flow may also provide a restriction on the amount of deformation and rotation that occurs. The slow rate of flow even at these high densities only results in small boulders being extruded (0.1–1.0 m in length). This suggests that the force of the flowing mud is not capable of moving blocks of the largest scale (20 m) observed in the feeder complexes.

Stoping

Stoping in its igneous context is the mechanical disintegration of the country rock surrounding the intrusion,

typically through fracturing due to pressure increases associated with thermal expansion of the host rock in proximity of the interface with the melt (Pinotti *et al.*, 2002). Fracture networks begin to propagate through the country rock closest to the intrusion. Once fractures are formed, melt and volatiles typically invade, widening the fracture and promoting the foundering of host rock blocks (Marsh, 1982). Once suspended in the melt, 'stoped' blocks may either sink or float depending upon the density of the block relative to that of the melt (Marsh, 1982; Kopf & Behrmann, 2000).

This process is not directly applicable to mud volcano systems as the upwelling fluids are usually between 11 to 26 °C (Guliyev *et al.*, 1994, 2000) and so would have no significant effect on the thermal expansion of the surrounding country rock. However, upwards-propagation of a fracture network driven by overpressured mud could set up a similar situation to igneous stoping (Barber *et al.*, 1986; Morley *et al.*, 1998; Kopf & Behrmann, 2000; Morley, 2003). Blocks isolated by this means would become suspended in the mud and allowed to rotate freely.

Once the initial failure of the rock occurs at depth more mud can intrude along the fractures and the stoping process slowly propagates to the surface of the edifice, with the majority of the fracture network being produced by hydrofractures (Jolly & Lonergan, 2002; Planke, 2003). This highly intruded zone of country rock now forms a 'stoping column' (Fig. 10c) (Geshi *et al.*, 2002). Breaching the surface would release fluids and with it some of the overpressure from the source of fluids at depth (Geshi *et al.*, 2002). The evacuation of material would cause a void to form at depth resulting in lack of support for the country rock above (Fig. 10d). As more fluids are expelled, the overburden would increase and may induce piecemeal caldera collapse into the void left in the vent (Fig. 10d) (Cole *et al.*, 2005).

The stoping hypothesis assumes a general downwards movement of stoped blocks, a feature that is not demonstrable in our case studies. Stoping models also, often, contain an element of block melting and mixing to preserve the volume of the system. This is not an option in mud volcano systems due to the low temperature of the intruding mud.

Rotation due to multiple intrusive episodes

After the major stoping event the intrusion of mud, occurring as a result of the stoping process, would also exert forces on the blocks of 'stoped' country rock. As mud forces its way between the stoped blocks it pushes them away from the flow (Fig. 9b). Each time a new intrusion of mud occurs up the conduits more force is exerted rotating the blocks further. This is a similar process found in dykes swarms in ophiolites and spreading centres (Moores & Vine, 1971). Igneous dykes intrude up the centre of pre-existing dykes, forcing each half of the intruded dyke to opposite sides of the new dyke (Moores & Vine, 1971). If one area of the mud volcano has a higher rate of intrusion than others then the blocks will be pushed and rotated towards areas that are more quiescent.

Caldera Collapse

Both trap-door and piston caldera collapses have been identified on the underwater mud volcanoes in the Caspian Sea (Cole *et al.*, 2005; Stewart & Davies, 2006; Evans *et al.*, 2008). In these onshore examples the dominant morphology is the piecemeal collapse (Fig. 9a). The evacuation of the mud from a chamber or source at a shallow depth would cause a void to be formed. This would enable the strata above to collapse into the chamber. The effect of this would be enhanced by the increased overburden of erupted mud on top of the country rock causing more subsidence. This collapse would not have occurred as one event, instead a piecemeal collapse results in the country rock collapsing at different rates and times. This varying collapse rate would enable different blocks of rock to collapse and rotate at different times and to varying degrees of rotation.

The discrepancy with the piecemeal caldera collapse arises with the large differences in strike angles within such a small area. Piecemeal collapses usually only allow bedding rotations of a few degrees (0–20°) rather than the observed rotations (0–90°) (Cole *et al.*, 2005). This suggests that caldera collapse cannot be the singular cause of the block rotations seen at the centre of the feeder complexes.

Diapirs

Hovland *et al.* (1998) define a piercement shale diapir as a positive topographical feature constructed mainly of clay-sized sediments that periodically or continuously move from the sub-surface and upwards towards and through the sea floor. This would be on a scale of hundreds to thousands of metres in depth and width. The diapir itself would be composed almost entirely of mud or shale on a ratio of 80 : 20 (mud : xenoliths). We follow Cooper (2001) and Davies & Stewart (2005) in discounting large-scale mud diapirism on the basis of there being no observations of that phenomenon in the basin, instead we find piercing mud volcano feeder complexes that have a geometry similar to sill and dyke complexes in igneous volcanic systems (Davies & Stewart, 2005).

IMPLICATIONS

We expect the identification of structural sub-domains to be of utility for the study of other exhumed intrusive complexes. Similar and additional sub-domains could be identified in other exhumed feeder complexes and with improved seismic reflection technology, it is conceivable that similar zones may be detectable in the sub-surface. The blocks of country rock within these complexes are heavily fractured and cut by dense networks of mud intrusions. This dramatically reduces the reservoir potential of these segments within the vent as the country rock has become extremely compartmentalized. Commercially the compartmentalization of the country rock will be significantly increased by the intrusion of the mud dyke systems.

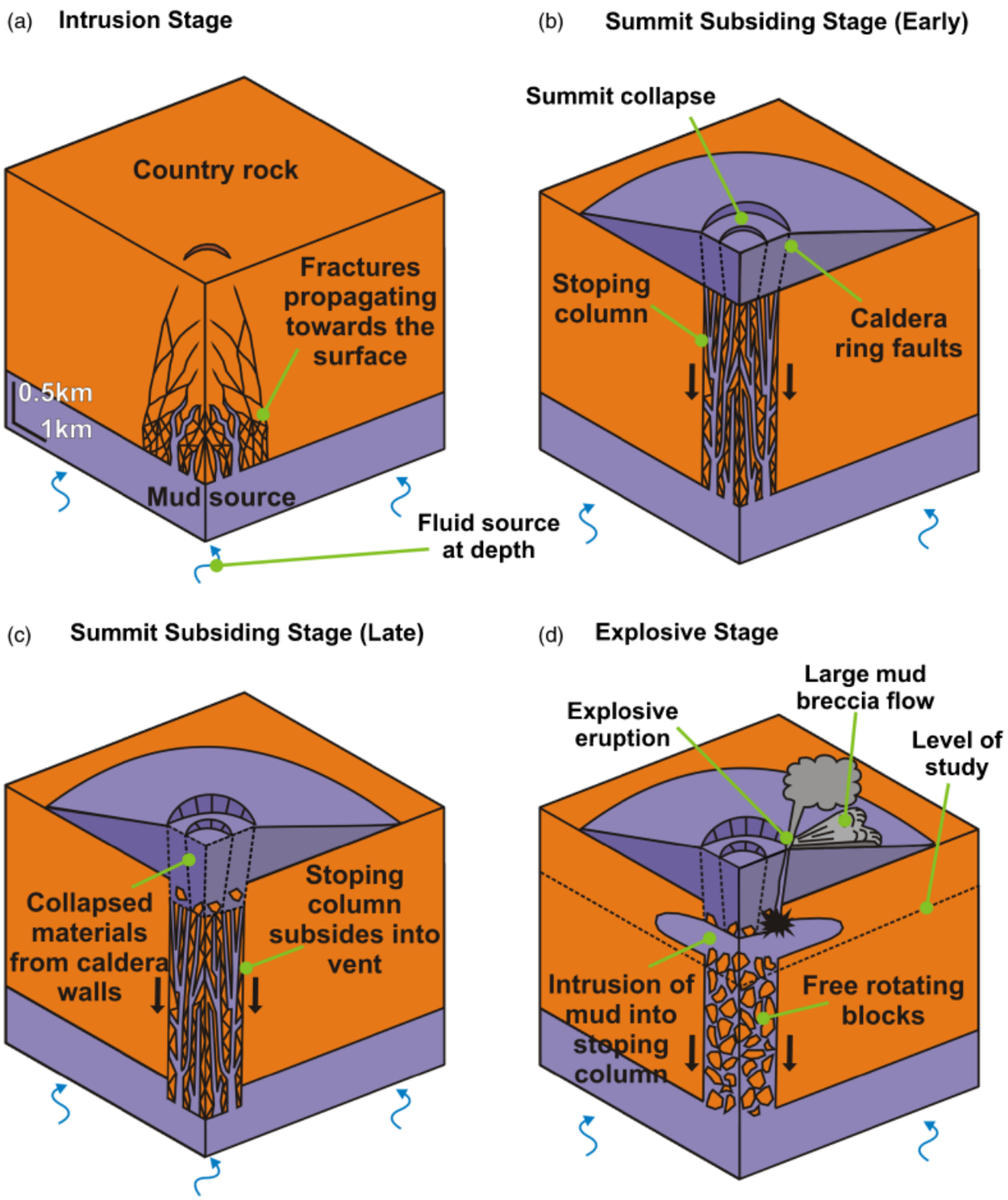

Fig. 10. Schematic of the 'hybrid stoping' mechanism modified from Geshi *et al.* (2002). (a) Intrusion stage before the surface collapse. Evacuation of mud from the reservoir caused stoping of the roof rock of the reservoir. Underground stoping formed a cavity at the top of the stoping column. (b) The early stage of summit subsidence. The roof rocks of the cavity can not carry their own weight and collapse into the cavity. Release of mud and fluids fills the cavity. (c) The late stage of the summit subsidence. Continuous evacuation of mud from the reservoir caused the subsidence of the roof of the reservoir. The top of the stoping column was filled with the collapsed materials from the outward migrating caldera wall. (d) Explosive stage. Invasion of fluids to the stoping column causes eruption and conduit consists of large blocks of country rock rotating freely within it.

Although these segments of country rock are not economic the observation that they are present and can be recognized by their change in strike compared with the surrounding country rock will improve identification of mud volcano systems when drilling. The evolution of this system over time should be considered when planning wells because old

feeder dykes may be encountered when drilling. The reservoirs surrounding mud volcano intrusive domains are commercially viable, however, large, seismic scale faults, seen during the mapping of Koturdag anticline, away from the intrusive zone within tight regional fold structures, may pose problems. These faults can often act as either baffles or aids to fluid flow from the reservoirs through which they penetrate creating problems when evaluating the reservoir potential in the region.

These interpretations will enable a better understanding of the processes governing fluid transport through the shallow crust and how the processes affect the surrounding country rock. Comparisons with igneous vent systems could be fruitful as they share some common morphological and mechanical process with mud volcanoes and there may be parallels with the mechanisms by which fluids travel to the surface. Further studies of piercement structures will help establish the common processes and products.

CONCLUSIONS

On the basis of field mapping, including collection of bedding orientations, fracture types and densities, we identify sub-domains within mud volcano feeder complexes. This represents the first study on mud volcano systems of its kind. These sub-domains consist of the 'active vent zone' where fluids are currently being extruded, the 'peripheral fracture zone' where both sinuous and conjugate fracture systems are found, the 'central zone of block rotation' where bedding strike measurements vary greatly from the surrounding anticlinal bedding and the 'un-intruded zone' which contains only conjugate faulting/fracturing. The 'active vent zone', 'peripheral fracture zone' and 'central intrusive zone', together comprise the mud volcano feeder complex itself, with the 'unintruded zone' lying outside the feeder complex. Further research could establish the existence of these sub-domains elsewhere, refine the characteristics for their identification and lead to the identification of new examples. Their delineation should also provide an objective method for the comparison of other mud volcano feeder complexes.

Overall we find the feeder complexes to consist of megabreccia of country rock surrounded by intruded mud and some long-lived fluid conduits. Our preferred model consists of a propagating fracture network that isolates blocks that become free to move as the smaller clasts become eroded by the mud–water–gas mix through time. This process has similarities with the better-known stoping process in igneous volcanic complexes. An initial stoping mechanism where an upward-propagating fracture network isolates a megabreccia of blocks up to 20 m in scale. Once the fracture system breaches the surface and becomes an anastomosing flow pathway, the smaller blocks within the breccia are eroded and extruded, creating space for widening of the flow conduits and settlement and rotation of the larger blocks whose size and weight prevent them from being carried upwards (Fig. 10). During periods of low mud flow rates, gravity driven compaction of the system may account for relatively low levels of water and gas eruption observed during 'quiescent' periods.

Furthermore in addition to supplying parameters for lithology and 3D porosity and permeability distribution in feeder complexes, our observations also provide a starting assumption for the dimensions of these structures in areas were seismic imaging does not clearly resolve their extent. These parameters will be useful in the cases of reserves assessment and drilling planning in the deeper parts of mud volcano systems.

ACKNOWLEDGEMENTS

We are very grateful to BP for funding K. S. Roberts' PhD and for logistical support during field seasons. S. Grant, M. Ireland, S. Richardson and R. Townsend are thanked for assistance during fieldwork. We thank C. K. Morley, M. Huuse and R. J. H. Jolly and an anonymous reviewer for their helpful comments. The technical conclusions presented do not necessarily represent the opinion of B. P.

REFERENCES

Abdullayev, N.R. (1998) Seismic stratigraphy of the upper pliocene and quaternary deposits in the South Caspian Basin. *J. Petrol. Sci. Eng.*, **28**(4), 207–226.

Abidin, H.Z., Davies, R.J., Kusuma, M.A., Andreas, H. & Deguchi, T. (2008) Subsidence and uplift of Sidoarjo (East Java) due to the eruption of the LUSI mud volcano (2006-present). *Environment. Geol.*, **57**(4), 833–844.

Aliyev, A., Guliyev, I.S. & Belov, I.S. (2002) *Catalogue of Recorded Eruptions of Mud Volcanoes of Azerbaijan*. Nafta Press, Baku.

Allen, M.B., Jones, S., Ismail-Zadeh, A., Simmons, M.D. & Anderson, L. (2002) Onset of subduction as the cause of rapid pliocene–quaternary subsidence in the South Caspian Basin. *Geology*, **30**(9), 775–778.

Allen, M.B., Vincent, S.J., Alsop, G.I., Ismail-Zadeh, A. & Flecker, R. (2003) Late Cenozoic deformation in the South Caspian Region: effects of a rigid basement block within a collision zone. *Tectonophysics*, **366**, 223–239.

Barber, A.J., Tjokrosapoetro, S. & Charlton, T.R. (1986) Mud volcanoes, shale diapirs, wrench faults, and mélanges in accretionary complexes, Eastern Indonesia. *Am. Assoc. Petrol. Geol. Bull.*, **20**(11), 1729–1741.

Brown, K.M. (1990) The nature and hydrogeological significance of mud diapirs and diatremes for accretionary prisms. *J. Geophys. Res.*, **95**, 8969–8982.

Cole, J.W., Milner, D.M. & Spinks, K.D. (2005) Calderas and caldera structures: a review. *Earth-Sci. Rev.*, **69**(1–2), 1–26.

Cooper, C. (2001) Mud volcanoes of Azerbaijan visualized using 3D seismic depth cubes: the importance of overpressured fluid and gas instead on non-existent diapirs. In: *Proceedings of EAGE Conference: Subsurface Sediment Mobilization*, **Vol. 71**, 71. Ghent, Belgium.

Davies, R.J. & Stewart, S.A. (2005) Emplacement of giant mud volcanoes in the South Caspian Basin: 3D seismic reflection imaging of their root zones. *J. Geol. Soc. Lond.*, **162**, 1–4.

Devlin, W.L., Gogswell, J., Gaskins, G., Isaksen, G., Pitcher, D., Puls, D., Stanley, K. & Wall, G. (1999) South Caspian Basin: young, cool, and full of promise. *GSA Today*, **9**, 1–9.

Evans, R.J., Stewart, S.A. & Davies, R.J. (2008) The structure and formation of mud volcano summit calderas. *J. Geol. Soc.*, **165**, 769–780.

Geshi, N., Shimano, T., Chiba, T. & Nakada, S. (2002) Caldera collapse during the 2000 eruption of Miyakejima Volcano, Japan. *Bull. Volcanol.*, **64**, 55–68.

Graue, K. (2000) Mud volcanoes in deep water Nigeria. *Mar. Petrol. Geol.*, **17**, 959–974.

Guliyev, I.S., Feizullayev, A.A. & Belov, I.S. (2000) *All About Mud Volcanoes*. Geology Institute, Azerbaijan Academy of Sciences, Azerbaijan.

Guliyev, I.S., Feizullayev, A.A., Nadirov, R.S., Rakhmanov, R.R., Aliev, A.D.A., Bagirov, E.B., Mukhtarov, A.S.H., Tagiev, M.F., Magerramova, F.S., Murtazaev, I.R., Archer, R., Casey, D.M., Gronlie, A., Huntley, A., Mitchell, G. & Simmons, M.D. (1994) Mud volcanoes of Azerbaijan: Report of the GIA, BP and Statoil joint study.

Hovland, M., Hill, A. & Stokes, D. (1997) The structure and geomorphology of the Dashgil mud volcano, Azerbaijan. *Geomorphology*, **21**, 1–15.

Hovland, M., Nygaard, E. & Thorbjørnsen, S. (1998) Piercement shale diapirism in the deep-water Vema Dome Area, Vøring Basin, Offshore Norway. *Mar. Petrol. Geol.*, **15**, 191–201.

Hudson, S.M., Johnson, C.L., Efendiyeva, M.A., Rowe, H.D., Feyzullayev, A.A. & Aliyev, C.S. (2008) Stratigraphy and geochemical characterization of the Oligocene–Miocene Maikop Series: implications for the paleogeography of Eastern Azerbaijan. *Tectonophysics*, **451**, 40–55.

Iverson, R.M. (1997) The physics of debris flows. *Rev. Geophys.*, **35**(3), 245–296.

Jackson, J., Priestley, K., Allen, M.B. & Berberian, M. (2002) Active tectonics of the South Caspian Basin. *Geophys. J. Int.*, **148**, 214–245.

Jolly, R. & Lonergan, L. (2002) Mechanisms and controls on the formation of sand intrusions. *Geol. Soc Lond.*, **159**, 605–617.

Kopf, A. (2002) Significance of mud volcanism. *Rev. Geophys.*, **40**, 1005.

Kopf, A. & Behrmann, J.H. (2000) Extrusion dynamics of mud volcanoes on the Mediterranean Ridge accretionary complex (2000). *Geol. Soc. Lond. Spec. Publ.*, **174**, 169–204.

Kroonenberg, S.B., Badyukova, E.N., Storms, J.E.A., Ignatov, E.I. & Kasimov, N.S. (2000) A full sea-level cycle in 65 years: barrier dynamics along Caspian shores. *Sediment. Geol.*, **134**, 257–274.

Marsh, B.D. (1982) On the mechanisms of igneous diapirism, stoping, and zone melting. *Am. J. Sci.*, **282**, 808–855.

Mazzini, A., Svensen, H., Akhmanov, G.G., Aloisi, G., Planke, S., Malthe-Sørenssen, A. & Istadi, B. (2007) Triggering and dynamic evolution of the LUSI mud volcano, Indonesia. *Earth Planet. Sci. Lett.*, **261**, 375–388.

Milkov, A.V. (2000) Worldwide distribution of submarine mud volcanoes and associated gas hydrates. *Mar. Geol.*, **167**(1), 29–42.

Moores, E.M. & Vine, F.J. (1971) Troodos Massif, Cyprus and other ophiolites as ocean crust: evaluations and implications. *Philos. Transact. Roy. Soc. Lond. Serial A*, **268**, 443–446.

Morley, C.K. (2002) *Structural Geology of the Berakas Syncline Regional-Reservoir Scale Perspectives*. Universiti Brunei Darussalam, Department of Petroleum Geosciences. Fieldtrip for Brunei Shell, Brunei.

Morley, C.K. (2003) Outcrop examples of mudstone intrusions from the Jerudong Anticline. In: *Subsurface Sediment Remobilizatio* (Ed. by P. Vanrensenbergen, R.R. Hillis, A.J. Maltman & C.K. Morley), Geol. Soc. Lond. Spec. Publ., **216**, 381–394.

Morley, C.K., Crevello, P. & Ahmad, Z.H. (1998) Shale tectonics associated with active diapirism; The Jerudong Anticline, Brunei Darussalam. *J. Geol. Soc. Lond.*, **155**(3), 475–490.

Morley, C.K. & Guerin, G. (1996) Comparison of gravity-driven deformation styles and behaviour associated with mobile shales and salt. *Tectonics*, **15**(6), 1154–1170.

Planke, S., Svensen, H., Hovland, M. & Banks, D.A. (2003) Mud and fluid migration in active mud volcanoes in Azerbaijan. *Geo Mar. Lett.*, **23**, 258–268.

Pinotti, L.P., Coniglio, J.E., Esparza, A.M., Eramo, F.J. & Llambías, E.J. (2002) Nearly circular plutons emplaced by stoping at shallow crustal levels, Cerro Aspero Batholith, Sierras Pampeanas de Córdoba, Argentina. *J. South Am. Earth Sci.*, **15**, 251–265.

Ramsay, J.G., Huber, M.I. & Lisle, R. (1987) *The Techniques of Modern Structural Geology: Folds and Fractures*. Academic Press, London.

Reading, H.G. (1996) *Sedimentary environments: processes, facies and stratigraphy* (Ed. by H.G. Reading), 3rd ed., Blackwell Science, Oxford.

Reynolds, A.D., Simmons, M.D., Bowman, B.J., Henton, J., Brayshaw, A.C., Ali-Zade, A.A., Guliyev, I.S., Suleymanova, S.F., Ataeva, E.Z., Mamedova, D.N. & Koshkarly, R.O. (1998) Implications of outcrop geology for reservoirs in the Neogene productive series: Apsheron peninsula, Azerbaijan. *AAPG Bull.*, **82**, 25–47.

Robertson, A.H.F. & Kopf, A. (1998) Tectonic setting and processes of mud volcanism on the Mediterranean Ridge accretionary complex: evidence from Leg 160. In: A.H.F. Robertson, K.–C. Emeis, C. Richter & A. Camerlengthi, (eds), *Proceedings of the Ocean Drilling Program, Scientific Results*, **160**. Ocean Drilling Program, College Station, TX, 665–680.

Stewart, S.A. & Davies, R.J. (2006) Structure and emplacement of mud volcano systems in the South Caspian Basin. *AAPG Bull.*, **90**(5), 771–786.

Yusifov, M. & Rabinowitz, P.D. (2004) Classification of mud volcanoes in the South Caspian Basin, offshore Azerbaijan. *Mar. Petrol. Geol.*, **21**(8), 965–975.

Manuscript received 23 January 2009; Manuscript accepted 8 September 2009.

Sector collapse of mud volcanoes, Azerbaijan

Katie S. Roberts, Simon A. Stewart, Richard J. Davies, et al.

Journal of the Geological Society 2011; v. 168; p. 49-60
doi: 10.1144/0016-76492010-115

Journal of the Geological Society, London, Vol. **168**, 2011, pp. 49–60. doi: 10.1144/0016-76492010-115.

Sector collapse of mud volcanoes, Azerbaijan

KATIE S. ROBERTS[1]*, SIMON A. STEWART[2], RICHARD J. DAVIES[1] & ROBERT J. EVANS[3]
[1]*CeREES (Centre for Research into Earth Energy Systems), Department of Earth Sciences, Durham University, Science Laboratories, South Road, Durham DH1 3LE, UK*
[2]*Institute of Petroleum Engineering, Heriot-Watt University, Edinburgh EH14 4AS, UK*
[3]*3DLab, School of Earth, Ocean and Planetary Sciences, Cardiff University, Cardiff CF10 3YE, UK*
**Corresponding author (e-mail: k.s.roberts@dur.ac.uk)*

Abstract: Field data collected from mud volcanoes in Azerbaijan are used to describe a process in mud volcano development that involves portions of the constructional edifices collapsing outwards in 'thin-skinned' slides. These events create kilometre-scale scarps that are tens of metres in height, arcuate in plan view, elongate and facing downdip. Similar morphological features occur on igneous volcanoes and have been described as 'sector collapse' structures. The largest sector collapses in igneous volcanoes involve some 10^{12} tons of mobilized material; equivalent structures in mud volcanoes are several orders of magnitude smaller. We employ a shape parameter that can be utilized in field and satellite-based mapping, to distinguish between slope failure and eruptive deposits. Three mud volcanoes with kilometre-scale sector collapses are described and controlling mechanisms are reviewed. The updip domains of these collapses are characterized by fluid escape, showing that there is also linkage to deeper mud volcano structure. The observations are reconciled in a model consisting of a deflating mud chamber that triggers thin-skinned sector collapse. The updip domain of the sector collapse is localized above a deep-seated zone of volume loss and the downdip domain of the collapse runs down the edifice flank onto the surrounding plain.

Mud volcanoes range in size from 0.01 to 5 km in diameter and occur in a range of tectonic settings, yet there are relatively few detailed descriptions of the morphology of kilometre-scale edifices (Milkov 2000; Kopf 2002; Planke *et al.* 2003; Yusifov & Rabinowitz 2004). Mud volcanoes are similar to igneous volcanoes in that they both form constructional edifices when erupting at the surface and can develop structural elements such as calderas and ring faulting (Evans *et al.* 2008). The structural development of mud volcano edifices has received some attention (Hovland *et al.* 1997; Davies & Stewart 2005; Mazzini *et al.* 2007, 2008; Evans *et al.* 2008; Roberts *et al.* 2010) but has been studied far less than igneous equivalents (Fisher 1990; Kokelaar & Romagnoli 1995; Lipman 1997; Leyrit 2000; Geshi *et al.* 2002; Masson *et al.* 2002; Kennedy *et al.* 2004; Cole *et al.* 2005).

The aim of this study is to describe kilometre-scale collapse phenomena and related morphological features seen on mud volcano edifices based on field mapping in Azerbaijan, and to identify the most likely trigger mechanisms for collapse events. A particular difficulty in the study of mud volcanoes is distinguishing between features that are dominantly due to slope failure and those that are largely the product of incision and erosion of the flanks during an eruptive event. We distinguish between these processes on the basis of geomorphological criteria and the overall dimensions of the deposits.

Geological setting

The South Caspian Basin is known for its abundant kilometre-scale mud volcano systems (Guliyev & Feizullayev 1995; Milkov 2000; Aliyev *et al.* 2002). This concentration of mud volcano systems occurs as a result of the presence of the argillaceous Maykop Formation of Oligocene to Miocene age (Hudson *et al.* 2008), which has become overpressured as a result of disequilibrium compaction and mobilized by the addition of fluids from depth (Kopf *et al.* 2003). The Maykop Formation is *c.* 1 km thick and is buried to a depth of 3.5–5 km in the area of this study (Allen *et al.* 2003). Mud volcano edifices are the extrusive termination of steep intrusive feeder complexes that are created by pressure at depth exceeding the lithostatic pressure, resulting in hydrofracturing. This leads to intrusion of fluids and mud, resulting in eventual stoping of the surrounding country rock (Stewart & Davies 2006; Deville & Guerlais 2009; Roberts *et al.* 2010).

Methods and datasets

The edifices studied were Akhtarma-Karadag, Pilpilya and Lökbatan mud volcanoes, all located in Azerbaijan along the west coast of the Caspian Sea (Fig. 1). Mapping was carried out using a handheld global positioning system (GPS) receiver, with a positional accuracy of 5 m. Structural readings such as bedding, fracture and fold orientations were measured using a compass clinometer. The GPS coordinates with their corresponding structural datasets were integrated as layers in ArcMap software. The coordinate system for the data was input using spheroid WGS 1984. Aerial imagery is from Digital Globe and IKONOS via Google Earth, and all aerial imagery has a resolution of 6.5–23 m.

Observations

A number of mud volcano edifices from the South Caspian Basin feature elongate collapse scars on their flanks. We provide a detailed description of two representative collapse structures and their associated deposits, plus one feature interpreted as an incipient collapse structure. Locations are shown in Figure 1.

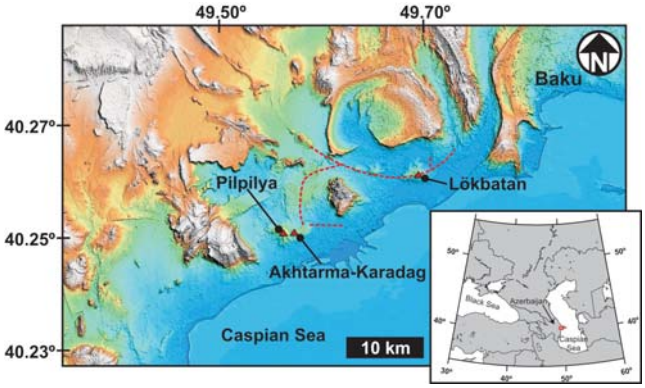

Fig. 1. Digital elevation map of the Caspian coastline in Azerbaijan showing the location of the study areas (localities marked with red triangles). Red dashed lines indicate presence of faults. White colouring indicates highest topographic areas; blue represents the lowest topographic areas. Inset regional map shows main map location as red box.

Lökbatan mud volcano

Lökbatan is one of Azerbaijan's most active mud volcanoes, with 22 major eruptions from 1810 to 2010 (Aliyev *et al.* 2002); it is located 15 km SW of Baku (Fig. 1). Lökbatan is situated on the crest of an anticline of the same name, which trends east–west. The fold has a northern limb steeper (55–60°) than its relatively gentle southern limb (30–35°), and its crest is faulted. The plan-view shape of the mud volcano edifice is elongate, in contrast to many other examples documented in the area (Evans *et al.* 2008). Its plan-view dimensions are *c*. 1.6 km by 0.9 km (Fig. 2) and its crest is 130 m above the level of the Caspian Sea.

The western flank of Lökbatan is characterized by an arcuate, elongate failure scarp measuring 1.62 km long in the dip direction. This feature was first described by Planke *et al.* (2003) as a 'western trending graben collapse structure'. The failure has a maximum width of 0.48 km and is 6 m high at the crest of the edifice (Fig. 2). The failure structure is oriented coaxially with the mud volcano edifice. Where the fault scarp is exposed it dips at 60–80° towards the collapse structure. There is no scarp at the downdip limit of the

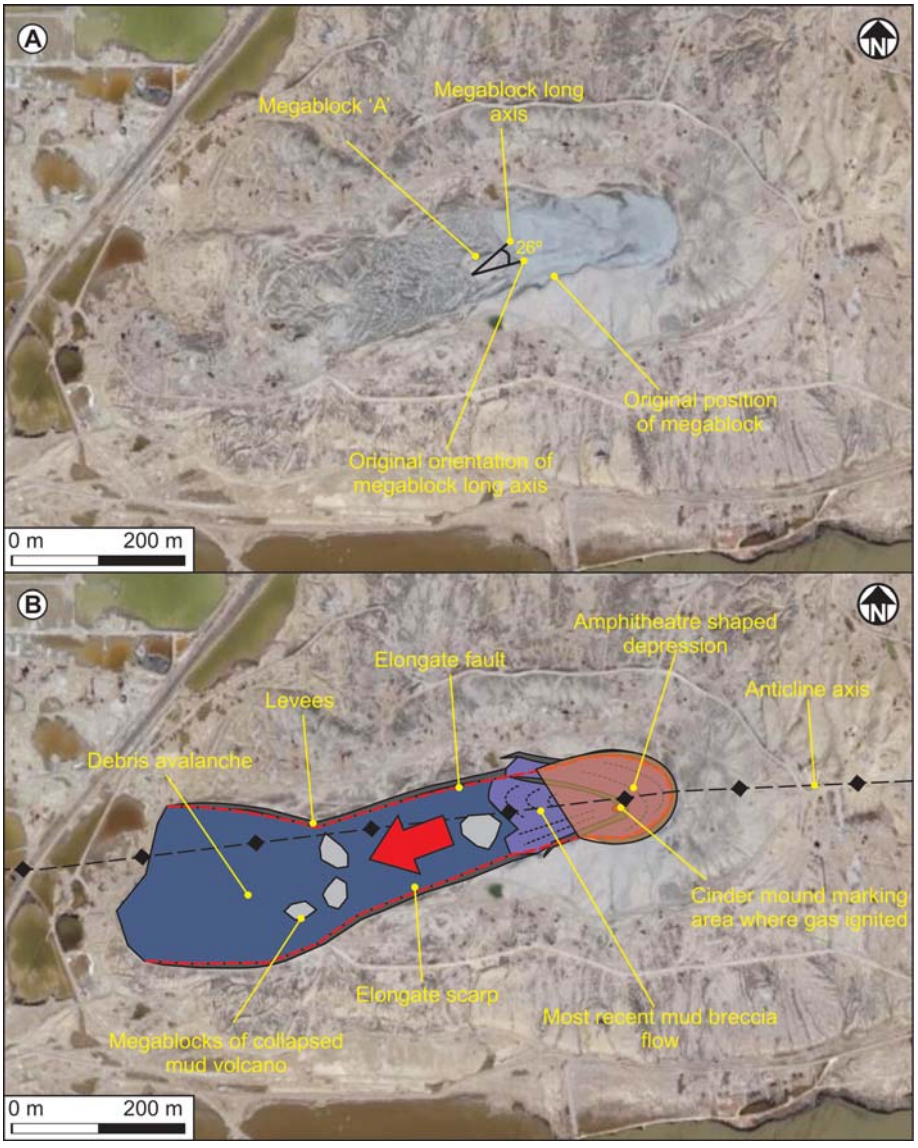

Fig. 2. (**a**) Lökbatan mud volcano, Baku, Azerbaijan. (**b**) The western flank of this volcano collapsed in 2001 during an eruption. Red arrow indicates the direction of the main failure. Amphitheatre-shaped depression is shaded in orange. Old mud breccia flows are coloured in purple. Levees are dark brown. Edges of collapse structure are marked by the dashed red line. Image © 2010 DigitalGlobe, © 2010 Google.

collapse structure. At the base of the scarp, 1–2 m high elongate mounds of mud breccias demarcate the sides of the failure.

Freshly erupted mud breccias occupy an area of *c*. 0.096 km^2 in the upper reaches of the area enclosed by this scarp. The contrast in colour and texture of the mud breccias, and their field relationships with the scarp, indicate that these were erupted some time after the main collapse structure developed (Fig. 2). Scholte *et al.* (2003) referred to this as a 'breccia field'. 'Megablocks' (Siebert 1984) occur within the main flow, measuring up to 110 m in length (Fig. 2). The megablocks display a similar light grey colour to those of the flanks of the volcano when compared with the darker grey flow deposit within the collapse structure and the blue–grey of the younger mud breccia flows (Fig. 2). One indicator that these megablocks are not *in situ* is that they rise 2–5 m above the height of the flanks in their present location, suggesting that they came from a location further updip, where the fault scarp is higher. Also, in Figure 2a, a wedge-shaped megablock (Megablock 'A') can be 'fitted' back to where its height corresponds to the volcano flanks. A 'long axis' of this block is determined on the basis of variations in thickness of the block, with a view to establishing whether the block has rotated about a steep or vertical axis (Fig. 2a). This method suggests that the block has moved 160 m down the flank and has been rotated 26° from its original long axis orientation (Fig. 2a).

Akhtarma-Karadag and Pilpilya mud volcanoes

These volcanoes are located on an east–west-trending anticlinal structure 87 km SW of Baku. Akhtarma-Karadag and Pilpilya are essentially two summits of a single elongate mud volcano (Fig. 3a), the summits being separated by a col tens of metres below the elevation of the adjacent highs. Each elongate summit area is characterized by kilometre-scale failures that face in opposite directions to one another and are a few hundred metres apart at their closest approach.

Pilpilya, the westerly half of the mud volcano, has an almost circular plan-view shape measuring *c*. 2.06 km by 1.90 km (Fig. 3b). The main active vent zone on the summit is found at the eastern end of the edifice. Although no vents are currently active on the volcano itself, a single, 200 m diameter active gryphon is located 500 m west of the mud volcano (Fig. 3b). Pilpilya has a failure structure *c*. 1.58 km in length and *c*. 240 m wide that has failed in a westerly direction (Fig. 3b).

The head-scarp at the top of the edifice is arcuate and *c*. 170 m wide. At the top of the edifice the scarp is 5.5 m high, reducing to 20 cm at the base of the mud volcano flanks. The sides of the scarp dip steeply at 30–40° towards the collapse structure on all sides of the failure. At the base of the scarp 1–2 m high elongate mounds of breccias mark the sides of the failure. A major mud breccia eruption has occurred subsequent to the failure, as a large breccia flow oversteps the debris avalanche (Fig. 3b).

Akhtarma-Karadag volcano is elongate and measures *c*. 2.15 km by 0.8 km in areal extent, and is 96 m in elevation (Fig. 3c). The main active vent zone on the summit occurs at the western end of the edifice (Fig. 3c). This feature was first observed using satellite imagery that identified a closed, kilometre-scale elongate structure (Fig. 3c). Field mapping demonstrated the western end of this feature to be an arcuate fault (Fig. 3d). Displacement decreases from *c*. 1.5 m at the west end of the structure to a centimetre-scale fracture zone at the east end,

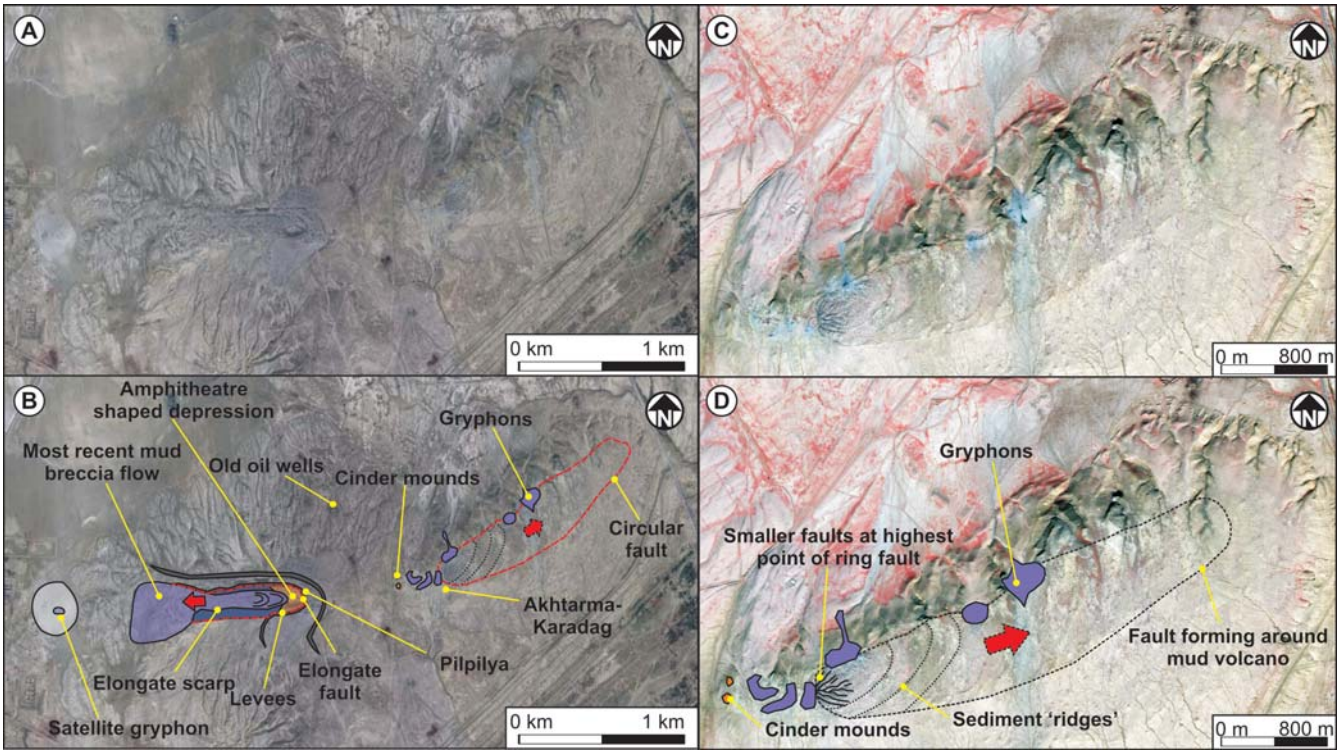

Fig. 3. (**a**) Google Earth image of Akhtarma-Karadag mud volcano and west of it Pilpilya mud volcano with a collapse structure. Image © 2010 GeoEye, © 2010 Google. (**b**) Interpretation of (**a**). Red arrow indicates the direction in which the main slope failure has occurred or could occur. On Pilpilya the collapse and most recent flow can be seen to fail down the volcano's western flank. (**c**) IKONOS image of Akhtarma-Karadag mud volcano. (**d**) Interpretation of (**c**). Dotted black line shows fault trace. Purple areas represent gryphons and orange areas indicate regions where cinder mounds are present. Image © 2010 GeoEye.

barely perceptible in the prevailing outcrop conditions (Fig. 4). The head of the break in slope at the western end of the volcano is arcuate and has several smaller fractures radiating from it in east–west orientations (Fig. 3d). There are several centimetre- to metre-scale kinematic shear sense indicators that have been identified from the incipient fault. The most prominent of these shear indicators are en echelon fractures (Fig. 4b, inset) showing lateral movement towards the NE. Freshly exposed plant root systems span the main open fracture, and many gryphons and salses are coincident with the fracture zone (Fig. 4a and b). Another kinematic indicator is the 'sediment ridges' that occur within the structure, similar in form to pressure ridges seen in lava flows (Fig. 3; Sigurdsson *et al.* 2000). These also indicate movement to the NE.

Interpretation

The main features described are elongate scarps on the flanks of mud volcanoes, mud breccia levees; arcuate-amphitheatre-shaped craters and allochthonous megablocks. All of these features are consistent with thin-skinned failure of the margins of the mud volcano flanks (as opposed to deep-rooted caldera collapse) and are described below, drawing parallels to equivalent structures documented on igneous volcanoes. Where possible, we follow the nomenclature used in igneous context by Ui *et al.* (2000).

Amphitheatre

The volume encompassed by an arcuate, updip part of a scarp that delimits a sector collapse is termed the 'amphitheatre' as the scar forms a 'horseshoe' shape (Fig. 5; Leyrit 2000). This morphology is accentuated when the collapse is accompanied or overprinted by eruptive activity (Leyrit 2000). The walls of the amphitheatre are steep and reach several hundreds of metres height in igneous volcanoes. At Lökbatan and Pilpilya mud volcanoes these walls are steep but reach only 2–10 m in height.

The edge of the amphitheatre is defined by the footwall high of the sector collapse fault. Its height is controlled by the amount of fault displacement and the amount of material removed by the debris avalanche. Our examples suggest that amphitheatre height in mud volcanoes is restricted to a maximum of *c*. 10 m.

Sector collapse fault

The margin of the amphitheatre is marked by either an inward-dipping scarp or a slope with a pronounced break at its base. This defines the 'elongate scarp' marking the limits of failure. This scarp varies in height from *c*. 10 m in the amphitheatre to less than 1 m at the downdip limit.

At Akhtarma-Karadag this fault is interpreted to be in an incipient stage at present. The elongate shape of this ring fault is

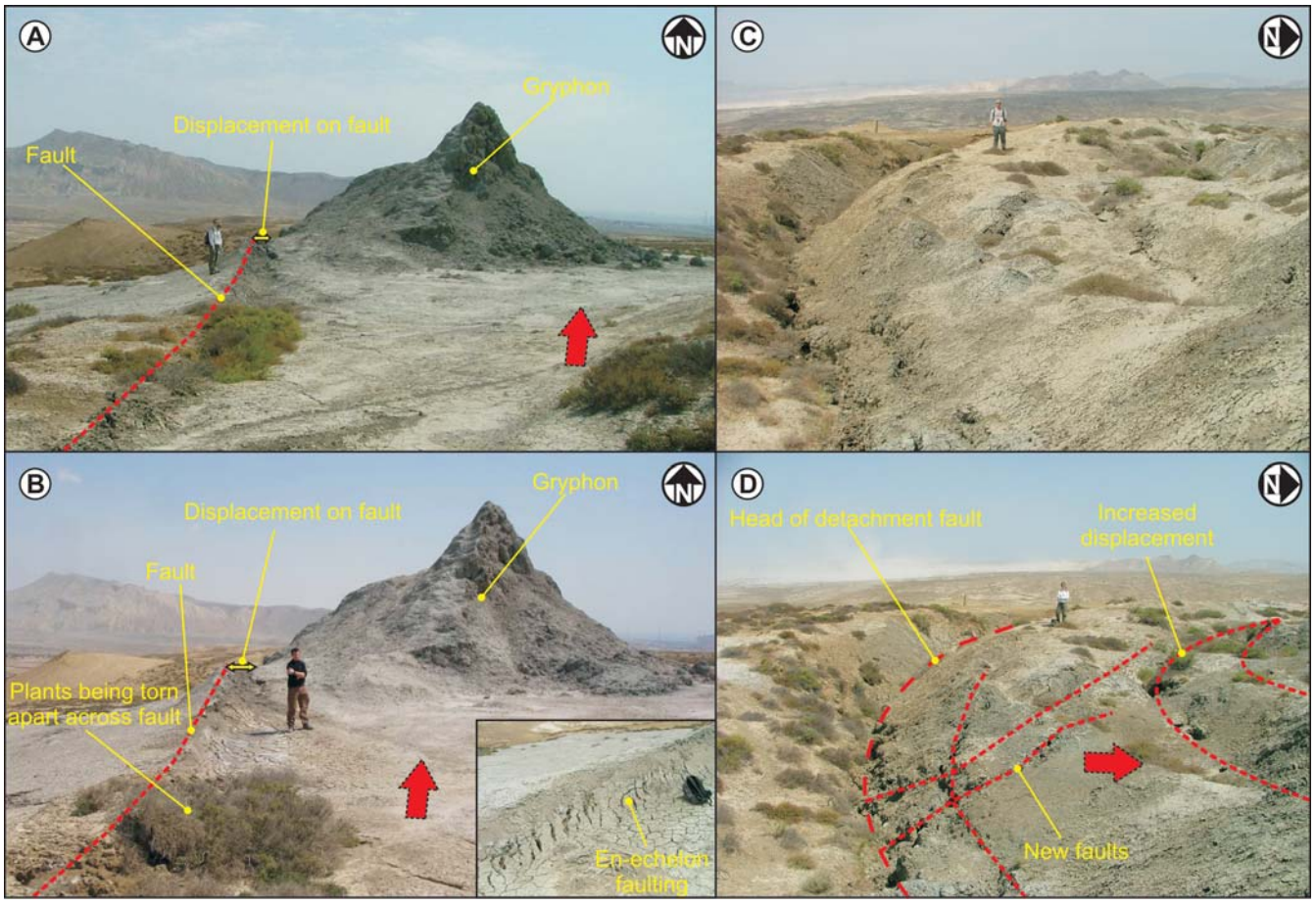

Fig. 4. Photographs of the Akhtarma-Karadag mud volcano. (**a**, **b**) At northern side of ring fault, (**a**) June 2006 and (**b**) April 2009, with an inset photograph of en echelon faulting seen along the main ring fault. The photographs show a section of the ring fault (marked by the dashed red line) that has an offset on it. There is also a large gryphon that is erupting along this fault line. (**c**) Photograph taken at the head of the ring fault in June 2005. (**d**) Photograph taken at the head of the ring fault in June 2006.

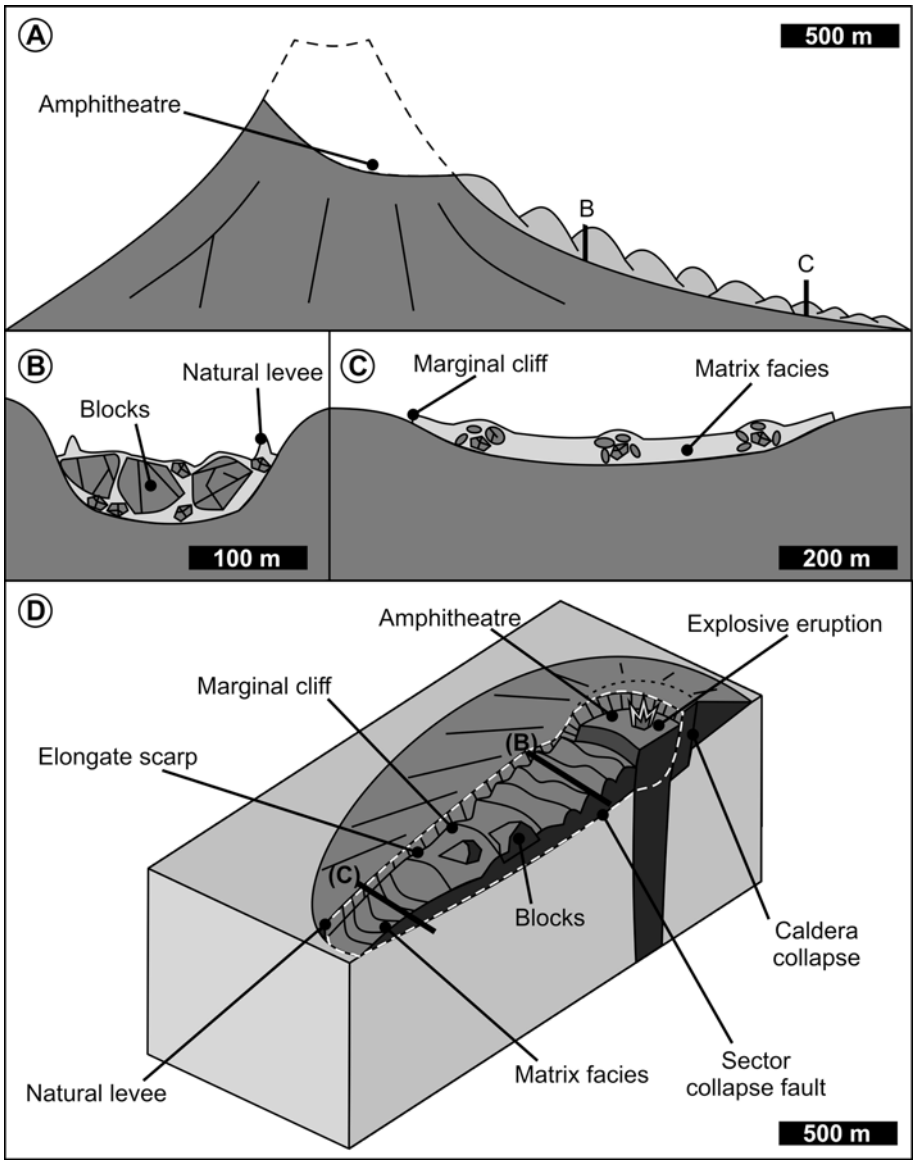

Fig. 5. Schematic illustration of sector collapse of an igneous volcano after Ui *et al.* (2000). (**a**) Longitudinal section of a sector collapse. The dashed line indicates the previous morphology of the volcano before the collapse took place. (**b**) Cross-section across the debris avalanche high on the flanks of the volcano; 'debris avalanche block facies', location B. (**c**) Cross-section across the debris avalanche low on the flanks of the volcano; 'debris avalanche matrix facies', location C. (**d**) A 3D schematic illustration of mud volcano sector collapse with localities of cross-sections B and C indicated. White dashed line marks sector collapse fault.

similar in plan-view form to the failure at Lökbatan mud volcano. The dimensions of this structure are *c*. 1.2 km length and *c*. 400 m width, similar to the collapses mapped at Lökbatan and Pilpilya. The fault is currently active on the basis of exposed and broken plant root systems found spanning open fractures, en echelon fracturing and sediment ridges (Fig. 4b, inset). Gryphons and salses coincident with this fault demonstrate active fluid flow preferentially localizing onto the fault surface. This link between fluid flow and faulting argues against a purely thin-skinned interpretation along the whole length of the sector collapse fault (Fig. 4a and b).

We distinguish between caldera collapse and sector collapse in terms of bounding fault geometry. The lower tips of faults associated with calderas and ring complexes occur at depth in the subsurface below or within a volcanic edifice and could be described as 'thick-skinned' collapse (Fig. 6a). On the other hand, the lower tip line of a fault or shear zone bounding a sector collapse crops out at the surface on the volcano flank and can be considered as 'thin-skinned' failure (Fig. 6b). Therefore in terms of peripheral, bounding structures (as opposed to internal structures), sector collapse structures should have a downdip domain characterized by surface expression of compression (which may be an overthrust or flow over lateral equivalent units), whereas caldera structures do not.

Planke *et al.* (2003) described the elongate portion of the sector collapse fault at Lökbatan as a 'graben collapse structure'. They suggested that this was caused by the presence of an elongated, shallow mud chamber within the crest of the anticline and that during an eruption mud was drained from the chamber, resulting in subsidence and collapse of the roof, essentially viewing the whole structure as an elongate caldera. We propose an alternative interpretation, that the scarp was produced by a process of 'thin-skinned', detached collapse only indirectly linked to a deeper-seated deflating chamber. A critical piece of evidence supporting our interpretation is the presence of hummocky terrain, enclosed by the downdip portion of the elongate ring fault.

Levees

These morphological features form on the downthrown side of the elongate scarp and mark the edges of the debris avalanche field. They can be seen at both Lökbatan and Pilpilya. At the

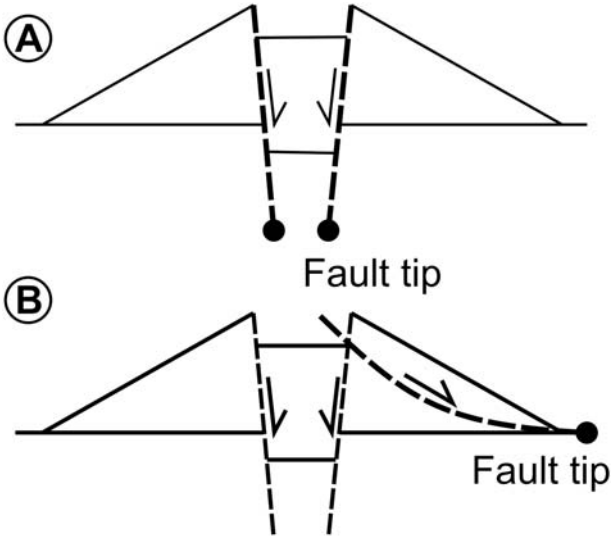

Fig. 6. Schematic diagrams showing (**a**) the positions of fault tips during caldera collapse and (**b**) fault forming as a result of sector collapse of mud volcanoes.

updip (headscarp) end of the collapse, the levees are between 2 and 4 m in height and towards the foot of the edifice they decrease to less than 1 m in height. In cross-section they have a wedge shape and in three dimensions this wedge is sinuous, defining the edges of the debris avalanche deposit. This morphology is similar to debris avalanche levees common on igneous volcano sector collapse deposits (Siebert 1984), and also fluvial or alluvial levees (Adams *et al.* 2004). This similarity suggests that these processes share a common mode of formation. Levees form on mud volcano sector collapse flows as opposed to eruptive flows because sector collapse flows are geologically instantaneous, catastrophic events involving very poorly sorted material. As this debris avalanche moves downslope and outwards the levees build up in areas where flow boundary conditions are markedly non-uniform as flow energy decreases towards the outer edges of the avalanche. This process does not occur in eruptive flows, as they often flow at an average rate of 0.5–2 m a^{-1} and are composed of a mass of mud breccia that flows downhill almost as a coherent block.

Debris avalanche deposits

These produce hummocky deposits of fragmented debris towards the base of volcanoes (Figs 5d and 7b). Early igneous workers variously interpreted these hummocks as glacial moraines, phreatic blisters on the surface of gas-rich lava flows, small independent volcanic vents, lahars, or man-made features (Siebert 1984). Debris avalanche deposits in the case studies considered here consist primarily of the mud breccia that originally formed the mud volcano edifice. Table 1 shows that the volumes of debris avalanches are comparable with those of the missing sectors of the cone, indicating that the dominant process is not input of new, erupted material, but slope failure of a pre-existing portion of the volcanic edifice.

Debris avalanche deposits are poorly sorted and the dominant constituent is material of the volcanic edifice. Some freshly erupted material may be present, although this is hard to

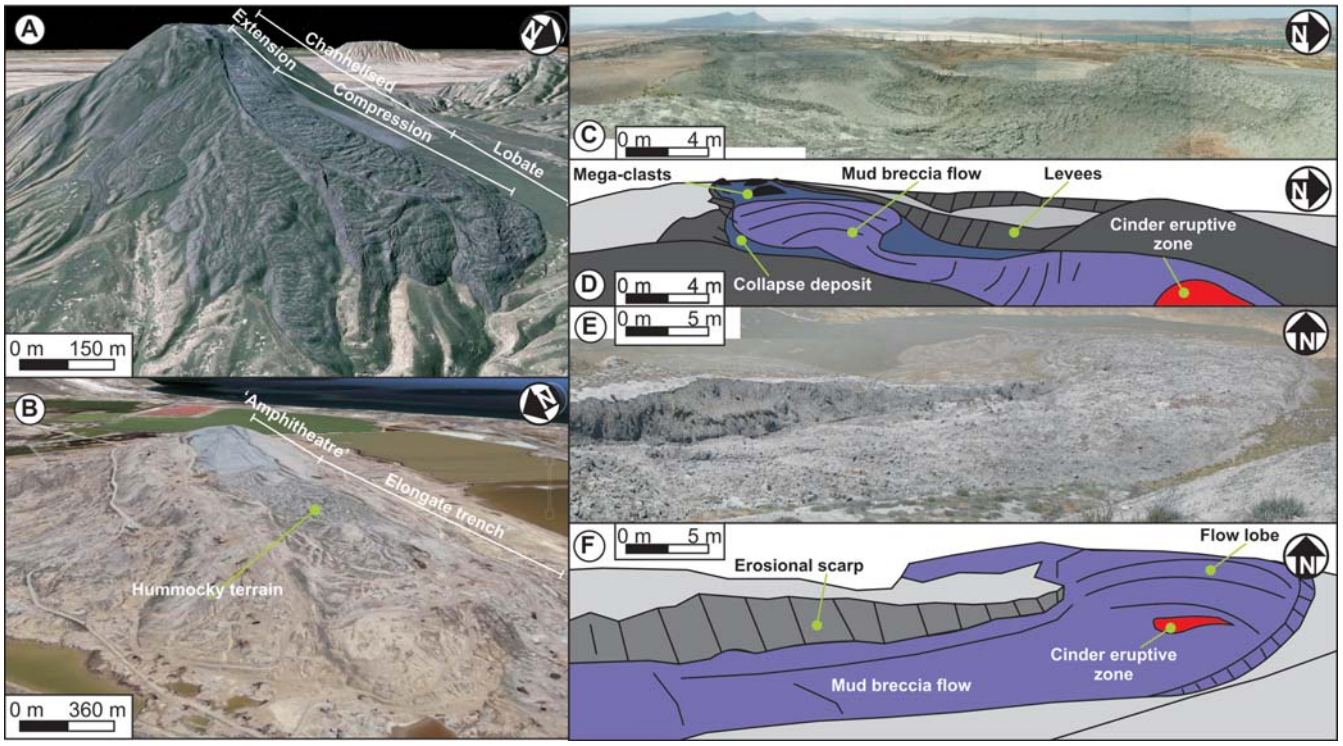

Fig. 7. Structure of mud breccia flows compared with collapse deposits. (**a**) Mud breccia flow emanating from Koturdag crater (3 × vertical exaggeration). Koturdag mud volcano is located 30 km SW of Pilpilya. Image © 2010 GeoEye, © 2010 Google. (**b**) Elongate collapse structure on Lökbatan (3× vertical exaggeration). Image © 2010 DigitalGlobe, © 2010 Google. (**c**) Photograph of the elongate collapse structure on Lökbatan. (**d**) Schematic illustration of structural features seen in (**c**). (**e**) Photograph of the mud breccia flow emanating from Koturdag crater. (**f**) Schematic illustration of the structural features seen in (**e**).

Table 1. *Dimensions of sector collapse structures discussed in the text*

Mud volcano	Angle of sector (°)	Length of elongate scarp (km)	Volume of debris avalances (m^3)	Volume of scarp (m^3)	Angle of repose (°)	Width of elongate scarp (km)	Area of volcano (km^2)
Akhtarma-Karadag	35	1.6	–	–	6	0.9	5.79
Pilpilya	29	1.75	*c.* 7.43×10^6	*c.* 7.29×10^6	10	0.8	6.75
Lökbatan	28	1.65	*c.* 7.42×10^6	*c.* 6.32×10^6	10	0.8	5.75
Mount St. Helens	36	15.44	2.3×10^9	–	15	3.45	70.37

distinguish in mud volcanic eruptions if the deposits are old. Large fragments of the volcanic edifice, tens of metres in size or larger, termed 'megablocks' (Siebert 1984), can be incorporated in debris avalanches (e.g. at Lökbatan). Debris avalanche deposits display surface morphology with textural and morphological features characteristic of landslide deposits (Fig. 5; Siebert 1984). In particular, hummocky topography with numerous hills, closed depressions, and longitudinal and transverse ridges occur at both Lökbatan and Pilpilya (Figs 5d and 7b). Mud volcano debris avalanches are more easily eroded than those at igneous volcanoes and so are relatively inconspicuous.

Eruptive flow versus sector collapse

It is not necessarily straightforward to distinguish between scarps produced by sector collapse and those excavated by erosive flow of erupted mud. However, there appear to be morphological differences between the kilometre-scale structures produced by these processes (Fig. 7). Mud breccia flows tend to be narrow, point-sourced phenomena originating near the top of the mud volcano edifice (Fig. 7a, e and f; Chow *et al.* 2006). As they reach lower-lying, gentler slopes they spread out into wider, lobate deposits. In contrast, sector collapses involve a whole segment of the flank moving downslope (Figs 5 and 7b–d). The dimensions of eight sector collapses and 21 mud breccia flows were measured from aerial imagery and are plotted in Figure 8. Flows in this dataset were characterized on the basis of fieldwork and/or diagnostic features recognized on aerial imagery (levees, megablocks, sinuosity and colour; Fig. 7). The results show that the ratio of 'Bottom Width' (width at the most distal termination of the structure) to 'Middle Width' (width halfway down the structure) of the structures effectively distinguishes between the two failure modes, with sector collapse ratio being about unity and flows ratio being greater than unity (typically two or more; Fig. 8).

We identify three end members of failure and resulting deposits on mud volcano flanks based on scale, and relative importance of slope failure versus eruptive processes (Fig. 9). Erosive flow of a mud breccia deposit can involve relatively long, meandering tongues of mud breccia that cut into the flanks of the volcano from which they emanate. They tend to spread out once they meet the plain on which the edifice is building (Figs 7 and 8). At the foot of the flows pressure ridges build up, giving them an appearance similar to 'ropy' lava flows (Fig. 7a; Sigurdsson *et al.* 2000).

Sector collapse deposits have a low to moderate length and a uniform width throughout their length. Their internal structure resembles that of a debris avalanche, with an extensional zone at the top and a compressional zone at the bottom of the deposit. Surface morphology of sector collapse deposits includes hummocky terrain and megablocks of the flanks of the volcano. Small slope failures (5–30 m length) also occur on the flanks of these volcanoes and structurally resemble the larger sector

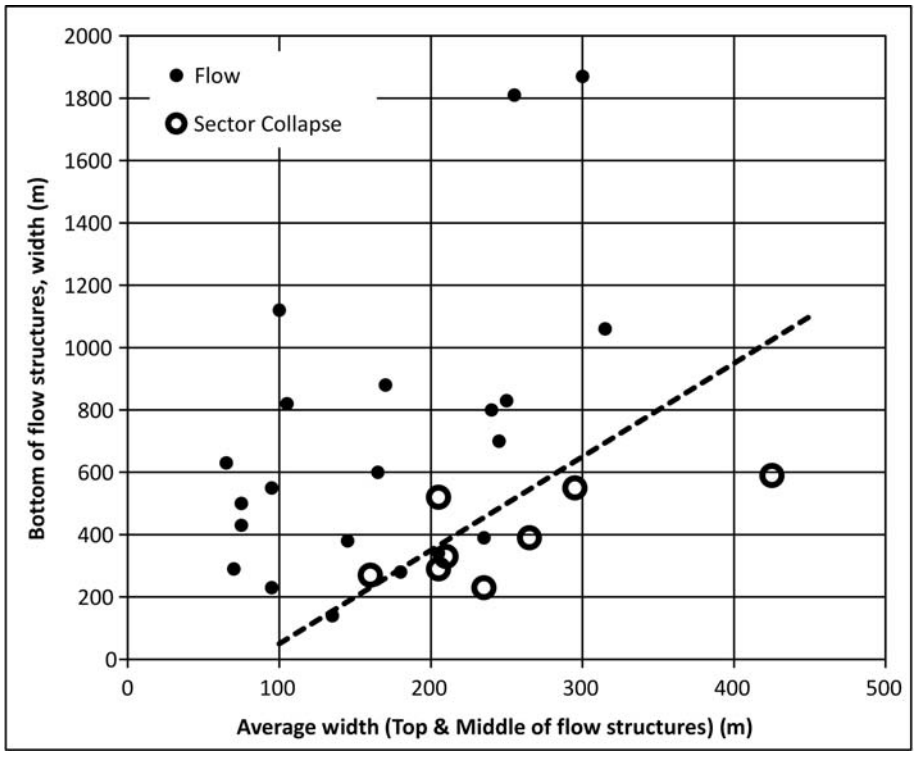

Fig. 8. Graph showing the relationship between lengths and widths of various flow structures on mud volcano edifices. Dashed line represents the transition zone between mud breccia flows and sector collapse geometries.

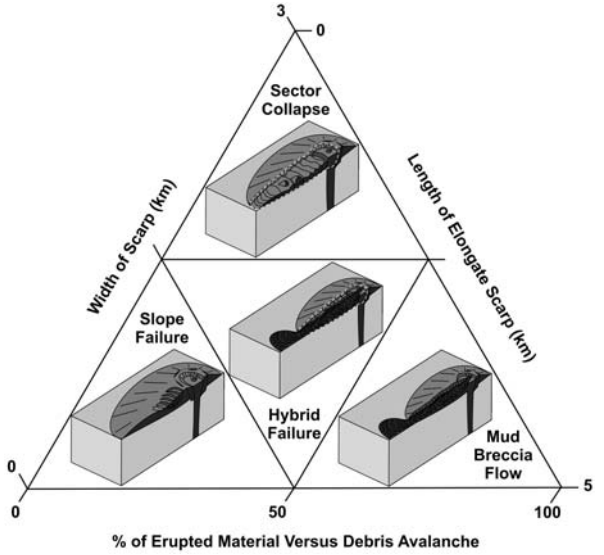

Fig. 9. Schematic ternary diagram showing the positions of mud breccia flows, sector collapses, slope failures and hybrid failures occurring on mud volcanoes in relation to the scarp length and width and the size of the feature. The internal structure of each deposit can also be seen in the block diagrams.

collapse deposits. They have short downslope length and are relatively wide compared with their length.

Discussion: mechanisms for mud volcano sector collapse

Sector collapses are well documented in the context of igneous volcanoes (Siebert *et al.* 1987; Van Wyk de Vries *et al.* 2000; Lundgren *et al.* 2003). In relation to igneous volcanoes these structures are in excess of tens of kilometres in extent; some of the largest examples involve *c*. 10^{12} tons of mobilized material (Masson *et al.* 2002). Mud volcanoes are generally smaller than igneous volcanoes, so sector collapses of mud volcano edifices occupy a different scale range. The lower cut-off for length scale of sector collapse in mud volcanoes employed here is 1 km, on the basis that these are substantial structures that are relatively easy to identify in the field and on seismic reflection data, and are of a scale to pose significant risk to subsea infrastructure.

A range of possible mechanisms may be involved in triggering sector collapse in mud volcanoes; it may be that actual events result from combinations of such factors. A brief review is presented here based in part on processes that have been discussed in relation to sector collapse in igneous settings (Fig. 10; Voight & Elsworth 1997). The most likely mechanisms for mud volcano sector collapse are as follows.

Oversteepening. Oversteepening of the summit region of the volcano (e.g. tumescence owing to mud injection) could produce gravitational instability (Fig. 10a). Slope angles in the case studies reported here range from 6 to 10° (Table 1). On igneous volcanoes the majority of collapses occur on slopes of 28–30° (Voight & Elsworth 1997). The slope failures reported here from Azerbaijan do not, however, occur on the steepest parts of the edifice.

Regional stress. Siebert *et al.* (1987) stated that the location of sector collapses within the igneous volcanic edifice can be influenced by local and regional stress regimes. Swarms of mud

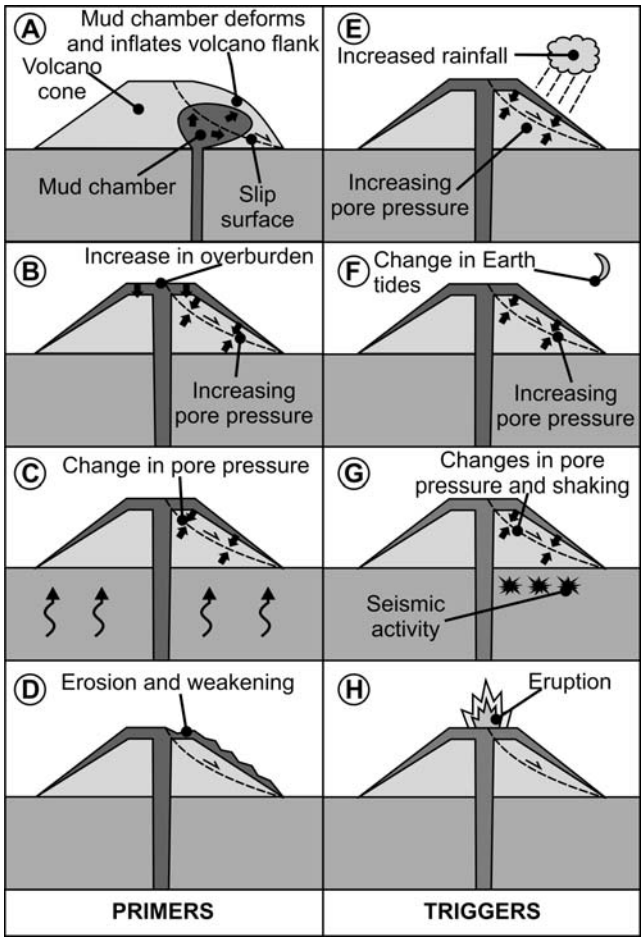

Fig. 10. Schematic diagrams showing primers and triggers of mud volcano sector collapse events. (**a**) Inflation of mud chamber and volcano causing instability. (**b**) Addition of overburden when mud breccia is erupted onto the volcano flanks. (**c**) Change in pore pressure within the mud volcano. (**d**) Erosion and removal of support. (**e**) Precipitation increasing pore fluid and loading and therefore pore pressures. (**f**) Earth tides exerting different gravitational forces on the mud source, causing more or less violent eruptions. (**g**) Seismicity shaking the ground and changing pore pressure in the mud volcanoes. (**h**) Eruption of mud volcano.

volcano vents often occur parallel to the regional maximum horizontal compression (Roberts *et al.* 2010), resulting in the elongation of the volcanic edifice in that direction. In the Azerbaijani examples mud breccia flows show weak clustering in a NE or SW direction, generally flowing down the steepest topography (Fig. 11b). In contrast, the sector collapse failures occur parallel to the direction of mud volcano edifice elongation, generally an east–west trend that is also parallel to the anticline axis at each location (Fig. 11c). This relationship suggests that, although the sector collapses may be related to some aspect of mud volcano edifice geometry, they are not directly related to regional stress.

Loading. Loading of the volcano flanks by erupted mud breccia may cause increase in pore pressure resulting in collapse (Fig. 10b). Rainfall could be another significant loading factor in the onshore Azerbaijani mud volcanoes. The climate is arid for much of the year and the mud flows become heavily fractured as they dry out; appreciable water load is absorbed in the wet season.

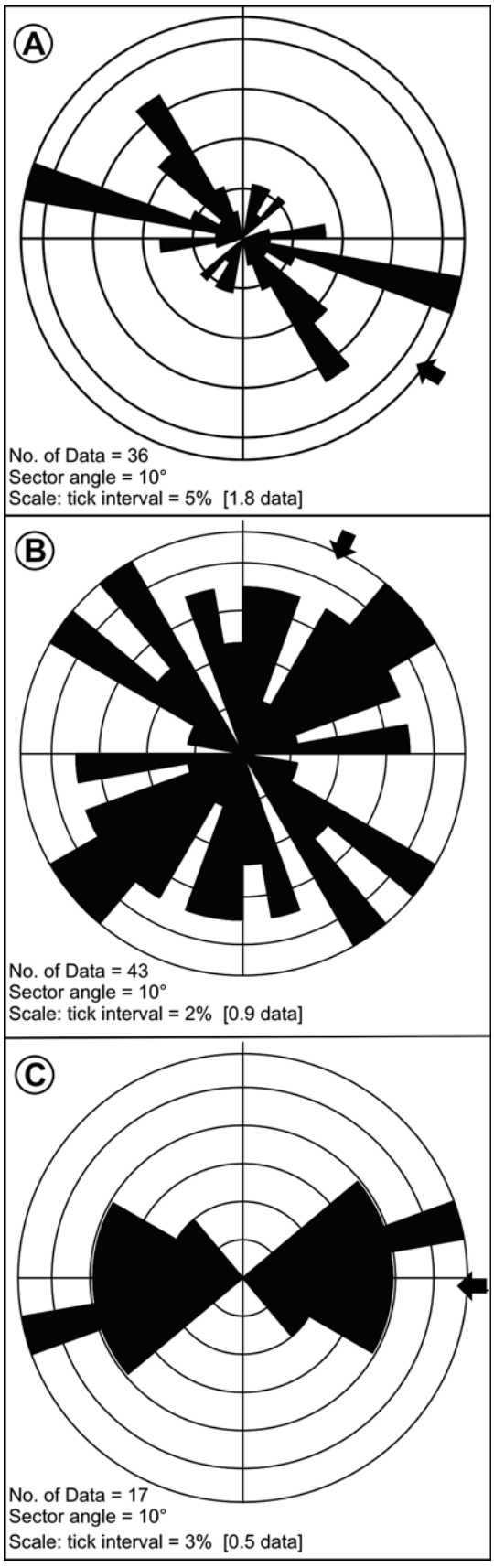

Fig. 11. Rose diagrams of orientations of (**a**) long axes of mud volcano calderas, (**b**) mud breccia flows and (**c**) sector collapse troughs.

Overpressure. Overpressure of pore fluids in and around the mud volcano edifice may cause failure (Fig. 10c). If the sediments are sealed, pore pressure within them will increase, reducing the effective normal stress as well as shear strength of the sediment. No additional trigger is necessarily required; pore pressure can simply increase until the downslope component of the gravitational force is greater than the shear strength of the sediment and its cohesion, at which point failure occurs.

Erosion. This can create steeper zones that are susceptible to destabilization (Fig. 10d). It may also remove lateral support to slopes and so induce collapse.

Hydrothermal alteration. Hydrothermal alteration along regional fracture sets also may be an important process in the localization of sector collapse features (López & Williams 1993; Reid *et al.* 2001; Reid 2004). Circulation of fluids (meteoric and hydrothermal) can result in an increase in pore water pressure.

Seismic activity. This is a documented triggering factor of both igneous and mud volcano eruptions and collapses (Fig. 10g; Manga 2007; Manga *et al.* 2009). Continuous monitoring of Lökbatan mud volcano has indicated the occurrence of weak earthquakes during eruptions but it is not clear whether these are a cause or effect of the eruption process.

Earth tides. These have been linked with both mud volcano and igneous volcano eruptive periodicity (Fig. 10f; Mauk & Johnston 1973; Aliyev *et al.* 2002).

Eruptions and fluid activity. These are involved in some 50% of all igneous sector collapses (Leyrit 2000). Lökbatan's first recorded eruption took place in 1864 (Aliyev *et al.* 2002). The 2001 eruption involved ignited gas jets 50–60 m in height (Aliyev *et al.* 2002; Kadirov & Mukhtarov 2004) and 304 m^3 of erupted mud breccia (Aliyev *et al.* 2002). Sector collapse at Lökbatan may have coincided with the eruption on 23 February 1935. Aliyev *et al.* (2002) documented this eruption as 'taking place without noise, gas and breccia emanation'. Aliyev *et al.* (2002) noted that step-like subsidence occurred with landslides, which were most probably the result of a collapse of the western portion of the volcano. The centre of the volcano then subsided up to 22 m and numerous fractures formed that then began to emit gas and breccia that covered up to 25 000 m^2 (Aliyev *et al.* 2002).

A broader summary of factors that may relate to sector collapse is tabulated in Table 2.

Mapping in this study has revealed apparently conflicting structural evidence in relation to mechanism of the kilometre-scale elongate collapse structures on mud volcanoes in Azerbaijan. On one hand, there is good morphological evidence of mass flow on shallow detachment with many similarities to sector collapse structures in igneous volcanoes. On the other hand, we observe alignments of fluid expulsion features along the bounding faults, particularly in the updip domains, of these structures. Reconciling these observations leads us to a preferred model that is essentially a development of that previously published by Planke *et al.* (2003). We adopt their idea of an elongate mud chamber at relatively shallow (<1 km) level. However, rather than the elongate fault-bounded structures at the surface directly representing a collapsing roof of a deflating mud chamber, we suggest that the observed sector collapse structures are thin-skinned sector collapses triggered and localized by mud chamber deflation, as shown in Figure 12. This ring fault provides a

Table 2. *Causes of mud volcano collapse, adapted from Voight & Elsworth (1997)*

Inherent causes
Initial composition
Texture: loose, porous, weak materials are slide prone
Bedding attitude relative to slope face
Layering sequences in relation to strength, permeability
Discontinuity systems: faults, joints, bedding planes
Slope-forming process history, movement history; bedding slip and fault slip history and orientation of movement
Initial physicochemical setting; conditions of weathering and alteration
History of seismicity and seismic damage
Ambient (seasonal) groundwater conditions
Causes of increased shear strength
Removal of lateral or underlying support of slopes
Erosional processes producing, steepening, or undercutting natural slopes
Prior mass movements
Eruptions near base of slope
Static loading
Natural deposition: slope or river sedimentation
Weight of water added by natural precipitation or by exsolved volatiles
Seepage pressures and joint water pressures
Mud or fluid pressure
Swelling pressures in expansive clays
Dynamic loading
Regional or local tectonic earthquakes
Vibrations from volcanic earthquakes, explosion and eruptive processes
Vibrations from adjacent, rapidly moving landslides
Increase of surface slope
Mud or fluid intrusion-related deformation
Regional tectonics
Slope changes owing to depositional processes
Causes that reduce shear strength
Physicochemical factors
Hydrothermal alteration
Softening of clays
Hydration of clay minerals
Ion exchange of clays
Weathering
Solution of grain cement
Decomposition of organic materials
Physicochemical fracturing
Pore fluid pressure enhancement
Heavy rainfall or rapid snowmelt
Changes in groundwater flow regime
Pore pressure changes owing to hydrothermal processes
Thermal expansion of pore fluid owing to frictional slip
Vibration-induced pore fluid pressure rise
Shear deformation-induced pressure rise
Consolidation seepage induced by surcharge
Base-level changes in reservoirs, lakes or oceans
Flow boundary condition changes
Changes in structure
Disturbance
Particle reorientation owing to slip or dynamic loading; peak to residual strength loss
Grain collapse in altered deposits
Fracturing and loosening of valley walls, stress relief
Deep-seated fracturing associated with fluid intrusion, stress relief, physicochemical alteration
Adjustments to groundwater flow paths; slope drainage enhanced or impeded

pathway for fluids and so results in vents aligning along the fault itself (Fig. 12b). Ring fault formation may be enhanced by fluid flow up crestal faulting parallel to the anticline axis (Roberts *et al.* 2010), which would explain why failure sometimes occurs on the shallowest slopes.

Subsea examples of igneous sector collapse have also been identified in both seismic reflection and multibeam (swath) bathymetric sonar data (Mattioli *et al.* 1995; Leat *et al.* 2010), as well as possible unidentified sector collapse structures on mud volcanoes in subsea seismic reflection data from the South Caspian Basin (e.g. Corthay & Aliyev 2000). These structures also share the same 'shape parameters' that we believe identify sector collapse. Using this study to identify similar subsurface structures could aid a better understanding of the processes at depth as well as determining areas that may be at risk to these potential geohazards (Corthay & Aliyev 2000; Leat *et al.* 2010).

Conclusions

Elongate trench-like depressions bounded by shallow inward-facing faults trending from the summit to the base of some mud volcanoes in Azerbaijan, and displaying evidence of downdip lateral movement, are termed 'mud volcano sector collapses'. Examples mapped in the field are in the range of *c.* 180–200 m

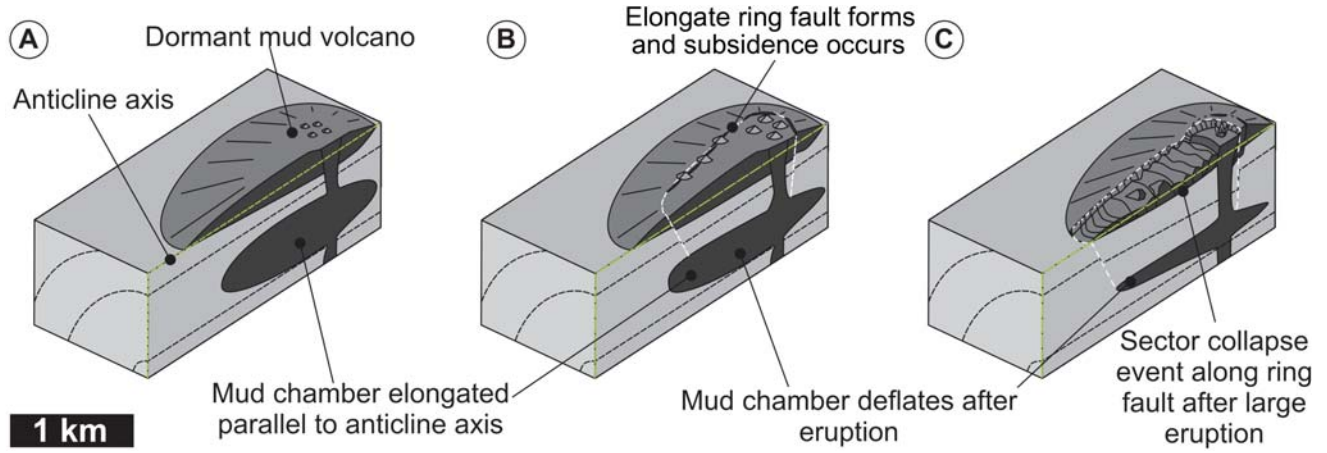

Fig. 12. Schematic sector collapse formation. (**a**) Dormant mud volcano edifice. (**b**) Ring fault forms after small eruption and evacuation of material from depth. (**c**) Large eruption causes subsidence to occur as a result of expulsion of fluids at the surface, resulting in sector collapse along ring fault. Green dashed line indicates position of anticline axis.

in width and 1–2 km in length, each representing up to 10^6 tons of mobilized material assuming depth to detachment averaging 10–20 m. Field observations include an elongate trough that is fault-bounded on three sides (open downdip), with an updip 'amphitheatre' depression, levees, and a downdip domain with hummocky morphology. The bounding fault system shows kinematic evidence of lateral movement. However, the presence of fluid escape structures in the updip parts of these collapses also indicate a relationship with the deeper-seated structure of the mud volcano. We reconcile the observations in a model where a deflating, perhaps elongate, shallow mud chamber (<1 km) triggers detached sector collapse. This model could account for the range of observations plus the curious spatial relationship of the sector collapses; namely, they occur on the gentler slopes (i.e. elongate crest) of the mapped mud volcano edifices. Our model also allows the sector collapse to be more extensive than any underlying mud chamber, potentially running out beyond the edifice onto the surrounding plain.

A by-product of our study is recognition that sector collapse flows tend to have a different planform shape relative to eruptive flows, the latter having a pronounced lobe at the base of slope. This criterion allows these structures to be distinguished on remote-sensed data. The observations of sector collapse made herein can also be applied in risk assessments; for instance, it should not be assumed that mud flow hazard is restricted to areas downdip of the steepest sides of mud volcanoes. This can equally be applied in submarine settings.

We are grateful to BP for funding K.S.R.'s PhD and for logistical support during field seasons. S. Grant, T. Evans, S. Bull, M. Ireland, S. Richardson and R. Townsend are thanked for assistance during fieldwork. The reviewers, T. Needham and R. Jones are also thanked for their helpful comments. We are also grateful for the use of ArcGIS, Google Earth software and IKONOS for use of satellite imagery.

References

Adams, P.N., Slingerland, R.L. & Smith, N.D. 2004. Variations in natural levee morphology in anastomosed channel flood plain complexes. *Geomorphology*, **61**, 127–142, doi:10.1016/j.geomorph.2003.10.005.

Aliyev, A.A., Guliyev, I.S. & Belov, I.S. 2002. *Catalogue of recorded eruptions of mud volcanoes of Azerbaijan (for period of years 1810–2001)*. Nafta Press, Baku.

Allen, M.B., Vincent, S.J., Alsop, G.I., Ismail-Zadeh, A. & Flecker, R. 2003. Late Cenozoic deformation in the South Caspian region: Effects of a rigid basement block within a collision zone. *Tectonophysics*, **366**, 223–239, doi:10.1016/S0040-1951(03)00098-2.

Chow, J.J., Chang, S.-K. & Yu, H.-S. 2006. GPR reflection characteristics and depositional models of mud volcanic sediments—Wushanting mud volcano field, south western Taiwan. *Journal of Applied Geophysics*, **60**, 179–200, doi:10.1016/j.jappgeo.2006.03.001.

Cole, J.W., Milner, D.M. & Spinks, K.D. 2005. Calderas and caldera structures: A review. *Earth-Science Reviews*, **69**, 1–26, doi:10.1016/j.earscirev.2004.06.004.

Corthay, J.E. & Aliyev, A.A. 2000. Delineation of a mud volcano complex, surficial mudflows, slump blocks, and shallow gas reservoirs, offshore Azerbaijan. *In: Offshore Technology Conference, 1 May–4 May 2000, Houston, TX*, **12066-MS**, doi:10.4043/12066-MS.

Davies, R.J. & Stewart, S.A. 2005. Emplacement of giant mud volcanoes in the South Caspian Basin: 3D seismic reflection imaging of their root zones. *Journal of the Geological Society, London*, **162**, 1–4.

Deville, E. & Guerlais, S.-H. 2009. Cyclic activity of mud volcanoes: evidences from Trinidad (SE Caribbean). *Marine and Petroleum Geology*, **26**, 1681–1691, doi:10.1016/j.marpetgeo.2009.03.002.

Evans, R.J., Stewart, S.A. & Davies, R.J. 2008. The structure and formation of mud volcano summit calderas. *Journal of the Geological Society, London*, **165**, 769–780, doi:10.1144/0016-76492007-118.

Fisher, R.V. 1990. Transport and deposition of a pyroclastic surge across an area of high relief: The 18 May 1980 eruption of Mount St. Helens, Washington. *Geological Society of America Bulletin*, **102**, 1038–1054, doi:10.1130/0016-7606.

Geshi, N., Shimano, T., Chiba, T. & Nakada, S. 2002. Caldera collapse during the 2000 eruption of Miyakejima Volcano, Japan. *Bulletin of Volcanology*, **64**, 55–68, doi:10.1007/s00445-001-0184-z.

Guliyev, I.S. & Feizullayev, A.A. 1995. *All about mud volcanoes*. Nafta Press, Baku.

Hovland, M., Hill, A. & Stokes, D. 1997. The structure and geomorphology of the Dashgil mud volcano, Azerbaijan. *Geomorphology*, **21**, 1–15.

Hudson, S.M., Johnson, C.L., Efendiyeva, M.A., Rowe, H.D., Feyzullayev, A.A. & Aliyev, C.S. 2008. Stratigraphy and geochemical characterization of the Oligocene–Miocene Maikop series: implications for the paleogeography of Eastern Azerbaijan. *Tectonophysics*, **451**, 40–55, doi:10.1016/j.tecto.2007.11.045.

Kadirov, F.A. & Mukhtarov, A.S.H. 2004. Geophysical fields, deep structure, and dynamics of the Lökbatan mud volcano. *Izvestiya, Physics of the Solid Earth*, **40**, 327–333.

Kennedy, B., Stix, J., Vallance, J.W., Lavallée, Y. & Longpré, M.-A. 2004. Controls on caldera structure: results from analogue sandbox modeling. *Geological Society of America Bulletin*, **116**, 515–524, doi:10.1130/B25228.1.

Kokelaar, P. & Romagnoli, C. 1995. Sector collapse, sedimentation and clast population evolution at an active island-arc volcano: Stromboli, Italy. *Bulletin of Volcanology*, **57**, 240–262, doi:10.1007/BF00265424.

Kopf, A. 2002. Significance of mud volcanism. *Reviews of Geophysics*, **40**, 1005, doi:10.1029/2000RG000093.

Kopf, A., Deyhle, A., *et al.* 2003. Isotopic evidence (He, B, C) for deep fluid and mud mobilization from mud volcanoes in the Caucasus continental collision zone. *International Journal of Earth Sciences*, **92**, 407–425, doi:10.1007/s00531-003-0326-y.

Leat, P.T., Tate, A.J., Tappin, D.R., Day, S.J. & Owen, M.J. 2010. Growth and mass wasting of volcanic centres in the northern South Sandwich arc, South Atlantic, revealed by new multibeam mapping. *Marine Geology*, **275**, 110–126, doi:10.1016/j.margeo.2010.05.001.

Leyrit, H. 2000. Flank collapse and debris avalanche deposits. *In:* Leyrit, H. & Montenat, C. (eds) *Volcaniclastic Rocks, from Magmas to Sediments*. Gordon & Breach, New York, 111–130.

Lipman, P.W. 1997. Subsidence of ash-flow calderas: relation to caldera size and magma-chamber geometry. *Bulletin of Volcanology and Geothermal Research*, **59**, 198–218, doi: 10.1007/s004450050186.

López, D.L. & Williams, S.N. 1993. Catastrophic volcanic collapse: relation to hydrothermal processes. *Science*, **260**, 1794–1796.

Lundgren, P., Berardino, P., *et al.* 2003. Coupled magma chamber inflation and sector collapse slip observed with synthetic aperture radar interferometry on Mt. Etna volcano. *Journal of Geophysical Research*, **108**, 2247, doi:10.1029/2001JB000657.

Manga, M. 2007. Did an earthquake trigger the May 2006 eruption of the Lusi Mud Volcano? *EOS Transactions, American Geophysical Union*, **88**, doi:10.1029/2007EO180009.

Manga, M., Brumm, M. & Rudolph, M. L. 2009. Earthquake triggering of mud volcanoes. *Marine and Petroleum Geology*, **26**, 1785–1798.

Masson, D.G., Watts, A.B., Gee, M.J.R., Urgeles, R., Mitchell, N.C., Le Bas, T.P. & Canals, M. 2002. Slope failures on the flanks of the western Canary Islands. *Earth-Science Reviews*, **57**, 1–35, doi:10.1016/S0012-8252(01)00069-1.

Mattioli, G.S., Jansma, P.E., Jaramillo, L. & Smith, A.L. 1995. Sector collapse in island arc volcanoes: a digital topographic and bathymetric investigation of the Qualibou Depression, St. Lucia, Lesser Antilles. *Caribbean Journal of Science*, **31**, 163–173.

Mauk, F.J. & Johnston, M.J.S. 1973. On the triggering of volcanic eruptions by Earth tides. *Journal of Geophysical Research*, **78**, 3356–3362, doi:10.1029/JB078i017p03356.

Mazzini, A., Svensen, H., Akhmanov, G.G., Aloisi, G., Planke, S., Malthe-Sørenssen, A. & Istadi, B. 2007. Triggering and dynamic evolution of the LUSI mud volcano, Indonesia. *Earth and Planetary Science Letters*, **261**, 375–388, doi:10.1016/j.epsl.2007.07.001.

Mazzini, A., Svensen, H., Planke, S., Guliyev, I., Akhmanov, G.G., Fallik, T. & Banks, D. 2008. When mud volcanoes sleep: insights from seep geochemistry at the Dashgil mud volcano, Azerbaijan. *Marine and Petroleum Geology*, **26**, 1704–1715, doi:10.1016/j.marpetgeo.2008.11.003.

Milkov, A.V. 2000. Worldwide distribution of submarine mud volcanoes and associated gas hydrates. *Marine Geology*, **167**, 29–42, doi:10.1016/S0025-3227(00)00022-0.

Planke, S., Svensen, H., Hovland, M., Banks, D.A. & Jamtveit, B. 2003. Mud and fluid migration in active mud volcanoes in Azerbaijan. *Geo-Marine Letters*, **23**, 258–268, doi:10.1007/s00367-003-0152-z.

Reid, M.E. 2004. Massive collapse of volcano edifices triggered by hydrothermal pressurization. *Geology*, **32**, 272–376.

Reid, M.E., Sisson, T.W. & Brien, D.L. 2001. Volcano collapse promoted by hydrothermal alteration and edifice shape, Mount Rainier, Washington. *Geology*, **29**, 779–782, doi:10.1130/0091-7613(2001)029.

Roberts, K.S., Davies, R.J. & Stewart, S.A. 2010. Structure of exhumed mud volcano feeder complexes, Azerbaijan. *Basin Research*, **22**, 439–451, doi:10.1111/j.1365-2117.2009.00441.x.

Scholte, K.H., Hommels, A., *et al.* 2003. Subsurface resistivity in combination with hyperspectral field and satellite data for mud volcano dynamics, Azerbaijan. *In: Geoscience and Remote Sensing Symposium, 2003, IGARSS'03 Proceedings, 2003 IEEE International*, **5**, 3395–3397.

Siebert, L. 1984. Large volcanic debris avalanches: characteristics of source areas, deposits, and associated eruptions. *Journal of Volcanology and Geothermal Research*, **22**, 163–197, doi:10.1016/0377-0273(84)90002-7.

Siebert, L., Glicken, H. & Ui, T. 1987. Volcanic hazards from Bezymianny- and Bandai-type eruptions. *Bulletin of Volcanology*, **49**, 435–459, doi:10.1007/BF01046635.

Sigurdsson, H., Houghton, B., McNutt, S.R., Rymer, H. & Stix, J. (eds) 2000. *Encyclopedia of Volcanoes*. Academic Press, New York, 617–626.

Stewart, S.A. & Davies, R.J. 2006. Structure and emplacement of mud volcano systems in the South Caspian Basin. *AAPG Bulletin*, **90**, 771–786, doi:10.1306/11220505045.

Ui, T., Takarada, S., Yoshimoto, M. 2000. Debris avalanches. *In:* Sigurdsson, H., Houghton, B., McNutt, S.R., Rymer, H. & Stix, J. (eds) *Encyclopedia of Volcanoes*. Academic Press, New York, 617–626.

Van Wyk de Vries, B., Kerle, N. & Petley, D. 2000. Sector collapse forming at Casita volcano, Nicaragua. *Geology*, **28**, 167–170, doi:10.1130/0091-7613.

Voight, B. & Elsworth, D. 1997. Failure of volcano slopes. *Géotechnique*, **47**, 1–31.

Yusifov, M. & Rabinowitz, P.D. 2004. Classification of mud volcanoes in the South Caspian Basin, offshore Azerbaijan. *Marine and Petroleum Geology*, **21**, 965–975, doi:10.1016/j.marpetgeo.2004.06.002.

Received 1 July 2010; revised typescript accepted 13 September 2010.
Scientific editing by Tim Needham.

Journal of the Geological Society, London, Vol. **168**, 2011, pp. 1–18. doi: 10.1144/0016-76492010-158.

Structural controls on mud volcano vent distributions: examples from Azerbaijan and Lusi, east Java

KATIE S. ROBERTS[1]*, RICHARD J. DAVIES[1], SIMON A. STEWART[2] & MARK TINGAY[3]

[1]*CeREES (Centre for Research into Earth Energy Systems), Department of Earth Sciences, Durham University, Science Laboratories, South Road, Durham, UK*

[2]*Institute of Petroleum Engineering, Heriot–Watt University, Edinburgh EH14 4AS, UK*

[3]*Australian School of Petroleum Geoscience, University of Adelaide, Adelaide, SA, Australia*

**Corresponding author (e-mail: K.S.Roberts@Durham.ac.uk)*

Abstract: Structural mapping, nearest neighbour and two-point azimuth statistical analysis of mud volcano vent distributions from nine examples in Azerbaijan and the Lusi mud volcano in east Java are described. Distributions are non-random, forming alignments subparallel to faults within anticlines, ring faults, conjugate faults and detachment faults; this finding confirms a spatial relationship and supports a model for subsurface flow along these features as well as showing fractionation at depth. As fracture and fault orientations are related to structures such as anticlines and the *in situ* stress state they are therefore predictable. We use vent distributions in Azerbaijan, where the structural geology is well constrained, to propose what controls the distribution of 169 vents at the Lusi mud volcano. This mud volcano system shows evidence for initial eruptions along a NE–SW trend, parallel to the Watukosek fault, changing to eruptions that follow east–west trends, subparallel to regional fold axes. Our analysis indicates that regions east and west of the Lusi mud volcano are more likely to be affected by new vents than those to the north and south, owing to probable onset of elongate caldera collapse within a 10 km diameter of the central vent.

Mud volcano systems are a dynamic type of piercement structure that are integral components of many sedimentary basins globally (e.g. Kopf 2002). However, because of the ephemeral nature of the fluid flow the structural pathways exploited during their intrusion are poorly defined. Fine-grained sediment and fluid can be transported from depths exceeding 8 km (Kopf 2002) resulting in eruption at the surface producing edifices that can potentially reach 25 km^3 in volume (Davies & Stewart 2005). The driving force is generally considered to be excess pore fluid pressure (e.g. Davies *et al*. 2011) but how mud is entrained and the pathways for this fluid are poorly understood. It has been proposed that folds, faults and fractures may be some of the dominant controls on fluid migration pathways during the intrusion of mud volcano systems (e.g. Morley 2003; Roberts *et al*. 2010) but this has not been tested. Analysis of surface vent patterns and their spatial relationships to these structures represents one type of test, which has successfully been carried out for igneous volcanoes but not for their mud volcano counterparts.

Alignments of point-like geological features such as volcanic cones, hydrothermal vents, fluid expulsion pipes and springs have often been shown to follow underlying structures, such as dykes, faults or joints (e.g. Hammer 2009; Moss & Cartwright 2010; Paulsen & Wilson 2010). Igneous vent patterns have been studied in great detail both on Earth (Lutz 1986; Wadge & Cross 1988; Connor 1990; Hammer 2009; Paulsen & Wilson 2010) and on extraterrestrial bodies (Bleacher *et al*. 2009). Time-dependent changes in igneous vent distributions have never been considered, mainly because these changes tend to occur over longer time scales than mud volcanoes, over thousands to millions of years (Paulsen & Wilson 2010).

Here we use eight mud volcanoes in Azerbaijan to statistically analyse the distribution of vents and relate these to well-exposed geologically mapped structures such as folds, faults and fractures (Hovland *et al*. 1997; Guliyev *et al*. 2000; Planke *et al*. 2003). These examples provide confidence in assessing the controls on vent distributions that can then be applied to the Lusi mud volcano in east Java (Fig. 1). This has continuously erupted since 2006, displacing 13 000 families, but the structural geology that could be influencing vent locations is not well constrained. At the time of writing Lusi has 169 vents, which erupt and sometimes ignite without warning in the surrounding densely populated area (Tingay 2010). Our analysis allows for a general assessment of the pathways for fluid and gas in mud volcanoes. In the case of Lusi, it provides a better understanding of where vents are more likely to occur in the future.

Mud volcanoes and vent populations

A mud volcano system includes an intrusive domain containing the feeder complex; a source domain, which comprises the source of water, gas and mud; and an extrusive domain, which is dominated by the eruptive edifice (Stewart & Davies 2006; Roberts *et al*. 2010). Mud volcano eruptions can be violent with quiescent inactive stages during which eruptions from multiple, small vents are the dominant process (Guliyev *et al*. 2000). Dormant mud volcano edifices can have anything from one to thousands of vents of differing morphologies erupting varying compositions of mud, water and gas (Table 1; Fig. 2). Vent types include cinder mounds, which are the result of *c*. 100% gaseous phase eruptions. Mud breccia flows consist of *c*. 90–100% mud that has the rheology of a Bingham body (Iverson 1997). Salses contain suspensions of <30% mud particles in water and gryphons have a composition of 30–90% mud particles in water that are either thixotrophic or shear thinning (Yassir 1990, 2003; Mueller *et al*. 2010). Herein the pattern of vents on edifices is

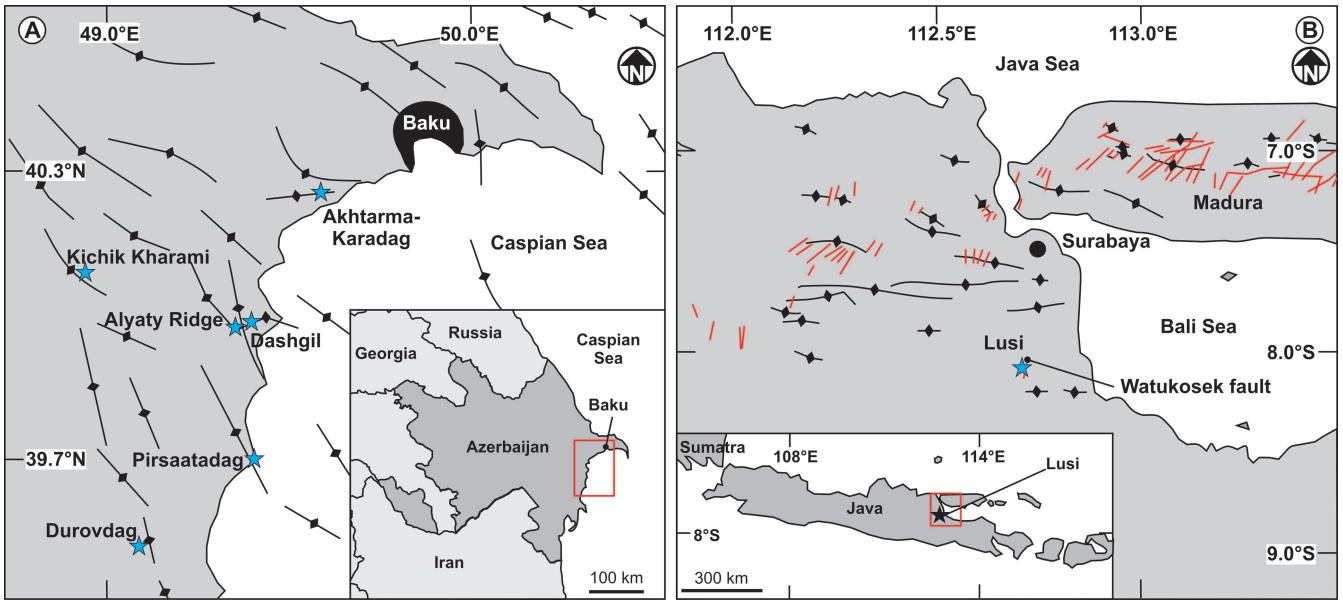

Fig. 1. (**a**) Major structural elements of eastern Azerbaijan after Jackson *et al*. (2002), showing the location of the mud volcanoes in this study (localities marked with blue stars; see inset for global location). (**b**) Major structural elements of the east Java Basin, after Geological Survey of Indonesia (1963), showing the location of Lusi mud volcano (marked with a star) and main faults marked in red (see inset for global location).

Table 1. *Classification of vents mapped during the study*

Vent type	Composition	Height (m)	Width (m)	Clasts?	Morphology	Fluid type
Gryphons	>30–90% mud: <30% fluids	0.02–10	0.05–360	Yes	'Cones' of mud breccias with bubbling pools of mud in their crater	Shear thinning or thixotropic
Salses	<30% mud: >70–100% fluids	0.02–2	0.05–80	No	Shallow-sided 'cones' of mud breccias with a large pool of watery mud at the summit and several bubbling centres	Mud suspensions
Cinder mounds	100% gaseous	0–3	1–50	Yes	Mounds of red, orange or brown glassy mud breccia	Gaseous
Breccia pipes	>30–90% mud: <30% fluids	0.5–1.5	0.5–10	Yes	Clusters of salses surrounded by damp mud containing clasts of country rock	–
Mud plugs	90–100% mud	4	30–100	Yes	Large flows of mud breccia emanating from one vent	Bingham
Pools	100% water	0.01	<0.05	No	Small vents that cluster round gryphons and salses only erupting water and/or gas	–

termed 'vent populations'. The area that is most densely populated with vents is termed the active vent zone (Roberts *et al*. 2010).

Geological settings

Azerbaijan

Azerbaijan's mud volcanoes probably form as a result of rapid sedimentation during the last 5.5 Ma, tectonic compression, the presence of a thick overpressured mudstone (Maykop Formation) at 5–8 km depth and hydrocarbon maturation (Davies & Stewart 2005; Evans *et al*. 2008). All the mud volcanoes are located along or near the crests of anticlines and most are thought to have initiated in the Pliocene (*c*. 3.5 Ma; Narimanov 1993; Yusifov & Rabinowitz 2004). The mud volcano systems may also incorporate fluids rising from below the Maykop Formation (Kopf 2002; Hovland *et al*. 2006).

The region has undergone 2.4 km of tectonic subsidence since *c*. 5.5 Ma (Allen *et al*. 2003). Several kilometres of sediment accumulated during the Pliocene and have subsequently been folded, with these structures having a dominant NW–SE fold axis orientation (Allen *et al*. 2003; Yusifov & Rabinowitz 2004).

Lusi, Sidoarjo, east Java

This mud volcano erupted in the east Java basin in May 2006 (Davies *et al*. 2007; Mazzini *et al*. 2007). During the Eocene, NE–SW-oriented rift basins formed and filled with continental clastic rocks that host both source rock and productive reservoirs (Kusumastuti *et al*. 2002). In the Oligocene to early Miocene east–west-trending normal faults formed (Kusumastuti *et al*. 2002; Istadi *et al*. 2009). Carbonate platforms developed on some palaeo-basement highs. Carbonate reefs are located beneath the Lusi mud volcano and have an east–west orientation (Kusumastuti *et al*.

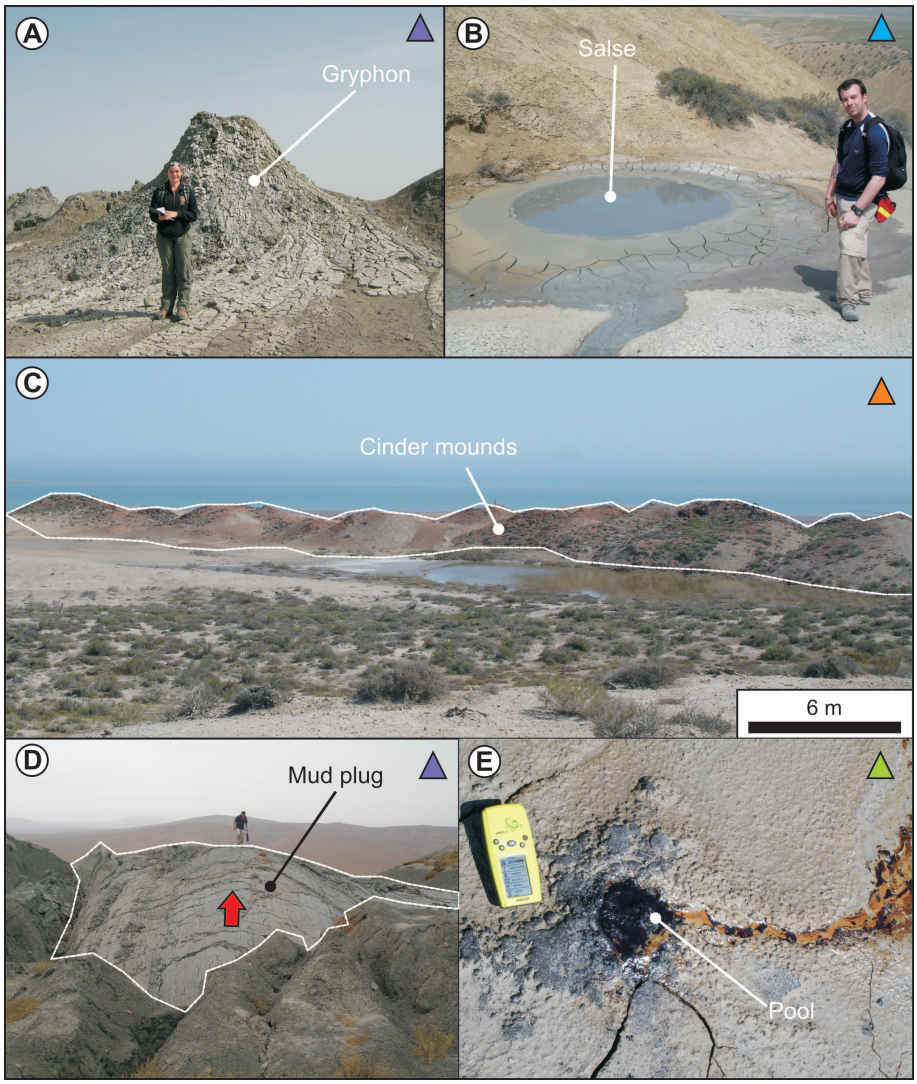

Fig. 2. (**a**) Gryphons (purple triangles in Figs 3, 5, 6 and 7). Conical vents erupting mud, a few centimetres to 4 m high. (**b**) Salses (blue triangles in Figs 3, 5, 6 and 7). 'Lakes' of muddy water, with cones 1–2 m high and diameters of a few centimetres to over 50 m (Guliyev *et al*. 2000). (**c**) Cinder mounds (orange triangles in Figs 3, 5, 6 and 7). These erupt only gaseous phases, and resemble heaps of fired clay. They are up to 4 m high and 10–20 m long, with an orangey-red ceramic appearance (Hovland *et al*. 1997; Planke *et al*. 2003). (**d**) Mud plugs (purple triangle labelled in Fig. 3a). Breccia with a putty-like malleable consistency extruding from craters like 'paste from a tube', on Koturdag A mud volcano (Guliyev *et al*. 2000; Planke *et al*. 2003). (**e**) Pools (green triangles in Figs 3, 5, 6 and 7). Bubbling pools of fluid, less than 2 cm in diameter (Mazzini *et al*. 2009) on extinct or dormant vents (black triangles in Figs 3, 5, 6 and 7).

2002). Compression during the late Miocene–Pleistocene resulted in inversion associated with east–west-trending fault movement (Istadi *et al*. 2009). This produced the east–west orientation of the anticline structures (Istadi *et al*. 2009). Subsequent Pliocene–Pleistocene sedimentation consisted of an eastward-prograding mudstone-dominated volcaniclastic wedge derived from the Java volcanic arc (Istadi *et al*. 2009). The mudstone of the Pleistocene Kalibeng Formation is overpressured at 900–1870 m depth at Lusi (Istadi *et al*. 2009). This is the source of the mud that makes up the solid fraction of the erupted liquid mud (Mazzini *et al*. 2007). The water is most likely to have been sourced from the Miocene carbonates (2833–3500 m; Tanikawa *et al*. 2010; Tingay 2010; Davies *et al*. 2011) with a contribution from the remobilized Upper Kalibeng Formation (Davies *et al*. 2007). Some fluids may also be sourced from shallow aquifers in the Pleistocene Pucangan Formation at 280–900 m depth (Tingay *et al*. 2008).

New vents form frequently and several have ignited causing injury. For example, the Porong highway, near the Lusi mud volcano, developed metre-long cracks leaking methane on 2 July 2010, with the highway surface increasingly sloping toward the mud embankments used to limit the spread of the mud. It has been predicted that it will take 26 years for the flow rate to reduce to 10% of its initial rate (Davies *et al*. 2011). Therefore more vents will form and the subsidence (Abidin *et al*. 2008; Istadi *et al*. 2009) will continue for decades.

Database and methods

Structural mapping

Mapping of vent populations was carried out using a handheld global positioning system (GPS) receiver, with a positional accuracy of 5 m (Azerbaijan) and 5–12 m (Lusi data, courtesy of Badan Penanggulangan Lumpur Sidoarjo (BPLS)). Bedding, fracture and fold orientations were plotted using GEOrient software onto stereographic and rose projections. The GPS coordinates and corresponding structural data were integrated in ArcMap software. The coordinate system for these data was input using spheroid WGS 1984.

Vents were classified as either gryphons, salses, cinder mounds, mud plugs or pools (Fig. 2; Table 1; Hovland *et al*. 1997; Guliyev *et al*. 2000; Mazzini *et al*. 2009). Each is marked onto satellite imagery with different symbols (Fig. 2). The potential spatial relationships between folds, faults and fractures and vent populations should be clear, as exposure is >60%.

Structural data from outcrop and 2D seismic coverage for Lusi mud volcano are limited.

Statistical analyses

Two statistical approaches, adapted from igneous vent systems, are used to characterize spatial patterns within vent populations. At igneous vent systems these techniques have revealed that magmatic volcanic vents often form clusters and define alignments at several scales from tens of metres to over 1000 km (Bleacher *et al*. 2009; Paulsen & Wilson 2010). As the GPS accuracy is 5 m, vent alignments have 5 m accuracy.

The nearest neighbour technique (Clark & Evans 1954) tests randomness in spatial distributions by calculating the ratio of the observed mean distance to the expected mean distance for a hypothetical random distribution to determine whether the points are clustered. A ratio of unity is a random distribution and a ratio of <1 is clustered; the nearer to zero the more clustered the distribution. This analysis was carried out using ArcGIS, which measures the distance from every vent point to its nearest neighbouring vent point.

The two-point azimuth technique (Lutz 1986; Bleacher *et al*. 2009) is used as a measure of the significance of alignments between vents. The technique quantitatively identifies trends within vent populations and has been widely used in studies on the structural geology of igneous volcanoes (Wadge & Cross 1988; Connor 1990; Bleacher *et al*. 2009). The azimuths of line segments that connect each vent to all other vents east of its location were calculated (Bleacher *et al*. 2009). Only points to the east of each vent were measured so as not to duplicate any measurements. Histograms of azimuth values ($0° =$ north, $90° =$ east, $180° =$ south) were produced with 10° bins. Peaks in the frequency distribution of the azimuths result from preferred formation of vents in response to structural controls (Bleacher *et al*. 2009). In this study the 'dominant' alignment refers to the azimuthal trend with the highest frequency of azimuths. Sub-alignments include smaller peaks in azimuth frequency less significant than that of the 'dominant' alignment. Different vent types are separated and the azimuth alignments of each of the vent fluid types displayed (i.e. mud, water and gas) are analysed. The 'overall' azimuth alignments, which include all vent types for each volcano, are also plotted to identify larger scale influences on vent alignments of the whole edifice. On each of the graphs 'Y' indicates the orientation of the anticline axis in the region, 'X' the orientation of any faulting measured during mapping and 'A' any anomalous values that may be the result of external factors, such as human influences (e.g. loading induced fluid flow around manmade dams (e.g. Londe 1987)).

Observations

Alyaty Ridge

This ridge is an anticline that extends for 12 km in a NW–SE orientation and hosts several mud volcano systems. Koturdag A has a single, 240 m diameter caldera on its summit, which is 500 m to the north of the anticline axis (Fig. 3a). The most recent mud breccia flow has been continuing for *c*. 50 years and is currently extruding mud breccia from a 20 m wide vent at a rate of 2–6 cm day^{-1}. The flow has areas of oxidized mud breccia and cinder, which are the result of escaping gases igniting mud during eruptions (Fig. 2c; Hovland *et al*. 1997; Guliyev *et al*. 2000). The 20 m wide vent has a 1 m high gryphon 5 m away from it.

This contrasts with the extrusive features seen at Koturdag B and C, at which gryphons, salses and breccia pipes are present (Fig. 2a and b). Koturdag B has a high concentration of salses, 0.2–5 m in diameter, compared with the increased concentration of 1–2 m high gryphons found at Koturdag C (Fig. 3a). Koturdag C is located at 100 m higher elevation than Koturdag B and has twice as many gryphons. In contrast, Koturdag B has twice as many salses as Koturdag C. Both Koturdag B and C edifices have long axes that align with the anticline axis at 130°N (Fig. 3a).

The orientations of fractures in the area are subparallel to the anticline axis at 130–140°N with another peak at 90° to this, at *c*. 050°N (Fig. 3b). When including all the vent positions along Alyaty Ridge as a whole the observed frequencies of azimuths derived from the two-point azimuth technique show preferential alignment in the direction of 120–130°N (Fig. 3c). Koturdag B (Fig. 3d) and C (Fig. 3e) share this dominant 130°N trend. Koturdag B also shows a peak in salse alignment at this orientation whereas Koturdag C shows a peak in gryphon alignment (Fig. 3d and e).

Kichik Kharami mud volcano

This is 1 km to the south of a NW–SE-trending anticline axis and is roughly circular in plan view (Figs 1a and 4a, b). Minor amounts of mud are being expelled in the form of salses, although a 1.2 km long mud flow to the south of the feeder complex is evidence for a significant eruption of mud breccia within the past few hundred years (Fig. 4a). The salses have a circular arrangement at the centre of the volcano (Fig. 4b), and at 100 m from the centre of the volcano they orient themselves in NW–SE and NE–SW linear trends (Fig. 4b).

Fractures are dominantly arranged subparallel to the anticline axis at 120–130°N with a set perpendicular to this at 030°N. There are also smaller fracture alignments at 100°N and 160°N, which form two planes, each at roughly 30° to the fold axis (Fig. 4c). The dominant azimuthal frequency at Kichik Kharami is 130–140°N (Fig. 4). There are also secondary alignments, for example at 090°N (Fig. 4), which do not share a common orientation with any structures in the area. The salses show a dominant azimuth subparallel to that of the strongest fracture orientation at 130°N.

Pirsaatadag mud volcano

This is located on the axis of a NW–SE-trending anticline and has an elliptical shape, the long axis of which is aligned with the anticline axis at 150°N (Figs 1a and 5). Minor amounts of mud are being expelled in the form of salses and pools. The mud volcano is heavily eroded so exposure of country rock at its centre allows easy measurement of structures. The active vent zone of the volcano is offset to the northwestern end of the edifice and displays a slight circular arrangement of vents at its centre (Fig. 5a).

The dominant orientation of fractures is at 030°N, with the second most prevalent fracture orientation being subparallel to the fold axis at 150°N (Fig. 5b). The dominant azimuthal frequency at Pirsaatadag is 180°N (Fig. 5c and d); however, there is also a high azimuth frequency subparallel to the anticline axis at 150°N. There is a lack of azimuths at *c*. 090°N.

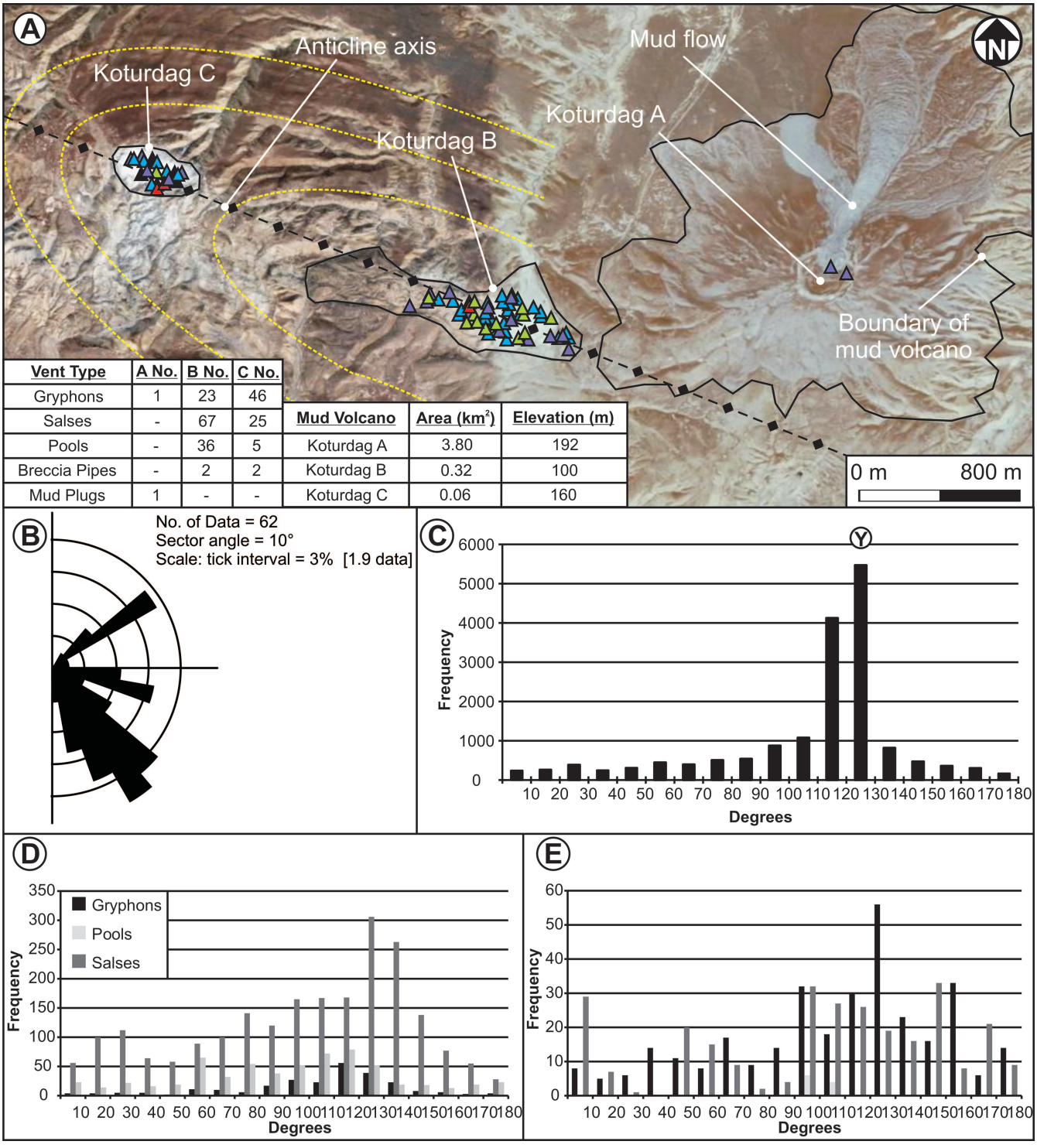

Vent Type	A No.	B No.	C No.
Gryphons	1	23	46
Salses	-	67	25
Pools	-	36	5
Breccia Pipes	-	2	2
Mud Plugs	1	-	-

Mud Volcano	Area (km^2)	Elevation (m)
Koturdag A	3.80	192
Koturdag B	0.32	100
Koturdag C	0.06	160

Fig. 3. (**a**) Part of Alyaty Ridge with three mud volcanoes intruded along its axis. Koturdag A is located 0.6 km north of the fold axis. Yellow dashed lines represent the bedding orientation. Triangles: purple, gryphons; orange, cinder mounds; black, extinct vents; blue, salses; green, pools. Image © 2010 DigitalGlobe, © 2010 GeoEye and © 2010 Geocentre Consulting, © 2010 Google. (**b**) Rose diagram of fault and fracture orientations measured along Alyaty Ridge. (**c**) Histogram of frequencies of azimuthal direction for two-point azimuth technique for all vent types grouped together for Koturdag A, B and C. (**d**) Histogram of frequencies of azimuthal direction for two-point azimuth technique, showing the distribution of each vent type for Koturday B. (**e**) Histogram of frequencies of azimuthal direction for two-point azimuth technique, showing the distribution of each vent type for Koturday C.

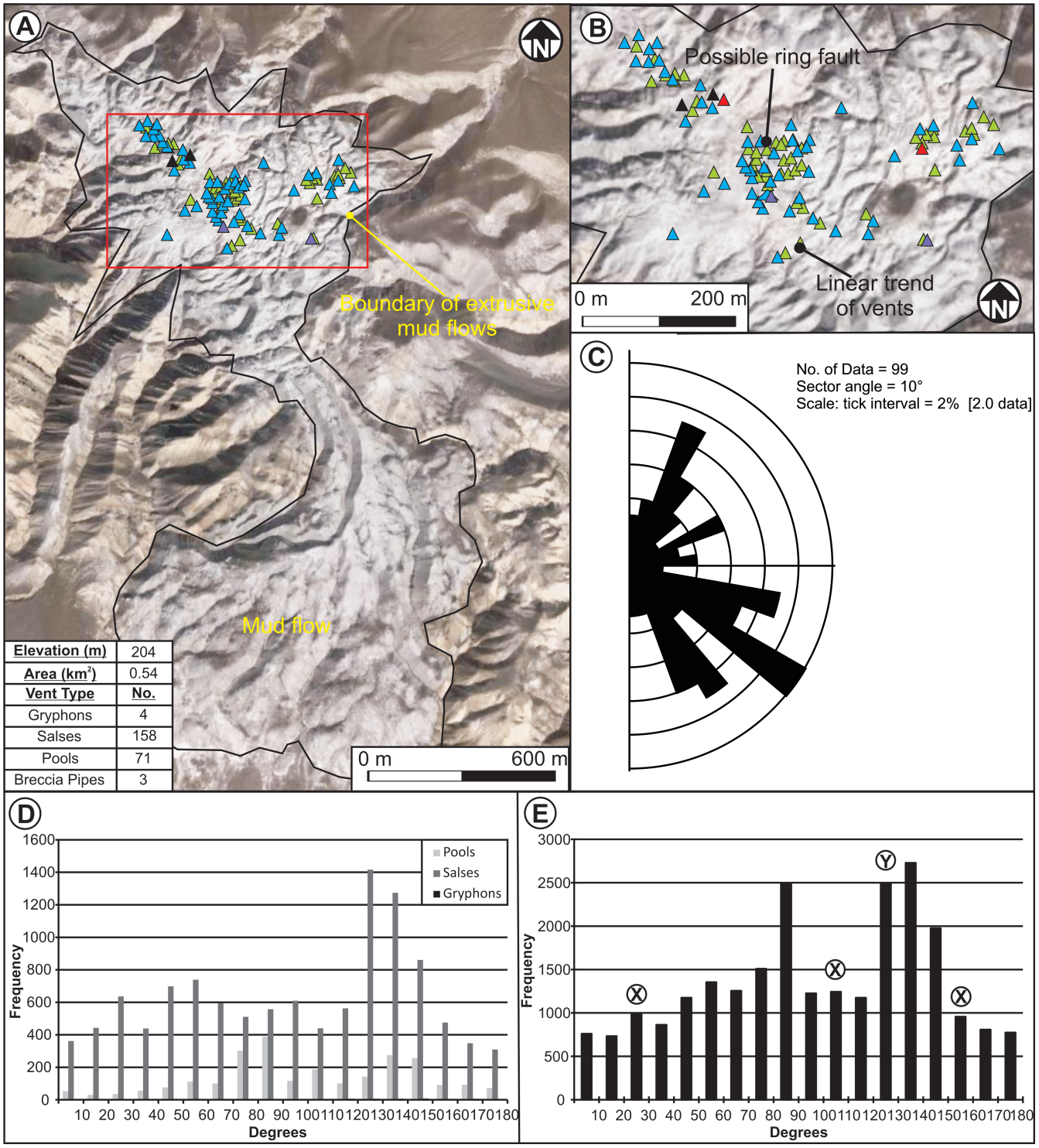

Fig. 4. (**a**) Kichik Kharami mud volcano. (**b**) Close-up view of the centre of the mud volcano seen in (**a**). Vents can be seen clustering in concentric rings at the centre of the volcano whereas they form along lines oriented NW–SE and NE–SW further out from the centre of the volcano. Symbols as in Figure 3. Images © 2010 DigitalGlobe and © 2010 Geocentre Consulting, © 2010 Google. (**c**) Rose diagram of fault and fracture orientations from country rock in and around Kichik Kharami. (**d**) Histogram of frequencies of azimuthal direction for two-point azimuth technique, showing the distribution of each vent type. (**e**) Histogram of frequencies of azimuthal direction for two-point azimuth technique, for all vent types grouped together.

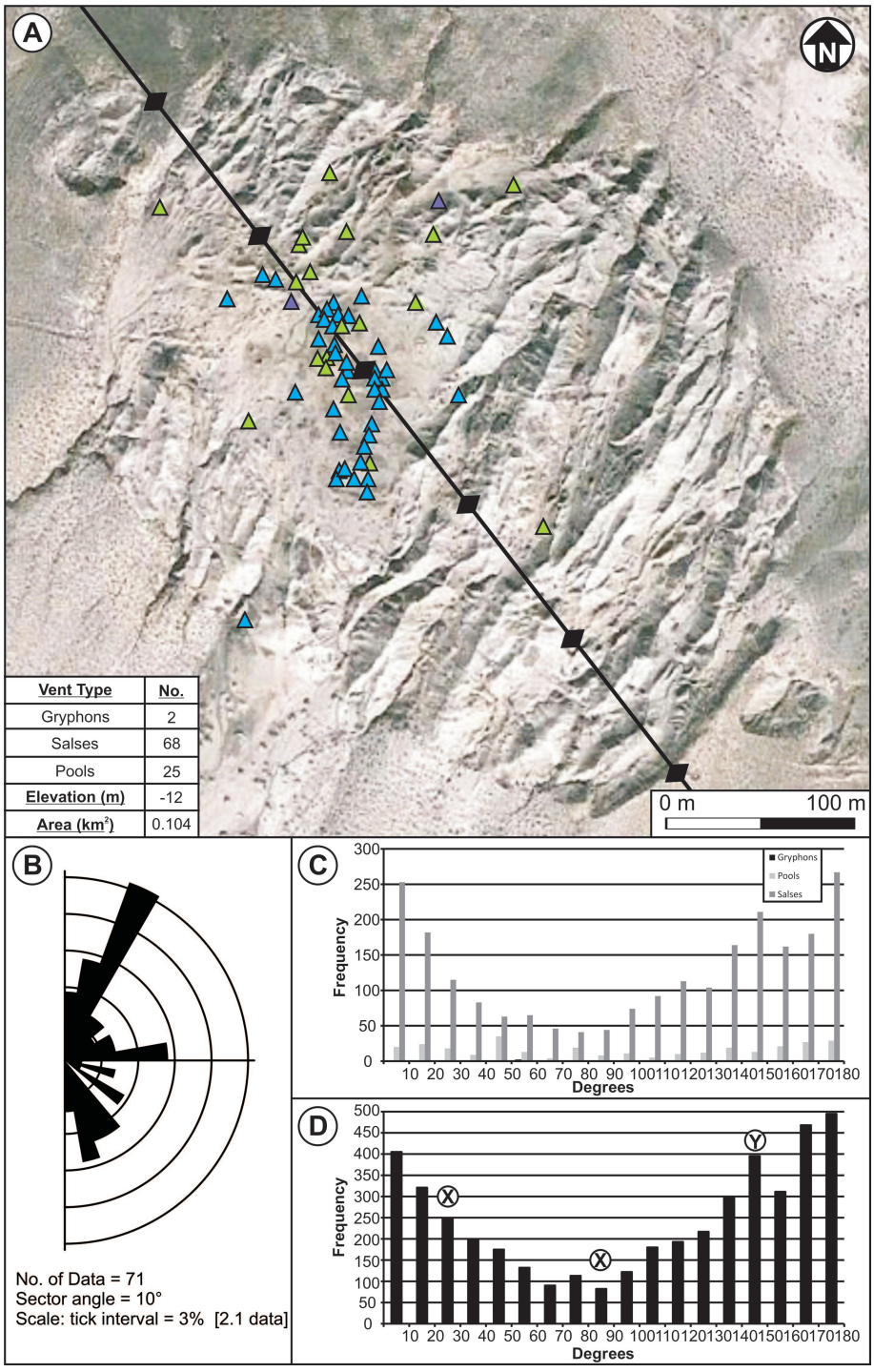

Fig. 5. (**a**) Pirsaatadag mud volcano. Symbols as in Figure 3. Image © 2010 GeoEye and © 2010 Geocentre Consulting, © 2010 Google. (**b**) Rose diagram of fault and fracture orientations from country rock in and around Pirsaatadag. (**c**) Histogram of frequencies of azimuthal direction for two-point azimuth technique, showing the distribution of each vent type. (**d**) Histogram of frequencies of azimuthal direction for two-point azimuth technique, for all vent types grouped together.

Akhtarma-Karadag mud volcano

Akhtarma-Karadag crops out along an ENE–WSW-trending anticline axis and is also elongate parallel to this anticline axis (Figs 1a and 6a). The active vent zone on the summit is found at the western end of the edifice (Fig. 6a). It has three eruptive compositions: cinder mounds, salses and gryphons.

There are three cinder mounds at the western edge of the mud volcano (Fig. 6a), only 1 m in height and diameter. The salses are towards the centre of the edifice and have a maximum diameter of 10 m. The main concentration of gryphons is closer (*c.* 6 m) to the cinder mounds. There are also numerous dormant gryphons (Fig. 6a). The two-point azimuth technique shows a dominant azimuth frequency for gryphons and salses at 030°N whereas the pools tend to align at 120°N (Fig. 6b). When including all vent types, the dominant alignment can be seen to be at 070°N, which does not align with the anticline axis oriented at 090°N (Fig. 6).

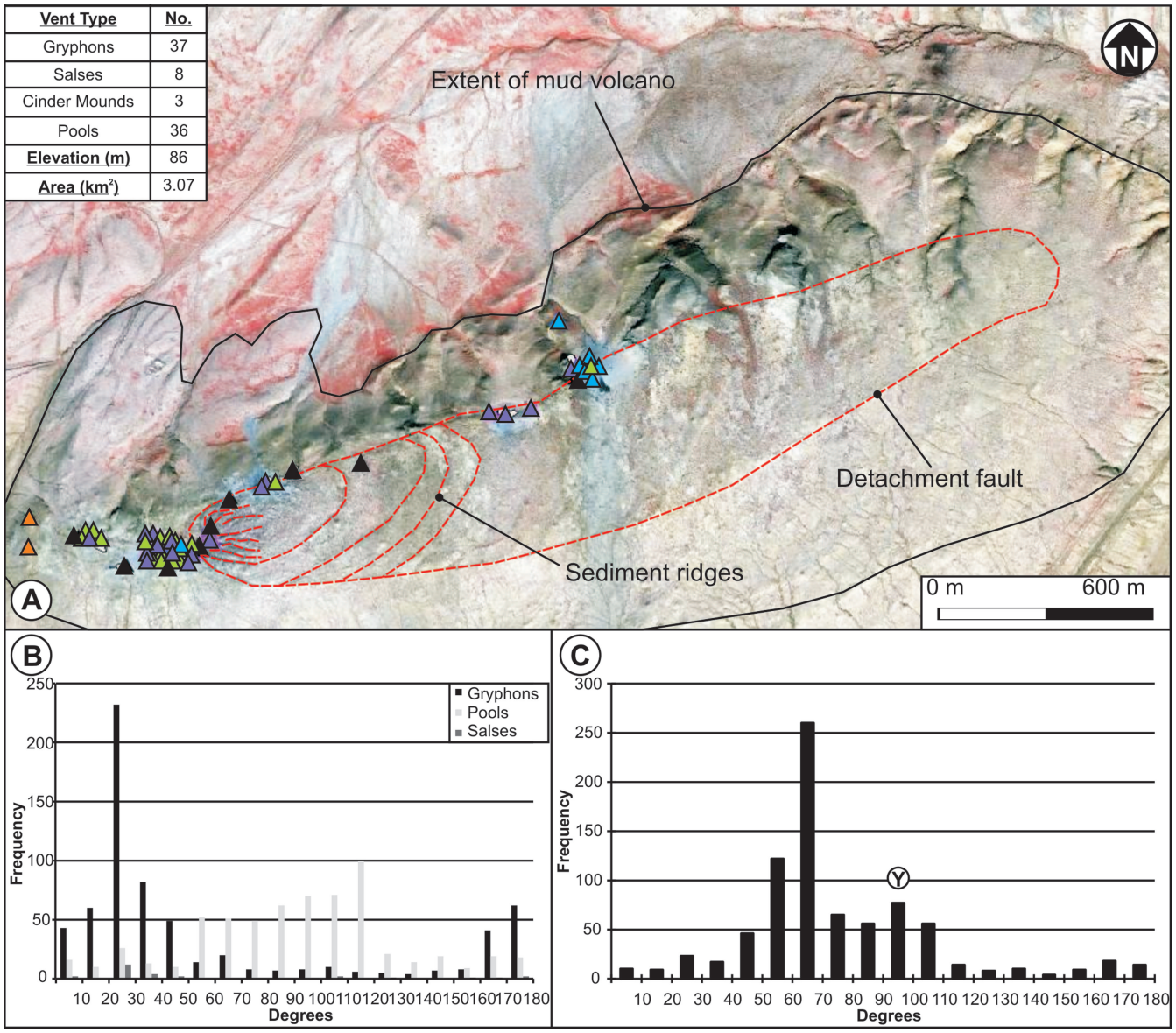

Fig. 6. (**a**) Akhtarma-Karadag mud volcano. This volcano is dominated by gryphons at its western edge next to two small cinder mounds. The majority of the salses and larger gryphons extrude along an elongate ring detachment fault found along the length of the edifice (Roberts *et al*. 2011). The salses are found furthest away from the main centre of eruption further to the east of the volcano. Symbols as in Figure 3. Image © 2010 GeoEye. (**b**) Histogram of frequencies of azimuthal direction for two-point azimuth technique, showing the distribution of each vent type. (**c**) Histogram of frequencies of azimuthal direction for two-point azimuth technique, for all vent types grouped together.

Dashgil mud volcano

This is on the crest of the Dashgil fold (Fig. 1a), which is 6–8 km long, 3.5–4 km wide and trends in an east–west direction. The active vent zone is offset to the western end of the edifice (Fig. 7a). There is a concentration of gryphons, 2–3 m in height, clustering at the centre of 200 m diameter crater to the west of the volcano (Fig. 7a). A 200 m long row of 2–3 m high, 4–5 m wide cinder mounds trends in an east–west direction. These are found only in the southeastern section of the volcano and form a sharp, straight boundary to the edge of the active vent zone. Dashgil also has two salses 20–30 m in diameter on its summit in the eastern portion of the mud volcano. These are composed of several bubbling centres. There is also a small cluster of dormant gryphons in the northern section of the volcano.

Both the combined and separate vent type two-point azimuth results show that the dominant orientation in this system is at 050°N with sub-orientations at 100°N and 170°N (Fig. 7c). When separating different vent types from each other three ‘peaks’ in azimuth frequency can be seen for both gryphons and salses at 060°N, 110°N and 170°N, whereas pools only have one dominant trend at 060°N (Fig. 7b).

Durovdag mud volcano

The crest of the volcano is dominated by gryphons and salses, which are <2 m in height (Figs 1a and 8a). There is a concentration of gryphons at the northern end of the volcano, with an average vent spacing of 5 m. Owing to the unstable nature of this region separate readings could not be taken and so

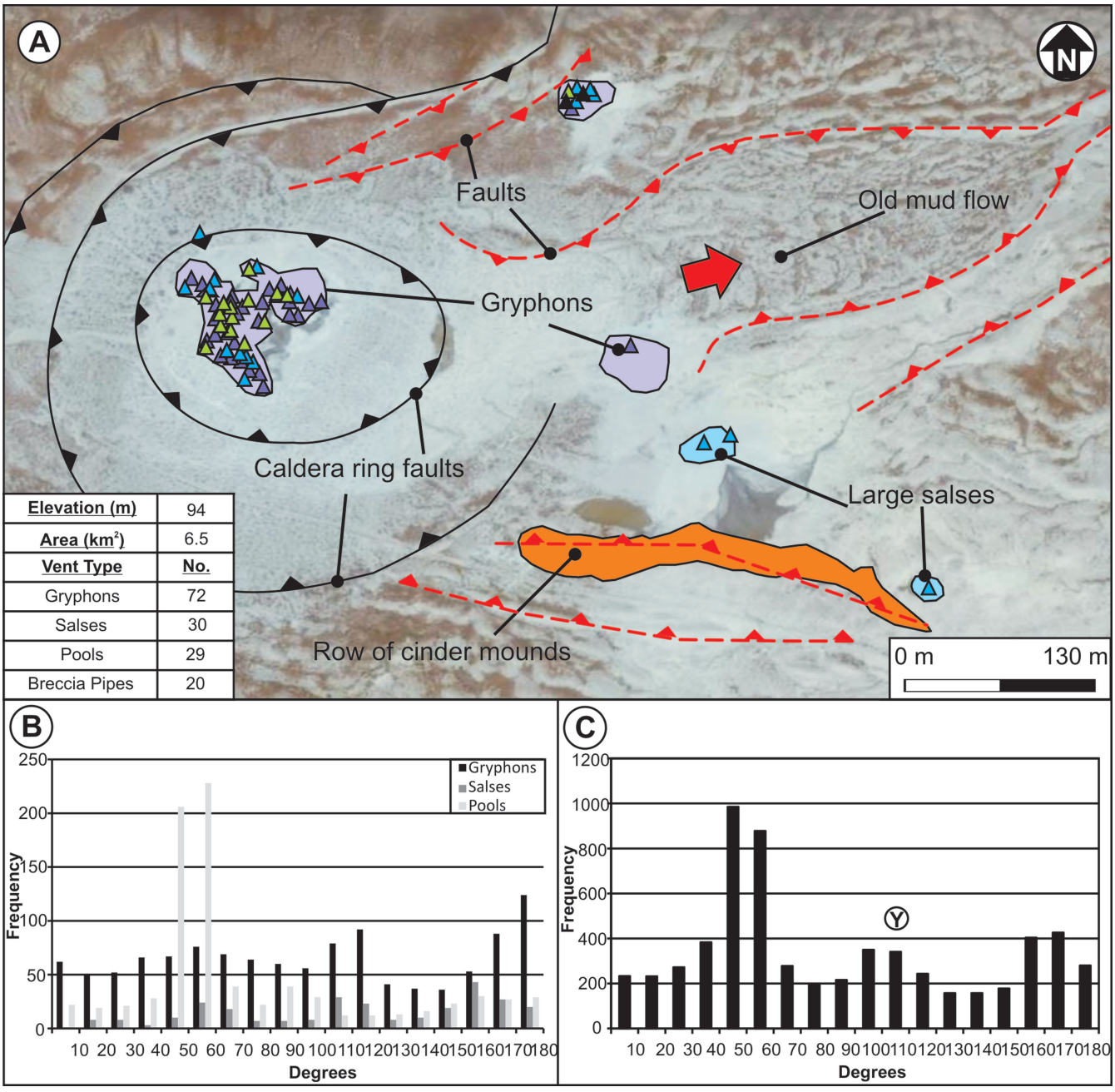

Fig. 7. (**a**) Dashgil mud volcano; close-up view of the active vent zone. Gryphons can be seen clustering in the western section of the volcano. Cinder mounds form an elongate ridge at the southern limit of the active vent zone and two large salses are found at the SE end of the volcano. Symbols as in Figure 3. Red lines show faults and black lines show breaks in slope, with triangles pointing towards the downthrown side. Image © 2010 GeoEye and © 2010 Geocentre Consulting, © 2010 Google. (**b**) Histogram of frequencies of azimuthal direction for two-point azimuth technique, showing the distribution of each vent type. (**c**) Histogram of frequencies of azimuthal direction for two-point azimuth technique, for all vent types grouped together.

the area has been considered as one large vent in the statistical analysis. The majority (*c*. 92%) of the remaining vents on the summit are found around the outer edge of the mud volcano, forming an 800 m diameter 'ring' (Fig. 8a). The vents also align at tens of metre scale, along linear conjugate paths within this 'ring' zone.

Durovdag volcano has a wide spread of vent azimuth frequencies, which is also seen on a smaller scale at the centre of Kichik Kharami volcano (Fig. 4). The dominant orientation in this system is at 160°N with sub-orientations at 100°N and 020°N (Fig. 4).

Lusi mud volcano, east Java

The Lusi edifice is 3.4 km by 2.6 km in areal extent (Fig. 9). The main active vent is 100 m in diameter and located at the centre of the edifice (Fig. 9). The first seven vents at Lusi formed roughly aligned in a NE–SW direction during first week of

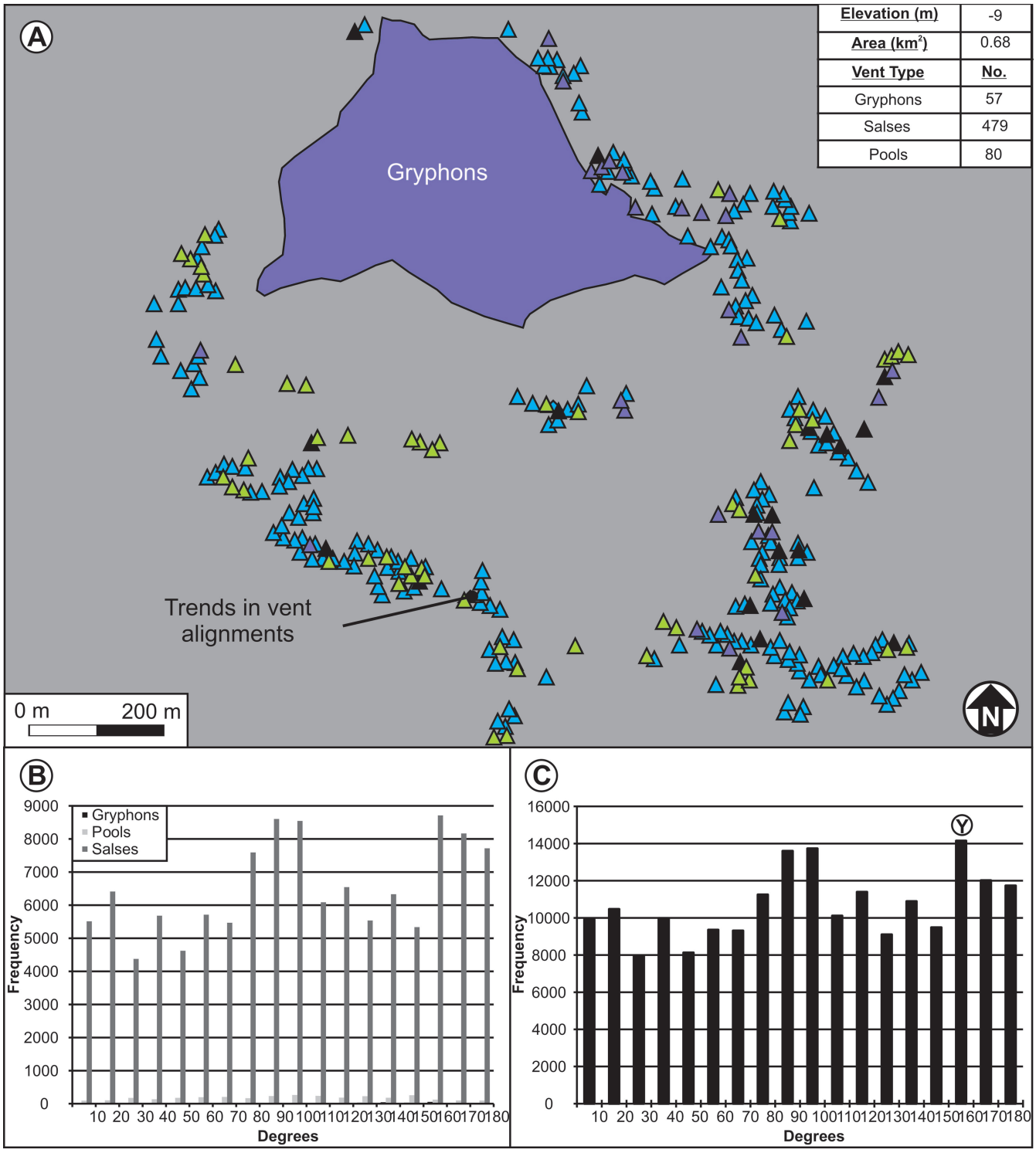

Fig. 8. (**a**) Durovdag mud volcano. This volcano is dominated by gryphons at its northern edge. This area had such a large concentration of gryphons that the whole of this area has been coloured purple to represent the intense number of gryphons found in this region, approximately one gryphon every 5 m^2. Because of the unstable nature of this area separate readings could not be taken and so the area has been considered as one large vent. The majority of the salses cluster in a ring around the outer edge of the mud volcano with only a few small vents and extinct vents at the centre of the edifice. Symbols as in Figure 3. (**b**) Histogram of frequencies of azimuthal direction for two-point azimuth technique, showing the distribution of each vent type. (**c**) Histogram of frequencies of azimuthal direction for two-point azimuth technique, for all vent types grouped together.

Fig. 9. Lusi mud volcano, east Java. (**a**) November, 2006. Histogram of frequencies of azimuthal direction for two-point azimuth technique for active vents in 2006. (**b**) 30 September 2009. Histogram of frequencies of azimuthal direction for two-point azimuth technique for active vents in 2009. (**c**) January 2010. Histogram of frequencies of azimuthal direction for two-point azimuth technique for active vents in 2010. Blue dashed line shows trace of Kendensari River. The blue triangles represent 'bubbles' that are or were currently active at that time. Red dashed lines indicate faults described by Istadi *et al*. (2009). Images courtesy of CRISP.

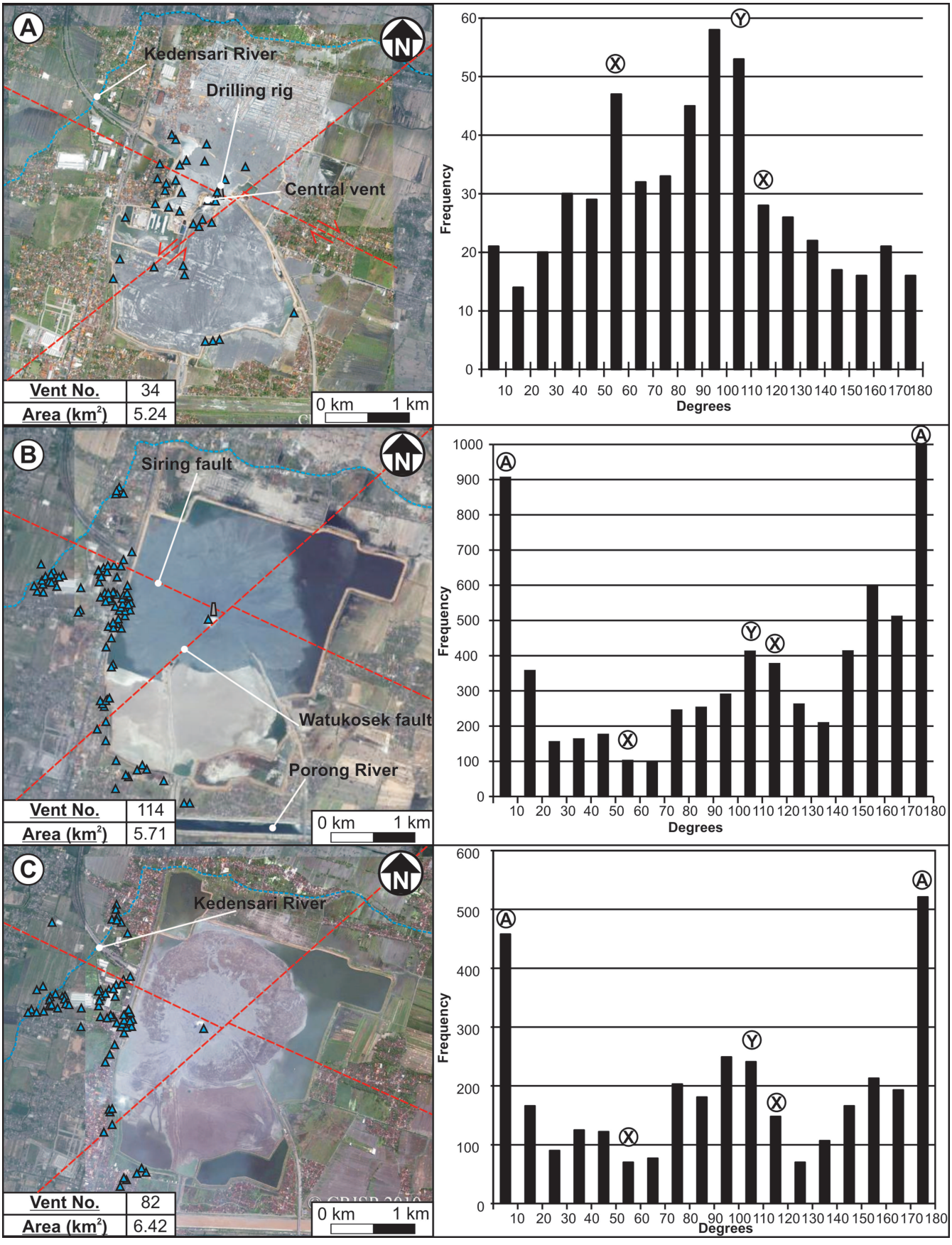
A
Kedensari River
Drilling rig
Central vent
N
Vent No. 34
Area (km²) 5.24
0 km 1 km
Frequency
Degrees
B
Siring fault
Watukosek fault
Porong River
N
Vent No. 114
Area (km²) 5.71
0 km 1 km
Frequency
Degrees
C
Kedensari River
N
Vent No. 82
Area (km²) 6.42
0 km 1 km
Frequency
Degrees

eruption (29 May 2006; Mazzini *et al*. 2007). This increased to 34 in November 2006, also in a NE–SW orientation. A fracture hundreds of metres long and tens of centimetres wide was observed a few days after the eruption, which also had a NE–SW orientation (Mazzini *et al*. 2007). This was interpreted as being the Watukosek fault, which is interpreted to cross the area (Fig. 9; Mazzini *et al*. 2007). Most of the early 'sandy' eruption sites discussed by Mazzini *et al*. (2007) were buried during the second week of June 2006, by the mud erupting from the main vent. New smaller vents started erupting in November 2006 *c*. 1 km to the SW of the main crater (Mazzini *et al*. 2007). Currently there are 169 active vents (BPLS) although not all vent occurrences can be documented owing to limited access to the majority of the edifice and because some are short lived. The vents near the main central vent had a roughly concentric pattern (Fig. 9a) whereas vents further away are closer to the observed faults in the region (Fig. 9a). Newer vents occur further away from the central vent and are now clustering close to the Kendensari River to the west of Lusi (Fig. 9b and c). These eruption sites erupt gas or suspensions of <20% mud in water.

The two-point azimuth data for Lusi mud volcano (Fig. 9) show the vent distribution in 2006, a few months after it first erupted, compared with the vent distributions seen in 2009 and 2010. In 2006 the dominant azimuth frequency is WNW–ESE (100°N), with two smaller trends at 060°N in a NE–SW orientation and 120°N in a NW–SE orientation (Fig. 9a). There is also a large spread in azimuth frequencies apart from the dominant trends (Fig. 9a). In 2009 there are two dominant azimuthal trends at 010°N and 180°N with two less dominant trends at 100°N and 120°N (Fig. 9b). The 060°N NE–SW azimuthal orientation of vents in 2006 has now decreased in frequency. In 2010 this trend continues with the decreasing influence of the 060°N and 120°N alignments and increasing frequency of alignments at 010°N, 180°N and 100°N (Fig. 9c).

Nearest neighbour analysis

The two-point azimuth and nearest neighbour analyses show that all mud volcanoes have vent populations that are statistically 'clustered' to a significant value of <0.05 (Table 2) and have a strong spatial relationship to folds, fractures and folds. The results also indicate that there is a significant alignment of vents along mapped structural features. These statistical analyses indicate that fluid flow along structural features (faults, fractures and anticlines) may be enhanced in certain regions, causing regions of vent clustering along the structures. Where vent spacing is <5 m the alignments identified are less reliable. However, there are clear visual and statistical alignments in vents that are consistent and geologically sensible in areas where the vent spacing drops below 5 m.

Discussion

Alignments

Alignment along anticline crests. It has previously been noted that kilometre-scale mud volcano systems align along the crest and hinges of anticlines (Fig. 10d; Devlin *et al*. 1999; Planke *et al*. 2003; Bonini 2007, 2008) and this observation is also made here. However, the two-point azimuth technique also identifies a clear trend of both the kilometre-scale mud volcano systems and the metre-scale vents aligning on crests, and subparallel to the anticlinal trend evident in all mud volcano systems in this study (Figs 3–8).

Koturdag B and C are located on the crest of the Alyaty Ridge at 130°N (Fig. 3a). Dominant trends at each of these volcanoes are also at 130°N, showing that both the mud volcano systems as a whole and the metre-scale vent populations align in the same orientation as anticline axes. Fluids are most probably taking advantage of pathways produced by increased compressive shear failure in the anticlinal cores, and outer arc crestal faulting along the anticlines (Ramsay & Huber 1987). The folding has brought the overpressured Maykop Formation to a shallower depth in the subsurface and allowed thickening of these strata in the anticlinal hinges (Allen *et al*. 2003). This, as well as the unloading of the anticlines during exhumation onshore and decreased overburden load, would decrease the force needed for the overpressured Maykop Formation to overcome the vertical stress and the tensile strength of the overburden (Magara 1981; Yassir & Bell 1996). These factors significantly increase the potential for the mud–water–gas mix to travel to the surface and erupt along these planes of weakness (Yusifov & Rabinowitz 2004).

Mud volcanoes also tend to become elongate in the direction of the anticline axis, as seen for many of the examples in this study (Figs 3–8). Elongation of edifices is also seen in igneous volcanoes and is generally parallel to the maximum horizontal stress (Nakamura 1977; Paulsen & Wilson 2010). This is attributed to formation of vents along feeder dykes that orient parallel to the maximum stress and open perpendicular to the minimum horizontal stress (σ_{Hmin}; Paulsen & Wilson 2010). In mud volcano systems and their vent populations this is not the case, as they all extrude along or subparallel to anticline axes, which form perpendicular to the maximum horizontal stress (σ_{Hmax}; Fig. 11). This is to be expected, as the 'source' of the fluids and any mud chambers feeding the edifices would also become elongate perpendicular to the maximum horizontal stress (Fig. 11). The result of this is that vent populations on mud

Table 2. *Nearest neighbour statistical analysis results for mud volcanoes*

Mud volcano	Observed mean distance (km)	Clustered or dispersed	Significance value	Critical value	Z score	Nearest neighbour observed mean distance (km)	Expected mean distance (km)	Nearest neighbour index
Dashgil	0.29	Clustered	0.01	−2.58	−14.34	0.000047	0.000161	0.291484
Durovdag	0.34	Clustered	0.01	−2.58	−31.44	0.000025	0.000072	0.34203
Akhtarma-Karadag	0.82	Clustered	0.05	−1.96	−2.22	0.000237	0.00029	0.818488
Kichik Kharami	0.55	Clustered	0.01	−2.58	−12.92	0.00007	0.000128	0.546609
Koturdag B	0.71	Clustered	0.01	−2.58	−6.18	0.000106	0.000149	0.714539
Koturdag C	0.51	Clustered	0.01	−2.58	−6.95	0.000047	0.000091	0.514191
Lusi	0.39	Clustered	0.01	−2.58	−12.39	0.0034637	0.008802	0.393561

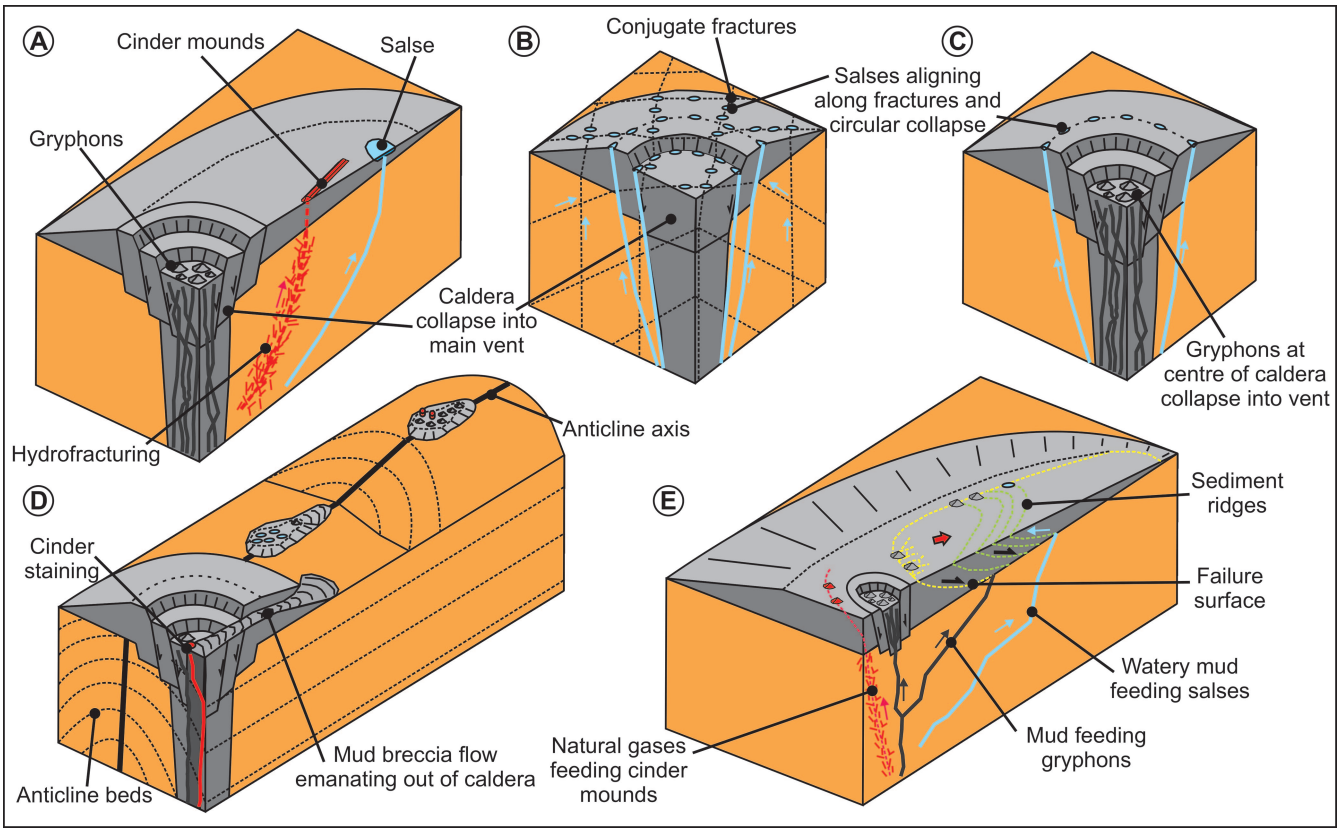

Fig. 10. Schematic illustrations of the structures that may cause the varying vent distributions. (**a**) Dashgil type, where some form of phase segregation is occurring at depth, allowing the gryphons to erupt in the area of caldera collapse, the cinder mounds to follow a linear area of weakness and so erupt in a line, and the watery salses to erupt further away from the main vent zone. (**b**) Kichik Kharami type, where small salses line up along pre-existing conjugate fractures and also concentrically at the centre of the edifice, where caldera collapse may be initiating. (**c**) Durovdag type, where some form of phase segregation is occurring at depth, allowing the gryphons to erupt in the central zone of caldera collapse beneath the main vent, with the watery salses erupting further away from the main vent zone along concentric ring faults produced during caldera collapse. (**d**) Koturdag type, where mud volcanoes can be seen aligning along anticline axes but have varying vent fluid compositions along the length of the anticline. (**e**) Akhtarma-Karadag type, where some form of phase segregation is occurring at depth, allowing the gryphons to erupt in the area of caldera collapse, the cinder mounds to follow a linear area of weakness and so erupt in a line, and the watery salses to erupt further away from the main vent zone along the detachment fault.

volcano edifices provide a good indicator of both palaeo- and current regional stress regimes.

Alignment with fractures. Fault and fracture networks can act to either enhance or prevent fluid flow depending on their relative permeability compared with that of the surrounding country rock (Aydin 2000; Eichhubl & Boles 2000; Faulkner *et al*. 2011). When faults and fractures have high permeabilities they are able to act as pathways allowing fluids to utilize them as a conduit to the surface (e.g. Sibson 1996; Faulkner *et al*. 2011). A prominent characteristic of mud volcano systems is high fluid pressures, which may result in the formation of hydrofractures and shearing producing open fractures and dilatant faults (e.g. Aydin 2000). By comparing vent alignment orientations with structures mapped in close proximity it is possible to identify which fault and fracture systems have the highest permeability in a certain region. The cinder mounds on Dashgil are found only in a discrete elongate zone and so probably form when gas venting from the mud volcano feeder complex travels along a pre-existing fault plane (Fig. 10a). This faulted zone may intersect a mud chamber that has separated phases of gas, water and mud within it. Periodically the pressure in this chamber would become high enough to overcome the tensile strength and minimum horizontal stress, producing new hydrofractures in a similar way to fault-valve behaviour, allowing fluids to erupt at the surface as discrete events (Sibson 1990, 1992). This fault may even be an anticline crestal fault, as the cinder mounds can be seen oriented in an east–west direction similar to that of the Dashgil Fold (Fig. 7a).

Kichik Kharami mud volcano is similar to Durovdag at its centre, with a 10 m diameter ring of salses forming along a circular collapse structure. However, 100 m out from the centre, the salses are aligned in rows in NW–SE (160°N) and NE–SW (100°N) directions (Fig. 4d and e). These orientations are coincident with the orientation of shear fractures (Fig. 4c) found on anticline flanks (Ramsay & Huber 1987) and both occur at 30° from the anticline axis orientation of 130°N. This implies that these have the highest permeability compared with other structures in the region (Fig. 10b). Dashgil also displays these fault arrangements (Fig. 7), with 'peaks' in both gryphon and salse azimuths occurring at 060°N and 170°N fracture orientations occurring at 60° to the anticline axis orientation (110°N).

Detachment fault alignment. Both active and extinct gryphons and salses on the Akhtarma-Karadag mud volcano align along a linear offset that can be traced around the summit of the volcano, which is interpreted here as a detachment fault (Figs 6 and 10e; Roberts *et al*. 2011). Pressure ridges of sediment can be seen at the centre of the detachment fault, suggesting that the mud

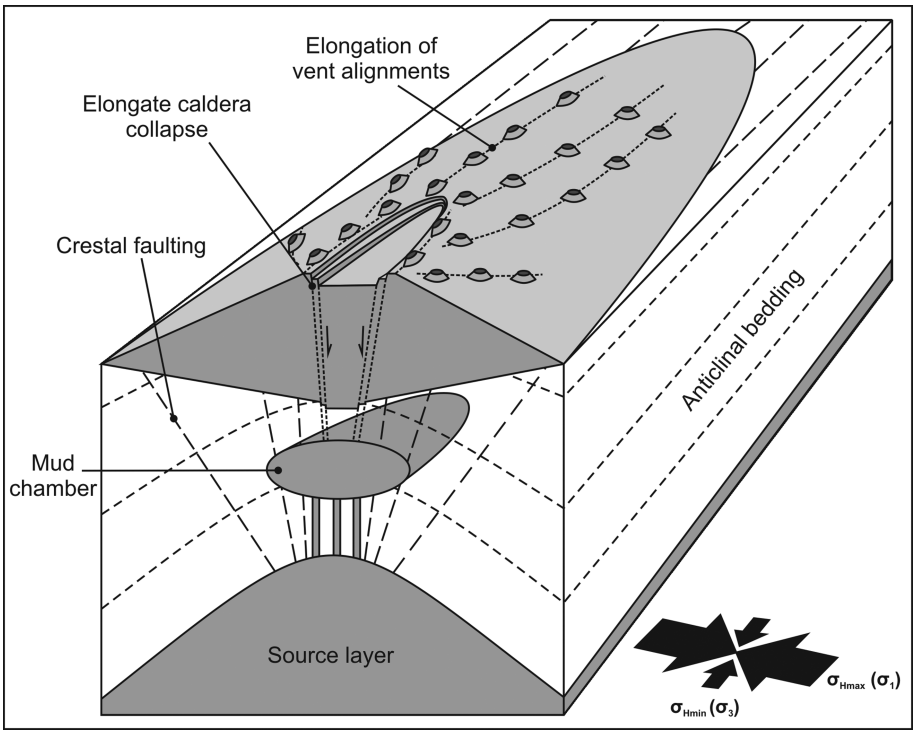

Fig. 11. Schematic model depicting mud volcano elongation, elongated vent distributions, mud chamber elongation and summit caldera elongation patterns. Mud dykes preferentially trend perpendicular to σ_{Hmax} taking advantage of the crestal faulting along the anticline. Summit calderas and mud chambers also become elongate perpendicular to σ_{Hmax}. After Paulsen & Wilson (2010).

volcano appears to be failing to the NE (Fig. 6a). This movement is confirmed by the presence of plants being torn across the head of the detachment fault and en echelon fracturing. This is again supported by the two-point azimuth statistics, which show that the vents have a dominant orientation similar to that of the detachment fault at 070°N (Fig. 6c).

Ring fault alignment. Durovdag displays clear alignment of its vents, with 92% of the gryphons and salses erupting around the periphery of the edifice (Fig. 8). This alignment is to be expected for a caldera collapse system (Stewart & Davies 2006; Evans *et al*. 2008), with the majority of the vents forming a 'ring' around the outer edge of the mud volcano (Fig. 10c). These fluids are taking advantage of ring faulting that is forming as a result of the gravitational collapse of the mud volcano. This distribution is displayed as a large spread of alignments on the two-point azimuth histograms, as well as showing the slightly more dominant anticline axis alignment (160°N) and less dominant alignments that may be caused by fracture alignments (100°N and 020°N; Fig. 10c). On a metre scale vents align in a conjugate pattern similar to shear fracturing on anticline limbs (Ramsay & Huber 1987). These metre-scale alignments occur around the trace of the kilometre-scale 'ring' fault itself (Fig. 8a). It is likely that these metre-scale conjugate vent alignments formed first aligning with the pre-existing anticline fractures. After this, caldera collapse initiated and formed the more recent ring fault alignments, which then overprinted the conjugate alignments to produce the dominant azimuth frequency. The concentration of gryphons to the north of the volcano indicates that there may be a large mud chamber beneath this area.

Distributions: fractionation of vent eruptive phases

Dashgil and Akhtarma-Karadag both produce three eruptive compositions: gaseous (cinder mounds), watery mud (salses) and viscous mud–water mix (gryphons). They also show a similar spatial distribution of erupting fluid types. Dashgil is dominated by gryphons on its westerly side, salses to the east and cinder mounds to the south of the active zone of the edifice (Fig. 7a). Akhtarma-Karadag has cinder mounds in the most westerly section, 5–10 m from an area of gryphons at the centre of the active zone, and then salses at the easterly end of the volcano (Fig. 6a). From these observations it is possible to ascertain that these three phases must be separating at depth and travelling to their points of eruption via different pathways. This has been noted by others in past studies at Dashgil mud volcano (Mazzini *et al*. 2009). Mazzini *et al*. (2009) found that the water geochemistry highlights different water sources and reactions that occur at gryphons, pools and salses. Gryphons have a signature of deep-rising fluids, whereas pools and salses show the imprint of meteoric fluids and a solute content increased by *in situ* evaporation (Mazzini *et al*. 2009). When integrating this with the observations it can be assumed that gryphons may be fed directly from a mud chamber in the main feeder complex of the mud volcano at depth, whereas salses and cinder mounds are most probably sourced from shallow, smaller chambers that remain 'stagnant' for periods of time, allowing them to interact with the surrounding meteoric fluids. The azimuth frequencies for each vent type show that gryphons and salses often display common orientations, indicating that they may share similar fluid flow pathways in the subsurface (Figs 3, 6 and 7). Pools show no correlation with other vent types, in agreement with Mazzini *et al*. (2009), who suggested that these are only shallow fluid flow pathways that are not influenced by regional structure (Figs 3, 6 and 7).

Time-dependent changes, Lusi mud volcano

The dominant 010°N and 180°N vent azimuth orientations seen at Lusi in 2009 may result from local loading by the earth dams in this region, which share this alignment. Loading would allow focused fluid flow in this orientation (e.g. Londe 1987) or could

be the result of sampling bias, as these locations are more readily reported by residents of Sidoarjo. Because of these possible influences we focus on the second most dominant azimuth orientations, which change from NE–SW to east–west vent alignments.

During the first eruptive phase in 2006 vents were aligned in a NE–SW orientation (Fig. 9a) at *c*. 30° to the present-day maximum horizontal stress (σ_1, σ_{Hmax}) orientation of NNE–SSW (Mazzini *et al*. 2009; Sawolo *et al*. 2009; Tingay *et al*. 2010). This is consistent with fluids initially travelling up the highest permeability paths, which were optimally oriented for sinistral shear failure in a strike-slip faulting stress regime, and originating from the Miocene carbonates at >2800 m depth (Fig. 12a; Davies *et al*. 2008; Tingay 2010). Analogous to this is the formation of Miocene shale dykes along faults in the Jerudong Anticline of Brunei (Tingay *et al*. 2005). It is well documented that faults can transmit significant volumes of fluids when active (Barton *et al*. 1995; Sibson 1996) especially if they have a higher permeability than the surrounding country rock. However, this in no way indicates that reactivation of the fault triggered the initial eruption (see Davies *et al*. in preparation).

The second phase of eruption during 2009 showed the east–west (100°N) vent azimuth alignments becoming even more prominent, and these became increasingly dominant in 2010 (Fig. 9c). Evolution of these vent populations has occurred in only 9 months and implies that the fluid pathways themselves are developing during a similar time period. It also suggests that an important east–west-trending, regional-scale anticlinal structure influences the feeder system architecture, reducing the importance of the local NE–SW fault. The fact that so few vents are erupting the same fluid as the main Lusi vent, and that most are thought to be very shallow rooted, implies that the source for the main vent and the smaller vents may differ. One preferred interpretation is that many of the water eruptions are coming from *c*. 290–900 m deep aquifers (Tingay *et al*. 2008) that have become faulted owing to subsidence, resulting in seal breakage and fluid flow. From studies of mud volcanoes in Azerbaijan it is possible to make the assumption that older feeder systems naturally take advantage of pre-existing structures in the region (Fig. 12b). It is proposed that this change in orientation occurred as a result of a drop in pore fluid pressure in the system once the majority of the main source of overpressured fluid had been erupted. The decreased pore fluid pressure was lower than the tensile strength and minimum principal stress required to keep the original hydrofractures open, resulting in closure of these pathways and a decrease in their permeability (e.g. Jolly & Lonergan 2002).

A ring-like arrangement of vents is observed around the main central vent at Lusi (Fig. 9a) and is similar to the pattern seen at Durovdag (Fig. 8). This could indicate that a ring fault has formed as a result of subsidence in the region owing to the evacuation of large volumes of fluid from depth (Fukushima *et al*. 2009). Abidin *et al*. (2008) and Fukushima *et al*. (2009) both used time-lapse synthetic aperture radar interferograms from 1 year after the start of the Lusi mud eruption in May 2006 to show subsidence over an ellipsoidal area of 12 km^2 centred on the main eruptive vent. Depletion of material and decrease of fluid pressure at depth were described as being the dominant cause of the subsidence. Fukushima *et al*. (2009) found that deflation of an oblate spheroid lying shallower than 1 km explains the observed displacements. This observation is supported by the 2010 azimuth data (Fig. 9c), which show a wider spread of azimuth trends than seen in 2009.

Mode of formation: 2008–present. The Miocene carbonates are proposed as the primary source of the fluids driving the eruption from the main vent (Davies *et al*. 2007, 2008; Tanikawa *et al*. 2010). However, other studies have suggested that the shallower Upper Kalibeng clays are the source of the majority of the fluids (Mazzini *et al*. 2007). We speculate that from 2008 to the present, subsidence up to 10 km away from the main vent, resulting from the evacuation of large quantities of remobilized mud (Abidin *et al*. 2008), may have been accommodated by the reactivation of the east–west-trending crestal faulting along an anticlinal structure. During reactivation these faults would have breached aquifers located in the Pucangan Formation (280–900 m depth; Fig. 12b; Tingay *et al*. 2008). Overpressured fluids from these aquifers would use these high-permeability, reactivated faults as conduits to the surface. This is supported by the relatively low height of eruptions (1–3 m) at satellite vents, indicating modest overpressure and that the pore fluid is not hydraulically connected to the source of fluid for the main vent, where eruptions can be tens of metres in height. The Miocene carbonate deposits also trend in an east–west orientation (Carter *et al*. 2005) and so subsequent subsidence in the vicinity of the reefal mounds could also result in localized reactivation of pre-existing east–west faults. Almost none of the satellite vents are erupting mud; indeed, a very large number are erupting fluids consisted of methane, CO_2 and a mixture of thermogenic and biogenic hydrocarbons (Mazzini *et al*. 2007; Sawolo *et al*. 2009). As the main vent continues to remobilize mud from the Kalibeng Formation (900–1870 m), this will load the surface and more subsidence will occur, resulting in more faulting, aquifer breaches and new vent formation. When the system evolves further an elongate caldera collapse could develop, similar to the Porong collapse identified 8 km to the NE of Lusi (Fig. 12c; Istadi *et al*. 2009). This will produce a vent azimuth distribution similar to that seen at Durovdag mud volcano; indeed, the 2010 vent azimuth histogram is already exhibiting ring fault distribution, to a greater extent than in previous years.

Differences between mud volcanism in Azerbaijan and at Lusi

It should be noted that the alignments seen at Lusi may differ from those in Azerbaijan as it is almost certainly not a naturally occurring mud volcano. The temperature of the fluids erupting at Lusi are around 70–100 °C (Tingay 2010) whereas mud volcano fluids in Azerbaijan are classically around 10–20 °C (Guliyev *et al*. 2000). This may be due to relatively rapid fluid ascent rates at Lusi compared with those in Azerbaijan, where fluid flow pathways have been present for thousands of years. Lusi had an average mud and fluid flow rate of *c*. 64 000 m^3 day^{-1} over the first 3 years (Istadi *et al*. 2009; Tingay 2010), differing dramatically from most naturally occurring mud volcano systems. In Azerbaijan flow rates of only a few tens to hundreds of cubic metres per day occur, but occasionally there are eruptions that are short-lived (1–14 days) and extremely violent (100 000–1 000 000 m^3 day^{-1}; Tingay 2010). When compared with mud volcanoes in Azerbaijan, Lusi is an extremely rapidly evolving system, but this does not mean that the structural influences will differ, and ultimately regional structure will govern both areas.

Conclusions

The orientation of regional folds, faults and local metre- to kilometre-scale fractures, detachment and ring faults are the key control to the vent patterns in the mud volcanoes studied here.

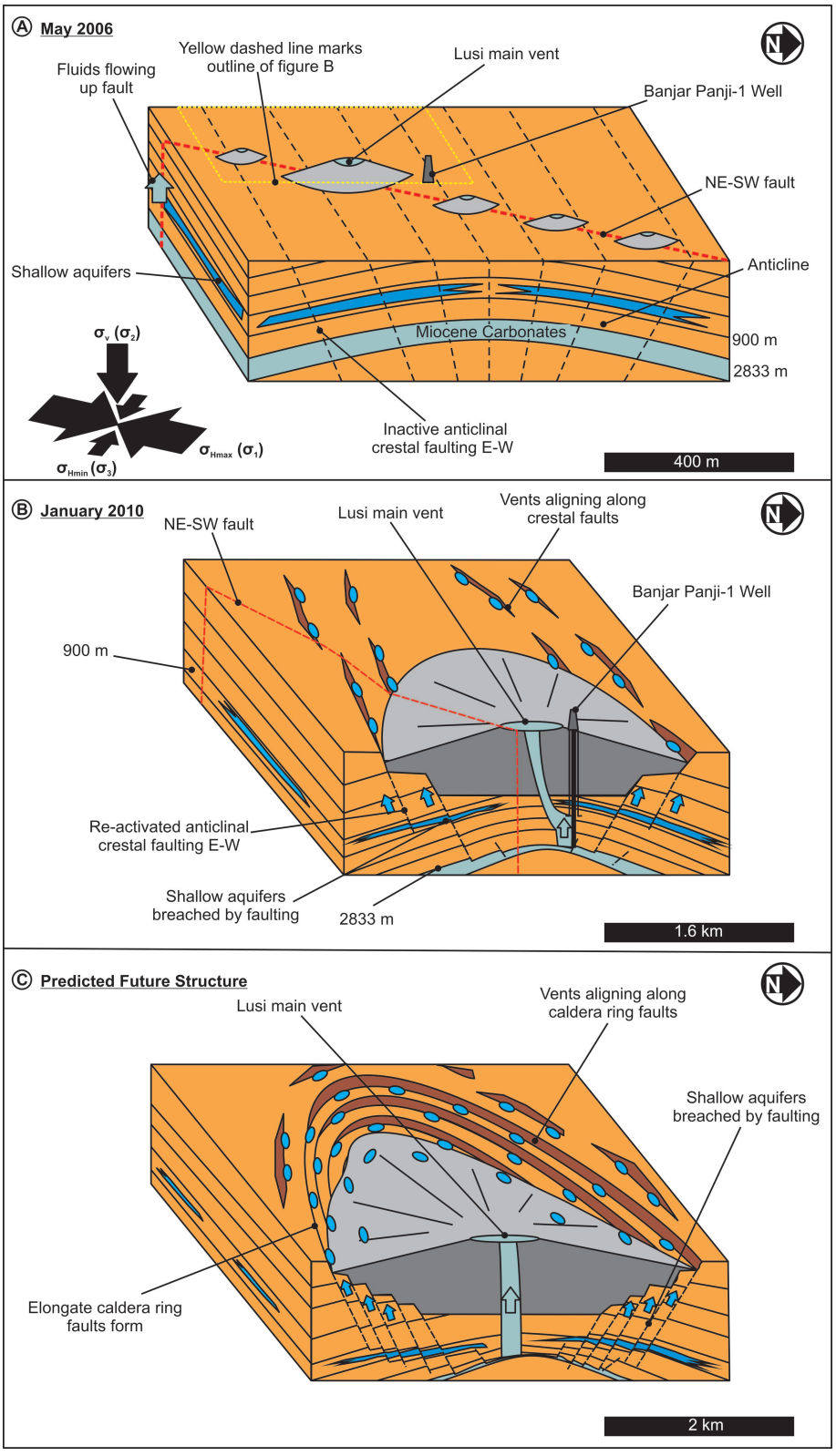

Fig. 12. Schematic diagram of the mode of formation of Lusi mud volcano and how its vent systems have evolved through time. (**a**) November 2006 with its initial NE–SW vent alignment. (**b**) January 2010 with the initiation of caldera collapse with vents aligning along reactivated east–west-trending anticline crestal faulting. (**c**) Predicted future development including elongate caldera collapse structure with vents aligning along caldera ring faults.

The most dominant vent orientations occur subparallel to anticline axes, causing elongation of the volcanic edifice perpendicular to the regional maximum horizontal stress. If later detachment or ring faulting forms this will overprint the original subparallel anticline crestal faulting. Zonation of eruptive phase types also occurs, implying that there is some form of fractionation beneath the edifices in either one large chamber or a network of smaller linked chambers. The composition of the fluids being erupted and alignment of vents along anticline axes are significant as these characteristics will dictate how the edifice itself will accrete over time.

Mud volcano alignments can occur on a range of scales from

metre-scale vents that erupt along crestal fractures to the 1–4 km systems that align along anticline axes. Lusi mud volcano is an example of how fluid flow pathways evolve through time from a localized kilometre-scale fault zone and hydrofracture system in 2006 to exploiting pre-existing pathways in the larger regional anticlinal structural control in 2009 and 2010. This evolution is likely to continue along this trend and in a similar ring fault style to that seen in Azerbaijan, which could have major implications for the local population. It can be predicted that the flux of fluid flow up east–west-oriented structures at Lusi will be more important than NE–SW faulting, and that as more subsidence occurs in the region more hazardous vents will form, eventually producing multiple ring fault alignments and ultimately elongate caldera collapse up to 10 km away from the main vent, as seen in palaeo-collapse structures in the region.

References

Abidin, H.Z., Davies, R.J., Kusuma, M.A., Andreas, H. & Deguchi, T. 2008. Subsidence and uplift of Sidoarjo (East Java) due to the eruption of the Lusi mud volcano (2006–present). *Environmental Geology*, doi:10.1007/s00254-008-1363-4.

Allen, M.B., Vincent, S.J., Alsop, G.I., Ismail-Zadeh, A. & Flecker, R. 2003. Late Cenozoic deformation in the South Caspian Region: Effects of a rigid basement block within a collision zone. *Tectonophysics*, **366**, 223–239, doi:10.1016/S0040-1951(03)00098-2.

Aydin, A. 2000. Fractures, faults, and hydrocarbon entrapment, migration and flow. *Marine and Petroleum Geology*, **17**, 797–814, doi:10.1016/S0264-8172(00)00020-9.

Barton, C.A., Zoback, M.D. & Moos, D. 1995. Fluid flow along potentially active faults in crystalline rock. *Geology*, **23**, 683–686, doi:10.1130/0091-7613(1995)023<0683:FFAPAF>2.3.CO;2.

Bleacher, J.E., Glaze, L.S., *et al.* 2009. Spatial and alignment analyses for a field of small volcanic vents south of Pavonis Mons and implications for the Tharsis province, Mars. *Journal of Volcanology and Geothermal Research*, **185**, 96–102, doi:10.1016/j.jvolgeores.2009.04.008.

Bonini, M. 2007. Interrelations of mud volcanism, fluid venting, and thrust–anticline folding: Examples from the external northern Apennines (Emilia-Romagna, Italy). *Journal of Geophysical Research*, **112**, B08413, doi:10.1029/2006JB004859.

Bonini, M. 2008. Elliptical mud volcano caldera as stress indicator in an active compressional setting (Nirano, Pede-Apennine Margin, Northern Italy). *Geology*, **36**, 131–134, doi:10.1130/G24158A.1.

Carter, D.C., Mandhiri, D., *et al.* 2005. Interpretation methods in the exploration of Oligocene–Miocene carbonate reservoirs, offshore Northwest Madura, Indonesia. *In: Proceedings, Indonesian Petroleum Association, Thirtieth Annual Convention and Exhibition*, IPA05-G-003.

Clark, P.J. & Evans, F.C. 1954. Distance to nearest neighbour as a measure of spatial relationships in populations. *Ecology*, **35**, 445–453, doi:10.2307/1931034.

Connor, C.B. 1990. Cinder cone clustering in the TranMexican volcanic belt: Implications for structural and petrologic models. *Journal of Geophysical Research—Solid Earth*, **95**, 19395–19405, doi:10.1029/JB095iB12p19395.

Davies, R.J. & Stewart, S.A. 2005. Emplacement of giant mud volcanoes in the South Caspian Basin: 3D seismic reflection imaging of their root zones. *Journal of the Geological Society, London*, **162**, 1–4, doi:10.1144/0016-764904-082.

Davies, R.J., Swarbrick, R.E., Evans, R.J. & Huuse, M. 2007. Birth of a mud volcano: East Java, 29 May 2006. *GSA Today*, **17**, 4–9.

Davies, R.J., Brumm, M., Manga, M., Rubiandini, R., Swarbrick, R.E. & Tingay, M. 2008. The East Java mud volcano (2006 to present): An earthquake or drilling trigger? *Earth and Planetary Science Letters*, **272**, 627–638.

Davies, R.J., Mathias, S.A., Swarbrick, R.E. & Tingay, M.J. 2011. Probabilistic longevity estimate for the LUSI mud volcano, East Java. *Journal of the Geological Society, London*, **168**, 000–000.

Devlin, W.L., Gogswell, J., *et al.* 1999. South Caspian Basin: young, cool, and full of promise. *GSA Today*, **9**, 1–9.

Eichhubl, P. & Boles, J.R. 2000. Focused fluid flow along faults in the Monterey Formation, coastal California. *Geological Society of America Bulletin*, **112**, 1667–1679, doi:10.1130/0016-7606(2000)112<1667:FFFAFI>2.0.CO;2.

Evans, R.J., Stewart, S.A. & Davies, R.J. 2008. The structure and formation of mud volcano summit calderas. *Journal of the Geological Society, London*, **165**, 769–780, doi:10.1144/0016-76492007-118.

Faulkner, D.R., Jackson, C.A.L., Lunn, R.J., Schlische, R.W., Shipton, Z.K., Wibberley, C.A.J. & Withjack, M.O. 2011. A review of recent developments concerning the structure, mechanics and fluid flow properties of fault zones. *Journal of Structural Geology* (in press), doi:10.1016/j.jsg.2010.06.009.

Fukushima, Y., Mori, J., Hashimoto, M. & Kano, Y. 2009. Subsidence associated with the LUSI mud eruption, East Java, investigated by SAR interferometry. *Marine and Petroleum Geology*, **26**, 1740–1750, doi:10.1016/j.marpetgeo.2009.02.001.

Geological Survey of Indonesia 1963. *Geological map of Djawa and Madura*. Geological Survey of Indonesia.

Guliyev, I.S., Feizullayev, A.A. & Belov, I.S. 2000. *All about mud volcanoes*. Geology Institute, Azerbaijan Academy of Sciences.

Hammer, Ø. 2009. New statistical methods for detecting point alignments. *Marine and Petroleum Geology*, **35**, 659–666, doi:10.1016/j.cageo.2008.03.012.

Hovland, M., Hill, A. & Stokes, D. 1997. The structure and geomorphology of the Dashgil mud volcano, Azerbaijan. *Geomorphology*, **21**, 1–15, doi:10.1016/S0169-555X(97)00034-2.

Hovland, M., Fichler, C., Rueslåtten, H. & Johnsen, H.K. 2006. Deep-rooted piercement structures in deep sedimentary basins—manifestations of super-critical water generation at depth? *Journal of Geochemical Exploration*, **89**, 157–160, doi:10.1016/j.gexplo.2005.11.056.

Istadi, B.P., Pramono, G.H., Sumintadireja, P. & Alam, S. 2009. Modeling study of growth and potential geohazard for LUSI mud volcano: East Java, Indonesia. *Marine and Petroleum Geology*, **26**, 1724–1739, doi:10.1016/j.marpetgeo.2009.03.006.

Iverson, R.M. 1997. The physics of debris flows. *Reviews of Geophysics*, **35**, 245–296, doi:10.1029/97RG00426.

Jackson, J., Priestley, K., Allen, M.B. & Berberian, M. 2002. Active tectonics of the South Caspian Basin. *Geophysical Journal International*, **148**, 214–245, doi:10.1046/j.1365-246X.2002.01588.x.

Jolly, R. & Lonergan, L. 2002. Mechanisms and controls on the formation of sand intrusions. *Journal of the Geological Society, London*, **159**, 605–617, doi:10.1144/0016-764902-025.

Kopf, A. 2002. Significance of mud volcanism. *Reviews of Geophysics*, **40**, 1005, doi:10.1029/2000RG000093.

Kusumastuti, A., Van Rensbergen, P. & Warren, J.K. 2002. Seismic sequence analysis and reservoir potential of drowned Miocene carbonate platforms in the Madura Strait, East Java, Indonesia. *AAPG Bulletin*, **86**, 213–232.

Londe, P. 1987. Malpasset dam failure. *Engineering Geology*, **24**, 295–329.

Lutz, T.M. 1986. An analysis of the orientations of large scale crustal structures: A statistical approach based on areal distributions of pointlike features. *Journal of Geophysical Research*, **91**, 421–434, doi:10.1029/JB091iB01p00421.

Magara, K. 1981. Mechanisms of natural fracturing in a sedimentary basin. *AAPG Bulletin*, **65**, 123–132.

Mazzini, A., Svensen, H., Akhmanov, G.G., Aloisi, G., Planke, S., Malthe-Sørenssen & Istadi, B. 2007. Triggering and dynamic evolution of the LUSI mud volcano, Indonesia. *Earth and Planetary Science Letters*, **261**, 375–388, doi:10.1016/j.epsl.2007.07.001.

Mazzini, A., Svensen, H., Planke, S., Guliyev, I., Akhmanov, G.G.M., Fallik, T. & Banks, D. 2009. When mud volcanoes sleep: insights from seep geochemistry at the Dashgil mud volcano, Azerbaijan. *Marine and Petroleum Geology*, **26**, 1704–1715, doi:10.1016/j.marpetgeo.2008.11.003.

Morley, C.K. 2003. Outcrop examples of mudstone intrusions from the Jerudong Anticline. *In:* Van Rensenbergen, P., Hillis, R.R., Maltman, A.J. & Morley, C.K. (eds) *Subsurface Sediment Remobilization*. Geological Society, London, Special Publications, **216**, 381–394.

Moss, J.L. & Cartwright, J. 2010. The spatial and temporal distribution of pipe formation, offshore Nambia. *Marine and Petroleum Geology*, **27**, 1216–1234, doi:10.1016/j.marpetgeo.2009.12.013.

Mueller, S., Llewellin, E.W. & Mader, H.M. 2010. The rheology of suspensions of solid particles. *Proceedings of the Royal Society of London, Series A*, **466**, 1201–1228, doi:10.1098/rspa.2009.0445.

Nakamura, K. 1977. Volcanoes as possible indicators of tectonic stress orientation—principle and proposal. *Journal of Volcanology and Geothermal Research*, **2**, 1–16, doi:10.1016/0377-0273(77)90012-9.

Narimanov, A.A. 1993. The petroleum systems of the South Caspian Basin. *In:* Doré, A.G., Augustson, J.H., Hermanrud, C., Stewart, D.J. & Sylta, O. (eds) *Basin Modeling Advances and Applications*. Norwegian Petroleum Society, Special Publications, **3**, 599–608.

Paulsen, T.S. & Wilson, T.J. 2010. New criteria for systematic mapping and reliability assessment of monogenetic volcanic vent alignments and elongate volcanic vents for crustal stress analyses. *Tectonophysics*, **482**, 16–28, doi:10.1016/j.tecto.2009.08.025.

Planke, S., Svensen, H., Hovland, M. & Banks, D.A. 2003. Mud and fluid migration in active mud volcanoes in Azerbaijan. *Geo-Marine Letters*, **23**, 258–268, doi:10.1007/s00367-003-0152-z.

Ramsay, J.G. & Huber, M.I. 1987. *The Techniques of Modern Structural Geology: Folds and Fractures*. Academic Press, New York.

Roberts, K.S., Davies, R.J. & Stewart, S.A. 2010. Structure of exhumed mud volcano feeder complexes, Azerbaijan. *Basin Research*, **22**, 439–451, doi:10.1111/j.1365-2117.2009.00441.x.

Roberts, K.S., Stewart, S.A., Davies, R.J. & Evans, R.J. 2011. Sector collapse of mud volcanoes, Azerbaijan. *Journal of the Geological Society, London*, **168**, 1–12, doi:10.1144/0016-76492010-115.

Sawolo, N., Sutrioni, E., Istadi, B.P. & Darmoyo, A.B. 2009. The LUSI mud volcano triggering controversy: Was it caused by drilling? *Marine and Petroleum Geology*, **26**, 1766–1784, doi:10.1016/j.marpetgeo.2009.04.002.

Sibson, R.H. 1990. Conditions for fault-valve behaviour. *In:* Knipe, R.J. & Rutter, E.H. (eds) *Deformation Mechanisms, Rheology and Tectonics*. Geological Society, London, Special Publications, **54**, 15–28, doi:10.1144/GSL.SP.1990.054.01.02.

Sibson, R.H. 1992. Implications of fault-valve behaviour for rupture nucleation and recurrence. *Tectonophysics*, **211**, 283–293, doi:10.1016/0040-1951(92)90065-E.

Sibson, R.H. 1996. Structural permeability of fluid-driven fault-fracture meshes. *Journal of Structural Geology*, **18**, 1031–1042, doi:10.1016/0191-8141(96)00032-6.

Stewart, S.A. & Davies, R.J. 2006. Structure and emplacement of mud volcano systems in the South Caspian Basin. *AAPG Bulletin*, **90**, 771–786.

Tanikawa, W., Sakaguchi, M., Wibowo, H.T., Shimamoto, T. & Tadai, O. 2010. Fluid transport properties and estimation of overpressure at the Lusi mud volcano, east Java Basin. *Engineering Geology*, **116**, 73–85, doi:10.1016/j.enggeo.2010.07.008.

Tingay, M. 2010. Anatomy of the 'Lusi' mud eruption, east Java. *ASEG Extended Abstracts*, 1–6, doi:10.1071/ASEG2010ab241.

Tingay, M., Hillis, R.R., Morley, C.K., Swarbrick, R.E. & Drake, S.J. 2005. Present-day stress orientation in Brunei: a snapshot of 'prograding tectonics' in a Tertiary delta. *Journal of the Geological Society, London*, **162**, 39–49, doi:10.1144/0016-764904-017.

Tingay, M., Heidbach, O., Davies, R.J. & Swarbrick, R.E. 2008. Triggering of the Lusi mud eruption: Earthquake versus drilling initiation. *Geology*, **36**, 639–642, doi:10.1130/G24697A.1.

Tingay, M., Morley, C.K., King, R.E., Hillis, R.R., Hall, R. & Coblentz, D. 2010. The Southeast Asian Stress Map. *Tectonophysics*, **482**, 92–104, doi:10.1016/j.tecto.2009.06.019.

Wadge, G. & Cross, A. 1988. Quantitative methods for detecting aligned points: An application to the volcanic vents of the Michoacan–Guanajuato volcanic field, Mexico. *Geology*, **16**, 815–818, doi:10.1130/0091-7613(1988)016<0815:QMFDAP>2.3.CO;2.

Yassir, N. 1990. The undrained shear behaviour of fine-grained sediments. *In:* Knipe, R.J. & Rutter, E.H. (eds) *Deformation Mechanisms, Rheology and Tectonics*. Geological Society, London, Special Publications, **54**, 399–404, doi:10.1144/GSL.SP.1990.054.01.36

Yassir, N. 2003. The role of shear stress in mobilizing deep-seated mud volcanoes: geological and geomechanical evidence from Trinidad and Taiwan. *In:* Van Rensbergen, P., Hillis, R.R., Maltman, A.J. & Morley, C.K. (eds) *Subsurface Sediment Mobilization*. Geological Society, London, Special Publications, **216**, 461–474, doi:10.1144/GSL.SP.2003.216.01.30.

Yassir, N. & Bell, J. 1996. Abnormally high fluid pressures and associated porosities and stress regimes in sedimentary basins. *SPE Formation Evaluation*, **11**, 5–10.

Yusifov, M. & Rabinowitz, P.D. 2004. Classification of mud volcanoes in the South Caspian Basin, offshore Azerbaijan. *Marine and Petroleum Geology*, **21**, 965–975, doi:10.1016/j.marpetgeo.2004.06.002.

Received 5 October 2010; revised typescript accepted 21 January 2011.
Scientific editing by Tim Needham.

1: Address 1 - please add postcode
2: Address 3 - please add postal code
3: Should text be changed to 'histograms, which also show'?
4: Davies et al. - this should be included in reference list only if it can be updated
5: Should there be an Acknowledgements section at end of main text?
6: Carter et al. - if possible, please give publication details (editor/s, publisher's name and location, and page numbers of paper)
7: Faulkner et al. - please update if possible
8: Geological Survey of Indonesia - please add publisher's location
9: Guliyev et al. - please add location of publisher
10: Mazzini et al. - please add initial/s for Malthe-Sørenssen
11: Fig. 12, part a - 'November 2006' in caption but 'May 2006' in figure. Please amend caption or figure as necessary

References

Abdullayev, N.R. 2000. Seismic stratigraphy of the Upper Pliocene and Quaternary deposits in the South Caspian Basin. *Journal of Petroleum Science and Engineering*, **28**, 207-226, DOI: 10.1016/S0920-4105(00)00079-6.

Abidin, H.Z., Davies, R.J., Kusuma, M.A., Andreas, H. & Deguchi, T. 2008. Subsidence and uplift of Sidoarjo (East Java) due to the eruption of the LUSI mud volcano (2006-present). *Environmental Geology*, **57**, 833-844, DOI: 10.1007/s00254-008-1363-4.

Abikh, G.H. 1863. New islands on the Caspian Sea and the cognition of mud volcanoes of the Caspian Region. Memoirs of Academic Sciences, Petersburg.

Abrams, M.A. & Narimanov, A.A. 1997. Geochemical evaluation of hydrocarbons and their potential sources in the western South Caspian depression, Republic of Azerbaijan. *Marine and Petroleum Geology*, **14**, 451-468, DOI: 10.1016/S0264-8172(97)00011-1.

Abriutski, V. 1853. Eruption of mud volcanoes in the Taman Peninsula, in August 1853. *Gorn. Jurn.*, **4**, 271–277. In Russian.

Acocella, V. 2007. Understanding caldera structure and development: an overview of analogue models compared to natural calderas. *Earth-Science Reviews*, **85**, 125–160, DOI: 10.1016/j.earscirev.2007.08.004.

Acocella, V., Korme, T., Salvini, F. & Funiciello, R. 2003. Elliptical calderas in the Ethiopian Rift: control of pre-existing structures. *Journal of Volcanology and Geothermal Research*, **119**, 189-203, DOI: 10.1016/S0377-0273(02)00342-6.

Adams, P.N., Slingerland, R.L. & Smith, N.D. 2004. Variations in natural levee morphology in anastomosed channel flood plain complexes. *Geomorphology*, **61**, 127-142, DOI: 10.1016/j.geomorph.2003.10.005.

Aliyev, A.K. 1960. *Geology and hydrocarbons of the Kura-Araks region*. Azerbaijan State Publisher of Hydrocarbon Literature, Baku, 361.

Aliyev, A.A., Guliyev, I.S. & Belov, I.S. 2002. *Catalogue of recorded eruptions of mud volcanoes of Azerbaijan (for period of years 1810-2001)*. Publishing House 'Nafta-Press', Baku.

Allen, M.B., Jones, S., Ismail-Zadeh, A., Simmons, M.D. & Anderson, L. 2002. Onset of subduction as the cause of rapid Pliocene-Quaternary subsidence in the South Caspian Basin. *Geology*, **30**, 775-778, DOI: 10.1130/0091-7613(2002)030<0775:OOSATC>2.0.CO;2.

Allen, M.B., Vincent, S.J., Alsop, G.I., Ismail-Zadeh, A. & Flecker, R. 2003. Late Cenozoic deformation in the South Caspian Region: effects of a rigid basement block within a collision zone. *Tectonophysics*, **366**, 223-239, DOI: 10.1016/S0040-1951(03)00098-2.

Anderson, E.M. 1936. The dynamics of the formation of cone-sheets, ring-dykes, and caldron subsidences. *Proceedings of the Royal Society, Edinburgh*, **56**, 128–157.

Anderson, J.G.C. 1937. Intrusions of the Glen Falloch Area. *Geological Magazine*, **74**, 458-468, DOI: 10.1017/S0016756800088968.

Ansted, D.T. 1866. On the mud volcanoes of the Crimea, and on the relation of these and similar phenomena to deposits of petroleum. *Proceedings of the Royal Institute Great Britain*, *IV*, 628–640.

Arhangelski, A. 1932. Some words about genesis of mud volcanoes on the Apsheron Peninsula and Kerch–Taman area. *Bulletin of the MOIP, Series Geology*, **3**, 269–285. In Russian.

Aydin, A. 2000. Fractures, faults, and hydrocarbon entrapment, migration and flow. *Marine and Petroleum Geology*, **17**, 797-814, DOI: 10.1016/S0264-8172(00)00020-9.

Barber, A.J., Tjokrosapoetro, S. & Charlton, T.R. 1986. Mud volcanoes, shale diapirs, wrench faults and melanges in accretionary complexes, Eastern Indonesia. *AAPG Bulletin*, **70**, 1729-1741.

Barton, C.A., Zoback, M.D. & Moos, D. 1995. Fluid flow along potentially active faults in crystalline rock. *Geology*, **23**, 683-686, DOI: 10.1130/0091-7613(1995)023<0683:FFAPAF>2.3.CO;2.

Best, M. 2003. *Igneous and metamorphic petrology*. 2nd edition. Wiley-Blackwell Science Ltd, Oxford, 729.

Bleacher, J.E., Glaze, L.S., Greeley, R., Hauber, E., Baloga, S.M., Sakimoto, S.E.H., Williams, D.A. & Glotch, T.D. 2009. Spatial and alignment analyses for a field of small volcanic vents south of Pavonis Mons and implications for the Tharsis province, Mars. *Journal of Volcanology and Geothermal Research*, **185**, 96-102, DOI: 10.1016/j.jvolgeores.2009.04.008.

Boehm, A. & Moore, J.C. 2002. Fluidized sandstone intrusions as an indicator of palaeostress orientation, Santa Cruz, California. *Geofluids*, **2**, 147-161, DOI: 10.1046/j.1468-8123.2002.00026.x.

Bonini, M. 2007. Interrelations of mud volcanism, fluid venting, and thrust-anticline folding: examples from the external northern Apennines (Emilia- Romagna, Italy). *Journal of Geophysical Research*, **112**, B08413, DOI: 10.1029/2006JB004859.

Bonini, M. 2008. Elliptical mud volcano caldera as stress indicator in an active compressional setting (Nirano, Pede-Apennine Margin, Northern Italy). *Geology*, **36**, 131-134, DOI: 10.1130/G24158A.1.

Bonini, M. & Mazzarini, F. 2010. Mud volcanoes as potential indicators of regional stress and pressurized layer depth. *Tectonophysics*, **494**, 32-47, DOI: 10.1016/j.tecto.2010.08.006.

Bosworth, W., Burke, K. & Strecker, M. 2003. Effect of stress fields on magma chamber stability and the formation of collapse calderas. *Tectonics*, **22**, 1042, DOI: 10.1029/2002TC001369.

Bouska, J. & Johnston, R. 2005. The first 3D/4C ocean bottom seismic surveys in the Caspian Sea: acquisition design and processing strategy. *The Leading Edge*, **24**, 910-922, DOI: 10.1190/1.2056392.

Bristow, C.R., Gale, I.N., Fellman, E., Cox, B.M., Wilkinson, I.P. & Riding, J.B. 2000. The lithostratigraphy, biostratigraphy and hydrogeological significance of the mud springs at Templars Firs, Wootton Bassett, Wiltshire. *Proceedings of the Geologists Association*, **111**, 231-245.

Brown, K.M. 1990. The nature and hydrogeological significance of mud diapirs and diatremes for accretionary prisms. *Journal of Geophysical Research*, **95**, 8969-8982, DOI: 10.1029/JB095iB06p08969.

Brown, K.M. 1994. Fluids in deforming sediments. *In:* Maltman, A.J. (ed.) *The Geological Deformation of Sediments*. Chapman & Hall, London, 205-237.

Brown, K.M. & Orange, D.L. 1993. Structural aspects of diapiric mélange emplacement; the Duck Creek diapir. *Journal of Structural Geology*, **15**, 831-847, DOI: 10.1016/0191-8141(93)90179-E.

Bruno, B.C., Taylor, G.J., Rowland, S.K. & Baloga, S.M. 1994. Quantifying the effect of rheology on lava-flow margins using fractal geometry. *Bulletin of Volcanology*, **56**, 193-206, DOI: 10.1007/BF00279604.

Buryakovsky, L.A., Chilingar, G.V. & Aminzadeh, F. 2001. Petroleum geology of the South Caspian Basin. Gulf Professional Publishing, Butterworth-Heinemann, Boston, USA, 442.

Calvès, G., Schwab, A., Huuse, M., Van Rensbergen, P., Clift, P.D., Tabrez, A.R. & Inam, A. 2010. Cenozoic mud volcano activity along the Indus Fan: offshore Pakistan. *Basin Research*, **22**, 398-413, DOI: 10.1111/j.1365-2117.2009.00448.x.

Carter, D.C., Mandhiri, D., Park, R.K., Asjhari, I., Basyuni, S., Birdus, S., Bradfield, J.P., Iriawan, A., Nasfiah, M. & Nugroho, M.A.A. 2005. Interpretation methods in the exploration of Oligocene-Miocene carbonate reservoirs, offshore Northwest Madura, Indonesia. *Proceedings, Indonesian Petroleum Association*, Thirtieth Annual Convention & Exhibition, **IPA05-G-003**.

Cartwright, J.A. 2007. The impact of 3D seismic data on the understanding of compaction, fluid flow and diagenesis in sedimentary basins. *Journal of the Geological Society, London*, **164**, 881-894, DOI: 10.1144/0016-76492006-143.

Cartwright, J.A., Huuse, M. & Aplin, A. 2007. Seal bypass systems. *AAPG Bulletin*, **91**, 1141-1166, DOI: 10.1306/04090705181.

Chow, J.J., Chang, S.-K. & Yu, H.-S. 2006. GPR reflection characteristics and depositional models of mud volcanic sediments- Wushanting mud volcano field, south-western Taiwan. *Journal of Applied Geophysics*, **60**, 179-200, DOI: 10.1016/j.jappgeo.2006.03.001.

Clari, P., Cavagna, S., Martire, L. & Hunziker, J. 2004. A Miocene mud volcano and its plumbing system: a chaotic complex revisited (Monferrato, NW Italy). *Journal of Sedimentary Research*, **74**, 662-676, DOI: 10.1306/022504740662.

Clark, P.J. & Evans, F.C. 1954. Distance to nearest neighbor as a measure of spatial relationships in populations. *Ecology*, **35**, 445-453, DOI: 10.2307/1931034.

Cole, J.W., Milner, D.M. & Spinks, K.D. 2005. Calderas and caldera structures: a review. *Earth-Science Reviews*, **69**, 1-26, DOI: 10.1016/j.earscirev.2004.06.004.

Connor, C.B. 1990. Cinder cone clustering in the TransMexican volcanic belt: implications for structural and petrologic models. *Journal of Geophysical Research – Solid Earth*, **95**, 395-405, DOI: 10.1029/JB095iB12p19395.

Cooper, C. 2001. Mud volcanoes of Azerbaijan visualized using 3D seismic depth cubes: the importance of overpressured fluid and gas instead on non-existent diapirs. *In: Proceedings of EAGE Conference: Subsurface Sediment Mobilization*, Ghent, Belgium, **71**.

Corthay, J.E. & Aliyev, A.A. 2000. Delineation of a mud volcano complex, surficial mudflows, slump blocks, and shallow gas reservoirs, offshore Azerbaijan. *Offshore Technology Conference*, 1 May-4 May 2000, Houston, Texas, **12066-MS**, DOI: 10.4043/12066-MS.

Cosgrove, J.W. 2001. Hydraulic fracturing during the formation and deformation of a basin: a factor in the dewatering of low permeability sediments. *AAPG Bulletin*, **85**, 737-748, DOI: 10.1306/8626C997-173B-11D7-8645000102C1865D.

Dadashev, A.A. 1963. Hydrocarbon gases of mud volcanoes of Azerbaijan. Azerneshr, Baku. In Russian.

Davies, R.J., Brumm, M. Manga, M., Rubiandini, R., Swarbrick, R.E. & Tingay, M. 2008. The East Java mud volcano (2006 to present): an earthquake or drilling trigger? *Earth and Planetary Science Letters*, **272**, 627-638, DOI: 10.1016/j.epsl.2008.05.029.

Davies, R.J. & Stewart, S.A. 2005. Emplacement of giant mud volcanoes in the South Caspian Basin: 3D seismic reflection imaging of their root zones. *Journal of the Geological Society, London*, **162**, 1-4, DOI: 10.1144/0016-764904-082.

Davies, R.J., Swarbrick, R.E., Evans, R.J. & Huuse, M. 2007. Birth of a mud volcano: East Java, 29 May 2006. *GSA Today*, **17**, 4-9.

Davison, I., Alsop, I. & Blundell, D. 1996. Salt tectonics: some aspects of deformation mechanics. *Geological Society, London, Special Publications*, **100**, DOI: 10.1144/GSL.SP.1996.100.01.01.

Day, S.J., Carracedo, J.C., Guillou, H. & Gravestock, P. 1999. Recent structural evolution of the Cumbre Vieja volcano, La Palma, Canary Islands: volcanic rift zone reconfiguration as a precursor to volcano flank instability? *Journal of Volcanology and Geothermal Research*, **94**, 135-167, DOI: 10.1016/S0377-0273(99)00101-8.

Delaney, P.T., Pollard, D.D., Ziony, J.I. & McKee, E.H. 1986. Field relations between dikes and joints: emplacement processes and palaeostress analysis. *Journal of Geophysical Research*, **91**, 4920-4938, DOI: 10.1029/JB091iB05p04920.

Delisle, G., Von Rad, U., Andruliet, H., Von Daniels, C.H., Tabrez, A.R. & Inam, R. 2001. Active mud volcanoes on- and offshore Makran, Pakistan. *International Journal of Earth Sciences*, **91**, 93-110, DOI: 10.1007/s005310100203.

Deville, E. & Guerlais, S.-H. 2009. Cyclic activity of mud volcanoes: evidences from Trinidad (SE Caribbean). *Marine and Petroleum Geology*, **26**, 1681-1691, DOI: 10.1016/j.marpetgeo.2009.03.002.

Deville, E., Guerlais, S-H., Callec, Y., Griboulard, R., Huyghe, P., Lallemant, S., Mascle, A., Noble, M. & Schmitz, J. 2006. Liquefied vs. stratified sediment mobilization processes: insight from the South of the Barbados accretionary prism. *Tectonophysics*, **428**, 33-47, DOI: 10.1016/j.tecto.2006.08.011.

Deville, E., Guerlais, S.-H., Lallemant, S. & Schneider, F. 2010. Fluid dynamics and subsurface sediment mobilization processes; and overview from Southeast Caribbean. *Basin Research*, **22**, 361-379, DOI: 10.1111/j.1365-2117.2010.00474.x.

Devlin, W.L., Gogswell, J. Gaskins, G., Isaksen, G., Pitcher, D., Puls, D., Stanley, K. & Wall, G. 1999. South Caspian Basin: young, cool, and full of promise. *GSA Today*, **9**, 1-9.

Dimitrov, L.I. 2002. Mud volcanoes- the most important pathway for degassing deeply buried sediments. *Earth-Science Reviews*, **59**, 49-76, DOI: 10.1016/S0012-8252(02)00069-7.

Eichhubl, P. & Boles, J.R. 2000. Focused fluid flow along faults in the Monterey Formation, coastal California. *Geological Society of America Bulletin*, **112**, 1667-1679, DOI: 10.1130/0016-7606(2000)112<1667:FFFAFI>2.0.CO;2.

Etiope, G., Caracausi, A., Favara, R., Italiano, F. & Baciu, C.L. 2002. Methane emission from the mud volcanoes of Sicily (Italy). *Geophysical Research Letters*, **29**, 1215, DOI: 10.1029/2001GL014340.

Etiope, G., Feyzullayev, A., Baciu, C.L. & Milkov, A.V. 2004. Methane emission from mud volcanoes in eastern Azerbaijan. *Geology*, **32**, 465-468, DOI: 10.1130/G20320.1.

Etiope, G. & Klusman, R.W. 2002. Geologic emissions of methane to the atmosphere. *Chemosphere*, **49**, 777-789, DOI: 10.1016/S0045-6535(02)00380-6.

Etiope, G. & Milkov, A.V. 2004. A new estimate of global methane flux from onshore and shallow submarine mud volcanoes to the atmosphere. *Environmental Geology*, **46**, 997-1002, DOI: 10.1007/s00254-004-1085-1.

Evans, R.J. 2008. *The structure, evolution and geophysical expression of mud volcano systems from the South Caspian Basin*. Ph.D. thesis, Cardiff University.

Evans, R.J., Davies, R.J. & Stewart, S.A. 2006. Internal structure and eruptive history of a kilometre-scale mud volcano system. *Basin Research*, **19**, 153-163, DOI: 10.1111/j.1365-2117.2007.00315.x.

Evans, R.J., Stewart, S.A. & Davies, R.J. 2007. Phase-reversed seabed reflections in seismic data: examples related to mud volcanoes from the South Caspian Sea. *Geo-Marine Letters*, **27**, 203-212, DOI: 10.1007/s00367-007-0073-3.

Evans, R.J., Stewart, S.A. & Davies, R.J. 2008. The structure and formation of mud volcano summit calderas. *Journal of the Geological Society, London*, **165**, 769-780, DOI: 10.1144/0016-76492007-118.

Faulkner, D.R., Jackson, C.A.L., Lunn, R.J., Schlische, R.W., Shipton, Z.K., Wibberley, C.A.J. & Withjack, M.O. 2010. A review of recent developments concerning the structure, mechanics and fluid flow properties of fault zones. *Journal of Structural Geology*, In press, DOI: 10.1016/j.jsg.2010.06.009.

Fisher, R.V. 1990. Transport and deposition of a pyroclastic surge across an area of high relief: the 18 May 1980 eruption of Mount St. Helens, Washington. *Geological Society of America Bulletin*, **102**, 1038-1054, DOI: 10.1130/0016-7606(1990)102<1038:TADOAP>2.3.CO;2.

Fortes A.D. & Grindrod, P.M. 2006. Modelling of possible mud volcanism on Titan. *Icarus*, **182**, 550-558, DOI: 10.1016/j.icarus.2005.11.013.

Fowler, S.R., Mildenhall, J., Zalova, S., Riley, G., Elsley, G., Desplanques, A. & Guliyev, F. 2000. Mud volcanoes and structural development on Shah Deniz. *Journal of Petroleum Science and Engineering*, **28**, 189-206, DOI: 10.1016/S0920-4105(00)00078-4.

Francis, P. & Wells, A. 1988. LANDSAT the 2854 matic mapper observations of debris avalanche deposits in the central Andes. *Bulletin of Volcanology*, **50**, 258–278.

Fukushima, Y., Mori, J., Hashimoto, M. & Kano, Y. 2009. Subsidence associated with the LUSI mud eruption, East Java, investigated by SAR interferometry. *Marine and Petroleum Geology*, **26**, 1740-1750, DOI: 10.1016/j.marpetgeo.2009.02.001.

Geshi, N., Shimano, T., Chiba, T. & Nakada, S. 2002. Caldera collapse during the 2000 eruption of Miyakejima Volcano, Japan. *Bulletin of Volcanology*, **64**, 55-68, DOI: 10.1007/s00445-001-0184-z.

Gorkun, V.N. & Siryk, I.M. 1968. Calculating depth of deposition and volume of gas expelled during eruptions of mud volcanoes in southern Sakhalin. *International Geology Review*, **10**, 4–12.

Goubkin, I.M. & Fedorov, S.F. 1938. Mud volcanoes of the Soviet Union and their connection with the genesis of petroleum fields in Crimea-Caucasus geologic province. *USSR Academy of Science*. In Russian.

Graue, K. 2000. Mud volcanoes in deep water Nigeria. *Marine and Petroleum Geology*, **17**, 959-974, DOI: 10.1016/S0264-8172(00)00016-7.

Guliyev, I.S., Feizullayev, A.A., Nadirov, R.S., Rakhmanov, R.R., Aliyev, A.A., Bagirov, E.B., Mukhtarov, A.SH., Tagiev, M.F., Magerramova, F.S., Murtazaev, I.R., Archer, R., Casey, D.M., Gronlie, A., Huntley, A., Mitchell, G. & Simmons, M.D. 1994. *Mud volcanoes of Azerbaijan*. Report of the GIA, BP and Statoil joint study.

Guliyev, I.S., Feizullayev, A.A. & Belov, I.S. 2000. *All about mud volcanoes*. Geology Institute, Azerbaijan Academy of Sciences, 'Nafta Press', Baku.

Guliyev, I.S. & Panahi, B. 2004. Geodynamics of the deep sedimentary basin of the Caspian Sea region: paragenetic correlation of seismicity and mud volcanism. *Geo-Marine Letters*, **24**, 169-176, DOI: 10.1007/s00367-004-0174-1.

Hammer, Ø. 2009. New statistical methods for detecting point alignments. *Computers & Geosciences*, **35**, 659-666, DOI: 10.1016/j.cageo.2008.03.012.

Hansen, D.M. 2006. The morphology of intrusion-related vent structures and their implications for constraining the timing of intrusive events along the NE Atlantic margin. *Journal of the Geological Society, London*, **163**, 789-800, DOI: 10.1144/0016-76492004-167.

Hansen, J.P.V., Cartwright, J.A., Huuse, M. & Clausen, O. 2005. 3D seismic expression of fluid migration and mud remobilization on the Gjallar Ridge, offshore mid-Norway. *Basin Research*, **10**, 1365-2117, DOI: 10.1111/j.1365-2117.2005.00257.x.

Hedberg, H. 1974. Relation of methane generation to undercompacted shales, shale diapirs and mud volcanoes. *AAPG Bulletin*, **58**, 661-673, DOI: 10.1306/83D91466-16C7-11D7-8645000102C1865D.

Holmes, A.T. 1998. Igneous intrusions. *In:* Duff, D. (eds) *Holmes principles of physical geology.* 4th edition. Stanley Thornes (Publishers) Ltd, Cheltenham, 176-206.

Holohan, E.P., Troll, V.R., Walter, T.R., Münn, S., McDonnell, S. & Shipton, Z.K. 2005. Elliptical calderas in active tectonic settings: An experimental approach. *Journal of Volcanology and Geothermal Research*, **144**, 119-136, DOI: 10.1016/j.jvolgeores.2004.11.020.

Hovland, M. 1990. Suspected gas-associated clay diapirism on the seabed off Mid Norway. *Marine and Petroleum Geology*, **7**, 267-276, DOI: 10.1016/0264-8172(90)90004-Z.

Hovland, M., Hill, A. & Stokes, D. 1997. The structure and geomorphology of the Dashgil mud volcano, Azerbaijan. *Geomorphology*, **21**, 1-15, DOI: 10.1016/S0169-555X(97)00034-2.

Hovland, M., Nygaard, E. & Thorbjørnsen, S. 1998. Piercement shale diapirism in the deep-water Vema Dome Area, Vøring Basin, Offshore Norway. *Marine and Petroleum Geology*, **15**, 191-201, DOI: 10.1016/S0264-8172(98)80004-4.

Hovland, M., Fichler, C., Rueslåtten, H. & Johnsen, H.K. 2006. Deep-rooted piercement structures in deep sedimentary basins — manifestations of supercritical water generation at depth? *Journal of Geochemical Exploration*, **89**, 157-160, DOI: 10.1016/j.gexplo.2005.11.056.

Hudson, S.M., Johnson, C.L., Efendiyeva, M.A., Rowe, H.D., Feyzullayev, A.A. & Aliyev, C.S. 2008. Stratigraphy and geochemical characterization of the Oligocene-Miocene Maikop Series: Implications for the paleogeography of Eastern Azerbaijan. *Tectonophysics*, **451**, 40-55, DOI: 10.1016/j.tecto.2007.11.045.

Hunt, J.M. 1979. *Petroleum geochemistry and geology*. San Francisco, Freeman, 617.

Hurst, A., Cartwright, J., Huuse, M., Jonk, R., Schwab, A., Duranti, D. & Cronin, B. 2003a. Significance of large-scale sand injectites as long-term fluid conduits: evidence from seismic data. *Geofluids*, **3**, 263-274, DOI: 10.1046/j.1468-8123.2003.00066.x.

Hurst, A., Cartwright, J.A. & Duranti, D. 2003b. Fluidization structures produced by upward injection of sand through a sealing lithology. *In:* Van Rensenbergen, P., Hillis, R.R., Maltman, A.J. & Morley, C.K. (eds) *Subsurface sediment remobilization*. Geological Society, London, Special Publications, **216**, 123-137.

Huuse, M., Jackson, C.A.-L., Van Rensbergen, P., Davies, R.J., Flemings, P.B. & Dixon, R.J. 2010. Subsurface sediment remobilization and fluid flow in sedimentary basins: an overview. *Basin Research*, **22**, 342-360, DOI: 10.1111/j.1365-2117.2010.00488.x.

Huuse, M., Cartwright, J., Hurst, A. & Steinsland, N. 2007. Seismic characterization of large-scale sandstone intrusions. *In:* Hurst, A. & Cartwright, J. (eds) *Sand Injectites: Implications for Hydrocarbon Exploration and Production*, *AAPG Memoirs*, **87**, 21-35.

Huuse, M., Shoulders, S.J., Netoff, D.I. & Cartwright, J. 2005. Giant sandstone pipes record basin-scale liquefaction of buried dune sands in the Middle Jurassic of SE Utah. *Terra Nova*, **17**, 80-85, DOI: 10.1111/j.1365-3121.2004.00587.x.

Istadi, B.P., Pramono, G.H., Sumintadireja, P. & Alam, S. 2009. Modeling study of growth and potential geohazard for LUSI mud volcano: East Java, Indonesia. *Marine and Petroleum Geology*, **26**, 1724-1739, DOI: 10.1016/j.marpetgeo.2009.03.006.

Iverson, R.M. 1997. The physics of debris flows. *Reviews of Geophysics*, **35**, 245-296, DOI: 10.1029/97RG00426.

Jackson, J., Priestley, K., Allen, M.B. & Berberian, M. 2002. Active tectonics of the South Caspian Basin. *Geophysical Journal International*, **148**, 214-245, DOI: 10.1046/j.1365-246X.2002.01588.x.

Jolly, R.J.H., Cosgrove, J.W. & Dewhurst, D.N. 1998. Thickness and spatial distributions of clastic dykes, northwest Sacramento Valley, California. *Journal of Structural Geology*, **20**, 1663-1672, DOI: 10.1016/S0191-8141(98)00053-4.

Jolly, R. & Lonergan, L. 2002. Mechanisms and controls on the formation of sand intrusions. *Journal of the Geological Society, London*, **159**, 605-617, DOI: 10.1144/0016-764902-025.

Jonk, R., Hurst, A., Duranti, D., Parnell, J., Mazzini, A. & Fallick, A.E. 2005. Origin and timing of sand injection, petroleum migration, and diagenesis in Tertiary reservoirs, south Viking Graben, North Sea. *AAPG Bulletin*, **89**, 329-357, DOI: 10.1306/10260404020.

Judd, A.G. & Hovland, M. 1992. The evidence of shallow gas in marine sediments. *In:* Davies, A.M. (ed.) *Methane in marine sediments*. Continental Shelf Research, **12**, 1081-1097.

Judd, A.G. & Hovland, M. 2007. *Seabed fluid flow*. Cambridge University Press, 475, DOI: 10.2277/0521819504.

Kadirov, F.A. & Mukhtarov, A.SH. 2004. Geophysical fields, deep structure, and dynamics of the Lökbatan mud volcano. *Izvestiya. Physics of the Solid Earth*, **40**, 327-333.

Kalinko, M.K. 1964. *Osnovnye zakonomernosti raspredeleniya nefti i gaza v zemnoi kore* (Main trends in the distribution of oil and gas in the Earth's crust). Moscow: Nedra. In Russian.

Kennedy, B., Stix, J., Vallance, J.W., Lavallée, Y. & Longpré, M-A. 2004. Controls on caldera structure: results from analogue sandbox modeling. *GSA Bulletin*, **116**, 515-524, DOI: 10.1130/B25228.1.

Knapp, C.C., Knapp, J.H. & Connor, J.A. 2004. Crustal-scale structure of the South Caspian Basin revealed by deep seismic reflection profiling. *Marine and Petroleum Geology*, **21**, 1073-1081, DOI: 10.1016/j.marpetgeo.2003.04.002.

Kokelaar, P. & Romagnoli, C. 1995. Sector collapse, sedimentation and clast population evolution at an active island-arc volcano: Stromboli, Italy. *Bulletin of Volcanology*, **57**, 240-262, DOI: 10.1007/BF00265424.

Kopf, A. 2002. Significance of mud volcanism. *Reviews of Geophysics,* **40**, 1005, DOI: 10.1029/2000RG000093.

Kopf, A. & Behrmann, J.H. 2000. Extrusion dynamics of mud volcanoes on the Mediterranean Ridge accretionary complex. *Journal of the Geological Society, London, Special Publications,* **174**, 169-204, DOI: 10.1144/GSL.SP.1999.174.01.10.

Kopf, A., Deyhle, A., Lavrushin, V.Y., Polyak, B.G., Gieskes, J.M., Buachidize, G.I., Wallmann, K. & Eisenhauer, A. 2003. Isotopic evidence (He, B, C) for deep fluid and mud mobilization from mud volcanoes in the Caucasus continental collision zone. *International Journal of Earth Sciences,* **92**, 407-425, DOI: 10.1007/s00531-003-0326-y.

Kopf, A., Stegmann, S., Delisle, G., Panahi, B., Aliyev, C.S. & Guliyev, I. 2009. In situ cone penetration tests at the active Dashgil mud volcano, Azerbaijan: evidence for excess fluid pressure, updoming, and possible future violent eruption. *Marine and Petroleum Geology*, **26**, 1716-1723, DOI: 10.1016/j.marpetgeo.2008.11.005.

Kusumastuti, A., Van Rensbergen, P. & Warren, J.K. 2002. Seismic sequence analysis and reservoir potential of drowned Miocene carbonate platforms in the Madura Strait, East Java, Indonesia. *AAPG Bulletin*, **86**, 213-232, DOI: 10.1306/61EEDA94-173E-11D7-8645000102C1865D.

Lagmay, A.M.F. & Valdivia, W. 2006. Regional stress influence on the opening direction of crater amphitheaters in Southeast Asian volcanoes. *Journal of Volcanology and Geothermal Research*, **158**, 139–150, DOI: 10.1016/j.jvolgeores.2006.04.020.

Leat, P.T., Tate, A.J., Tappin, D.R., Day, S.J. & Owen, M.J. 2010. Growth and mass wasting of volcanic centres in the northern South Sandwich arc, South Atlantic, revealed by new multibeam mapping. *Marine Geology*, **275**, 110-126, DOI: 10.1016/j.margeo.2010.05.001.

Lerche, I. & Bagirov, E. 1999. *Impact of natural hazards on oil and gas extraction, the South Caspian Basin.* Kluwer Academic/Plenum Publishers, 353.

Lerche, I., Bagirov, E., Nadirov, F., Tagliyev, M. & Guliyev, I.S. 1997. *Evolution of the South Caspian Basin: geologic risks and probable hazards*. Institute of Geology of Azerbaijan Academy of Sciences, Baku, 580.

Leyrit, H. 2000. Flank collapse and debris avalanche deposits. *In:* Leyrit, H. & Montenat, C. (eds) *Volcaniclastic rocks, from magmas to sediments*. Gordon and Breach Science Publishers, 111-130.

Lipman, P.W. 1997. Subsidence of ash-flow calderas: relation to caldera size and magma-chamber geometry. *Bulletin of Volcanology and Geothermal Research,* **59**, 198-218, DOI: 10.1007/s004450050186.

Lipman, P.W. 2000. Calderas. *In*: Sigurdsson, H., Houghton, B.F., McNutt, S.R., Rymer, H. & Stix, J. (eds) *Encyclopedia of volcanoes*. Academic Press, San Francisco, 642-662.

Londe, P. 1987. Malpasset dam failure. *Engineering Geology*, **24**, 295-329.

López, D.L. & Williams, S.N. 1993. Catastrophic volcanic collapse: relation to hydrothermal processes. *American Association for the Advancement of Science*, **260**, 1794-1796, DOI: 10.1126/science.260.5115.1794.

Lorenz, V. 1986. On the growth of maars and diatremes and its relevance to the formation of tuff rings. *Bulletin of Volcanology*, **48**, 265-274, DOI: 10.1007/BF01081755.

Løseth, H., Wensaas, L., Anrntsen, B., Hanken, N., Basire, C. & Graue, K. 2001. 1000 m long gas blow-out pipes. *In: EAGE 63rd Conference and Technical Exhibition*. Amsterdam, The Netherlands.

Lowe, D.R. 1975. Water escape structures in coarse grained sediments. *Journal of Sedimentary Petrology*, **44**, 484-501, DOI: 10.1111/j.1365-3091.1975.tb00290.x.

Lundgren, P., Berardino, P., Coltelli, M., Fornaro, G., Lanari, R., Puglisi, G., Sansosti, E. & Tesauro, M. 2003. Coupled magma chamber inflation and sector collapse slip observed with synthetic aperture radar interferometry on Mt. Etna volcano. *Journal of Geophysical Research*, **108**, 2247, DOI: 10.1029/2001JB000657.

Lutz, T.M. 1986. An analysis of the orientations of large scale crustal structures: A statistical approach based on areal distributions of pointlike features. *Journal of Geophysical Research*, **91**, 421-434, DOI: 10.1029/JB091iB01p00421.

Macedonio, G., Dobran, F. & Augusto, N. 1994. Erosion processes in volcanic conduits and application to the AD 79 eruption of Vesuvius. *Earth and Planetary Science Letters*, **121**, 137-152, DOI: 10.1016/0012-821X(94)90037-X.

Magara, K. 1981. Mechanisms of natural fracturing in a sedimentary basin. *AAPG Bulletin*, **65**, 123-132, DOI: 10.1306/2F919783-16CE-11D7-8645000102C1865D.

Maltman, A.J. 1994. Introduction and overview. *In:* Maltman, A.J. (ed.) *The geological deformation of sediments*. Chapman and Hall, London, 1-35.

Maltman, A.J. & Bolton, A. 2003. How sediments become mobilized. *In:* Van Rensbergen, P., Hillis, R.R., Maltman, A.J. & Morley, C.K. (eds) *Subsurface sediment mobilization.* Geological Society, London, Special Publications, **216**, 9-20.

Manga, M. 2007. Did an earthquake trigger the May 2006 eruption of the Lusi Mud Volcano? *Eos Transactions, AGU*, **88**, DOI: 10.1029/2007EO180009.

Manga, M. & Brodsky, E.E. 2006. Seismic triggering of eruptions in the far field: volcanoes and geysers. *Annual Review of Earth Planetary Sciences*, **34**, 263–291, DOI: 10.1146/annurev.earth.34.031405.125125.

Manga, M., Brumm, M. & Rudolph, M.L. 2009. Earthquake triggering of mud volcanoes. *Marine and Petroleum Geology*, **26**, 1785-1798, DOI: 10.1016/j.marpetgeo.2009.01.019.

Marsh, B.D. 1982. On the mechanisms of igneous diapirism, stoping, and zone melting. *American Journal of Science*, **282**, 808-855, DOI: 10.2475/ajs.282.6.808.

Martinelli, G. & Judd, A. 2004. Mud volcanoes of Italy. *Geological Journal*, **39**, 49-61, DOI: 10.1002/gj.943.

Masson, D.G., Watts, A.B., Gee, M.J.R., Urgeles, R., Mitchell, N.C., Le Bas, T.P. & Canals, M. 2002. Slope failures on the flanks of the western Canary Islands. *Earth Science Reviews*, **57**, 1-35, DOI: 10.1016/S0012-8252(01)00069-1.

Mattoli, G.S., Jansma, P.E., Jaramillo, L. & Smith, A.L. 1995. Sector collapse in island arc volcanoes: a digital topographic and bathymetric investigation of the Qualibou Depression, St. Lucia, Lesser Antilles. *Caribbean Journal of Science*, **31**, 163-173.

Mauk, F.J. & Johnston, M.J.S. 1973. On the triggering of volcanic eruptions by Earth tides. *Journal of Geophysical Research*, **78**, 3356-3362, DOI: 10.1029/JB078i017p03356.

Mazzini, A., Svensen, H., Akhmanov, G.G., Aloisi, G., Planke, S., Malthe-Sørenssen, A. & Istadi, B. 2007. Triggering and dynamic evolution of the LUSI mud volcano, Indonesia. *Earth and Planetary Science Letters*, **261**, 375-388, DOI: 10.1016/j.epsl.2007.07.001.

Mazzini, A., Svensen, H., Planke, S., Guliyev, I., Akhmanov, G.G.M. Fallik, T. & Banks, D. 2009. When mud volcanoes sleep: insights from seep geochemistry at the Dashgil mud volcano, Azerbaijan. *Marine and Petroleum Geology*, **26**, 1704-1715, DOI: 10.1016/j.marpetgeo.2008.11.003.

McGuire, W.J. & Pullen, A.D. 1989. Location and orientation of eruptive fissures and feeder dykes at Mount Etna; influence of gravitational and regional tectonic stress regimes. *Journal of Volcanology and Geothermal Research*, **38**, 325-344, DOI: 10.1016/0377-0273(89)90046-2.

Mellors, R., Kilb, D., Aliyev, A., Gasanov, A. & Yetirmishli, G. 2007. Correlations between earthquakes and large mud volcano eruptions. *Journal of Geophysical Research*, **112**, 11, DOI: 10.1029/2006JB004489.

Milkov, A.V. 2000. Worldwide distribution of submarine mud volcanoes and associated gas hydrates. *Marine Geology*, **167**, 29–42, DOI: 10.1016/S0025-3227(00)00022-0.

Milkov, A.V., Sassen, R., Apanasovich, T.V. & Dadashev, F.G. 2003. Global gas flux from mud volcanoes: a significant source of fossil methane in the atmosphere and the ocean. *Geophysical Research Letters*, **30**, 1037, DOI: 10.1029/2002GL016358.

Mitchell, A. 2005. The ESRI guide to GIS analysis. Volume 2: Spatial measurements and statistics: ESRI Press, California, 238.

Moores, E.M. & Vine, F.J. 1971. Troodos Massif, Cyprus and other ophiolites as ocean crust: evaluations and implications. *Philosophical Transactions of the Royal Society of London*, Serial A, **268**, 443-446, DOI: 10.1098/rsta.1971.0006.

Morley, C.K. 2002. *Structural geology of the Berakas Syncline regional-reservoir scale perspectives*. Universiti Brunei Darussalam, Department of Petroleum Geosciences. Fieldtrip for Brunei Shell.

Morley, C.K. 2003. Outcrop examples of mudstone intrusions from the Jerudong Anticline. *In:* Van Rensenbergen, P., Hillis, R.R., Maltman, A.J. & Morley, C.K. (eds) *Subsurface sediment remobilization*. Geological Society, London, Special Publications, **216**, 381-394.

Morley, C.K., Crevello, P. & Ahmad, Z.H. 1998. Shale tectonics associated with active diapirism; the Jerudong Anticline, Brunei Darussalam. *Journal of the Geological Society, London*, **155**, 475-490, DOI: 10.1144/gsjgs.155.3.0475.

Morley, C.K. & Guerin, G. 1996. Comparison of gravity-driven deformation styles and behaviour associated with mobile shales and salt. *Tectonics*, **15**, 1154-1170, DOI: 10.1029/96TC01416.

Moss, J.L. & Cartwright, J. 2010. The spatial and temporal distribution of pipe formation, offshore Nambia. *Marine and Petroleum Geology*, **27**, 1216-1234, DOI: 10.1016/j.marpetgeo.2009.12.013.

Mueller, S., Llewellin, E.W. & Mader, H.M. 2010. The rheology of suspensions of solid particles. *Proceedings of the Royal Society A: Mathematical, Physical and Engineering Sciences,* **466**, 1201-1228, DOI: 10.1098/rspa.2009.0445.

Murton, B.J. & Biggs, J. 2003. Numerical modelling of mud volcanoes and their flows using constraints from the Gulf of Cadiz. *Marine Geology*, **195**, 223-236, DOI: 10.1016/S0025-3227(02)00690-4.

Nadirov, R.S., Bagirov, E., Tagiyev, M. & Lerche, I. 1997. Flexural plate subsidence, sedimentation rates, and structural development of the super-deep South Caspian Basin. *Marine and Petroleum Geology*, **14**, 383-400, DOI: 10.1016/S0264-8172(96)00054-2.

Nakamura, K. 1977. Volcanoes as possible indicators of tectonic stress orientation- principle and proposal. *Journal of Volcanology and Geothermal Research*, **2**, 1-16, DOI: 10.1016/0377-0273(77)90012-9.

Narimanov, A.A. 1993. The petroleum systems of the South Caspian Basin. *In:* Doré, A.G., Augustson, J.H., Hermanrud, C., Stewart, D.J. & Sylta, O. (eds) *Basin Modeling Advances and Applications*. Norwegian Petroleum Society, Special Publications, **3**, 599–608.

Oehler, D.Z. & Allen, C.C. 2010. Evidence for pervasive mud volcanism in Acidalia Planitia, Mars. *Icarus*, **208**, 636-657, DOI: 10.1016/j.icarus.2010.03.031.

Osborne, M.J. & Swarbrick, R.E. 1997. Mechanisms for driving overpressure in sedimentary basins: a reevaluation. *AAPG Bulletin*, **81**, 1023-1041.

Parize, O. & Friès, G. 2003. The Vocontian clastic dykes and sills: a geometric model. *Geological Society, London, Special Publications*, **216**, 51-72, DOI: 10.1144/GSL.SP.2003.216.01.05.

Paulsen, T.S. & Wilson, T.J. 2010a. New criteria for systematic mapping and reliability assessment of monogenetic volcanic vent alignments and elongate volcanic vents for crustal stress analyses. *Tectonophysics*, **482**, 16-28, DOI: 10.1016/j.tecto.2009.08.025.

Paulsen, T.S. & Wilson, T.J. 2010b. Evolution of Neogene volcanism and stress patterns in the glaciated West Antarctic Rift, Marie Byrd Land, Antarctica. *Journal of the Geological Society, London*, **167**, 401-416, DOI: 10.1144/0016-76492009-044.

Petford, N. 1996. Dykes or Diapirs? *In:* Brown, M., Candela, P.A., Peck, D.L., Stephens, W.E., Walker, R.J. & Zen, E-an (eds) *The third Hutton symposium on the origin of granites and related rocks*. The Geological Society of America, Special Papers, **315**, 105-114.

Pickering, K.T., Agar, S.M. & Ogawa, Y. 1988. Genesis and deformation of mud injections containing chaotic basalt-limestone-chert associations: examples from the southwest Japan forearc. *Geology*, **16**, 881-885, DOI: 10.1130/0091-7613(1988)016<0881:GADOMI>2.3.CO;2.

Pinotti, L.P., Coniglio, J.E., Esparza, A.M., Eramo, F.J. & Llambías, E.J. 2002. Nearly circular plutons emplaced by stoping at shallow crustal levels, Cerro Aspero Batholith, Sierras Pampeanas de Córdoba, Argentina. *Journal of South American Earth Sciences*, **15**, 251-265, DOI: 10.1016/S0895-9811(02)00033-0.

Planke, S., Svensen, H., Hovland, M. & Banks, D.A. 2003. Mud and fluid migration in active mud volcanoes in Azerbaijan. *Geo-Marine Letters,* **23**, 258-268, DOI: 10.1007/s00367-003-0152-z.

Ramsay, J.G. & Huber, M.I. 1987. *The techniques of modern structural geology, Volume 2: folds and fractures*. Academic Press, London, 391.

Reading, H.G. 1996. *Sedimentary environments: processes, facies and stratigraphy*. Wiley-Blackwell Science, Oxford, 704.

Reid, M.E. 2004. Massive collapse of volcano edifices triggered by hydrothermal pressurization. *Geology*, **32**, 272-376, DOI: 10.1130/G20300.1.

Reid, M.E., Sisson, T.W. & Brien, D.L. 2001. Volcano collapse promoted by hydrothermal alteration and edifice shape, Mount Rainier, Washington. *Geology*, **29**, 779-782, DOI: 10.1130/0091-7613(2001)029.

Reilly, M.J. & Flemings, P.B. 2010. Deep pore pressures and seafloor venting in the Auger Basin, Gulf of Mexico. *Basin Research*, **22**, 380-397, DOI: 10.1111/j.1365-2117.2010.00481.x.

Reynolds, A.D., Simmons, M.D., Bowman, B.J., Henton, J., Brayshaw, A.C., Ali-Zade, A.A., Guliyev, I.S., Suleymanova, S.F., Ataeva, E.Z., Mamedova, D.N. & Koshkarly, R.O. 1998. Implications of outcrop geology for reservoirs in the Neogene Productive Series: Apsheron peninsula, Azerbaijan. *AAPG Bulletin,* **82**, 25–49.

Roberts, K.S., Davies, R.J. & Stewart, S.A. 2010. Structure of exhumed mud volcano feeder complexes, Azerbaijan. *Basin Research*, **22**, 439-451, DOI: 10.1111/j.1365-2117.2009.00441.x.

Roberts, K.S., Davies, R.J., Stewart, S.A. & Tingay, M. *Accepted for publication*. Structural controls on mud volcano vent distributions: examples from Azerbaijan and Lusi, east Java. *Journal of the Geological Society, London,* DOI: 10.1144/0016-76492010-158.

Roberts, K.S., Stewart, S.A., Davies, R.J. & Evans, R.J. 2011. Sector collapse of mud volcanoes, Azerbaijan. *Journal of the Geological Society, London*, **168**, 1–12, DOI: 10.1144/0016-76492010-115.

Robertson, A.H.F. & Kopf, A. 1998. Tectonic setting and processes of mud volcanism on the Mediterranean Ridge accretionary complex: Evidence from Leg 160. *In*: Robertson, A.H.F., Emeis, K.–C., Richter, C. & Camerlengthi, A. (eds) *Proceedings of the Ocean Drilling Program, Scientific Results*. Ocean Drilling Program, College Station, Texas, **160**, 665-680.

Sawolo, N., Sutrioni, E., Istadi, B.P. & Darmoyo, A.B. 2009. The LUSI mud volcano triggering controversy: was it caused by drilling? *Marine and Petroleum Geology*, **26**, 1766-1784, DOI: 10.1016/j.marpetgeo.2009.04.002.

Scholte, K.H., Hommels, A., Van Der Meer, F.D., Slob, E.C., Kroonenberg, S.B., Aliyeva, E., Huseynov, D. & Guliyev, I. 2003. Subsurface resistivity in combination with hyperspectral field and satellite data for mud volcano dynamics, Azerbaijan. *Geoscience and Remote Sensing*

Symposium, 2003, IGARSS'03 Proceedings, 2003 IEEE International, **5**, 3395-3397, DOI: 10.1109/IGARSS.2003.1294794.

Schroot, B.M., Klaver, G.T. & Schüttenhelm, R.T.E. 2005. Surface and subsurface expressions of gas seepage to the seabed- examples from the Southern North Sea. *Marine and Petroleum Geology*, **22**, 499-515, DOI: 10.1016/j.marpetgeo.2004.08.007.

Sibson, R.H. 1990. Conditions for fault-valve behaviour. *Geological Society of London, Special Publication*, **54**, 15-28, DOI: 10.1144/GSL.SP.1990.054.01.02.

Sibson, R.H. 1992. Implications of fault-valve behaviour for rupture nucleation and recurrence. *Tectonophysics*, **211**, 283-293, DOI: 10.1016/0040-1951(92)90065-E.

Sibson, R.H. 1996. Structural permeability of fluid-driven fault-fracture meshes. *Journal of Structural Geology*, **18**, 1031-1042, DOI: 10.1016/0191-8141(96)00032-6.

Siebert, L. 1984. Large volcanic debris avalanches: characteristics of source areas, deposits, and associated eruptions. *Journal of Volcanology and Geothermal Research*, **22**, 163-197, DOI: 10.1016/0377-0273(84)90002-7.

Siebert, L., Glicken, H. & Ui, T. 1987. Volcanic hazards from Bezymianny- and Bandai-type eruptions. *Bulletin of Volcanology*, **49**, 435-459, DOI: 10.1007/BF01046635.

Sigurdsson, H., Houghton, B., McNutt, S.R., Rymer, H. & Stix, J. 2000. *Encyclopedia of volcanoes*. Academic Press, 1417.

Skinner, J.A. & Tanaka, K.L. 2009. Evidence for and implications of sedimentary diapirism and mud volcanism in the southern Utopia highland-lowland boundary plain, Mars. *Icarus*, **186**, 41-59, DOI: 10.1016/j.icarus.2006.08.013.

Snead, R.J. 1964. Active mud volcanoes of Baluchistan, West Pakistan. *The Geographical Review*, **54**, 545–560.

Somoza, L., Díaz-Del-Río, V., León, R., Ivanov, M., Fernandez-Puga, M.C., Gardner, J.M., Hernandez-Molina, F.J., Pinheiro, L.M., Rodero, J., Lobato, A., Maestro, A., Vazquez, J.T., Medialdea, T. & Fernandez-Salas, L.M. 2003. Seabed morphology and hydrocarbon seepage in the Gulf of Cadiz mud volcano area: acoustic imagery, multibeam and ultra-high resolution seismic data. *Marine Geology*, **195**, 153-176, DOI: 10.1016/S0025-3227(02)00686-2.

Stewart, S.A. 1999. Seismic interpretation of circular geological structures. *Petroleum Geoscience*, **5**, 273-285.

Stewart, S.A. 2006. Implications of passive salt diapir kinematics for reservoir segmentation by radial and concentric faults. *Marine and Petroleum Geology*, **23**, 843-853, DOI: 10.1016/j.marpetgeo.2006.04.001.

Stewart, S.A. & Davies, R.J. 2006. Structure and emplacement of mud volcano systems in the South Caspian Basin. *AAPG Bulletin*, **90**, 771-786, DOI: 10.1306/11220505045.

Tibaldi, A. 1995. Morphology of pyroclastic cones and tectonics. Journal of Geophysical Research, **100**, 24,521-24,535, DOI: 10.1029/95JB02250.

Tingay, M. 2010. Anatomy of the 'Lusi' Mud Eruption, East Java. *ASEG Extended Abstract*, 1-6, DOI: 10.1071/ASEG2010ab241.

Tingay, M., Heidbach, O., Davies, R.J. & Swarbrick, R.E. 2008. Triggering of the Lusi mud eruption: earthquake versus drilling initiation. *Geology*, **36**, 639-642, DOI: 10.1130/G24697A.1.

Tingay, M., Hillis, R.R., Morley, C.K., Swarbrick, R.E. & Drake, S.J. 2005. Present-day stress orientation in Brunei: a snapshot of 'prograding tectonics' in a Tertiary delta. *Journal of the Geological Society, London*, **162**, 39-49, DOI: 10.1144/0016-764904-017.

Tingay, M., Morley, C.K., King, R.E., Hillis, R.R., Hall, R. & Coblentz, D. 2010. Present-day stress field of Southeast Asia. *Tectonophysics*, **482**, 92-104, DOI: 10.1016/j.tecto.2009.06.019.

Ui, T., Takarada, S. & Yoshimoto, M. 2000. Debris avalanches. *In:* Sigurdsson, H., Houghton, B., McNutt, S.R., Rymer, H. & Stix, J. (eds) *Encyclopedia of volcanoes*. Academic Press, 617-626.

Van Rensbergen, P. & Morley, C.K. 2003. Re-evaluation of mobile shale occurrences on seismic sections of the Champion and Baram deltas, offshore Brunei. *In:* Van Rensbergen, P., Hillis, R.R., Maltman, A.J. & Morley, C.K. (eds) *Subsurface sediment mobilization.* Geological Society, London, Special Publications, **216**, 395-411, DOI: 10.1144/GSL.SP.2003.216.01.26.

Van Rensbergen, P., Morley, C.K., Ang, D.W., Hoan, T.Q. & Lam, N.T. 1999. Structural evolution of shale diapirs from reactive rise to mud volcanism: 3D seismic data from the Baram delta, offshore Brunei Darussalam. *Journal of the Geological Society*, **156**, 633-650, DOI: 10.1144/gsjgs.156.3.0633.

Van Wyk De Vries, B., Kerle, N. & Petley, D. 2000. Sector collapse forming at Casita volcano, Nicaragua. *Geology*, **28**, 167-170, DOI: 10.1130/0091-7613.

Vendeville, B.C. & Jackson, M.P.A. 1992. The rise of diapirs during thin-skinned extension. *Marine and Petroleum Geology*, **9**, 331-354, DOI: 10.1016/0264-8172(92)90047-I.

Voight, B. & Elsworth, D. 1997. Failure of volcano slopes. *Geotechníque,* **47**, 1-31.

Von Rad, U., Berner, U., Delisle, G., Doose-Rolinski, H., Fechner, N., Linke, P., Lückge, A., Roeser, H.A., Schmaljohann, R. & Wiedicke, M. 2000. Gas and fluid venting at the Makran accretionary wedge off Pakistan. *Geo-Marine Letters*, **20**, 10-19, DOI: 10.1007/s003670000033.

Wadge, G. & Cross, A. 1988. Quantitative methods for detecting aligned points: an application to the volcanic vents of the Michoacan-Guanajuato volcanic field, Mexico. *Geology*, **16**, 815-818, DOI: 10.1130/0091-7613(1988)016<0815:QMFDAP>2.3.CO;2.

Wiedicke, M., Neben, S. & Spiess, V. 2001. Mud volcanoes at the front of the Makran accretionary complex, Pakistan. *Marine Geology*, **172**, 57-73, DOI: 10.1016/S0025-3227(00)00127-4.

Winslow, M.A. 1983. Clastic dike swarms and the structural evolution of the foreland fold and thrust belt of the southern Andes. *Geological Society of America Bulletin*, **94**, 1073-1080, DOI: 10.1130/0016-7606(1983)94<1073:CDSATS>2.0.CO;2.

Yassir, N. 1990. The undrained shear behaviour of fine-grained sediments. *Geological Society, London, Special Publications,* **54**, 399-404, DOI: 10.1144/GSL.SP.1990.054.01.36.

Yassir, N. 2003. The role of shear stress in mobilizing deep-seated mud volcanoes: geological and geomechanical evidence from Trinidad and Taiwan. *In:* Van Rensbergen, P., Hillis, R.R., Maltman, A.J. & Morley, C.K. (eds) *Subsurface sediment mobilization.* Geological Society, London, Special Publications, **216**, 461-474, DOI: 10.1144/GSL.SP.2003.216.01.30.

Yassir, N. & Bell, J. 1996. Abnormally high fluid pressures and associated porosities and stress regimes in sedimentary basins. *SPE Formation Evaluation*, **11**, 5-10, 10.2118/28139-PA.

Yusifov, M. 2004. *Seismic interpretation and classification of mud volcanoes of the South Caspian Basin, offshore Azerbaijan*. MSc thesis, Texas A & M University.

Yusifov, M. & Rabinowitz, P.D. 2004. Classification of mud volcanoes in the South Caspian Basin, offshore Azerbaijan. *Marine and Petroleum Geology*, **21**, 965-975, DOI: 10.1016/j.marpetgeo.2004.06.002.

The Geological Survey of Indonesia 1963. Geological map of Djawa and Madura. *Geological Survey of Indonesia.*